

Geologic Studies in Alaska by the U.S. Geological Survey, 1991

DWIGHT C. BRADLEY and CYNTHIA DUSEL-BACON, Editors

U.S. GEOLOGICAL SURVEY BULLETIN 2041

U.S. DEPARTMENT OF THE INTERIOR
MANUEL LUJAN, JR., Secretary



U.S. GEOLOGICAL SURVEY
Dallas L. Peck, Director

Any use of trade, product, or firm names
in this publication is for descriptive purposes only
and does not imply endorsement by the U.S. Government

UNITED STATES GOVERNMENT PRINTING OFFICE, WASHINGTON : 1992

For sale by
Book and Open-File Report Sales
U.S. Geological Survey
Federal Center, Box 25286
Denver, CO 80225

COVER: Aerial view looking southwest from Muldrow Glacier toward Mount McKinley (elevation 6,193 m), the summit of which is covered by an ice cloud. The combination of more than 4,000 m vertical relief and granitoid bedrock containing minerals suitable for fission-track dating is ideal for determination of uplift rates (see article by Plafker and others, page 202). Photograph by George Plafker, July 1976.

CONTENTS

Introduction 1

Dwight C. Bradley and Cynthia Dusek-Bacon

MINERAL RESOURCE STUDIES — ARTICLES

Fluid-inclusion study of the Rock Creek area, Nome Mining District, Seward Peninsula, Alaska 3

Lori E. Apodaca

Geochemistry of lode-gold deposits, Nuka Bay district, southern Kenai Peninsula 13

J. Carter Borden, Richard J. Goldfarb, Carol A. Gent, Robert C. Burruss, and Bruce H. Roushey

Placer gold of the Kenai lowland 23

Barrett A. Cieutat, Richard J. Goldfarb, Dwight C. Bradley, and Bruce H. Roushey

Summary of results of the mineral resource assessment of the Bethel and southeastern part of the Russian Mission 1° by 3° quadrangles, Alaska 30

Thomas P. Frost, Stephen E. Box, and Elizabeth J. Moll-Stalcup

Comparison of the effectiveness of stream-sediment, heavy-mineral-concentrate, aquatic-moss, and stream-water geochemical sample media for the mineral assessment study of the Iditarod quadrangle, Alaska 49

John E. Gray, Philip L. Hageman, and Jean L. Ryder

Geochemically anomalous areas in the west-central part of the Howard Pass quadrangle, National Petroleum Reserve, Alaska: Evidence for sediment-hosted Zn-Pb-Ag-Ba mineralization 60

Karen D. Kelly, J. Carter Borden, Elizabeth A. Bailey, David L. Fey, Jerry M. Motooka, and Bruce H. Roushey

A followup geochemical survey of base-metal anomalies in the Ward Creek/Windfall Harbor and Gambier Bay areas, Admiralty Island, Southeast Alaska 70

Cliff D. Taylor, Barrett A. Cieutat, and Lance D. Miller

Experimental abrasion of detrital gold in a tumbler 86

Warren Yeend

MINERAL RESOURCE STUDIES — GEOLOGIC NOTES

Gold in the Usibelli Group coals, Nenana Coal Field, Alaska 93

Gary D. Stricker, Richard B. Tripp, John B. McHugh, Ronald H. Affolter, and John B. Cathrall

Rare earth minerals in "thunder eggs" from Zarembo Island, southeast Alaska 98

John Philpotts and John R. Evans

GEOLOGIC FRAMEWORK STUDIES — ARTICLES

- Upper Devonian shallow-marine siliciclastic strata and associated fauna and flora, Lime Hills D-4 quadrangle, southwest Alaska 106
Robert B. Blodgett and Wyatt G. Gilbert
- Petrography and provenance of sandstones from the Nation River Formation (Devonian) and the Step Conglomerate (Permian), Kandik region, east-central Alaska 116
Thomas Brocculeri, Michael B. Underwood, and David G. Howell
- Magnetic susceptibilities and iron content of plutonic rocks across the coast plutonic-metamorphic complex near Juneau, Alaska 125
James L. Drinkwater, Arthur B. Ford, and David A. Brew
- High-pressure amphibolite-facies metamorphism and deformation within the Yukon-Tanana and Taylor Mountain terranes, eastern Alaska 140
Cynthia Dusel-Bacon and Vicki L. Hansen
- Some facies aspects of the upper part of the Kenai Group, southern Kenai Peninsula 160
Romeo M. Flores and Gary D. Stricker
- Sedimentology of the Bay of Pillars and Point Augusta Formations, Alexander Archipelago, Alaska 171
Susan M. Karl and Closey F. Giffen
- Depositional environments and some aspects of the fauna of middle Ordovician rocks of the Tetsitna Formation, northern Kuskokwim Mountains, Alaska 186
Elizabeth A. Measures, David M. Rohr, and Robert B. Blodgett
- Cenozoic uplift history of the Mount McKinley area in the central Alaska Range based on fission-track dating 202
George Plafker, Charles W. Naeser, Robert A. Zimmerman, John S. Lull, and Travis Hudson
- Isotopic variations in calcite veins from the Kandik region of east-central Alaska 213
Kevin L. Shelton, Michael B. Underwood, Deborah Bergfeld, and David G. Howell
- Statistical comparison between illite crystallinity and vitrinite reflectance, Kandik region of east-central Alaska 222
Michael B. Underwood, Thomas Brocculeri, Deborah Bergfeld, David G. Howell, and Mark Pawlewicz

GEOLOGIC FRAMEWORK STUDIES — GEOLOGIC NOTE

- The Arctic Alaska superterrane 238
Thomas E. Moore

BIBLIOGRAPHIES

- U.S. Geological Survey reports on Alaska released in 1991 245
Compiled by Ellen R. White
- Reports about Alaska in non-USGS publications released in 1991 that include USGS authors 250
Compiled by Ellen R. White

CONTRIBUTORS TO THIS BULLETIN

Anchorage

U.S. Geological Survey
4200 University Drive
Anchorage, Alaska 99508-4667

Bailey, Elizabeth A.
Bradley, Dwight, C.
Karl, Susan M.

Denver

U.S. Geological Survey MS-
Box 25046 Denver Federal Center
Lakewood, Colorado 80225-0046

Affolter, Ronald H. MS 972
Apodaca, Lori E. MS 973
Borden, J. Carter MS 973
Burruss, Robert C. MS 973
Cathrall, John B. MS 973
Cieutat, Barrett A. MS 973
Fey, David L. MS 973
Flores, Romeo M. MS 972
Gent, Carol A. MS 973
Goldfarb, Richard J. MS 973
Gray, John E. MS 973
Hageman, Philip L. MS 973
Kelley, Karen D. MS 973
McHugh, John B. MS 973
Motooka, Jerry M. MS 973
Naeser, Charles W. MS 963
Pawlewicz, Mark MS 940
Roushey, Bruce H. MS 973
Ryder, Jean L. MS 973
Stricker, Gary D. MS 972
Taylor, Cliff D. MS 973
Tripp, Richard B. MS 973
Zimmerman, Robert A. MS 905

Menlo Park

U.S. Geological Survey MS-904
345 Middlefield Road
Menlo Park, California 94025

Brew, David A.
Drinkwater, James L.
Dusel-Bacon, Cynthia
Ford, Arthur B.
Howell, David G.
Lull, John S.
Moore, Thomas E.
Plafker, George
White, Ellen R. (MS 955)
Yeend, Warren

Reston

U.S. Geological Survey
National Center, MS-
12201 Sunrise Valley Drive
Reston, Virginia 22092

Blodgett, Robert B. MS 970
Evans, John R. MS 957
Moll-Stalcup, Elizabeth J. MS 959
Philpotts, John MS 923

Spokane

U.S. Geological Survey
W 920 Riverside Ave, Rm. 656
Spokane, WA 99201

Box, Stephen E.
Frost, Thomas P.

Outside

Bergfeld, Deborah
Brocculeri, Thomas
Shelton, Kevin L.
Underwood, Michael B.
Department of Geological Sciences
University of Missouri
Columbia, Missouri 65211

Giffen, Closey F.
North Pacific Mining Corporation
121 W. Fireweed Road, Suite 102
Anchorage, Alaska 99503

Gilbert, Wyatt G.
Alaska Division of Geological and Geophysical Surveys
794 University Avenue
Fairbanks, Alaska 99708

Hansen, Vicki L.
Department of Geological Sciences
Southern Methodist University
Dallas, Texas 75275

Hudson, Travis
ARCO Alaska Inc.
P.O. Box 100360
Anchorage, Alaska 99510

Measures, Elizabeth A.
Department of Geology
University of Idaho
Moscow, Idaho 83843

Miller, Lance D.
Department of Geosciences
University of Arizona
Tucson, Arizona 85721

Rohr, David M.
Department of Geology
Sul Ross State University
Alpine, Texas 79832

Geologic Studies in Alaska by the U. S. Geological Survey, 1991

Dwight C. Bradley and Cynthia Dusel-Bacon, *Editors*

INTRODUCTION

This collection of twenty-one papers continues the annual series of U.S. Geological Survey reports on the geology of Alaska. These contributions, which include full-length Articles and shorter Geologic Notes, are grouped under two broad headings: Mineral Resource Studies (ten papers) and Geologic Framework Studies (eleven papers). Reports on mineral resources discuss exploration geochemistry in the Howard Pass quadrangle, Iditarod quadrangle, and Admiralty Island, a mineral resource appraisal of the Bethel quadrangle, a fluid-inclusion study in the Nome Gold District, geochemistry of lode-gold deposits in the Seldovia quadrangle, a new occurrence of placer gold in the Seldovia quadrangle, gold in coal in the Healy quadrangle, experimental abrasion of detrital gold, and a new occurrence of rare-earth minerals in southeastern Alaska. Under the heading of Geologic Framework Studies are reports on sedimentology and (or) stratigraphy in the Seldovia, Lime Hills, and Medfra quadrangles, the Kandik region, and the Alexander terrane in southeastern Alaska. Other papers report on the isotope geochemistry of veins and thermal maturity of the Kandik region, metamorphism and deformation of the Yukon-Tanana and Taylor Mountain terranes in east-central Alaska, magnetic susceptibilities of plutonic rocks in southeastern Alaska, terrane nomenclature in northern Alaska, and uplift of Mt. McKinley. These studies span nearly the entire State from the North Slope and Brooks Range to interior, western, southwestern, south-central, and southeastern Alaska (fig. 1).

Two bibliographies on Alaskan geology at the end of the volume list (1) reports about Alaska in USGS publications released in 1991, and (2) reports about Alaska by USGS authors in publications outside the USGS in 1991.

Manuscript approved for publication July 9, 1992.

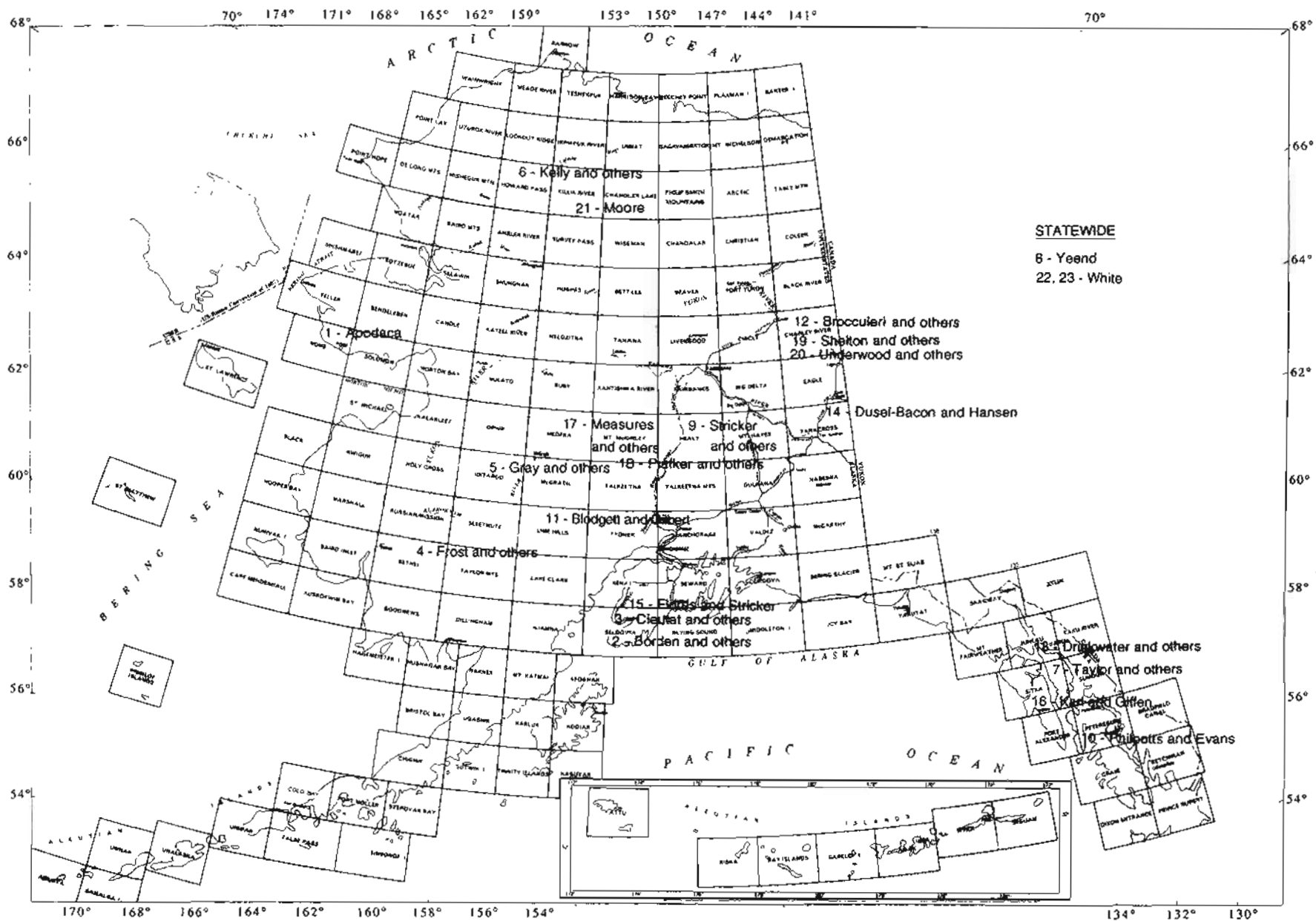


Figure 1. Index map of Alaska showing 1:250,000-scale quadrangles and general locations of study areas discussed in this bulletin. Numbers are approximately located in center of study area and indicate order of papers in this volume; names of authors follow numbers.

Fluid-Inclusion Study of the Rock Creek Area, Nome Mining District, Seward Peninsula, Alaska

By Lori E. Apodaca

Abstract

Microthermometry and mass spectrometry were used to study fluid inclusions in quartz veins concordant to the metamorphic foliation and gold-bearing quartz veins in greenschist-facies metamorphic rocks of the Rock Creek area, Nome Mining District. Fluids from both vein types are characterized by a $\text{H}_2\text{O}-\text{CO}_2-\text{NaCl}\pm\text{N}_2\pm\text{CH}_4$ composition. The fluids that formed the auriferous quartz veins were emplaced postkinematically as indicated by the observation that the veins crosscut the metamorphic foliation of their host rocks. These veins are composed of quartz, with albite, chlorite, carbonate, and sulfides occurring along the vein selvages. Mineralized veins formed at minimum temperatures of 184°C to 272°C compared with 259°C to 312°C for concordant veins. Minimum pressures during vein formation are inferred to be 1 kbar and 1.4 kbar for the mineralized and concordant quartz, respectively, and it was possible that immiscibility was involved in the vein-forming processes.

INTRODUCTION

Since the discovery of placer gold in 1898 on the Seward Peninsula, western Alaska, placer production has exceeded 6.2 million oz of gold, of which about 75 to 80 percent is from the Nome Mining District. Lode-gold deposits on the Seward Peninsula have remained relatively unexploited. The only recorded lode production is from the Big Hurrah Mine located 65 km east of Nome, with a reported production of 27,000 oz of gold, principally between 1903 and 1907 (Read and Meinert, 1986).

Largely owing to the poor bedrock exposure, the geology and geochemistry of the lode-gold deposits of the Nome Mining District are not well understood. Characterization of the ore-bearing fluids, vein mineral assemblages, and alteration is important in understanding the genesis of gold-bearing, low-sulfide quartz veins. As part of the investigation of the gold-bearing veins, a fluid-inclusion study has been undertaken to place constraints on the pressure, temperature, and composition of ore deposition within the Rock Creek area of the Nome Mining District.

Previous work in the Nome district has concentrated on geologic mapping, but little work has been done on the geochemistry of the gold-bearing quartz veins. However, Read and Meinert (1986), in a study of the Big Hurrah Mine, discussed the genesis of the gold-bearing veins during a fluid-inclusion study of the different generations of quartz veins. Their fluid-inclusion data do not clearly define significant geochemical differences between vein types (that is, mineralized vs. premineralized conditions) owing to the limited measurements of primary inclusions in the different vein stages at the Big Hurrah Mine.

The Rock Creek area is located in the Nome mining district approximately 14 km north of Nome, Alaska (fig. 1). Known lode-gold deposits occur as quartz-sulfide veins from Anvil Creek northward to Lindblom Creek within greenschist-facies metasedimentary rocks.

Samples collected for fluid-inclusion studies from the Rock Creek area include vein material from Anvil Creek on the south end, north to Lindblom Creek; the highest concentration of samples was obtained from Sophie Gulch. These samples include mineralized quartz veins that cut the metamorphic foliation and earlier unmineralized quartz veins parallel to the metamorphic foliation.

GEOLOGY

Metamorphic rocks in the southwestern part of the Seward Peninsula are composed of the 4.5-km-thick Nome Group, which consists of (1) a basal quartz-rich pelitic schist unit, (2) a mixed unit consisting predominantly of quartz-graphite schist and marble with minor lenses of mafic schists, (3) mafic or chlorite-rich schist with calcareous components, and (4) a chloritic marble (Till, 1984). These rocks were originally lower Paleozoic sediments that underwent regional blueschist metamorphism during the Jurassic, followed by Late Jurassic to Early Cretaceous overprinting under greenschist-facies metamorphic conditions during decompression of the metamorphic pile (Patrick and Evans, 1989).

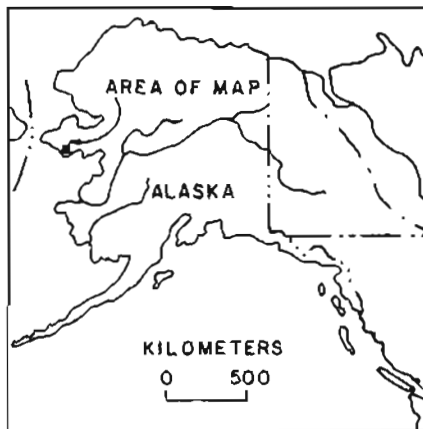
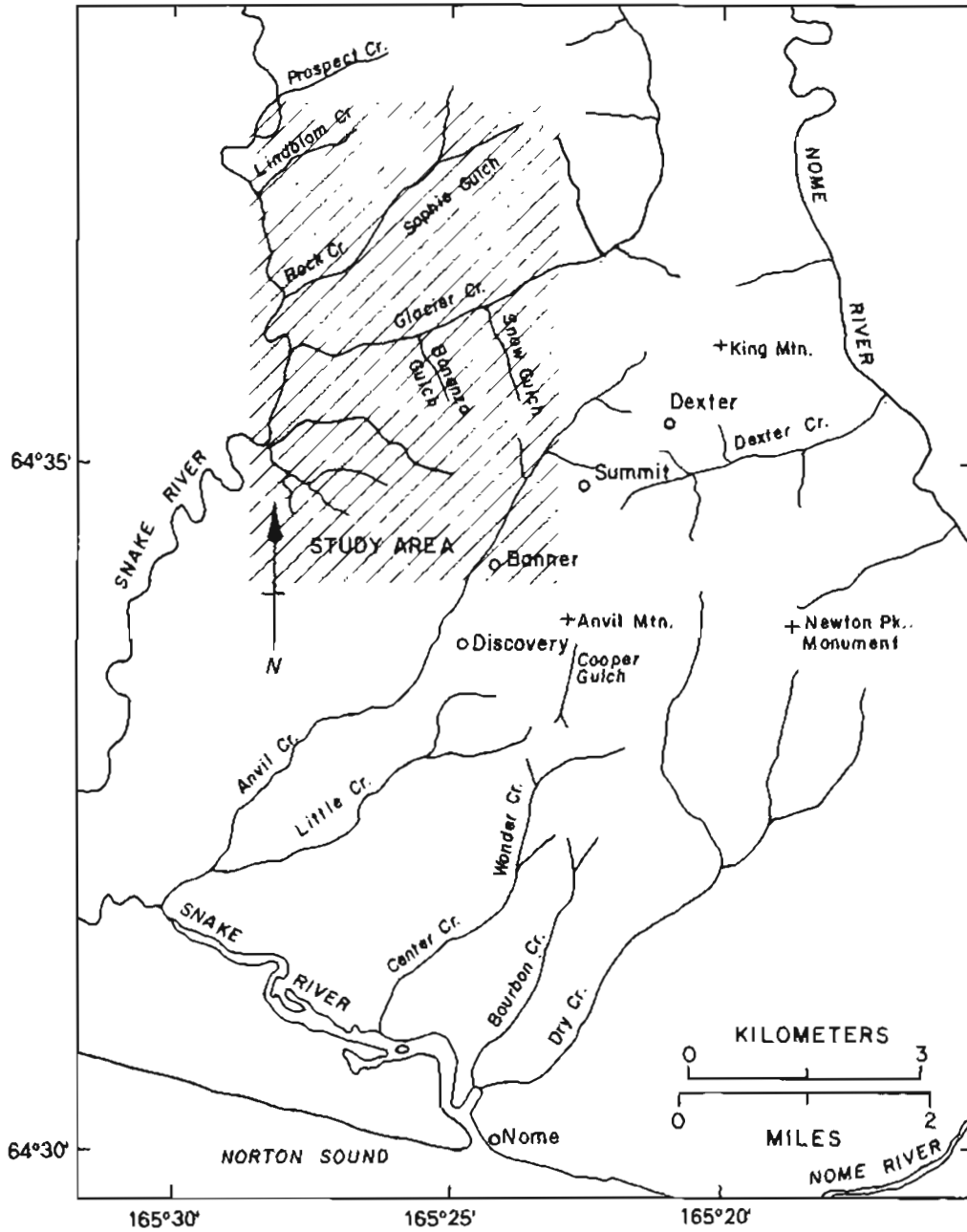


Figure 1. Rock Creek study area in Nome Mining District, Seward Peninsula, Alaska.

Amphibolite- to granulite-facies rocks of the east-west-trending Kigluaik Mountains, approximately 40 km north of the Rock Creek area, form the northern boundary of the Nome Mining District. Intrusive rocks are not present in the Rock Creek area, but granitic intrusions are common in the Kigluaik Mountains to the north. A granitic stock of Cretaceous age is located at Cape Nome, 25 km southeast of the Rock Creek area. The Cape Nome stock has a weakly foliated texture parallel to the regional metamorphic fabric (Gillette, 1989).

In the Nome Mining District, the gold-bearing quartz veins are preferentially hosted in the mixed unit of the Nome Group. Schists within the district are composed of quartz, muscovite, chlorite, and carbonate with some zones of albite porphyroblasts in which chlorite typically replaces the albite. Accessory minerals in the host rocks consist of pyrrhotite, pyrite, and carbon (Gillette, 1989).

VEIN TYPES

Three distinct generations of veins occur in the Rock Creek area (from oldest to youngest). First-generation veins consist of barren quartz emplaced as lenses and bands parallel to the metamorphic foliation generally not exceeding a few centimeters in width. The second-generation consists of low-sulfide gold-bearing quartz veins that crosscut the metamorphic foliation at high angles. The third-generation consists of barren carbonate-pyrite veins that fill fractures and cut both the first- and second-generation veins. Minor scheelite in drill-core samples appears to be younger than the second-generation veins, as it fills fractures in these veins.

Veins containing gold mineralization are confined to the second-generation and typically range in size from a few millimeters to about 10 cm in width. These low-sulfide gold-bearing quartz veins are inferred to be later than the barren concordant quartz lenses and bands, as they cut the lensoidal quartz.

Mineralized veins tend to occur in swarms (fig. 2). These veins have a core composed of milky quartz, with vein margins consisting of quartz, carbonate (dolomite to ankerite), chlorite, albite, gold, and sulfides (arsenopyrite, pyrite, galena, sphalerite, and stibnite). Gold occurs in the second-generation quartz veins as free gold within fractures in the quartz and in sulfides, and near or attached to sulfide grains.

Several silicified fault zones up to 90 cm thick are seen in drill core, containing fragments of second-generation veins. These faults are often high grade owing to the fragments of second-generation veins in them. The silica that forms the matrix in these fault zones is not mineralized.

FLUID-INCLUSION MICROTHERMOMETRY

A study of fluid inclusions has been carried out to characterize the fluids associated with the mineralizing and earlier metamorphic event. Inclusions were measured in generation I and II quartz. A modified U.S. Geological Survey gas-flow fluid-inclusion stage was used. Temperature range for the stage is from -196°C to $+700^{\circ}\text{C}$ at a temperature resolution of 0.1°C . Accuracy for the stage is $\pm 0.2^{\circ}\text{C}$ between -60.0°C and 0°C , and $\pm 5^{\circ}\text{C}$ up to 400°C (Werre and others, 1979).

The fluid inclusions studied in mineralized vein material were isolated inclusions trapped near sulfide grain embayments. Fluid inclusions found in sphalerite have gas/liquid ratios similar to inclusions found in quartz, but because of the opacity of the sphalerite, microthermometric measurements of these inclusions were difficult to obtain. In the mineralized veins, fluid inclusions may be secondary or pseudosecondary inclusions that were trapped along fractures and later healed.



Figure 2. Surface exposure of gold-sulfide veins at Sophie Gulch.

The inclusions in quartz are compositionally similar to those analyzed in sphalerite, which may also be secondary inclusions. Thus, they are presumed to be associated with sulfide deposition. In the unmineralized quartz first-generation veins, isolated inclusions and groups of inclusions that are believed to be primary were measured.

Gold-Sulfide Vein Quartz

Fluid inclusions were measured in quartz from second-generation veins and in fragments of second-generation veins from the silicified fault zones. Three types of inclusions have been identified in the mineralized vein quartz. Type I inclusions are single-phase, primary fluid inclusions of CO₂ liquid and (or) other gases (fig. 3A). Type II inclusions are two- and three-phase, primary inclusions. At room temperature, type II two-phase inclusions contain CO₂ liquid and other gases plus low-salinity water (fig. 3B), while type II three-phase in-

clusions contain CO₂ liquid, CO₂ gas, and H₂O liquid (fig. 3C). Vapor to liquid ratios are fairly consistent within groups of inclusions, with the vapor occupying approximately 75 to 90 volume percent for these inclusions. The density of the CO₂-rich phase in the inclusions determines whether these inclusions exhibit two or three phases at room temperature.

Type III inclusions are aqueous two-phase inclusions of vapor and low-salinity water, with the vapor occupying approximately 10 volume percent (fig. 3D). These inclusions are believed to be secondary because they often occur in trails within the quartz.

Measured fluid inclusions ranged in size from 5 to 13 μm . In addition to CO₂, type I and II inclusions contain minor CH₄ and (or) N₂ gases as indicated by the depression of the triple point for pure CO₂. Type I and II inclusions had measured $T_m\text{CO}_2$ (melting temperature of CO₂) that ranged from -59.8°C to -56.8°C and $T_h\text{CO}_2$ (homogenization temperature of CO₂) ranged from 0.3°C to 29.2°C with homogenization to a liquid. Type I inclusions had lower $T_h\text{CO}_2$ than

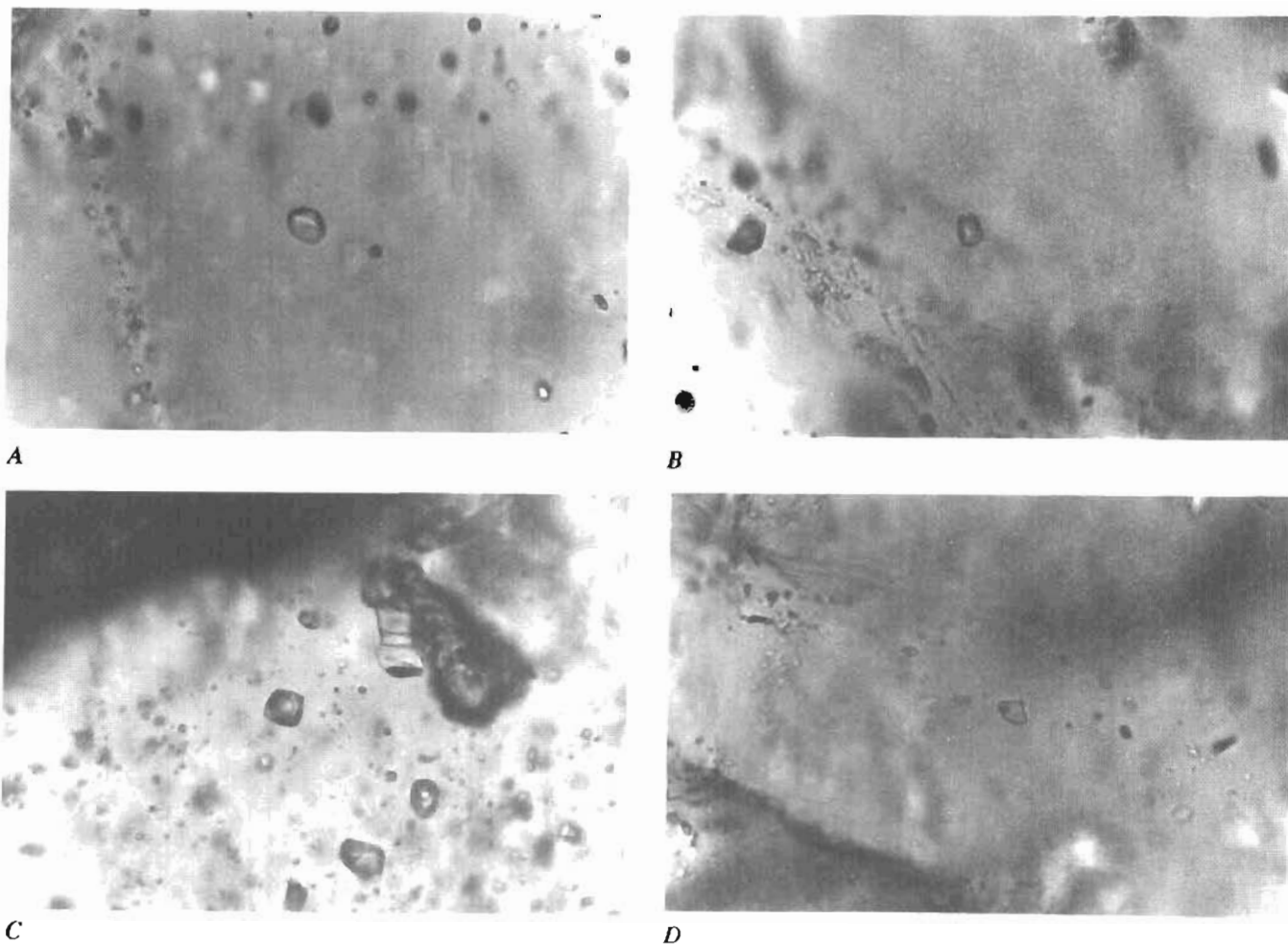


Figure 3. Fluid inclusions in vein and concordant quartz, Rock Creek area. A, Single-phase CO₂-rich fluid inclusions. B, Two-phase CO₂-rich fluid inclusion. C, Three-phase CO₂ (liquid, vapor)-H₂O fluid inclusions. D, Trail of H₂O-rich secondary inclusions. Field of view 0.16 mm.

type II inclusions. For type II inclusions, $T_{m, \text{clathrate}}$ (melting temperature of clathrate) values ranged from 7.9°C to 11.4°C. Depression of the $T_{m, \text{clathrate}}$ values from that expected for pure CO₂ indicate a salinity of less than 5 equivalent weight percent NaCl for inclusions with relatively high T_{m, CO_2} (Collins, 1979).

Final T_h (temperature of homogenization) for individual inclusions was often not reproducible, suggesting that microfracturing or leakage of the inclusions may have occurred during heating. For those inclusions that had reproducible values, T_h ranged from 184°C to 272°C. Type II inclusions homogenized to a liquid. Observing the final homogenization to a liquid along with the small sizes of the inclusions made it difficult to determine final T_h .

Type III secondary inclusions have $T_{m, \text{ice}}$ (melting temperature of ice) of -2.1°C to -1.3°C, which yields salinity values of <4 equivalent weight percent NaCl, based on the freezing-point depression in the H₂O-NaCl system (Roedder, 1984). Type III inclusions homogenized to a liquid, with T_h values ranging from 118°C to 179°C.

Coeval CO₂-rich and H₂O-rich inclusions would indicate immiscibility. This evidence for immiscibility is not observed in the samples studied. If it is assumed that immiscibility did not occur, then homogenization temperatures are minimum trapping temperatures.

Concordant Vein Quartz

Fluid inclusions in the concordant quartz first-generation veins contain the same three types of inclusions as described in the gold-bearing quartz veins. Type I and II inclusions had T_{m, CO_2} values ranging from -59.3°C to -57.1°C, and T_h, CO_2 values of 0.3°C to 23.7°C. Type II inclusions had $T_{m, \text{clathrate}}$ of 9.4°C to 10.5°C. Salinity values cannot be estimated from $T_{m, \text{clathrate}}$ of type II inclusions owing to the presence of other gases (Collins, 1979). In the gold-sulfide quartz veins, many type II inclusions did not provide reproducible T_h values because of microfracturing or leakage. A few inclusions decrepitated before homogenization was reached. For those type II inclusions that did not decrepitate or leak, T_h values to a liquid ranged from 259°C to 312°C.

Type III secondary inclusions consisted of water and 10 volume percent vapor, with $T_{m, \text{ice}}$ ranging from -0.4°C to -1.8°C (<4 equivalent weight percent NaCl). Secondary inclusions homogenized to a liquid at T_h ranging from 147°C to 228°C.

Comparisons Between Different Generations of Quartz

The data for T_{m, CO_2} , $T_{m, \text{ice}}$, $T_{m, \text{clathrate}}$, T_h, CO_2 , and T_h in figure 4 have been compiled for fluid inclusions in

the concordant quartz veins and in the gold-bearing quartz veins. The histograms include data for both primary and secondary inclusions. For type II inclusions, T_{m, CO_2} and $T_{m, \text{clathrate}}$ values are within the same range for both types of quartz (fig. 4A, C). T_h, CO_2 values are slightly lower for concordant quartz relative to gold-bearing vein quartz (fig. 4D), which may indicate that a denser fluid formed the concordant quartz. Type III inclusions (secondary inclusions) are the only inclusions in which ice melt could be determined; the range of $T_{m, \text{ice}}$ is the same for both types of quartz (fig. 4B).

T_h for concordant quartz occurs at temperatures >256°C, whereas values for gold-bearing vein quartz range from ~200°C to 235°C. Differences in trapping pressures or composition may explain the temperature differences between the concordant and gold-bearing vein quartz, as the T_h values are minimum temperatures.

FLUID-INCLUSION MASS SPECTROMETRY

Microthermometry analyses provide semiquantitative information on the composition of the gaseous phase in inclusions. A quadrupole mass spectrometer was used to quantitatively determine the volatile composition (H₂O, CO₂, CH₄, N₂, and H₂S) of the fluid inclusions (Landis and others, 1987). Fluid inclusions in quartz were thermally decrepitated during ramped heatings (30°C intervals) over a temperature range of 110°C to 410°C. Although thermal decrepitation releases gases from different generations of inclusions, monitoring of the gases released at decrepitation allows for a quantitative study of the ore fluid at a level comparable to results obtained from individual inclusions. The gas released is profiled as a function of temperature, allowing different fluid-inclusion populations to be defined.

Gold-Sulfide Vein Quartz

Thermal decrepitation of gold-bearing quartz vein material has shown a bimodal population of inclusions having a mode of 68 mole percent CO₂, along with another less well-defined population having a mode of 5 mole percent CO₂ (fig. 5). There is also a faint indication of a third population having a mode of 40 mole percent CO₂. In measured inclusions within sphalerite, a single population shows an identical high CO₂ mode.

Higher values of CH₄ and N₂ are found in CO₂-rich inclusions than in H₂O-rich inclusions, with both CH₄ and N₂ having a mode at 10 mole percent. Trace amounts of H₂S were also detected in a few larger inclusions.

In the H₂O-rich inclusions, CH₄ and N₂ are present in very low amounts, generally around 0 to 2 mole percent. No H₂S was found in H₂O-rich inclusions.

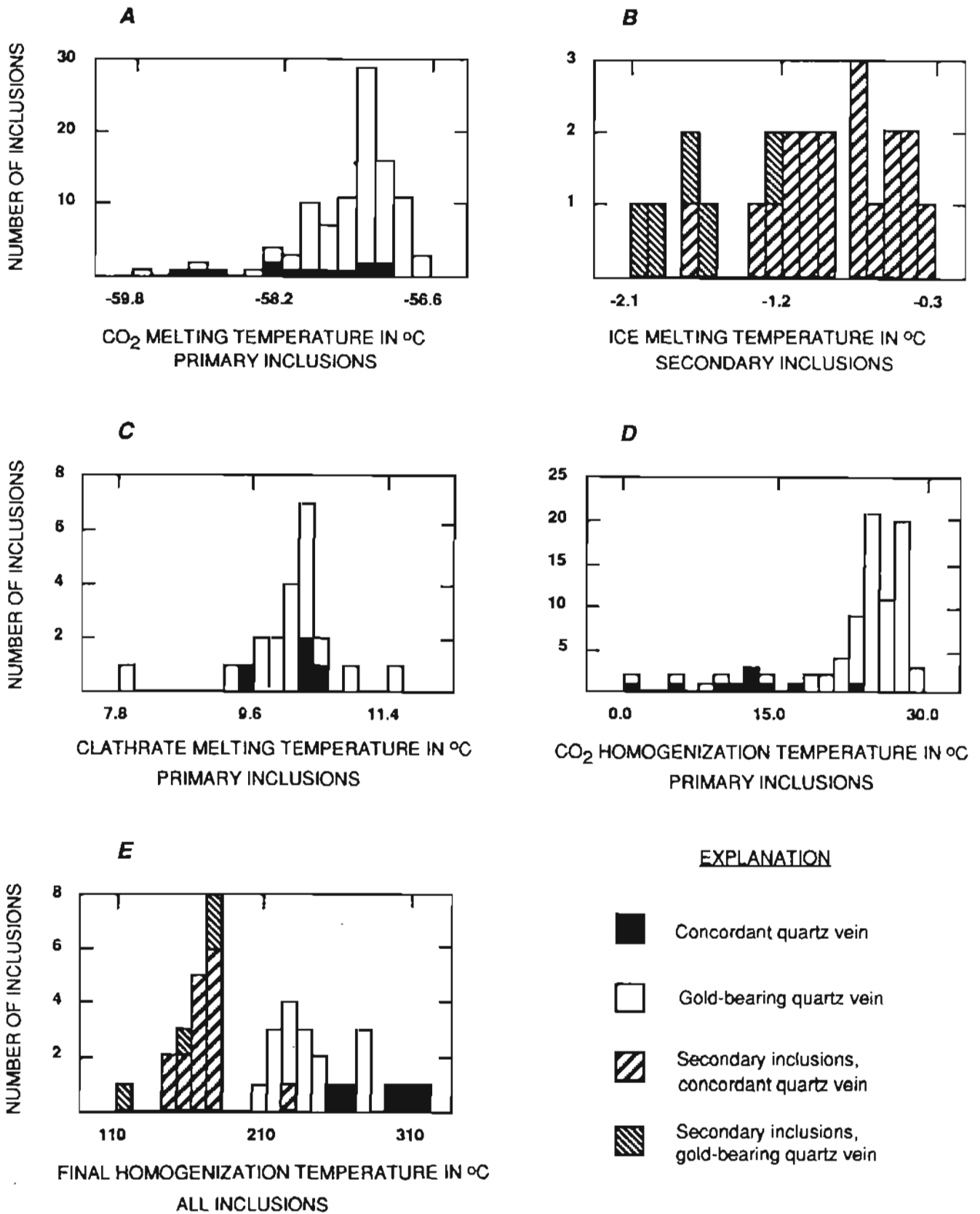


Figure 4. Microthermometric data for (A) melting of CO₂, (B) melting of ice, (C) melting of clathrate, (D) homogenization of CO₂, and (E) final homogenization temperatures for concordant and gold-bearing quartz veins.

Concordant Vein Quartz

Inclusions in the concordant quartz also exhibit a bimodal distribution, with two modes present in the histogram plot of CO₂—one at 68 mole percent CO₂ and the other at 2 mole percent CO₂ (fig. 5). H₂O has modes at 15 and 97 mole percent, CH₄ has a mode at 2.5 mole percent, and N₂ exhibits modes at 1 and 15 mole percent, with the higher values corresponding to CO₂-rich inclusions. H₂S was not present in any of the inclusions in the concordant quartz.

Comparisons Between Different Generations of Quartz and Sphalerite

The fairly consistent CO₂/H₂O ratios between the inclusions measured in the gold-bearing vein quartz, sphalerite, and concordant quartz suggest that these inclusions might have been trapped above the CO₂-H₂O-NaCl solvus (fig. 6). However, the bimodal CO₂ and H₂O populations in the quadrupole mass spectrometer

data hint that the inclusions may represent end members of an unmixed parent CO₂-H₂O fluid.

PRESSURE AND TEMPERATURE CONDITIONS

Limits on pressure (*P*) and temperature (*T*) conditions of ore deposition can be estimated from the density of the fluids in the fluid inclusions and known experimental data on the CO₂-H₂O system. If the fluid inclusions in the one-phase field were trapped above the CO₂-H₂O-NaCl solvus (for example, because of the consistent gas/liquid ratios for groups of inclusions), then isobaric densities of 0.84 g/cm³ for the concordant quartz and 0.74 g/cm³ for the gold-bearing vein quartz (using calculations in Shepherd and others, 1985) can be used to put constraints on the *P-T* conditions of formation. Using homogenization temperatures and densities of the inclusions, minimum trapping pressures of about 1 kbar and 1.4 kbar are estimated for the gold-bearing vein quartz and concordant quartz, respectively (fig. 7). Actual trapping *P-T* conditions would lie to the right of the

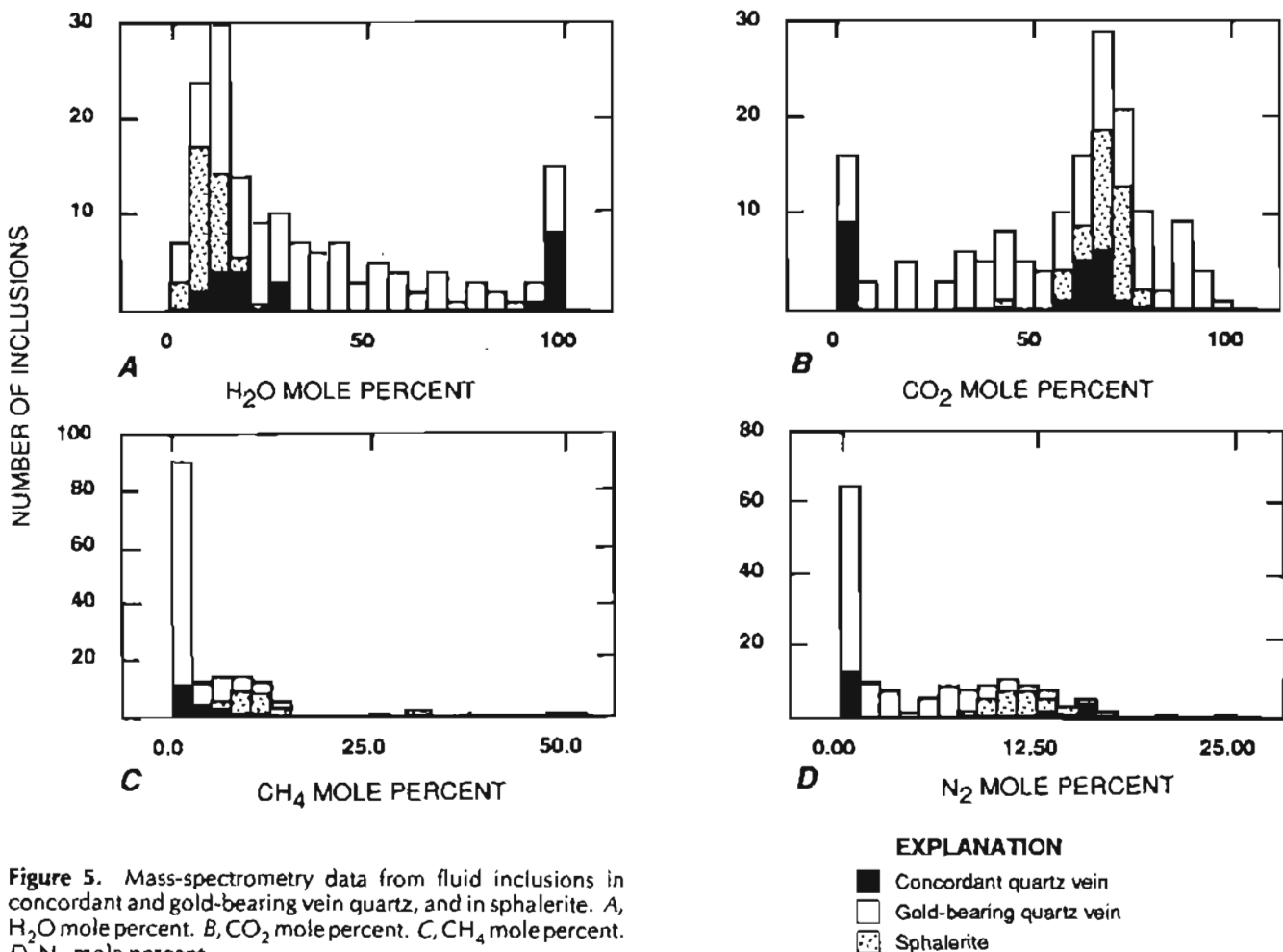


Figure 5. Mass-spectrometry data from fluid inclusions in concordant and gold-bearing vein quartz, and in sphalerite. A, H₂O mole percent. B, CO₂ mole percent. C, CH₄ mole percent. D, N₂ mole percent.

solvus along the isochores. Since small amounts of salt, CH₄ and/or N₂ will substantially shift a solvus to higher temperatures and pressures, the trapping pressure of 1 kbar would be the minimum trapping pressure. These pressures correspond to minimum depths of formation of 2.8 to 3.9 km, assuming lithostatic pressure.

From the work of Patrick and Evans (1989), maximum temperature and pressure can be estimated to be 500°C and 12 kbar for peak *P-T* conditions of metamorphism of the host rocks. Since the barren concordant vein quartz could not have formed at a temperature greater than 500°C and the mineralized vein quartz was clearly emplaced after peak metamorphism of the surrounding host rocks, these veins formed in the stippled region of figure 7, assuming immiscibility did not occur. Microthermometric data and estimates of the fluid density suggest a path of evolution of the fluid along the solvus from A to B in figure 7.

On the other hand, bulk fluid compositions of CO₂- and H₂O-dominated inclusions derived from mass spectrometry may indicate trapping of end members of an immiscible fluid that separated under lower *P-T* conditions. This implies a parent fluid having a composition

that falls between the end members' composition, as seen in figure 6. The parent fluid would have been trapped above the CO₂ solvus. It is not possible to precisely estimate the bulk composition of the unmixed parent fluid. From homogenization temperatures from the gold-bearing vein quartz, minimum pressure have been estimated to be 1.5 kbar, but the presence of dissolved salts and CH₄ and (or) N₂ will shift the solvus to higher temperatures.

DISCUSSION

Fluid-inclusion data from the Rock Creek area indicate that this deposit is similar to a number of greenschist-hosted lode-gold deposits in southern Alaska, such as deposits in the Juneau Gold Belt (Goldfarb and others, 1989) and those of the Chugach-Kenai Mountains (Goldfarb and others, 1986). These data are also similar to those from California Mother Lode deposits (Bohlke, 1989) and mesothermal Canadian Cordillera gold deposits (Nesbitt and Muehlenbachs, 1989). Indeed, the similarity between the fluid-inclusion data from different

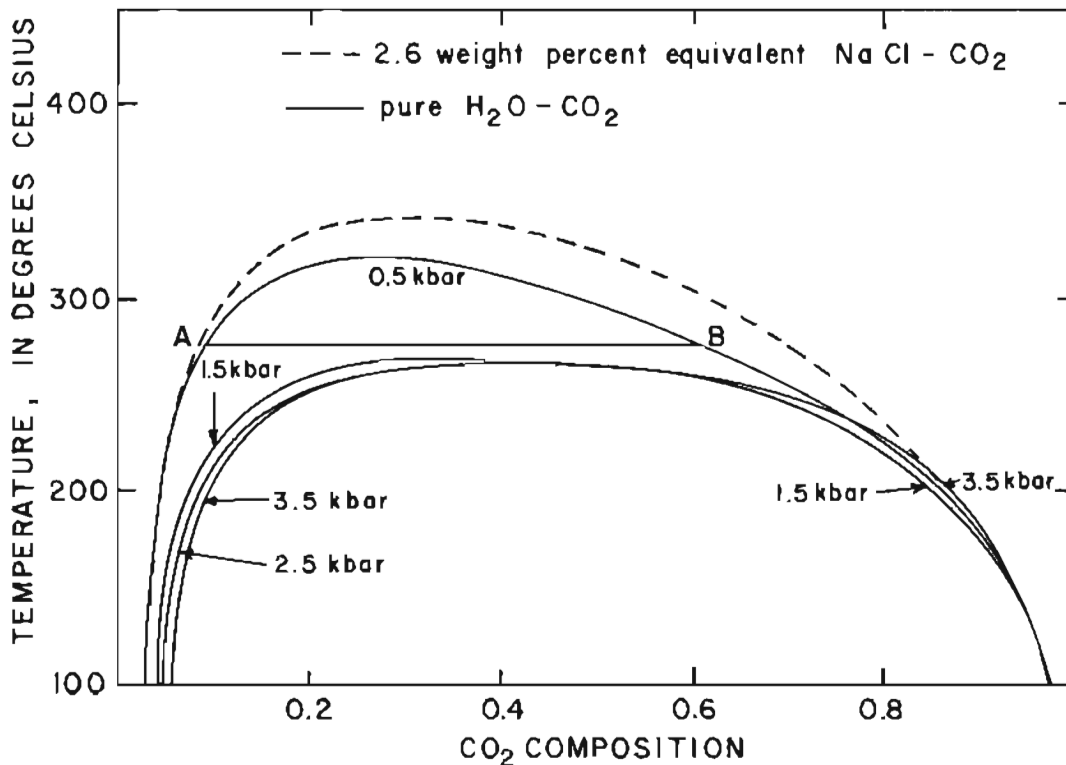


Figure 6. Selected solvi in the CO₂-H₂O-NaCl system at various pressures (Crawford, 1981). Below a solvus, two immiscible fluids coexist; above a solvus, a single homogeneous fluid is present. Addition of salts and other volatiles such as N₂ greatly expands two-phase field. At 270°C and pressure greater than or equal to 1.5 kbar, a single homogeneous fluid is present. Reduction in the confining pressure to 0.5 kbar results in fluid immiscibility with end-member compositions at points A and B. Reduction in confining pressures can be achieved by uplift and erosion, structural dilation of fracture by tectonic activity, or by hydrofracturing, among other means (Leach and others, 1987). CO₂ composition is in weight percent.

mesothermal gold deposits is one of the most consistent features of these deposits.

High CO_2 contents were seen in fluid inclusions associated with ore deposition at the Alaska-Juneau, Ibex, and Reagan deposits in the Juneau Gold Belt (Goldfarb and others, 1989). At these deposits, unmixing of the CO_2 -rich parent fluid is assumed to have accompanied ore deposition. The ore fluids are defined as being low-salinity (<5 equivalent weight percent NaCl) aqueous fluids containing 3 to 10 mole percent $\text{CO}_2 \pm (\text{CH}_4, \text{H}_2\text{S}, \text{N}_2)$ at temperatures of 200°C to 350°C.

In the Mother Lode area of California, gold-bearing quartz veins are also found in greenschist-facies metamorphic terranes. These deposits are similar to the Rock Creek deposit. Bohlke (1989) described them as structurally discordant synmetamorphic to postmetamorphic gold-quartz veins with low base metals contents that formed from low-salinity, CO_2 -rich, aqueous fluids at approximately 250°C to 450°C and 0.5 to 3+ kbar. The lower CO_2 contents (maximum of 10 mole percent) noted in the Mother Lode deposits by Bohlke (1989) may be the result of fluids derived from chemically different host rocks than in the Rock Creek area. Calcareous rocks of the Nome Group may account for the higher CO_2 content in the inclusions from Rock Creek.

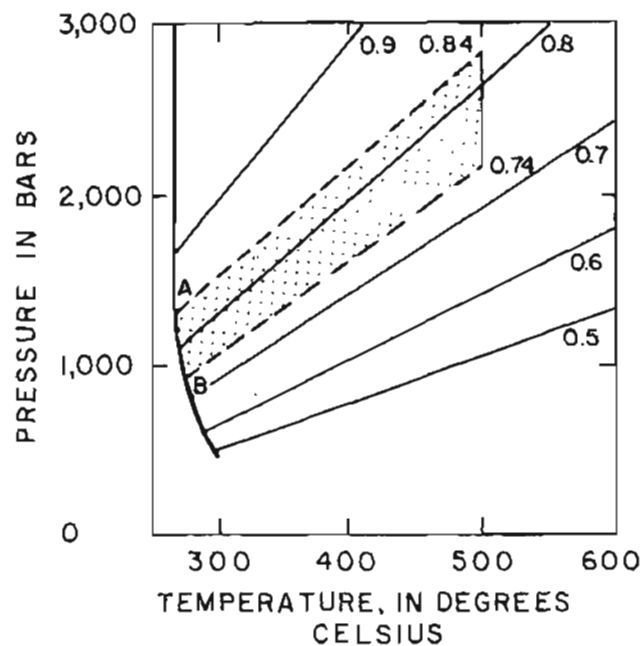


Figure 7. Pressures and temperatures of homogenization for a fluid of 60 mole percent CO_2 . Heavy line is solvus, with a one-phase fluid to right and a two-phase fluid to left. Light lines are isochores, in grams per cubic centimeter (Shepherd and others, 1985). If fluids were one-phase when they were trapped, they would fall to the right of solvus, whereas a fluid that was two-phase at time of trapping would fall to the left of solvus. Stippled area represents most likely region of conditions of formation.

Mesothermal Canadian Cordillera gold deposits exhibit characteristics similar to other mesothermal gold deposits, having formation temperatures of 250°C to 350°C, pressures of 1 ± 0.3 kbar, and salinities from 1 to 5 equivalent weight percent NaCl. CO_2 is found in inclusions in all of the Canadian Cordillera mesothermal gold deposits, ranging from 5 to 100 mole percent CO_2 , with average values of 10 to 20 mole percent CO_2 . Co-existing CO_2 -rich and H_2O -rich inclusions in these deposits indicate that phase separation has occurred (Nesbitt and Muehlenbachs, 1989).

The trapping of two end members of an immiscible fluid may explain the bimodal nature of the data from the Rock Creek area. Alternatively, several generations of inclusions with an initial CO_2 -rich liquid may have been trapped. The spectrum of values for CO_2 - H_2O compositions between the modes may represent leakage or necking of the inclusions. The presence of high- CO_2 inclusions in sphalerite and in the gold-bearing quartz veins may indicate either that only one end member of an immiscible fluid was trapped or that the ore fluid may have contained high amounts of CO_2 .

Touret (1981) suggested that high-density, carbonic fluids are ubiquitous in high-grade metamorphic rocks and granulites. However, such fluids are not recognized to be associated with mesothermal gold veins, perhaps owing to a lack of gold-complexing H_2S in the fluids. Fluids with a composition (X) of $\text{CO}_2 = 0.6$ at Rock Creek argue for fluid production occurring during high-grade metamorphism, such as amphibolite- or granulite-facies conditions. Rocks of this metamorphic grade are widespread in the Kigluaik Mountains 40 km to the north and could underlie the Rock Creek area at depth. Alternatively, high-grade rocks that are not recognized in the Rock Creek area may be absent at depth, and in that case the CO_2 -rich inclusions could indicate that immiscibility occurred.

CONCLUSIONS

The results of this study indicate that in the Rock Creek area, Nome Mining District, the gold-bearing quartz veins were deposited at minimum temperatures between 184°C and 272°C. The mineralizing fluid was a CO_2 rich- $\text{H}_2\text{O} \pm \text{CH}_4 \pm \text{N}_2$ fluid. CO_2 , CH_4 , and N_2 gases present in the inclusions may have been derived from the carbonaceous matter often seen in the wallrock.

Minimum pressure has been estimated at approximately 1 kbar for 60 mole percent CO_2 inclusions observed in this study. This corresponds to a minimum depth of formation of approximately 2.8 km. If the 60 mole percent CO_2 inclusions represent an end member of an unmixed fluid, minimum P - T estimates would shift to lower values.

Microthermometric studies show minimum trapping temperature of inclusions in concordant quartz veins with T_h of 259°C to 312°C, and of inclusions in gold-bearing vein quartz with T_h of 184°C to 272°C. Differences in trapping pressures or composition may explain the temperature differences between the metamorphic and gold-bearing vein quartz, as the T_h values are minimum temperatures.

The bimodal nature of CO₂-H₂O compositions indicates that immiscibility may have been present during ore deposition. The high CO₂ content of the inclusions may not indicate immiscibility if the fluid was produced during high-grade metamorphism, although evidence of this is not present in the Rock Creek area.

Acknowledgments.—I wish to thank G.P. Landis for the use of the quadrupole mass spectrometer. This work could not have been possible without the help and support of C.B. Gillette (Placer Dome U.S.), T. Eggleston and G.P. Parsley (Tenneco Minerals), and R.V. Bailey (Aspen Exploration).

REFERENCES CITED

- Bohlike, J.K., 1989, Comparison of metasomatic reactions between a common CO₂-rich vein fluid and diverse wall rocks: Intensive variables, mass transfers, and Au mineralization at Alleghany, California: *Economic Geology*, v. 84, p. 291-327.
- Collins, P.L.F., 1979, Gas hydrates in CO₂-bearing fluid inclusions and the use of freezing data for estimation of salinity: *Economic Geology*, v. 74, p. 1435-1444.
- Crawford, M.L., 1981, Fluid inclusions in metamorphic rocks—Low and medium grade, in Hollister, L.S., and Crawford, M.L., eds., *Short course in fluid inclusions applications to petrology*: Mineralogical Association of Canada Short Course Handbook, v. 6, p. 157-181.
- Gillette, C.B., 1989, Geology and mineralization of the Rock Creek Deposit, Nome Alaska: Northwest Mining Association 95th Annual Convention and Trade Show, December 6-8, 1989, Spokane Wash., p. 34-41.
- Goldfarb, R.J., Leach, D.L., Miller, M.L., and Pickthorn, W.J., 1986, Geology, metamorphic setting, and genetic constraints of epigenetic lode-gold mineralization within the Cretaceous Valdez Group, south-central Alaska, in Keppie, J.D., Boyle, R.W., and Haynes, S.J., eds., *Turbidite-hosted gold deposits*: Geological Association of Canada Special Paper 32, p. 87-105.
- Goldfarb, R.J., Leach, D.L., Rose, S.C., and Landis, G.P., 1989, Fluid inclusion geochemistry of gold-bearing quartz veins of the Juneau gold belt, southeastern Alaska: Implication for ore genesis: *Economic Geology*, Monograph 6, p. 363-375.
- Landis, G.P., Hofstra, A.H., Leach, D.L., and Rye, R.O., 1987, Quantitative analysis of fluid-inclusion gases-application to the study of ore deposits [abs.]: U.S. Geological Survey Circular 995, p. 38-39.
- Leach, D.L., Goldfarb, R.J., and Light, T.D., 1987, Fluid inclusion constraints on the genesis of the Alaska-Juneau gold belt, in Elliot, I.L., and Smee, B.W., eds., *GeoExpo 86: Exploration in the North American Cordillera*: Rexdale, Ontario, Canada, Association of Exploration Geochemistry, p. 150-159.
- Nesbitt, B.E., and Muehlenbachs, K., 1989, Geology, geochemistry, and genesis of mesothermal lode gold deposits of the Canadian Cordillera: Evidence of ore formation from evolved meteoric water: *Economic Geology*, Monograph 6, p. 553-563.
- Patrick, B.E., and Evans, B.W., 1989, Metamorphic evolution of the Seward Peninsula blueschist terrane: *Journal of Petrology*, v. 30, p. 531-555.
- Read, J., and Meinert, L.D., 1986, Gold-bearing quartz vein mineralization at the Big Hurrah Mine, Seward Peninsula, Alaska: *Economic Geology*, v. 81, p. 1760-1774.
- Roedder, E., 1984, Fluid inclusions: *Mineralogical Society of America Reviews in Mineralogy*, v. 12, 644 p.
- Shepherd, T.J., Rankin, A.H., and Alderton, D.H.M., 1985, A practical guide to fluid inclusion studies: London, Blackie, 239 p.
- Touret, J.L.R., 1981, Fluid inclusions in high grade metamorphic rocks, in Hollister, L.S., and Crawford, M.L., eds., *Short course in fluid inclusions applications to petrology*: Mineralogical Association of Canada Short Course Handbook, v. 6, p. 182-208.
- Till, A.B., 1984, Low grade metamorphic rocks of the Seward Peninsula, Alaska [abs.]: *Geological Society of America Abstracts with Programs*, v. 16, no. 5, p. 337.
- Werre, R.W., Jr., Bodnar, R.J., Bethke, P.M., and Barton, P.B., Jr., 1979, A novel gas-flow fluid inclusion heating/freezing stage [abs.]: *Geological Society of America Abstracts with Programs*, v. 11, p. 539.

Reviewers: David L. Leach and Richard J. Goldfarb

Geochemistry of Lode-Gold Deposits, Nuka Bay District, Southern Kenai Peninsula

By J. Carter Borden, Richard J. Goldfarb, Carol A. Gent, Robert C. Burruss, and Bruce H. Roushey

Abstract

Gold-bearing quartz veins in the Nuka Bay district of the southern Kenai Peninsula fill joints and faults within graywacke of the Upper Cretaceous Valdez Group and within Tertiary felsic dikes. The veins commonly contain abundant free gold and anomalous concentrations of Ag, As, Bi, Cd, Co, Cu, Hg, Fe, Pb, Sb, Te, and Zn-rich sulfide-bearing phases. $\delta^{18}\text{O}$ values for the quartz in these veins range from 14.0 to 17.4 per mil; $\delta^{34}\text{S}$ data for the sulfide minerals range from -1.2 to +1.8 per mil. Fluid-inclusion studies indicate that the ore-forming fluid had an approximate composition of 90 to 92 mole percent H_2O , 6 to 8 mole percent CO_2 , and 1 to 2 mole percent CH_4 and N_2 . The veins were formed at temperatures of at least 250°C to 300°C and pressures of at least 2.3 to 3.0 kbar. Data are compatible with an ore fluid produced during dehydration and decarbonation reactions of metasedimentary rocks deeper within the accretionary prism.

INTRODUCTION

The Nuka Bay gold district (fig. 1) is located along the eastern side of the southern Kenai Peninsula, approximately 55 km east of the town of Homer. Small, east-west trending, gold-bearing quartz veins are widespread in metasedimentary rocks near Surprise Bay, the North Arm of Nuka Bay, Quartz Bay, Yalik Bay, and Beauty Bay. These veins compose the southernmost of a series of small lode-gold districts scattered throughout the Chugach-Kenai Mountains of south-central Alaska. Other significant and similar districts include Hope-Sunrise (Tuck, 1933), Moose Pass (Tuck, 1933), Port Valdez (Johnson, 1915), Port Wells (Johnson, 1914), and Girdwood (Park, 1933). Epigenetic lodes in all districts are hosted in structurally deformed turbidite deposits of the Late Cretaceous Valdez Group, the major component of the Chugach terrane.

The gold-bearing veins in the Nuka Bay district have been described in Grant and Higgins (1910), Shepard (unpublished data, 1925), Pilgrim (unpublished data, 1931), Smith (1938), and Richter (1970). The

veins were discovered in the early 1900's, and peak mining activity occurred in the 1930's. Dollar estimates by Richter (1970) suggest combined gold production of 5,000 to 6,000 oz. from five mines. There has been no recorded production from any of the mines for the past 50 years. However, active claim work is still ongoing at the Goyne prospect and the Sonny Fox Mine near Surprise Bay and at the Little Creek prospect near the head of Beauty Bay.

This paper presents new geochemical data for some of the larger gold-bearing veins in the Nuka Bay district. Atomic absorption analyses of gold-bearing vein samples provide trace-element signatures for the vein deposits. The first stable-isotope and fluid-inclusion analyses for samples from the Nuka Bay district are also presented. These data provide important constraints on the pressure, temperature, and composition conditions of mineralization.

GEOLOGY

The Nuka Bay district occurs within marine turbidites of the Upper Cretaceous Valdez Group. The Valdez Group consists mainly of turbiditic graywacke and slate, which has been tightly to isoclinally folded, thrust faulted, and in places disrupted to form type I melange. Metamorphic biotite in thin sections from the North Arm of Nuka Bay (T.M. Kusky and D.C. Bradley, oral commun., 1992) indicates mid-greenschist-facies metamorphism in the Nuka Bay Mining District. The Valdez Group is the major component of the Chugach terrane, the Mesozoic part of south-central Alaska's accretionary prism. It has been interpreted as having been deposited in a deep-sea trench during the latest Cretaceous (Nilsen and Zuffa, 1982); within a few million years of deposition, the Valdez Group was incorporated into the Chugach accretionary prism. Flysch sequences of the Orca Group, composing the Prince William terrane, were thrust below rocks of the Chugach terrane during Paleogene time (Winkler and Plafker, 1975; Plafker and others, 1977).

Granodiorite dikes and, less commonly, sills cut metasedimentary rocks of the Valdez Group throughout the study area. The igneous intrusions are part of a belt of Paleogene granites, granodiorites, and tonalites termed the Sanak-Baranof plutonic belt (Hudson and others, 1979), which rims much of the Gulf of Alaska. These igneous rocks have not been isotopically dated in Nuka Bay but are probably Eocene in age. Monazite from a pluton about 15 km east of Nuka Bay yielded a 56-Ma U-Pb age, and amphiboles from an intermediate dike to the west near Seldovia have an Ar-Ar age of 57 Ma (W. Clendenen, quoted in Bradley and Kusky, 1992).

GOLD-BEARING VEINS

Gold-bearing quartz veins of the Nuka Bay district cut graywacke and the slate of the Valdez Group; locally, they also cut dikes and sills. Richter (1970) noted a spatial association of the veining with more competent metagraywacke and igneous rocks relative to the less competent fine-grained metasedimentary rocks. Veining is observed to both parallel cleavage and to cut the foliation. The latter observation indicates mineralization postdates regional metamorphism of the immediate host rocks. Mineralized veins consistently strike east-west at

a high angle to regional strike, and they dip steeply to vertically. East-west-trending veins may occupy tensional cross joints, as suggested by Richter (1970). In addition, veins may occupy late brittle cross faults of the set described by Bradley and Kusky (1992) in the McHugh Complex of the Chugach terrane. Bradley and Kusky determined dextral motion on the structures to be coeval with felsic and intermediate dike emplacement; such extension may also have been coeval with the gold veining. The gold-bearing veins are irregular and discontinuous, with pinching and swelling suggesting that some deformation postdates mineralization. Larger quartz veins tend to reach about 100 m in length and 3 m in width.

Arsenopyrite with lesser pyrite, chalcopyrite, galena, sphalerite, and free gold are commonly visible. Smith (1938) noted that the visible gold was often spectacular and abundant, with up to 15 oz/ton of gold in one 5-ton ore shipment from the Sonny Fox Mine. Tetrahedrite, covellite, chalcocite, sylvanite, native silver, and native copper have also been observed in the veins (Smith, 1938). Carbonization, sulfidization, and silicification characterize wall rock adjacent to the veins. Sericitization of metasedimentary wall rocks is common at the Little Creek prospect. An $^{40}\text{Ar}/^{39}\text{Ar}$ age of 55.6 ± 0.17 Ma was obtained on muscovite from within

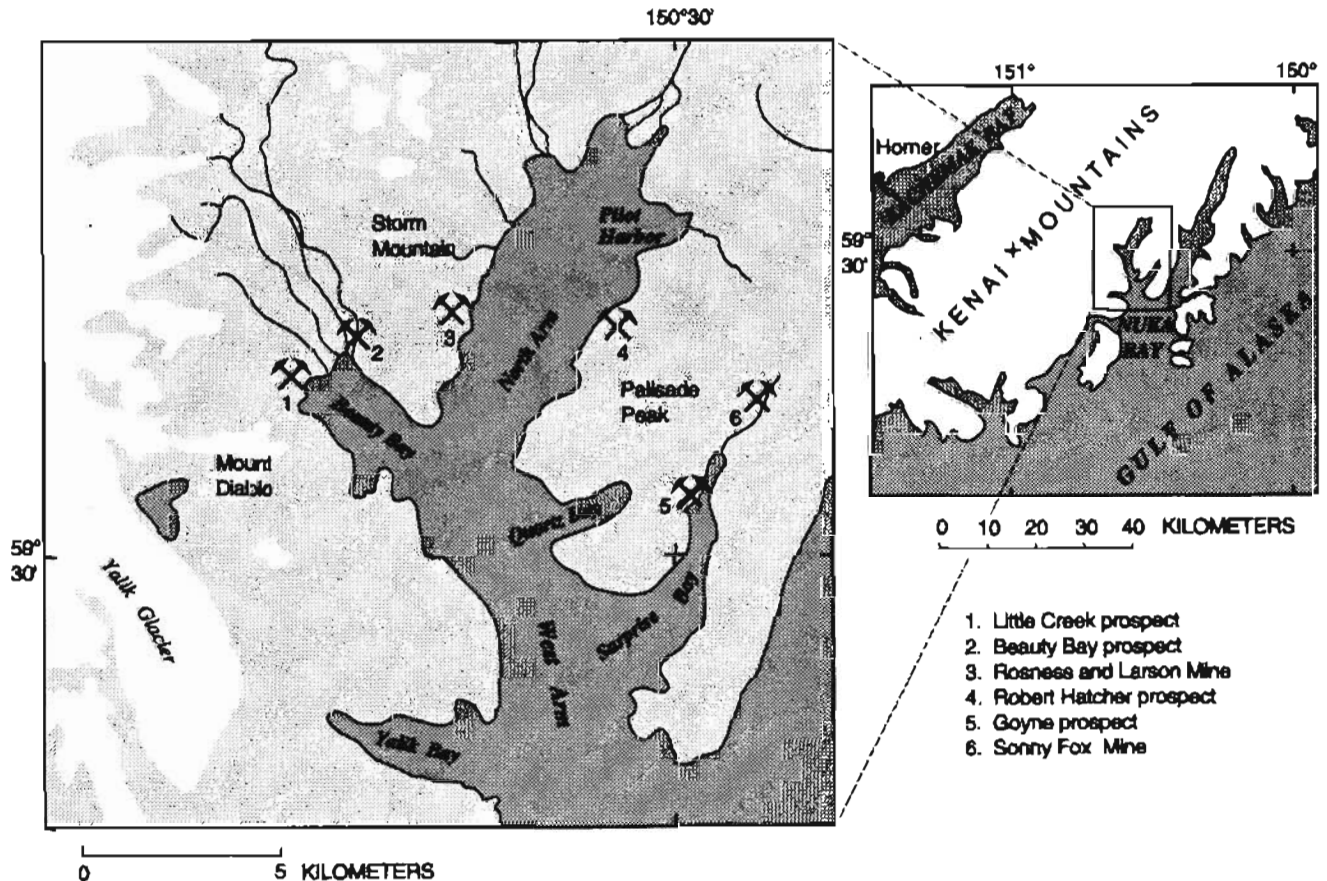


Figure 1. Locations of mines and prospects within Nuka Bay gold district.

the vein quartz at the Little Creek prospect (Larry Snee, oral commun., 1992) and is believed to represent the age of gold mineralization.

Richter (1970) presented atomic absorption analyses for gold and tellurium, colorimetric analyses for arsenic, and semiquantitative emission spectrographic data for Ag, B, Ba, Co, Cr, Cu, Ni, Pb, Sb, V, and Zn. Results of analyses show samples with as much as 304 ppm Au, 6,000 ppm As, 30 ppm Ag, 200 ppm Cu, 1,500 ppm Pb, 300 ppm Sb, and 700 ppm Zn. More sensitive atomic absorption analyses for many of the ore-related elements are listed in table 1. Sulfide-rich quartz-vein grab samples from mines and prospects around Nuka Bay were determined to contain as much as 48 ppm Au, 200 ppm Ag, 8.7 percent As, 107 ppm Bi, 220 ppm Cd, 200 ppm Co, 1,000 ppm Cu, 7.6 ppm Hg, 30 percent Fe, 2 percent Pb, 260 ppm Sb, 19 ppm Te, and 6,500 ppm Zn. Elements B, Ba, Mo, and W do not exceed background levels in any of the ore samples.

ISOTOPE GEOCHEMISTRY

Hydrothermal quartz separates from gold-bearing veins were collected from the Sonny Fox and Rosness and Larson Mines, and from the Goyne, Robert Hatcher, and Little Creek prospects. In addition, a quartz sample was obtained from small, unmineralized veinlets that cut a granodiorite dike on the north side of Pilot Harbor. Oxygen for $\delta^{18}\text{O}$ measurements was liberated by reaction of the quartz separates with ClF_3 in nickel bombs at 550°C, as described by Borthwick and Harmon (1982). Sphalerite, pyrite, and arsenopyrite were separated from gold-bearing quartz collected at the Rosness and Larson Mine and at the Goyne and Little Creek prospects. $\delta^{34}\text{S}$ values were determined following oxidation of these sulfide minerals to sulfur dioxide by cupric oxide combustion (Grinenko, 1962; Fritz and others, 1974). The standard error for each analysis is approximately ± 0.2 per mil for both oxygen and sulfur.

Oxygen Isotopes

Oxygen-isotope values for gold-bearing quartz from mines and prospects of the Nuka Bay district range from 14.0 to 17.4 per mil (table 2). Samples from two different veins at the Little Creek prospect are statistically identical. At the

Table 1. Chemical analyses from Nuka Bay mines and prospects

(All data are in parts per million (ppm) except for Fe, which is in percent. Lower determination limit listed in parentheses beneath element. "N" indicates element was not detected at lower determination limit)

Au (0.05)	Ag (0.5)	As (10)	B (10)	Ba (20)	Bi (1)	Cd (0.1)	Co (5)	Cu (5)	Hg (0.02)	Fe (0.05)	Mo (5)	Ni (5)	Pb (10)	Sb (2)	Te (0.05)	W (0.5)	Zn (5)	
Little Creek prospect																		
5.00	.5	60,000	<10	70	N	3.0	10	300	0.70	7	N	N	30	104	1.1	<.5	155	
3.40	200.0	67,000	<10	20	61	220.0	20	1,000	7.60	30	N	5	20,000	260	9.0	N	6,100	
16.00	15.0	48,000	<10	<20	8	2.7	30	300	1.80	7	N	10	20,000	102	7.8	.5	150	
7.10	7.0	43,000	N	<20	5	9.9	200	500	.32	20	N	50	20,000	80	6.0	<.5	700	
1.50	3.0	11,000	N	20	N	.4	100	1,000	.08	30	N	20	100	22	2.9	<.5	25	
Robert Hatcher prospect																		
.55	<0.5	11,000	30	30	1	N	10	<5	.06	.7	N	N	<10	18	4.4	<.5	N	
Rosness and Larson Mine																		
3.70	.5	40,000	10	1,000	2	58.0	30	10	1.70	7	N	10	50	48	.7	2.5	6,500	
5.70	3.0	28,000	50	500	1	41.0	50	20	.70	10	N	20	300	50	1.4	2.0	4,400	
Goyne prospect																		
26.00	7.0	31,000	<10	150	3	6.1	10	10	>10.00	5	N	N	500	34	16.0	.5	135	
31.00	100.0	55,000	N	200	107	26.0	<5	7	>10.00	30	N	N	20,000	62	19.0	2.0	5	
32.00	15.0	45,000	<10	<20	18	3.9	<5	<5	2.4	15	<5	N	3,000	38	10.8	.5	N	
24.00	15.0	87,000	<10	500	3	0.1	100	150	2.6	20	N	N	100	102	12.0	.3	5	
Sonny Fox Mine																		
.35	<.5	1,000	10	150	N	N	<5	<5	.08	.15	N	N	20	2	--	1.0	5	
2.60	2.0	18,000	150	1,000	N	.8	50	50	.40	7	N	30	20	56	.4	3.0	80	
.20	<.5	23,000	20	700	1	.5	30	<5	.10	1	N	15	300	4	--	.5	15	
48.00	15.0	1,000	<10	<20	N	N	<5	N	.18	.15	N	N	N	2	--	N	15	

Table 2. Oxygen-isotope data for quartz-vein samples

Occurrence	$\delta^{18}\text{O}$ (per mil)
Goyne prospect	14.0
Sonny Fox Mine	15.5
Little Creek prospect	16.1, 16.2
Robert Hatcher prospect	17.4, 17.0, 17.2, 17.0
Rosness and Larson Mine	17.3
Vein cutting felsic dike, Pilot Harbor	17.3

Robert Hatcher prospect, quartz separates were obtained from adjacent bands of white, flesh-colored, and sulfide-rich blue quartz. Oxygen-isotope analysis of each of the three distinct quartz bands resulted in statistically indistinguishable values, suggesting that pulses of vein forming fluids were in isotopic equilibrium with rocks of similar compositions and that temperatures of vein formation remained constant for each pulse. Oxygen-isotope values for quartz from the Nuka Bay district are identical to those from other gold districts within the Chugach terrane. Quartz $\delta^{18}\text{O}$ values range from 13.9 to 17.0 per mil for other gold districts in the Kenai-Chugach Mountains (Goldfarb and others, 1986) and from 16.5 to 17.3 per mil for gold-bearing quartz from the Chichagof district in southeastern Alaska (Goldfarb and others, 1988).

Differences in $\delta^{18}\text{O}$ of 3.4 per mil between vein quartz from the different gold occurrences in the Nuka Bay district reflect either differences in ore fluid compositions or in temperatures of quartz precipitation. A temperature difference of about 100°C between fluids responsible for quartz precipitation at the Goyne prospect ($\delta^{18}\text{O}_{\text{quartz}} = 14.0$ per mil) and at the Robert Hatcher prospect ($\delta^{18}\text{O}_{\text{quartz}} = 17.4$ per mil) would explain the range in the data. The most gold- and sulfide-rich samples were obtained from the Little Creek and Goyne prospects and the Sonny Fox Mine, and these samples have slightly lighter $\delta^{18}\text{O}$ values. The heavier $\delta^{18}\text{O}$ values for samples from the Robert Hatcher prospect and Rosness and Larson Mine could reflect lower temperature conditions that are less favorable for significant gold and base-metal sulfide precipitation. Conversely, differences in actual ore-fluid isotopic values may reflect differences in fluid source areas or fluid pathways. A fluid originating within, or having greater contact along its pathway with, ^{18}O -rich argillite of the Valdez Group would be slightly heavier than a fluid that is derived from, or passes through, graywacke or conglomerate.

If one assumes vein formation at 300°C and applies the quartz-water fractionation relationship of Matsuhiya and others (1979), then $\delta^{18}\text{O}$ values of 6.0 to 9.4 per mil are calculated for vein-forming fluids. This range is permissive of a fluid with a crustal origin, including both a magmatic and a metamorphic source. These data are not consistent with a meteoric fluid source, as Tertiary mete-

Table 3. Sulfur-isotope data for sulfide minerals

Occurrence	Mineral	$\delta^{34}\text{S}$ (per mil)
Rosness and Larson Mine	sphalerite	-0.5
Rosness and Larson Mine	pyrite	-1.0
Little Creek prospect	pyrite	-1.2
Little Creek prospect	arsenopyrite	0.1, 0.2
Goyne prospect	arsenopyrite	1.6, 1.8, 1.7

oric water in south-central Alaska had a $\delta^{18}\text{O}$ value of approximately -15 per mil as estimated from δD contours originally shown in Taylor (1974). If the ore fluids were meteoric in origin, they would have had to have undergone an oxygen shift of approximately 20 to 25 per mil requiring unlikely water-to-rock ratios of less than 0.1. The relatively narrow range in the $\delta^{18}\text{O}_{\text{quartz}}$ values is indicative of a fluid-dominant ore system with significantly higher water-to-rock ratios (Kerrick, 1987). Quartz veins hosted by granodiorite dikes at the Goyne prospect and near Pilot Harbor have similar isotopic compositions to those hosted by metasedimentary rocks and would have noticeably lighter isotopic ratios if igneous rock-dominant conditions prevailed.

Sulfur Isotopes

Eight sulfide minerals from three of the gold-bearing vein occurrences in the Nuka Bay district have a narrow $\delta^{34}\text{S}$ range between -1.2 and +1.8 per mil (table 3). This is consistent with the only other sulfur-isotopic data from gold veins hosted by rocks of the Valdez Group; these data were obtained by Pickthorn (1982) from the Port Valdez district. Eight sulfide minerals from four mines in that district also had $\delta^{34}\text{S}$ values tightly clustered around 0 per mil, ranging from -2.3 to +2.2 per mil.

Under mesothermal vein-forming temperatures, cogenetic pyrite and sphalerite should have a $\Delta^{34}\text{S}_{\text{py-sl}}$ value of about +1 to +2 per mil using the relationship of Sakai (1968). The determined $\Delta^{34}\text{S}_{\text{py-sl}}$ value of -0.5 per mil indicates a lack of isotopic equilibrium between the sulfide phases at the Rosness and Larson Mine and suggests either deposition at different temperatures or post-depositional sulfur-isotopic exchange.

The narrow range for sulfide $\delta^{34}\text{S}$ values is consistent with an isotopically uniform sulfur source. The thick sequence of Valdez Group flysch is a very likely source. Leaching of sulfides, or desulfidization reactions associated with prograde metamorphism, could release sulfur into ore-carrying fluids. The abundance of arsenopyrite in the gold-bearing veins and the absence of significant negative $\delta^{34}\text{S}$ values favor relatively reducing conditions for ore deposition.

FLUID-INCLUSION GEOCHEMISTRY

Microthermometry

Microthermometric data were obtained from doubly polished thin sections of gold-bearing quartz veins from five mines and prospects (Little Creek prospect, Robert Hatcher prospect, Rosness and Larson Mine, Sonny Fox Mine, and Goynes prospect). Measurements of fluid inclusions in the quartz were made on a modified U.S. Geological Survey gas-flow heating and cooling stage. Temperatures were determined, whenever possible, for CO₂ melting (T_m CO₂), CO₂ homogenization (T_h CO₂), ice melting (T_m ice), clathrate melting (T_m clath), and final homogenization (T_h final). All measurements were reproducible to $\pm 0.2^\circ\text{C}$, except for final homogenization temperatures, which were reproducible to $\pm 3^\circ\text{C}$.

Two types of fluid inclusions were found in all samples except for those from the Robert Hatcher prospect, which had inclusions too small to be examined. Type I inclusions (fig. 2) are isolated toward the center of clear quartz crystals, range from 2.5 to 10 μm in diameter, and tend to be rectangular to oval in shape; these observations suggest that the inclusions formed during precipitation of the bulk of the quartz. Type II inclusions are aqueous, range in size up to 8 μm , have smaller bubbles, show no evidence of gas, and are found in late trails and closer to the edges of quartz crystals. These inclusions appear to have been trapped paragenetically late and long after the bulk of the vein material formed. All examined sections exhibit fluid inclusions that were trapped above the appropriate solvus in a one-phase field. Variable gas-to-liquid ratios, where present, reflect necking down or autodecrepitation of inclusions; there is no evidence for fluid immiscibility.



Figure 2. Typical type I inclusion from Little Creek prospect, showing three phases at -10°C . Type I inclusions contain 90–92 mole percent H₂O, 6–8 mole percent CO₂, 1 mole percent CH₄, and <1 mole percent N₂. Inclusion is 10 μm in diameter.

In all the samples, type I inclusions are two-phase at room temperature. However, when cooled below room temperature, inclusions from the Little Creek prospect and Rosness and Larson Mine exhibit three phases consisting of liquid water and separate CO₂-dominant liquid and gaseous phases. T_m CO₂ values are between -63.6°C to -59.1°C (table 4), suggesting that CO₂ is the dominant gas phase but with significant contamination from CH₄ and (or) N₂ (Swanenberg, 1979). One inclusion from the Rosness and Larson Mine melted an additional solid phase at -109°C and homogenized to a liquid at -85°C . The latter temperature suggests that the major contaminant is CH₄ owing to its proximity to the methane critical temperature of -82°C . Further indication of the presence of CH₄ is the range of T_m clath values between 11.3°C and 21.6°C (table 4); these values are significantly higher than the CO₂-H₂O hydrate melting temperature of 10.0°C .

Values for T_h CO₂ range between -16.5°C and $+9.8^\circ\text{C}$ (table 4), and homogenization is consistently into the liquid phase. Calculated densities would be between 0.88 and 1.00 g/cm³, assuming pure CO₂. Higher density values in this range reflect increased contamination of the CO₂ phase with other gases. This conclusion is supported by the fact that the only two inclusions with T_h CO₂ above 0°C are among the least contaminated inclusions; that is, they have relatively high T_m CO₂ values. Therefore, the lower end of the range of possible densities is interpreted to best reflect true CO₂ densities in type I inclusions.

Due to the presence of gas-hydrate formation in type I fluid inclusions, observations of ice melting were generally obscured. In three inclusions, T_m ice values of -1.4°C to -1.2°C (table 4) was obtained in the presence of coexisting solid clathrate. Such values indicate a fluid salinity of 2.5 weight percent equivalent NaCl. However, the presence of coexisting clathrate, trapping water in an additional solid phase, suggests that the salinity is only a maximum value, and that the true value will be significantly lower (Collins, 1979).

The T_h final of the aqueous solution in type I inclusions varies between 155°C and 248°C (table 4). Difficulties in measuring T_h final arose from stretching of inclusions in quartz upon repeated heating or, more commonly, from decrepitation of fluid inclusions prior to final homogenization. Most type I inclusions in a sample would decrepitate during a single heating cycle, rendering the sample useless for additional measurements. The consistent decrepitation activity prior to final homogenization and the presence of empty or deformed, autodecrepitated inclusions indicate high internal pressures. Depending on the fluid-inclusion size, decrepitation occurred between 242°C and 299°C (table 4).

Type II inclusions range up to 8 μm in diameter and have smaller vapor bubbles than type I inclusions. Type

Table 4. Fluid-inclusion data from Nuka Bay mines and prospects

[All data, except volume percent, are in degrees Celsius]

Mine or prospect	T_{mCO_2}	T_{mice}	T_{mclath}	T_{fCO_2}	Vol %	T_{ffinal}
Type I inclusions						
Little Creek	-59.5		11.3		10	211
Little Creek	-60.4		12.4	-2.7	15	243
Little Creek	-59.4		11.6	9.8	10	
Little Creek	-60.1			-5.5	20	
Little Creek	-62.1	-1.4	14.0	-10.7	20	
Little Creek	-63.0		11.8		10	
Little Creek	-61.6		13.8	-4.2	10	
Little Creek	-62.2		15.1	-9.4	20	
Little Creek	-63.6		14.0	-10.3	10	
Little Creek						248
Little Creek	-59.1		11.6	7.8	20	
Little Creek	-59.3			-12.4	15	
Little Creek						² 242
Little Creek						² 261
Little Creek						² 278
Rosness-Larson	-63.1			-10.3	20	
Rosness-Larson	-63.2		17.0	-12.5	30	
Rosness-Larson			21.6		30	
Rosness-Larson	-62.5		15.5	-16.5	40	
Rosness-Larson	-63.4		16.6	-9.5	40	
Rosness-Larson ¹	-60.5					
Sonny Fox			14.6		2	
Sonny Fox			15.4		2	
Sonny Fox			18.2		10	
Sonny Fox						² 262
Sonny Fox						² 299
Sonny Fox						² 295
Sonny Fox						² 258
Goyne			13.9		5	
Goyne		-1.4	13.7		5	155
Goyne			13.5		2	
Goyne		-1.2	13.9		10	164
Type II inclusions						
Little Creek		-2.9			7	
Little Creek		-3.0			2	
Little Creek		-2.7			2	
Little Creek		-2.4			2	
Little Creek		-2.8			1	
Little Creek						196
Little Creek						140
Goyne		-1.5			5	

¹An inclusion containing CH₄ phase; T_{mCH_4} is -109°C and T_{fCH_4} is -85°C.

²Temperatures that indicate decrepitation prior to final homogenization.

II inclusions in samples from the Rosness and Larson and Sonny Fox Mines could not be measured because the inclusions were too small, appeared to have experienced leaking, or consistently exhibited metastable be-

havior. The T_{mice} in measured inclusions ranged from -3.0°C to -1.5°C (table 4), suggesting salinities from 2 to 5 weight percent equivalent NaCl (Roedder, 1962). Many samples had T_{mice} that oscillated upon repeated

heatings from -1°C to $+3^{\circ}\text{C}$ (table 4), indicating that the inclusions are metastable. The occurrence of metastable superheated ice at high "negative pressures" is not unusual for low-salinity, low to moderate-temperature aqueous inclusions (Roedder, 1984, p. 298). Metastable inclusions were most prevalent throughout the samples from the Sonny Fox Mine. The $T_{h\text{final}}$ of the type II inclusions were 140°C to 196°C (table 4).

Pressure-Temperature-Composition Conditions of Vein Formation

Microthermometric data indicate that type I inclusions are in the $\text{H}_2\text{O}+\text{CO}_2+\text{CH}_4+\text{NaCl}\pm\text{N}_2$ system. Type I inclusions are clearly "more primary" than type II inclusions and appear to have been trapped during precipitation of the bulk of the quartz and metals. Estimates of 85 to 92 mole percent water ($X_{\text{H}_2\text{O}}=0.85-0.92$) in type I inclusions for the Little Creek prospect and for the Rosness and Larson Mine were determined using the graphical method of Burruss (1981) and temperatures of CO_2 homogenization assuming the vein-forming fluid is in a binary $\text{H}_2\text{O}-\text{CO}_2$ system. The lowest estimates are likely an artifact of calculations based on the latter assumption. Inclusions with highest apparent CO_2 densities also have significant X_{CH_4} , which causes errors in calculation of $X_{\text{H}_2\text{O}}$. Therefore, ore fluids most likely had a composition of 90 to 92 mole percent H_2O , 7 to 9 mole percent gas, and no more than 1 to 2 mole percent salt (3-6 weight percent equivalent NaCl).

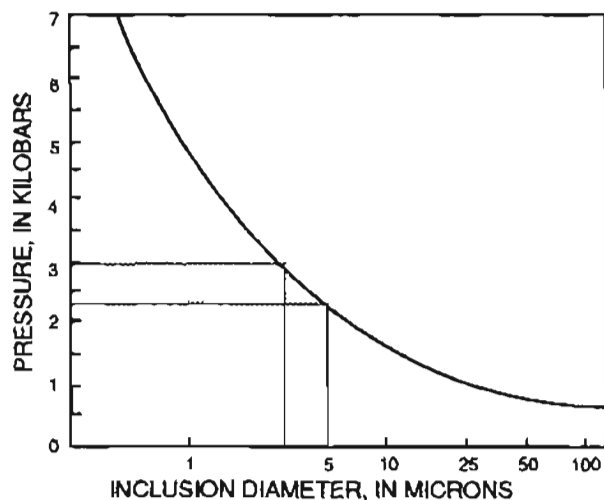


Figure 3. Internal pressure required for decrepitation of fluid inclusions in quartz according to size of inclusion at 1 atm (curve from Bodnar and others, 1989). A 5-micron inclusion decrepitating prior to final homogenization will have been trapped at a pressure of at least 2.3 kbar; decrepitation of a 2.5-micron inclusion suggests a minimum trapping pressure of 3 kbar.

The dominant species in the gas phase of the ore fluids is clearly CO_2 ; clathrate melting data suggest that CH_4 is the dominant contaminant. Values of 0.14 to >0.30 mole percent CH_4 in the gas phase were determined using both Swanenberg's (1979) technique, which plots X_{CH_4} versus degree of fill, and a $V_{\text{bulk}}-X_{\text{CH}_4}$ diagram (Burruss, 1981) using the $T_h\text{CO}_2$ values. Both methods for calculating X_{CH_4} assume that the fluid is a binary CO_2-CH_4 system and that the presence of H_2O has a nominal effect upon the volatile phase.

Lasar Raman microprobe spectroscopy was used to confirm the presence of all volatiles within the inclusions in the quartz crystals. A few selected inclusions were scanned with the microprobe for CO_2 , CH_4 , H_2S , and N_2 . Resulting data indicate that CH_4 makes up 14 to 15 mole percent of the gas phase. Nitrogen was detected but never exceeded 1 percent of the gas phase. Hydrogen sulfide was not identified in any of the examined type I inclusions. A quadrupole mass spectrometer system (Landis and others, 1987) was used to more quantitatively determine the volatile composition of the inclusions from the Little Creek prospect. Analyses of gases released from individual or small groups of inclusions during thermal decrepitation indicated roughly equivalent amounts of CH_4 and N_2 in the ore fluids.

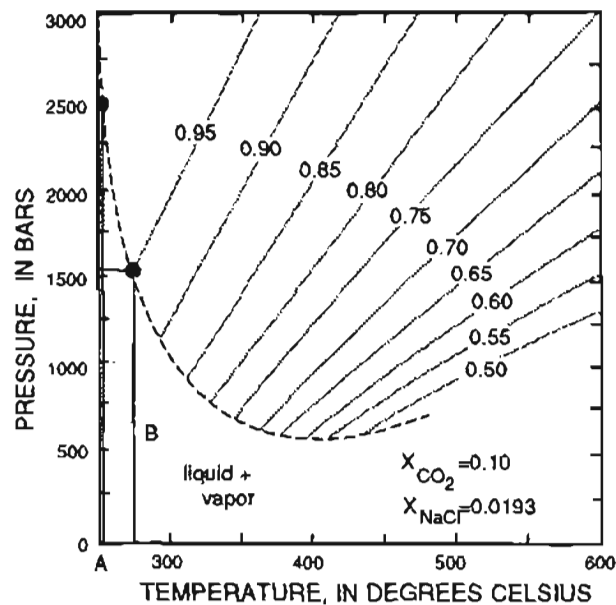


Figure 4. Solvus and isochores for fluids approximate in composition to type I fluid inclusions (from Bowers and Helgeson, 1983). All inclusions were trapped above experimentally determined solvus. Line A indicates that fluid inclusions with minimum trapping temperatures of 250°C are characterized by minimum trapping pressures of 2.5 kbar. Line B indicates that temperature estimates of 275°C suggest minimum trapping pressures of 1.5 kbar. An inclusion exhibiting $T_{h\text{final}} = 275^{\circ}\text{C}$ would have been trapped somewhere along the 0.95 g/cm^3 isochore, thus extending above the solvus.

H₂S was also detected in the analysis of the largest inclusion burst.

Two independent approaches can be used to estimate minimum trapping pressures for the ore fluids. Type I inclusions as small as 4.7 μm³ in samples from the Little Creek prospect and as small as 2.5 μm in diameter in samples from the Sonny Fox Mine decrepitated at 278°C and 299°C, respectively, prior to final homogenization (table 4). Using the relationship between inclusion size and the internal pressure needed to decrepitate inclusions in quartz under one atmosphere confining pressure (Bodnar and others, 1989), one can determine that the decrepitated inclusions would have been trapped at pressures in excess of 2.3 to 3.0 kbar (fig. 3). An alternative approach uses appropriate isochores on a pressure-temperature diagram and minimum trapping temperatures determined from microthermometry to estimate minimum trapping pressures. Based on calculated isochores for the H₂O-CO₂-NaCl system determined by Bowers and Helgeson (1983), a fluid similar in composition to that of the Nuka Bay district ore fluids would have minimum trapping pressures of 2.5 kbar and 1.5 kbar for homogenization (or decrepitation prior to homogenization) temperatures of 250°C and 275°C, respectively (fig. 4).

The consistent decrepitation of type 1 fluid inclusions between 250°C and 300°C throughout all the samples gives a minimum estimate of vein formation temperatures. The few measured homogenizations (table 4) occur at significantly lower temperatures, but these are rare observations and likely reflect deformed and (or) leaked inclusions. Minimum trapping pressures of 2.3 to 3.0 kbar from the quartz decrepitation data also indicate minimum trapping temperatures of 250°C using the compositional relationships shown in figure 4.

DISCUSSION

Stable-isotope and fluid-inclusion data from Nuka Bay are essentially identical to those from other districts hosted by rocks of the Valdez Group (Pickthorn, 1982; Goldfarb and others 1986, 1988.) The ore solutions were low-salinity C-O-H-N-S fluids typical in composition of those observed in low- to medium-grade metamorphic environments (Crawford and Hollister, 1986). Our data suggest that H₂O in the ore-forming fluids is a product of dehydration reactions within the metasedimentary rock pile. Minerals such as chlorite and epidote release significant volumes of H₂O during prograde greenschist-facies metamorphic reactions. The CO₂ in the ore fluids is similarly controlled by prograde decarbonation reactions. Significant amounts of CH₄ and N₂ measured in Nuka Bay samples might reflect the late stage breakdown of organic materials during the meta-

morphism of the metasedimentary rocks. Alternatively, these species could be derived locally at the site of vein deposition through reduction of CO₂ in the ore fluid and oxidation of ammonia in silicates to form N₂.

Oxygen- and sulfur-isotope compositions are also consistent with derivation from metamorphic rocks in the Nuka Bay area. Although hydrogen-isotope data have not yet been obtained for hydrogen-bearing minerals from the Nuka Bay deposits, similar gold districts in rocks of the Valdez Group are characterized by isotopically heavy fluids of -20 to -35 per mil (Pickthorn and others, 1987). Such fluids are normally incompatible with a meteoric source and are more indicative of derivation from metamorphic country rocks. A quartz sample with relatively few type II secondary inclusions from the Little Creek prospect was crushed to release fluid inclusion waters. Isotopic analysis of these waters yielded a δD value of -65 per mil. Whereas such a value clearly reflects a mixture of primary ore fluids and secondary waters trapped during later uplift (Pickthorn and others, 1987), it is still about 50 per mil heavier than local meteoric water. This provides further support for a deep crustal origin for the ore fluids.

In addition to the isotopic data and fluid chemistry, the minimum trapping pressures also weigh strongly against the involvement of meteoric waters in the ore-forming process. Under the assumption of lithostatic pressure, the veins are inferred to have formed at depths of at least 8.0 to 10.5 km, the deepest estimates to date for any of the Valdez Group-hosted gold deposits. It is unlikely, especially when noting the lack of any major extensional structures in the Nuka Bay area, that surface water would have circulated to such depths within the metasedimentary rocks.

The available data best support a model in which ore-forming fluids were produced during regional medium-grade metamorphic reactions in sedimentary rock. Such reactions are possible either at deeper levels within the rocks of the Valdez Group or in units of the underthrust Prince William terrane. Coeval ages for veining and igneous activity suggest that both were products of the same, relatively high temperature tectonic episode. Ore fluids migrated upward into retrograding parts of the Valdez Group, either immediately after devolatilization or subsequent to periods of ponding below impermeable units. In the latter case, a reduction of the confining pressure associated with uplift of the Kenai Mountains could have led to hydraulic fracture and fluid release.

CONCLUSION

Mesothermal gold-bearing quartz veins of the Nuka Bay district were emplaced into metasedimentary rocks of the Valdez Group at 55.6 Ma. The C-O-H-N-S ore fluids had a δ¹⁸O composition of 6.0 to 9.4 per mil and a

$\delta^{34}\text{S}$ composition of about 0 per mil. The data are consistent with fluids produced via prograde metamorphic reactions within rocks of either the Valdez Group or the underthrust Orca Group. They migrated upward to retrograding parts of the metamorphic pile at depths no shallower than 8 to 10.5 km and precipitated quartz and metals at temperatures of at least 250°C to 300°C.

REFERENCES CITED

- Bodnar, R.J., Binns, P.R., and Hall, D.L., 1989, Synthetic fluid inclusions—VI. Quantitative evaluation of the decrepitation behavior of fluid inclusions in quartz at one atmosphere confining pressure: *Journal of Metamorphic Geology*, v. 7, p. 229-242.
- Borthwick, J., and Harmon, R.S., 1982, A note regarding ClF_3 as an alternative to BrF_3 for oxygen isotope analysis: *Geochimica et Cosmochimica Acta*, v. 46, p. 1665-1668.
- Bowers, T.S., and Helgeson, H.C., 1983, Calculation of the thermodynamic and geochemical consequences of nonideal mixing in the system $\text{H}_2\text{O}-\text{CO}_2-\text{NaCl}$ on phase relations in geological systems—Metamorphic equilibria at high pressures and temperatures: *American Mineralogist*, v. 68, p. 1059-1075.
- Bradley, D.C., and Kusky, T.M., 1992, Deformation history of the McHugh Complex, Seldovia quadrangle, south-central Alaska, in Bradley, D.C., and Ford, A.B., eds., *Geological studies in Alaska by the U.S. Geological Survey, 1990*: U.S. Geological Survey Bulletin 1999, p.17-32.
- Burruss, R.C., 1981, Analysis of phase equilibria in C-O-H-S fluid inclusions: *Mineralogical Association of Canada Short Course Handbook*, v. 6, p. 39-74.
- Collins, P.L.F., 1979, Gas hydrates in CO_2 -bearing fluid inclusions and the use of freezing data for estimation of salinity: *Economic Geology*, v. 74, p. 1435-1444.
- Crawford, M.L., and Hollister, L.S., 1986, Metamorphic fluids—The evidence from fluid inclusions, in Walther, J.V., and Wood, B.J., eds., *Fluid-rock interactions during metamorphism, v. 5 of Advances in physical geochemistry*: Springer-Verlag, New York, p. 1-35.
- Fritz, P., Drimmie, R.J., and Nowicki, V.J., 1974, Preparation of sulfur dioxide for mass spectrometer analyses by combustion of sulfides with copper oxide: *Analytical Chemistry*, v. 46, p. 164-166.
- Goldfarb, R.J., Leach, D.L., Miller, M.L., and Pickthorn, W.J., 1986, Geology, metamorphic setting, and genetic constraints of epigenetic lode-gold mineralization within the Cretaceous Valdez Group, south-central Alaska, in Keppie, J.D., Boyle, R.W., and Haynes, S.J., eds., *Turbidite-hosted gold deposits: Geological Association of Canada Special Paper 32*, p. 87-105.
- Goldfarb, R.J., Leach, D.L., and Pickthorn, W.J., 1988, Accretionary tectonics, fluid migration, and gold genesis in the Pacific Border Ranges and Coast Mountains, southern Alaska, in Kisvarsanyi, G., and Grant, S.K., eds., *North American Conference on Tectonic Control of Ore Deposits and the Vertical and Horizontal Extent of Ore Systems, 1988 Proceedings: Volume, Rolla, Mo., University of Missouri-Rolla*, p. 67-79.
- Grant, U.S., and Higgins, D.F., Jr., 1910, Preliminary report on the mineral resources of the southern part of the Kenai Peninsula: U.S. Geological Survey Bulletin 442-D, p. 166-178.
- Grinenko, V.A., 1962, Preparation of sulfur dioxide for isotope analysis: *Zhurnal Neorganicheskoi Khimii*, v. 7, p. 2478-2483.
- Hudson, T., Plafker, G., and Peterman, Z.E., 1979, Paleogene anatexis along the Gulf of Alaska margin: *Geology*, v. 7, p. 573-577.
- Johnson, B.L., 1914, The Port Wells gold-lode district: U.S. Geological Survey Bulletin 592, p. 195-235.
- 1915, The gold and copper deposits of the Port Valdez district: U.S. Geological Survey Bulletin 622, p. 141-187.
- Kerrick, R., 1987, The stable isotope geochemistry of Au-Ag vein deposits in metamorphic rocks: *Mineralogical Association of Canada Short Course Handbook*, v. 13, p. 287-336.
- Landis, G.P., Hofstra, A.H., Leach D.L., and Rye, R.O., 1987, Quantitative analysis of fluid-inclusion gases—Application to the study of ore deposits (abs.): U.S. Geological Survey Circular 995, p.38-39.
- Matsubisa, Y., Goldsmith, J.R., and Clayton, R.N., 1979, Oxygen isotopic fractionation in the system quartz-albite-anorthite-water: *Geochimica et Cosmochimica Acta*, v. 43, p. 1131-1140.
- Nelson, S.W., Dumoulin, J.A., and Miller, M.L., 1985, Geological map of the Chugach National Forest, Alaska: U.S. Geological Survey Miscellaneous Field Studies Map MF-1645-B, 18 p., 1 sheet, scale 1:250,000.
- Nilsen, T.H., and Zuffa, G.G., 1982, The Chugach terrane, a Cretaceous trench-fill deposit, southern Alaska: in Legget, J.K., ed., *Trench-forearc geology—Sedimentation and tectonics on modern and ancient active plate margins*: London, Blackwells, p. 213-227.
- Park, C.F., Jr., 1933, The Girdwood district, Alaska: U.S. Geological Survey Bulletin 849-G, p. 381-424.
- Pickthorn, W.J., 1982, Stable isotope and fluid inclusion study of the Port Valdez district, southern Alaska: Los Angeles, Calif., University of California, M.S. thesis, 66 p.
- Pickthorn, W.J., Goldfarb, R.J., and Leach, D.L., 1987, Comment on "Dual origin of lode gold deposits in the Canadian Cordillera": *Geology*, v. 15, p. 471-472.
- Plafker, G., Jones, D.L., and Pessagno, E.A., Jr., 1977, A Cretaceous accretionary flysch and melange terrane along the Gulf of Alaska margin, in Blean, K.M., ed., *The U.S. Geological Survey in Alaska—Accomplishments during 1976*: U.S. Geological Survey Circular 751-B, p. B41-B43.
- Richter, D.H., 1970, Geology and lode-gold deposits of the Nuka Bay area, Kenai Peninsula, Alaska: U.S. Geological Survey Professional Paper 625G, 16 p.
- Roedder, E., 1962, Studies of fluid inclusions I—Low temperature application of a dual-purpose freezing and heating stage: *Economic Geology*, v. 57, p. 1045-1061.
- 1984, Fluid inclusions: *Mineralogical Society of America Reviews in Mineralogy*, v. 12, 644 p.
- Sakai, H., 1968, Isotopic properties of sulfur compounds in hydrothermal processes: *Geochemical Journal*, v. 2, p. 29-49.

- Smith, P.S., 1938, Mineral industry of Alaska in 1936: U.S. Geological Survey Bulletin 897-A, p. 1-107.
- Swanenberg, H.E.C., 1979, Phase equilibria in carbonic systems and their application to freezing studies in fluid inclusions: Contributions to Mineralogy and Petrology, v. 68, p. 303-306.
- Taylor, H.P., Jr., 1974, The application of oxygen and hydrogen isotope studies to problems of hydrothermal alteration and ore deposition: Economic Geology, v. 69, p. 843-883.
- Tuck, R., 1933, The Moose Pass-Hope district, Kenai Peninsula, Alaska: U.S. Geological Survey Bulletin 849-I, p. 469-530.
- Tysdal, R.G., and Case, J.E., 1979, Geologic map of the Seward and Blying Sound quadrangles, Alaska: U.S. Geological Survey Miscellaneous Field Studies Map I-1150, 12 p., 1 sheet, scale 1:250,000.
- Winkler, G.R. and Plafker, G., 1975, The Landlock fault—Part of a major early Tertiary plate boundary in southern Alaska in Yount, M.E., ed., U.S. Geological Survey Alaskan Program, 1975: U.S. Geological Survey Circular 722, p. 49.

Reviewers: Lori Apodoca and John E. Gray

Placer Gold of the Kenai Lowland

By Barrett A. Cieutat, Richard J. Goldfarb, Dwight C. Bradley, and Bruce H. Roushey

Abstract

A geochemical survey of the Kenai lowland, Cook Inlet basin, Alaska, produced stream-sediment and heavy-mineral-concentrate samples that were consistently anomalous in gold. Stream-sediments with as much as 2.8 ppm Au and heavy-mineral-concentrate samples with up to 700 ppm Au are believed to reflect reworked material from Quaternary glacial deposits and (or) from the upper part of the Tertiary Kenai Group. Gold grains are generally concentrated in the -35-mesh to +230-mesh size fractions. Concentrations of heavy minerals from an outcrop of Quaternary or Tertiary partly lithified conglomerate along the Fox River reveal that at least some of the gold was derived from the Chugach terrane to the east. Although no specific placer or lode occurrences that have resource potential have been identified, geomorphic processes in the Kenai lowland may have formed small, locally economic, undiscovered placer concentrations.

INTRODUCTION

Metallic mineral resources are largely unrecognized within the southern Kenai lowland of south-central Alaska (fig. 1). The only confirmed mineral production in the study area (fig. 1) is from a small placer gold occurrence mined intermittently from 1889 to 1911 at the mouth of the Anchor River (Cobb, 1973). Fine gold was found in thin layers of gravel <1 m below the surface of the beach (Martin and others, 1915). Platinum was rumored to occur with the gold (Cobb, 1973). Martin and others (1915) also reported placer activities in the Kenai lowlands to the north of the present study area, near Ninilchick and between the Killey River and Kenai, but the success of these operations is unknown. Presently, placer-gold claims exist along Cook Inlet at Anchor Point and about 2 km north of the mouth of Diamond Creek (U.S. Bureau of Mines MAS deposit listings). A lode-gold claim is also recorded from the beach within 1 km of the mouth of Diamond Creek. Little is known about this claim, but it most likely includes rocks of the Tertiary Kenai Group and (or) overlying Quaternary gravels exposed in the beach cliffs.

As part of the Alaska Mineral Resources Appraisal Program (AMRAP) study of the Seldovia 1° by 3° quadrangle, we conducted geological and geochemical studies in the southern Kenai lowland. Results from the studies indicate a widespread distribution of detrital gold grains in stream alluvium. This report details and discusses the significance and possible origin of widespread, anomalous gold values in stream-sediment and rock samples from this area. These findings are surprising because previous reports of gold in this populated region are restricted to the beach claims described above.

REGIONAL GEOLOGY

The Kenai lowland is part of the Cook Inlet Basin, an active forearc basin of the present day Aleutian-Alaska Range subduction zone (Magoon and Egbert, 1986). The basin is flanked to the west by active volcanoes that are built on older arc basement and to the east by an uplifted Mesozoic accretionary prism (the Chugach terrane) composed mainly of mafic volcanic rocks, chert, argillite, and graywacke. The Kenai lowland is characterized by gentle to flat topography, except near shoreline escarpments, and by an abundance of fair to poorly drained marshland. The lowland is covered by Quaternary alluvial and glacial deposits that are underlain by sedimentary rocks of the Tertiary Kenai Group (Magoon and others, 1976). Only the two youngest formations of the Kenai Group—the Beluga Formation and the overlying Sterling Formation—are exposed within our study area.

The Miocene Beluga Formation consists of up to 1,525 m (5,000 ft) of claystone, siltstone, thin sandstone, and subbituminous coal (Hartman and others, 1972). The Beluga Formation crops out in cliffs along the shore of Kachemak Bay to the northeast of Homer and along the shore of Cook Inlet northwest of Homer. Only the upper few hundred meters are exposed; the remainder is known from subsurface studies (Hayes and others, 1976). Paleocurrent directions are toward the west-northwest (Rawlinson, 1984). The most abundant sandstone

framework grains in the Beluga Formation are weakly metamorphosed sedimentary rocks comparable to those exposed in the Kenai Mountains to the east (Hayes and others, 1976). The heavy-mineral assemblage, which is dominated by epidote, garnet, apatite, and zircon, also is consistent with an easterly source (Hayes and others, 1976). Flores and Stricker (this volume) interpreted the Beluga Formation as having been deposited by an anastomosing fluvial system; alternatively, Hayes and others (1976) and Rawlinson (1984) interpreted it as having been deposited by braided streams.

The late Miocene and Pliocene Sterling Formation consists of more than 3,050 m (10,000 ft) of massive sandstone and conglomerate, which are interbedded with thin claystone and lignite (Hartman and others, 1972). Rocks of the Sterling Formation are intertongued with those of the underlying Beluga Formation. Extensive exposures of the Sterling Formation occur along Kachemak Bay, along the Fox River north of Kachemak Bay, and around Epperson Knob and Lookout Mountain in the Anchor River drainage. Only the lowest 700 m of the Sterling Formation crops out, the remainder being known in the subsurface. Evidence summarized by

Hayes and others (1976) indicates that the Sterling Formation was mainly derived from sources to the west. West-northwesterly paleocurrent directions measured at Kachemak Bay near the eastern basin margin, however, also indicate a sediment source in the Kenai Mountains (Rawlinson, 1984). Sandstone framework grains in the Sterling Formation consist of quartz, plagioclase, biotite, and glassy volcanic rock fragments and suggest derivation from the magmatic arc to the west (Hayes and others, 1976). The heavy-mineral assemblage, which is dominated by hornblende and pyroxene, also suggests an arc source (Kirschner and Lyon, 1973; Hayes and others, 1976). A meandering stream depositional environment has been widely accepted for the Sterling Formation (Hayes and others, 1976; Rawlinson, 1984; Flores and Stricker, this volume).

Quaternary surficial deposits form a discontinuous mantle that unconformably overlies the Kenai Group. These deposits of till, outwash, and glaciolacustrine mud vary in thickness from 0 to 320 m; the thickest Quaternary section is in an exploratory well near Kenai (Calderwood and Fackler, 1972). At least five major Pleistocene and two minor post-Pleistocene glaciations

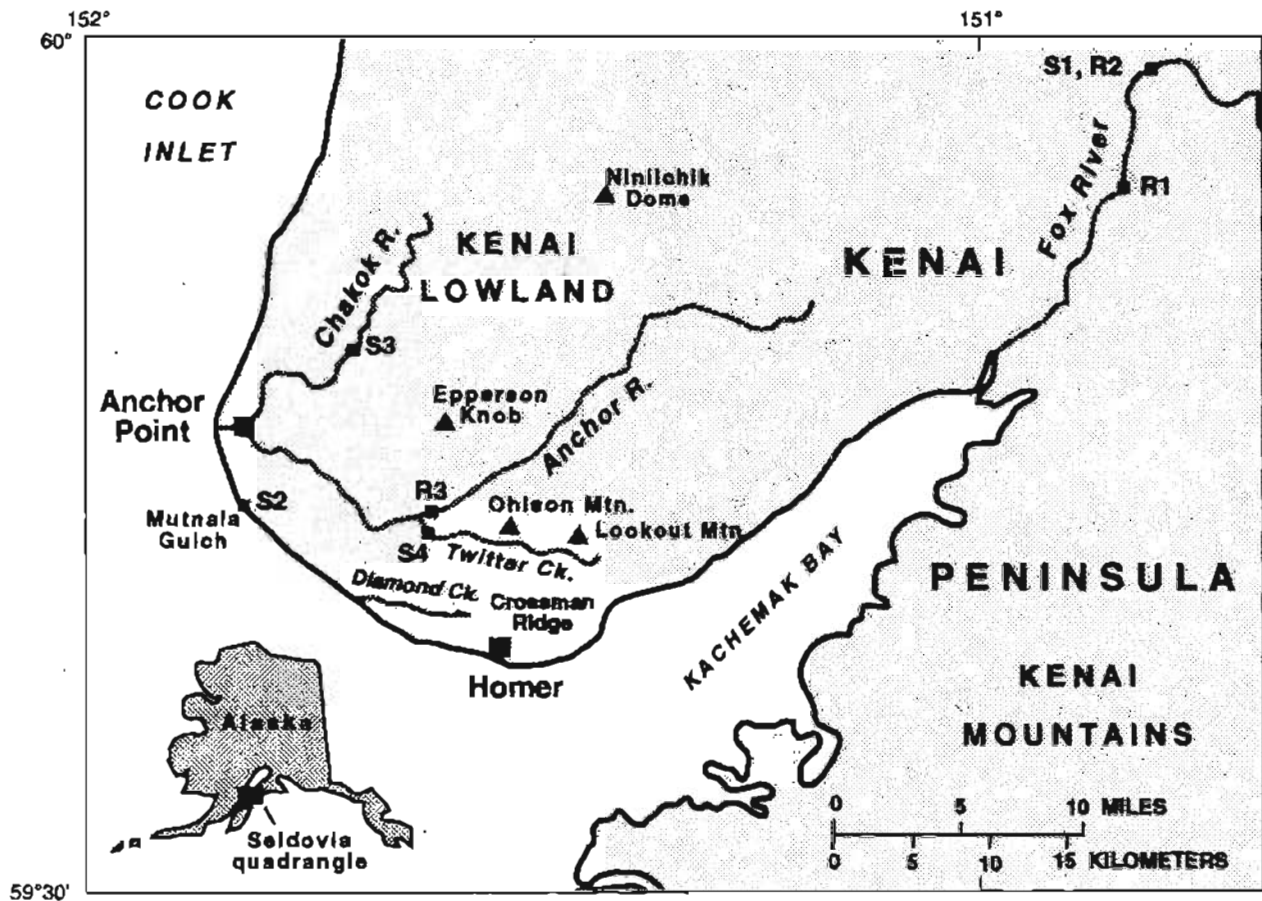


Figure 1. Site location map for sluice-concentrate and rock samples in Kenai lowland.

have been identified in the Kenai lowland (Karlstrom, 1964). In the Seldovia quadrangle, direct evidence for four Pleistocene ice advances is provided by moraines and related ice-marginal deposits of the Caribou Hills, Eklutna, Knik, and Naptowne (listed from oldest to youngest; Karlstrom, 1964).

Tertiary strata in the Kenai lowland generally can be discriminated from the Quaternary deposits on the basis of two characteristics—the presence of coal, and partial to complete lithification. However, a problematic succession of variably lithified, gold-bearing gravel and conglomerate occurs in 50-m-high bluffs along the upper part of the Fox River at location S1 (fig. 1); these deposits deserve special mention. Weakly stratified, clast-supported gravels occur in beds up to 10 m thick and are associated with thick beds (several meters thick) and thinner lenses of weakly lithified to unlithified sand. Some conglomerate beds are sufficiently lithified to occur as talus blocks at the foot of the bluff. Clasts (the largest are about 20 cm long) include melange, graywacke, and greenstone; chert of the McHugh Complex; and hornfelsed metapelite of the Valdez Group. The clasts indicate an easterly sediment source in the Kenai Mountains. Bedding dips about 15° W. Similar deposits that fill paleovalleys among the the southeastern shore of Kachemak Bay have been assigned to the Tertiary Kenai Group on the basis of abundant plant fossils (Magoon and others, 1976). However, published maps of the regional bedrock geology (Magoon and others, 1976) and surficial geology (Karlstrom, 1964) have assigned the unfossiliferous upper Fox River outcrops to the Quaternary. In light of bedding dips, degree of lithification, and similarities to known Tertiary strata along the Kenai Mountain front, we favor the interpretation that the upper Fox River gravels are Tertiary in age and represent proximal alluvial-fan deposits that are laterally equivalent to fluvial deposits of the Beluga and (or) Sterling Formations. However, the possibility that the gold-bearing conglomerates and gravels are indeed Quaternary remains viable.

REGIONAL GEOCHEMISTRY

Stream-sediment and heavy-mineral-concentrate samples were collected at 75 sites within the Kenai lowland as part of an extensive regional geochemical reconnaissance survey of the Seldovia 1° by 3° quadrangle. Samples were collected between Cook Inlet and the Fox River, with the majority located south of Ninilchik Dome along first- and second-order tributaries to the Chakok and Anchor Rivers. At least five grab samples were collected at each site along a 9-m stretch of stream channel. The grab samples were composited into a single sample, air-dried, sieved in the laboratory using a

stainless-steel 80-mesh screen, and pulverized prior to chemical analysis. Heavy-mineral-concentrate samples were collected at all sediment sites using a 14-in.-diameter gold pan. Typically, 3 to 4 kg of composited sediment were collected and panned, yielding the desired 30 to 60 g of concentrate. Remaining lightweight material was separated by floatation in bromoform (specific gravity 2.86), and the resulting heavy-mineral fraction was separated into magnetic, semimagnetic, and nonmagnetic fractions using a Frantz Isodynamic Separator.

Both the stream-sediment sample and the nonmagnetic heavy-mineral-concentrate fraction were analyzed for minor and trace elements by emission spectrography according to the method outlined by Grimes and Marranzino (1968). Owing to the relatively high lower limits of detection for emission spectrography, more sensitive analytical methods were used on stream-sediment samples. They were analyzed for Ag, As, Au, Bi, Cd, Cu, Mo, Pb, Sb, and Zn by inductively coupled plasma spectroscopy (ICP) following the method of Motooka (1988). Lower determination limits for the method for gold and silver are 0.045 and 0.15 ppm, respectively. Gold concentrations were also determined by flame atomic absorption (Thompson and others, 1968) for about half the stream-sediment samples and by graphite furnace atomic absorption spectrophotometry (Meier, 1980) for the remaining stream-sediment samples. Samples that registered below the lower determination limit for flame atomic absorption were analyzed using the graphite furnace method. Lower determination limits are 0.05 and 0.002 ppm for the two methods, respectively.

Anomalous concentrations of gold were identified in stream-sediment samples from 27 of the 75 sampled sites. Graphite furnace atomic absorption data indicate an anomaly threshold value of 0.007 ppm for gold in stream sediments from the Kenai lowland. Fourteen of the sediment samples contain at least 0.012 ppm Au, and eight of these contain 0.3 to 2.8 ppm Au. Highest values were found in samples collected just above the beach in Mutnaia Gulch (1.0 ppm), along a tributary to the Anchor River in sec. 22, R. 14 W., T. 5 S. (1.8 ppm), and from another tributary to the Anchor River along the east side of the Sterling highway about 1.5 km north of the Anchor River campground (2.8 ppm). No other anomalous metals were found consistently in stream-sediment samples containing anomalous gold. Silver concentrations for all 75 stream-sediment samples were at background levels, ranging from not detected at the 0.045-ppm lower determination limit to 0.080 ppm. A few samples with anomalous gold values contained 30 to 40 ppm As, but most arsenic values were below 20 ppm.

Sixteen of 71 heavy-mineral-concentrate samples contained anomalous gold concentrations ranging from 20 ppm to 700 ppm. In addition, three other samples had detectable gold but at levels below the 20 ppm

lower determination level. Small flakes of gold were commonly visible in these samples when viewed with a 10X hand lens in the field. The majority of these samples were from sites that lacked anomalous gold concentrations in corresponding stream sediments. Similarly, most sites with anomalous gold concentrations in stream-sediment samples yielded heavy-mineral-concentrate samples that lacked anomalous gold. The lack of correlation suggests that (1) gold grains are relatively fine and easily lost during the panning process, and (2) gold grains likely occur in many other heavy-mineral-concentrate samples but in concentrations below the 20-ppm lower determination level. Anomalous silver values of 1 to 20 ppm in heavy-mineral-concentrate samples characterize most of the sites with gold anomalies in stream-sediment or heavy-mineral-concentrate samples. Molybdenum, tin, and tungsten are commonly found at anomalous levels in many of the heavy-mineral-concentrate samples from throughout the Kenai lowland. Most of these samples contain microscopically visible scheelite; molybdenite was identified in one sample (Richard Tripp, unpub. data). Whereas these metals show no distinct correlation with the gold and silver anomalies, they do suggest a strong igneous component within the Tertiary sedimentary rocks that are the source for much of the stream sediment.

The regional geochemical data indicate a widespread distribution of gold grains in the Kenai lowland. The distribution, as well as the commonly delicate morphology of gold flakes viewed with a hand lens, suggest an extensive, locally derived source. Brooks (1911) speculated that the gold was derived either from rocks of the Tertiary Kenai Group or from overlying glaciofluvial gravels; our data allow both possibilities.

FOLLOWUP INVESTIGATION

Sediments

Three stream channel localities that contained samples with anomalous gold collected during the regional investigation were revisited for more detailed study of the placer material. Bulk samples were collected at Mutnaia Gulch (site S2), on Chakok River (site S3), and on Twitter Creek (site S4). These sites (fig. 1) had yielded samples with anomalous concentrations of gold in sediment only, both concentrate and sediment, and concentrate only, respectively.

In an effort to better estimate the amount of gold at the three sites, sixteen 14-in.-diameter gold pans of alluvium were sluiced at each site. The sixteen pans approximately equal one-sixteenth of a cubic yard of alluvium. This quantity is sufficient to remove the "nugget effect" from analyses (S. Fechner, oral commun.,

Table 1. Concentrations of gold in nonmagnetic fractions of sluice concentrates from selected stream sample sites in the Kenai lowland, Alaska

(Values in parts per million)

Sample	S2	S3	S4
Mesh size:			
-10 to +18	<0.002	<0.002	<0.002
-18 to +35	<0.002	<0.002	<0.002
-35 to +80	920	120	700
-80 to +230	840	520	380
-230 ^a	8.6	5.2	160

^aValues include combination of magnetic, semimagnetic, and nonmagnetic fractions because -230-mesh fraction was too small for effective use of the magnetic separator.

1991). The alluvium was sieved using a 10-mesh (2.0-mm) stainless-steel screen prior to being placed into the sluice. The sluice was arranged in each stream so that water velocity carried a 1-in.-diameter pebble through at a slow, steady rate. Material that did not wash away was saved for analysis. A thorough cleaning of the sluice between samples ensured minimal contamination.

Site S2, S3, and S4 samples were air dried in the laboratory before being sieved into five size fractions (-10-mesh to +18-mesh, -18-mesh to +35-mesh, -35-mesh to +80-mesh, -80-mesh to +230-mesh, and -230-mesh). Lightweight material from each fraction was separated by floatation in bromoform (specific gravity 2.86), and the resulting heavy-mineral fraction was split into magnetic, semimagnetic, and nonmagnetic fractions using a Frantz Isodynamic Separator. Semimagnetic and magnetic fractions were analyzed for gold by emission spectrography using the method outlined by Grimes and Marranzino (1968). The nonmagnetic fraction was analyzed for gold using flame atomic absorption (Thompson and others, 1968). The lower determination limits for the two are 20 and 0.050 ppm, respectively.

The semimagnetic and magnetic fractions contained no detectable gold at any site in any of the five sieve categories. The nonmagnetic fraction, however, contained gold in three of the size fractions for sites S2, S3, and S4: -35-mesh to +80-mesh, -80-mesh to +230-mesh, and -230-mesh (table 1). The -35-mesh to +80-mesh and the -80-mesh to +230-mesh fractions contained the bulk of the gold, whereas no gold was found in the -10-mesh to +18-mesh and the -18-mesh to +35-mesh fractions. Sample site S2 had the greatest concentrations of gold with 920, 840, and 8.6 ppm in the -35-mesh to +80-mesh, -80-mesh to +230-mesh, and -230-mesh fractions, respectively. All of the sluice samples contained visible gold when viewed with a 10X hand lens in the field.

Site S2 is located at the mouth of Mutnaia Gulch on the shore of Cook Inlet. It is a small, steeply stream

(<2 m across) of moderate gradient with water depth never exceeding 0.3 m in the sampling area. The sample was obtained from the drainage above possible tidal influence. The Beluga Formation crops out at the beach and on both sides of the gulch. Site S3 on Chakok River predominantly drains Quaternary sediments. However, within its drainage basin to the east is Epperson Knob, which consists of the Sterling Formation. The sampled stream is 3 to 4 m across, with depths to 1.5 m on some cutbanks. It has a low gradient, meanders, and has alluvium ranging in size from silt to cobble. Site S4 is located on Twitter Creek just north of Homer. It mainly drains the Sterling Formation of Ohlson Mountain, Crossman Ridge, and Lookout Mountain, but the Beluga Formation is present on some of the lower stretches near the Anchor River. It is of low to moderate gradient, 1.5 to 3 m across, and 0.3 to 1 m deep.

Table 2. Concentrations of gold of rock samples from the Kenai lowland, Alaska

[Values in parts per million. N, not detected at indicated lower determination limit; L, detected but below indicated lower determination limit; Do., ditto]

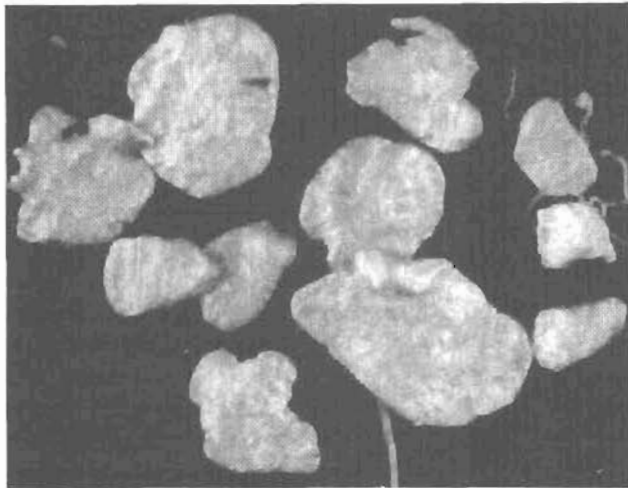
Sample	Concentration	Location	Source
R1-1 -----	L(.002)	T. 3 S., R. 9 W.,	conglomerate
R1-2 -----	L(.002)	sec. 16, SE ¹ / ₄	cong. matrix
R1-3 -----	L(.002)		Do.
R1-4 -----	L(.002)		Do.
R1-5 -----	L(.002)		Do.
R2B-1 -----	.004	T. 2 S., R. 9 W.,	conglomerate
R2B-2 -----	.004	sec. 24, NW ¹ / ₄	cong. matrix
R2B-3 -----	.004		Do.
R2B-4 -----	.006		Do.
R2B-5 -----	.004		Do.
R2A-1 -----	.004		Do.
R2A-2 -----	.002		Do.
R2A-3 -----	.002		Do.
R3-1 -----	.014	T. 5 S., R. 14 W.,	claystone
R3-2 -----	N(.002)	sec. 26, NW ¹ / ₄	coaly coarse ss
R3-3 -----	N(.002)		coal
R3-4 -----	L(.002)		< 2 mm clastics
R3-5 -----	L(.002)		< 2 mm clastics

Prior to analysis the gold grains from site S2 were hand picked (fig. 2A) for examinations of gold morphology; the gold was returned to the sample before chemical analysis. Site S2 grains are generally flat and rounded to irregular, with the largest grain being 0.95 mm at its longest dimension. With increasing distance of mechanical transport, gold-grain morphology changes from delicate, through irregular and abraded, to rounded, while grain size is progressively diminished (Grant and others, 1991). The studied gold grains in all likelihood have undergone at least secondary fluvial and possibly glacial transport. The range in shape from round to irregular suggests either that the gold has weathered out at different locations along the flowpath of the stream, or that morphologic differences among gold grains are inherited from prior fluvial histories, or both.

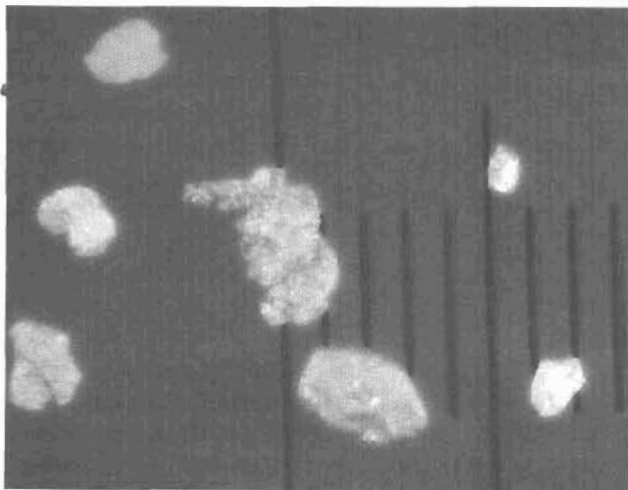
Rocks

The only available background gold values for the Kenai Group are from three conglomerates analyzed in the present study (table 2). Owing to relatively weak lithification, we were able to remove coarse material (cobbles to boulders) by hand. The samples then were sieved and the +35-mesh fraction was discarded.

Sample R1 is from the Sterling Formation along the Fox River. The outcrop consists of conglomerate with a coarse sandstone matrix and interlayered siltstones and



A



B

Figure 2. Gold grains from two sluice-concentrate sites within Kenai lowland. A, Grains from sample site S2. Longest gold grain is approximately 1 mm across. B, Grains from sample site S1.

claystones. The -35-mesh fraction was crushed, ground, and analyzed for low-level gold by graphite furnace atomic absorption spectrophotometry (Meier, 1980). None of the five splits from site R1 measured above the lower determination limit.

Sample R3 is from the Beluga Formation about 10 km northwest of Homer along the south bank of the Anchor River. The outcrop consists of conglomerate, claystone, coaly iron-stained coarse sandstone, and coal. The conglomerate matrix contained detectable gold below the determination limit. The claystone contained 0.014 ppm gold, the highest value for any rock sample. No gold was detected in the sandstone or coal.

Sample R2 is from the undifferentiated (Tertiary or Quaternary) gravel and conglomerate along the upper Fox River (fig. 3). Eight splits of the sample were analyzed for gold; values ranged from 0.002 to 0.006 ppm. Sample S1 was taken from the same location and was crushed prior to being sieved, sluiced, prepared, and analyzed in similar fashion to the sediment samples S2, S3, and S4 mentioned previously. For sample S1, the semimagnetic and magnetic fractions from all sieve categories were barren of detectable gold at the 20-ppm determination limit using an optical emission spectrograph according to the method outlined by Grimes and Marranzino (1968). Also barren were the -10-mesh to +18-mesh, -18-mesh to +35-mesh, and -35-mesh to +80-mesh sieve sizes of the nonmagnetic fraction. The -80-mesh to +230-mesh size fraction contained 5.6-ppm gold, while the -230-mesh size fraction contained 0.3-ppm gold.

Gold from the sluice concentrate from site S1 was hand picked (fig. 2B) to examine morphology. Gold grains are smaller and more delicate than those from site S2. The largest grain is approximately 0.45 mm on its longest dimension. Since the sample at site S1 was taken directly from outcrop, the gold has not undergone reworking by present fluvial activity. Therefore, barring chemical transport and reprecipitation of gold, it appears likely that the lack of present-day mechanical transport is responsible for the more delicate nature of gold grains at site S1.

DISCUSSION AND CONCLUSIONS

Placer gold is extensive throughout the Kenai lowland. Of 75 sampled drainages, 27 were anomalous for gold in stream sediment and 16 were anomalous for gold in heavy-mineral concentrates from stream sediment. A sluice box was used to assess the placer-gold potential of three streams. Of the three stream locations (sites S2, S3, and S4) where the sluice was used to concentrate larger volumes of material, none contained significant gold quantities. The fine size (generally <0.2 mm) and lack of concentration of the gold deflate any hope of a minable resource at this time.

Whether the gold has been reworked from the Quaternary deposits or the Tertiary Kenai Group, or both, remains unresolved. The two bedrock sites in unequivocal Sterling and Beluga Formations lack significant gold,



Figure 3. Outcrop of Tertiary or Quaternary conglomerate and gravel along upper Fox River where sluice sample S1 and rock sample R2 were taken.

but more sampling would likely be necessary to locate significant quantities. In addition, it is possible that the placer gold was derived from the coarser fraction of conglomerates—the fraction that was discarded prior to chemical analysis. Although gold was recovered from bluffs of gravel and conglomerate along the upper Fox River (samples R2, S1), the stratigraphic position is ambiguous. Regardless of whether the strata are Tertiary or Quaternary, the occurrence of paleoplacer gold in alluvium derived from the Kenai Mountains does indicate that at least some of the placer gold was ultimately derived from the east.

An analogous situation to the gold in the Kenai lowland may be the placer deposits along the Gulf of Alaska coastline from Cape Yakataga to Icy Bay. There, the Yakataga Formation is the principal source of gold, which is being reworked and concentrated by recent fluvial systems and by longshore currents (Reimnitz and Pfalker, 1976; Eyles, 1990). Eyles (1990) cited glaciers as playing a major role in transporting detrital gold over such large areas and noted that postglacial shallow-marine and fluvial activity concentrated the gold. Eyles (1990) also pointed out that gold shows a noticeable size reduction as it moves away from its source river along the beach.

REFERENCES CITED

- Boss, R.F., Lennon, R.B., and Wilson, B.W., 1976, Middle Ground Shoal oil field, Alaska, in Braunstein, Jules, ed., North American oil and gas fields: American Association of Petroleum Geologists Memoir 24, p. 1-22.
- Brooks, A.H., 1911, The Mount McKinley region, Alaska, with descriptions of the igneous rocks and of the Bonfield and Kantishna districts: U.S. Geological Survey Professional Paper 70, 234 p.
- Calderwood, K.W., and Fackler, W.C., 1972, Proposed stratigraphic nomenclature for Kenai Group, Cook Inlet basin, Alaska: American Association of Petroleum Geologists Bulletin, v. 56, no. 4, p. 739-754.
- Cobb, E.H., 1973, Placer deposits of Alaska: U.S. Geological Survey Bulletin 1374, 213 p.
- Eyles, N., 1990, Glacially derived, shallow-marine gold placers of the Cape Yakataga district, Gulf of Alaska: Sedimentary Geology, v. 68, p. 171-185.
- Eyles, N., and Kocsis, S.P., 1989, Sedimentological controls on gold in a late Pleistocene glacial placer deposit, Cariboo Mining District, British Columbia, Canada: Sedimentary Geology, v. 65, p. 45-68.
- Grant, A.H., Lavin, O.P., and Nichol, I., 1991, The morphology and chemistry of transported gold grains as an exploration tool: Journal of Geochemical Exploration, v. 40, p. 73-94.
- Grimes, D.J., and Marranzino, A.P., 1968, Direct-current arc and alternating-current spark emission spectrographic field methods for the semiquantitative analysis of geologic materials: U.S. Geological Survey Circular 591, 6 p.
- Hartman, D.C., Pessel, G.H., and McGee, D.L., 1972, Preliminary report on stratigraphy of Kenai Group, upper Cook Inlet, Alaska: Alaska Division of Geological and Geophysical Surveys, Special Report 5, 4 p., 7 maps, scale 1:500,000, 1 pl.
- Hayes, J.B., Harms, J.C., and Wilson, T.W., 1976, Contrasts between braided and meandering stream deposits, Beluga and Sterling Formations (Tertiary), Cook Inlet, Alaska, in Miller, T.P., ed., Recent and ancient sedimentary environments in Alaska: Anchorage, Alaska Geological Survey, p. J1-J27.
- Karlstrom, T., 1964, Quaternary geology of the Kenai lowland and glacial history of the Cook Inlet region, Alaska: U.S. Geological Survey Professional Paper 443, 69 p.
- Kirschner, C.E., and Lyon, C.A., 1973, Stratigraphic and tectonic development of Cook Inlet petroleum province, in Pitcher, M.G., ed., Arctic geology: American Association of Petroleum Geologists' Memoir 19, p. 396-407.
- Magoon, L.B., Adkinson, W.L., and Egbert, R.M., 1976, Map showing geology, wildcat wells, Tertiary plant-fossil localities, K-Ar age dates, and petroleum operations, Cook Inlet area, Alaska: U.S. Geological Survey Miscellaneous Geologic Investigations Map I-1019, 3 sheets, scale 1:250,000.
- Magoon, L.B., and Egbert, R.M., 1986, Framework geology and sandstone compositions, in Magoon, L.B., ed., Geologic studies of the lower Cook Inlet COST No. 1 Well, Alaska outer continental shelf: U.S. Geological Survey Bulletin 1596, p. 65-90.
- Martin, G.C., Johnson, B.L., and Grant, U.S., 1915, Geology and mineral resources of the Kenai Peninsula, Alaska: U.S. Geological Survey Bulletin 587, 243 p.
- Meier, A.L., 1980, Flameless atomic absorption determination of gold in geologic materials: Journal of Geochemical Exploration, v. 13, p. 77-85.
- Motooka, J.M., 1988, An exploration geochemical technique for the determination of preconcentrated organometallic halides by ICP-AES: Applied Spectroscopy, v. 42, p. 1293-1296.
- Rawlinson, S.E., 1984, Environments of deposition, paleocurrents, and provenance of Tertiary deposits along Kachemak Bay, Kenai Peninsula, Alaska: Sedimentary Geology, v. 38, p. 421-442.
- Reimnitz, E., and Pfalker, G., 1976, Marine gold placers along the Gulf of Alaska margin: U.S. Geological Survey Bulletin 1415, 16 p.
- Thompson, C.E., Nakagawa, H.M., and VanSickle, G.H., 1968, Rapid analysis for gold in geological materials, in Geological Survey research 1968: U.S. Geological Survey Professional Paper 600-B, p. B130-B132.

Reviewers: Robert Eppinger and Greg Lee

Summary of Results of the Mineral Resource Assessment of the Bethel and Southeastern Part of the Russian Mission 1° by 3° Quadrangles, Alaska

By Thomas P. Frost, Stephen E. Box, and Elizabeth J. Moll-Stalcup

Abstract

A synthesis of geologic, geochemical, and geophysical data from the Bethel and southern part of the Russian Mission quadrangles in southwestern Alaska were used to estimate the mineral potential of the region. In the map area, the potential for undiscovered gold placer deposits is high, the potential for epithermal mercury and polymetallic vein deposits is moderate, and the potential for other metallic mineral resources is low.

Five tracts, distinguished on the basis of their basement geology, are identified as favorable for the discovery of gold placers in the eastern half of the Bethel 1:250,000 map area. The most important geologic criterion for the delineation of the gold placer tracts is the presence of granitoid plutons. Tracts favorable for epithermal mercury or simple antimony deposits have either shallow granitoid plutons or rhyolitic volcanic rocks present in them. Tracts favorable for silica-carbonate mercury deposits contain altered serpentinites along major terrane-bounding faults. Two types of gold-bearing polymetallic quartz veins are recognized in the map area: one contains significant base metals along with gold and silver; the other is lacking in base-metal enrichments. Both gold-bearing vein subtypes are associated with granitoid plutons or rhyolitic dikes and domes. Tourmaline-quartz replacement of volcanic rocks is locally present in the map area; the replacement zones are variably enriched in Au, Ag, base metals, Sn, and W. Quartz veins with anomalous Sn and W are also present near some granitoid plutons.

INTRODUCTION

The Bethel region has been an important placer gold-producing region in southwestern Alaska; over 250,000 oz of gold have been produced through 1989 (Bundtzen and others, 1989). The potential for undiscovered placer gold remains high in streams that drain areas underlain by granitoid plutons and their wall rocks. No other metallic minerals have been produced from the region, although

there is low to moderate potential for epithermal mercury and polymetallic veins containing gold.

A geological mapping program and reconnaissance geochemical survey were conducted as part of the Alaska Mineral Resource Assessment Program (AMRAP) during 1987–89 in the Bethel and southeastern part of the Russian Mission 1° by 3° quadrangles (referred to hereafter as the Bethel map area or simply map area) of southwest Alaska. The western half of the Bethel map area is underlain by unconsolidated Quaternary deposits of glacial, fluvial, lacustrine, and eolian origin; this area is not considered in this report. This report is a summary of the complete mineral resource assessment, which will appear as a separate U.S. Geological Survey Bulletin.

Products to date from the Bethel AMRAP include a geologic map (Box and others, in press); gravity and aeromagnetic maps (Phillips and Morin, 1992); studies of prospects and mineral occurrences (Frost, 1990; Gray and others, 1990; Goldfarb and others, 1990; Frost and Box, 1991a, b); isotopic, petrographic, and geochemical studies (Frost and others, 1988, 1992a, b; Moll-Stalcup and others, 1989; Box and others, 1990, in press; Moll-Stalcup and Box, 1992; Roeske and Box, 1992); geochemical sampling of mines, prospects, and altered and unaltered bedrock (Frost and others, 1992a); stream-sediment and heavy-mineral-concentrate data (Bradley and Frost, in press); and tectonic, sedimentologic, and fossil studies (Box and Murphy, 1987; Box and Elder, 1992; Elder and Box, 1992; Box, 1992).

GEOLOGIC SUMMARY

Pre-Late Cretaceous Tectonostratigraphic Terranes

The Bethel map area (fig.1) is underlain by five accreted tectonostratigraphic terranes, separated from

one another by major faults (Jones and others, 1987), although many boundaries are covered by sedimentary rocks of the Upper Cretaceous Kuskokwim Group (Box and others, in press). The terranes, from east to west, are briefly described below.

A structurally complex assemblage of Paleozoic and Mesozoic chert and Devonian to Triassic limestone, basalt, and clastic rocks form the Tikchik terrane (Mertie, 1938; Hoare and Coonrad, 1959a; 1978; Box and others, in press). The right-lateral Togiak fault marks the boundary between the Tikchik terrane and the Togiak terrane to the west (Box and Murphy, 1987; Box and others, in press).

Rocks of the Togiak terrane (fig. 1) are complexly deformed andesitic arc volcanic and volcanoclastic rocks of Late Triassic through Early Cretaceous age (Box and others, in press). The boundary between the rocks of the Togiak terrane and the Goodnews terrane to the west is covered by sedimentary rocks of the Upper Cretaceous Kuskokwim Group (Box and others, in press).

The Goodnews terrane is exposed in erosional windows through the unconformably overlying Upper Cretaceous Kuskokwim Group (fig. 1). The Goodnews terrane is a structurally complex assemblage of variably foliated metabasalt, low-grade schist, marble, chert, graywacke, and slate (Hoare and Coonrad, 1959a, 1978; Box and Murphy, 1987). Fossils are Ordovician to Early Cretaceous in age (Hoare and Coonrad, 1978; Box and others, in press).

Proterozoic orthogneiss, amphibolite, and quartz-mica schist of the Kilbuck terrane crop out in a narrow tectonic sliver east of the Golden Gate fault (fig. 1) (Box and others, 1990). The Kilbuck terrane is unconformably overlain by conglomerates of the Upper Cretaceous Kuskokwim Group that contain clasts derived in part from rocks of the Kilbuck terrane (Box and Murphy, 1987).

Middle and Upper Jurassic andesitic volcanic rocks and volcanoclastic sandstones of the Nyac terrane (Box and Murphy, 1987) are the westernmost basement rocks exposed in the Bethel map area. The contact between the Nyac terrane and other pre-Late Cretaceous terranes is not exposed. The contact with the Upper Cretaceous Kuskokwim Group to the east is marked by the Sawpit fault (fig. 1) or its equivalent in the southern part of the Bethel map area (Hoare and Coonrad, 1959a, b; Box and others, in press). Late Cretaceous and (or) early Tertiary volcanic and plutonic rocks appear to overlap and intrude, respectively, the Sawpit fault (Box and others, in press).

Cretaceous Sedimentary Rocks

The Upper Cretaceous Kuskokwim Group (fig. 1) consists of a thick sequence of shale, siltstone, sandstone, and basal conglomerate that was deposited unconformably on all older rocks except those of the Nyac terrane (Hoare and Coonrad, 1959a, b, 1978; Box

and Murphy, 1987; Elder and Box, 1992; Box, 1992). The Kuskokwim Group is composed predominantly of marine turbidites in most of the map area, and of shallow marine and nonmarine conglomerates and sandstones in the southwestern part of the map area (Box, 1992; Box and others, in press).

Cretaceous and Early Tertiary Plutonic and Volcanic Rocks

Early Cretaceous (120–102 Ma) granitoid plutons are restricted to the Nyac terrane west of the Sawpit fault (fig. 1); granitoid plutons and volcanic fields that intrude or overlie other terranes and the Kuskokwim Group are Late Cretaceous to Tertiary (72–55 Ma) in age (Shew and Wilson, 1981; Robinson and Decker, 1986; Frost and others, 1988, 1992b; Box and others, in press). Hornblende-biotite granodiorite through granite is most common, although augite-biotite quartz monzodiorite, quartz diorite, diorite, and gabbro also are present (Robinson and Decker, 1986; Frost and others, 1988; Box and others, in press). The rocks are porphyritic or coarse grained; many contain miarolytic cavities. Most plutons are surrounded by a biotite-cordierite-bearing hornfels zone. Textures and hornfels mineralogy suggest emplacement depths of less than 2 km to subvolcanic levels.

Late Cretaceous to early Tertiary volcanic rocks crop out in several geographically distinct calc-alkalic volcanic fields (fig. 1). These rocks consist mainly of bedded andesitic to dacitic flows and tuffs, minor basaltic flows, volcanoclastic sedimentary rocks, and scattered felsic domes (Hoare and Coonrad, 1959a; Box and others, in press). The domes are composed of biotite rhyolite and dacite that contain partially resorbed quartz phenocrysts. Intermediate to felsic dikes cut all older rock types.

Mildly alkalic Eocene basalt and andesite flows and tuffs, as well as rhyolite tuffs and domes, crop out in the Nukluk volcanic field (Moll-Stalcup and others, 1992), overlapping the Sawpit fault in the western part of the map area (fig. 1)

Quaternary Deposits

The western third of the Bethel quadrangle is covered by thick loess, lacustrine, outwash, and moraine deposits. All known placers in the quadrangle are localized in alluvial deposits of active rivers or streams, where they are incised in bedrock, or in terrace gravels within a few tens of meters above the present channels. Glaciation in the eastern half of the quadrangle has been of both mountain and valley type, and for the most part it appears to have disrupted preexisting placers (Hoare and Coonrad, 1959a; Hoare and Cobb, 1977).

GEOCHEMICAL STUDIES

A total of 1,486 stream-sediment, 1,104 heavy-mineral-concentrate samples from first- and second-order streams, and 1,773 rock samples were collected and analyzed (Bradley and Frost, 1992; Frost and others, 1992a). These sample media provide a representative

composite of the transported material of a stream or drainage basin; the composition of the samples ideally represents the bedrock exposed in the drainage basin. Both unaltered and altered rock samples were collected to identify background chemical signatures of the various geologic units and to identify element suites associated with mineralization processes.

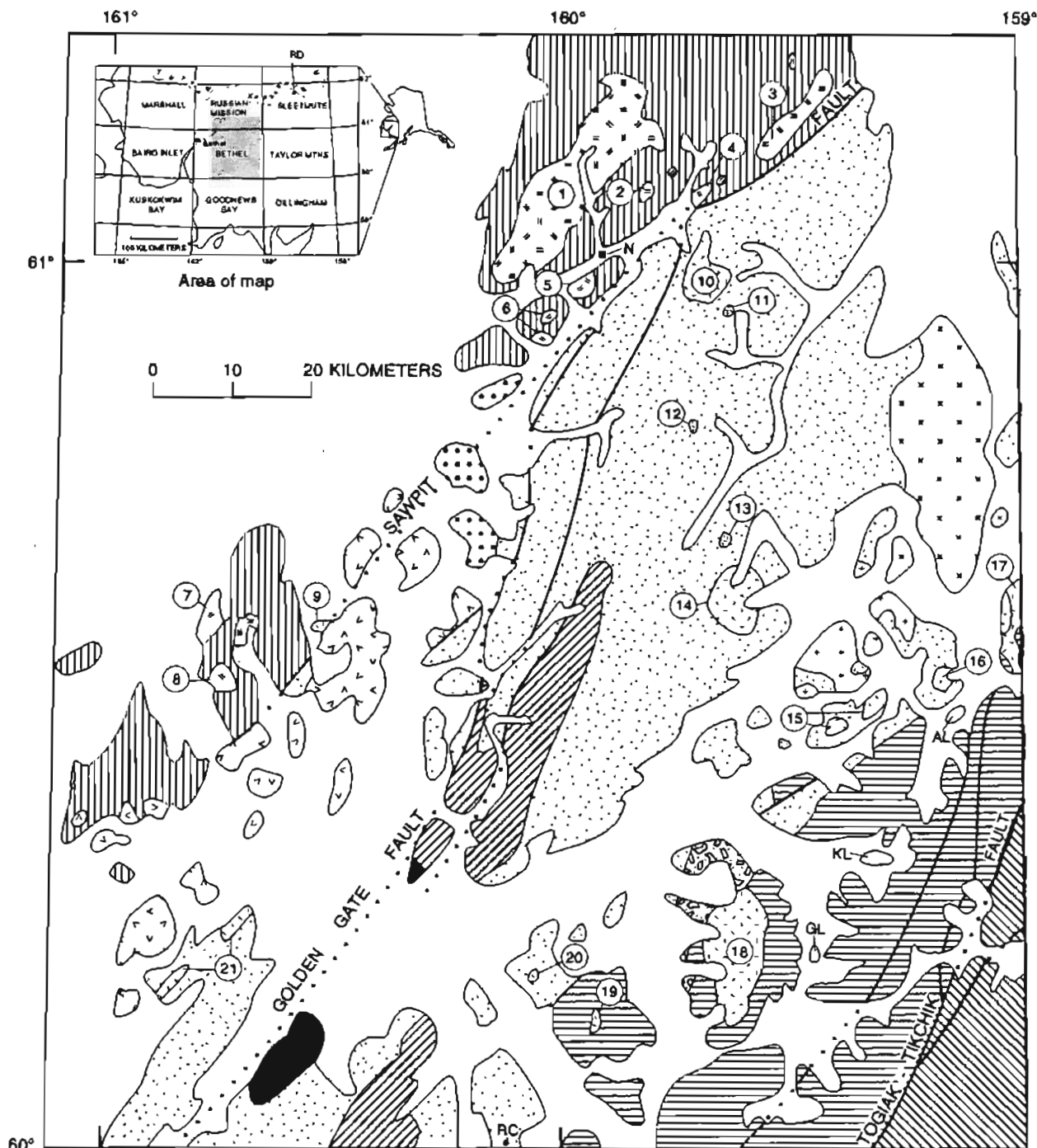


Figure 1. Simplified geologic map of Bethel area. Geographic names as used in this report are indicated. Shaded area in inset shows area of this and subsequent figures. Adapted from Frost and others (1988), Frost (1990), and Box and others (in press). Pluton descriptions in tables 1-3.

MINERAL RESOURCES OF THE BETHEL MAP AREA

This mineral resource assessment follows in principle the protocols developed by the U.S. Geological Survey in assigning to geographic tracts varying degrees of certainty of discovery of mineral resources with geologic and geochemical similarities to known mineral deposits (for example, Cox and Singer, 1986). A mineral occurrence is defined as a "concentration of a mineral *** that is considered valuable by someone somewhere, or that is of scientific or technical interest" (John and others, in press). A mineral deposit is a "mineral occurrence of sufficient size and grade that it might, under the

most favorable circumstances, be considered to have economic potential" (John and others, in press). Permissive tracts are areas in which the geologic, geochemical, and geophysical evidence does not eliminate the possibility of occurrence of a given mineral deposit type. Favorable tracts are areas in which there is positive indication that mineral deposits may be found. For example, presence of known occurrences, presence of plutons known to be associated with a given deposit type, or presence of an appropriate suite of anomalous elements in geochemical data are positive indicators that mineralization processes have occurred in a tract. In the interest of brevity, only favorable tracts for most deposit types are discussed in the following sections.

EXPLANATION

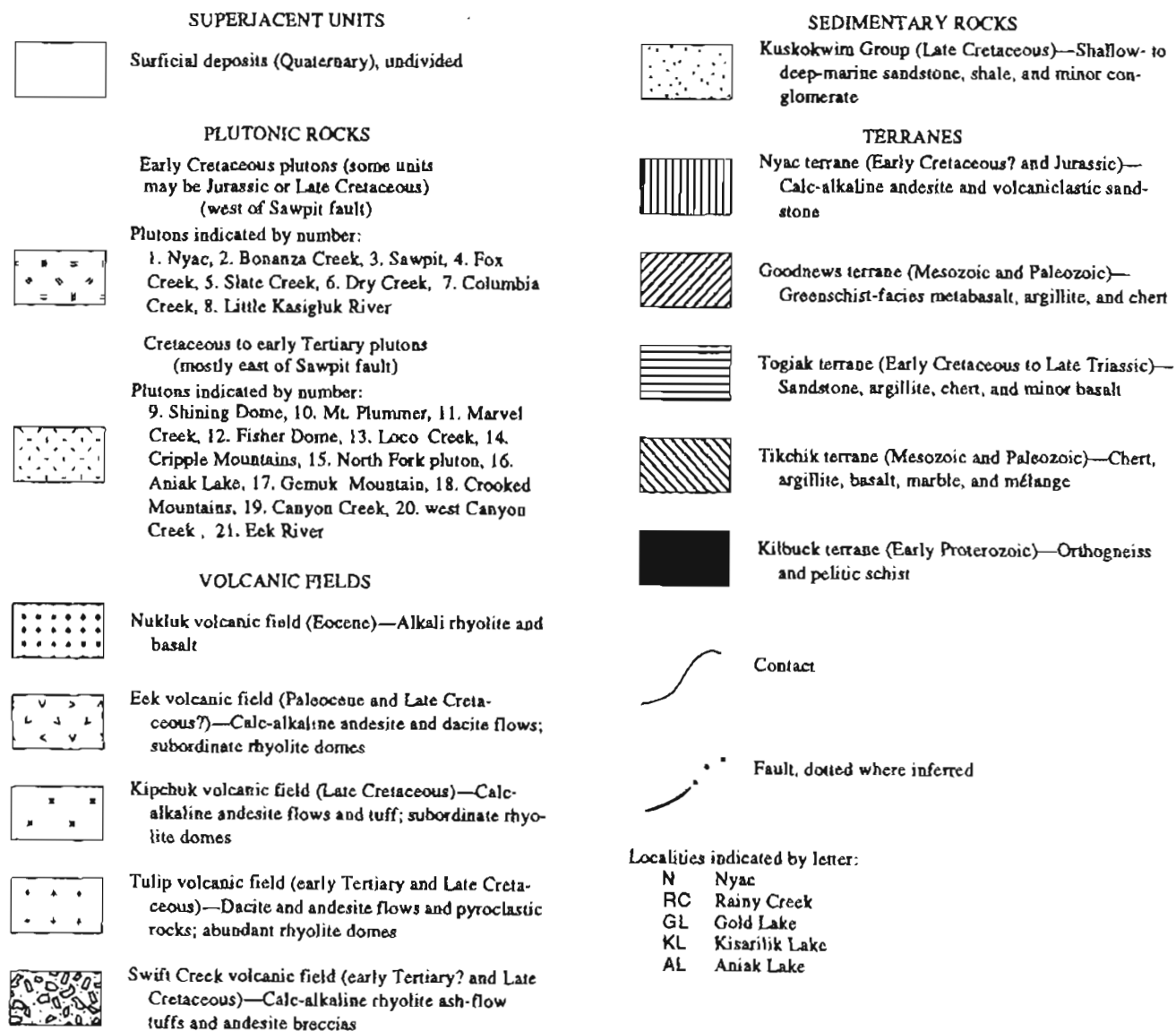


Figure 1. Continued.

Gold Placers

The Bethel region has produced over 250,000 oz of placer gold (Bundtzen and others, 1989), mostly from streams draining areas underlain by granitoid plutons. Placer gold remains the commodity with the greatest potential for undiscovered deposits. Most placer occurrences that have had production were discovered before 1930 (Hoare and Cobb, 1977). Known occurrences and mines are discussed for each favorable tract below.

Favorable Tracts

Five geologically or geochemically distinct tracts are favorable for undiscovered gold placers (fig. 2). Known gold placers, and most stream sediment or heavy-mineral-concentrate samples that contain gold, are in streams that drain areas underlain by granitoid plutons and their hornfelsed wall rocks. Gold-bearing quartz veins associated with the plutons (discussed below) appear to be a significant source of gold in the favorable tracts. A summary of the criteria for the tracts is shown in table 1.

Tract P1 (fig. 2, table 1) consists of two geologically similar areas, separated by thick unconsolidated deposits. The tract is underlain by Jurassic to Early Cretaceous island arc volcanic and volcanoclastic rocks of the Nyac terrane, which are cut by 102- to 120-Ma granitoid plutons (Box and others, in press). Gold-bearing quartz veins locally are present in the tract (see later discussion). Placers in the tract, mostly along the Tuluksak River and its tributaries (fig. 2), have yielded at least 250,000 oz of gold through 1989 (Bundtzen and others, 1989). Twenty-three percent of heavy-mineral-concentrate samples in the tract contain gold; such samples are mostly in and near the Tuluksak River or its tributaries, or in the southern subarea near Columbia Creek (fig. 2). Tract P1 is considered to have high potential for undiscovered gold placers.

Tract P2 (fig. 2, table 1) consists of two subareas, separated by unconsolidated Quaternary deposits. The tract has several placers with recorded production, including Marvel, Eureka, Cripple, and Rainy Creeks, and the Salmon River (Hoare and Cobb, 1977). The tract is underlain by sandstones and shales of the Upper Cretaceous Kuskokwim Group; Late Cretaceous and early Tertiary felsic granitic plutonic and hypabyssal felsic rocks intrude the Kuskokwim Group at Mt. Plummer, Fisher Dome, and the Cripple Mountains (figs. 1, 2). Gold-bearing quartz veins are present cutting the Mt. Plummer pluton and in quartz-stibnite veins cutting the biotite granite porphyry of Fisher Dome (figs. 1, 2) (Frost, 1990). Gold content in stream sediment and heavy-mineral-concentrate samples (Bradley and Frost, in press) correlates with presence or absence of plutons in well-integrated drainages. Tract P2

is considered to have high potential for undiscovered gold placers.

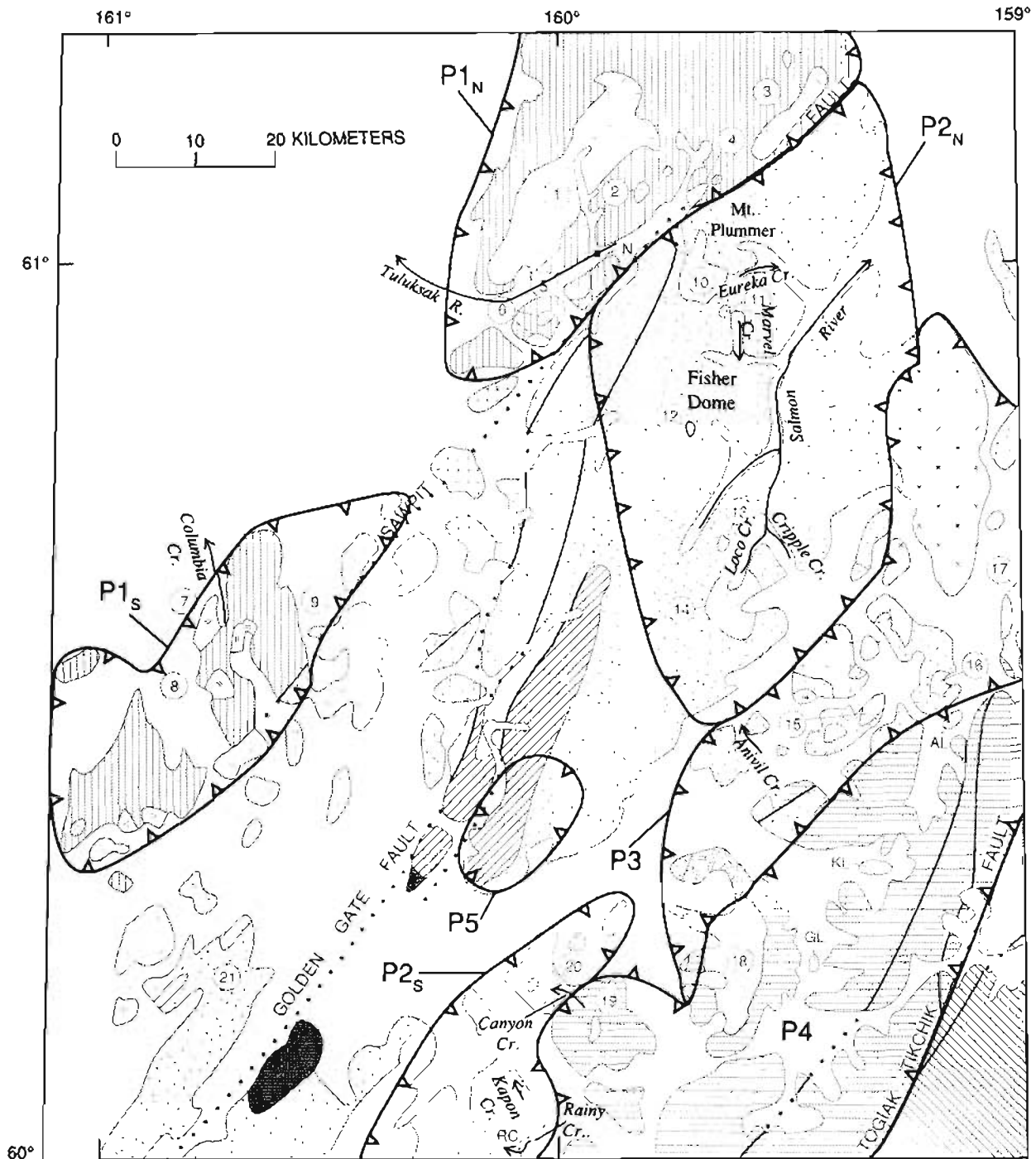
Tract P3 (fig. 2, table 1) is similar to tract P2 except that it contains volcanic fields of Late Cretaceous to early Tertiary age in addition to sedimentary rocks of the Kuskokwim Group and felsic to intermediate plutonic rocks (Box and others, in press). Quartz-vein samples (see following section) contain as much as 0.3 ppm Au (Frost, 1990). Twenty percent of heavy-mineral-concentrate samples contain at least 0.5 ppm Au (Bradley and Frost, in press). Owing to the lack of generally well-integrated drainages, and to the presence of extensive glacial outwash and moraine deposits in much of the area, we infer that tract P3 has a low potential for undiscovered gold placers.

Tract P4 (fig. 2, table 1) contains the placer mine at Canyon Creek and several prospects. The tract is underlain by Upper Triassic to Lower Cretaceous marine volcanoclastic rocks of the Togiak terrane (Box and others, in press). Late Cretaceous granodiorite and granite plutons are present, as well as subordinate augite-biotite quartz diorite through augite gabbro intrusions (Frost and others, 1988). Quartz veins associated with pyritiferous rhyolite dike complexes contain variable amounts of Ag, Au, Pb, and Zn (Frost, 1990). Gold is present in stream-sediment and heavy-mineral-concentrate samples, especially in unglaciated valleys near the Canyon Creek pluton (figs. 1, 2), and in 25 percent of heavy-mineral-concentrate samples in the northern half of the tract (Bradley and Frost, in press). Pleistocene mountain and valley glaciation modified most valleys in the high country underlain by most of tract P4. Largely owing to the effects of glaciation, the potential for placers is regarded as low.

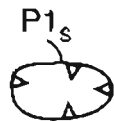
Tract P5 (fig. 2, table 1) is underlain by sandstones, slates, and greenschist-facies metachert and phyllite of Paleozoic to Mesozoic age of the Goodnews terrane, unconformably overlain by basal conglomerates and shales of the Upper Cretaceous Kuskokwim Group (Box and others, in press). Gold is present in several heavy-mineral-concentrate samples in the area, as are scattered anomalous concentrations of Ag, Hg, Sn, Pb, and Zn (Bradley and Frost, in press). The narrow canyons and low amount of alluvium in most canyons suggest a low probability of placer deposits in tract P5.

Silica-Carbonate Mercury

Mercury deposits fitting the silica-carbonate model of Cox and Singer (1986) are localized in altered serpentinites and sedimentary rocks in and near major faults in accreted terranes. Cinnabar and native mercury, along with minor base-metal sulfides, are common ore mineral assemblages which are present along with quartz and carbonate. No serpentinite-hosted mercury deposits fitting the silica-carbonate model of Cox and Singer



EXPLANATION



Favorable tracts for gold placer deposits

Figure 2. Simplified map showing favorable tracts for gold placer deposits. Favorable tracts are as indicated in table 1 and discussed in text. Tracts P1 and P2 each have northern (N) and southern (S) subarea; for each tract, it is probable that geologic units that define subareas are continuous under intervening Quaternary cover. Geologic units as in figure 1.

Table 1. Summary of favorable tracts for placer gold

[Tracts and localities shown on figures 1 and 2. See text for discussion]

Tract	Area	Host rock types	Terrane	Criteria	Mines and prospects	Magmatism	Composition	Age (Ma)	References
P1	Nyac	volcanic-arc andesites, volcaniclastic sandstones	Nyac	1,2,3,5,6,7,8,9	Nyac district Columbia Ck. area	Nyac p. Sawpit p. Bonanza Ck. p. Fox Creek p. Slate Creek p. Dry Creek p. Nukluk v.f. Columbia Ck. p. Kasigluk p. Shining Dome p.	hbl-bio gr, grd bio gr bio-hbl qtz mzd, grd gr, gab, dio bio-hbl grd, qtz mzd rhy. porphyry basalt-rhy. hbl-bio grd, qtz mzd cpx gab, dio cpx-bio qtz dio.	102-120 (K-Ar) Early Cretaceous(?) Early Cretaceous(?) Early Cretaceous(?) Early Cretaceous(?) Jurassic to Tertiary 55 (Ar-Ar) 115 (K-Ar bio) Early Cretaceous(?) Late Cret. to early Tert.	1,2,3,4,5,6,7
P2	Kuskokwim Mtns. Salmon River	sandstone and shale	Kuskokwim Group	1,2,4,5,6,7,8	Marvel, Eureka, Cripple, Fisher, Rainy Cks., Salmon R.	Mt. Pfumner p. Marvel Creek p. Fisher Dome p. Loco Creek p. Cripple Mtns p. W. Canyon Ck. p.	bio-hbl grd, qtz mzd bio gr porphyry bio gr bio gr porphyry bio grd, gr bio grd, mzd	65-67 (K-Ar) Late Cret. to early Tert. Late Cret. to early Tert. Late Cret. to early Tert. 62 (K-Ar) Late Cretaceous(?)	1,2,3,4,5,6,7
P3	Tulip-Kipchuk	volcanic flows and domes sandstone and shale	Tulip-Kipchuk v.f. Kuskokwim Group	1,2,4,5,6,7,8	Anvil Ck.	North Fork p. Aniak Lake p. Crooked Mtns p. Kipchuk v.f. Tulip v.f.	cpx qtz dio, bio grd, bio gr hb-bio grd, bio gr and, dac and, rhy	64 (Ar-Ar) 61 (Ar-Ar) 70 (Ar-Ar) 70 (Ar-Ar) Late Cret. to early Tert.	1,2,3,4,5,6,7
P4	Togiak	marine clastic rocks, chert, and basalt	Togiak	1,2,5,7,8,9	Canyon, Kapon Cks.	Canyon Creek p. Crooked Mtns p. Swift Creek v.f.	cpx-bio qtz dio, grd hb-bio grd, bio gr and, rhy	70 (Ar-Ar) 70 (Ar-Ar) 74 (Ar-Ar)	1,2,3,4,5,6,7
P5	Kuskokwim Mtns. Kisarilik River	sandstone and shale	Kuskokwim Group	7,8	dikes	intermediate	Late Cret. to early Tert.	3, 4	

Criteria: 1, known deposits; 2, known prospects; 3, Early Cretaceous granites; 4, Late Cretaceous granites; 5, hydrothermally altered rock; 6, gravity low; 7, gold in pan-concentrate samples; 8, gold in stream-sediment samples; 9, gold in quartz veins in bedrock.

Abbreviations used: bio, biotite; hbl, hornblende; cpx, clinopyroxene; qtz, quartz; gr, granite; grd, granodiorite; mzd, monzodiorite; dio, diorite; gab, gabbro; and, andesite; dac, dacite; rhy, rhyolite; p., pluton; v.f., volcanic field.

References: 1, Frost (1990); 2, Box and others (in press); 3, Frost and others (1988); 4, Bradley and Frost (1992); 5, R. Tripp, U.S. Geological Survey, written commun. (1988-89); 6, Phillips and Morin (1992); 7, Hoare and Cobb (1977).

(1986) have been identified in southwestern Alaska to date.

In the Bethel map area, a favorable tract for silica-carbonate Hg is present along the northern part of the Sawpit and Golden Gate faults (S-C on fig. 3). Present along the presumed trace of the faults are scattered unvegetated, reddish-orange- to black-weathering areas as large as 1 km². The areas are composed of frost-heaved blocks of silica-carbonate rock, gabbro, serpentinite, and peridotite, apparently in a scaly serpentinite-mélange matrix. In silica-carbonate rock, protolith assemblages were replaced by serpentine-group minerals, followed by partial to complete replacement by quartz, calcite, and (or) iron-rich carbonate, followed by brecciation and quartz veining (Frost, 1990).

Altered silica-carbonate rock samples from the tract (S-C, fig. 3) contain as much as 1 ppm Ag, 450 ppm As, 2,000 ppm Cr, 1,500 ppm Ni, 1,000 ppm Zn, and 41 ppm Sb (Frost, 1990; Frost and others, 1992a). Mercury content in these samples averages 4 ppm, but the Hg content of several samples exceeds the detection limit of 36 ppm (Frost and others, 1992a). The tract has moderate potential for silica-carbonate mercury deposits.

Epithermal Mercury

Southwestern Alaska epithermal mercury deposits are believed to form in shallow (<1 km) hydrothermal systems (Miller and others, 1989; Frost, 1990; Goldfarb and others, 1990) related to Late Cretaceous to early Tertiary magmatism (Gray and others, 1992). Such deposits contain cinnabar, pyrite, and native mercury, with or without arsenic and antimony sulfides, in quartz veins and disseminations in altered host rocks. The alteration and sulfide mineral assemblages in southwestern Alaska epithermal mercury deposits are similar to those of the silica-carbonate mercury deposit model of Cox and Singer (1986), although serpentinites are not associated with Alaskan examples. The Red Devil deposit in the Sleetmute quadrangle (fig. 1) is the largest of such deposits in Alaska, having shipped about 32,000 flasks of mercury (Miller and others, 1989). No other deposits in southwestern Alaska have shipped more than a few hundred flasks (Sainsbury and MacKevett, 1965). Criteria for the delineation of favorable tracts are summarized in table 2.

Known Occurrences

The Rainy Creek prospect (fig. 3), hosted in shales and sandstones of the Upper Cretaceous Kuskokwim Group, is the only mercury lode in the map area (Rutledge, 1948; Sainsbury and MacKevett, 1965; Berg and Cobb, 1967; Frost, 1990; Goldfarb and others, 1990). There has been no production, although 2,000 lb of cinnabar were concentrated from the gold placer

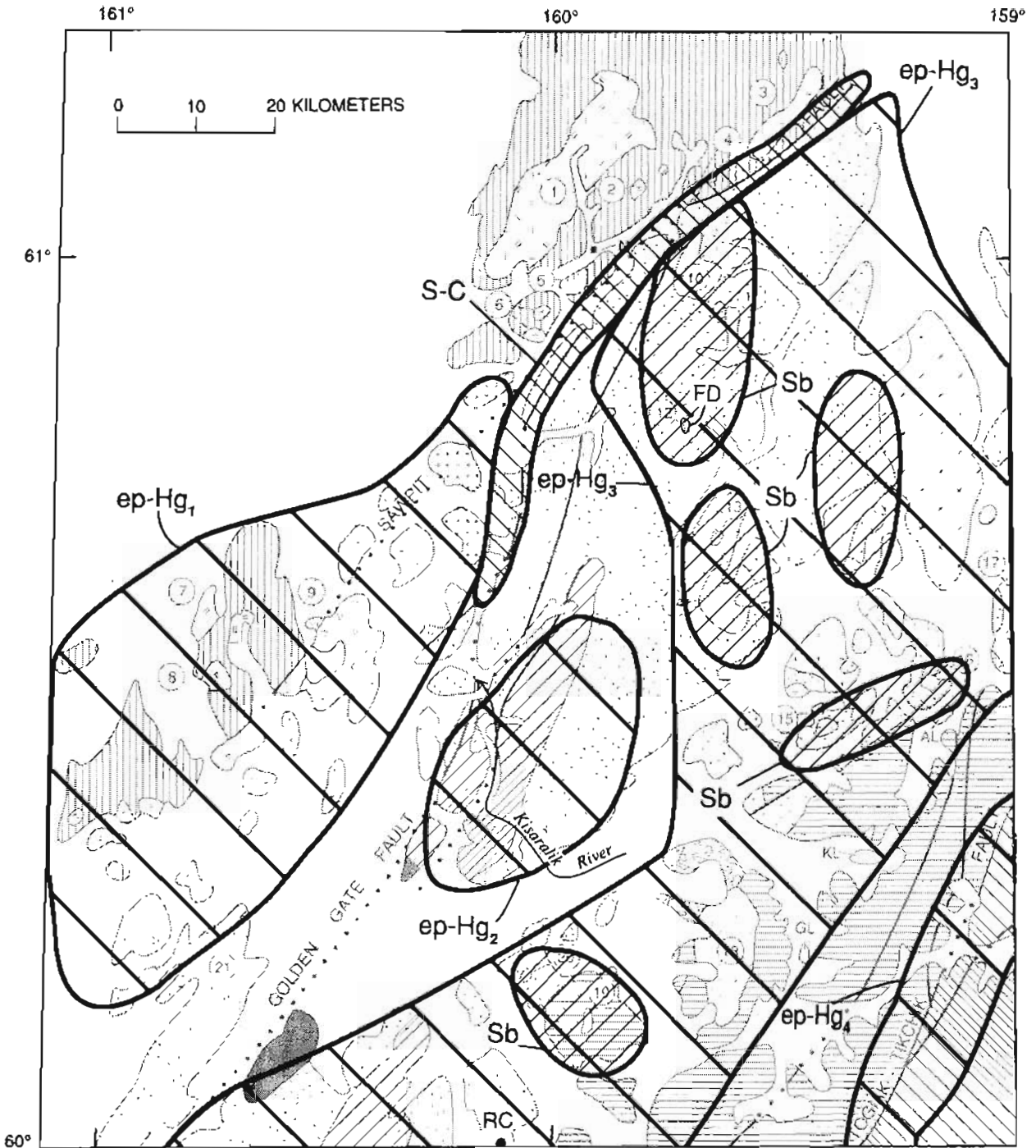
downstream (Sainsbury and MacKevett, 1965). Two distinct textural types of mercury-bearing quartz veins are present: dilational quartz veins as wide as 10 cm that contain minor cinnabar and stibnite, and anastomosing realgar- and orpiment-rich veins (as much as 75 percent sulfides) and stockworks with minor cinnabar (Frost, 1990). Gold is present at levels as high as 0.05 ppm in the As-Sb-dominated veins (Frost, 1990; Gray and others, 1990).

Favorable Tracts


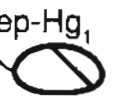

Tract ep-Hg₁ (table 2, fig. 3) is defined by Late Cretaceous to early Tertiary felsic domes and flows and granitoid plutons, which unconformably overlie and intrude, respectively, marine sedimentary rocks of the Kuskokwim Group and Jurassic andesitic arc volcanic rocks of the Nyac terrane (Box and others, in press). Samples of silicic to intermediate volcanic rocks, sedimentary rocks of the Kuskokwim Group, and quartz veins contain as much as 2 ppm Hg (Frost and others, 1992a). Stream sediment samples contain as much as 7 ppm Hg (Bradley and Frost, in press). Tract ep-Hg₁ is considered to have moderate potential for epithermal mercury deposits.

Tract ep-Hg₂ (table 2, fig. 3) has a low potential for undiscovered epithermal mercury deposits. The tract consists of greenschist- to blueschist-facies rocks of the Goodnews terrane. Lithologies include variably deformed metabasalt, metachert, marble, and phyllitic rocks of Paleozoic and Mesozoic age. Unconformably overlying the rocks of the Goodnews terrane are basal conglomerates of the Upper Cretaceous Kuskokwim Group, which grade upward in a few hundred meters to deep-water, fine-grained sandstones and shales. Altered andesite and dacite dikes are common in the Kuskokwim Group in the tract; in most dikes, plagioclase and mafic minerals are replaced by chlorite, calcite, and quartz. There is little in the lithologies or rock geochemical data (Box and others, in press; Frost and others, 1992a) in the tract to suggest the presence of epithermal mercury deposits, but cinnabar is present in some heavy-mineral-concentrate samples (R.B. Tripp, U.S. Geological Survey, written commun.), and mercury was detected at levels as high as 1.5 ppm in stream-sediment samples (Bradley and Frost, in press).

Tract ep-Hg₃ (table 2, fig. 3) has high potential for epithermal Hg deposits. It contains the occurrence at Rainy Creek (Sainsbury and MacKevett, 1965; Frost, 1990) and has many of the structural, stratigraphic, and volcano-plutonic associations of other Alaskan Hg deposits, including Red Devil in the Sleetmute quadrangle (fig. 1) and Cinnabar Creek in the Taylor Mountains quadrangle (Sainsbury and MacKevett, 1965; Miller and others, 1989; Frost, 1990; Goldfarb and others, 1990).



EXPLANATION

- 
S-C
Favorable tracts for silica-carbonate mercury deposits
- 
ep-Hg₁
Favorable tracts for epithermal mercury deposits
- 
Sb
Favorable tracts for simple antimony deposits

The southwestern part of tract ep-Hg₃ consists of argillaceous mélange with blocks of limestone, basalt, and chert of Paleozoic to Mesozoic age, overlain by Lower Cretaceous turbidites of the Goodnews terrane (fig. 3) (Box and others, in press). Upper Jurassic to Lower Cretaceous tuffaceous cherts and argillites and Lower Cretaceous volcanoclastic rocks of the Togiak terrane make up the eastern part of the tract (Box and others, in press). All of these rocks are unconformably overlain by the Upper Cretaceous Kuskokwim Group, which in this area is composed mostly of conglomerates, sandstones, and shales of turbidite origin (Box and others, in press).

Late Cretaceous to early Tertiary felsic to intermediate plutons and batholiths intrude the older terranes and the Kuskokwim Group (Frost and others, 1988; Frost, 1990; Box and others, in press) in tract ep-Hg₃ (fig. 3). Late Cretaceous to early Tertiary andesite and dacite flows and tuffs, as well as rhyolite domes, flows, and ash flows (Box and others, in press), locally overlie all older rocks. Tract ep-Hg₃ does not extend as far west as do the westernmost outcrops of the Kuskokwim Group or as far east as do the easternmost parts of the Togiak terrane; the geochemical anomalies, which, in part, define the tract, appear to be associated with the magmatic-hydrothermal systems of the plutonic and volcanic rocks rather than the underlying rocks.

Anomalous concentrations of Hg, As, Sb, and, to a lesser extent, Au, Ag, Pb, and Zn are present in samples from tract ep-Hg₃ (Bradley and Frost, 1992; Frost and others, 1992a). Liesegang-banded rhyolite samples from rhyolite domes in the Tulip volcanic field in tract ep-Hg₃ (fig. 3) contain as much as 15 ppm Hg, 140 ppm As, and 0.30 ppm Au (Frost, 1990). Mercury content is greater than 5 ppm in 17 stream-sediment samples (6 percent of samples) and is greater than 36 ppm in 9 samples (Bradley and Frost, in press). Cinnabar is present in 35 percent of heavy-mineral-concentrate samples (R.B. Tripp, U.S. Geological Survey, written commun.). Stream-sediment samples contain as much as 690 ppm As (Bradley and Frost, in press); corresponding heavy-mineral-concentrate samples contain arsenopyrite. Stream-sediment samples contain as much as 20 ppm Sb (Bradley and Frost, in press); most of the Sb is in stibnite. Polymetallic quartz veins (see later section) are also present in the tract. Tract ep-Hg₃ has high potential for epithermal Hg deposits.

Tract ep-Hg₄ straddles the Togiak fault (fig. 3, table 2). Mercury is present in some stream-sediment samples,

←

Figure 3. Simplified map showing favorable tracts for silica-carbonate mercury, epithermal mercury deposits, and simple antimony deposits. Criteria for epithermal mercury deposit tracts summarized in table 2. Fisher Dome and Rainy Creek localities shown by FD and RC, respectively. Geologic units as in figure 1.

and cinnabar is present in heavy-mineral-concentrate samples (Bradley and Frost, in press). Samples of brecciated argillite along the trace of the Togiak fault, of argillite east of the fault, and of a diabase contain 0.25 to 4.0 ppm Hg and as much as 720 ppm As and 18 ppm Sb (Frost and others, 1992a). The tract has low potential for epithermal mercury deposits.

Simple Antimony Veins

Simple antimony veins (Cox and Singer model 27d) are present in orogenic areas and are characterized by quartz and stibnite veins or disseminations associated with pyrite, base-metal sulfides, cinnabar, silver, gold, or scheelite. A single occurrence that fits the simple Sb model is present in the Bethel map area, where a quartz-stibnite vein cuts the biotite quartz porphyry of Fisher Dome (figs. 1, 3). Massive and bladed stibnite as long as 7 cm comprises 5 to 50 percent of the vein; the remainder is composed of vuggy quartz. Samples of the vein contain as much as 1.0 ppm Au, 7.0 ppm Ag, and 1,500 ppm As; Hg content is less than 5 ppm (Frost, 1990).

Favorable Tracts

Five tracts are delineated as favorable for simple Sb veins in the Bethel region (Sb on fig. 3). Indicators of mineralization in the tracts include presence of felsic plutons, anomalous contents of certain elements in heavy-mineral-concentrate samples (15,000 ppm Sb, >5,000 ppm As, 700 ppm Ag, and 10,000 ppm W in concentrate samples; Bradley and Frost, 1992), and gold, stibnite, arsenopyrite, and scheelite in heavy-mineral-concentrate samples (R.B. Tripp, U.S. Geological Survey, written commun., 1989). Quartz vein and host rock samples from a biotite granite porphyry at Loco Creek (13 on fig. 1) contain as much as 90 ppm Sb and 200 ppm As (Frost and others, 1992a). The probability of occurrence of simple Sb deposits is low.

Polymetallic Veins

In the Bethel map area, two types of polymetallic veins are present: a gold-silver quartz vein type without elevated base metals, and a gold-silver base-metal type. The base-metal-rich veins are referred to as the Gold Lake type after the prospect discovered in 1987 near Gold Lake (figs. 1, 4) (Frost, 1990); known occurrences are present in rocks of pre-Late Cretaceous terranes that are overlain by sedimentary rocks of the Kuskokwim Group. Gold Lake type vein systems may crop out over areas as large as several square kilometers. The type lacking elevated base metals crops out over areas less

Table 2. Favorable tracts for epithermal mercury deposits

[Tracts and localities shown on figures 1 and 3. See text for discussion]

Tract	Area	Host rock types	Terrane	Criteria	Mines and prospects	Magmatism	Composition	Age (Ma)	References
ep-Hg ₁	Western volcanic	rhyolite to dacite domes and flows shale and sandstone andesitic arc volcanic rocks	Eek and Nukluk v.f. Kuskokwim Group Nyac	2,3,4,5	none	Eek v.f. Nukluk v.f. Columbia Ck. p. Kasigluk R. p.	Andesite, dacite alkali rhy hbl-bio grd, qtz mzd cpx gab, dio	59 (K-Ar) 55 (Ar-Ar) 115 (K-Ar bio) Early Cretaceous(?)	1,2,3,4,5,6
ep-Hg ₂	Kisarilik River	metabasalt, metachert marble, phyllite conglomerate and sandstone	Goodnews Kuskokwim Group	3,4,5	none	dikes	and, dac, rhy	Late Cret. to early Tert.	1,2,4,5,6
ep-Hg ₃	Central mercury belt	argillaceous melange sandstone and shale chert, argillite, and sandstone	Goodnews Kuskokwim Group Togiak	1,2,3,4,5	Rainy Creek	Mt. Plummer p. Marvel Creek p. Fisher Dome p. North Fork p. Aniak Lake p. Crooked Mtns. p. Cripple Mtns. p. Canyon Creek p. W. Canyon Ck. p. Kipchuk v.f. Tulip v.f. dikes	bio-hbl grd bio gr. porphyry bio gr cpx dio, bio grd bio gr hb-bio grd, bio gr bio grd cpx-bio qtz dio, grd grd, mzd and, dac and, rhy and, dac, rhy	65-67 (K-Ar) Late Cret. to early Tert. Late Cret. to early Tert. 64 (Ar-Ar) 61 (Ar-Ar) 70 (Ar-Ar) 62 (K-Ar) 70 (Ar-Ar) Late Cretaceous(?) 70 (Ar-Ar) Late Cret. to early Tert. Late Cret. to early Tert.	1,2,3,4,5,6,7
ep-Hg ₄	Togiak fault	Togiak fault zone	Togiak-Tikchik boundary	3,4,5	none	dikes	hbl dio	Late Cretaceous(?)	2,4,5

Criteria: 1, shallow plutons; 2, volcanic rocks; 3, cinnabar in concentrate samples; 4, mercury detected in stream sediments; 5, mercury detected in bedrock.

Abbreviations used: bio, biotite; hbl, hornblende; cpx, clinopyroxene; qtz, quartz; gr, granite; grd, granodiorite; mzd, monzodiorite; dio, diorite; gab, gabbro; and, andesite; dac, dacite; rhy, rhyolite; p., pluton; v.f., volcanic field.
References: 1, Frost (1990); 2, Box and others (in press); 3, Frost and others (1988); 4, Bradley and Frost (1992); 5, R. Tripp, U.S. Geological Survey, written commun. (1988-89); 6, Phillips and Morin (1992); 7, Hoare and Cobb (1977).

than a few tens of square meters and are referred to as the simple gold subtype. Simple gold veins may be present in any bedrock type, including the Kuskokwim Group (Frost, 1990). The absolute ages of the two types are unknown, but both are spatially associated with Late Cretaceous to early Tertiary magmatic rocks. Although the favorable tracts for the polymetallic vein types are delineated separately on figure 4, a continuum between the two types is possible. The criteria for delineation of favorable tracts for polymetallic veins in the Bethel area are summarized in table 3.

Known Occurrences of Gold Lake-Type Polymetallic Veins

The veins northeast of Gold Lake and north of Kisarilik Lake (fig. 4) were first described by Frost (1990). Oxidized pyrite-bearing rhyolite dikes and sulfide-bearing quartz veins cut argillite, sandstone, and volcanic and volcanoclastic rocks of the Togiak terrane at the Gold Lake and Kisarilik Lake occurrences. Most of the dike and vein networks are exposed over areas of less than a few tens of square meters, but some larger zones extend erratically over several square kilometers. The dikes are erosionally resistant and are as wide as 3 m. The dike and vein networks have anomalous concentrations of various combinations of Ag, As, Au, Cu, Hg, Mo, Pb, Sb, and W (Frost, 1990; Frost and others, 1992a). The highest concentrations of Au, Ag, and As are in quartz veins associated with rhyolite dikes (Frost, 1990).

The altered rhyolite dikes contain partially resorbed quartz phenocrysts and pyrite cubes as large as 3 mm. The groundmass of the dikes is replaced by sericite or illite and quartz. Relict plagioclase phenocrysts are replaced by albite and sericite. Altered rhyolite samples contain as much as 7.0 ppm Ag, 3,000 ppm As, 0.23 ppm Au, 100 ppm Mo, and 100 ppm Sb (Frost, 1990).

Several generations of quartz veins with cores containing as much as 20 per cent galena cut all rock types at the Gold Lake prospect. Argillite and sandstone wall rocks and rhyolite dikes are incipiently to extensively altered to quartz, sericite, calcite, and iron-oxide minerals near quartz veins. Quartz, quartz+calcite, quartz+(chlorite), quartz+iron oxides, quartz+pyrite, and quartz+galena are common vein assemblages. Most veins are less than 2 cm wide, although some are as wide as 12 cm. Quartz forms euhedral prisms as long as 1 cm. Two generations of carbonate are present in the veins; both postdate crystallization of most of the quartz. The earliest carbonate is a brown, fine-grained aggregate that is intergrown with fine-grained quartz and galena. A later generation of coarse-grained, clear calcite fills vugs. Quartz veins contain as much as 7 ppm Ag, 7,000 ppm As, 2.0 ppm Au, 30 ppm Bi, 300 ppm Pb, 150 ppm Sb, and 70 ppm W (Frost, 1990; Frost and others, 1992a). Hydrothermal breccias composed of pale greenish-gray clays, quartz clasts, and oxide minerals have gold contents as high as 2.0 ppm (Frost, 1990).

Favorable Tracts for Gold Lake-Type Polymetallic Veins

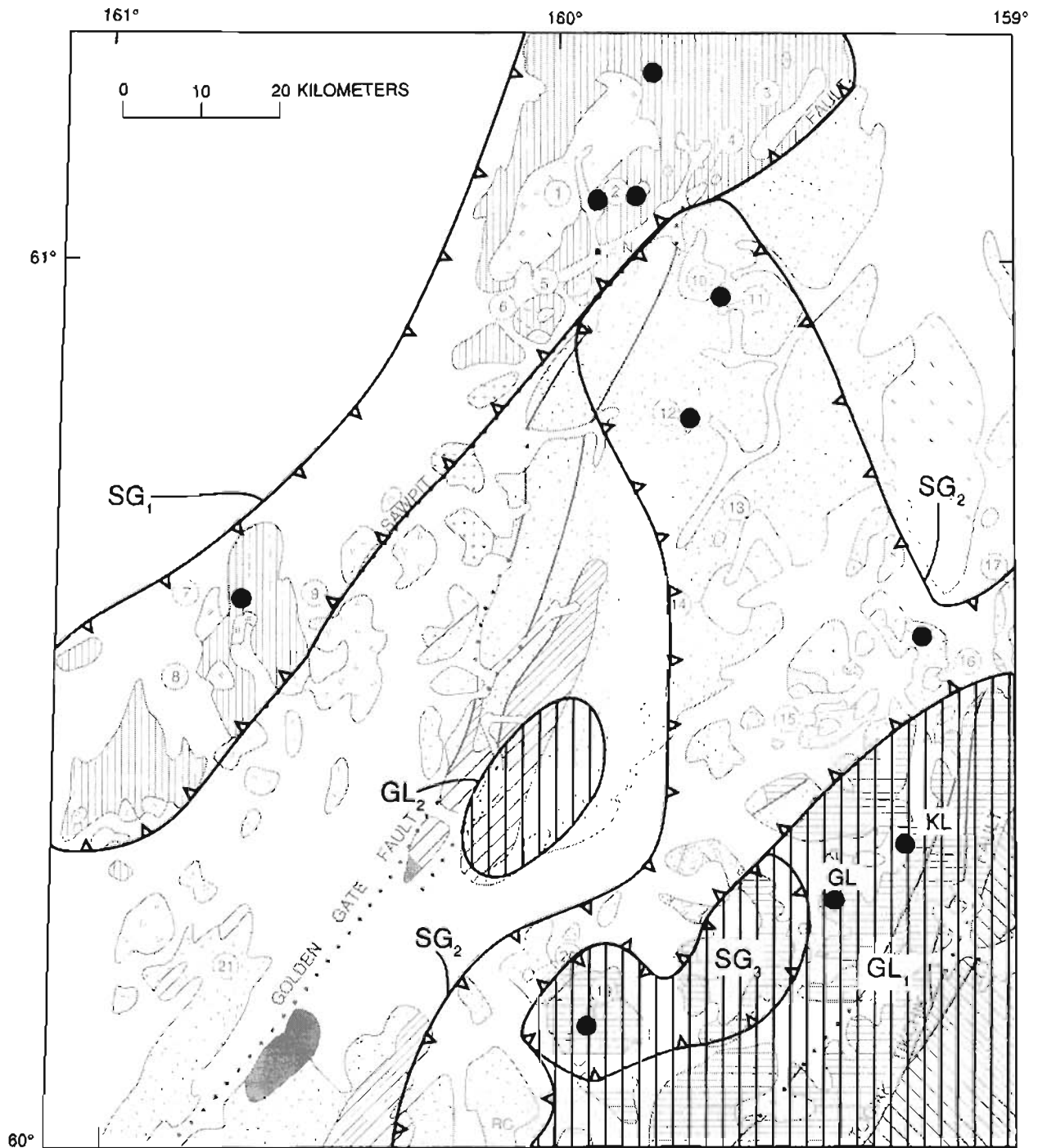
Dike and vein networks similar to those at Gold and Kisarilik Lakes are present throughout the southeastern corner of the Bethel map area in rocks of the Togiak and Tikchik terranes (tract GL1, fig. 4), but most have surface expressions of less than a few tens of square meters, and most do not have anomalous contents of all the elements Ag, As, Au, Bi, Pb, Sb, and W (Frost, 1990). Contents of As and Sb are as high as 180 ppm and 28 ppm, respectively, in stream-sediment samples in drainages from the Togiak and Tikchik terranes (Bradley and Frost, in press). Heavy-mineral-concentrate samples from the same areas are as high as 5,000 ppm As, 15,000 ppm Sb, 200 ppm Pb, 5,000 ppm W, and 2,000 ppm Zn (Bradley and Frost, in press). These data indicate that additional Gold Lake vein occurrences are present in the tract, although the size of most occurrences probably are small.

Anomalous As, Au, Ag, Hg, and Pb contents in rock and stream-sediment samples in areas underlain by the Togiak and Tikchik terranes in the Goodnews, Taylor Mountains, and Dillingham quadrangles (Coonrad and others, 1978; Hessin and others, 1978a, b; Kilburn and others, in press) suggest that these areas also are favorable for Gold Lake-type mineralization.

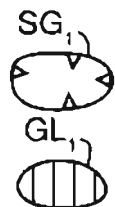
The geochemical and mineralogical data suggest the possibility of occurrence of polymetallic veins in tract GL2 (fig. 4), although no evidence was observed in the field. The tract is underlain by arkosic sandstones and slates, and greenschist-facies metachert and phyllite of Paleozoic to Mesozoic age of the Goodnews terrane, unconformably overlain by basal conglomerates and shales of the Upper Cretaceous Kuskokwim Group. Intermediate composition dikes are common and locally constitute as much as 10 percent of exposure in outcrops of Kuskokwim Group rocks in the tract. Gold is present in several heavy-mineral concentrate samples in the area, as are scattered anomalous concentrations of Ag, Hg, Sn, Pb, and Zn (Bradley and Frost, in press). Stibnite, cinnabar, cassiterite, pyrite, barite, arsenopyrite, and scheelite are present in heavy-mineral-concentrate samples (R. Tripp, U.S. Geological Survey, written commun., 1988, 1989).

Known Occurrences of Simple Gold Polymetallic Veins

The simple gold polymetallic veins in the Bethel map area are gold-bearing quartz veins that lack base-metal anomalies but may contain As and Sb (Frost, 1990). No example crop out over a strike length of more than a few meters; veins are less than 35 cm wide. Hand-picked specimens of pyrite- and iron oxide-bearing quartz and calcite veins from prospect pits in the Nyac terrane (fig. 4) contain as much as 20 ppm Au (Frost, 1990). Gold-bearing quartz veins from the Nyac



EXPLANATION



Favorable tracts for simple gold polymetallic vein deposits

Favorable tracts for Gold Lake-type polymetallic vein deposits

Figure 4. Simplified map showing favorable tracts for occurrence of polymetallic veins. Boundaries for both Gold Lake subtype and simple subtype are indicated. Criteria for tracts are summarized in table 3. Gold Lake and Kisarilik Lake prospect areas are shown by subareas GL and KL, respectively. Other localities with gold content of at least 0.05 ppm in bedrock samples marked with a dot (from Frost, 1990). Geologic units as in figure 1.

Table 3. Favorable tracts for polymetallic veins

{Tracts and localities shown on figures 1 and 4. See text for discussion}

Tract	Area	Host rock types	Vein types	Terrane	Criteria	Mines and prospects	Magmatism	Composition	Age (Ma)	References
Gold Lake polymetallic veins										
GL1	Gold Lake	argillite, sandstone, intermediate volcanic rocks	sulfide-bearing qtz veins silicified rhyolite hydrothermal breccias	Togiak, Tikchik	1,2,3,4	Gold Lake Kisarilik Lake	Crooked Mtns. p. Canyon Ck p. Gemuk Mtn p. dikes dikes	hb-bio grd, bio gr cpx-bio qtz dio, grd cpx-bio qtz gab, dio hbl dio, qtz dio rhy	70 (Ar-Ar) 70 (Ar-Ar) Late Cretaceous(?) Late Cretaceous Late Cretaceous(?)	1,2,4,5,6,7
GL2	Goodnews/ Kuskokwim	sandstone, metachert, phyllite conglomerate, sandstone	none	Goodnews Kuskokwim Group	3,4	none	dikes	and	Late Cretaceous(?)	4,5
Simple gold polymetallic veins										
SG1	Nyac	volcanic arc andesites and clastic rocks	quartz veins	Nyac	1,2,3,4	several unnamed	Nyac p. Sawpit p. Bonanza Creek p. Fox Creek p. Slate Creek p. Columbia Creek p. Little Kasigluk p.	hbl-bio gr, grd bio gr bio-hbl qtz mzd, grd gr, gab, dio bio-hbl grd, qtz mzd hbl-bio grd, qtz mzd cpx gab, dio	120-101 (K-Ar) Early Cretaceous Early Cretaceous Early Cretaceous Early Cretaceous(?) 115 (K-Ar bio) Early Cretaceous(?)	1,2,3,4,5,6
SG2	Kuskokwim	sandstone and shale	quartz veins	Kuskokwim Group	1,2,3,4	several unnamed	Mt. Plummer p. Marvel Creek p. Fisher Dome p. Cripple Mtns. p. North Fork p. W. Canyon Ck. p. Aniak Lake p. Gemuk Mtn. p. Kipchuk v.f. Tulip v.f.	bio-hbl grd bio gr porphyry bio gr hbl-bio grd, bio gr cpx qtz dio, bio grd bio grd, mzd bio gr cpx-bio qtz gab, dio and, dac and, rhy	67-65 (K-Ar) Late Cret. to early Tert. Late Cret. to early Tert. 62 (K-Ar) 64 (Ar-Ar) Late Cretaceous(?) 61 (Ar-Ar) Late Cretaceous(?) 60-69 (K-Ar) Late Cret. to early Tert.	1,2,3,4,5,6,7
SG3	Togiak	basalt, chert, argillite	quartz veins	Togiak	1,2,3,4	none	Crooked Mtns. p. Canyon Ck. p.	hb-bio grd, bio gr cpx-bio qtz dio, grd	70 (Ar-Ar) 70 (Ar-Ar)	3,4,5

Criteria: 1, presence of gold-bearing quartz veins; 2, felsic plutonic rocks; 3, gold in nonmagnetic heavy-mineral-concentrate samples; 4, gold detected in stream-sediment samples.

Abbreviations used: bio, biotite; hbl, hornblende; cpx, clinopyroxene; qtz, quartz; gr, granite; grd, granodiorite; mzd, monzodiorite; dio, diorite; gab, gabbro; and, andesite; dac, dacite; rhy, rhyolite; p., pluton; v.f., volcanic field.

References: 1, Frost (1990); 2, Box and others (in press); 3, Frost and others (1988); 4, Bradley and Frost (1992); 5, R. Tripp, U.S. Geological Survey, written commun. (1988-89); 6, Phillips and Morin (1992); 7, Frost and others (1992a).

terrane contain 0.6 to 2.3 ppm Hg; one sample contains 500 ppm As and 10 ppm Ag (Frost, 1990). Simple gold veins containing as much as 0.35 ppm Au also are present east of the Sawpit fault, cutting Late Cretaceous to early Tertiary granitoid plutons and their wall rocks, which may include sedimentary rocks of the Kuskokwim Group or low-grade metasedimentary rocks of the Togiak terrane (fig. 4) (Frost, 1990; Frost and others, 1992a).

Euhedral vuggy quartz, calcite, chlorite, and, locally, pyrite are gangue minerals in the simple gold veins. Several generations of quartz veins may be present at any locality; all may contain gold. The veins are less than 30 cm thick; most are anastomosing or en echelon and are exposed over strike lengths of less than 5 m. The spatial association between veins and plutons suggests that the plutons provided at least a heat source to circulate hydrothermal fluids that deposited the gold.

Favorable Tract for Simple Polymetallic Gold Veins

The favorable tract for simple gold veins includes all of the Nyac terrane, the Kuskokwim Group where it is cut by granitoid plutons, and part of the Togiak terrane (fig. 4, table 3). The Nyac terrane is included in the favorable tract due to the widespread presence of plutonic and volcanic rocks (Box and others, in press), gold in heavy-mineral-concentrate samples (Bradley and Frost, in press), and gold in quartz veins (Frost, 1990; Frost and others, 1992a). Kuskokwim rocks where there is field or geophysical evidence for plutons, gold in quartz veins (Frost, 1990), and gold in heavy-mineral-concentrate and stream-sediment samples, are included in the favorable tract (Bradley and Frost, in press). Areas in the Togiak terrane that host plutons are also favorable for simple gold quartz veins. There is a high probability of undiscovered simple gold vein occurrences in the favorable tract, although the small size of the known occurrences suggests that any undiscovered deposits are of similarly small size.

Base- and Precious-Metal Anomalies Associated with Tourmaline Replacement

Known Occurrences

Partial to complete replacement of subaerial volcanic and lacustrine volcanoclastic rocks by quartz-tourmaline-iron oxide assemblages is present at two localities in the northeastern part of the map area (fig. 5). Tourmalinized rocks contain as much as 70 ppm Ag, 2,000 ppm As, 0.1 ppm Au, 300 ppm Bi, 30 ppm Cd, 700 ppm Cu, >36 ppm Hg, 11,000 ppm Pb, 1,500 ppm Sb, 100 ppm Sn, 30 ppm W, and >10,000 ppm Zn, although no individual sample is anomalous in all elements (Frost, 1990; Frost and others, 1992a).

The replacement occurrences appear to be broadly stratiform, having gradational contacts with footwall rocks and with laterally equivalent rocks. In partially replaced rocks, relict porphyritic textures are present; plagioclase and mafic phenocrysts are replaced by tourmaline and iron oxides, and the groundmass is replaced by granular aggregates of quartz+tourmaline+oxides. Modally and (or) size-graded layering 1 to 10 mm thick is common. The original attitude of the layers with respect to layering in the host rocks is not known, but the layers are tourmaline rich at their sharp "lower" contacts and grade "up" to finer grained quartz-rich rock. Layering is planar but locally may be convoluted. Orbicular patches as large as 15 cm across are common and are defined by alternating quartz- and tourmaline-rich shells texturally similar to the layered rocks. Iron oxide- and quartz-cemented tourmaline-quartz breccias are present locally. Base- and precious-metal-bearing phases include, but are not limited to, iron oxides, pyrite, arsenopyrite, sphalerite, and galena.

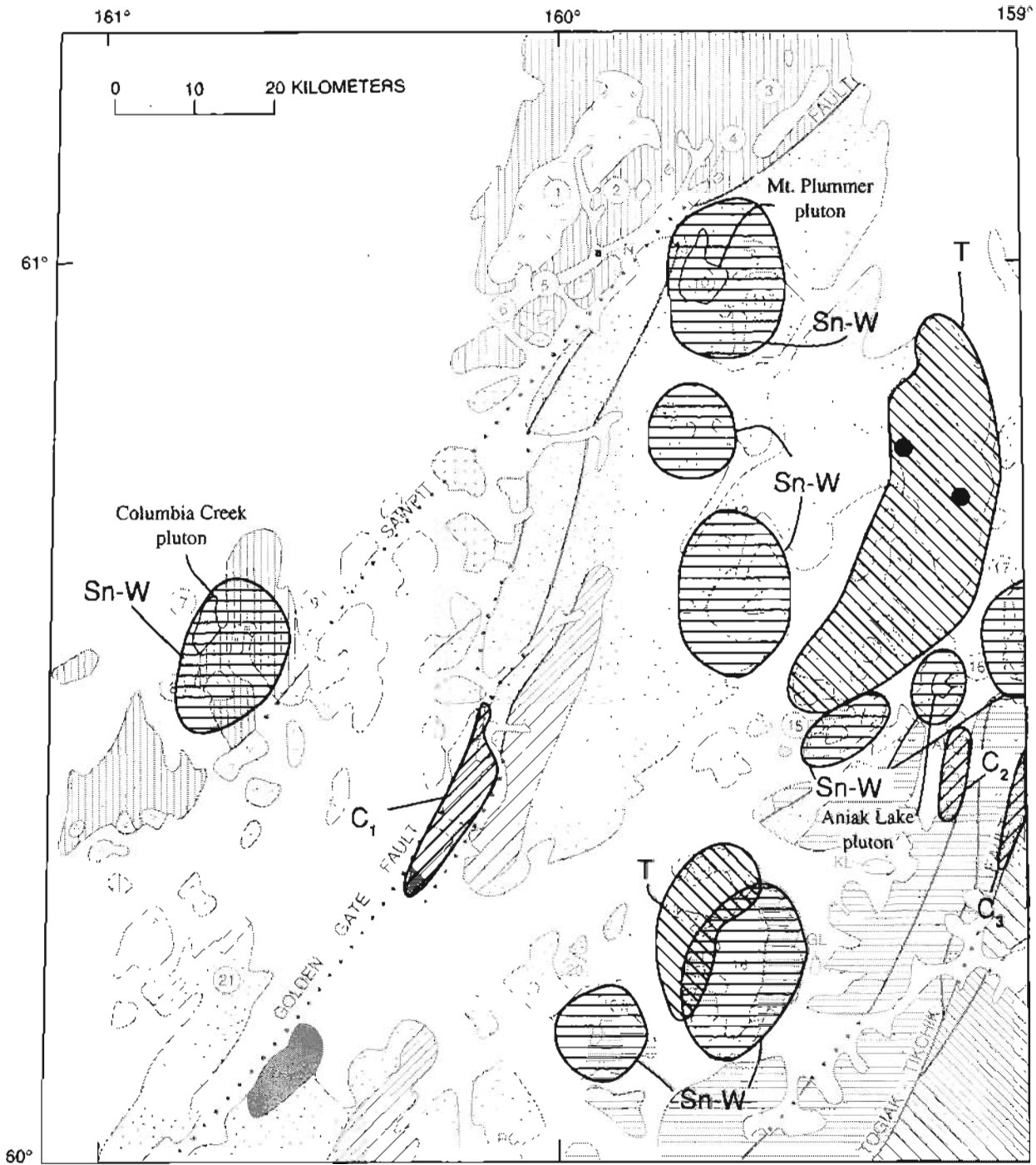
The tourmaline replacement may represent parts of hydrothermal systems related to emplacement and cooling of plutons at depth or to the volcanic host rocks (Frost, 1990). Mineralogically similar Ag-Sn-B-enriched mineralized systems with anomalous Bi, Zn, and Pb are reported from elsewhere in southwestern Alaska. Most are described as greisens, veins, shear zones, stockworks, or breccia pipes (Bundtzen and Gilbert, 1983; Bundtzen and Laird, 1982, 1983, 1990; Miller and others, 1989; Nokleberg and others, 1987) and are associated with intermediate volcanic and (or) hypabyssal intermediate to felsic plutonic rocks (Bundtzen and Laird, 1990). Sulfide-tourmaline-quartz intrusive "greisen" veins in the northernmost part of the Russian Mission 1° by 3° quadrangle, associated with the Russian Mountain pluton, yield fluid-inclusion closing temperatures of 280°C to 410°C (Bundtzen and Laird, 1990). It is not clear whether or not the tourmaline-quartz replacement zones in the Kipchuk volcanic field are similar to the veins described by Bundtzen and Laird (1990) or instead represent a distinct occurrence type.

Permissive tracts

The two tourmaline replacement zones are localized in intermediate volcanic rocks and volcanoclastic sedimentary rocks; similar lithologies would be appropriate exploration targets and are outlined as permissive tracts on figure 5. Lack of similar geochemical anomaly patterns in Late Cretaceous or Tertiary volcanic and plutonic rocks elsewhere in the map

⇒

Figure 5. Permissive terranes for tourmaline-quartz replacement zones, tin-tungsten veins, and Cypress massive sulfide deposits. See text for explanation. Geologic units as in figure 1.



EXPLANATION

- Tourmaline-quartz replacement locality
- T- (diagonal hatching) Permissive terrane for tourmaline-quartz replacement deposits
- Sn-W (horizontal hatching) Permissive terrane for tin-tungsten veins
- C₁ (diagonal hatching) Permissive terrane for Cypress massive sulfide

area (Frost and others, 1992a) suggests a low probability of additional occurrences.

Tin-Tungsten Veins

Tungsten concentrations as high as 100 ppm are present in quartz veins cutting many plutons or the hornfels surrounding them (Frost and others, 1992a). Quartz veins that contain anomalous W may also contain as much as 100 ppm Sn. Two Sn-W-bearing quartz vein samples, one from the Columbia Creek pluton and one from the Mt. Plummer pluton (10 on fig. 1), also contain 0.1 to 0.4 ppm Au (Frost, 1990). Some of the Sn-W-bearing quartz veins, especially those cutting rocks of the Togiak terrane, may be part of the polymetallic vein association. Pyritiferous rhyolite dikes cutting the Aniak Lake pluton (figs. 1, 5) contain as much as 100 ppm Sn, 940 ppm As, and 10 ppm Sb, without detectable (<20 ppm) W (Bradley and Frost, in press). Cassiterite and scheelite are present in heavy-mineral-concentrate samples from streams draining all the granitoid plutons that cut shales and sandstones of the Kuskokwim Group, as well as in streams draining granitoids that cut arc volcanic and volcanoclastic rocks of the Niyac terrane (R. Tripp, U.S. Geological Survey, written commun., 1988, 1989). Tin and W are present at levels exceeding detection limits (2,000 ppm and 20,000 ppm, respectively) in many heavy-mineral-concentrate samples (Bradley and Frost, in press) in a zone coincident with the locus of Late Cretaceous to early Tertiary plutonism and volcanism in the map area. The Sn-, W-, and locally Au-bearing quartz veins may represent polymetallic veins similar to the Gold Lake type. Areas permissive for Sn-W bearing quartz veins are shown on figure 5.

Massive Sulfide

Cypress massive Cu-Zn sulfide deposits are localized in pillow basalt sections of ophiolites (Cox and Singer, 1986, model 24a). Ophiolites represent tectonically dismembered oceanic crust and overlying sedimentary rocks incorporated in accreted terranes. Associated deposits consist of massive deposits and stockworks of pyrite, chalcopyrite, sphalerite, and (or) pyrrhonite that are commonly associated with deep-water sedimentary rocks including cherts and phyllite. Rock types permissive for the occurrence of Cypress massive sulfide deposits crop out locally in the map area.

Foliated greenschist-facies metabasalt is present in the Goodnews terrane (tract C1, fig. 5). Quartz veins that cut the metabasalts contain as much as 500 ppm Cu and average 200 ppm Zn (Frost and others, 1992a). Variably foliated and deformed massive and pillow

basalts and basaltic breccias interbedded with and overlain by thin-bedded tuffaceous chert and shale of Late Triassic age (Box and others, in press) are present in the Togiak terrane (tracts C2 and C3, fig. 5). No anomalous concentrations of Cu or Zn are present in rock, stream-sediment, or heavy-mineral-concentrate samples in tracts C2 and C3 (maximum for any sample media: 100 ppm Cu, 120 ppm Zn; Bradley and Frost, 1992; Frost and others, 1992a). The probability of occurrence of Cypress massive sulfide deposits is very low.

DISCUSSION AND CONCLUSIONS

The Bethel region has produced over 250,000 oz of placer gold, mostly from streams draining areas underlain by Early Cretaceous to early Tertiary granitoid plutons. Gold is also present in quartz veins cutting the granitoid plutons and their wall rocks. There is a strong correlation between the locus of plutonism in the eastern part of the map area and favorable tracts for placer deposits and (or) lode-gold occurrences (figs. 2, 4). Gold appears to be mobilized by and deposited from the hydrothermal systems associated with the emplacement and crystallization of the plutons. Erosion of scattered gold-bearing quartz veins associated with the plutons provides a mechanism for the concentration of gold in placers. The potential for lode gold deposits that would fall on the grade and tonnage curves of Cox and Singer (1986) is low in all terranes in the map area. The potential for placer-gold occurrences that would fall on the grade and tonnage curves of Bliss and others (1987) is moderate to high.

The potential for epithermal mercury deposits is high in areas underlain by Late Cretaceous to early Tertiary plutonic rocks where they intrude the Kuskokwim Group or the rocks of the Togiak terrane. Stable isotope data suggest that many mercury occurrences in southwestern Alaska, including those in the Bethel region, formed from ore fluids derived from dehydration of sedimentary rocks due either to burial metamorphism or to localized igneous activity (Goldfarb and others, 1990). The spatial association of mercury anomalies in volcanic rocks and granitoid plutons in the map area suggests that heat provided by Late Cretaceous to early Tertiary magmatism is the driving mechanism for mercury mobilization. Gray and others (1992) have obtained a 72 Ma ^{40}Ar - ^{39}Ar age on hydrothermal mica in cinnabar-bearing veins in the Sleetmute quadrangle, which corroborates the magmatism-driven mineralization model.

Gold is present in some Hg-As veins in the map area. The data suggest that the zonation observed at other mercury deposits—from mercury dominated at shallow levels, to antimony dominated and gold dominated at deeper levels (Gumiel and Arribas, 1987;

Seward, 1984; Miller and others, 1989)—may be telescoped in the Bethel occurrences, and (or) that higher gold contents may be present at deeper levels (Frost, 1990; Gray and others, 1990).

REFERENCES CITED

- Berg, H.C., and Cobb, E.H., 1967, Metalliferous lode deposits of Alaska: U.S. Geological Survey Bulletin 1246, 254 p.
- Bliss, J.D., Orris, G.J., and Menzie, W.D., 1987, Changes in grade, volume and contained gold during the mining life-cycle of gold placer deposits: CIM (Canadian Institute of Mining) Bulletin, v. 80, no. 903, p. 75-80.
- Box, S.E., 1992, Evidence for basin-margin right-slip faulting during Kuskokwim Group deposition, southwestern Alaska [abs.]: Geological Society of America Abstracts with Programs, v. 24, no. 5, p.9.
- Box, S.E., and Elder, W.P., 1992, Depositional and biostratigraphic framework of the Upper Cretaceous Kuskokwim Group, southwestern Alaska, in Bradley, D.C., and Ford, A.B., eds., Geologic studies in Alaska by the U.S. Geological Survey, 1990: U. S. Geological Survey Bulletin 1999, p 8-16.
- Box, S.E., Moll-Stalcup, E.J., Frost, T.P., and Murphy, J.R., in press, Preliminary geologic map of the Bethel and southern part of the Russian Mission 1:250,000 quadrangles, Alaska: U.S. Geological Survey Miscellaneous Field Studies Map.
- Box, S.E., Moll-Stalcup, E.J., Wooden, J.L., and Bradshaw, J.Y., 1990, Kilbuck terrane: oldest known rocks in Alaska: *Geology*, v. 18, p. 1219-1222.
- Box, S.E., and Murphy, J.M., 1987, Late Mesozoic structural and stratigraphic framework, eastern Bethel quadrangle, southwestern Alaska, in Hamilton, T.D., and Galloway, J.P., eds., Geologic studies in Alaska by the U.S. Geological Survey during 1986: U.S. Geological Survey Circular 998, p. 78-82.
- Bradley, Leon, and Frost, T.P., in press, Analytical results and sample locality maps of stream sediment and heavy-mineral-concentrate samples from the Bethel and part of the Russian Mission quadrangles, southwestern Alaska: U.S. Geological Survey Open-File Report .
- Bundtzen, T.K., and Gilbert, W.G., 1983, Outline of the geology and mineral resources of the upper Kuskokwim region, Alaska: *Journal of the Alaska Geological Society*, v. 3, p. 101-117.
- Bundtzen, T.K., and Laird, G.M., 1982, Geologic map of the Iditarod D-2 and eastern D-3 quadrangles, Alaska: Alaska Division of Geological and Geophysical Surveys Geologic Report 72, scale 1:63,360.
- 1983, Geologic map of the Iditarod D-1 quadrangle, Alaska: Alaska Division of Geological and Geophysical Surveys Professional Report 78, scale 1:63,360.
- 1990, Geology and mineral resources of the Russian Mission C-1 quadrangle, southwest Alaska: Alaska Division of Geological and Geophysical Surveys Public Data File 89-17, 28 p.
- Bundtzen, T.K., Swainbank, S.W., Deagen, J.R., and Moore, J.L., 1989, Alaska's mineral industries 1989, Alaska Division of Geological and Geophysical Surveys Special Report 44. 33 p.
- Coonrad, W.L., Hoare, J.M., Taufen, P.M., and Hessin, T.D., 1978, Geochemical analyses of rock samples in the Goodnews and Hagemester Island quadrangles region, southwestern Alaska: U.S. Geological Survey Open-File Report 78-9-H, 1 sheet, scale 1:250,000.
- Cox, D.P. and Singer, D.A., eds., 1986, Mineral deposit models: U.S. Geological Survey Bulletin 1693, 379 p.
- Elder, W.E., and Box, S.E., in press, Late Cretaceous inoceramid bivalves of the Kuskokwim Basin, southwestern Alaska, and their implications on basin evolution: *The Paleontological Society, Memoir* 26.
- Frost, T.P., 1990, Geology and geochemistry of mineralization in the Bethel quadrangle, southwestern Alaska, in Goldfarb, R.J., Nash, J.T., and Stoesser, J.W., eds., Geochemical studies in Alaska by the U.S. Geological Survey: U.S. Geological Survey Bulletin 1950, p. C1-C10.
- Frost, T. P. and Box, S.E., 1991a, Depth controls on magmatism-related gold and mercury mineralization, Bethel quadrangle, southwestern Alaska [abs.]: Geological Society of America Abstracts with Programs, v. 23, no. 2, p. 27.
- 1991b, Lithologic and tectonic controls on mercury mineralization in the Bethel 1°x3° quadrangle, southwestern Alaska [abs.], in Good, E.E., Slack, J.F., and Kotra, R.K., eds., USGS research on mineral resources—1991: Program and abstracts: U.S. Geological Survey Circular 1062, p. 29-31.
- Frost, T.P., Bradley, Leon, O'Leary, Rich, and Motooka, J., 1992a, Geochemical results and sample locality map for rock samples from the Bethel and southern part of the Russian Mission 1:250,000 quadrangles, Alaska: U.S. Geological Survey Open-file Report 92-316, 229 p.
- Frost, T.P., Calzia, J.P., Kistler, R.W., and Vivit, D.V., 1988, Petrogenesis of the Crooked Mountains pluton, Bethel quadrangle—A preliminary report, in Galloway, J.P., and Hamilton, T.D., eds., Geologic studies in Alaska by the U.S. Geological Survey during 1987: U.S. Geological Survey Circular 1016, p. 126-131.
- Frost, T.P., Moll-Stalcup, E.J., and Box, S.E., 1992b, Early Cretaceous and Late Cretaceous-Paleocene plutonism in the Bethel region, southwestern Alaska: Products of two magmatic arcs [abs.]: Geological Society of America Abstracts with Programs, v. 24, no. 5, p 25.
- Goldfarb, R.J., Gray, J.E., Pickthorn, W.J., Gent, C.A., Cieutat, B.A., 1990, Stable isotope systematics of epithermal mercury-antimony mineralization, southwestern Alaska, in Goldfarb, R.J., and Nash, J.T., eds., Geochemical studies in Alaska by the U.S. Geological Survey, 1989: U.S. Geological Survey Bulletin 1950, p. E1-E9.
- Gray, J.E., Frost, T.P., Goldfarb, R.J., and Detra, D.E., 1990, Gold associated with cinnabar- and stibnite-bearing deposits and mineral occurrences in the Kuskokwim River area, southwestern Alaska, in Goldfarb, R.J., and Nash, J.T., eds., Geochemical studies in Alaska by the U.S. Geological Survey, 1989: U.S. Geological Survey Bulletin 1950, p. D1-D6.
- Gray, J.E., Goldfarb, R.J., Snee, L.W., and Gent, C.A., 1992, Geochemical and temporal conditions for the formation of

- mercury-antimony deposits, southwestern Alaska [abs.]: Geological Society of America Abstracts with Programs, v. 24, no. 5, p. 28.
- Gumiel, P., and Arribas, A., 1987, Antimony deposits in the Iberian Peninsula: *Economic Geology*, v. 82, p. 1453-1463.
- Hessin, T.D., Taufen, P.M., Seward, J.C., Quintana, S.J., Clark, A.L., Grybeck, Donald, Hoare, J.M., and Coonrad, W.L., 1978a, Geochemical and generalized geological map showing distribution and abundance of lead in the Goodnews and Hagemeister Island quadrangles region, southwestern Alaska: U.S. Geological Survey Open-File Report 78-7-N, scale 1:250,000.
- 1978b, Geochemical and generalized geological map showing distribution and abundance of arsenic, gold, silver, and platinum in the Goodnews and Hagemeister Island quadrangles region, southwestern Alaska: U.S. Geological Survey Open-File Report 78-7-R, scale 1:250,000.
- Hoare, J.M., and Cobb, E.H., 1977, Mineral occurrences (other than mineral fuels and construction materials) in the Bethel, Goodnews, and Russian Mission quadrangles, Alaska: U.S. Geological Survey Open-File Report 77-156, 98 p.
- Hoare, J.M., and Coonrad, W.L., 1959a, Geology of the Bethel quadrangle, Alaska: U.S. Geological Survey Miscellaneous Investigations Map I-285, scale 1:250,000.
- 1959b, Geology of the Russian Mission quadrangle, Alaska: U.S. Geological Survey Miscellaneous Investigations Map I-292, scale 1:250,000.
- 1978, Geologic Map of the Goodnews and Hagemeister Island quadrangles, Alaska: U.S. Geological Survey Open-File Report 78-9-B, scale 1:250,000.
- John, D.A., Stewart, J.H., Kilburn, J.E., Silberling, N.J., and Rowan, L.C., in press, Geology and mineral resources of the Reno 1°x2° quadrangle, Nevada and California: U.S. Geological Survey Bulletin.
- Jones, D.L., Silberling, N.J., Coney, P.J., and Plafker, George, 1987, Lithotectonic terrane map of Alaska (west of the 141st meridian): U.S. Geological Survey Miscellaneous Field Studies Map MF-1874-A, scale 1:2,500,000.
- Kilburn, J.E., Goldfarb, R.J., Griscom, Andrew, Barnes, D.F., and Box, S.E., in press, Map showing areas of potential for mineral resources in the Goodnews Bay, Hagemeister Island, and Nushagak Bay 1°x3° quadrangles, southwest Alaska: U.S. Geological Survey Miscellaneous Field Studies Map.
- Mertie, J.B., Jr., 1938, The Nushagak district, Alaska: U.S. Geological Survey Bulletin 903, 96 p.
- Miller, M.L., Belkin, H.E., Blodgett, R.B., Bundtzen, T.K., Cady, J.W., Goldfarb, R.J., Gray, J.E., McGimsey, R.G., and Simpson, S.L., 1989, Pre-field study and mineral resource assessment of the Sleetmute quadrangle, southwestern Alaska: U.S. Geological Survey Open-File Report 89-363, 115 p.
- Moll-Stalcup, E.J., Box, S.E., and Lanphere, M.A., 1992, Eocene transition from arc to intraplate magmatism in southwestern Alaska [abs.]: Geological Society of America Abstracts with Programs, v. 24, no. 5, p. 71.
- Moll-Stalcup, E.J., Wooden, J.L., Box, S.E., and Frost, T.P., 1989, Preliminary Sr, Nd, and Pb isotopic evidence for magma sources in southwest Alaska: International Association of Volcanology and Chemistry of the Earth's Interior, Continental Magmatism, New Mexico Bureau of Mines and Mineral Resources Bulletin 131, p. 192.
- Nokleberg, W.J., Bundtzen, T.K., Berg, H.C., Brew, D.A., Grybeck, Donald, Robinson, M.S., Smith, T.E., and Yeend, Warren, 1987, Significant metalliferous lode deposits and placer deposits of Alaska: U.S. Geological Survey Bulletin 1786, 104 p.
- Phillips, J.D., and Morin, R.L., 1992, New aeromagnetic and gravity maps and interpretations for the Bethel 1°x3° quadrangle and part of the Russian Mission 1°x3° quadrangle, southwestern Alaska [abs.]: Geological Society of America Abstracts with Programs, v. 24, no. 5, p. 75.
- Robinson, M.S., and Decker, John, 1986, Preliminary age data and analytical data for selected igneous rocks from the Sleetmute, Russian Mission, Taylor Mountain, and Bethel quadrangles, southwestern Alaska: Alaska Division of Mining and Geological and Geophysical Surveys Public-Data File 86-98, 9 p.
- Roeske, S.M., and Box, S.E., 1992, Metamorphism and deformation of oceanic lithologies in a Cretaceous subduction/collision setting, southwestern Alaska [abs.]: Geological Society of America Abstracts with Programs, v. 24, no. 5, p. 79.
- Rutledge, F.A., 1948, Investigation of the Rainy Creek mercury prospect, Bethel district, southwestern Alaska: U.S. Bureau of Mines Report of Investigations 4361, 9 p.
- Sainsbury, C.L., and MacKevett, E.M., Jr., 1965, Quicksilver deposits of southwestern Alaska: U.S. Geological Survey Bulletin 1187, 89 p.
- Seward, T.M., 1984, The transport and deposition of gold in hydrothermal systems, in *Gold 82—The geology, geochemistry, and genesis of gold deposits*: Geological Society of Zimbabwe Special Publication 1, p. 165-181.
- Shew, Nora, and Wilson, F.H., 1981, Map and table showing radiometric ages of rocks in southwestern Alaska: U.S. Geological Survey Open-File Report 81-866, 26 p.

Reviewers: John E. Gray and Thomas Light

Comparison of the Effectiveness of Stream-Sediment, Heavy-Mineral-Concentrate, Aquatic-Moss, and Stream-Water Geochemical Sample Media for the Mineral Assessment Study of the Iditarod Quadrangle, Alaska

By John E. Gray, Philip L. Hageman, and Jean L. Ryder

Abstract

Samples of stream sediment, heavy mineral concentrate, aquatic moss, and stream water were collected during the mineral assessment study of the Iditarod quadrangle. Geochemical data were evaluated to determine the effectiveness of these media in the low and swampy terrain characteristic of much of southwestern Alaska. Results also were used to investigate the effectiveness of these media in the Iditarod AMRAP mineral assessment study.

Anomalous concentrations of Au, Ag, Hg, As, Cu, Pb, and Zn in stream-sediment samples are the most effective pathfinder elements for delineating ground favorable for metallic-mineral deposits in the Iditarod quadrangle. Anomalous concentrations of Au, Ag, Sb, As, Cu, Pb, and Zn, as well as the abundance of microscopic gold and cinnabar in heavy-mineral-concentrate samples, also are effective for delineating favorable areas for mineral deposits. These data identify 22 favorable areas for polymetallic Au vein deposits, polymetallic Cu-Ag-Sn vein deposits, or epithermal Hg-Sb vein deposits.

Aquatic-moss and stream-water samples are less effective geochemical sample media for identifying areas of metallic-mineral resource potential. Anomalous concentrations for Ag, Sb, As, Cu, Pb, or Zn in moss samples correspond with only 9 of the 22 areas favorable for mineral deposits. Similarly, stream-water samples were an ineffective geochemical sample medium, where As, Cu, Zn, SO_4^{2-} , or F^- anomalies only indicated 9 of the 22 areas delineated by the more effective stream-sediment and heavy-mineral-concentrate media. Most importantly, aquatic-moss and stream-water samples did not delineate any new areas favorable for metallic-mineral deposits that were not already identified by the stream-sediment and heavy-mineral-concentrate geochemical data.

INTRODUCTION

Southwestern Alaska is generally characterized by swampy terrain and low, rolling hills with broad, sediment-filled lowlands. This extensive region of low relief

presents a difficult problem not only for geologic mapping, but also for geochemical exploration. Therefore, the reconnaissance geochemical survey of the Iditarod quadrangle, conducted as part of the Alaska Mineral Resource Assessment Program (AMRAP), was designed to test less conventional sampling media and evaluate their effectiveness as exploration tools in this environment.

Regional geochemical reconnaissance studies typically use stream-sediment and heavy-mineral-concentrate samples to identify areas of geochemically anomalous ground favorable for mineral deposits. However, in areas of low relief, such as in the Iditarod quadrangle, some streams contain little detrital sediment, making such conventional sampling techniques difficult. Thus, alternative geochemical sample media were sought for this reconnaissance study.

Geochemical results from samples of aquatic moss (bryophytes) have shown promise as an exploration tool in some studies conducted near known mineral deposits (Whitehead and Brooks, 1969; Saether and Bølviiken, 1983; Erdman and Modreski, 1984; Jones, 1985). Aquatic mosses are perennial plants having many small leaves that are one cell in thickness, giving them a large reactive surface in relation to the mass of the plant (Shacklette, 1984). Mosses have high ion exchange capacities and effectively scavenge metals from the streams in which they grow. Aquatic mosses appear to concentrate metals continuously over their lifetime, effectively eliminating high- and low-flow seasonal fluctuations common in other sample media (Shacklette, 1984).

Water has also been used as a medium for geochemical exploration. Hydrogeochemical samples of stream water collected near mineral deposits have been shown to contain anomalous concentrations of ore-related cations and anions (Miller and others, 1982; Turner and Ikramuddin, 1982; Learned and others, 1985). Stream water is an advantageous sampling medium because it is widely present in humid regions, easy to collect, and needs little sample preparation prior to analysis.

Although several studies have tested specific geochemical sample media for their use in prospecting for a specific type of mineral deposit, few studies compare results for several sample media that are used over a broad region in prospecting for several mineral deposit types. Comparative reconnaissance geochemical studies on a regional scale in which several sample media are collected from the same sample sites are also rare. The purpose of this study is to compare and contrast the geochemistry of stream-sediment, heavy-mineral-concentrate, aquatic-moss, and stream-water samples collected during the reconnaissance geochemical survey of the Iditarod quadrangle.

GEOLOGY OF THE IDITAROD QUADRANGLE

Cretaceous sedimentary rocks of the Kuskokwim Group are the dominant bedrock in the Iditarod quadrangle (fig. 1). These rocks consist of thick sequences of intercalated sandstones, shales, and conglomerates (Cady and others, 1955). The Kuskokwim Group primarily is made up of deep-water turbidite facies, with lesser amounts of shallow shoreline facies rocks (Miller and Bundtzen, 1987). These rocks have been deformed into northeast-trending synclines and anticlines that are cut by numerous high-angle faults (McGimsey and others, 1988).

Late Cretaceous to early Tertiary volcano-plutonic complexes overlie or intrude sedimentary rocks of the Kuskokwim Group at many localities (Miller and Bundtzen, 1987). These complexes consist primarily of basalt and andesite that are in contact with or overlie monzonite plutons. Volcanic- and sedimentary-rock hornfels is commonly found near the contacts with the monzonite intrusions. Other igneous rocks coeval with the volcano-plutonic complexes include (1) an extensive field of felsic to mafic volcanic rocks that covers much of the western portion of the quadrangle, (2) small mafic to intermediate dikes that intrude country rock throughout the quadrangle, and (3) peraluminous granite porphyry dikes, sills, and small stocks (Miller and Bundtzen, in press).

Volumetrically minor pre-Cretaceous rocks are found in a narrow northeast-southwest-trending belt in the west-central part of the quadrangle. Metamorphic rocks of the Idono Complex with an Early Proterozoic protolith age are the oldest rocks in the quadrangle (Miller and others, 1991). A second unit in the belt consists of greenschist-facies metamorphic rocks of Paleozoic and Proterozoic(?) age (Angeloni and Miller, 1985). Mississippian to Triassic chert and volcanic rocks are found throughout the length of the belt (Miller and Bundtzen, in press). Finally, mafic and ultramafic rocks of the Dishna River area that are correlative with the Jurassic ophiolites of the Tozitna-Innoko belt are found

in the north-central portion of the quadrangle (Miller, 1990).

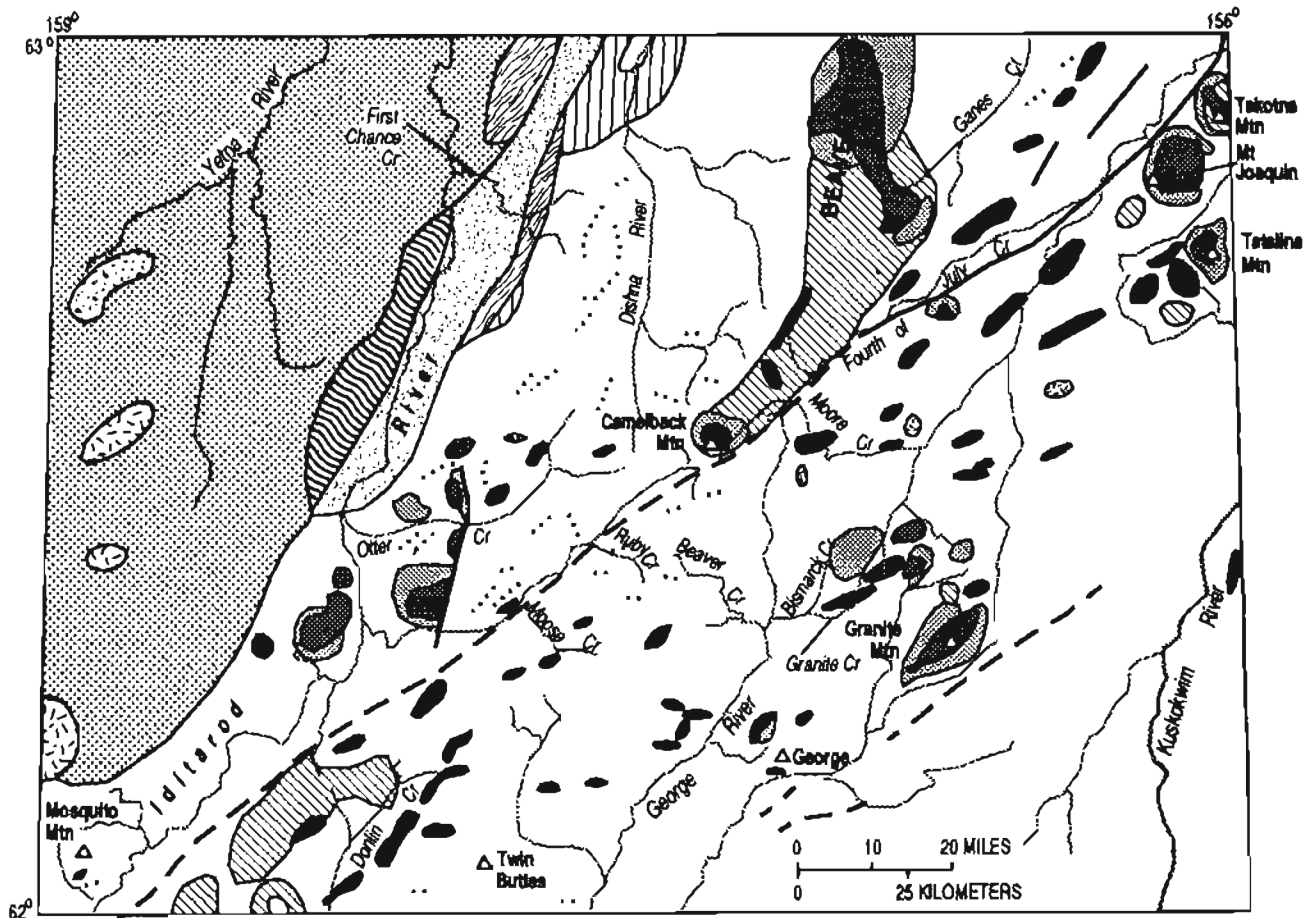
MINERAL DEPOSITS

Gold and Ag are the most economically significant commodities in the Iditarod quadrangle. Approximately 1,700,000 oz of Au and 240,000 oz of Ag have been produced from the area, mostly from placer mines (Bundtzen and others, 1987). The largest placer mines in the quadrangle are those in the Flat, Moore Creek, Donlin Creek, and Ganes Creek areas (fig. 2).

The source of placer gold in the Iditarod quadrangle has been linked to polymetallic Au veins spatially related to monzonite stocks (Kimball, 1969; Bundtzen and others, 1985; Miller and Bundtzen, 1987). The Golden Horn mine, near Flat, is the most well-known polymetallic Au deposit in the Iditarod quadrangle. Gold and scheelite are contained in quartz-carbonate veins, with lesser amounts of arsenopyrite, pyrite, chalcopyrite, sphalerite, galena, stibnite, and cinnabar (Bull, 1988). The mineralized veins are contained within faults and shear zones in the monzonite of a volcano-plutonic complex in this area (Bundtzen and Gilbert, 1983). Approximately 2,700 oz of Au, 2,600 oz of Ag, and minor Pb, Zn, and W have been recovered from Golden Horn (Bundtzen and others, 1988b). Samples of mineralized veins are anomalous in Au, Ag, Cu, Pb, Zn, Hg, Sb, As, W, Bi, and Cd (Bundtzen and others, 1988b).

The Broken Shovel lode (fig. 2) is a polymetallic Au vein deposit containing tetrahedrite, arsenopyrite, and scheelite in quartz-tourmaline veins that has been described by Bundtzen and others (1988a). Mineralized veins are hosted in a shear zone cutting an altered monzonite pluton in the Moore Creek area. Although native gold has not been identified in the lode, mineralized vein samples contain anomalous concentrations of Au and Ag, as well as Cu, Pb, Zn, As, Sb, W, Bi, and Bi (Bundtzen and others, 1988a).

Epithermal cinnabar- and stibnite-vein deposits representing significant Hg and Sb resources are found throughout the Kuskokwim River region, which includes a large portion of the Iditarod quadrangle (Sainsbury and MacKevett, 1965). These deposits are found primarily within sedimentary rocks of the Kuskokwim Group and mafic to felsic dikes, sills, or small stocks that intrude these sedimentary rocks (Bundtzen and others, 1987). Cinnabar and stibnite are the dominant ore minerals in these deposits, with lesser amounts of realgar, orpiment, native mercury, pyrite, hematite, limonite, and dickite (Sainsbury and MacKevett, 1965). The DeCourcy mine (fig. 2) is the most significant Hg mine in the Iditarod quadrangle, having produced approximately 1,500 flasks of Hg (M.L. Miller, written commun., 1992).



EXPLANATION

- Tertiary and Late Cretaceous monzonite, syenite, quartz monzonite, granodiorite, and granite stocks and plutons
- Tertiary and Late Cretaceous dacite to andesite intrusions
- Tertiary and Late Cretaceous hornfels of sedimentary and volcanic rock
- Tertiary and Late Cretaceous andesite, dacite, rhyolite, and minor basalt flows and tuffs of the Yetna River area
- Tertiary and Late Cretaceous granite porphyry sills, dikes, and plugs
- Tertiary and Late Cretaceous intermediate to mafic dikes generally less than 1 m wide
- Tertiary and Late Cretaceous andesite, basalt, and dacite volcanic flows, tuffs, volcanic breccia, and volcanoclastic sandstone
- Late Cretaceous sandstone, siltstone, shale, pebble conglomerate, and minor interbedded volcanic tuffs and flows, primarily of the Kuskokwim Group
- Early Cretaceous colluvial chips of sandstone, tuffaceous sandstone, and siltstone containing detrital potassium feldspar
- Tertiary and Cretaceous (?) amphibole-pyroxene-biotite alkali granite, poorly exposed
- Jurassic ultramafic and gabbroic rocks of the Dishna River area, probably part of the Tozitna-Innokko ophiolite belt
- Triassic to Mississippian recrystallized chert, volcanic rocks; metasilstone, and minor limestone correlative with the Innoko terrane
- Paleozoic and Proterozoic (?) greenschist-facies metaigneous and metasedimentary rocks correlative with the Ruby terrane
- Proterozoic metamorphic rocks, including orthogneiss, schist, and amphibolite of the Idono Complex
- Faults, dashed where inferred

Figure 1. Iditarod quadrangle geology (simplified from Miller and Bundtzen, in press).

Stibnite-rich veins are known near Snow Gulch in the Donlin Creek area (Cady and others, 1955), and a similar occurrence (the Wyrick lode) is found on Granite Creek (fig. 2) (Bundtzen and others, 1986). These lodes consist of small quartz-carbonate veins and vug fillings containing stibnite that are hosted in granite porphyry dikes, in the adjacent siltstone and graywacke of the Kuskokwim Group, or at contacts between the two rock types. Stibnite-rich samples from the Snow Gulch and the Wyrick lode are anomalous in Au and Ag (Cady and others, 1955; Bundtzen and others, 1986; McGimsey and others, 1988; Gray and others, 1990). Stibnite-rich veins spatially related to granite porphyry are an important deposit type in the Iditarod quadrangle and throughout the Kuskokwim River region.

Polymetallic Cu-Ag-Sn veins containing chalcopyrite, sphalerite, galena, tetrahedrite, arsenopyrite, cassiterite, and wolframite were discovered in the Beaver Mountains by Bundtzen and Laird (1982). Gangue minerals include quartz, tourmaline, axinite, and fluorite. The veins are found in faults, shear zones, or breccias within the cupolas of the monzonite stocks, or in sedimentary- and volcanic-rock hornfels aureoles surrounding the igneous rocks (Bundtzen and Gilbert, 1983; Bundtzen and others, 1987). The most consistent pathfinder elements associated with these polymetallic veins are Cu, Pb, Zn, Sn, W, Au, and Ag, but anomalous Hg, Sb, As, Bi, Cd, and B may also be associated with some of the deposits (Bundtzen and Laird, 1982; McGimsey and others, 1988).

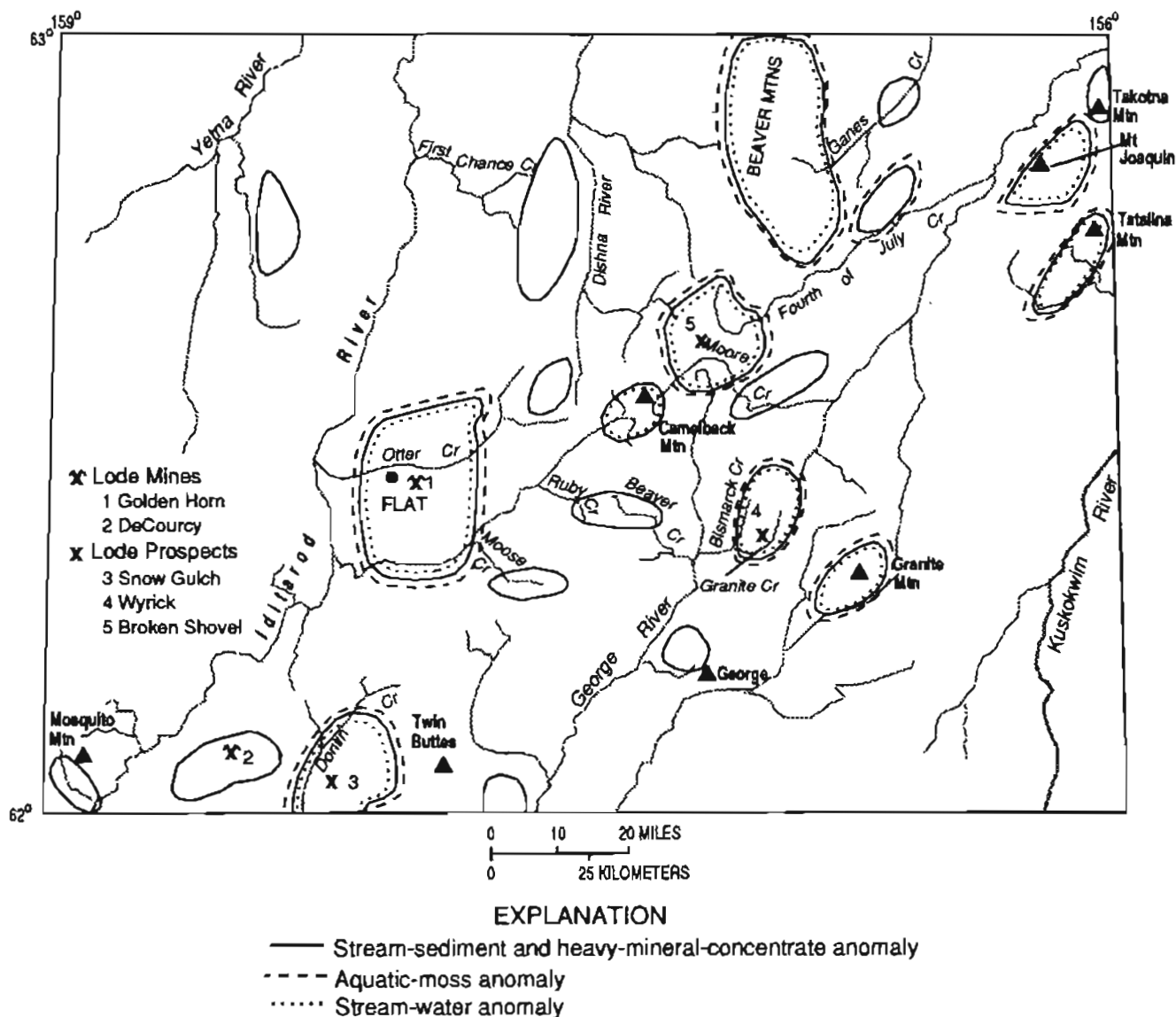


Figure 2. Geochemical anomaly map of Iditarod quadrangle. As described in text and shown here, only nine areas contain moss geochemical anomalies and nine areas contain stream-water geochemical anomalies, compared with 22 anomalies defined by the stream-sediment and heavy-mineral-concentrate data.

GEOCHEMICAL STUDIES

Methods and Data Evaluation

Stream-sediment, heavy-mineral-concentrate, stream-water, and aquatic-moss (bryophyte) samples were collected from active channels of perennial first- and second-order streams. The area of most drainage basins ranged from 1 mi² (2.6 km²) to about 5 mi² (13 km²). The stream-sediment sampling density was approximately 1 sample site per 9 mi² (23 km²).

The stream-sediment samples were sieved to minus-80-mesh (0.17 mm) and chemically analyzed. The panned-concentrate samples were sieved to minus-30-mesh (0.60 mm), separated in bromoform, and further separated magnetically to obtain a nonmagnetic, heavy-mineral-concentrate sample. The nonmagnetic, heavy-mineral-concentrates were split using a multiple-plate splitter. One split was hand ground for geochemical analysis, and the other split was saved for mineralogical identification.

Aquatic-moss samples were preferentially collected near the current water level from boulders or dead-fall vegetation in the active stream channel. However, when moss on the stream bottom could not be found, moss from the channel walls or overbank was collected. The moss and the sediment trapped within the moss were collected together, and the sediment was later removed by agitating the samples in water (Arbogast and others, 1991), which can be a time-consuming and labor-intensive procedure. When all of the sediment was removed, the moss samples were dried, ground in a mill, and ashed at 500°C. The ashed material was used for geochemical analysis.

Stream water filtered through a 0.45- μ m membrane was acidified with concentrated HNO₃ and used for cation analysis. Unfiltered water samples were also collected and used for anion analysis. No further preparation was required on the stream-water samples prior to analysis.

There were 1,151 stream-sediment samples collected in this study. A total of 799 heavy-mineral concentrates were collected and microscopically examined for their mineralogical content. However, some of the heavy-mineral concentrates collected contained an insufficient amount of material necessary for geochemical analysis, and only 662 concentrates were chemically analyzed. Aquatic mosses could not be located at some sites, and thus only 863 mosses were collected. There were 1,050 stream-water samples collected during this study.

Stream-sediment, heavy-mineral-concentrate, and moss samples were analyzed for multielement suites by semiquantitative emission spectrography. Stream-sediment samples were also analyzed for selected elements by inductively coupled plasma (ICP) and atomic absorption spectrophotometry (AAS) analysis. Stream-water samples were analyzed by ion chromatography, ICP, and AAS

analysis. The presence of gold and cinnabar was determined microscopically in the nonmagnetic, heavy-mineral-concentrate samples. Geochemical results for the stream sediments and heavy-mineral concentrates are listed in Gray and others (1988a) and Hopkins and others (1991). Mineralogy results for this study appear in Bennett and others (1988). Geochemical results for the moss samples are found in Arbogast and others (1991), and results for the stream waters appear in Gray and others (1988b).

INTERPRETATION OF GEOCHEMICAL RESULTS

Anomalous concentrations of Au, Ag, Hg, As, Cu, Pb, and Zn in stream-sediment samples and anomalous concentrations of Au, Ag, Sb, As, Cu, Pb, and Zn, as well as visual estimation of the abundance of gold and cinnabar, in heavy-mineral-concentrate samples are useful pathfinders for delineating areas favorable for mineral deposits in the Iditarod quadrangle. In aquatic-moss samples, anomalous concentrations of Ag, Sb, As, Cu, Pb, and Zn are also helpful for identifying areas favorable for mineral deposits. The moss samples were analyzed for Au, but none were found to contain Au above the lower limit of determination (2 ppm) by the spectrographic method. Thus, Au in the mosses was not useful in this study and is not discussed further. In stream-water samples, anomalous concentrations of As, Cu, Zn, SO₄²⁻, and F⁻ are the most useful.

Anomalies in all data sets were defined by identifying breaks in the frequency distribution of each data set. Anomaly selections were based on the ability to explain a large population of the data with a minimum of single-site anomalies. For example, the 98th percentile concentration of 3 ppm Ag in moss was selected as anomalous because 58 percent of the anomalous samples cluster into specific areas, whereas the 95th percentile concentration of 2 ppm Ag in moss has numerous single-site anomalies and only 39 percent of the data can be explained by clusters of samples forming geochemical anomalies. The anomalous values selected are generally near the 98th percentile. However, slightly lower percentiles were used as anomalous concentrations for some elements in the stream-sediment data and are a function of the larger number of these samples clustering into specific areas defining geochemical anomalies. A summary of the data used in this study is presented in table 1.

Stream-Sediment and Heavy-Mineral-Concentrate Samples

Stream-sediment and heavy-mineral-concentrate samples are the most useful sample media for delineating areas geochemically favorable for the mineral

Table 1. Summary of stream-sediment, heavy-mineral-concentrate, aquatic-moss, and stream-water geochemical data

[N, not detected at the concentration shown; L, detected but less than the concentration shown; G, greater than the concentration shown; —, not applicable. All concentrations shown are parts per million (ppm), except detection ratio, N, L, G, and the cinnabar and gold mineralogy results (in percent), and percent of anomalies in areas]

	Detection ratio ¹	N ²	L ³	G ⁴	Minimum	50th	Percentile concentrations			Maximum	Selected anomalies ⁵	Percent of anomalies in areas
							90th	95th	98th			
Stream sediments												
Au -----	0.30	0	758	0	0.005L	0.005L	0.006	0.01	0.05	1.55	0.01	69
Ag -----	.03	1,084	30	0	.5N	.5N	.5N	.5L	.5	3	.5L	85
Hg -----	.99	9	0	4	.02	.14	.45	.77	3.6	34G	.80	78
As -----	.46	508	89	0	2.0N	3.2	10	15	50	210	15	78
Cu -----	1.00	0	0	0	5	20	30	30	50	200	100	92
Pb -----	.72	103	218	0	10N	10	20	30	50	200	70	89
Zn -----	.11	352	675	0	200N	200L	200L	200L	200	500	300	81
Concentrates												
Au -----	.02	645	1	3	20N	20N	20N	20N	70	1,000G	20	80
Ag -----	.05	629	1	0	1N	1N	1N	1N	20	500	1	80
Sb -----	.03	640	1	0	200N	200N	200N	200N	700	10,000	200	83
As -----	.005	659	0	0	500N	500N	500N	500N	500N	1,500	1,000	100
Cu -----	.62	7	247	0	10N	10	30	50	100	1,000	300	56
Pb -----	.62	110	147	0	20N	20	70	150	200	5,000	300	85
Zn -----	.005	619	8	0	500N	500N	500N	500L	1,000	20,000	1,500	58
Gold -----	.01	790	—	—	N	N	N	N	N	1%	Gold ⁶	89
Cinnabar -----	.25	598	—	—	N	N	<1%	1-5%	1-5%	20-50%	1-5%	79
Mosses												
Ag -----	.88	68	32	0	.1N	.5	1.5	2	3	20	3	58
Sb -----	.03	829	12	0	50N	50N	50N	50N	50	200	50	77
As -----	.04	810	18	0	200N	200N	200N	200L	700	5,000	200	76
Cu -----	1.00	0	0	0	5	200	500	500	1,000	2,000	1,000	23
Pb -----	.97	0	22	0	10L	20	50	50	100	500	100	83
Zn -----	.99	1	6	0	100N	500	1,500	2,000	2,000	7,000	2,000	12
Waters												
As -----	.58	351	86	0	.001N	.001	.003	.003	.004	.019	.004	33
Cu -----	.30	91	647	0	.001N	.001L	.005	.006	.007	.015	.007	16
Zn -----	.42	163	446	0	.001N	.002L	.006	.008	.015	.080	.10	25
SO ₄ ²⁻ -----	.86	78	70	0	.15	1.5	6.5	8.7	10	210	10	41
F ⁻ -----	.56	184	276	0	.01N	.04	.14	.15	.20	.54	.18	26

¹Detection ratio is the number of uncensored values divided by the total number of samples analyzed.

²N is the number of samples in which concentrations could not be detected at the lower limit of determination.

³L is the number of samples in which concentrations were reported as observable but were less than the lower limit of determination.

⁴G is the number of samples in which concentrations were reported as observable but were greater than the upper limit of determination.

⁵Anomalous concentrations were selected by identifying breaks in the frequency distribution of each data set.

⁶Any amount of visible gold in heavy-mineral-concentrate samples is anomalous.

deposit types in the Iditarod quadrangle. Twenty-two areas were identified as favorable for the presence of metallic-mineral resources based solely on clusters of geochemical or mineralogical anomalies in stream-sediment or heavy-mineral-concentrate samples (fig. 2; table 2). These areas range from large, covering numerous drainage basins (for example, the Beaver Mountains), to small, covering only one or two drainage basins (for example, Ruby-Beaver Creeks). However, no areas were delineated on the basis of an anomaly at a single site. Over 75 percent of the geochemical and mineralogy anomalies in stream-sediment and heavy-mineral-concentrate samples are included in the delineated areas (table 1), except for anomalous concentrations of Au in stream-sediment samples (69 percent included in areas), Zn anomalies in concentrates (58 percent included in areas), and Cu anomalies in concentrates (56 percent included in areas).

Geochemical anomalies in samples of stream-sediment and heavy-mineral concentrate cluster around known placer-gold mines such as Flat, Moore Creek, and Donlin Creek. Stream-sediment and heavy-mineral-concentrate samples with geochemical anomalies are also found downstream from polymetallic Cu-Ag-Sn veins in the Beaver Mountains and the Broken Shovel lode, in polymetallic Au vein deposits near Flat, and in the epithermal Hg-Sb deposit at DeCourcy. In addition, several new areas favorable for mineral deposits were also delineated by identifying geochemical anomalies in stream-sediment and heavy-mineral-concentrate samples in the quadrangle (table 2).

Aquatic-Moss Samples

Aquatic-moss samples are less useful than stream-sediment or heavy-mineral-concentrate samples for identifying areas that are geochemically favorable for mineral deposits in the Iditarod quadrangle. However, some of the collected moss samples are highly metalliferous. For example, 3 moss samples contain 5,000 ppm As, 2 have 2,000 ppm Cu, and 2 contain 7,000 ppm Zn. Unfortunately, only the 3 mosses with As anomalies are found in areas delineated as geochemically anomalous by the stream-sediment and heavy-mineral-concentrate samples. The 4 mosses with the highest concentrations of Cu and Zn are found as single-site anomalies that do not coincide with any of the 22 delineated anomalous areas. Furthermore, only 2 of the 17 mosses with the highest concentrations of Zn and 5 of the 22 mosses with the highest concentrations of Cu are found in areas delineated as anomalous by the stream-sediment and heavy-mineral-concentrate data. Multiple-site anomalies for Cu, Pb, or Zn in moss samples are found in only the Beaver Mountains, Granite Mountain, and Bismarck

Creek areas and are consistent with the areas defined by the stream-sediment and heavy-mineral-concentrate data that are favorable for polymetallic Cu-Ag-Sn vein deposits (table 2). These results suggest that anomalous concentrations of Cu, Pb, and Zn in moss samples are not completely reliable for identifying areas in the quadrangle that are favorable for mineral deposits.

Anomalous concentrations of Ag, Sb, and As in the mosses are consistent with some areas favorable for the presence of mineral deposits in the quadrangle. Using concentrations listed in table 1, 58 percent of the Ag, 77 percent of the Sb, and 76 percent of the As anomalies in moss samples are found within the 22 delineated areas. However, Ag, Sb, or As anomalies in moss are not found in the DeCourcy, First Chance Creek, George River-Moore Creek, southeast of Twin Buttes, Moose Creek, Mosquito Mountain, north of George, Ruby-Beaver Creeks, and Yetna River areas where Au-Ag or Hg-Sb-As anomalies in stream-sediment or heavy-mineral-concentrate samples are found. The lack of moss anomalies in some of these areas may be because the mosses were not analyzed for Hg. However, most of these areas contain stream-sediment and heavy-mineral-concentrate samples anomalous in Ag, Sb, or As but do not have Ag, Sb, or As anomalies in the mosses. These results suggest that identifying areas that are geochemically favorable for epithermal Hg-Sb vein deposits at a regional reconnaissance scale is more difficult using aquatic-moss samples than it is by using stream-sediment or heavy-mineral-concentrate samples.

Only 9 of the 22 areas outlined contain more than 1 moss sample with anomalous concentrations of Ag, Sb, As, Cu, Pb, or Zn. No areas favorable for the mineral deposit types in the Iditarod quadrangle were delineated based solely on the geochemical data from the mosses. These results suggest that collecting aquatic moss samples as a geochemical exploration medium in regional reconnaissance studies in southwestern Alaska offers no particular advantage over stream-sediment and heavy-mineral-concentrate sampling.

Stream-Water Samples

Anomalous concentrations of As are found in epithermal Hg-Sb vein deposits (Gray and others, 1990) and Au and Cu-Ag-Sn polymetallic vein deposits in the quadrangle (Bundtzen and Laird, 1982; Bundtzen and others, 1988a). Polymetallic Au and polymetallic Cu-Ag-Sn veins also contain anomalous concentrations of F^- or the mineral fluorite (Bull and Bundtzen, 1987; McGimsey and others, 1988). In addition, elevated concentrations of Cu, Zn, and SO_4^{2-} in surface waters near ore deposits has been attributed to the oxidation of sulfide minerals (Miller and others, 1982; Learned and others,

Table 2. Summary of stream-sediment, heavy-mineral-concentrate, aquatic-moss, and stream-water anomalies of selected areas in the Iditarod quadrangle

[SS, stream-sediment samples; H-M-C, nonmagnetic, heavy-mineral-concentrate samples. Data is for elements shown unless otherwise indicated. N/A, not applicable because mosses could not be located at this site and were not sampled]

Location	Number of anomalies												Known or favorable deposit types
	Au-Ag				Hg-Sb-As				Cu-Pb-Zn				
	SS	H-M-C	Moss ¹	Water ²	SS ³	H-M-C ⁴	Moss ⁵	Water ⁶	SS	H-M-C	Moss	Water ⁷	
Beaver Mountains -----	19	3	8	0	25	0	13	1	26	3	16	3	Cu-Ag-Sn polymetallic vein
Moore Creek Area -----	4	5	0	2	11	7	8	1	0	2	0	2	Au and Cu-Ag-Sn polymetallic vein
Flat Area -----	7	8	0	3	7	10	4	2	1	2	0	3	Au and Cu-Ag-Sn polymetallic vein
Mount Joaquin -----	4	1	0	0	4	3	2	4	1	0	0	2	Au polymetallic vein
Tatalina Mountain -----	2	2	1	2	4	9	4	3	2	0	0	1	Cu-Ag-Sn polymetallic vein
Granite Mountain* -----	8	5	2	0	3	2	5	2	3	2	3	0	Cu-Ag-Sn polymetallic vein
DeCourcy area -----	0	3	0	0	5	1	0	0	0	0	0	0	epithermal Hg-Sb vein
Donlin Creek -----	3	0	0	3	4	0	4	0	0	0	0	1	Au polymetallic vein
Camelback Mountain ----	0	0	0	3	6	2	1	1	2	0	1	0	Cu-Ag-Sn polymetallic vein
First Chance Creek* ----	4	1	0	0	5	4	0	0	2	3	0	0	epithermal Hg-Sb vein
George R.-Moore Ck.* ---	2	2	0	0	6	8	0	0	0	5	1	0	epithermal Hg-Sb vein
North of George* -----	1	0	0	0	3	0	0	0	0	0	0	0	epithermal Hg-Sb vein
SE of Twin Buttes* -----	0	0	0	0	2	2	0	0	0	0	0	1	epithermal Hg-Sb vein
Moose Creek* -----	0	0	0	0	1	2	0	0	0	0	0	0	epithermal Hg-Sb vein
Dishna R.-Otter Ck.* ----	0	0	0	1	2	1	1	0	1	0	0	0	epithermal Hg-Sb vein
Mosquito Mtn.* -----	0	5	0	0	1	0	0	0	0	0	0	0	Au polymetallic vein
Ruby-Beaver Creeks ----	3	1	0	0	0	0	0	0	0	0	0	1	epithermal Hg-Sb vein
Yetna River* -----	3	4	N/A	0	0	0	N/A	0	0	0	N/A	0	Au polymetallic vein
Bismarck Creek* -----	21	6	0	8	1	3	1	0	5	2	2	0	Cu-Ag-Sn polymetallic vein
Takotna Mtn. -----	0	0	0	0	1	0	0	1	0	1	0	0	Cu-Ag-Sn polymetallic vein
Ganes Creek -----	1	1	0	0	0	0	0	0	0	0	0	0	Au polymetallic vein
Fourth of July Ck.* -----	0	0	0	0	1	1	2	0	0	0	0	0	Au polymetallic vein

¹Anomalous concentrations of Ag only.²Anomalous concentrations of SO₄²⁻ and F⁻.³Anomalous concentrations of Hg and As.⁴Anomalous concentrations of cinnabar, Sb, and As.⁵Anomalous concentrations of Sb and As.⁶Anomalous concentrations of As only.⁷Anomalous concentrations of Cu and Zn.

* New areas with no reported mines, prospects, or mineral occurrences.

1985). Anomalous concentrations of As, Cu, Zn, F⁻, and SO₄²⁻ in stream waters should therefore be useful for identifying areas favorable for these types of mineral deposits in the Iditarod quadrangle. The concentration of Ag in stream water should also be a useful pathfinder, but the Ag content in samples of stream and lake water collected during a previously conducted National Uranium Resource Evaluation (NURE) survey was found to be ineffective for locating mineral deposits in the Iditarod quadrangle (Miller and others, in press). Therefore, the concentration of Ag in stream water was not determined during this study.

The geochemistry of the stream waters is the most difficult data set to interpret. Only about 28 percent of the samples with anomalous concentrations of As, Cu, Zn, SO₄²⁻, and F⁻ in the stream-water samples (table 1) are found in areas identified to be geochemically favorable for mineral deposits in the quadrangle. One complication is that water chemistry in this region of Alaska can be highly variable due to rapid fluctuations in discharge, related to frequent summer precipitation.

Sulfate has the highest reliability, with 41 percent of the stream-water samples having concentrations greater than 10 ppm being found within areas designated as favorable for the occurrence of mineral deposits. Anomalous SO₄²⁻ in stream-water samples are found in the Moore Creek, Flat, Donlin Creek, Camelback Mountain, and Bismarck Creek areas, where polymetallic vein or epithermal Hg-Sb vein deposits are known (table 2). Unfortunately, no stream-water samples with anomalous SO₄²⁻ were found in the Beaver Mountains, where several veins containing base-metal sulfides are known. It is unclear why anomalous SO₄²⁻ was not found in stream-water samples collected in the Beaver Mountains, as well as in 15 other areas favorable for mineral deposits in the quadrangle.

Only 33 percent of the stream-water samples with anomalous As (table 1) are found in areas geochemically favorable for mineral deposits in the quadrangle. Anomalous concentrations of As are found in stream-water samples collected in 8 areas favorable for polymetallic vein deposits, although 4 of these areas contain only 1 As anomaly. Similarly, only 26 percent of the stream-water samples with anomalous F⁻ (table 1) are found in the areas outlined, including the Tatalina Mountain, Otter Creek-Dishna River, and Bismarck Creek areas. Mineralized veins in the Granite Mountain area contain anomalous F⁻ (McGimsey and others, 1988), but the stream-water samples collected in this area do not. In addition, fluorite has been described in greisen veins in the Flat area, but only 1 stream-water sample contains anomalous F⁻ in this area.

Copper has the poorest reliability of the stream-water samples, with only 16 percent of the waters having concentrations greater than 0.007 ppm being found in

areas designated as geochemically favorable for mineral deposits in the quadrangle. Even more discouraging for Cu is the fact that only 1 of the most anomalous 11 stream-water samples (concentrations greater than or equal to 0.009 ppm) is found in an area outlined as favorable for mineral deposits; the other samples are found as single-site anomalies that are difficult to explain. Anomalous Zn in stream water is slightly more reliable; 25 percent of the samples that contain at least 0.010 ppm Zn are located in areas favorable for mineral deposits. However, only 6 of the 16 samples of stream water with the highest concentrations of Zn (greater than 0.020 ppm) are found in areas favorable for mineral deposits. Similar to Cu, the other 10 water samples with the highest Zn concentrations are found as single-site anomalies with no apparent association to mineral deposits. In the Beaver Mountains, only 1 water sample with anomalous Cu and 2 samples with anomalous Zn are found, which is not particularly impressive for an area with several known polymetallic base-metal vein deposits. More significantly, no Cu or Zn anomalies in stream waters are found in the Camelback Mountain area, where polymetallic vein deposits containing anomalous base metals are also known (Bundtzen and others, 1988a). Multiple-site stream-water Cu or Zn anomalies are consistent with only 4 of 14 areas favorable for polymetallic Cu-Ag-Sn or polymetallic Au vein deposits (table 2).

Stream-water samples are not as reliable as stream-sediment and heavy-mineral-concentrate samples for identifying geochemically favorable ground for mineral deposits in the Iditarod quadrangle. Similar to the aquatic-moss samples, no areas were delineated solely on the basis of geochemical data from the stream waters.

CONCLUSIONS

1. In the Iditarod quadrangle, geochemical data from stream-sediment and heavy-mineral-concentrate samples are reliable for identifying favorable areas for polymetallic Au, polymetallic Cu-Ag-Sn, and epithermal Hg-Sb vein deposits. Over 75 percent of the stream-sediment and heavy-mineral-concentrate samples with anomalous concentrations of pathfinder elements are included in these areas. Data suggest that stream-sediment and heavy-mineral-concentrate samples are effective geochemical exploration media in low-energy stream environments such as the swampy and low, rolling hills terrain in southwestern Alaska.

2. Some aquatic-moss samples collected in the Iditarod quadrangle contain high concentrations of metals. However, the moss data are difficult to interpret because mosses containing geochemical anomalies do not cluster well into areas that are favorable for the mineral deposit types in the quadrangle. Approximately 58

percent of the Ag, 77 percent of the Sb, 76 percent of the As, and 83 percent of the Pb anomalies in the moss samples were found within areas designated to be favorable for mineral deposits.

Geochemical results suggest that aquatic-moss sampling offered no particular advantage during the mineral assessment study in the Iditarod quadrangle other than to confirm the existence of anomalies already identified with stream-sediment and heavy-mineral-concentrate data. The results also suggest that had only moss sampling been conducted, over 50 percent of the areas favorable for the occurrence of mineral deposits in the quadrangle would have been overlooked. Furthermore, the aquatic-moss sampling design was adversely affected because mosses could not be found at all sites, whereas stream sediment is nearly always present. In addition, cleaning, sample preparation, and processing of mosses is time consuming and labor intensive.

3. Stream-water samples collected during the geochemical survey of the Iditarod quadrangle contain low concentrations of metals. Stream waters with geochemical anomalies show the greatest amount of scatter of all of the geochemical sample media used in the Iditarod study. Less than 28 percent of the samples with anomalous concentrations of As, Cu, Zn, SO_4^{2-} , and F^- in the stream waters are found in areas delineated as favorable for the presence of mineral deposits. More importantly, multiple sample-site anomalies for As, Cu, Zn, SO_4^{2-} , and F^- in the stream waters are found in only 9 of 22 of these areas. Thus, stream waters are the least reliable medium for identifying areas favorable for mineral deposits in the Iditarod quadrangle.

4. In no instances were aquatic-moss or stream-water samples exclusively beneficial for identifying areas favorable for mineral deposits. That is, in the Iditarod quadrangle, no geochemical anomalies were discovered solely on the basis of the aquatic-moss or stream-water data, and therefore they offered no particular advantage during the mineral assessment study of the quadrangle. This study does not imply that hydrogeochemical or aquatic-moss sampling cannot prove beneficial in some exploration programs. However, the regional reconnaissance survey used in the Iditarod quadrangle suggests stream-sediment and heavy-mineral-concentrate sampling are the most effective method for identifying geochemically anomalous ground in the swampy and low topographic terrain in southwestern Alaska.

Acknowledgments.—The authors would like to recognize the assistance of Delmont Hopkins, John Bullock, Belinda Arbogast, Jerry Motooka, Rick Sanzalone, John McHugh, Bruce Roushey, and Walt Ficklin with chemical analyses; Cliff Taylor and Greg Bennett for mineralogy identifications; Pete Folger, James McNeal, Scott Rose, Robert Carlson, Jerry Gaccetta, Wendy Gerstel, Martha L.

Miller, and Karen D. Kelly for sample collection; and Olga Erlich, Barbara Erickson, Tom Peacock, Pete Theodorakos, and Greg Thurston for sample preparation.

REFERENCES CITED

- Angeloni, L.M., and Miller, M.L., 1985, Greenschist facies metamorphic rocks of north-central Iditarod quadrangle, in Bartsch-Winkler, Susan, ed., *The U.S. Geological Survey in Alaska—Accomplishments during 1984: U.S. Geological Survey Circular 967*, p. 19-21.
- Arbogast, B.F., Erickson, B.M., Gray, J.E., and McNeal, J.M., 1991, Analytical results and sample locality map of moss, moss-sediment, and willow samples from the Iditarod quadrangle, Alaska: U.S. Geological Survey Open-File Report 91-380-A, 101 p., 1 pl., scale 1:250,000.
- Bennett, G.J., Gray, J.E., and Taylor, C.D., 1988, Mineralogy and sample locality map of the nonmagnetic, heavy-mineral-concentrate samples, Iditarod quadrangle, Alaska: U.S. Geological Survey Open-File Report 88-32, 37 p., 1 pl., scale 1:250,000.
- Bull, K.F., 1988, Genesis of the Golden Horn and related mineralization in the Flat area, Alaska: Fairbanks, University of Alaska, M.S. thesis, 149 p.
- Bull, K.F., and Bundtzen, T.K., 1987, Greisen and vein Au-W mineralization of the Black Creek stock, the Flat area, west-central Alaska [abs.]: Geological Society of America Abstracts with Programs, v. 19, p. 362.
- Bundtzen, T.K., Cox, B.C., and Veach, N.C., 1987, Heavy mineral provenance studies in the Iditarod and Innoko districts, western Alaska, in Process Mineralogy VII, SME/AIME joint meeting, Denver, Colorado: Metallurgical Society, p. 221-245.
- Bundtzen, T.K., and Gilbert, W.G., 1983, Outline of geology and mineral resources of upper Kuskokwim region, Alaska: *Journal of the Alaska Geological Society*, v. 3, p. 101-119.
- Bundtzen, T.K., and Laird, G.M., 1982, Geological map of the Iditarod D-2 and eastern D-3 quadrangles, Alaska: Alaska Division of Geological and Geophysical Surveys Geologic Report 72, 1 pl., scale 1:63,360.
- Bundtzen, T.K., Laird, G.M., and Lockwood, M.S., 1988a, Geologic map of the Iditarod C-3 quadrangle, Alaska: Alaska Division of Geological and Geophysical Surveys Professional Report 96, 13 p., 1 pl., scale 1:63,360.
- Bundtzen, T.K., Miller, M.L., Bull, K.F., and Laird, G.M., 1988b, Geology and mineral resources of the Iditarod mining district, Iditarod B-4 and B-5 quadrangles, westcentral Alaska: Alaska Division of Geological and Geophysical Surveys Public-Data File 88-19, 44 p., 1 pl., scale 1:63,360.
- Bundtzen, T.K., Miller, M.L., and Kline, J.T., 1985, Geology of heavy mineral placer deposits of the Iditarod and Innoko precincts, western Alaska, in Madonna, J.A., ed., *Conference on Alaskan Placer Mining, 7th, Proceedings: Fairbanks, Alaska, Alaska Prospectors Publishing Company*, p. 35-41.
- Bundtzen, T.K., Miller, M.L., and Laird, G.M., 1986, Prospect

- examination of the Wyrick placer/lode system, Granite Creek, Iditarod-George mining district, Iditarod B-2 quadrangle, Alaska: Alaska Division of Geological and Geophysical Surveys Public-Data File 86-29, 10 p., 1 pl., scale 1:63,360.
- Cady, W.M., Wallace, R.E., Hoare, J.M., and Webber, E.J., 1955, The central Kuskokwim region, Alaska: U.S. Geological Survey Professional Paper 268, 132 p.
- Erdman, J.A., and Modreski, P.J., 1984, Copper and cobalt in aquatic mosses and stream sediments from the Idaho cobalt belt: *Journal of Geochemical Exploration*, v. 20, p. 75-84.
- Gray, J.E., Arbogast, B.F., and Hudson, A.E., 1988a, Geochemical results and sample locality map of the stream-sediment and nonmagnetic, heavy-mineral-concentrate samples for the Iditarod quadrangle, Alaska: U.S. Geological Survey Open-File Report 88-221, 69 p., 1 pl., scale 1:250,000.
- Gray, J.E., Frost, T.P., Goldfarb, R.J., and Detra, D.E., 1990, Gold associated with cinnabar- and stibnite-bearing deposits and mineral occurrences in the Kuskokwim River region, southwestern Alaska, in Goldfarb, R.J., Nash, T.J., and Stoesser, J.W., eds., *Geochemical studies in Alaska*: U.S. Geological Survey Bulletin 1950, p. D1-D6.
- Gray, J.E., Ryder, J.L., Sanzolone, R.F., McHugh, J.B., and Ficklin, W.H., 1988b, Analytical data and sample locality map for stream water samples from the Iditarod quadrangle, Alaska: U.S. Geological Survey Open-File Report 88-55, 23 p., 1 pl., scale 1:250,000.
- Hopkins, D.M., Gray, J.E., McDougal, C.M., and Slaughter, K.E., 1991, Mercury, gold, thallium, and tellurium data and sample locality map of stream-sediment samples from the Iditarod quadrangle, Alaska: U.S. Geological Survey Open-File Report 91-283-A, 37 p., 1 pl., scale 1:250,000.
- Jones, K.C., 1985, Gold, silver and other elements in aquatic bryophytes from a mineralised area of North Wales, U.K.: *Journal of Geochemical Exploration*, v. 24, p. 237-246.
- Kimball, A.L., 1969, Reconnaissance sampling of decomposed monzonite near Flat, Alaska: U.S. Bureau of Mines Open-File Report 6-69, 39 p.
- Learned, R.E., Chao, T.T., and Sanzolone, R.F., 1985, A comparative study of stream water and stream sediment as geochemical exploration media in the Rio Tanama porphyry copper district, Puerto Rico: *Journal of Geochemical Exploration*, v. 24, p. 175-195.
- McGimsey, R.G., Miller, M.L., and Arbogast, B.F., 1988, Paper version of analytical results, and sample locality map for rock samples from the Iditarod quadrangle, Alaska: U.S. Geological Survey Open-File Report 88-421-A, 110 p., 1 pl., scale 1:250,000.
- Miller, M.L., 1990, Mafic and ultramafic rocks of the Dishna River area, north-central Iditarod quadrangle, west-central Alaska, in Dover, J.H., and Galloway, J.P., eds., *Geologic studies in Alaska by the U.S. Geological Survey, 1989*: U.S. Geological Survey Bulletin 1946, p. 44-50.
- Miller, M.L., Bradshaw, J.Y., Kimbrough, D.L., Stern, T.W., and Bundtzen, T.K., 1991, Isotopic evidence for Early Proterozoic age of the Idono Complex, west-central Alaska: *Journal of Geology*, v. 99, p. 209-223.
- Miller, M.L., and Bundtzen, T.K., 1987, Geology and mineral resources of the Iditarod quadrangle, west-central Alaska [abs.], in Sachs, J.S., ed., *U.S.G.S. research on mineral resources, 1987—Programs and abstracts*: U.S. Geological Survey Circular 995, p. 46-47.
- in press, Geologic map of the Iditarod quadrangle, Alaska: U.S. Geological Survey Miscellaneous Field Studies Map, scale 1:250,000.
- Miller, M.L., Bundtzen, T.K., and Gray, J.E., in press, Mineral resource assessment of the Iditarod quadrangle, Alaska: U.S. Geological Survey Miscellaneous Field Studies Map, scale 1:250,000.
- Miller, W.R., Ficklin, W.H., and Learned, R.E., 1982, Hydrogeochemical prospecting for porphyry copper deposits in the tropical-marine climate of Puerto Rico: *Journal of Geochemical Exploration*, v. 16, p. 217-233.
- Saether, O.M., and Bölviken, B., 1983, Anomalous metal contents of aquatic bryophytes at Tverrfjellet and Snertingdal, central Norway [abs.], in Björklund, A., and Koljonen, T., eds., *10th International Geochemical Exploration Symposium: Espoo/Helsinki, Finland*, Geological Survey of Finland, p. 69.
- Sainsbury, C.L., and MacKevett, E.M., Jr., 1965, Quicksilver deposits of southwestern Alaska: U.S. Geological Survey Bulletin 1187, 89 p.
- Shacklette, H.T., 1984, The use of aquatic bryophytes in prospecting: *Journal of Geochemical Exploration*, v. 21, p. 89-93.
- Turner, L.D., and Ikramuddin, Mohammed, 1982, Electrothermal atomic absorption determination of gold, silver, and arsenic in stream waters and their relationship to gold-silver occurrences in the Republic Graben, N.E. Washington, in Levinson, A.A., ed., *Precious metals in the northern Cordillera: Vancouver, British Columbia, Canada, Symposium Proceedings of the Association of Exploration Geochemists*, p. 79-88.
- Whitehead, N.E., and Brooks, R.R., 1969, Aquatic bryophytes as indicators of uranium mineralization: *Bryologist*, v. 72, p. 501-507.

Reviewers: Clifford J. Taylor and Richard J. Goldfarb

Geochemically Anomalous Areas in the West-Central Part of the Howard Pass Quadrangle, National Petroleum Reserve, Alaska: Evidence for Sediment-Hosted Zn-Pb-Ag-Ba Mineralization

By Karen D. Kelley, J. Carter Borden, Elizabeth A. Bailey, David L. Fey, Jerry M. Motooka and Bruce H. Roushey

Abstract

A detailed geochemical survey was conducted in 1991 in the west-central part of the Howard Pass quadrangle in the vicinity of three geochemically anomalous drainage basins that were delineated during a previous geochemical survey. These basins have similar geologic settings and geochemical signatures to those surrounding the Red Dog deposit in the westernmost Brooks Range. The Red Dog deposit is a zinc-lead-silver massive sulfide and barite deposit hosted in black shale of the Lower or Middle Pennsylvanian to Lower Mississippian Kuna Formation.

The three drainage basins are characterized by highly anomalous concentrations of Ag, As, Ba, Cd, Sb, and Zn in minus-30-mesh stream-sediment samples. One of these was collected from Drenchwater Creek, which was subsequently found to contain sulfide and barite mineralization similar to that at Red Dog. Two other samples—from Twistem Creek and an unnamed tributary of the Kiligwa River—represent basin areas of approximately 20 to 26 km². The goal of the detailed geochemical sampling conducted in 1991 was to more accurately locate the mineralized areas and to possibly locate sources of the anomalies.

Several geochemically anomalous basins between Twistem Creek and the easternmost tributaries of the Kiligwa River were located that were not sampled during the regional survey; two samples, representing basin areas of less than 13 km², contain highly anomalous concentrations of Ag (2 ppm), Ba (>5,000 ppm), Cd (2.7–4.8 ppm), and Zn (700–1,000 ppm) that are comparable to many of the samples from the Red Dog and Drenchwater Creek areas. These high values in sediment samples probably reflect sulfide and barite mineralization, although sulfide minerals other than pyrite have not yet been identified.

INTRODUCTION

The Howard Pass quadrangle is located in the western Brooks Range, partially within the southern National

Petroleum Reserve in Alaska (NPRA) (fig. 1). It lies within an east-west-trending fold-thrust belt of Paleozoic and Mesozoic sedimentary rocks that extends along the entire western and central Brooks Range. Mississippian rocks within this belt host several massive base-metal sulfide and barite mineral occurrences and deposits (fig. 1). Largest among these is the Red Dog deposit in the westernmost Brooks Range, a shale-hosted stratiform zinc-lead-silver-barite deposit now in production (Plahuta, 1978; Moore and others, 1986; Lange and Nokleberg, 1987).

In 1977–78, a regional geochemical survey was conducted as part of the mineral resource assessment of the southern NPRA (Churkin and others, 1978), which included most of the Howard Pass quadrangle. Stream-sediment samples were collected at a sample density of approximately 1 sample per 25 km² (Theobald and Barton, 1978). Although not within the NPRA, nine samples were also collected from Red Dog Creek and other drainages surrounding the Red Dog deposit in order to characterize the geochemical associations and concentrations of elements characteristic of this deposit type. Several sediment samples from drainage basins within the Howard Pass quadrangle that are underlain by lithologies similar to those that host the Red Dog deposit contain anomalous concentrations of base metals and barium. One of these geochemically anomalous areas is Drenchwater Creek in the west-central part of the Howard Pass quadrangle. Followup studies led to the discovery of the Drenchwater Creek deposit (fig. 1), a base-metal sulfide deposit in Mississippian(?) chert and shale (Nokleberg and Winkler, 1978; Churkin and others, 1978; Jansons and Baggs, 1980).

The 1977–78 regional geochemical survey also identified two drainage basins east of Drenchwater Creek containing the same geochemical signature. The basins are relatively large areas (approximately 20–26 km²),

and therefore locating the source of the anomalies may be difficult, particularly if the source is poorly exposed. In the summer of 1991, detailed geochemical sampling was conducted in the vicinity of these two anomalous drainage basins in order to better define the anomalous areas, and to possibly locate sources of the anomalies. Rock samples were collected from float and outcrop, and streams were sampled at an average density of 1 sample per 7 km², primarily from first- or second-order basins. This paper presents an interpretation of the geochemical results of the detailed sampling program.

METHODS

During the regional geochemical survey in 1977-78, 583 stream sediments were collected, dried, and sieved to minus-30-mesh. Heavy-mineral-concentrate samples were also collected by panning bulk stream sediment at each site. Magnetic and heavy-liquid separations were used to obtain a nonmagnetic heavy-mineral-concentrate fraction. The minus-30-mesh stream-sediment and nonmagnetic heavy-mineral-concentrate samples were analyzed for 31 elements by semiquantitative emission spectrography (ES) (Grimes and Marranzino, 1968). Re-

sults of the ES analyses are included in Theobald and Barton (1978). In 1990, the same samples were submitted for additional analyses by inductively coupled plasma-atomic emission spectrography (ICP-AES) using an organometallic halide partial extraction method (Motooka, 1988), which was developed as an exploration method for low-level analysis of 10 ore-related elements (Ag, As, Au, Bi, Cd, Cu, Mo, Pb, Sb, and Zn). Analytical results of the ICP-AES analyses are included in Kelley and others (1990).

During the detailed sampling program in 1991, 47 stream-sediment and nonmagnetic heavy-mineral-concentrate samples were collected from within the study area and prepared by methods similar to those used for the regional survey. In addition, 32 rock samples were collected either from float in the stream drainages or from outcrop. All samples were analyzed for 31 elements by ES, and the minus-30-mesh stream sediments and rock samples were analyzed for 10 elements using the organometallic halide partial extraction of Motooka (1988). In addition, the samples were analyzed for 40 elements by ICP-AES, using a low-temperature multiacid digestion (Crock and others, 1983), resulting in total dissolution of the sample as opposed to the partial extraction used in the 10-element ICP-AES method.

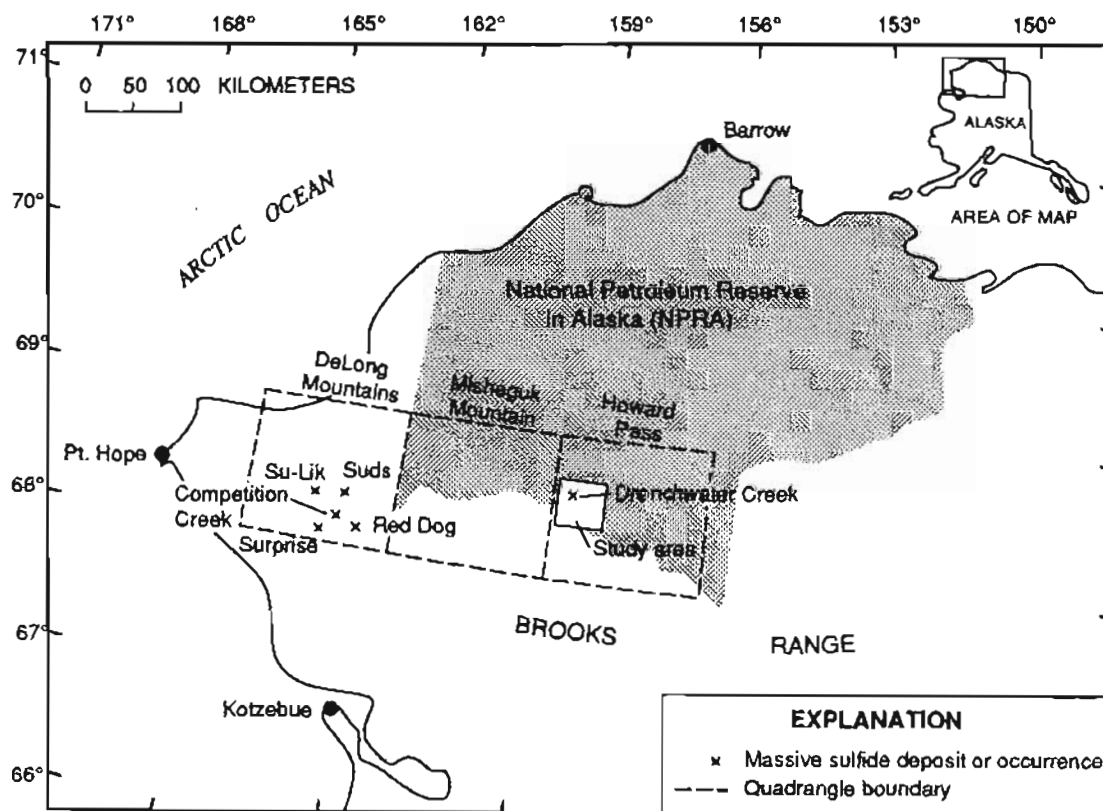


Figure 1. Location of study area, western Brooks Range, Alaska.

GEOLOGY

The Brooks Range is a fold and thrust belt trending east-west for approximately 800 km across northern Alaska that formed during an orogenic event that began in Late Jurassic time and culminated during the mid-Cretaceous. During this orogeny, a stable continental shelf that contained Devonian to Lower and Middle Jurassic sedimentary rocks was broken up and telescoped northward by numerous thrust sheets (Mayfield and others, 1983). The presence of these stacked and folded Paleozoic and Mesozoic allochthonous thrust sequences has been recognized by several authors, including Ellersieck and others (1979), Mull (1982), Mayfield and others (1983), and Moore and others (1986). In the western Brooks Range, at least seven major sedimentary and igneous allochthons have been recognized (Mayfield and others, 1983; Moore and others, 1986). The five structurally lowest allochthons are composed dominantly of sedimentary rocks, whereas the two highest allochthons are composed mainly of volcanic and plutonic rocks. The allochthons dominated by sedimentary rocks are composed of Mississippian through Cretaceous chert, shale, limestone, and sandstone (Mayfield and others, 1983). The lowest is termed the Brooks Range allochthon in the western Brooks Range and the Endicott Mountains allochthon in the central Brooks Range. It is continuously exposed in erosional windows as far west as the Red Dog Creek area in the DeLong Mountains quadrangle, across the Misheguk Mountain quadrangle, and in parts of the Howard Pass quadrangle. All of the known massive sulfide occurrences and deposits are hosted by Mississippian to Pennsylvanian chert and shale of this lowermost allochthon (Nokleberg and Winkler, 1982; Moore and others, 1986).

The study area comprises mainly rocks of the lowermost allochthon, consisting primarily of Mississippian to Jurassic sedimentary rocks (fig. 2). The oldest rocks include Mississippian to Pennsylvanian dark-gray to black chert, siliceous shale, and silicified mudstone (Tailleur and others, 1966); these rocks are probably lithologically equivalent to the Kuna Formation of the Lisburne Group (Mull and others, 1982; Young and Moore, 1987), which hosts the Red Dog deposit (Moore and others, 1986). Locally in the Drenchwater Creek area, volcanic and volcanoclastic rocks are found within this Mississippian and Pennsylvanian section (Nokleberg and Winkler, 1982; Lange and others, 1985).

Disconformably overlying the Mississippian and Pennsylvanian rocks are rocks of the Etivluk Group (Mull and others, 1982). Within the lowermost allochthon, the Etivluk Group consists of the Permian Siksikpuk Formation and the Lower Triassic to Middle Jurassic Otuk Formation (Mull and others, 1982), rocks formerly assigned to the Shublik Formation (Tailleur and

others, 1966). The Siksikpuk Formation is composed of a 100 to 150 m thick sequence of gray to maroon siltstone, mudstone, and chert, with an upper gray shale horizon. The overlying Otuk Formation is about 100 to 150 m thick and consists of dark-gray to black shale that grades up successively into dark-gray to black, thinly interbedded, siliceous limestone and shale containing abundant pelecypod fossils (Mull and others, 1982).

Locally in the southwest and northeast parts of the study area, chert and shale of Pennsylvanian to Jurassic age contain numerous mafic sills and dikes. These sedimentary and intrusive rocks are shown as a separate unit on figure 2.

REGIONAL GEOCHEMICAL SURVEY

During the 1977-78 regional geochemical survey of the southern NPRA, 583 minus-30-mesh stream-sediment and nonmagnetic heavy-mineral-concentrate samples were collected from the Howard Pass and Misheguk Mountain quadrangles, and 9 samples were collected from drainages surrounding the Red Dog massive sulfide deposit in the DeLong Mountains quadrangle (Theobald and Barton, 1978). The following generalizations can be made, based on data from the Red Dog area, regarding geochemical exploration specifically for stratabound sediment-hosted Zn-Pb-Ag deposits in the arctic environment:

1. Minus-30-mesh stream-sediment samples are better at targeting mineralized areas than nonmagnetic heavy-mineral-concentrate samples. None of the heavy-mineral concentrates surrounding Red Dog contain detectable Ag (1 ppm lower determination limit), two contain high concentrations of Zn (500-700 ppm), and three contain high concentrations of Pb (500-5,000 ppm) (Theobald and Barton, 1978). Stream-sediment samples, on the other hand, contain extremely high concentrations of all three elements. For example, one sediment sample collected near the discovery outcrop contains >20,000 ppm Pb and 2,000 ppm Zn (Tailleur, 1970), and immediately downstream from the deposit (less than 2.5 km), samples contain as much as 10 ppm Ag, 10,000 ppm Pb, and 6,000 ppm Zn (Theobald and Barton, 1978; Kelley and others, 1990). These data suggest that either (1) weathering of this deposit type in the arctic environment is primarily chemical, resulting in a higher degree of hydromorphic dispersion relative to mechanical dispersion, or (2) the sulfide minerals are so fine grained (clay sized) that they are removed during panning. Only minus-30-mesh stream-sediment data are considered further.
2. Zinc and Ag are the best pathfinder elements, but As, Ba, Cd, and Sb are also reasonably good. Lead is not a good pathfinder element in minus-30-mesh stream-sediment samples. Except for samples collected immediately downstream from the deposit, most sediment

samples contain background concentrations of Pb (25–30 ppm) (Kelley and others, 1990). Lead is typically considered to be less mobile than Zn or Ag, and thus is not transported as readily during chemical weathering (Levinson, 1974). High concentrations of Zn and Ag, and not Pb, in minus-30-mesh stream-sediment samples is further evidence that hydromorphic processes are important in this environment.

For this study, the regional-scale minus-30-mesh stream-sediment data from the Misheguk Mountain and Howard Pass

quadrangles were evaluated statistically and by means of histograms showing the frequency distribution of the data. Threshold concentrations for selected elements in minus-30-mesh stream-sediment samples were determined by evaluation of the histograms and of the spatial distribution of the data, and by comparison with concentrations in sediment samples from the vicinity of the Red Dog deposit (table 1). Concentrations equal to or greater than these threshold concentrations are considered to be anomalous and probably related to mineralizing processes.

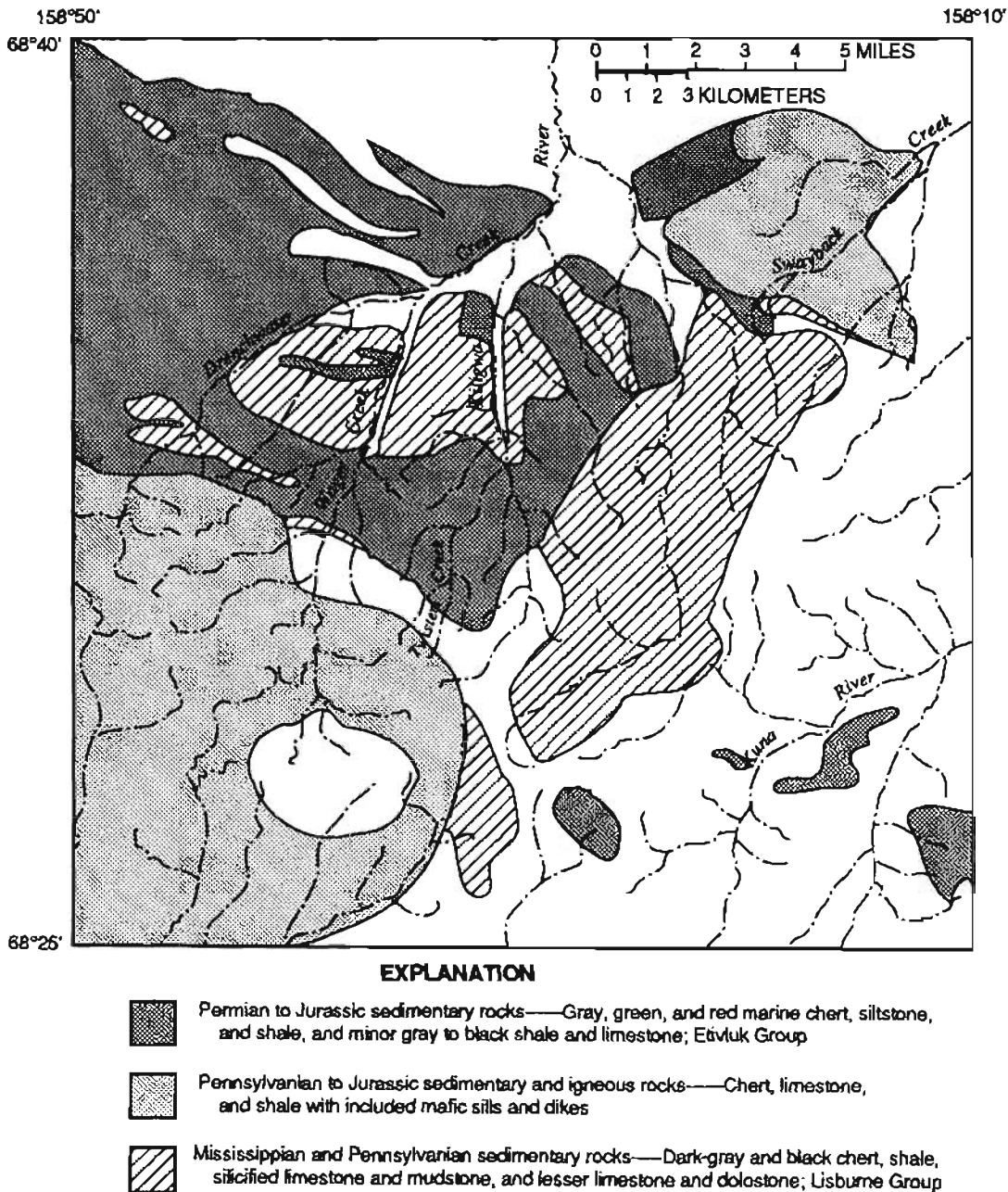


Figure 2. Generalized bedrock geologic map showing Mississippian to Jurassic units in study area [compiled by J.S. Schmidt and others, written commun. (1990) from previously published maps (Tailleur and others, 1966)].

Anomalous concentrations of Ag, As, Ba, Cd, Sb, and Zn occur in minus-30-mesh sediment samples surrounding the Drenchwater Creek deposit (table 1; fig. 3). The best indicators of mineralization appear to be Ag (0.72–1.4 ppm), Ba (7,000–>20,000 ppm), and Zn (460–800 ppm), although most of the samples also contain anomalous As (14–15 ppm), Cd (1.4–3.6 ppm), and Sb (1.9–2.7 ppm). Manganese, which is considered to be a good pathfinder element for some sediment-hosted massive sulfide deposits (Maynard, 1983, 1991), is also anomalous in two of the samples. Lead concentrations are mostly below threshold values, although one sample contains 90 ppm. Two additional drainages east of Drenchwater Creek are delineated by the same geochemical association (fig. 3), and are underlain by Mississippian to Jurassic shale and chert (fig. 2). These drainages are Twistem Creek and an unnamed tributary of the Kiligwa River east of Twistem Creek (fig. 3). The basin areas represented are relatively large (approximately 20–26

km²), and therefore detailed studies were conducted in order to more accurately locate mineralized areas.

DETAILED GEOCHEMICAL SURVEY

During the 1991 detailed geochemical survey, stream sediment samples were collected from the tributaries of Wager and Twistem Creeks and from the Kiligwa and Kuna Rivers (fig. 4). Most of the samples collected between Twistem Creek and the tributaries of the Kiligwa River are anomalous in Ag and Zn, and many also contain high concentrations of As, Ba, Cd, and Sb (table 1; fig. 4). Two samples contain 2 ppm Ag, 2.7–4.8 ppm Cd, and 700–1,000 ppm Zn; these values are comparable to many of the highly anomalous samples from the Red Dog area and are equal to or greater than those from Drenchwater Creek (table 1). These high values most likely reflect mineralization.

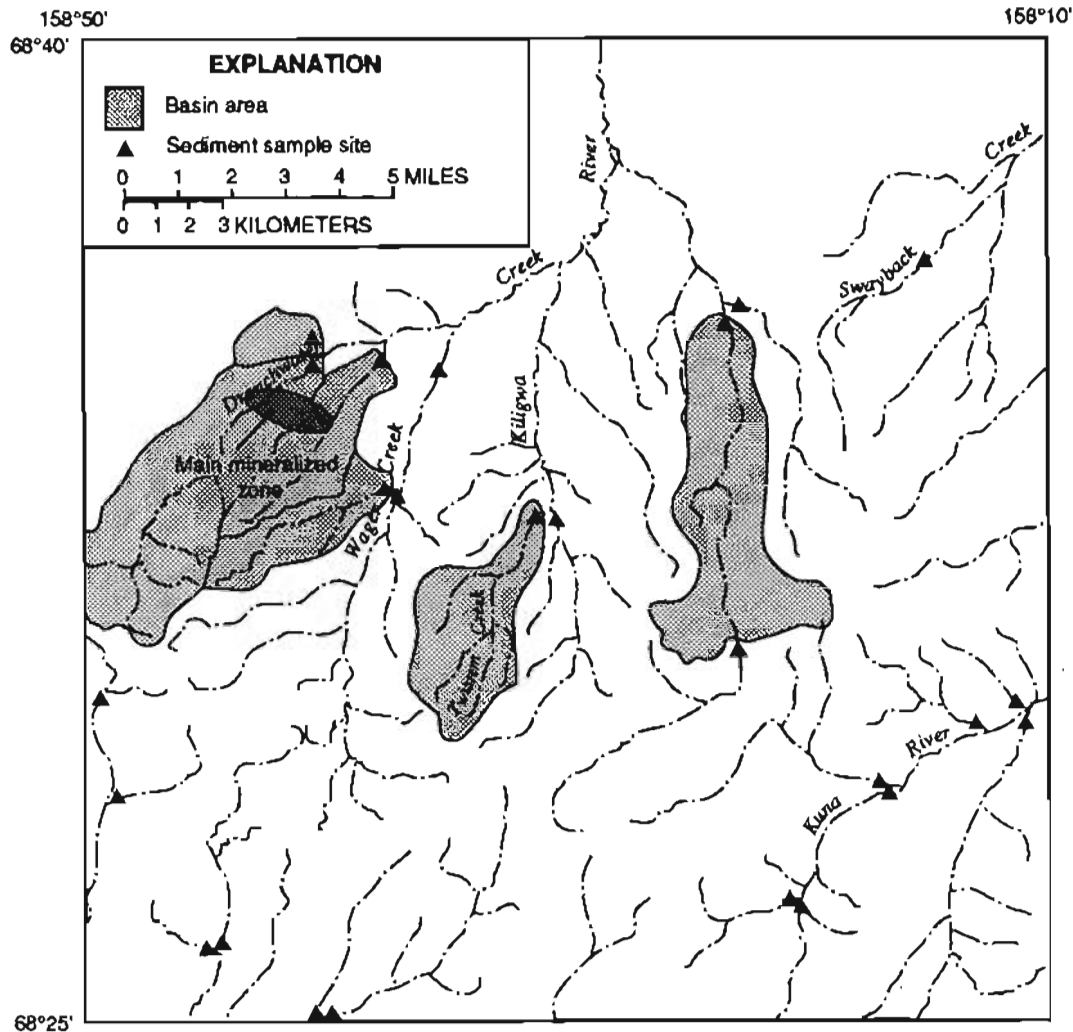


Figure 3. Stream-sediment sampling localities from regional 1977–78 geochemical survey and drainage basins anomalous in Ag, As, Ba, Cd, Sb, and Zn. (Threshold values for these elements listed in table 1.)

One of these samples is from a small first-order tributary of Twistem Creek representing a basin area of only about 1.3 km². The other is from a tributary of the Kiligwa River that was not sampled during the regional survey. The basin area represented by this sample is about 13 km² (fig. 4).

Almost all other stream-sediment samples collected in the Twistem Creek-Kiligwa River area contain relatively lower but anomalous concentrations of Ag, As, Cd, Sb, and Zn (fig. 4; table 1). All of these geochemically anomalous basins also contain anomalous concentrations of Ba ($\geq 5,000$ ppm, the upper determination limit by ES for this study). Manganese concentrations are also anomalous (3,000–9,800 ppm) in most of these samples. High concentrations of Ni (150–300 ppm) and Co (70–150 ppm) in several samples (table 1) probably reflect the presence of abundant pyrite, which often contains anomalously high concentrations of these elements (Levinson, 1974).

The entire area between Twistem Creek and the headwaters of the Kuna River is underlain by shale and chert (fig. 2), rock types that are permissive for hosting massive sulfide deposits. Chert and shale samples were collected from float or outcrop in several localities (fig. 5) and analyzed geochemically. Concentrations of selected elements are listed in table 2. For comparison, average worldwide concentrations of chert and shale are listed in table 3. Most samples collected from the study area contain concentrations of Ag and Zn that are comparable to average concentrations in shale or chert as reported in the literature. However, several samples contain relatively high concentrations of selected elements. For example, one chert sample (KWR007R) collected from outcrop contains high Ag (10 ppm by ES), Mn (5,000 ppm), and Zn (200 ppm). In addition, black pyritic shale collected from float in the same drainage (KWR005R) contains 1 ppm Ag, 260 ppm As and 100 ppm Cu. Silty shale collected from float farther west

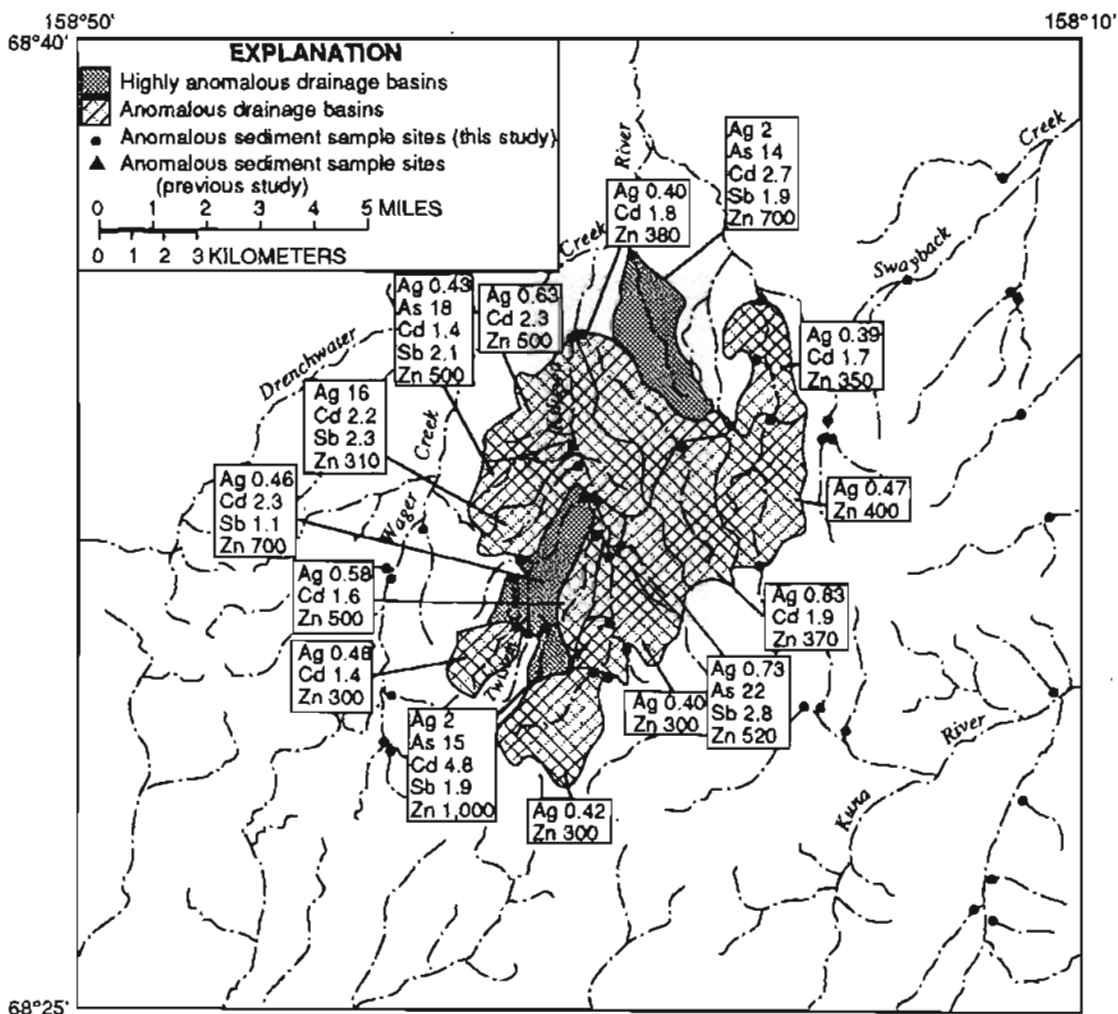


Figure 4. Drainage basin areas delineated during this study that are geochemically anomalous in Ag, As, Cd, Sb, and Zn. All of these basins are also anomalous in Ba ($\geq 5,000$ ppm). Values in parts per million.

(KWR033R) contains 10 ppm As and 270 ppm Zn. Several samples of gray chert and greenish-gray shale contain visible barite and have correspondingly anomalous concentrations of Ba (>5,000 ppm). Sulfide minerals other than pyrite have not yet been positively identified. Petrographic studies on many of the shale and chert samples with high concentrations of base metals are in progress.

CONCLUSIONS

Minus-30-mesh stream-sediment samples are more effective than nonmagnetic heavy-mineral-concentrate samples in delineating stratiform massive sulfide mineralization at the Red Dog and Drenchwater Creek deposits. Silver and Zn are the most reliable pathfinder elements, although As, Ba, Cd, and Sb are also effective; lead is not an effective pathfinder element for this type of deposit in the arctic environment. The anomalous geochemical association (Ag-As-Ba-Cd-Sb-Zn) is also

present in samples collected between Twistem Creek and the easternmost tributaries of the Kiligwa River. Several geochemically anomalous basins were located that were not delineated by the regional survey owing to the low sample density. Two of these contain concentrations of Ag, As, Cd, Co, Mn, Ni, Sb, and Zn that are equal to or greater than concentrations in samples from Drenchwater Creek and similar to most samples from the Red Dog area. These high concentrations most likely reflect sulfide mineralization, although only pyrite was observed in the field. The two basin areas represented by these high concentrations are less than 13 km² in area, compared with the previously delineated basins that were 20 to 26 km² in area. Several chert or shale samples collected during this study contain high concentrations of Ag (up to 10 ppm), As (23–260 ppm), Ba (>5,000 ppm), Mn (3,000–5,000 ppm), and Zn (200–270 ppm). These values are relatively high compared with average concentrations of these elements in unaltered and unmineralized chert and shale as reported in the literature and may reflect sulfide mineralization.

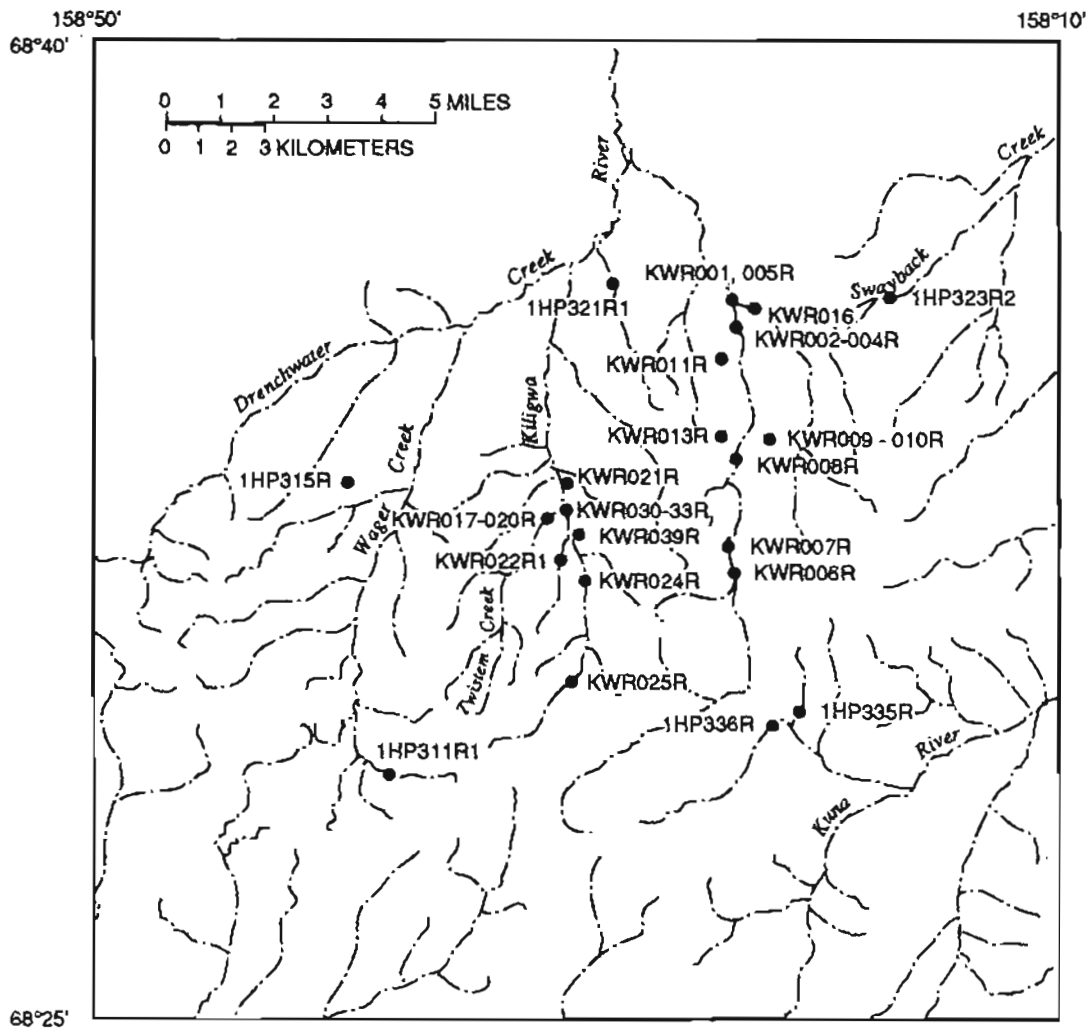


Figure 5. Locations of rock samples collected from study area.

Table 1. Threshold concentrations and ranges of anomalous concentrations of selected elements in minus-30-mesh stream-sediment samples from this study and comparison with results from the Red Dog and Drenchwater Creek areas

{All values in parts per million (ppm); n, number of samples}

Element	Threshold concentration	Range in concentrations in sediment samples from this study* (n=47)	Red Dog Creek area (n=9)	Drenchwater Creek area (n=4)
Ag-----	0.3	0.3-2	0.55-6.1	0.72-1.4
As -----	14	14-22	19-46	14-15
Ba ¹ -----	5,000	5,000->5,000	>20,000	7,000->20,000
Cd-----	1.4	1.4-4.8	1.4-25	1.4-3.6
Co-----	70	70-150	not anomalous	not anomalous
Cu-----	150	150-200	150	200
Mn -----	3,000	3,000-9,800	not anomalous	3,000
Ni-----	150	150-300	not anomalous	150
Pb-----	30	30-50	30-3,400	30-90
Sb-----	1.1	1.1-2.8	1.3-35	1.9-2.7
Zn-----	300	300-1,000	300-6,000	460-800

*Most anomalous concentrations are from a sample collected <2.5 km downstream from deposit where exposed at the surface.

¹Includes only concentration ranges equal to or greater than threshold values

¹Upper limit of determination for Ba is 20,000 ppm in the regional survey (Theobald and Barton, 1978) and 5,000 ppm for this study.

Acknowledgments.—We wish to thank John Gray and Gary Nowlan for their constructive and helpful reviews of this manuscript. Discussions with Gil Mull of the Alaska Division of Geological and Geophysical Surveys greatly improved our understanding of the geology of the area. We would also like to thank our helicopter pilot, Jim Tasakos, for getting us safely to and from the study area, often in spite of some typically unpredictable weather conditions.

REFERENCES CITED

- Adachi, M., Yamamoto, K., and Sugisaki, R., 1986, Hydrothermal chert and associated siliceous rocks from the northern Pacific: Their geologic significance as indication of ocean ridge activity: *Sedimentary Geology*, v. 47, p. 125-148.
- Churkin, Michael, Jr., Mayfield, C.F., Theobald, P.K., Barton, H.N., Nokleberg, W.J., Winkler, G.R., and Huie, C., 1978, Geological and geochemical appraisal of metallic mineral resources, southern National Petroleum Reserve in Alaska: U.S. Geological Survey Open-File Report 78-70A, 82 p.
- Crock, J.G., Lichte, F.E., and Briggs, P.H., 1983, Determination of elements in National Bureau of Standards Geologic Reference Material SRM 278 obsidian and SRM 688 basalt by inductively coupled argon plasma-atomic emission spectrometry: *Geostandards Newsletter*, v. 7, p. 335-340.
- Ellersieck, I., Mayfield, C.F., Tailleux, I.L., and Curtis, S.M., 1979, Thrust sequences in the Misheguk Mountain quadrangle, Brooks Range, Alaska: U.S. Geological Survey Circular 804-B, p. B8-B9.
- Grimes, D.J., and Marranzino, A.P., 1968, Direct-current arc and alternating-current spark emission spectrographic field methods for the semiquantitative analysis of geologic materials: U.S. Geological Survey Circular 591, 6 p.
- Jansons, Uldis, and Baggs, D.W., 1980, Mineral investigations of the Misheguk Mountain and Howard Pass quadrangles, Alaska: U.S. Bureau of Mines Open-File Report 38-80, 76 p.
- Kelley, K.D., Slaughter, K.E., and Motooka, J.M., 1990, Results of inductively coupled plasma-atomic emission spectroscopy of minus 30-mesh stream sediment samples from within and adjacent to the National Petroleum Reserve, Alaska: U. S. Geological Survey Open-File Report 90-501, 19 p., 1 sheet, scale 1:500,000.
- Lange, I.M., and Nokleberg, W.J., 1987, Geologic setting, petrology, and geochemistry of stratiform sphalerite-galena-barite deposits, Red Dog Creek and Drenchwater Creek areas, northwestern Brooks Range, Alaska—A Reply to Young and Moore, 1987: *Economic Geology*, v. 82, no. 4, p. 1079-1081.
- Lange, I.M., Nokleberg, W.J., Plahuta, J.T., Krouse, H.R., and Doe, B.R., 1985, Geologic setting, petrology, and geochemistry of stratiform sphalerite-galena-barite deposits, Red Dog Creek and Drenchwater Creek areas, northwestern Brooks Range, Alaska: *Economic Geology*, v. 80, p. 1896-1926.
- Levinson, A.A., 1974, Introduction to exploration geochemistry: Calgary, Alberta, Canada, Applied Publishing Ltd., 612 p.

Table 2. Concentrations of selected elements in rock samples from the study area

{All values in parts per million (ppm); all samples from float unless otherwise noted by oc (outcrop). Abbreviations: ICP-P, inductively coupled plasma-atomic emission spectrography, partial digestion; ICP-T, inductively coupled plasma-atomic emission spectrography, total digestion; ES, emission spectrography; N, not detected at the lower limit of determination shown}

Sample Number	Ag ^(ICP-P)	Ag ^(ES)	As ^(ICP-P)	As ^(ICP-T)	Ba ^(ES)	Cd ^(ICP-P)	Cu ^(ICP-T)	Mn ^(ICP-T)	Sb ^(ICP-P)	Pb ^(ICP-P)	Zn ^(ICP-T)	Rock description
1HP311R1	.40	N .5	2.0	<10	700	.34	7	1,500	N .67	5.2	86	chert; oc
1HP315R	N .067	N .5	3.4	<10	>5,000	.042	70	3,000	.71	6.1	110	shale
1HP321R1	2.7	3	3.6	<10	500	.25	30	150	1.6	3.9	59	shale
1HP323R2	.64	1	2.0	<10	1,500	.18	30	100	N .67	2.3	49	chert
1HP335R	N .067	N .5	N .67	<10	>5,000	.055	50	3,000	N .67	2.7	110	chert
1HP336R	.48	.5	N .67	<10	700	.15	30	150	N .67	1.9	53	black chert; oc
KWR001R	N .067	N .5	1.8	<10	700	.25	30	700	N .67	3.6	100	black chert
KWR002R	.30	.7	1.1	<10	1,000	.080	30	1,000	N .67	2.8	54	black chert
KWR003R	N .067	.5	11	23	3,000	.032	150	300	.84	14	92	silicified rock with pyrite
KWR004R	.12	<.5	1.2	<10	1,500	.033	7	70	N .67	1.4	25	boxwork silica/chert fragments
KWR005R	.32	1	41	260	500	.17	100	100	2.1	7.1	10	black shale with pyrite
KWR006R	.28	.7	1.3	<10	1,500	.082	15	300	N .67	1.5	63	chert
KWR007R	2.5	10	4.5	10	1,000	.24	50	5,000	.93	3.1	200	chert with Fe/Mn stain; oc
KWR008R	1.2	2	3.0	<10	1,000	.32	50	700	.81	1.8	100	black chert; oc
KWR009R	.30	.5	4.1	<10	2,000	.049	20	2,000	.98	5.7	72	chert with Fe/Mn stain; oc
KWR010R	.35	2	2.2	<10	1,000	.041	30	30	.85	.77	14	gray-blue chert; oc
KWR011R	.073	N .5	2.6	<10	5,000	N .020	10	70	.99	.78	8	chert with Fe stain; oc
KWR013R	.082	N .5	6.8	10	>5,000	N .020	30	100	1.1	4.1	39	gray chert; oc
KWR016R	.074	N .5	1.0	<10	2,000	.51	30	3,000	N .67	1.2	56	cherty limestone; oc
KWR017R	.86	1.5	4.9	10	500	.035	20	50	N .67	1.6	21	black chert with Fe stain
KWR018R	N .067	N .5	N .67	<10	700	.31	20	700	N .67	1.5	56	gray chert
KWR019R	.076	N .5	.74	<10	>5,000	.065	30	200	N .67	1.2	26	gray chert
KWR020R	N .067	N .5	N .67	<10	>5,000	N .020	70	200	N .67	6.3	71	siltstone
KWR021R	N .067	N .5	N .67	<10	>5,000	.024	50	500	N .67	13	130	greenish gray silty shale; oc
KWR022R1	N .067	N .5	N .67	<10	>5,000	.22	30	1,000	N .67	7.8	230	shale; oc
KWR024R	.074	N .5	1.5	<10	1,500	N .020	20	70	N .67	2.2	15	chert with Fe stain
KWR025R	N .067	N .5	N .67	<10	5,000	.026	20	200	N .67	7.1	130	chert; oc
KWR030R	N .067	N .5	N .67	<10	2,000	.037	100	500	N .67	3.6	130	chert with pyrite
KWR031R	N .067	N .5	N .67	<10	>5,000	.90	15	700	N .67	4.0	38	chert
KWR033R	N .067	N .5	3.0	10	700	.31	30	700	N .67	6.3	270	silty shale
KWR037R	N .067	N .5	3.4	<10	2,000	.96	30	700	.68	3.0	74	chert
KWR039R	.075	N .5	1.9	<10	5,000	.025	50	300	N .67	4.8	29	chert with pyrite; oc

Table 3. Average worldwide abundances of selected trace elements in unaltered and unmineralized shale and chert

[All values in parts per million (ppm). nd, no data. References: (1) Levinson, 1974; (2) Vine and Tourtelot, 1970; (3) Maynard, 1991; (4) Adachi and others, 1986]

Rock type and reference	Ag	As	Ba	Cd	Co	Cr	Cu	Mn	Ni	Pb	Sb	Zn
Shale (1)—————	0.05	15	700	0.2	20	100	50	850	70	20	1	100
Black shale (2)—————	< 1	nd	300	nd	10	100	70	150	50	20	nd	300
Host shale of Pb- and Zn-rich deposits (3)——	nd	nd	6,550	nd	3	nd	28	330	40	24	nd	129
Host chert of Pb- and Zn-rich deposits (3)——	nd	nd	5,047	nd	2	nd	18	123	16	13	nd	35
Oceanic chert (4)—————	nd	nd	450	nd	7	nd	130	2700	26	12	nd	35
Continental chert (4)—————	nd	nd	140	nd	4	nd	59	253	14	8	nd	29

Mayfield, C.F., Tailleir, I.L., and Ellersieck, I., 1983, Stratigraphy, structure, and palinspastic analysis of the western Brooks Range, northwestern Alaska: U.S. Geological Survey Open-File Report 83-779, 58 p.

Maynard, J.B., 1983, Geochemistry of sedimentary ore deposits: Springer-Verlag, New York, 305 pp.

———1991, Shale-hosted deposits of Pb, Zn, and Ba: Syngenetic deposition from exhaled brines in deep marine basins, in Force, E.R., Eidel, J.J., and Maynard, J.B., eds., Sedimentary and diagenetic mineral deposits: A basin analysis approach to exploration: Reviews in Economic Geology, v. 5., p. 177-183.

Moore, D.W., Young, L.E., Modene, J.S., and Plahuta, J.T., 1986, Geologic setting and genesis of the Red Dog zinc-lead-silver deposit, western Brooks Range, Alaska: Economic Geology, v. 81, p. 1696-1727.

Motooka, J.M., 1988, An exploration geochemical technique for the determination of pre-concentrated organometallic halides by ICP-AES: Applied Spectroscopy, v. 42, p. 1293-1296.

Mull, C.G., 1982, Tectonic evolution and structural style of the Brooks Range, Alaska: An illustrated summary, in Powers, R.B., ed., Geological studies of the Cordilleran thrust belt: Denver, Colorado, Rocky Mountain Association of Geologists, v. 1, p. 1-45.

Mull, C.G., Tailleir, I.L., Mayfield, C.F., Ellersieck, I., and Curtis, S., 1982, New upper Paleozoic and lower Mesozoic stratigraphic units, central and western Brooks Range, Alaska: American Association of Petroleum Geologists Bulletin, v. 66, p. 348-362.

Nokleberg, W.J., and Winkler, G.R., 1978, Geologic setting of the lead and zinc deposits, Drenchwater Creek area, Howard Pass quadrangle, western Brooks Range, Alaska: U.S. Geological Survey Open-File Report 78-70C, 16 p.

———1982, Stratiform zinc-lead deposits in the Drenchwater Creek area, Howard Pass quadrangle, northwestern Brooks Range, Alaska: U.S. Geological Survey Professional Paper 1209, 22 p., 2 sheets, scale 1:19,800.

Plahuta, J.T., 1978, Geologic map and cross sections of the Red Dog prospect, DeLong Mountains, northwestern Alaska: U.S. Bureau of Mines Open-File Report 65-78, 11 p., scale 1:20,000.

Tailleir, I.L., 1970, Lead-, zinc, and barite-bearing samples from the western Brooks Range, Alaska: U.S. Geological Survey Open-File Report 70-445, p. 1-16.

Tailleir, I.L., Kent, B.H., Jr., and Reiser, H.N., 1966, Outcrop geologic maps of the Nuka-Etivluk region, northern Alaska: U.S. Geological Survey Open-File Report 66-128, scale 1:63,360.

Theobald, P.K., and Barton, H.N., 1978, Basic data for the geochemical evaluation of National Petroleum Reserve, Alaska: U.S. Geological Survey Open-File Report 78-70D, 15 p.

Vine, J.D., and Tourtelot, E.B., 1970, Geochemistry of black shale deposits—A summary report: Economic Geology, v. 65, p. 253-272.

Young, L.E., and Moore, D.W., 1987, A discussion of "Geologic setting, petrology, and geochemistry of stratiform sphalerite-galena-barite deposits, Red Dog Creek and Drenchwater Creek areas, northwestern Brooks Range, Alaska": Economic Geology, v. 82, no. 4, p. 1077-1079.

Reviewers: John E. Gray and Gary Nowlan

A Followup Geochemical Survey of Base-Metal Anomalies in the Ward Creek/Windfall Harbor and Gambier Bay Areas, Admiralty Island, Southeast Alaska

By Cliff D. Taylor, Barrett A. Ciéutat, and Lance D. Miller

Abstract

A followup geochemical study was carried out on Admiralty Island to more accurately locate and, if possible, to identify the sources of anomalies characteristic of Kuroko-type volcanogenic massive sulfide deposits similar to the nearby Greens Creek and Pyrola deposits. Detailed rock, stream-sediment, and panned-concentrate sampling in the Ward Creek/Windfall Harbor area delineates a narrow belt of weakly anomalous samples that are restricted to a sequence of Permian to Late Triassic mafic volcanic and flysch-type sedimentary rocks exposed along most of the eastern shore of the island. We interpret the distribution of anomalous samples to indicate that high background concentrations of ore-related elements are a characteristic of this rock sequence. Several highly anomalous samples may indicate the presence of small mineralized occurrences. Detailed sampling in the Gambier Bay area led to the discovery of a structurally controlled Cu-Zn-Ag-Ba mineral occurrence of unknown extent. The occurrence is located on the north shore of Gambier Bay at the transition between the basal sedimentary to mafic volcanic units of the Late Triassic Hyd Group.

INTRODUCTION

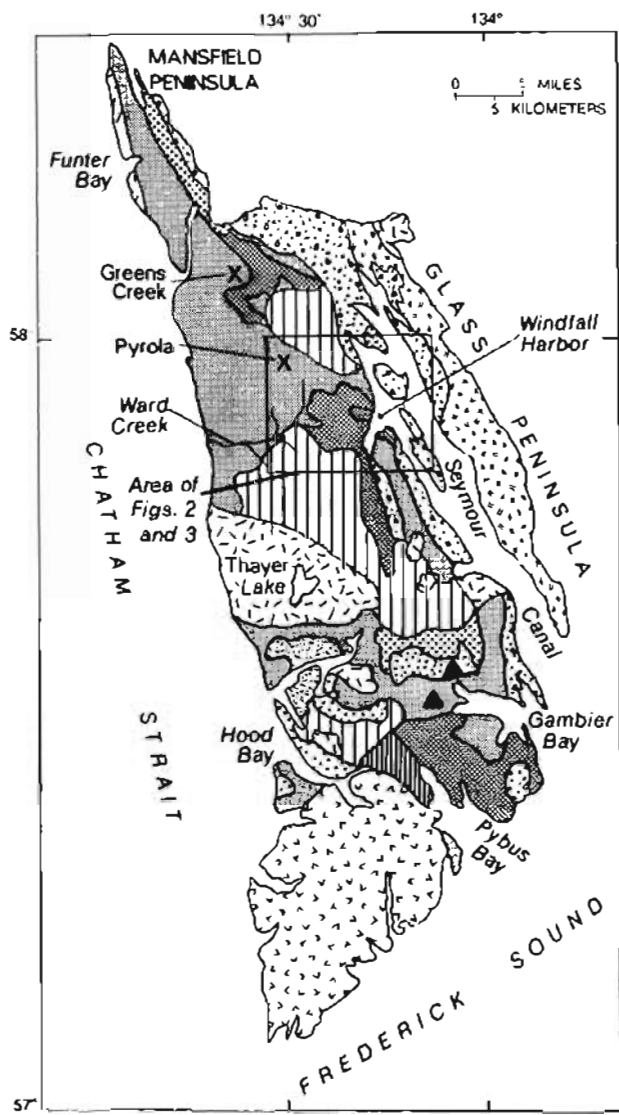
Admiralty Island is located 15 km south of Juneau in southeast Alaska (fig. 1). The island is 135 km by 50 km and is elongate in a north-south direction. Statistical analysis of the stream- and lake-sediment geochemical data collected during the National Uranium Resource Evaluation (NURE) program identified three anomalous areas that have geochemical characteristics interpreted to represent volcanogenic massive sulfide (VMS) mineral occurrences (Kelley, 1990). One of these areas encompasses the drainages in the vicinity of the Greens Creek Kuroko-type VMS deposit (fig. 1). The other two areas—Ward Creek/Windfall Harbor and Gambier/Pybus Bay—contain no known VMS occurrences. All three

areas lie within a sequence of Permian and Triassic mafic volcanic and flysch-type sedimentary rocks. This sequence trends northwest across the length of the island and is part of a belt of Permian and Triassic arc-related volcano-sedimentary rocks extending 300 km from Juneau to Ketchikan that hosts numerous VMS occurrences and deposits (Berg and Grybeck, 1980; Goldfarb and others, 1987).














This paper presents the results of detailed followup geochemical sampling programs designed to further constrain and, if possible, to locate the source of geochemical anomalies in the Ward Creek/Windfall Harbor and Gambier/Pybus Bay areas. We also describe a structurally controlled Cu-Zn-Ag-Ba mineral occurrence of unknown extent discovered during the followup work in the Gambier/Pybus Bay area.

GEOLOGY

Most of Admiralty Island is part of the allochthonous Alexander terrane (Monger and Berg, 1987). The Gravina-Nutzotin belt overlap assemblage (fig. 1) is adjacent to and overlies the Alexander terrane and crops out on the Glass Peninsula and the islands in the Seymour Canal along the eastern side of the island (Berg and others, 1978; Rubin and Saleeby, 1991). The Alexander terrane consists of Ordovician to Late Triassic marine sedimentary, volcanic, and plutonic rocks formed during intermittent volcanic arc activity along a convergent continental margin (Gehrels and Saleeby, 1987; Rubin and Saleeby, 1991). The Gravina-Nutzotin belt (Berg and others, 1972) consists of Late Jurassic to mid-Cretaceous marine sedimentary rocks, intertonguing andesitic to basaltic volcanic rocks, and quartz diorite to dunite and peridotite plutonic rocks. They were formed adjacent to and upon the Alexander terrane following a brief period of Late Triassic rifting. Rifting is thought to have occurred as a result of back-arc spreading (Rubin



EXPLANATION

-  **Tertiary rocks**—Andesitic basalt flows; Admiralty Island Volcanics
-  **Tertiary rocks**—Conglomerate, sandstone, shale, coal; Kootznahoo Formation
-  **Cretaceous rocks**—Intermediate, mafic, and ultramafic plutonic rocks
-  **Cretaceous and Jurassic rocks**—Argillite, conglomerate, and graywacke; Seymour Canal Formation
-  **Cretaceous and Jurassic rocks**—Basaltic or andesitic flow breccia; Douglas Island Volcanics
-  **Triassic and Permian rocks**—Volcanic and sedimentary rocks
-  **Triassic rocks**—Chert, argillite, graywacke, carbonate rocks, and intermediate to mafic volcanic rocks. Consists of the Hyd Group, as mapped, and the Retreat Group and Gambier Bay Formation
-  **Permian rocks**—Argillite, graywacke, chert, and minor conglomerate, limestone, and volcanic rocks; Cannery Formation
-  **Devonian rocks**—Marble enclosed tectonically within Gambier Bay Formation
-  **Silurian and Ordovician rocks**—Argillite, chert, graywacke, and minor volcanic rocks; includes Ordovician Hood Bay Formation and sedimentary rocks
-  **Mesozoic or Paleozoic rocks**—Metasedimentary and metaigneous rocks
-  Ag-Au-Pb-Zn deposit
-  Cu (±Au) occurrences

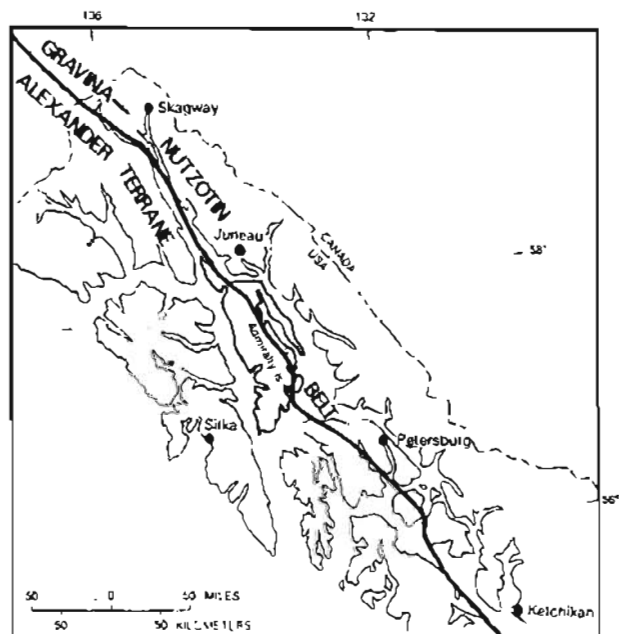


Figure 1. Geologic map of Admiralty Island. Generalized from Latham and others (1965) and Karl (1989); modified from Kelley (1990). Inset shows location of Admiralty Island and contact between Alexander terrane and Gravina-Nutzotin belt. Modified from Goldfarb and others (1987) and Monger and Berg (1987).

and Saleeby, 1991) or possibly pull-apart rifting in response to transcurrent (right lateral) movement of the volcanic arc prior to its accretion to the continental margin (Ford and Brew, 1988).

For the purposes of this paper, only the Early Permian to Late Triassic rocks favorable for VMS-type mineralization are described. However, rocks on the island range in age from Ordovician to Tertiary and are volcanic, plutonic, and sedimentary. Brief descriptions and the distribution of these rocks on the island are provided in figures 1-4. Excellent descriptions of all the rocks on Admiralty Island can be found in Loney (1964), Lathram and others (1965), and Ford and others (1989).

The Early Permian Cannery Formation consists of thin-bedded argillite, graywacke, chert, and minor volcanic flows and breccias representing a deep-water depositional environment and a period of submarine deposition (Ford and others, 1989). The Cannery Formation is present at the headwaters of Pack and Greens Creeks, in the vicinity of Windfall Harbor, and as a belt along the east side of Hasselborg Lake extending south from the head of Windfall Harbor (figs. 1-3). In the area of Pybus and Gambier Bays, the Cannery Formation is overlain by dolomite of the Permian Pybus Formation (fig. 4, inset). This unit is a light-brownish-gray, fossiliferous, cherty dolostone that is inferred to indicate a shallow-marine depositional environment (Ford and others, 1989).

Two probably correlative parts of a discontinuous sequence of Triassic rocks form most of the central and western parts of the island and stretch from the Mansfield Peninsula to the southern shore of Gambier Bay. A Cretaceous batholith at Thayer Lake divides the Retreat Group to the north from the Gambier Bay Formation to the south (Lathram and others, 1965). Several varieties of schist and lesser phyllite and argillite compose the rocks of this belt; the most common lithic types are chlorite-albite-epidote and calc-silicate schist. These rocks have been intensely deformed and variably metamorphosed up to greenschist facies. Originally thought to be Late Triassic(?) to Early Cretaceous(?) in age (Barker, 1957), the age of these rocks was revised to Middle(?) Devonian on the basis of poorly preserved fossils in the prominent marble exposures north and south of Hood Bay and north of Gambier Bay that were thought to be in depositional contact with the Gambier Bay Formation (Loney, 1964). Recent identification of fossils in argillites of the Retreat Group suggests a Late Triassic age for these rocks (Ford and others, 1989), and recent work suggests that the Devonian marbles may be olistostromal blocks (Brew and others, 1991). These rocks are thought to represent renewed volcanism and deposition of volcanic rocks and flysch-type sedimentary rocks in a relatively deep-water arc-slope environment (Ford and others, 1989).

The Late Triassic Hyd Group consists of a relatively undeformed sedimentary and volcanic section unconformably overlying Permian rocks along the eastern side of the island. The lithic components of the sedimentary and volcanic section are unequally distributed; volcanic rocks compose most of the section on the north shore of Gambier Bay. The sedimentary sequence consists of a basal sedimentary breccia of white chert and dolostone or green and red chert, overlain by a middle interval of brown limestone and an upper interval of thin-bedded argillite, chert, limestone, and minor spilitic lavas. The volcanic rocks are characterized by massive-to thick-bedded, jasper-bearing, red and green, amygdaloidal, altered, basic lava flows that thicken rapidly northward through Windfall Harbor. The sedimentary rocks of the section are most extensive in the Gambier/Pybus Bay area and thin rapidly northward (Lathram and others, 1965). The Hyd Group rocks are the youngest rocks of the Alexander terrane and are interpreted to represent a period of uplift and shallow-water carbonate sedimentation followed by rifting and basaltic volcanism prior to deposition of Gravina-Nutzotin belt sediments (Brew and Ford, 1984; Gehrels and Saleeby, 1987; Ford and others, 1989).

METHODS

During this study, 48 stream-sediment and panned-concentrate samples were collected from first- and second-order streams in the Ward Creek/Windfall Harbor area at a sampling density of 1 sample per 13 km². At each site, a composite sample from a 5- to 10-m section of the active channel was sieved through a 10-mesh (2.0 mm) screen. Approximately 1 to 2 kg was saved as a stream-sediment sample. A panned concentrate was produced by panning 6 to 8 kg of the screened material to remove most of the quartz, feldspar, and organic and clay-sized material. In addition, 64 rock samples with visible alteration, veining, and mineralization were collected from float and outcrop in an attempt to identify possible sources of the geochemical anomalies. In the Gambier/Pybus Bay area, 4 stream-sediment and panned-concentrate samples and 43 rock samples from float and outcrop were collected. Of the rock samples, only the 41 samples collected at the newly discovered mineral occurrence are discussed.

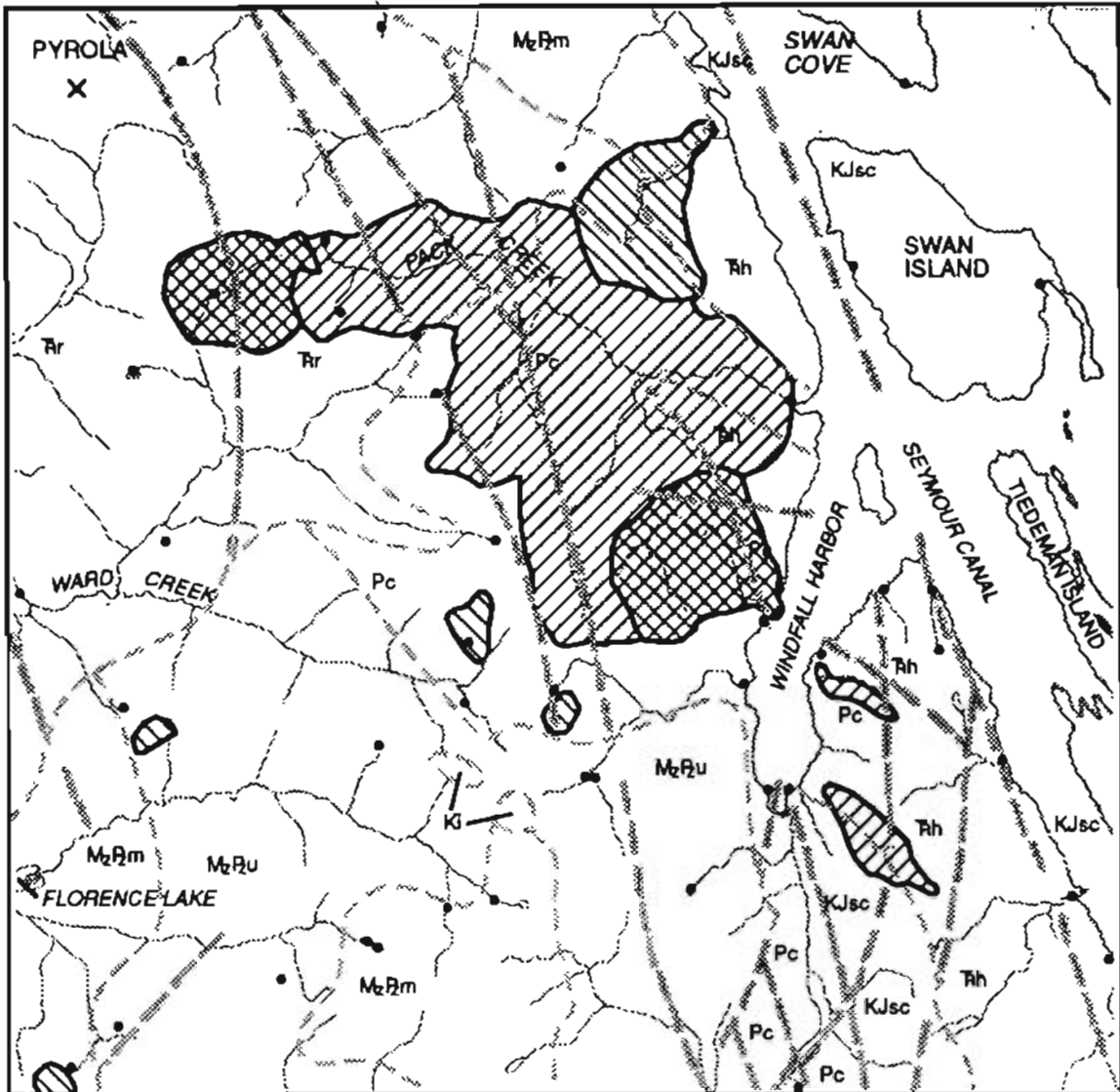
In the laboratory, stream sediments were sieved to -200 mesh (0.075 mm). Rock samples were first crushed and then pulverized using ceramic-plate grinders. The panned-concentrate samples were sieved to -35 mesh (0.5 mm) and separated magnetically and by heavy liquids to produce a nonmagnetic heavy-mineral-concentrate. The concentrate was split, and one fraction was hand ground for chemical analysis. The second split

134° 35'

134° 10'

57° 59'

57° 46'



Explanation



KI	Intrusive rocks (Cretaceous)
KJsc	Seymour Canal Formation (Cretaceous and Jurassic)
Trh	Hyd Group (Triassic)
Tr	Retreat Group (Triassic)
Pc	Cannery Formation (Permian)
MzPm	Metamorphic rocks (Mesozoic and Paleozoic)
MzPu	Sedimentary, metamorphic, and intrusive rocks, undivided (Mesozoic and Paleozoic)
•	NURE Sample site
---	Fault
~ ~ ~	Contact

	Factor 3 As-Ba-Zn-Ni
	Factor 5 Pb-Zn-Cu
	Factors 3 and 5

Figure 2. Location of geochemical anomalies resulting from statistical analysis of NURE stream- and lake-sediment data in Ward Creek/Windfall Harbor area. *R*-mode factors from Kelley (1990); geology generalized from Karl (1989).

was saved for detrital-grain mineral identification using a binocular microscope.

The stream-sediment and rock samples were analyzed by inductively coupled plasma-atomic emission spectrography for 40 elements (ICP-AES 40) using a low-temperature multi-acid total digestion (Crock and others, 1983), and for 10 elements (ICP-AES 10) using an organometallic halide partial-extraction method (Motooka, 1988). Gold (0.002-ppm lower limit) was determined by graphite furnace atomic absorption spectrophotometry (HGA-AAS; Thompson and others, 1968) and Hg (0.02-ppm lower limit) by cold vapor atomic absorption spectrophotometry (CV-AAS; Kennedy and Crock, 1987). The nonmagnetic heavy-mineral-concentrate samples were analyzed semiquantitatively for 37 elements by DC-arc atomic emission spectrography (DC-AES; Grimes and Marranzino, 1968). The lower limits of determination for each method and selected subsets of the elements analyzed for are shown in tables 1-3.

Percentages of ore and ore-related minerals in the heavy-mineral-concentrate samples are based on visual estimates. Mineralogical identification was augmented by single-grain X-ray diffraction (XRD) analyses. Occurrences and percentage estimates of ore and ore-related minerals are listed in table 2. No galena or sphalerite was found in any of the concentrates. However, sphalerite is especially difficult to identify due to its resemblance to rutile. In the rock samples from the mineral occurrence in the Gambier/Pybus Bay area, identification of bornite and silver-rich tetrahedrite (tetrahedrite slightly shifted toward fribergite; S. Sutley, oral commun., 1991) was made by single-grain XRD analyses. Identification of other phases was made by reflected-light microscopy.

GEOCHEMICAL STUDIES IN THE WARD CREEK/WINDFALL HARBOR AREA

The Ward Creek/Windfall Harbor area is roughly 625 km² in size and is characterized by steep, mountainous terrain. Most of the area is composed of Permian to Late Triassic volcanic and sedimentary strata favorable for VMS-type mineralization (figs. 2, 3). During the NURE sampling program, 42 samples were collected from this area at a density of about 1 sample every 15 km². Anomalous samples contained up to 517 ppm Zn, 267 ppm Cu, 72 ppm Pb, and 216 ppm As. A few samples also contained elevated concentrations of Ba, Fe, Mn, Ni, Cr, Co, Sb, and Bi (Kelley, 1990). *R*-mode factor analysis (Davis, 1986) identified two element associations that were interpreted to be indicative of VMS-type mineralization. One was As, Ba, Ni, and Zn, and the other was Pb, Zn, and Cu (factors 3 and 5, respectively, in fig. 2; Kelley, 1990). Anomalous scores for

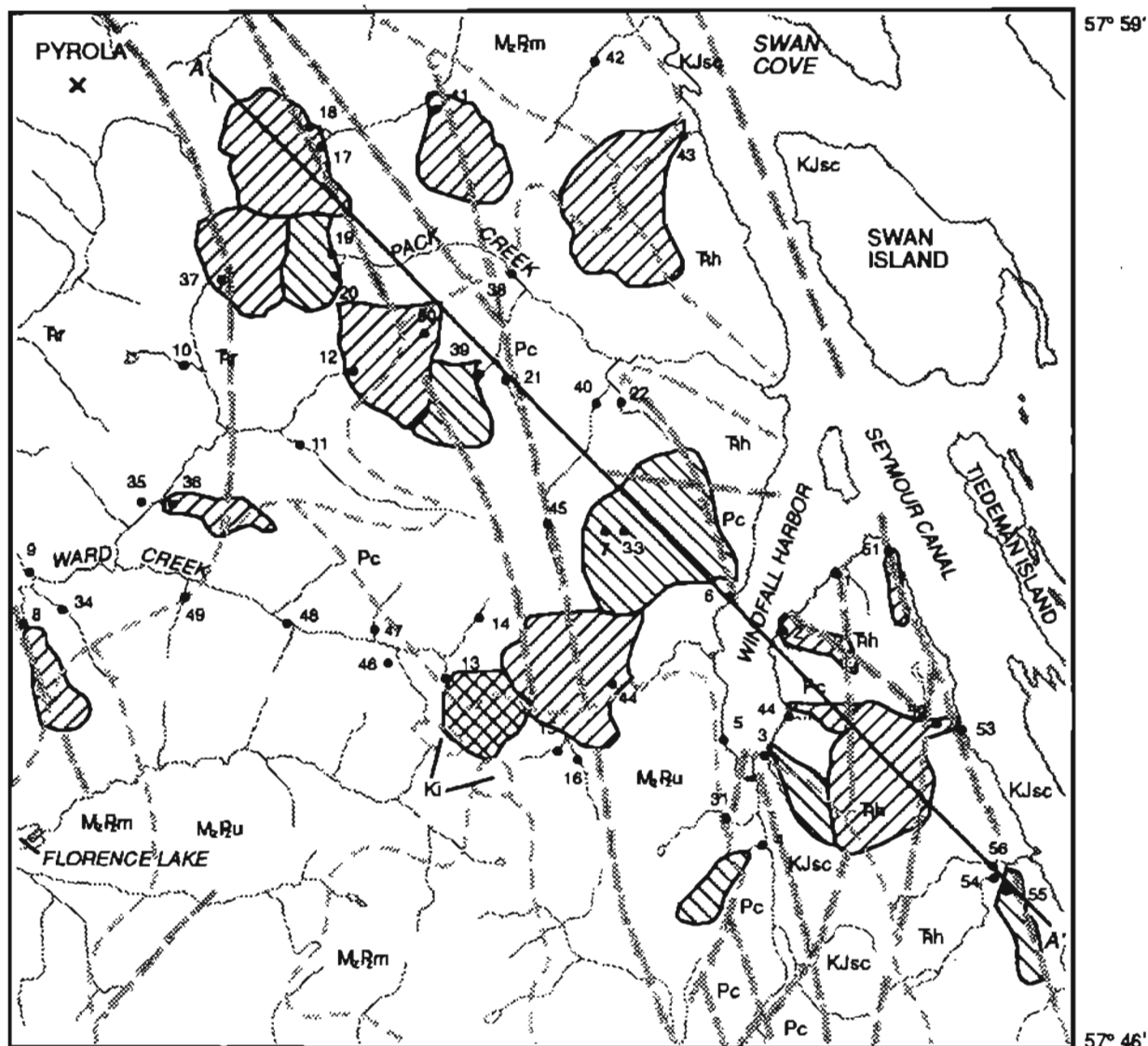
these two associations plotted at 1:63,360 occur in samples from the headwaters of Ward and Pack Creeks and in samples from creeks draining into Windfall Harbor (fig. 2).

Fourteen minor and trace elements that are expected to represent elements indicative of Kuroko-type VMS mineralization (Lambert and Sato, 1974; Kelley, 1990) were selected from the stream-sediment and nonmagnetic heavy-mineral-concentrate geochemical data sets for univariate statistical analysis. These elements are Fe, Mn, Ba, Ag, As, Bi, Cd, Cu, Mo, Pb, Sb, Zn, Au, and Hg. Threshold concentrations for each element were selected by comparing the 90th-percentile value to the corresponding histogram (histograms not shown). Univariate statistical summaries of the stream-sediment and nonmagnetic heavy-mineral-concentrate sample data and the threshold concentration selected for each element are shown in table 4A and 4B. The concentrations of the selected elements in anomalous stream-sediment samples and nonmagnetic heavy-mineral-concentrate samples from the Ward Creek/Windfall Harbor area are shown in tables 1 and 2, respectively. Only sites with two or more anomalous elements in the same sample media were considered in defining anomalous drainages. The resulting anomalous areas and sample-site locations are shown in figure 3.

Results and Interpretation of Geochemical Data

Interpretation of the data shows a distinct northwest-to southeast-trending zone of anomalous samples. From the headwaters of Pack Creek to the peninsula southeast of Windfall Harbor, stream-sediment and nonmagnetic heavy-mineral-concentrate samples are characterized by elevated values of Cu, Ni, Fe, Mn, Ag, Mo, Cd, and (or) Zn. Also, there appears to be a very subtle enrichment of As, Sb, Pb, and Ba in the northwest and Hg and Au in the southeast part of the study area. To show this graphically, sample sites along the anomalous zone were projected onto a NW-SE-oriented transect (A-A', fig. 3), and the stream-sediment concentrations of the six elements mentioned were plotted as a set of individual bar graphs (fig. 5). The slight zonation in the enrichment of these elements along the NW-SE transect also corresponds with the observed distribution of the mineralogy in the nonmagnetic heavy-mineral-concentrate samples as discussed below. The belt of anomalous samples is narrower and the zonation more apparent in the stream-sediment geochemistry. The anomalous area indicated by the heavy-mineral-concentrate geochemistry is wider and is less well zoned (fig. 3).

There is a distinct correlation between the trend of anomalous sample sites and the occurrence of ore and ore-related minerals in the heavy-mineral-concentrate



Explanation

KI	Intrusive rocks (Cretaceous)
KJsc	Seymour Canal Formation (Cretaceous and Jurassic)
Rh	Hyd Group (Triassic)
Tr	Retreat Group (Triassic)
Pc	Cannery Formation (Permian)
MzRm	Metamorphic rocks (Mesozoic and Paleozoic)
MzRu	Sedimentary, metamorphic, and intrusive rocks, undivided (Mesozoic and Paleozoic)
46 •	Sample site number and site location
	Fault
	Contact



	Anomalous stream sediments
	Anomalous concentrates
	Anomalous concentrates and stream sediments

Figure 3. Location of geochemical anomalies resulting from analysis of stream-sediment and nonmagnetic heavy-mineral-concentrate sample single-element plots from Ward Creek/Windfall Harbor area. A-A' cross-section refers to fig. 5. Geology generalized from Karl (1989).

samples (table 2). The concentrates contain mostly gray to flesh-colored silicates and rock fragments of phyllite and argillite reflecting the dominant lithology at the sample site. Commonly, they also contain variable amounts of semitranslucent to opaque white barite; tarnished, oxidized, and often goethite-replaced cubic and dodecahedral pyrite; and black and blood-red to yellow-orange rutile. Well-formed cubic pyrite is particularly abundant in areas where pyrite-bearing black slate and argillite are the dominant rock types.

From the headwaters of Pack Creek to the peninsula southeast of Windfall Harbor, the percentages of pyrite and barite in heavy-mineral-concentrate samples is 30 to 60 percent. In many of these samples cinnabar occurs in small quantities from a few grains to 2 percent. Sites 31 and 51 on the peninsula each contain a grain of chalcocopyrite. All of the samples to the northeast of this belt of anomalous samples contain 30 to 60 percent barite and several contain >30 percent pyrite. The occurrence of cinnabar and barite is distributed throughout the anomalous trend. However, the highest percentages of barite in concentrates occur at the northwest end of the trend, and the only samples containing more than 10 to 12 grains of cinnabar occur on the peninsula southeast of Windfall Harbor.

With a few notable exceptions, we regard the anomalous trend to be an indication of high background concentrations in the Permian and Triassic rocks rather than an indication of proximity to significant VMS-type mineralization. This conclusion is based on the observation that the geochemistry of nearly all the samples located in areas of Permian and Triassic rocks have a low level and fairly uniform enrichment of the elements examined in comparison to the surrounding country rock. As discussed, there may be subtle variations in the nature of elemental enrichment *within* this package of rock, but nearly all of the samples collected in areas characterized by country rock other than the Permian through Triassic rock package are not geochemically anomalous.

The exceptions are characterized by slightly above threshold concentrations of five to seven elements that may indicate small mineral occurrences are present. The sample from site 7 contains 2,200 ppm Mn, 350 ppm As, 93 ppm Cu, 34 ppm Pb, 5.2 ppm Sb, 190 ppm Zn, and 0.008 ppm Au in stream sediment and 1,000 ppm As and Pb in the heavy-mineral concentrate. Sample 33 contains 2,700 ppm Mn, 120 ppm As, 2.8 ppm Cd, 110 ppm Cu, 49 ppm Pb, 390 ppm Zn, and 0.014 ppm Au in stream sediment and 50 percent Fe, 7 ppm Ag, and 1,000 ppm Pb in the heavy-mineral concentrate. These two sites represent upper tributaries of the same stream and together give a strong suggestion that mineralization is present. A sample (site 6) taken at the mouth of the main stream 3 km distant contains 99 ppm As, 24 ppm

Pb, and 210 ppm Zn in stream sediment and 3 ppm Ag in the heavy-mineral concentrate. Sample 19 contains 2,000 ppm Mn, 2,100 ppm Ba, 120 ppm Ni, 0.67 ppm Ag, 9.8 ppm Sb, 180 ppm Zn, and 0.85 ppm Hg in stream sediment and 100 ppm Pb in the heavy-mineral concentrate. Sample 50, which was collected from an iron-stained area of sparse vegetation (a kill zone), contains 160 ppm Ni, 0.61 ppm Ag, 170 ppm As, 1.6 ppm Cd, 130 ppm Cu, 6.7 ppm Mo, 6.5 ppm Sb, and 0.55 ppm Hg in stream sediment and 100 ppm Pb in the heavy-mineral concentrate. Sample 51 contains 3,400 ppm Mn, 0.80 ppm Ag, 2 ppm Cd, 9.9 ppm Mo, and 180 ppm Zn in stream-sediment and 3 ppm Ag and 300 ppm Mn in the heavy-mineral concentrate. Although microscopic examination of the heavy-mineral-concentrate samples failed to identify sphalerite, the combination of 2,000 to 5,000 ppm Zn and 50 to 500 ppm Cd in samples 12, 17, 36, 37, 41, and 43 probably indicates its presence.

Geochemical analyses (not presented) obtained for rock samples collected in the Ward Creek/Windfall Harbor Area show that for the most part, the rock samples are unmineralized. However, there are a few exceptions that may relate to the anomalous trend shown by the stream-sediment and heavy-mineral-concentrate samples. A traverse was made from south to north along the divide between sites 13 and 15. At the south end, equigranular, fine crystalline, Cretaceous diorite is in contact with a monotonous sequence of undivided Paleozoic and Mesozoic argillites and phyllites. Pyrite is commonly disseminated throughout the diorite and is locally abundant. The intruded metamorphic rocks are iron stained and locally altered near the contact. At the northern end of the traverse, intrusive rocks are absent but the metamorphic rocks are similarly iron stained. Examination of the iron-altered material shows abundant pyrite on fracture surfaces. Both the pyritic diorite and the overlying metamorphic rocks contain anomalous concentrations of Cu (55 ppm) and Zn (45 ppm), and one sample of the diorite is enriched in As (170 ppm). The pyrite in the diorite and in the altered metamorphic rocks is probably the source of the anomalies shown at sites 13 and 44.

The area around site 50 is characterized by intense iron staining and lack of vegetation on flat rocky patches and along several small streams. The argillites(?) are brecciated and veined. Dissolution of the argillite clasts produces a boxwork texture of quartz and calcite. Intense iron staining is associated with pyrite on fracture surfaces, and analyses show that these rocks contain 2.2 ppm Ag and 83 ppm As.

At site 43, near Swan Cove, silicified material was found in float that contains minor chalcocopyrite and sphalerite. The sample contains 370 ppm Zn, 110 ppm Cu, and 0.5 ppm Ag and is probably the source of the anomalous heavy-mineral-concentrate sample. Site 43 is

Table 1. Concentrations of selected elements in anomalous stream-sediment samples from the Ward Creek/Windfall Harbor area

(Mn, Ba, and Ni analyses performed by ICP-AES 40; Au analyses by HGA-AAS, and Hg analyses by CV-AAS. All other analyses are by ICP-AES 10. Brackets indicate lower limit of determination. N, not detected at lower limit; <, detected at lower limit)

Sample	Mn (ppm) [4]	Ba (ppm) [1]	Ni (ppm) [2]	Ag (ppm) [0.045]	As (ppm) [0.60]	Bi (ppm) [0.60]	Cd (ppm) [0.05]	Cu (ppm) [0.05]	Mo (ppm) [0.09]	Pb (ppm) [0.60]	Sb (ppm) [0.60]	Zn (ppm) [0.05]	Au (ppm) [0.002]	Hg (ppm) [0.020]
01 ----	1700	1200	53	0.30	21	N 0.67	0.65	48	1.4	13	1.5	130	0.004	0.26
02 ----	1400	820	92	.37	30	N .67	.49	63	4.5	8.1	3.1	83	.004	.24
03 ----	1700	1600	64	.31	36	N .67	2.2	52	7.0	9.2	3.8	190	.004	.64
04 ----	1700	2100	63	.44	24	N .67	.87	72	1.8	31	2.3	110	.006	.44
06 ----	1500	770	47	.43	99	N .67	1.1	62	2.4	24	2.6	210	.006	.48
07 ----	2200	1300	53	.34	350	N .67	1.1	93	2.1	34	5.2	190	.008	.19
08 ----	1500	420	49	.11	12	N .67	.26	48	.94	4.3	.84	63	.002	.03
10 ----	2000	920	61	.25	18	N .67	.53	55	1.1	9.7	1.3	91	.002	.09
12 ----	1400	2100	99	.42	35	N .67	1.2	42	3.6	10	4.2	130	.004	.37
13 ----	1600	560	59	.16	200	N .67	.51	58	1.6	8.1	1.9	97	.013	.15
15 ----	1600	470	73	.11	7.5	N .67	.36	52	.75	7.6	.89	95	< .002	.07
16 ----	1600	450	69	.097	5.9	N .67	.25	52	.80	5.0	N .67	78	< .002	.11
17 ----	1300	1700	80	.38	29	N .67	.73	73	3.2	8.0	27	110	.003	.32
18 ----	1200	1300	92	.23	15	N .67	.41	61	1.2	9.1	2.6	88	.002	.19
19 ----	2000	2100	120	.67	49	N .67	1.4	69	4.7	10	9.8	180	.004	.85
20 ----	1800	1500	85	.88	47	N .67	1.9	53	5.0	12	9.0	180	.004	.51
21 ----	1500	2900	77	.30	60	N .67	.72	48	2.4	9.7	1.7	120	.003	.12
31 ----	1800	600	100	.27	16	1.1	.77	200	3.1	7.4	5.6	95	.006	.98
33 ----	2700	1100	71	.46	120	N .67	2.8	110	2.5	49	3.2	390	.014	.17
36 ----	1800	890	140	.28	28	N .67	.60	54	1.1	8.4	1.7	95	.004	.14
37 ----	1000	2000	73	.62	23	N .67	1.2	49	4.3	10	4.2	110	.005	.27
39 ----	1900	2600	100	.54	36	N .67	.90	62	3.4	8.4	2.1	130	.005	.20
41 ----	1300	1300	46	.25	27	N .67	1.3	46	6.1	9.4	3.2	110	.004	.39
43 ----	1400	2600	72	.35	39	N .67	.78	65	3.2	12	2.2	140	.004	.29
44 ----	1400	610	52	.29	16	N .67	.24	74	1.2	10	1.2	70	.016	.09
45 ----	1300	730	46	.26	20	.67	.24	72	1.2	7.4	1.1	68	.006	.06
50 ----	1500	200	160	.61	170	N .67	1.6	130	6.7	13	6.5	170	.003	.55
51 ----	3400	730	90	.80	18	N .67	2.0	57	9.9	13	2.0	180	.002	.44
53 ----	1600	1200	93	.27	16	N .67	.55	48	1.7	7.5	3.5	100	.012	2.0
55 ----	1500	610	93	.19	11	N .67	2.0	68	2.2	10	2.4	180	.002	.19

in the vicinity of a chalcopyrite-pyrrhotite occurrence in the Hyd Group reported by Lathram and others (1965). These workers also reported another occurrence in the volcanic rocks of the Hyd Group on the southeast shore of Windfall Harbor between sites 1 and 2 (fig. 3). Small amounts of chalcopyrite in iron-rich quartz-carbonate veins and stockworks were found cutting mafic volcanic rocks. A sample collected from the mineralized stockwork contains 0.46 percent Cu.

GEOCHEMICAL STUDIES IN THE GAMBIER/PYBUS BAY AREA AND THE DISCOVERY OF THE NORTH GAMBIER CU-ZN-AG-BA OCCURRENCE

During the followup geochemical sampling in the Gambier/Pybus Bay area, we conducted an examination of a NURE stream-sediment anomaly containing 2,366 ppm Ba, 361 ppm Zn, 103 ppm Cu, 27 ppm Pb, 55 ppm As, 9 ppm Sb, and 5 ppm Bi. The presence of chalcopyrite and barite in stream cobbles led to an outcrop discovery of Cu-

Zn-Ag-Ba mineralization that, to the best of our knowledge, has not been previously reported. The occurrence, here informally named the North Gambier occurrence, is located in the northwest corner of section 27 (Sitka B-1, U.S. Geological Survey 15-minute quadrangle), approximately 2 km north from the mouth of the stream that flows into Gambier Bay from the north shore (fig. 4). The earliest reports on the region (Wright and Wright, 1904; Wright, 1906, 1907) noted the occurrence and minor working of several claims near the west end of Gambier Bay. The Brown's prospect is located at 1,000-ft elevation on the north side of Cave Mountain, which separates the north and south arms of the bay. Mineralization consists of "brecciated limestone partly replaced by quartz stringers and by small masses of pyrite and chalcopyrite" along a northwest-striking "ledge" or structure that is continuous for more than 200 ft (Wright, 1906). Preliminary assays indicated low Cu-Au values. Two other Cu-Au-bearing "ledges" were also reported on the south (Cook Claim) and northeast slopes of Gambier Mountain, north of the Brown's prospect and several kilometers to the northwest of the North Gambier occurrence.

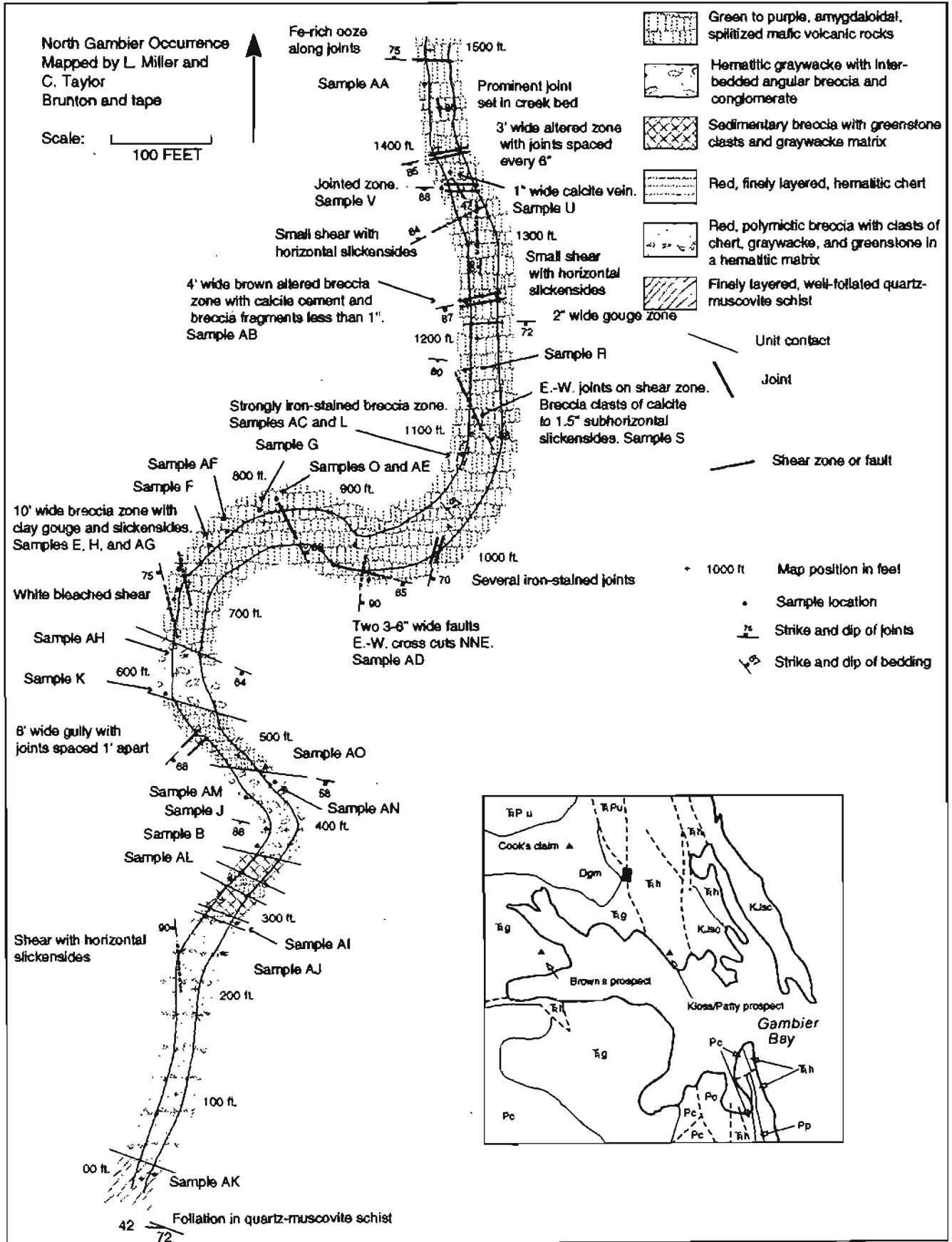


Table 2. Concentrations of selected elements in anomalous nonmagnetic heavy-mineral-concentrate samples from the Ward Creek/Windfall Harbor area

[All analyses by DC-AES. Brackets indicate lower limit of determination. N, not detected at lower limit; <, detected at lower limit. Abbreviations: bt, barite; py, pyrite; cn, cinnabar; cpy, chalcopyrite]

Sample	Fe (percent) {0.1}	Ag (ppm) {1}	As (ppm) {500}	Cd (ppm) {50}	Cu (ppm) {10}	Mn (ppm) {20}	Ni (ppm) {10}	Pb (ppm) {20}	Zn (ppm) {500}	Ore mineralogy values in percent
01 -----	5	N 1	N 500	N 50	30	200	20	< 20	N 500	40 bt
02 -----	30	N 1	N 500	N 50	700	300	300	30	N 500	50 py, cn
03 -----	5	N 1	N 500	N 50	100	200	20	N 20	1000	2 cn
04 -----	3	N 1	N 500	N 50	50	100	10	20	N 500	90 bt
06 -----	20	3	N 500	N 50	500	150	70	70	< 500	35 py, 40 bt
07 -----	15	< 1	1000	N 50	70	150	50	1000	1500	60 bt, cn
08 -----	20	N 1	1500	N 50	100	300	70	20	N 500	30 py
10 -----	1	3	N 500	N 50	200	100	20	70	N 500	
12 -----	7	< 1	N 500	50	200	100	70	20	2000	
13 -----	10	< 1	1500	N 50	150	300	20	20	N 500	
15 -----	2	N 1	N 500	N 50	50	300	15	30	N 500	
16 -----	1.5	N 1	N 500	N 50	50	300	15	30	N 500	
17 -----	20	1.5	N 500	70	1000	100	200	50	2000	30 py, 30 bt
18 -----	30	1	N 500	N 50	700	150	300	200	< 500	30 py, 30 bt, cn
19 -----	1.5	N 1	N 500	N 50	70	150	15	100	1000	30 bt, cn
20 -----	1.5	N 1	N 500	N 50	100	300	20	20	700	
21 -----	3	N 1	N 500	N 50	100	200	30	20	N 500	30 bt
31 -----	>50	3	N 500	N 50	1000	100	300	50	N 500	60 py, 30 bt, 2 cn, cpy
33 -----	50	7	N 500	N 50	300	200	200	1000	N 500	30 py, 30 bt
36 -----	30	5	N 500	< 50	700	200	500	70	2000	50 py
37 -----	50	5	< 500	50	1000	150	500	100	2000	75 py
39 -----	15	< 1	N 500	N 50	200	150	100	20	1500	50 bt
41 -----	50	1	500	500	500	200	500	30	5000	30 bt
43 -----	30	3	500	N 50	700	150	100	100	2000	30 py, 50 bt
44 -----	>50	3	N 500	N 50	300	200	150	100	N 500	60 py
45 -----	50	1	N 500	N 50	300	100	70	100	N 500	30 py, 50 bt
50 -----	5	1	N 500	N 50	100	150	30	100	< 500	
51 -----	20	3	N 500	N 50	200	300	100	20	700	40 bt, cpy
53 -----	50	< 1	N 500	< 50	500	200	150	20	3000	cn
55 -----	20	< 1	N 500	N 50	200	300	100	30	N 500	cn

These historic occurrences were noted in the reconnaissance mapping of Lathram and others (1965) and in the more detailed mapping of Pybus and Gambier Bays by Loney (1964). Numerous other publications (Berg and Cobb, 1967; Cobb, 1972a, b; Berg and others, 1981) list these as well. In addition they list several Cu-Ni prospects hosted by rocks of the Hyd Group on the north shore of Gambier Bay, downstream and east of the North Gambier occurrence. The Kloss and Patty prospects, de-

scribed in the literature as possibly being different names for the same occurrence, are cited to contain disseminated Cu-Ni oxides in a 150- to 200-ft-wide shear zone in the Hyd Group and a nearby parallel shear zone containing Cu mineralization (Berg and Cobb, 1967; Cobb, 1972a, b, 1978a, b).

A detailed stream-sediment geochemistry program conducted by the Alaska Division of Mines and Minerals in the Gambier/Pybus Bay area reported anomalous concentrations of Cu, Pb, Zn, and Mo in samples taken along the north shore of Gambier Bay in the vicinity of the North Gambier occurrence and suggested that Pb-Zn-Cu mineralization might be present. This report also noted Cu-Ni occurrences in the Hyd Group on the ridge to the east and made a vague reference to prospectors reporting a few copper occurrences in the area (Herbert and Race, 1965).

Berg and others (1981) made reference to an unpublished Bear Creek Mining Company report written in 1978, entitled "Significant Mineral Deposits and Anomalies, Southeast Alaska." Four occurrences are "located approximately" at different places on the south end of

Figure 4. Geology and locations of rock sample sites, North Gambier Cu-Zn-Ag-Ba occurrence. Inset: Gambier Bay area showing location of the North Gambier occurrence. Map units: Dgm, Devonian marble (olistostromal blocks) enclosed within Gambier Bay Formation (Triassic); Pp, dolomite of Pybus Formation (Permian); Pc, Cannery Formation (Permian); Tg, Gambier Bay Formation (Triassic); Th, Hyd Group (Triassic); APu, sedimentary, metamorphic, and intrusive rocks, undivided (Triassic and Permian); KJsc, Seymour Canal Formation (Cretaceous and Jurassic). Dashed lines indicate faults; black box indicates area of the main part of figure 4 (modified from Lathram and others, 1965).

Table 3. Concentrations of selected elements in rock samples from the North Gambier occurrence

[Shaded block indicates analyses performed by ICP-AES 40; Au analyses by HGA-AAS, and Hg analyses by CV-AAS. All other analyses are by ICP-AES 10. Brackets indicate lower limit of determination. N, not detected at lower limit; <, detected at lower limit. Abbreviations: Slcfd, silicified; brx, brecciated; volc, volcanic; rx, rocks; malzd, mineralized; bt, barite; cpy, chalcopyrite; py, pyrite; tetz, tetrahedrite; qtz, quartz; sph, sphalerite; gal, galena; bor, borite; cc, calcite; cov, covellite; carb, carbonate; aspy, arsenopyrite]

Sample	Fe (percent) [0.005]	Mn (ppm) [4]	Ni (ppm) [2]	Ag (ppm) [0.045]	As (ppm) [0.60]	Bi (ppm) [0.60]	Cd (ppm) [0.05]	Cu (ppm) [0.05]	Mo (ppm) [0.09]	Pb (ppm) [0.60]	Sb (ppm) [0.60]	Zn (ppm) [0.05]	Au (ppm) [0.002]	Hg (ppm) [0.020]	Sample description and ore mineralogy
A	8.9	4100	43	12	28	38	1.5	20000	6.3	120	55	130	0.006	1.81	Float, slcfd bt veined mafic volcanic, cpy, py
B	5.3	1500	35	N1.0	N10	N10	N0.30	44	1.6	N10	N10	24	.003	.11	Polymictic brx w/ clasts of chert and volc. rx., py
C	7.1	1400	150	N1.0	N10	N10	N.30	130	2.6	N10	N10	3	<.002	.18	Float, green chert w/ Fe carbonate, py, cpy
D	5.4	3600	12	2.8	N10	N10	1.5	3900	4.4	55	28	9	.007	1.2	Float, qtz-carbonate-bt veined wacke, cpy, py, tetz
E	21	11000	89	3.3	N10	N10	82	1300	5.9	420	13	12000	.003	30	Slcfd brx mafic volcanic w/ qtz, bt, sph, tetz, cpy
F	19	7000	170	6.5	13	N10	1.6	1800	2.6	870	N10	520	.002	2.0	Brx mafic volcanic w/py rimmed clasts
G	7.2	4700	24	4.9	N10	13	1.9	7100	3.1	310	29	150	<.002	1.10	2-in qtz-carbonate-bt vein in mafic volcanic, cpy
H	17	9000	47	2.4	N10	N10	65	3100	13	320	15	6200	.004	15.1	Slcfd brx w/ bladed bt., cpy, cut by qtz-sph-tetz-gal
I	4.1	1600	40	N1.0	N10	N10	.41	330	1.1	18	N10	27	.003	.13	Float, bladed bt w/ Fe carbonate, cpy, py matrix
J	7.4	2100	62	N1.0	N10	N10	.42	100	N.90	N10	N10	72	.003	N.02	Ferruginous graywacke
K	14	4200	68	N1.0	N10	N10	N.30	65	N.90	N10	N10	240	<.002	N.02	Green, altered wacke or tuff
L	8.3	5000	38	1.1	N10	N10	.87	680	N.90	10	N10	150	.003	.18	Brx mafic volcanic, carbonate-bladed bt matrix, cpy
M	2.3	2500	39	1.3	N10	N10	1.2	350	N.90	11	N10	53	<.002	.03	Float, bladed bt in brx Fe carbonate and green chert
N	.41	51	4	N1.0	N10	N10	N.30	15	1.4	N10	N10	3.6	<.002	.20	Float, massive white vein qtz w/ graphitic partings
O	8.3	5200	15	6.0	N10	18	1.2	9200	1.8	190	38	110	.005	.83	2-in qtz-carb vein in volcanics w/ cpy, py selvage
P	8.4	6100	58	N1.0	N10	N10	.86	82	N.90	12	N10	170	.005	.21	Float, volcanoclastic w/ green chert-Fe carb matrix
Q	9.2	7000	19	1.3	N10	N10	3.8	3500	2.3	13	25	73	.002	.44	Float, slcfd qtz-carbonate brx w/ cpy
R	9.5	2800	48	38	25	N10	2	6800	22	31	-	160	.030	.64	Qtz-carbonate vein in volcanics, cpy, bor, cov, tetz
S	7.5	3600	45	1.7	N10	N10	.47	2400	N.90	17	N10	170	.003	.16	Slcfd brx w/ chert and volcanoclasts, qtz-carb-bt-cpy
T	6.6	1200	84	7.4	N10	N10	89	120	4.2	6500	N10	11000	.005	9.7	Float, slcfd mafic volcanic qtz w/ carb-py-sph-gal-tetz
U	4.1	2500	56	1.7	N10	N10	.44	270	N.90	N10	N10	100	.003	.08	Fe carbonate altered mafic volcanic, bladed bt veins
V	9.1	2600	64	1.1	N10	N10	.52	59	N.90	13	N10	180	.003	N.02	Purple amygdular mafic volcanic w/ cc fillings
W	3.9	4200	20	2.0	N10	N10	3.8	1000	1.3	12	N10	150	<.002	.22	Slcfd brx w/ qtz-carbonate-bt-cpy matrix
X	10	5200	55	1.2	N10	N10	.62	36	N.90	12	N10	180	.002	N.02	1-in cc vein in amygdular mafic volcanic
Y	45	12000	10	1.1	39	N10	.84	110	1.7	20	N10	33	<.002	.19	Foot thick Fe-rich precipitate from seep
Z	5.5	110	5	N1.0	2000	N10	.33	2.3	2.0	42	72	9.9	<.002	10.8	Float, brx chert w/ py and aspy?
AA	15	3300	32	87	84	N10	39	200000	77	51	-	240	.040	40	Massive flow banded cpy-bor-py-qtz-cov-tetz
AB	12	7500	51	N1.0	N10	N10	.94	890	2.3	13	N10	110	.002	N.02	Slcfd brx w/ bar, cpy
AC	6.1	4700	22	N1.0	N10	N10	1.3	3700	8.7	40	16	77	<.002	.02	Slcfd brx w/ bar, cpy
AD	8.2	2600	71	N1.0	N10	N10	.45	12	1.6	N10	N10	670	.004	N.02	Altered mafic volcanic
AE	10	6500	47	N1.0	N10	N10	56	2000	6.1	130	12	3700	.040	13.2	Rock chip sample, bt, cpy, sph, tetz, py malzd
AF	8.3	4000	88	N1.0	N10	N10	.56	410	1.4	13	N10	190	<.002	N.02	Rock chip sample, unminlzd mafic volcanics
AG	15	6500	78	N1.0	N10	N10	8.3	690	1.5	220	N10	1300	<.002	3.9	Rock chip sample, bt, cpy, sph, tetz, py malzd
AH	6.9	2200	47	N1.0	N10	N10	.43	74	1.0	N10	N10	110	.003	N.02	Altered wacke or tuff
AI	3.9	230	8	N1.0	N10	N10	N.30	5.4	2.6	12	N10	7.0	<.002	.31	Finely layered ferruginous chert
AJ	9.5	1100	21	N1.0	13	N10	N.30	24	3.4	17	14	28	<.002	.02	Ferruginous polymictic sedimentary breccia
AK	4.1	990	15	N1.0	N10	N10	N.30	6.3	3.2	25	12	16	<.002	.13	Foliated and finely layered ferruginous qtz-musc schist
AL	11	3900	88	N1.0	N10	N10	N.30	170	1.5	N10	N10	86	<.002	N.02	Altered mafic volcanic or tuff
AM	15	8500	94	1.0	N10	N10	.34	110	1.8	N10	N10	140	<.002	.06	Slcfd brx, volcanoclasts in bt-cpy matrix
AN	6.4	4100	47	N.067	2.2	N.67	.19	45	.28	7.0	17	55	<.002	27.1	Ferruginous greywacke
AO	10	3400	260	.34	N.67	N.67	.10	460	.25	9.6	4.4	170	.003	12.3	Altered amygdular mafic volcanic w/ cc fillings

Admiralty Island, one of which is on the north shore of Gambier Bay. An excerpted quote from the unpublished report describes the four occurrences as "Major stratabound massive sulfide Cu-Zn prospects; stream-sediment anomalies up to 2 percent Zn; active claims and exploration; southward continuation of major stratabound massive sulfide belt containing deposit at locality (Greens Creek Mine)." This suggests that prior

documentation of a major stratabound Cu-Zn massive-sulfide occurrence in the same general area as the North Gambier occurrence may lie buried in old company files.

During this study we spent a day and a half mapping 1,500 ft of the creek where the North Gambier occurrence is located. Thirty-one outcrop and 10 float rock samples were collected for petrographic examination and geochemical analyses. The geologic map of the North

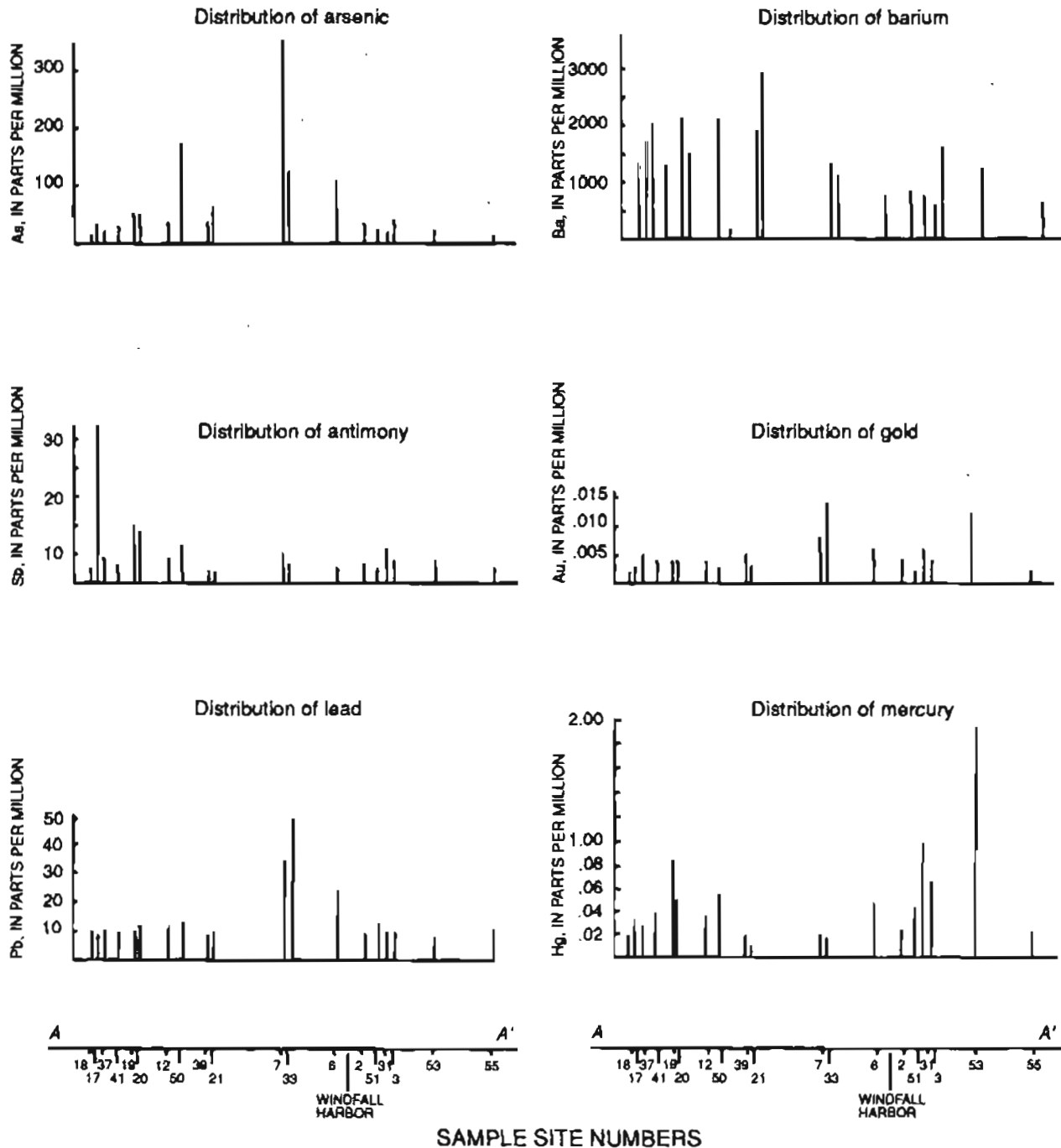


Figure 5. Distribution of selected elements from stream-sediment analyses in Ward Creek/Windfall Harbor area projected onto northwest to southeast transect (A-A', fig. 3).

Gambier occurrence with outcrop rock-sample locations is presented in figure 4. The position of features described below are given as distance in feet from the arbitrarily selected starting point of the map. Selected element concentrations of rock samples and brief descriptions are shown in table 3.

At the south end of the mapped section, the basal unit consists of hematitic, green-streaked, brick-red to purple, finely layered, well-foliated quartz-muscovite schist (sample AK). The unit has tight, centimeter-scale W-shaped folds, and elongation lineation plunges 42° to the west. This unit is in unconformable contact with a 250-ft-thick (measured horizontally up the stream bed) section of brick-red to purple, matrix-supported, polymictic breccia with subangular clasts up to several centimeters in size. The clasts consist of chert, graywacke, and mafic volcanic rocks in a dark red, hematitic matrix (sample AJ). This unit is in contact with a 10-ft-thick section of relatively unfolded, brick-red, finely laminated, hematitic chert (sample AI).

Upstream from the chert is 75 to 80 ft of reddish sedimentary breccia consisting of clasts of mafic volcanic rocks in a graywacke matrix. The breccia unit is divided by a 20-ft-thick section of soft, reddish-green, chlorite-altered mafic volcanic rocks or tuff (sample AL). Bedding in the sedimentary breccia has an irregularly laminated appearance and is folded and possibly faulted. This unit is in contact with a 120-ft-thick section of red, hematitic graywacke (samples J and AN) with interbedded layers of angular breccia (sample AM) and stretched, grain-supported chert-pebble conglomerate (sample B). Orientation of tension cracks and elongation of the chert pebbles indicate stretching in an east-west direction. The hematitic graywacke is overlain by 80 ft of altered mafic volcanic rocks (sample AO), which are in turn overlain by another 60 to 70 ft of hematitic graywacke (samples K and AH) and interbedded conglomerate layers.

From the 640-ft position to beyond the northern end of the mapped area, the country rock consists of a massive section of green to purple, aphanitic to porphyritic-aphanitic, amygdaloidal, spilitized, mafic volcanic rocks. The greenstone becomes silicic and ferruginous (as a result of the weathering of introduced sulfides) in brecciated areas and in proximity to the numerous shears and joints that occur along the creek. Amygdules are filled with calcite and an outer margin of a blue-green clay mineral.

Graded bedding occurs in the sedimentary section at the south end of the mapped area and seems to indicate an up direction to the north. However, the area is structurally complicated by faulting and folding that makes the sedimentologic information equivocal. Identifiable bedding surfaces are rare and are complicated by structural deformation and probable overturning. In general, the dip angle of bedding is steep (>60°). Based on our

observations and their similarity to descriptions of the Gambier Bay Formation and the basal sedimentary unit of the Hyd Group (Loney, 1964; Lathram and others, 1965; Rubin and Saleeby, 1991, p. 14,556), we suggest that the rocks in this area represent the lower sedimentary and middle volcanic intervals of the Hyd Group, which rest unconformably upon the Gambier Bay Formation.

There are three dominant structural trends. The oldest and most penetrative fabric trends northwest parallel to the regional structural trend. Previous mapping on the north shore of Gambier Bay (Loney, 1964; Lathram and others, 1965) shows a northwest-trending fault along the creek. The previously mentioned mineral occurrences are located on or near northwest-trending structures. This structural trend is exhibited by numerous faults and shear zones less than 1 ft to 10 ft wide. Rocks within these shear zones commonly have horizontal slickensides, gouge, and silicified, thoroughly ferruginized breccia. The second structural trend is oriented predominantly east-west and is present as small shear zones and joint sets with associated horizontal slickensides and breccia as described above. Shearing and brecciation are most intense in the central part of the mapped area. The intensity diminishes northward, where iron-stained joint sets predominate. The third, less pervasive structure strikes north to northeast and is present as small faults, joints, and calcite veins. At one location (site AD near the 900-ft position), an east-trending fault displaces a north-northeast-trending fault.

Mineralization occurs primarily within sheared and brecciated zones in the mafic volcanic rocks. Chalcopyrite and barite are the major constituents with lesser bornite, pyrite, sphalerite, galena, covellite, and silver-rich tetrahedrite. Chalcopyrite occurs (1) as clots up to several centimeters in diameter with associated coarse crystalline, bladed, white barite, (2) as millimeter-sized grains disseminated in the greenstone, and (3) as massive, flow-banded material that is intimately intergrown with bornite, covellite, tetrahedrite, and fine-grained pyrite and quartz. Covellite occurs as fine, hairlike needles and laths within the bornite. Tetrahedrite occurs as small blebs and fracture fillings within the chalcopyrite-bornite assemblage.

Quartz-carbonate veins 1 to 10 cm wide are commonly present in the mineralized shear and breccia zones. The veins contain pyrite, chalcopyrite, and bladed barite in their interiors. The barite is partially to completely replaced by quartz and iron-rich dolomite. The sulfides are present as thin (1 mm), deformed lines of crystals, similar in appearance to stylolites, near the outer edges of the veins or in selvages at the vein/country-rock contact. The veins range from concordant to highly discordant to the host rock.

A second, distinct mineral assemblage consists of breccia- and fracture-filling quartz, sphalerite, tetrahe-

Table 4A. Univariate statistical analysis of selected elements in -200-mesh stream-sediment samples and the threshold values selected for single-element plots

[All values in parts per million. Abbreviations: DV, number of determinant (unqualified) variables; N, number of variables below the lower limit of detection; L, number of variables detected at the lower limit of detection; G, number of variables greater than the upper limit of detection.]

Element	DV	N	L	Concentration		Percentile		Threshold value
				Minimum	Maximum	50th	90th	
Ba -----	52	0	0	200	2900	820	2100	2100
Ni -----	52	0	0	27	180	77	118	118
Ag -----	52	0	0	.08	.88	.26	.536	.5
As -----	52	0	0	5.7	350	21	120	90
Cd -----	52	0	0	.18	2.8	.65	1.68	1.6
Cu -----	52	0	0	42	250	58	81	80
Mn -----	52	0	0	980	3400	1500	1880	1880
Mo -----	24	0	28	2	19	2.1	4.94	4.9
Pb -----	49	0	3	4	48	9.2	13.8	13.8
Sb -----	49	3	0	.73	27	2	5.18	5.18
Zn -----	52	0	0	60	390	110	180	180
Au -----	48	0	4	.002	.016	.004	.008	.008
Hg -----	52	0	0	.03	2	.17	.542	.55

Table 4B. Univariate statistical analysis of selected elements in nonmagnetic heavy-mineral-concentrate samples and the threshold values selected for single-element plots

[All values in parts per million unless otherwise noted]

Element	DV	N	L	G	Concentration		Percentile		Threshold value
					Minimum	Maximum	50th	90th	
Fe (%) ----	50	0	0	2	1	50	15	50	50
Ni -----	52	0	0	0	10	500	70	300	300
Ag -----	19	22	11	0	1	7	0.7	3	3
As -----	5	45	2	0	500	1500	250	350	700
Cd -----	5	45	2	0	50	500	25	35	70
Cu -----	52	0	0	0	15	1000	150	700	700
Mn -----	52	0	0	0	100	500	200	300	300
Pb -----	44	1	7	0	20	1000	30	100	100
Zn -----	21	27	4	0	500	5000	250	2000	2000

drite and very minor galena. This assemblage has also been noted in float as disseminated grains in a quartz-veined and silicified mafic volcanic rock. In several well-brecciated, mineralized samples where crosscutting relationships can be seen, matrix material consisting of fine-grained chalcopyrite and large bladed crystals of barite are clearly crosscut by veinlets of quartz, sphalerite, tetrahedrite, and minor galena. This assemblage is present in the two prominent structures at the 700- and 800-ft positions near the transition from volcanic rocks to sedimentary rocks, and in a float sample (sample T) from the creek bed at the northern end of the mapped area.

The geochemistry of the mineralized samples (table 3) closely reflects the mineralogy. Most samples contain 0.1 to 1 percent Cu, 0.1 percent Zn, several ppm Ag, and highly anomalous concentrations of Mn, As, Cd, Mo, Pb, Sb, and Hg. The two most highly mineralized samples (samples AA and R) are examples of the first type of mineral assemblage and contain anomalously high Cu

(20 and 6.8 percent, respectively), Ag (84 and 38 ppm, respectively), and highly anomalous As, Mo, and Hg. Samples in which the second mineral assemblage is present contain high Zn and Pb concentrations with minor Cu. Sample T is the most extreme example of this, with 1.1 percent Zn, 0.65 percent Pb, and 7.4 ppm Ag.

In order to test the extent of mineralization within and away from the mineralized structures, we collected a composite chip sample from each of two mineralized shear zones that cross the creek at the 700- and 800-ft positions (samples AE and AG, fig. 4). A third composite chip sample (sample AF) was collected from the massive altered mafic volcanic rocks in-between. The analyses (presented in table 3) indicate strong enrichment of Cu, Pb, Zn, and associated trace elements in the mineralized structures and a distinct drop in concentration of the same elements in the unmineralized mafic volcanic rocks. These samples clearly show that the mineralization is confined to the structures.

DISCUSSION AND CONCLUSIONS

Analysis of the geochemical data from the Ward Creek/Windfall Harbor area clearly confirms and further constrains the presence of a belt of rocks that are prospective for VMS-type mineralization. This belt, which is characterized by stream-sediment and heavy-mineral-concentrate samples with anomalous concentrations of Mn, Ni, Ag, As, Cd, Sb, Mo, Ba, Cu, Pb, Zn and Hg (\pm Au), closely corresponds with exposures of Permian to Late Triassic mafic volcanic and flysch-type sedimentary rocks. Although there are a few stream-sediment and heavy-mineral-concentrate samples that may indicate the presence of small mineral occurrences, we interpret the belt of anomalous samples to be a reflection of the high background concentration of these elements in the Permian and Triassic rocks. This observation implies that the slight zonation in element enrichment of As, Sb, Pb, and Ba at the northwest end of the belt to enrichment of Au and Hg at the southeast end reflects a difference in the background concentrations of these elements in the Retreat Group and the Hyd Group. Such a difference might provide a means of distinguishing geochemically between the two groups of Triassic rocks in areas of poor exposure. It also suggests that the Retreat Group may be more likely to host Cu-Pb-Zn-Ag-Ba rich VMS-type deposits and the Hyd Group most likely to host Cu-Zn-Au-Ag deposits. However, further work is needed to clarify and (or) substantiate this suggestion.

We cannot speculate on the genesis of the North Gambier mineral occurrence. Further work will focus on determining the extent of mineralization, confirming its stratigraphic and structural setting, determining more completely the geochemical expression of the mineralization and associated alteration of country rock, and exploring the possibility that this occurrence may be continuous with previously noted mineralization on the ridge to the southeast and (or) with the prospects on Gambier Mountain.

Acknowledgments.—We wish to thank Karen Kelley and Al Hofstra for thorough reviews that greatly improved the paper; John Philpotts for his cheerful help in the field; Paul Briggs, Dave Fey, Jerry Motooka, Phil Hageman, and Bruce Roushey for their careful geochemical analyses; Steve Sutley for the XRD mineralogical determinations; and Karen Kelley for her never-ending help with the NURE data. Vivian Hoffman, the U.S. Forest Service manager for the Admiralty Island National Monument, was especially helpful in granting access to the study area. We also offer a special thanks to Dan Maurice and Tim Perry, our helicopter pilots. Without their steady flying this study would have been impossible.

REFERENCES CITED

- Barker, F., 1957, Geology of the Juneau (B-3) quadrangle, Alaska: U.S. Geological Survey Map GQ-100, scale 1:63,360.
- Berg, H.C., and Cobb, E.H., 1967, Metalliferous lode deposits of Alaska: U.S. Geological Survey Bulletin 1246, 254 p.
- Berg, H.C., Decker, J.E., and Abramson, B.S., 1981, Metallic mineral deposits of southeastern Alaska: U.S. Geological Survey Open-File Report 81-122, 1 sheet, scale 1:1,000,000, 136 p.
- Berg, H.C., and Grybeck, D., 1980, Upper Triassic volcanogenic Zn-Pb-Ag (-Cu-Au)-barite mineral deposits near Petersburg, Alaska: U.S. Geological Survey Open-File Report 80-527, 9 p.
- Berg, H.C., Jones, D.L., and Coney, P.J., 1978, Map showing pre-Cenozoic tectono-stratigraphic terranes of southeastern Alaska and adjacent areas: U.S. Geological Survey Open-File Report 78-1085, 2 sheets, scale 1:1,000,000.
- Berg, H.C., Jones, D.L., and Richter, D.H., 1972, Gravina-Nutzotin belt: Tectonic significance of an upper Mesozoic sedimentary and volcanic sequence in southern and southeastern Alaska: U.S. Geological Survey Professional Paper 800-D, p. D1-D24.
- Brew, D.A., and Ford, A.B., 1984, Tectonostratigraphic terranes in the Coast plutonic-metamorphic complex, southeastern Alaska, in Reed, K.M., and Bartsch-Winkler, S., eds., The United States Geological Survey in Alaska: Accomplishments during 1982: U.S. Geological Survey Circular 939, p. 90-93.
- Brew, D.A., Karl, S.M., Barnes, D.F., Jachens, R.C., Ford, A.B., and Horner, R., 1991, A northern Cordilleran ocean-continent transect: Sitka Sound, Alaska, to Atlin Lake, British Columbia. Canadian Journal of Earth Sciences, v. 28, no. 6, p. 840-853.
- Cobb, E.H., 1972a, Metallic mineral resources map of the Sitka quadrangle, Alaska: U.S. Geological Survey Miscellaneous Field Studies Map MF-467, 1 sheet, scale 1:250,000.
- 1972b, Metallic mineral resources map of the Sumdum quadrangle, Alaska: U.S. Geological Survey Miscellaneous Field Studies Map MF-425, 1 sheet, scale 1:250,000.
- 1978a, Summary of references to mineral occurrences (other than mineral fuels and construction materials) in the Sitka quadrangle, Alaska: U.S. Geological Survey Open-File Report 78-450, 124 p.
- 1978b, Summary of references to mineral occurrences (other than mineral fuels and construction materials) in the Sumdum and Taku River quadrangles, Alaska: U.S. Geological Survey Open-File Report 78-698, 64 p.
- Crock, J.G., Lichte, F.E., and Briggs, P.H., 1983, Determination of elements in National Bureau of Standards geologic reference material SRM 278 obsidian and SRM 688 basalt by inductively coupled argon plasma-atomic emission spectrometry: Geostandards Newsletter, v. 7, p. 335-430.
- Davis, J.C., 1986, Statistics and data analysis in geology (2d ed.): New York, Wiley, 646 p.
- Ford, A.B., and Brew, D.A., 1988, The Douglas Island Volcanics: Basaltic rift not island arc volcanics of the "Gravina-Nutzotin belt," northern southeastern Alaska [abs.]: Geological Society of America Abstracts with Programs, v. 20, no. 7, p. 111.
- Ford, A.B., Karl, S.M., Dutweiler, K.A., Sutphin, D.M., Finn, C.A., and Brew, D.A., 1989, Sitka quadrangle, Alaska—

- An AMRAP preassessment planning document: U.S. Geological Survey Administrative Report, 92 p.
- Gehrels, G.E., and Saleeby, J.B., 1987, Geologic framework, tectonic evolution and displacement history of the Alexander terrane: *Tectonics*, v. 6, p. 151-173.
- Goldfarb, R.J., Nelson, S.W., Berg, H.C., and Light, T.D., 1987, Distribution of mineral deposits in the Pacific Border Ranges and Coast Mountains of the Alaskan Cordillera, in Elliot, I.L., and Snee, B.W., eds., *Geoexpo/86—Exploration in the North American Cordillera: Vancouver, British Columbia, Canada, Association of Exploration Geochemists*, p. 19-41.
- Grimes, D.J., and Marranzino, A.P., 1968, Direct-current arc and alternating-current spark emission spectrographic field methods for the semi-quantitative analysis of geologic materials: U.S. Geological Survey Circular 591, 6 p.
- Herbert, C.F., and Race, W.H., 1965, Geochemical investigations of selected areas in southeastern Alaska, 1964 and 1965: Alaska Division of Mines and Minerals Geochemical Report 6, 65 p.
- Karl, S.M., 1989, Preliminary geologic map of the Sitka quadrangle, Alaska in Ford, A.B., Karl, S.M., Duttweiler, K.A., Sutphin, D.M., Finn, C.A., and Brew, D.A., Sitka quadrangle, Alaska—An AMRAP preassessment planning document: U.S. Geological Survey Administrative Report, plate 2, scale 1:250,000.
- Kelley, K.D., 1990, Interpretation of geochemical data from Admiralty Island, Alaska—Evidence for volcanogenic massive sulfide mineralization, in Goldfarb, R.J., Nash, J.T., and Stoesser, J.W., eds., *Geochemical studies in Alaska by the U.S. Geological Survey, 1989*: U.S. Geological Survey Bulletin 1950, p. A1-A9.
- Kennedy, K.R., and Crock, J.G., 1987, Determination of mercury in geological materials by continuous flow, cold vapor, atomic absorption spectrophotometry: *Analytical Letters*, v. 20, no. 6, p. 899-908.
- Lambert, I.B., and Sato, T., 1974, The Kuroko and associated ore deposits of Japan: A review of their features and metallogenesis: *Economic Geology*, v. 69, p. 1215-1236.
- Lathram, E.H., Pomeroy, J.S., Berg, H.C., and Loney, R.A., 1965, Reconnaissance geology of Admiralty Island, Alaska: U.S. Geological Survey Bulletin 1181-R, 48 p.
- Loney, R.A., 1964, Stratigraphy and petrography of the Pybus-Gambier area, Admiralty Island, Alaska: U.S. Geological Survey Bulletin 1178, 103 p.
- Monger, J.W.H., and Berg, H.C., 1987, Lithotectonic terrane map of western Canada and southeastern Alaska: U.S. Geological Survey Miscellaneous Field Studies Map MF-1874-B, scale 1:2,500,000.
- Motooka, J.M., 1988, An exploration geochemical technique for the determination of preconcentrated organometallic halides by ICP-AES: *Applied Spectroscopy*, v. 42, p. 1293-1296.
- Rubin, C.M., and Saleeby, J.B., 1991, The Gravina Sequence: Remnants of a mid-Mesozoic oceanic arc in southern southeast Alaska: *Journal of Geophysical Research*, v. 96, no. B9, p. 14,551-14,568.
- Thompson, C.E., Nakagawa, H.M., and Van Sickle, G.H., 1968, Rapid analysis for gold in geologic material: U.S. Geological Survey Professional Paper 600-B, p. B130-B132.
- Wright, C.W., 1906, A reconnaissance of Admiralty Island: U.S. Geological Survey Bulletin 287, p. 138-161.
- 1907, Lode mining in southeastern Alaska, 1907: U.S. Geological Survey Bulletin 314, p. 47-72.
- Wright, F.E., and Wright, C.W., 1904, Economic developments in southeastern Alaska: U.S. Geological Survey Bulletin 259, p. 47-68.

Reviewers: Karen D. Kelley and Al Hofstra

Experimental Abrasion of Detrital Gold in a Tumbler

By Warren Yeend

Abstract

Gold grains were tumbled with gravel for up to 150 h (200 km) at 1.33 and 3.00 km/h. The eroded products of both the gold and gravel were noted, and curves were plotted showing the breakdown of both gravel and gold with time (distance of travel). Comparison of these data with data gathered from an earlier study seems to indicate that the breakdown of gold increases markedly between a travel rate of 0.85 km/h and 1.33 km/h. The higher rate of gold breakdown associated with higher tumbler rates can be negated by the presence of friable gravel clasts, in that there appears to be an inverse relation between the breakdown of gravel and the included gold fragments—the faster the gravel breaks down, the slower the gold breaks down, and vice versa. A gold breakdown rate of 0.25 percent/km seems to be the average when tumbling at 1.33 to 3.0 km/h.

INTRODUCTION

Originally conceived in the early 1970's, this study sought to learn about the physical breakdown of native-gold fragments in a simulated high-energy, alluvial-like environment. It was thought that the malleable nature of gold would probably lead to much different rates of physical breakdown and produce different shapes as compared with the breakdown of readily fractured silicate-rich minerals and rocks. The results of this study should be useful for interpreting the geologic history of gold-containing alluvial deposits.

The first phase of this study was published in 1975 (Yeend, 1975). Subsequently, it was recognized that more work was needed to better understand the physical breakdown of gold in a high-energy environment. Although this study adds to the small body of knowledge dealing with physical breakdown of native gold, there is certainly more to learn. And, as is so typical of studies of this nature, more questions are raised than answered, and related subjects that should be studied become evident. The first study used a 5-gal polyethylene bottle commonly referred to as a "carboy," with indented handholds in the sides as the tumbler. In an attempt to remove any erosive effects produced by the tumbler

itself, a rock-polishing tumbler with a rubber liner was obtained for the present study. In the original experiment, reconstructions of various combinations of sand, pebbles, and cobbles were used as the erosive material. In the current experiments, actual samples of sand and gravel collected from placer-rich river systems in Alaska were used as the erosive material. It was thought that this would more accurately simulate actual stream-erosion conditions.

The study was conducted in the office using gold fragments obtained from placers in the Circle Mining District in Alaska. The methods used and the experimental results from five separate sample "runs" in the tumbler are described. Graphs show both the loss of weight (unrecoverable by panning) of the original gold fragments and the weight loss of the >2-mm-size gravel fraction with duration of tumbler travel. Photos show the before-and-after appearance of the gold fragments used in the tumbling experiments. Finally, an attempt is made to interpret the experimental data.

PREVIOUS WORK

I am unaware of any field or laboratory studies on the physical breakdown of gold since my earlier report (Yeend, 1975). Mention is made in that paper of abrasion studies done on minerals such as quartz, garnet, tourmaline, apatite, and hornblende, among others, and of work done on the chemical and colloidal properties of gold (particularly its solubility versus insolubility).

Several studies of a somewhat related nature to the present one have been published. Hallbauer and Utter (1977) studied the relationship between the transport distance and changes in the surface morphology as well as changes in the chemical composition of gold particles during transport. They were able to detect characteristic changes in the morphology to allow an estimate of transport distances in the 10- to 30-km range. Parker (1974), sampling the <1-mg gold flakes along mountain creeks in Colorado found a downstream gold-fragment size decrease of from 5 to 23 percent per kilometer. How much of this decrease was a result of physical abrasion and

how much was due to selective sorting because of a lessened carrying capacity of the stream as a result of a flatter gradient is not known.

METHODS

Gold flakes were tumbled with sand, gravel, and water for measured time intervals of 5 to 150 h and then recovered by panning. The gold fragments and gravel were separately weighed and the weight loss noted. Changes were made to the different runs in the tumbler; these included varying the tumbler speed, the amount of gold, and the gravel components, as is subsequently described. Graphs show the weight loss of gold fragments and gravel with progressive distance of tumbler travel.

The tumbler used in this study has a 40-lb, 4-gal capacity and uses a 1/3-hp (horsepower) electric motor (fig. 1). The tumbler rotation speed was altered by changing pulley size on the tumbler rollers, and, correspondingly, the drive-belt length running off the motor pulley. The two tumbler speeds used were 28 and 64 rpm (revolutions per minute). The tumbler interior is hexagonal in outline, 29 cm in depth, and 13 cm wide on each side of the hexagon, giving an interior circumference of 78 cm. Using this circumference and the 28- and 64-rpm tumbler speeds, travel rates for the material tumbled can be calculated at 1.33 and 3.00 km/h. The tumbler possesses a heavy rubber liner. One end of the tumbler is removable for easy loading and unloading. The removable end is covered on the interior by a heavy rubber gasket. Because of the complete rubber lining, all abrasive effects were a result of the interaction of the gravel, sand, and clay. When running at the slow (1.33

km/h) rate, the sound of the gravel being tumbled was barely discernible. At the faster rate (3 km/h), however, the noise level bordered on being objectionable in an office environment.

Gold fragments used in this study were obtained from streams in the Circle Mining District in east-central Alaska. Size of the fragments ranged from 1 to 5 mm in diameter. They were generally bright and shiny with no adhering minerals. For each run, 10 to 12 gold fragments were used. The total gold fragment weights used in each run ranged from 48 to 401 mg determined to the nearest milligram. Photos were taken of the gold fragments from selected runs both before and after tumbling to show the changes in shape and number of recoverable fragments.

Sand and gravel used in the tumbler runs was collected from the floodplains of several different gold-bearing creeks in the Circle Mining District in east central Alaska (Yeend, 1991). The gravel possessed subangular to subrounded clasts up to 7 cm in diameter. The clasts were predominantly quartzite and quartz-mica schist, with some white quartz and granite. In the initial run of this study, no records were kept of the weight loss of the gravel. Subsequently, it was determined that this information would be useful, so on the ensuing runs, the weight percentages of the gravel fraction greater than 2 mm was noted both before and after tumbling. The amount of abraded products produced provided some comparison of the energy levels of the different runs. The schist clasts broke down the fastest.

The tumbler runs of gravel and gold were designed to test the abrasion rates of gold in several different environments. The tumbler was rotated both at 1.33 km/h and at the increased travel rate of 3.00 km/h in order to test the effects of increased velocity as might be present in a steep-gradient creek or of increased volumes of runoff in storm conditions. My earlier work (Yeend, 1975) had shown a tenfold increase in abrasion rates with a fourfold increase in velocity. The rotation rates used in the current study were determined by the pulley diameters available.

The tumbler was stopped at selected intervals during a run (anywhere from 5 to 40 h), and the gold separated by panning from the gravels. The recovered gold fragments were counted and weighed. Fragments smaller than 0.25 mm were not recovered; thus, gold finer than this was considered the abraded, lost gold. In several of the runs, the gravel with all its abraded products was used throughout the run. In others, at selected intervals, the old gravel and its eroded products were replaced by a new batch of gravel. This, in effect, introduced coarse particles and removed the fine-grained sand, silt, and clay that was produced during tumbling. The effect of this change would be somewhat analogous to that caused by tributary creeks contributing a coarser fraction of

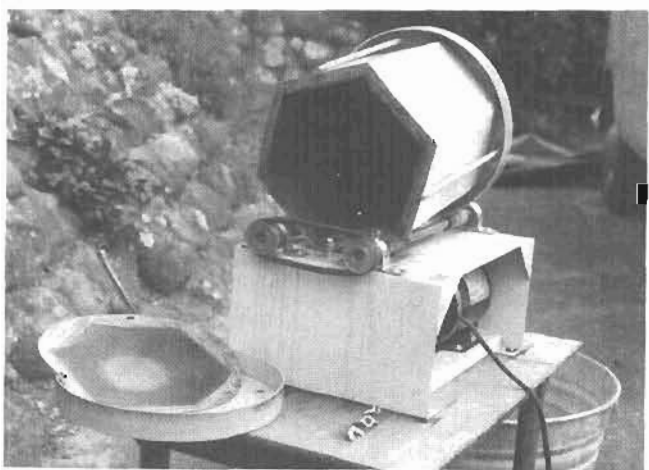


Figure 1. The 40-lb, 4-gal tumbler with 1/3-hp electric motor used in this study. Metal end and rubber gasket have been removed, showing hexagonal shape and rubber liner, having 78-cm internal circumference.

Table 1. Gold breakdown rate and averages for various tumbler runs, including previous study (Yeend, 1975)

Run /batch number (travel distance in km)	Rotation rate (km/h)	Gold breakdown rate during each run/batch (percent/ km)	Gold breakdown- rate averages (percent/ km)
Run 1 (151.8)-----	1.33	0.18	
Run 2 (198)-----	1.33	.25	
Run 3 (180)-----	3.00	.25	
Run 4			
batch 1 (45)-----	3.00	.29	
batch 2 (45)-----	3.00	.29	
batch 3 (45)-----	3.00	.27	
batch 4 (45)-----	3.00	.41	
total (180)-----	3.00		0.26
Run 5			
batch 1 (40)-----	1.33	.03	
batch 2 (46)-----	1.33	.01	
batch 3 (40)-----	1.33	.05	
batch 4 (40)-----	1.33	.08	
total (160)-----	1.33		.04
All runs at -----	1.33		.16
All runs at -----	3.00		.26
Yeend study (1975)---	.85		.02

gravel periodically to the trunk creek. These details are discussed in the description of the individual tumbler runs.

Graphs show the distance of tumbler travel plotted against gold and gravel weight loss percent. Because different weights of gold and gravel were used in the different runs, this method of graphical representation allows comparison between runs.

In each run, 2 to 3 liters of tap water were used to completely cover the gravel and contained gold. The same muddy water was used throughout a run, and no attempt was made to add clean water. Each run lasted from 60 to 150 h, the shorter times corresponding with the faster rotation rates. The total tumbler distance traveled in all runs varied from approximately 150 to 200 km. This seemed a sufficient distance to establish breakdown rates for the gold. The results of the tumbler runs are presented in the order in which they were done. A summary of the gold breakdown rates and comparison with the earlier study (Yeend, 1975) are presented in table 1.

TUMBLER RUNS

Run #1

Ten gold flakes 3 to 5 mm in diameter weighing 324 mg were tumbled with 4.437 kg of cobble gravel obtained from Mastodon Creek in the Circle Mining District, Alaska. The tumbler was rotated at a rate of 1.33 km/h. It was periodically stopped and the gold separated and weighed at the following time (distance) intervals: 5 h (6.6 km), 15 h (20.0 km), 35 h (46.2 km), 75 h (99 km), and 115 h (151.8 km). At the end of the run the recoverable, very flattened gold consisted of 9 fragments 2.0–4.0 mm; 2 fragments 1.0–2.0 mm; 4 fragments 0.5–1.0 mm; and 2 fragments 0.25–0.5 mm. The recovered gold weighed 236 mg, representing a 27.1 percent loss of weight, or 0.18 percent/km. This total weight loss was at a more-or-less uniform rate over the duration of the run, as the slope of the weight-loss curve shows (fig. 2).

Run #2

Small particles of gold weighing substantially <run #1 were used in run #2. Ten gold flakes 1 to 2 mm in greatest dimension weighed 48 mg. The gravel, obtained from Eagle Creek in the Circle Mining District, Alaska, was classified in two size fractions—>2-mm diameter, 3.83 kg; and <2-mm diameter, 0.43 kg. The tumbler was rotated at the rate of 1.33 km/h for 150 h. Gold was separated and weighed five times during the total run of 198 km. The ending gold weight of 24 mg was exactly 50 percent of the original weight and gives a weight-loss rate of 0.25 percent/km (fig. 2). At the end of the run, the gold consisted of 11 fragments 1.0–2.0 mm; 5 fragments 0.5–1.0 mm; and 3 fragments 0.5–0.25 mm. The coarse fraction of the gravel (>2 mm) had lost 55 percent of its weight (0.28 percent/km), most of

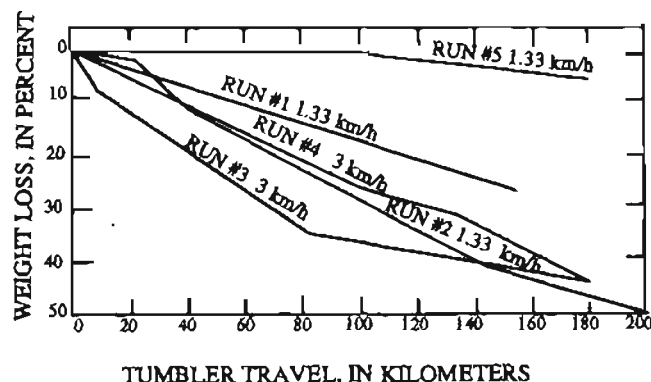


Figure 2. Curves showing weight loss of gold fragments with distance of tumbler travel for five different tumbler runs.

which was eroded to fine silt or clay-sized particles (fig. 3). The <2-mm-size fraction had increased by 6 times, and 95 percent of this was fine silt and clay.

Run #3

The rate of tumbler travel was increased to 3 km/hr in run #3. Gravel from Bottom Dollar Creek, Circle Mining District, Alaska, was tumbled with 10 fragments of gold that were 2–5 mm in greatest dimension and weighed 401 mg. The gravel clasts included 1.30 kg of <2-mm size, and 3.49 kg of greater than 2-mm size. Five of the gold fragments were obtained from the previous run and were very flat in shape; five fragments were newly introduced and were not particularly flattened but did have rounded edges. The gold-particle breakdown with progressive tumbling is as follows: 4 h (12 km), 10 fragments 2–5 mm, 4 fragments <1 mm; 12 h (36 km), 6 fragments >2 mm, 2 fragments 1–2 mm, 6 fragments <1 mm; 28 h (84 km), 8 fragments >2 mm, 3 fragments 1–2 mm, 4 fragments 0.25–1.0 mm, several hundred fragments <0.25 mm; 60 h (180 km), 10 fragments 1.5–3 mm, 11 fragments 0.25–1.5 mm, several hundred fragments <0.25 mm. The gold lost 46 percent of its original weight, or 0.25 percent/km. The >2-mm-size gravel fraction lost 73 percent of its original weight, or 0.40 percent/km. The <2-mm-size fraction increased 300 percent in weight, 98 percent of which was silt and clay.

Run #4

Run #4 varied from the previous runs by the introduction of a new batch of gravel at selected intervals. Gravel from the Ketchum Creek drainage, Circle Mining District, Alaska, was divided into four approximately

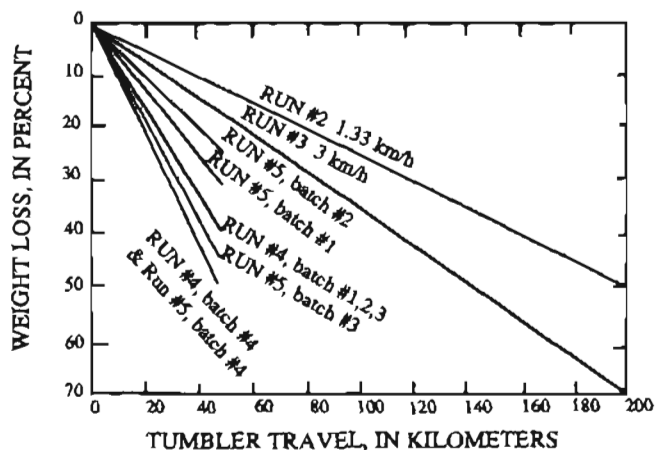


Figure 3. Curves showing gravel (>2-mm size) weight loss with distance of tumbler travel.

equal batches. After 15 h (45 km) of tumbler travel, the gold and gravel were separated and both were weighed. The gravel was discarded, and a new batch of gravel was added for the next 15-h (45 km) run. This would simulate the introduction of gravel by tributaries along a stream system. The same gold was used throughout the run. Twelve gold fragments 1.5–3.0 mm in diameter and weighing 190 mg were used for this run. At the beginning of the run, the 12 gold fragments consisted of 8 thin and very flattened fragments, 2 thicker but definitely flattened fragments, and 2 fragments that were ragged in outline, but not flattened.

Batch #1

The gravel-size fractions used consisted of 0.59 kg of <2-mm size and 1.96 kg of greater than 2-mm size. After 15 h (45 km) of tumbler travel, the gold weighed 165 mg, which represented a 13 percent weight loss, or 0.29 percent/km. The coarse gravel (>2 mm) weighed 1.18 kg, having lost 40.0 percent of its weight, or 0.89 percent/km, about 3 times the rate of the gold weight loss. The gold had broken down as follows: 6 fragments 1.5–3.0 mm; 6 fragments 1.0–1.5 mm; 15 fragments 0.5–1.0 mm; 15 fragments 0.25–0.5 mm; and 50 to 100 fragments <0.25 mm.

Batch #2

The gravel-size fractions were 1.79 kg of >2-mm size and 0.35 kg of <2-mm size. Following 15 h (45 km) of tumbling, the gold weighed 143 mg, having lost 13 percent of its starting weight, or 0.29 percent/km. The coarse-gravel fraction (>2 mm) had lost 40.0 percent of its original weight, or 0.89 percent/km. The gold particles included 5 fragments 1.5–3.0 mm; 8 fragments 1.0–1.5 mm; 10 fragments 0.5–1.0 mm; 13 fragments 0.25–0.5 mm; and 50 to 100 fragments <0.25 mm.

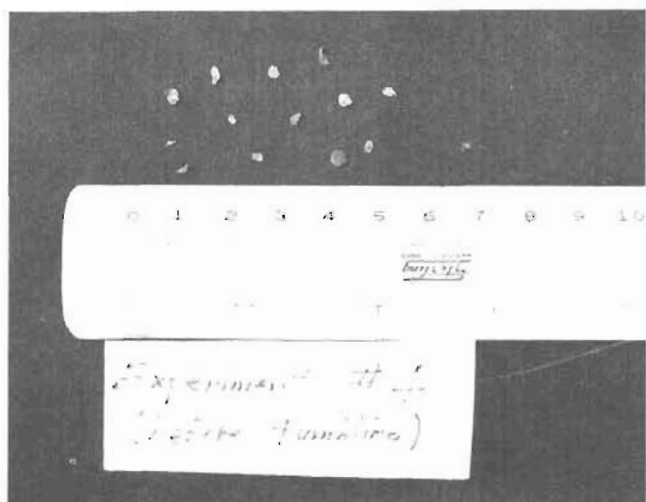
Batch #3

The starting gravel weights were 1.83 kg of >2-mm size and 0.45 kg of <2-mm size. After 15 h (45 km) of tumbling, the gold weighed 126 mg, which is equivalent to a 12 percent weight loss, or 0.27 percent/km. The coarse gravel lost 40.3 percent of its original weight, or 0.89 percent/km. The gold showed the following size classification: 5 fragments 1.5–3.0 mm; 6 fragments 1.0–1.5 mm; 20 fragments 0.5–1.0 mm; 6 fragments 0.25–0.5 mm; and 50 to 100 fragments <0.25 mm.

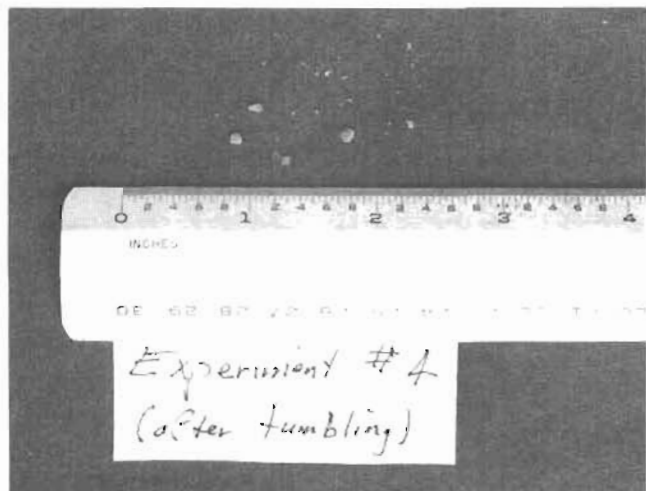
Batch #4

The recoverable gold in batch #4 was reduced to 103 mg which represented a loss of 18.3 percent from

the starting weight at the beginning of the batch run. This was the equivalent weight loss of 0.41 percent/km. The gravel lost 46.0 percent of its starting weight, or 1.02 percent/km. The final gold products were: 4 fragments 1.5–3.0 mm; 5 fragments 1.0–1.5 mm; 9 fragments 0.5–1.0 mm; 11 fragments 0.25–0.5 mm; and several hundred fragments <0.25 mm. Photos of the gold fragments before they were run with the first batch of gravel and after they were tumbled with the last batch of gravel are displayed in figure 4. For the entire length of run #4 (60 h, 180 km) the gold lost 45.0 percent of its original weight, or 0.26 percent/km, and the coarse gravel averaged 41.6 percent weight loss, or 0.92 percent/km.



A



B

Figure 4. Gold fragments used in run #4. A, Before tumbling. B, After 180 km of tumbler travel. Scale numbers are centimeters.

Run #5

Run #5 was characterized by slowing the tumbler back to the 1.33 km/h rate, and, similar to run #4, introducing equal amounts of fresh gravel and removal of the old gravel after each 30 h (40 km) of tumbling. Gravel composed exclusively of schist clasts from Switch Creek, Circle Mining District, Alaska, was used in the first two batches. Schist and granite gravel from an alluvial bench in Deadwood Creek, Circle Mining District, Alaska, was used in the final two batches. Ten gold fragments were introduced at the beginning of the run, and the same gold was used throughout the run.

Batch #1

The coarse-gravel fraction (>2 mm) weighed 1.71 kg. Ten flattened-gold fragments weighed 206 mg and were all 2 to 4 mm in diameter. After tumbling for 30 h (40 km), the gold had lost only 1.0 percent of its weight, while the coarse gravel (>2 mm) had lost 31.0 percent of its weight. The gold had broken down as follows: 10 fragments 2.0–4.0 mm; and 1 fragment 0.5–1.0 mm.

Batch #2

A fresh batch of Switch Creek gravel was introduced to the tumbler with the gold fragments from batch #1. After 30 h (40 km) of tumbling the coarse gravel fraction (>2 mm) had lost 26.5 percent of its weight, and the gold had lost only 0.5 percent of its weight. The gold fragments were made up of 10 fragments 2.0–4.0 mm; and 2 fragments 1.0–2.0 mm.

Batch #3

The gravel used in this batch was collected from a high-level bench in Deadwood Creek valley, Circle Mining District, Alaska. It was composed predominantly of schist with a few granitic and quartz clasts. The coarse fraction of 1.25 kg lost 42.0 percent of its weight following 30 h (40 km) of tumbling. The gold fragments lost 2.0 percent of their weight and were composed of 10 fragments 2.0–4.0 mm; and 2 fragments 1.0–1.5 mm.

Batch #4

The same kind of gravel as used in batch #3 was used here (Deadwood Creek bench gravel). The coarse fraction had a starting weight of 1.33 kg and lost 46.0 percent of its weight in 30 h (40 km) of tumbling. The gold lost 3 percent of its weight and ended the run as 10 fragments 2.0–4.0 mm; and 2 fragments 1.0–1.5 mm. For all of run #5, the gold lost 6.5 percent of its weight,

or 0.04 percent/km. The coarse gravel from Switch Creek used in batches #1 and #2 averaged a loss of 0.72 percent/km, while the coarse gravel obtained from the bench in Deadwood Creek used in batches #3 and #4 averaged a loss of 1.1 percent/km.

DISCUSSION

This study revealed two important variables in the physical breakdown rate of the gold fragments: the rate of tumbler rotation, and the durability of the coarse clasts making up the gravel. The data are summarized in table 1, which allows comparison of rotation rates with averages of gold breakdown including the 1975 (Yeend) study. There may be some threshold velocity above which the abrasion rate is markedly accelerated. In table 1, an eightfold increase in gold abrasion between the 0.85 km/h tumbler rotation and the 1.33 km/h tumbler rotation rate is observed; such a threshold velocity would seem to be within this range.

There appears to be an inverse relationship between the breakdown of the gravel and the gold—the faster the gravel breakdown, the slower the gold breakdown. This is logical in that a gravel with friable clasts composed mostly of mica schist breaks down to silt- and clay-size fragments quickly, and large clasts are not available to pound the gold fragments. In contrast, gravels rich in durable clasts such as quartz, quartzite, and granite break down slowly and retain their original coarse texture for a longer period of time, thus providing ample “pounding power” to break apart the gold fragments. This relationship is demonstrated in runs #2 and #3, which possessed the most durable gravel clasts. The gravels in these two runs broke down the slowest, as can be seen by the more gentle slope of the curve in figure 3. The gold in runs #2 and #3 broke down rather quickly, as can be seen in the steepness of their curves in figure 2 as compared with the other runs. Likewise, run #5 possesses very friable gravel and broke down extremely fast as the steepness of the curve in figure 3 shows. The gold in run #5 broke down extremely slowly (fig. 2). There is no explanation for this extremely slow abrasion rate of gold in run #5 other than the friability of the gravel. It should be pointed out that both the gravel and the gold in batches #3 and #4 broke down at a faster rate than the gravel or gold in batches #1 and #2. This would seem to have been caused by the presence of the durable granite clasts introduced in the gravel in batches #3 and #4. Batches #1 and #2 used gravel composed of only schist. It seems clear that the granite pulverized the schist and pounded the gold more thoroughly than did the schist clasts in batches #1 and #2.

Although the original aim of the study was to learn about the physical breakdown of gold, it became appar-

ent that the breakdown of the gravel was equally as interesting, and the factors affecting its breakdown were looked for. Certainly rate of tumbling was a factor. How the increase in rate of travel affects the breakdown of gravels with identical clast compositions and textures would be a worthwhile investigation. No attempt was made to do this in this study; however, another study focusing on such factors is contemplated. It seems quite clear that the velocity of travel does produce an increase in the gravel breakdown, but this correlation can be overwhelmed by the soft nature of the gravel clasts. This was demonstrated in runs #3 and #5. Here the faster tumbling rate of run #3, at 3.00 km/h, produced a lower rate of physical breakdown of the gravel composed predominately of quartzite and quartz and 10 percent or less schist—0.4 percent/km as compared to run #5 at 1.33 km/h and a breakdown rate of 0.8 percent/km. This was due to the highly friable nature of the gravel used in run #5, which was composed of both pure schist and a schist/granite mixture. The use of friable gravel here was not purposefully done but, rather, was ascertained after the fact as the factor responsible for this seemingly anomalous result.

Comparisons between the results of this study and those of the 1975 (Yeend) study are suspect for the following reasons. A plastic carboy was used as the tumbler in 1975, and the gravel used in that study was not a “real” gravel collected from a creek bed, but rather it was constructed from two size classes of clasts: cobbles (3–6 cm) and granules (2–5 mm). The extremely low abrasion rates of gold obtained in the 1975 experiment is, therefore, suspect when compared with the results of the current study, where a true tumbler and actual gravel collected from the floodplains of creeks were used. Perhaps the internal shape and hardness of the tumbler was a primary factor. The carboy used in 1975 was hard and round, allowing the contents to slide easily along the bottom during the rotation with little, if any, turbulence of the clastic particles. The tumbler used in the current study was hexagonal in outline with a soft rubber liner (fig. 1). During a run, the gravel and its contained gold would be carried by friction part way up the inside of the rotating barrel, causing the contents to fall back to the bottom. This action could have produced a higher energy environment than within the plastic carboy and may have been responsible for the higher abrasion rates obtained.

CONCLUSIONS

1. A threshold tumble rate above which the breakdown of gold fragments increases substantially (8 times) seems to be in the range of 0.85 km/h to 1.33 km/h.
2. Although a higher rate of tumbling generally produces

a higher rate of breakdown of gold, this is not always true. The higher rate of gold breakdown associated with higher tumbler rate can be negated by the presence of friable gravel clasts, thereby producing a low gold breakdown rate.

3. An average gold breakdown rate of approximately 0.25 percent/km is produced when tumbling at the 1.33 and 3.0 km/h rate with the quartzite schist-rich gravel, the predominant gravel type in creeks within the Circle Mining District; the gravel seems to break down at about 2 to 4 times the gold breakdown rate (0.59 to 1.00 percent/km).
4. There is an inverse relationship between the breakdown of gravel and the breakdown of associated gold fragments—the faster the gravel breakdown, the slower the gold breakdown, and vice versa.
5. The internal shape of the tumbler and the composition of the liner seem to be important factors in the breakdown rate of tumbled rocks and minerals.

REFERENCES CITED

- Hallbauer, K., and Utter, T. 1977, Geochemical and morphological characteristics of gold particles from recent river deposits and the fossil placers of Witwatersrand: *Mineralium Deposita*, no. 12, p. 293-306.
- Parker, B.H.Jr., 1974, Gold placers of Colorado: *Quarterly of the Colorado School of Mines*, no. 3, p. 37.
- Yeend, W.E., 1975, *Experimental abrasion of detrital gold*: U.S. Geological Survey Journal of Research, v. 3, no. 2, p. 203-212.
- 1991, *Gold placers of the Circle district, Alaska—Past, present, and future*: U.S. Geological Survey Bulletin 1943, 42 p., scale 1:63,360. 1 pl.

Reviewers: Robert A. Loney and Béla Csejtey, Jr.

Gold in the Usibelli Group Coals, Nenana Coal Field, Alaska

By Gary D. Stricker, Richard B. Tripp, John B. McHugh, Ronald H. Affolter, and John B. Cathrall

INTRODUCTION

Few data are available on gold content and distribution in U.S. coal, and even fewer data are available on the distribution or the occurrence of gold (Au) in Alaskan coal. Stone (1912) reported Au values as high as 17 parts per million (ppm) in coal ash from northeastern Wyoming. Finkleman (1981) detected 11 ppm Au in one sample of the Waynesburg coal ash from West Virginia. He also observed several flecks of Au in polished sections of the Upper Freeport coal from Pennsylvania and of the Ferron coal from Utah. Chyi (1982) reported that Au contents from 65 bituminous coal samples collected from western Kentucky, on a whole-coal basis, ranged from below the detection level to 1.8 parts per billion (ppb). Rao (1968, p. 2) noted a concentration of 4 ppm Au in the coal ash from one sample of the No. 2 bed at the Nenana coal field.

Gold contents in coal are commonly below the analytical detection limit that was used over 10 years ago. The present lower detection limits for the U.S. Geological Survey's coal-analysis package is 3 ppm on coal ash (Golightly and Simon, 1989). Prior to the early 1980's, the detection limit was 50 ppm on coal ash. The majority of Alaskan coal samples were analyzed at the 50 ppm detection limit. Therefore, all Au analytical values for Alaskan coal stored in the National Coal Resource Data System have been reported as "less than" or "not detected." Recent improvements in analytical methods have lowered the detection limits to 0.001 ppm (1 ppb) on coal ash (O'Leary and Meier, 1986).

Since 1984, we have been collecting face channel samples from the Nos. 3 and 4 beds of the Suntrana Formation that are exposed in the surface mine in the Lignite Creek coal basin, a small basin within the Nenana coal field, near Healy, Alaska (fig. 1). Twelve selected coal samples from these beds along with fly ash from the Golden Valley Electric Association, Inc. (GVEA) power plant at Healy were analyzed for Au content. Fly ash can be defined as all solids that are carried in the gas stream that are the result of the combustion of coal. These particles are collected in the stack recovery system at GVEA.

NENANA COAL FIELD

Since the first written record of utilization of Alaskan coal in 1786, more than half of the coal mined in Alaska has been produced from the Nenana coal field (Sanders, 1981). This field consists of 10 synclinal coal basins partially or completely separated by erosion. These basins extend about 200 km along the northern foothills of the Alaska Range and include, from west to east, the western Nenana, Healy Creek, Lignite Creek, Rex Creek, Tatlanika Creek, Mystic Creek, Wood River, West Delta, East Delta, and Jarvis Creek coal basins. The coals in these basins are in the Usibelli Group (Wahrhaftig, 1987), a sequence of five formations of poorly consolidated continental sedimentary rocks of late Eocene and early to late Miocene age (fig. 2).

The Usibelli Coal Mine is presently surface mining the Nos. 3, 4, and (occasionally) 6 beds from the Suntrana Formation and the Caribou and Moose beds from the Healy Creek Formation (fig. 2). The Caribou and Moose beds are not exposed in the type section near Suntrana Creek and are not shown on figure 2. These beds are found in the upper part of the Healy Creek Formation near the F and E beds (fig. 2). The bulk of the coal mined at the Usibelli Coal Mine is from the Nos. 3 and 4 beds. The specific coal that was burned to produce heat energy and fly ash is and will remain unknown. The power plant utilizes whichever coal is being mined by the Usibelli Coal Mine at the time the power plant's coal stockpile requires additional fuel.

ANALYTICAL PROCEDURE

Gold analyses for this investigation were determined by the procedure reported by O'Leary and Meier (1986). Depending upon the content, sufficient coal to produce 5 to 10 g of organic-free ash was ashed at 680°C for a 24-h period. The ash was then digested with concentrated hydrobromic acid (a 0.5-percent bromine solution), forming a gold-bromide complex that was extracted with methyl isobutyl ketone. This extract was analyzed with electrothermal

atomic-absorption spectrophotometry to determine gold to a lower detection limit of 1 ppb. Approximately 3,000 g of fly ash were collected at GVEA and three random 10 g splits were heated to 680°C to remove any remaining organic material. This organic-free fly ash was then analyzed for Au using the same method as described for coal ash.

ANALYTICAL RESULTS

Gold contents in coal ash for the 12 selected samples from the Nos. 3 and 4 beds of the Suntrana Formation range from 0.001 to 0.018 ppm (1 to 18 ppb). The arithmetic mean is 0.007 ppm with a standard deviation of 0.005 ppm. The analytical results for ash, gold values in

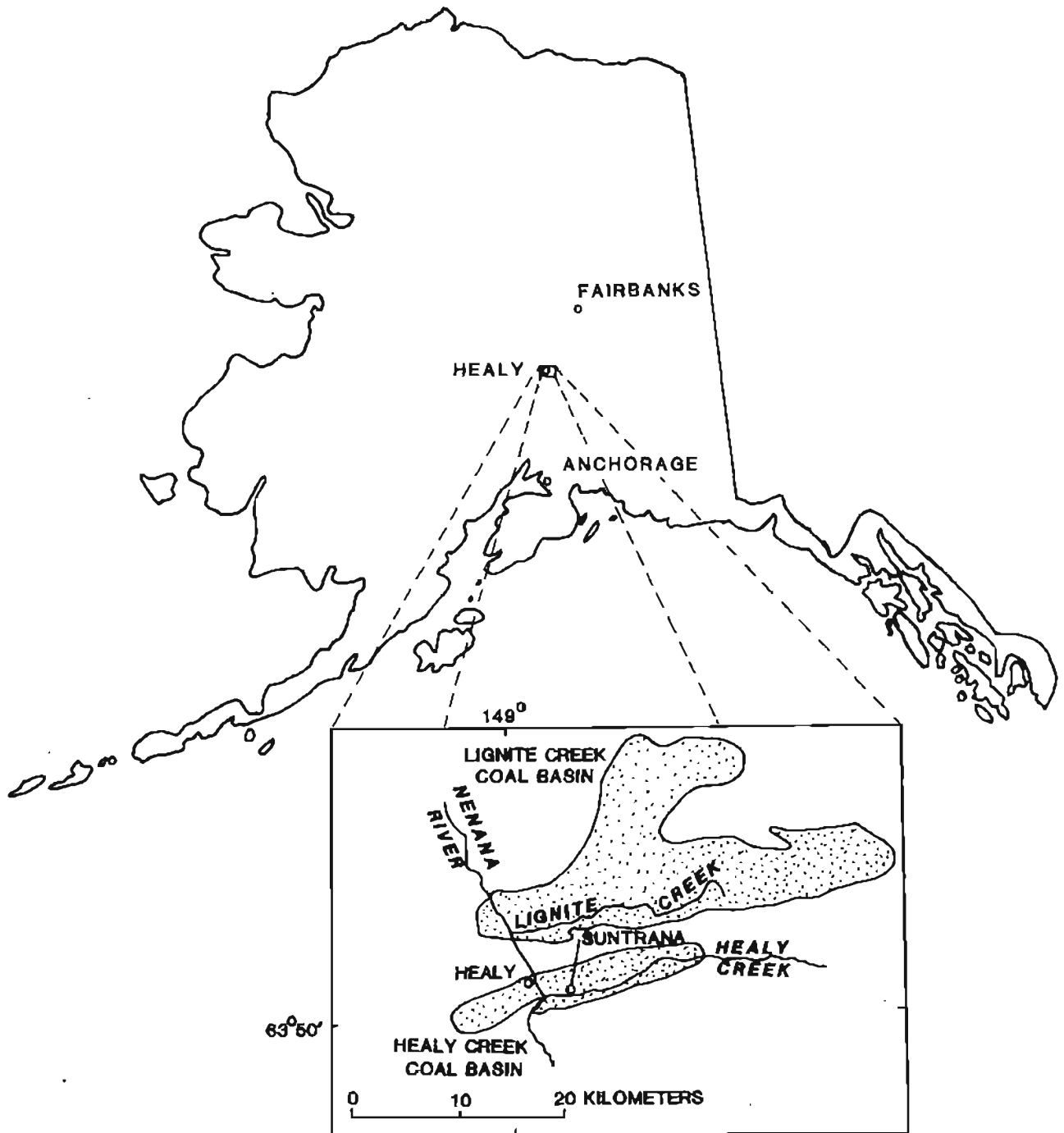


Figure 1. Location map of Lignite Creek and Healy Creek coal basins, Nenana coal field (modified from Wahrhaftig and others, 1969).

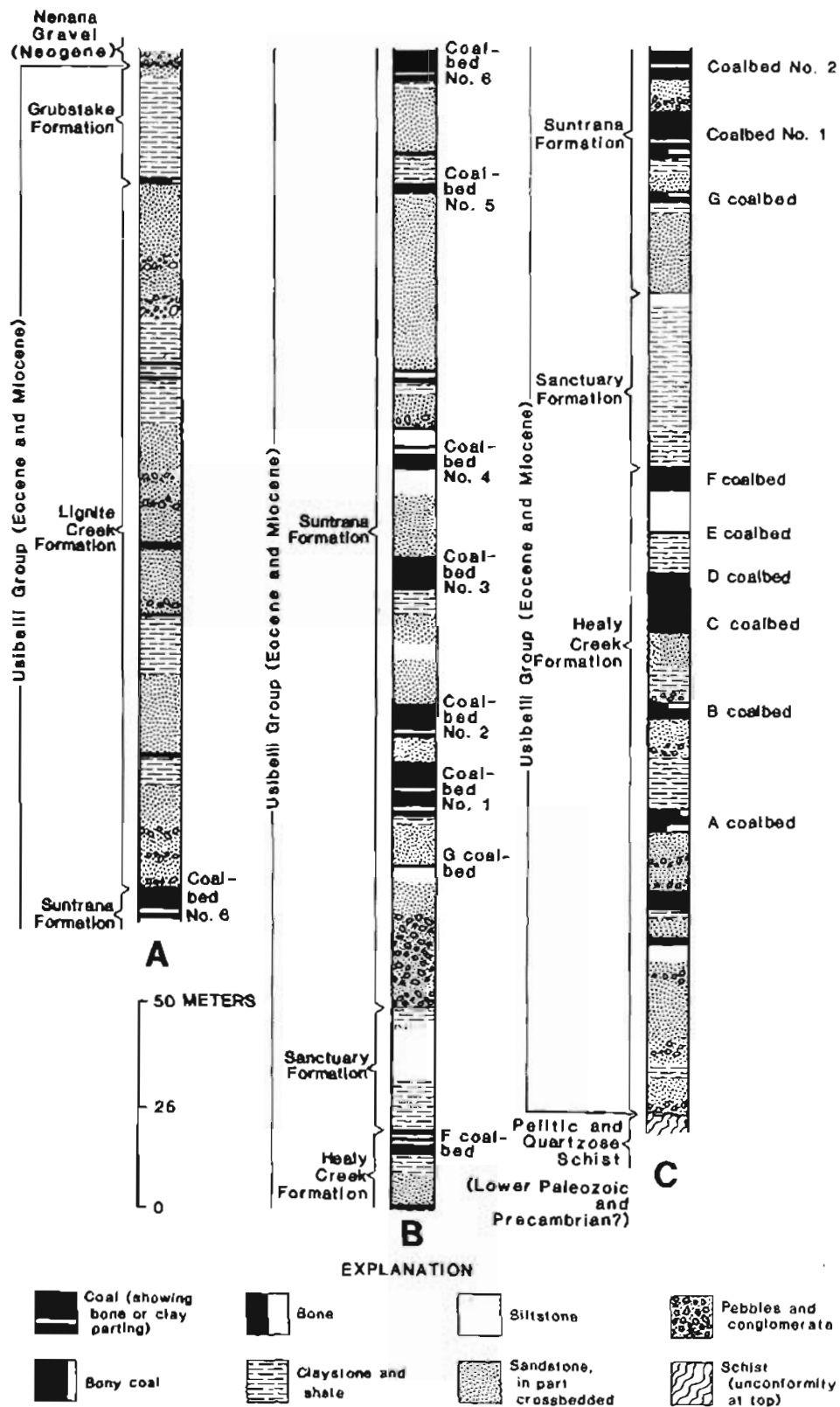


Figure 2. Generalized stratigraphic section of Usibelli Group, Nenana coal field, at Suntrana, Alaska. Sections A and B were measured along Suntrana Creek, and section C was measured on north bank of Healy Creek (modified from Wahrhaftig, 1987, and Frost and Stanley, 1991).

Table 1. Ash and gold contents, Nos. 3 and 4 coal beds, Suntrana Formation, Lignite Creek coal basin, Alaska

Coal bed*	Depth from top of bed (in meters)	Ash percent	Gold in ash (ppm)	Gold in whole coal (ppb)
3	0.1	10.80	0.0080	0.86
3	.4	10.80	.0040	.43
3	1.9	3.20	.0010	.032
3	2.5	5.48	.0130	.712
3	4.9	6.99	.0180	1.26
3	5.3	22.62	.0050	1.13
4	.1	51.80	.0060	3.10
4	.3	5.95	.0030	.17
4	2.6	8.72	.0070	.61
4	3.2	12.4	.0080	.995
4	7.4	6.67	.0060	.40
4	7.7	8.98	.0080	.718

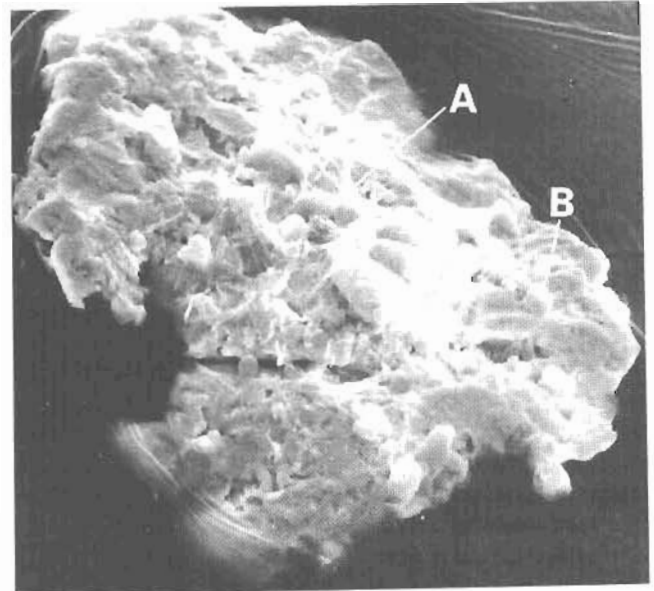
* The No. 3 bed is 5.4 m thick and the No. 4 bed is 7.8 m thick where sampled in 1987.

coal ash, and gold values in samples of whole coal from the Nos. 3 and 4 beds are shown in table 1. A correlation coefficient was computed between ash content and gold values in whole coal for the 12 samples in order to determine relationships of the Au to coal. The coefficient between ash content and Au content in whole coal is 0.92 (which is significant at the 95 percent level). Gold values for the three fly-ash splits are 0.076, 0.12, and 0.87 ppm.

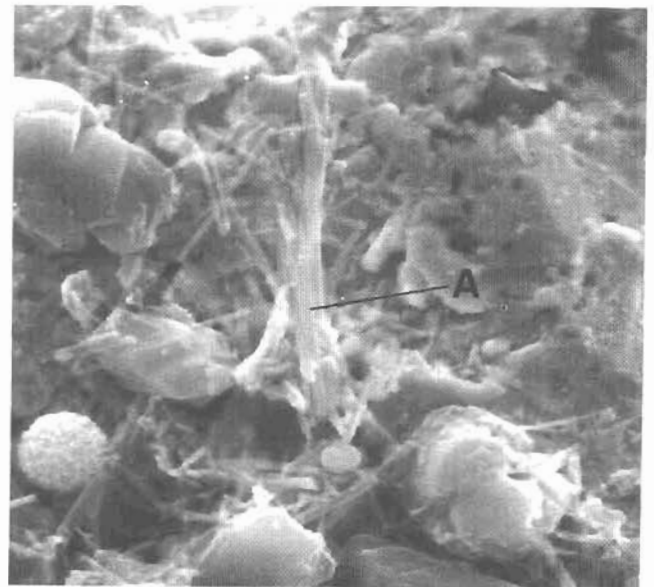
Individual grains of gold were identified on the scanning electron microscope (SEM). These grains were recovered from the GVEA fly ash. The gold appears to be a placer particle in that it is rough and irregular in outline (fig. 3). Parts of the particle are coated with bubbles of fused calcium-silicate glass, a result of the particle's trip through the GVEA's boiler. Other areas of the gold particle show new-growth gold in the form of sharply defined filament crystals and fine wires up to 7 μm long. The energy-dispersive system of the SEM determined that the gold wires are approximately 95 percent Au with 5 percent silver impurity.

The SEM photograph of a placer-shaped gold particle and a correlation coefficient of 0.92 between ash and Au content in whole coal suggest that there is some detrital Au in the Nos. 3 and 4 coal beds. However, it seems unreasonable that most of the Au in these coals would be detrital in origin. A vigorous flood of water capable of carrying detrital Au from the nearby alluvial system into the mire would also carry sufficient detritus to dilute the organic material and produce a carbonaceous shale. Gold is present in low-ash coal samples (table 1), and thus we must conclude that some of the Au presently found in the Nos. 3 and 4 beds must have entered the peat swamp in solution from ground or surface water during the peat-accumulating stage and precipitated within the peat/coal. Also, gold may have entered the coalbed both

during the coalification phase, when large volumes of water moved within the peat, and after coalification when ground water moved along cleats and fractures within the coal. Gold mobilization and crystallization is suggested by the existence of new-growth Au on the detrital grain (fig. 3). When the Au in solution entered the Nos. 3 and 4 beds is presently unknown.



A



B

Figure 3. Scanning electron micrographs of detrital gold found in fly ash, GVEA, Healy, Alaska. A, Detrital gold grain showing (A) new-growth gold filament and (B) bubbles of fused calcium-silicate glass. B, Enlargement of new-growth gold filament (A) shown in A.

CONCLUSIONS

This study of gold content of two coal beds of the Suntrana Formation utilizing a lower detection limit for Au provides a preliminary evaluation of gold in Alaska coals. With this improved detection limit, Au was detected in all samples studied from the Nos. 3 and 4 beds from the Lignite coal basin and in fly ash of the GVEA. The Nos. 3 and 4 coal beds of the Lignite Creek basin may have economic potential for the byproduct recovery of Au. Bagby and others (1986) report that the range for Au content in carbonate-hosted gold and silver deposits is from 0.7 to 8 ppm. Gold content of one fly-ash sample (0.87 ppm) is within the range for the above-mentioned carbonate-hosted Au and Ag deposits.

Our study has not addressed the vertical variability within the coal bed nor the modes of occurrence of the nondetrital Au. Work by Affolter and Stricker (1987) indicates that the coal beds at Healy have a significant vertical variability in the content of trace elements. This limited study indicates that further investigation into the occurrence and origin of Au in the Usibelli Group coals is warranted.

REFERENCES CITED

- Affolter, R.H., and Stricker, G.D. 1987, Variation in element distribution of coal from the Usibelli Mine, Healy, Alaska, in Rao, P.D., ed., *Focus on Alaska's coal, '86*: Fairbanks, Alaska, Mineral Industry Research Laboratory Report 72, p. 91-99.
- Bagby, W.C., Menzie, W.D., Mosier, D.L., and Singer, D.A., 1986, Grade and tonnage model of carbonate-hosted Au-Ag, in Cox, D.P., and Singer, D.A., eds., *Mineral deposit models*: U.S. Geological Survey Bulletin 1693, p. 176-177.
- Chyi, L.L., 1982, The distribution of gold and platinum in bituminous coal: *Economic Geology*, v. 77, p. 1592-1597.
- Finkleman, R.B., 1981, Modes of occurrence of trace elements in coal: U.S. Geological Survey Open-File Report 81-99, 301 p.
- Frost, G.M., and Stanley, R.G., 1991, Compiled geologic and Bouguer gravity map of the Nenana Basin area, central Alaska: U.S. Geological Survey Open-File Report 91-562, 30 p., 2 sheets, scale 1:250,000.
- Golightly, D.W., and Simon, F.O., 1989, Methods for sampling and inorganic analysis of coal: U.S. Geological Survey Bulletin 1823, 72 p.
- O'Leary, R.M., and Meier, A.L., 1986, Analytical methods used in geochemical exploration, 1984: U.S. Geological Survey Circular 948, 48 p.
- Rao, P. Dharma, 1968, Distribution of certain minor elements in Alaskan coal: Fairbanks, Alaska, Mineral Industry Research Laboratory, University of Alaska, Report 15, 47 p.
- Sanders, R.B., 1981, Coal resources of Alaska, in Rao, P.D., and Wolff, E.N., eds., *Focus on Alaska's coal '80*: Fairbanks, Alaska, Mineral Industry Research Laboratory Report 50, p. 11-31.
- Stone, R.W., 1912, Coal near Black Hills Wyoming-South Dakota: U.S. Geological Survey Bulletin 499, 66 p.
- Wahrhaftig, Clyde, 1987, The Cenozoic section at Suntrana, Alaska, in Hill M.L., ed. *The Cordilleran section of the Geological Society of America: Boulder, Colo., Geological Society of America, Centennial Field Guide 1*, p. 445-450.
- Wahrhaftig, Clyde, Wolfe, J.A., Leopold, E.B., and Lanphere, M.A., 1969, The coal-bearing group in the Nenana coal field, Alaska: U.S. Geological Survey Bulletin 1274-D, p. D1-D30.

Reviewers: Michael E. Brownfield and Romeo M. Flores

Rare Earth Minerals in "Thunder Eggs" from Zarembo Island, Southeast Alaska

By John Philpotts and John R. Evans

INTRODUCTION

Fluorite veining occurs at a locality (lat 56°16' N., long 132°56' W.) on the west side of Zarembo Island adjacent to Snow Passage in southeast Alaska (fig.1). Elevated Y and Nb levels were found in stream-sediment nonmagnetic heavy-mineral concentrate from this site in the field geochemistry assessment of Cathrall and others (1983). Yttrium minerals invariably have significant contents of rare earth elements (REE). In broader definitions, Y is often included as a REE; in this note, however, REE refers to the 15-element sequence from La to Lu. Fluorite veins are often associated with REE mineralization (for example, Salvi and Williams-Jones, 1990). Rare earth element mineralization is known to occur at several localities on the eastern side of Prince of Wales Island (fig.1), including Salmon Bay, which lies just 10 km to the west of the fluorite locality, on the west side of Clarence Strait (Grybeck and others, 1984). It was in this context that the fluorite locality was visited in the summer of 1991, and a suite of samples was collected for the specific purpose of looking for evidence of REE mineralization.

The general geology has been described by Buddington (1923, p. 54-55) as consisting of Tertiary volcanic flows, breccias, tuffs, and agglomerates, with some interbedded sedimentary rocks (sandstones and conglomerates) at the base (see also Brew and others, 1984). The lavas include basalt, andesite, and rhyolite. Amygdules, with fillings of chalcedony, chlorite, calcite, and epidote, are abundant in many of the lavas. The volcanic rocks, including amygdaloidal rhyolites, are host to numerous narrow breccia zones and seams filled with mammillary surfaces and drusy coatings of fine-grained quartz crystals or, less commonly, fluorite (Buddington, 1923, p. 75). Basalt fragments as large as a foot in diameter have been coated with chalcedony and then with pale-green fluorite. One fluorite vein ranges up to several feet in thickness. Grybeck and others (1984, p. 67) describe the fluorite as sparse, filling veins and coating chalcedony-encrusted breccia fragments over an area of at least 100 m in diameter in Tertiary volcanic rocks.

During the visit of July 31, 1991, both fluorite-silica vein samples and amygdaloidal samples were collected. The latter were found to be common among beach pebbles. A collection of such pebbles is shown in figure 2. Individual spheroids can be several centimeters across; many structures are compound. The spheroids resemble the small, siliceous, geodelike bodies that occur in welded tuff in Oregon and are known by the popular term "thunder eggs" (Staples, 1965). Based on examination of hand-specimens, two of these samples and three fluorite-silica samples were selected for further work. They were slabbed using a water-cooled diamond saw and prepared for study on a scanning electron microscope (SEM) equipped with an energy-dispersive X-ray fluorescence system (EDS). This note reports the results of the SEM study.

ANALYTICAL METHODS

Samples were hand polished on unused abrasive paper and then carbon coated. The SEM used is an Etec Autoscan with a Kevex Delta Microanalysis Energy-Dispersive System and Quantex software. Operating conditions of the SEM were accelerating voltage of 30 kV, filament current of 125 μ A, and working distance of 10 to 15 mm. Output was in the form of backscattered-electron images, in which grains of higher average atomic number tend to appear brighter, and X-ray spectra plots of relative intensity versus energy. Spectral assignments were made using the system's integral software. Because thick slabs were used in this SEM study in the interest of rapid sample preparation, there is very little control or knowledge of what is being analyzed at depth below the surface. Many of our EDS spectra are no doubt reflecting compositional data from more than one mineral. For this reason we have not attempted to make the corrections to raw peak intensities necessary to convert these into quantitative element abundances. Because of the geometric constraint, the lack of corrections to the intensity data, and other problems inherent to SEM-EDS analysis (especially for elements of lower atomic number),

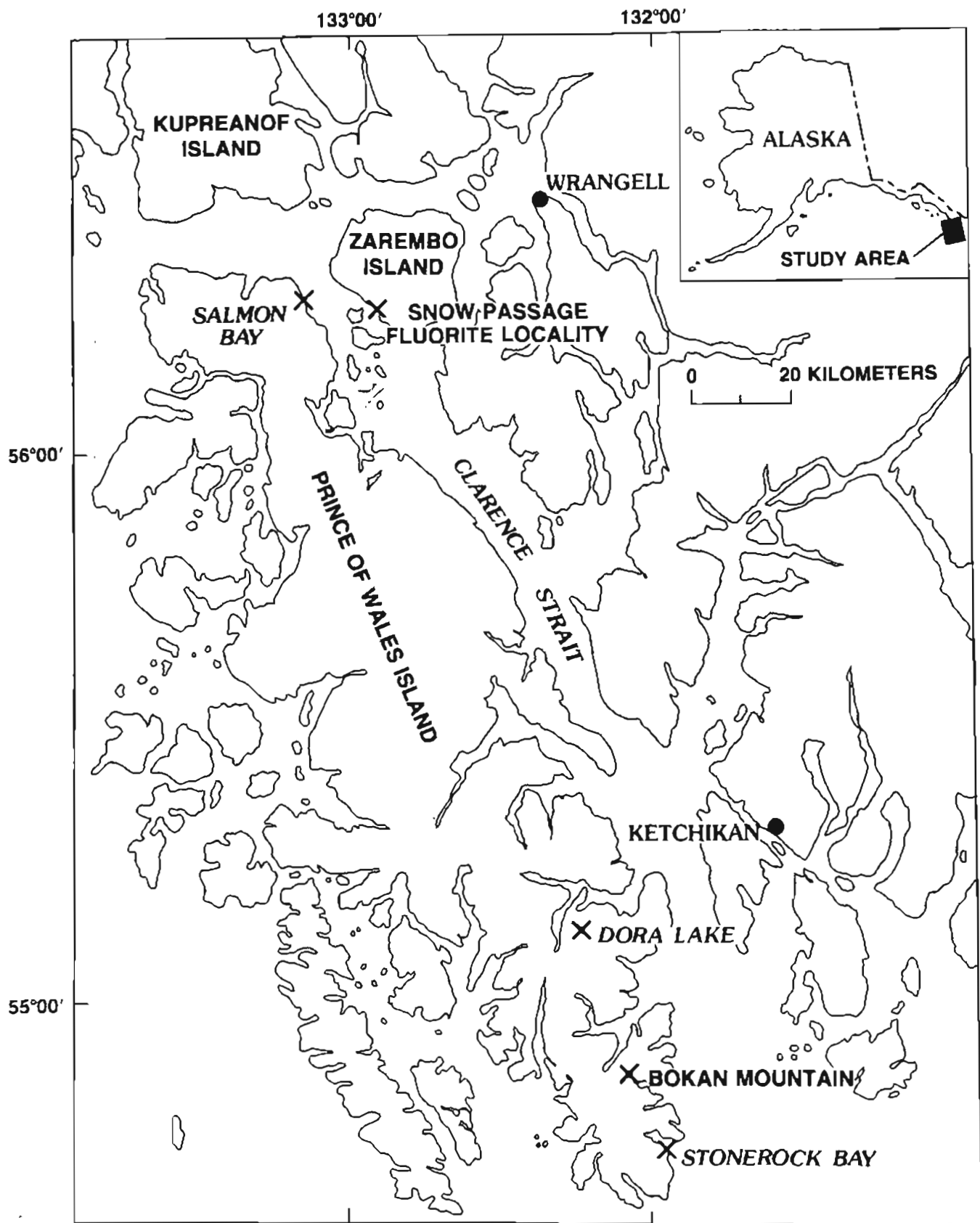


Figure 1. Locations of Snow Passage fluorite locality on Zarembo Island and of known rare earth element mineralization on neighboring Prince of Wales Island, southeast Alaska. Area covered by map shown on inset.

all mineral identifications and any intimations of exact compositions must be considered tentative (although hopefully reasonable) assignments.

SEM RESULTS

The three fluorite-silica samples examined revealed complex textures. Some textures suggest replacement or coprecipitation involving the two major phases. Other textures provide unambiguous evidence of a fluorite-precipitating phase invading brecciated silica. In hand specimen, some fluorite has a faint purple tint while most is greenish gray. EDS analysis revealed only Ca

and F in the spectra of both types. A variety of accessory minerals were found in these samples, including fairly abundant Fe-sulfide in the silica phase. However, no REE minerals were identified.

The amygdaloidal pebble samples proved more mineralogically diverse. The first sample examined contains amygdules in a light-green matrix. A cut section through this sample is shown in the upper left corner of figure 2. A low-magnification backscattered-electron image is shown in figure 3. The image shows the nature of the amygdules and the texture of the matrix. EDS analysis indicates that both the amygdules and the surrounding matrix are high in silica, usually with some showing of alkali feldspar. In addition to silica and

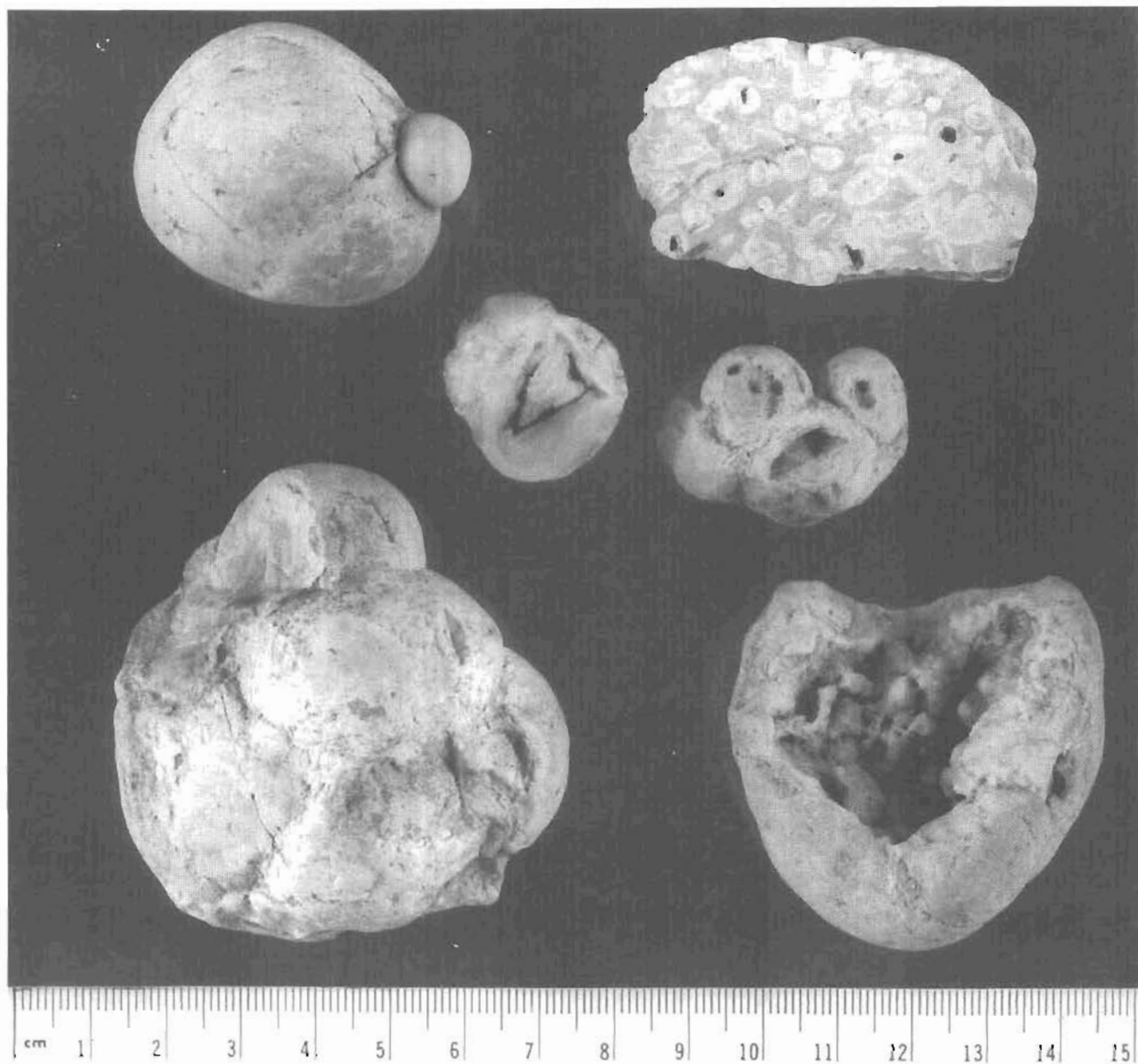


Figure 2. "Thunder egg" beach pebbles from Zarembo Island. Note centimeter scale.

alkali feldspar, EDS analysis indicates the presence of a number of accessory phases, including a matrix grain composed of Fe-sulfide and containing small blebs of galena. A titaniferous phase located at an amygdule margin contained minor Fe and Nb.

Of more interest for the present study are grains containing REE. The bright patch displayed at the center of figure 3, lying in the matrix near an amygdule margin, is rich in Y, Zr, and heavy REE (HREE—that is, REE with higher atomic mass or number). The patch is about 30 μm in diameter; it is composed of numerous small grains, several micrometers across, that appear to show variation in Y, Zr, and HREE content. The EDS spectrum for one of these grains is shown in figure 4.



Figure 3. Scanning electron microscope backscattered-electron image of amygdaloidal volcanic rock. Small brighter patch in center of image is composed of Y-HREE-Zr minerals. Field of view is approximately 4 mm.

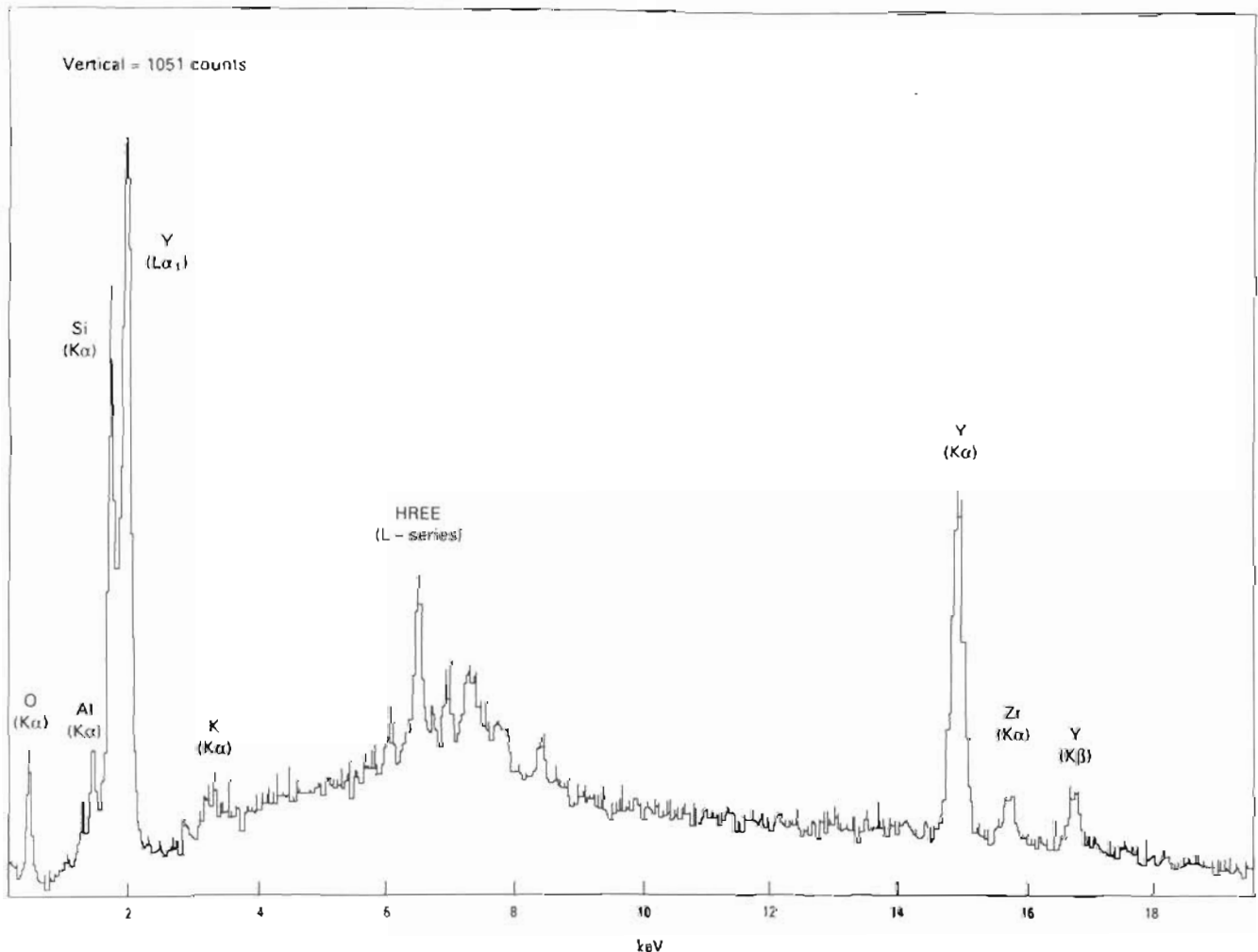


Figure 4. X-ray spectrum of relative intensity versus energy for a grain in figure 3 bright patch. Significant peaks are labeled in terms of major contributing X-ray lines.

Many of the peaks shown in figure 4 are composite and are identified only by the element believed to be making the major contribution. The HREE spectrum for this sample appears to be dominated by Gd, Dy, Er, and Yb. REE of even atomic number tend to be more abundant than neighboring odd atomic number REE because of their greater cosmic abundance. This particular grain may be a carbonate such as Y-bastnaesite $[(Y,REE)(CO_3)F]$ or possibly a silicate such as thalenite $[Y_3Si_3O_{10}(OH,F)]$ or tombarthite $[Y_4(Si_4H_4)O_{12-x}(OH)_{4+2x}]$. We did not find any light REE (LREE) in the amygdaloidal sample.

The other sample examined is a "thunder egg" containing a V-shaped central cavity in cut section (the lower of the two samples in the center of fig. 2). Based on EDS analysis the bulk of this sample is composed of silica and alkali feldspar. Accessory phases tentatively identified include apatite, zircon, and a TiO_2 -polymorph. These accessory minerals occur within the body of the "egg"; apatite also occurs in the central vug. The zircons show minor U content. Neither the apatite grains nor the zircon grains showed any detectable Y or REE. However, a TiO_2 -polymorph, about 75 μm in diameter, contains at its contact with siliceous matrix numerous small blebs, each a few micrometers across, that show Y and HREE abundances very similar to those found in the amygdaloidal sample. Elsewhere in the sample, an apparent assemblage of TiO_2 and potassium feldspar also shows Y and REE. Here the REE are more abundant relative to Y, and they are dominated by the intermediate REE Nd, Sm, and Dy. This appears to be a different mineral than the Y-rich one that yielded the spectrum shown in figure 4. The second assemblage also contains Nb, presumably in the titaniferous phase. The REE phosphate, monazite, is also tentatively identified within this "thunder egg." The REE spectrum is dominated by Ce with lesser La and Y.

Yet another REE abundance pattern occurs in grains and in areas both near the vug and in the interior of this second "thunder egg" sample. An example of the occurrence of these grains is shown in figure 5. The triangular shape occupied by the grains suggests that this area might be a filled pore space. The EDS spectrum is shown in figure 6. The REE are dominated by Ce. The only other REE detected is La, which shows up as a shoulder on the left flank of the major Ce peak. The Ce-rich mineral may be a carbonate. The presence of K-feldspar is also indicated by the spectrum. Ca is also present and may be in either or both of these phases.

A strikingly different LREE mineral occurs in and around the vug. Examples are the bright minerals shown in figure 7 along with dark quartz crystals lining the cavity. The EDS spectrum of the largest of the bright crystals is given in figure 8. This mineral also appears to be a LREE carbonate. However, in this case, the REE are

dominated by La and Nd. The small peak to the left of the main La peak is also contributed by La. As indicated by the trough between the two main La peaks, Ce, significantly, is absent.

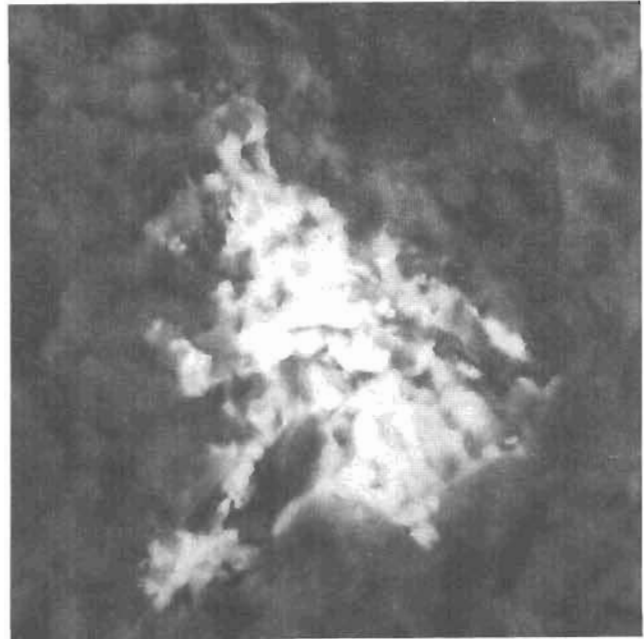
DISCUSSION

At the Zarembo Island fluorite locality, we found REE minerals not in the fluorite-silica vein material, but rather in beach pebbles of an amygdaloidal rock and of a concretionlike or geodelike "thunder egg" similar to the amygdules. The amygdaloidal rock is presumed to be volcanic. EDS analyses show the matrix surrounding the amygdules to be high in silica, and if the composition is primary, the rock would perhaps be a rhyolite. However, the amygdules likely have formed from a fluid that may also have altered the original composition of the matrix. The REE minerals within these samples show a variety of REE-abundance patterns. Rare earth patterns reflect both the REE abundances of the environment in which a mineral forms and any fractionation due to crystal-chemical constraints. Yttrium is similar in ionic radius to the HREE. Enrichment of HREE is expected, therefore, in Y-minerals such as the amygdule-matrix mineral represented by the figure 4 spectrum. The LREE-enriched patterns in the samples are not as readily explained.

An EDS spectrum of a monazite grain that displayed La and Ce peaks has been mentioned. Rare earth elements heavier than Ce are not present in this monazite at levels above EDS detection limits. This spectrum is what might be expected, in general, for a phase having enrichment of the LREE. In contrast, the REE spectrum shown in figure 6 shows only Ce and barely detectable La. This might represent a standard LREE-enrichment abundance pattern displaying a sharp maximum at Ce. Another explanation for the figure 6 spectrum, however, is suggested by the REE data shown in figure 8. This spectrum shows no Ce at all, but only La and Nd. Crystal-chemical constraints are *not* sufficiently discriminating to provide a REE pattern with bimodal abundance maxima at La and Nd and a minimum sufficient to exclude detection for Ce which is intermediate in ionic radius between La and Nd. This spectrum strongly suggests a Ce anomaly.

In igneous rocks, the REE represent a coherent geochemical group of trivalent ions that display small, regular differences in properties, principal of which is ionic radius. However, in sufficiently oxidizing sedimentary environments, the coherence breaks down as Ce, alone among the REE, becomes tetravalent. Tetravalent Ce is then the only REE entering Mn nodules and crusts in any great quantity, and this accounts for the negative Ce anomaly of seawater, fishbones, phos-

phorites, and so on. We believe that the REE data shown in figure 8 indicate that this mineral also has a negative Ce anomaly. This would require that Ce was tetravalent at some stage in the development of this mineral. A *positive* Ce anomaly would explain the high relative abundance of Ce indicated for the mineral yielding the spectrum in figure 6. The abundance data for this phase do not of themselves make as conclusive an argument for anomalous Ce as do the figure 8 data. However, the Ce-rich and Ce-deficient minerals do occur in close proximity within the "thunder egg," and it is likely that the unusual complementary abundances of Ce in both minerals have the same explanation (that is, stability of tetravalent Ce) rather than resulting from independent causes. In any case, we consider the evidence for a



⇒
Figure 5. Scanning electron microscope backscattered-electron image. Bright area is composed of LREE-enriched grains that may be filling pore space. Field of view is approximately 40 μm .

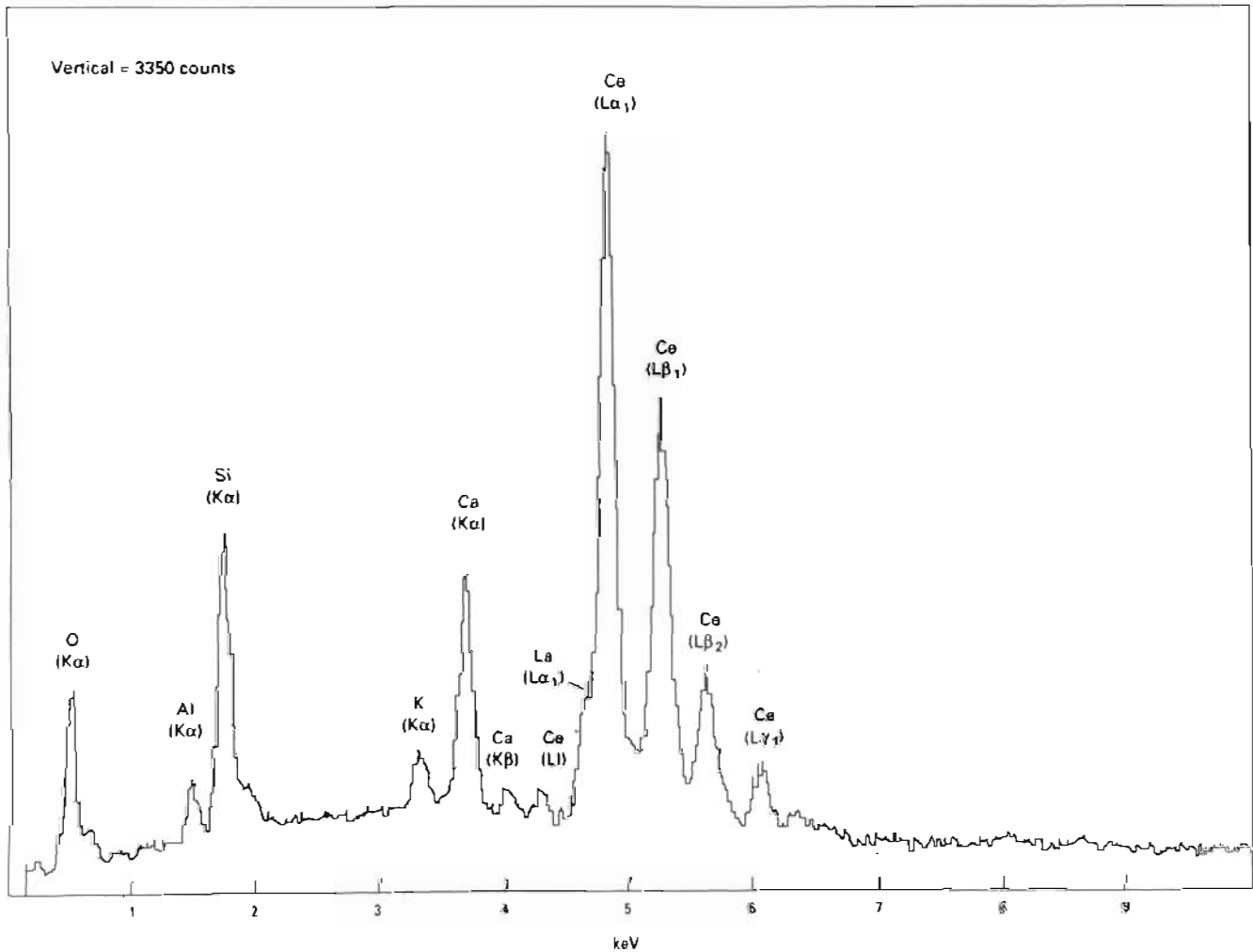


Figure 6. X-ray spectrum for a grain within figure 5 bright area. Ce is by far most abundant REE.

tetravalent-Ce effect to be very strong for the Ce-deficient mineral.

As mentioned above, Ce anomalies are features normally encountered in oxidized sedimentary environments, not in igneous rocks, so the questions arise as to what they represent within this "thunder egg" and at what stage they formed. The large crystal shown in figure 7 appears to demonstrate clearly that the Ce-deficient phase is not merely a surface coating within the vug but rather has a crystal form that is well defined within the enclosing siliceous matrix. It is possible that, during a period of oxidative weathering, Ce was preferentially leached as a tetravalent ion from the mineral. If this were the case, then these rocks might constitute a ready source of leachable Ce and one that might form eco-



⇒
Figure 7. Scanning electron microscope backscattered-electron image of REE minerals (bright) and quartz crystals (dark) around a "thunder egg" vug. Field of view is approximately 0.7 mm.

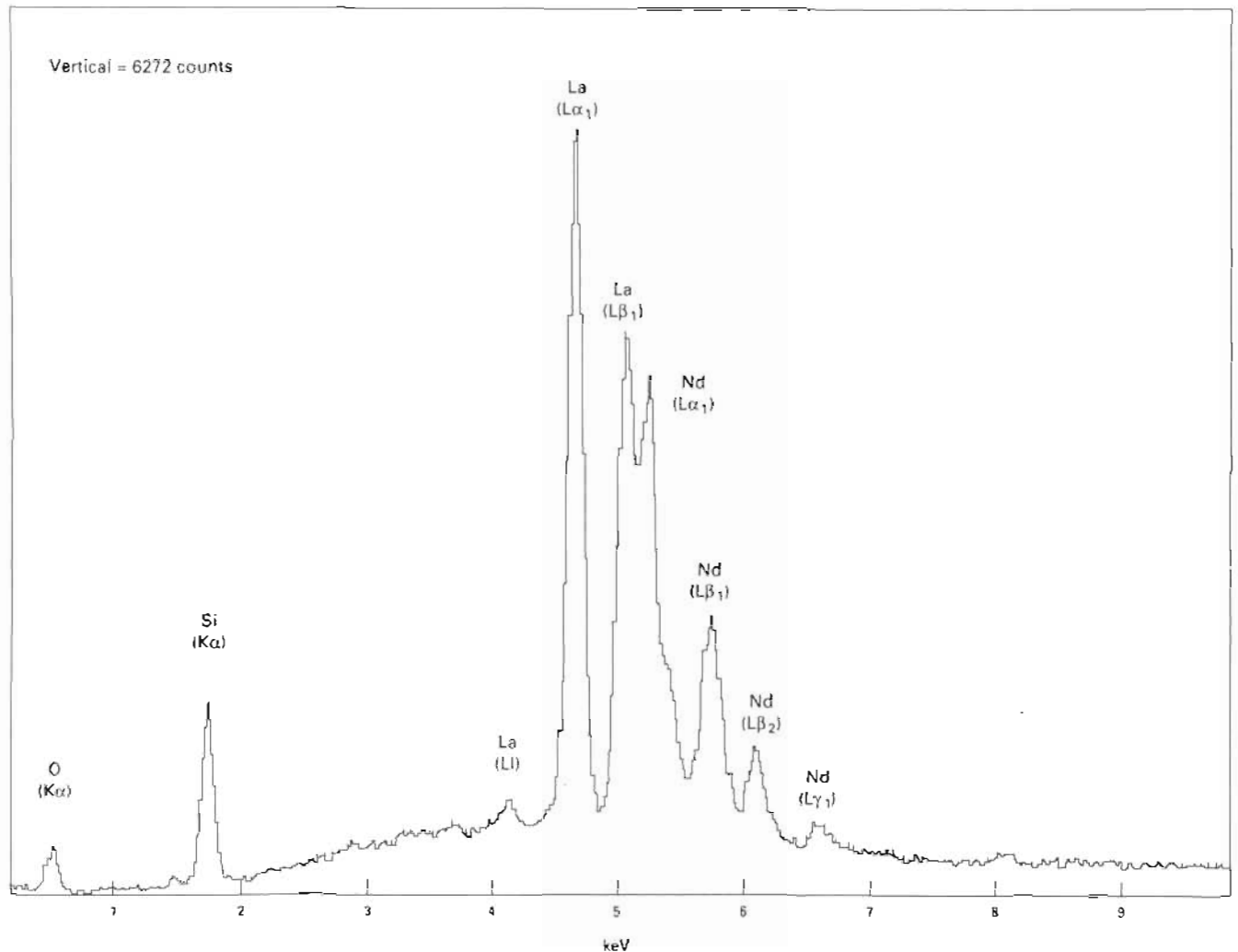


Figure 8. X-ray spectrum for large bright crystal in northeast quadrant of figure 7. Note absence of Ce.

nomie beach deposits. However, the occurrence of such an event is uncertain. For one thing, it would require that the nearby Ce-rich minerals have escaped such Ce loss. Further, this "thunder egg" is a typically well indurated sample, and it is not at all clear that its interior was open to weathering. For these reasons we currently favor the interpretation that Ce was tetravalent at the time that this phase formed, and that the Ce-deficient mineral crystallized at the same time as its siliceous surroundings during Tertiary or Quaternary hydrothermal activity. The identification of anomalous Ce in this process has genetic significance because it indicates hydrothermal conditions sufficiently oxidizing to stabilize tetravalent Ce.

Although we did not find REE minerals within samples of the fluorite-silica material, the presence of this veining offers at least the possibility of (re)mobilization of REE. Within the "thunder eggs," EDS analysis of minerals indicates that Ti, Nb, and Zr were mobile in addition to REE and Y. Very similar assemblages of mobile elements have been identified by Belkin (1991) for late-stage magmatic brine activity within a diabase in Pennsylvania and by Willis and others (1990) and Flohr (1991) for quartz-TiO₂ veins near Magnet Cove, Arkansas. This type of metasomatism also may have had a role in the enrichment of Y, Zr, and REE at major deposits such as Strange Lake, Quebec-Labrador (Salvi and Williams-Jones, 1990), and Thor Lake, N.W.T. (Pinckston and Smith, 1988).

REFERENCES CITED

- Belkin, H.E., 1991, Hydrothermal transport of zirconium in mafic igneous rocks: Evidence from fluid inclusions in ilmenite and implications for petrogenetic interpretation [abs.]: *Plinius*, v. 5, p. 19.
- Brew, D.A., Ovenshine, A.T., Karl, S.M., and Hunt, S.J., 1984, Preliminary reconnaissance geologic map of the Petersburg and parts of the Port Alexander and Sumdum 1:250,000 quadrangles, southeastern Alaska: U. S. Geological Survey Open-File Report 84-405, 43 p.
- Buddington, A.F., 1923, Mineral deposits of the Wrangell District, in Brooks, A.H., and others, Mineral resources of Alaska: U.S. Geological Survey Bulletin 739, p. 51-75.
- Cathall, J.B., Day, G.W., Hoffman, J.D., and McDanal, S.K., 1983, A listing and statistical summary of analytical results for pebbles, stream sediments, and heavy-mineral concentrates from stream sediments, Petersburg area, southeast Alaska: U.S. Geological Survey Open-File Report 83-420-A, 279 p.
- Flohr, M.J.K., 1991, Titanium-, vanadium-, and niobium mineralization at the Christy deposit, Magnet Cove alkaline igneous rock complex, Arkansas [abs.]: *Geological Society of America Abstracts with Programs*, v. 23, no. 5, p. A292.
- Grybeck, D.J., Berg, H.C., and Karl, S.M., 1984, Map and description of the mineral deposits in the Petersburg and eastern Port Alexander quadrangles, southeastern Alaska: U.S. Geological Survey Open-File Report 84-837, 87 p.
- Pinckston, D.R., and Smith, D.G.W., 1988, Mineralogy of the Lake Zone, Thor Lake, N.W.T. [abs.]: *Geologic Association of Canada Program with Abstracts*, v. 13, p. 99.
- Salvi, S., and Williams-Jones, A.E., 1990, The role of hydrothermal processes in the granite-hosted Zr, Y, REE deposit at Strange Lake, Quebec/Labrador: Evidence from fluid inclusions: *Geochimica et Cosmochimica Acta*, v. 54, p. 2403-2418.
- Staples, L.W., 1965, Origin and history of the thunder egg: *The Ore Bin*, v. 27, no. 10, p. 195-204.
- Willis, M.A., Pasteris, J.D., and Shock, E.L., 1990, Hydrothermal transport of titanium as exemplified by quartz-titanium dioxide veins near Magnet Cove, Arkansas [abs.]: *Geological Society of America Abstracts with Programs*, v. 22, no. 7, p. A363.

Reviewers: Marta J.K. Flohr and Philip A. Baedeker

Upper Devonian Shallow-Marine Siliciclastic Strata and Associated Fauna and Flora, Lime Hills D-4 Quadrangle, Southwest Alaska

By Robert B. Blodgett and Wyatt G. Gilbert

Abstract

A 103.6-m-thick section of Frasnian (lower Upper Devonian) siliciclastic strata in the Lime Hills D-4 quadrangle, southwestern Alaska, contains fauna and flora consistent with a shallow-water, nearshore depositional environment. This section occurs within the lower part of the Mystic sequence and represents a period of shallow-water deposition that followed deposition of deeper water shale and chert. The section is part of the Farewell terrane, which encompasses the Nixon Fork, Dillinger, and Mystic terranes of former usage. The fossil fauna of the measured section is dominated by brachiopods, followed secondarily in abundance by gastropods. Several species of the megafauna are also found in Frasnian fauna from the Shellabarger Pass area, northwestern Talkeetna quadrangle. Biogeographically, this fauna is allied with other Frasnian faunas from western North America, the Russian Platform, Novaya Zemlya, Taimyr, and Kolyma.

Locally, the uppermost strata of the underlying Dillinger sequence include deep-water turbiditic sandstone and shale, with minor carbonate debris flows yielding fauna of Lochkovian to Pragian (early Early to middle Early Devonian) age. The base of the overlying Mystic sequence is represented by Emsian (upper Lower Devonian) shallow-water platform carbonates. These are succeeded by deep-water shale and chert, followed by black shale, and succeeded in turn by Frasnian greenish-gray shale and interbedded orange siltstone and black shale of the measured section.

Regional correlation of Frasnian strata of the Lime Hills and McGrath quadrangles indicates the presence of a carbonate platform in the area of the Lyman Hills, which is correlative to the siliciclastic strata to the south and southeast in the Lime Hills D-4 quadrangle. The Frasnian siliciclastic strata may represent an orogenic clastic wedge derived from nearby tectonic highlands, probably situated to the southeast.

INTRODUCTION

In this paper we describe a measured stratigraphic section in Frasnian (lower Upper Devonian) siliciclastic strata in the Lime Hills D-4 quadrangle and discuss both

its contained fossil biota and its implications for the regional tectonic setting and correlation. Faunal data are also presented on some subjacent lithologic units. The research reported here results from a cooperative study between geologists of the U.S. Geological Survey (USGS) and the Alaska Division of Geological and Geophysical Surveys. Field work was conducted in the study area (Lime Hills D-4 and D-5 quadrangles) by W.G. Gilbert during the summers of 1989 and 1990; that of R.B. Blodgett was undertaken during the summer of 1990.

TERRANES AND SEQUENCES

The Paleozoic strata of the Lime Hills D-4 quadrangle are part of the Farewell terrane (Decker and others, in press), which encompasses the earlier described but obviously genetically related Dillinger, Nixon Fork, and Mystic terranes (fig. 1). Previously, strata of this quadrangle were included within the Dillinger terrane (Jones and Silberling, 1979; Jones and others, 1981, 1987). The Dillinger terrane was described by Jones and others (1981, p. 6-7) as a "coherent but complexly folded assemblage of lower and middle Paleozoic graptolitic shales, sandstone turbidites, and basal limestones of known Ordovician to Devonian age." The Mystic terrane was defined by Jones and others (1981, p. 6) to consist of "highly folded and partly disrupted shallow-water marine clastics and carbonate rocks of Late Devonian age overlain by radiolarian cherts and flyschlike graywacke, argillite and conglomerate of late Paleozoic age." Also included were Ordovician graptolitic shale associated with pillow basalt, blocks of Silurian platform rocks, and pillow basalts of presumed Triassic age.

Gilbert and Bundtzen (1984) considered the Dillinger and Mystic terranes to represent a single stratigraphic succession of Paleozoic to Triassic age, preferring to apply the term "sequence" to each. They considered the underlying Dillinger sequence to be a Cambrian to Lower Devonian deep-water succession that is followed *depositionally*

by the Mystic sequence, which consists of laterally variable Devonian to Triassic(?) shallow-water to nonmarine sedimentary rocks and intrusive and extrusive mafic and

ultramafic rocks. Both sequences are well exposed in the Lime Hills D-4 and D-5 quadrangles. The Nixon Fork terrane is now recognized to represent a predominantly

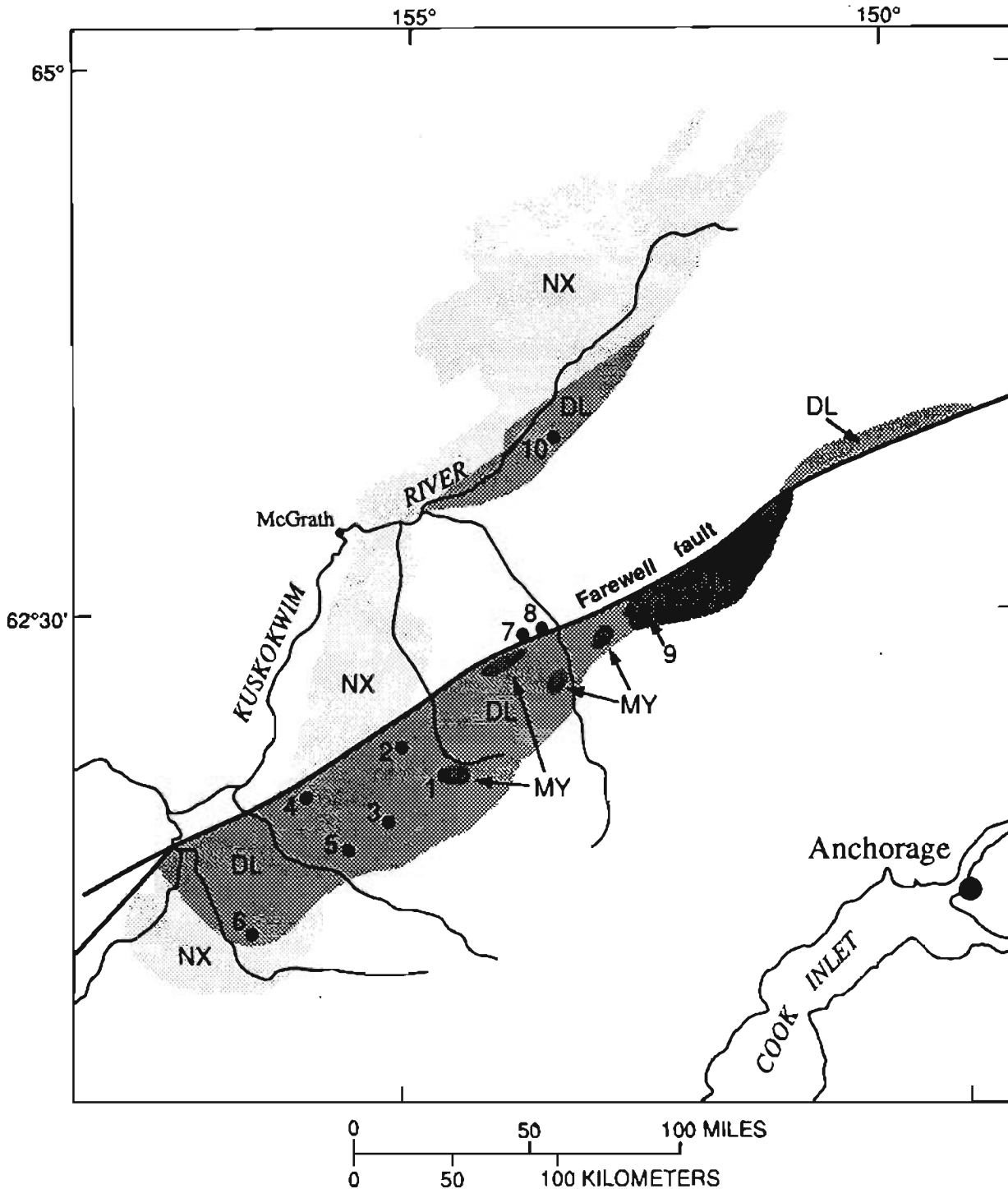


Figure 1. Generalized geologic map of southwestern Alaska showing location of cited place names and component "subterrane" (Dillinger, Nixon Fork, and Mystic) of the Farewell terrane. Map modified from Jones and others (1987). Dillinger "subterrane" here includes East Fork terrane of Dutro and Patton (1982). Map symbols: 1, study area; 2, Lyman Hills; 3, headwater region of the Gagaryah River; 4, VABM Steep; 5, North Lime Lake; 6, Door Mountains; 7, St. Johns Hill; 8, Farewell Mountain; 9, Shellabarger Pass; 10, East Fork Hills; NX, Nixon Fork terrane; DL, Dillinger terrane; MY, Mystic terrane.

shallow-water carbonate platform that is *laterally equivalent* to deeper water Cambrian to Devonian rocks of the Dillinger terrane exposed to the south (Blodgett, 1983; Blodgett and Gilbert, 1983; Bundtzen and Gilbert, 1983; Gilbert and Bundtzen, 1983; Blodgett and Clough, 1985).

DILLINGER SEQUENCE

The deep-water lower and middle Paleozoic strata of the Dillinger sequence occur throughout west-central and southwestern Alaska; this region includes the southeastern McGrath quadrangle (Bundtzen and others, 1982; Kline and others, 1986; Bundtzen and others, 1987; Gilbert and others, 1988, 1989), the northern Lime Hills quadrangle (Gilbert, 1981; Gilbert and others, 1990), and as far south as the western end of the Door Mountains (loc. 6 in fig. 1), east of the Hoholtna River in the Steetmute A-2 quadrangle (R.B. Blodgett, personal observations, 1984 and 1985). Similar deep-water strata occur in the East Fork Hills (loc. 10 in fig. 1) in the southern part of the Medfra quadrangle (East Fork Hills Formation of Dutro and Pauton, 1982) and have recently been recognized as far north as the Kantishna River C-5 quadrangle (R.B. Blodgett and W.G. Gilbert, personal observations, 1991).

In the study area (loc. 1 in fig. 1), the upper part of the Dillinger sequence includes deep-water turbiditic sandstone, siltstone, and shale. Limestone is uncommon and occurs either as carbonate turbidites (debris flows) or as platy, thin-bedded lime mudstone. The latter carbonate type probably represents times when siliciclastic sediment input was strongly reduced. One limestone debris flow (USGS locality 11940-SD) was sampled for conodonts. It consists of a thin limestone lens reaching up to 0.15 m (0.5 ft) in thickness that is laterally persistent for 4.5 m (15 ft). This lens is in an outcrop of steeply inclined, thinly interbedded shale and sandstone situated along the left bank of an unnamed northwest-flowing creek in SE $\frac{1}{2}$ NW $\frac{1}{4}$ sec. 7, T. 20 N., R. 28 W., Lime Hills D-4 quadrangle (lat 61°50'41" N., long 154°25'50" W.). A predominantly pelagic fauna is found in the limestone bed (USGS locality 11940-SD), consisting of abundant *dacryconarid* tentaculitids, orthoconic nautiloids, and an undetermined bivalve. Conodonts recovered from this limestone all belong to a single species, *Pandorinellina optima*, indicative of a Lochkovian (but not earliest Lochkovian) to Pragian age (Anita G. Harris and Robert Stamm, USGS, oral commun., 1991). The contact with the strata of the immediately overlying Mystic sequence has not been observed yet in the study area.

MYSTIC SEQUENCE

The type area of the Mystic sequence near Shellabarger Pass (loc. 9 in fig. 1) in the Talkeetna

quadrangle (Jones and others, 1981) includes Upper Devonian sandstone and limestone, uppermost Devonian and Mississippian radiolarian chert, and Pennsylvanian chert and argillite, succeeded structurally (and probably depositionally) by flyschlike rocks, including conglomerate that contains clasts of limestone and black cherty argillite (Jones and others, 1982). Middle Pennsylvanian plant fossils (identified by S.H. Mamay) were collected from a conglomerate lens at one locality; hence, these flyschlike rocks were presumed to be of late Paleozoic age. Older (pre-Devonian) lithologies reported by Jones and others (1981) are part of the Dillinger sequence (T.K. Bundtzen and W.G. Gilbert, personal observation, 1983). Late Paleozoic shallow-marine and nonmarine clastic rocks and Triassic(?) pillow basalt form isolated exposures that overlie the Dillinger sequence in the McGrath quadrangle (Bundtzen and others, 1982; Bundtzen and others, 1987; Gilbert and others, 1989).

The lowermost unit recognized in the Mystic sequence of the study area is a shallow-water, platform carbonate (Dl unit of Gilbert and others, 1990) that is at least 100 m thick. It consists of dark-gray lime mud-, wacke-, and grainstone bearing stromatoporoids, *Amphipora*, tabulate corals, and crinoid ossicles. This unit has been only cursorily examined for fossils. One locality that yielded both megafossils and conodonts is USGS locality 11941-SD, which is at the southeast end of a large limestone exposure atop a small hill (elevation 2001 ft) in NE $\frac{1}{4}$ SE $\frac{1}{4}$ SW $\frac{1}{4}$ sec. 15, T. 20 N., R. 29 W., Lime Hills D-5 quadrangle (lat 61°49'08" N., long 154°30'48" W.). The presence here of distinctive two-hole crinoid ossicles indicates an Emsian to early Eifelian age. Conodonts from this locality include *polygnathids* and *Pelekysgnathus* similar to Emsian species (Robert Stamm, USGS, oral commun., 1991). The combined ranges suggest an Emsian (late Early Devonian) age for strata of this locality.

This limestone is succeeded by the Dsc unit of Gilbert and others (1990), which consists of very thinly bedded chert, cherty argillite, and shale, and which hosts the Gagaryah barite deposit (Bundtzen and Gilbert, in press). This unit appears to have been deposited under deep-water conditions, in contrast to both the subjacent and superjacent units. The next succeeding unit is the Ds unit of Gilbert and others (1990), which is gradational with the underlying Dsc unit. Unit Ds includes the strata of the described measured section in its upper part.

Stratigraphic Section

The measured stratigraphic section is located (fig. 2) in SE $\frac{1}{4}$ SW $\frac{1}{4}$ SE $\frac{1}{4}$ sec. 12, T. 20 N., R. 29 W., Lime Hills D-4 quadrangle. The section extends uphill along a northwest-southeast-trending transect. Strata of this section be-

long to the upper part of the Ds unit of Gilbert and others (1990). The base of the measured section (fig. 3) was placed at the transition between underlying unfossiliferous, black shale and superjacent thin-bedded, grayish-green shale. It is situated at an elevation of approximately 2,850 ft (lat 61°49'56" N., long 154°26'51" W.). The top of the measured section is at the base of a thick, lithic sandstone interval that begins around an elevation of 3,200 ft (lat 61°49'52" N., long 154°26'38" W.) and forms the base of the uPzs unit of Gilbert and others (1990).

The lower part of the measured section consists of 32.0 m (105 ft) of greenish-gray shale (locally contorted). This shale lacks visible fossils for the most part, except near the top where crinoid ossicles and small brachiopods were recovered (USGS localities 11928-SD, 11929-SD). At 32.0 m above the base of the section, the greenish-gray shale grades into an overlying interval consisting of predominantly orange-brown-weathering siltstone interbedded with minor black shale. The latter lithology tends to predominate in the upper part of this interval. This interval extends from 32.0 m (105 ft) to 103.6 m (340 ft) above the base of the section [with a covered interval between 34.1 m (112 ft) and 39.0 m (128 ft)]. A silty limestone lens (USGS locality 11938-SD) was found at 86.6 m (284 ft) above the base. Open-marine fossils are found throughout this interval, both in

outcrop and in talus rubble. Brachiopods are the most common faunal element, followed in abundance by gastropods. Brachiopods include *Eleutherokomma* n. sp. (fig. 4.1–4.5), *Schizophoria* sp. (fig. 4.1, 4.6, 4.7), and *Spinatrypa* sp. (fig. 4.1). Gastropods include the following species: *Aglaoglypta* n. sp. (fig. 4.8), n. gen. aff *Acanthonema*, n. sp. (fig. 4.10, 4.11), and *Orecoxia* cf. *O. mccoyi* (Walcott, 1884) (fig. 4.9). Gyrogonites of the charophyte genus *Sycidium* (a green alga) (fig. 4.12, 4.13) are abundant at USGS locality 11930-SD.

A 15.3-m (50-ft) covered interval separates the fossiliferous siltstone and shale interval from an overlying interval of medium- to thick-bedded, fine- to medium-grained, brown, locally laminated lithic sandstone. The sandstone is predominantly fine grained, with subangular grains, and contains numerous small, angular shale chips. No visible fossil remains were noted from these beds. This upper lithic sandstone interval has been mapped by Gilbert and others (1990) as the lowermost part of their uPzs unit and was shown here to rest upon their Ds unit.

Age

An early Late Devonian (Frasnian) age is indicated by both the megafauna and conodonts collected from the strata of the measured section. The brachiopod genus *Eleutherokomma* Crickmay, 1950, occurs in strata of late Givetian (latest Middle Devonian) to middle Frasnian (middle early Late Devonian) age. This genus is represented here by a new species (fig. 4.1–4.5) that shows the rather distinctive microornament of the genus, consisting of strong, closely spaced concentric lamellae and subordinate radial capillae. This species differs from most of the described species in being somewhat larger than typical for the genus and in being considerably less mucronate. The new species appears to most closely resemble *Eleutherokomma reidfordi* Crickmay, 1950, from the basal part of the Hay River Formation of the District of Mackenzie, Northwest Territories. The latter species is of middle Frasnian age. The close relationship between these two species is supported by direct comparison with material of *E. reidfordi* that has been deposited in the National Museum of Natural History. They both share common features such as relatively large size, more numerous costae, and development of specimens that are weakly mucronate. The new species can be distinguished from *E. reidfordi* in having a more strongly rounded dorsal fold and in being less transverse. The brachiopod genera *Schizophoria* and *Spinatrypa* are both relatively long ranging, and until species-level affinities are elucidated, they provide no critical age resolution.

The gastropod genus *Orecoxia* is recognized only from the Frasnian. Among North American species, the Lime Hills form illustrated here (fig. 4.9) is most similar

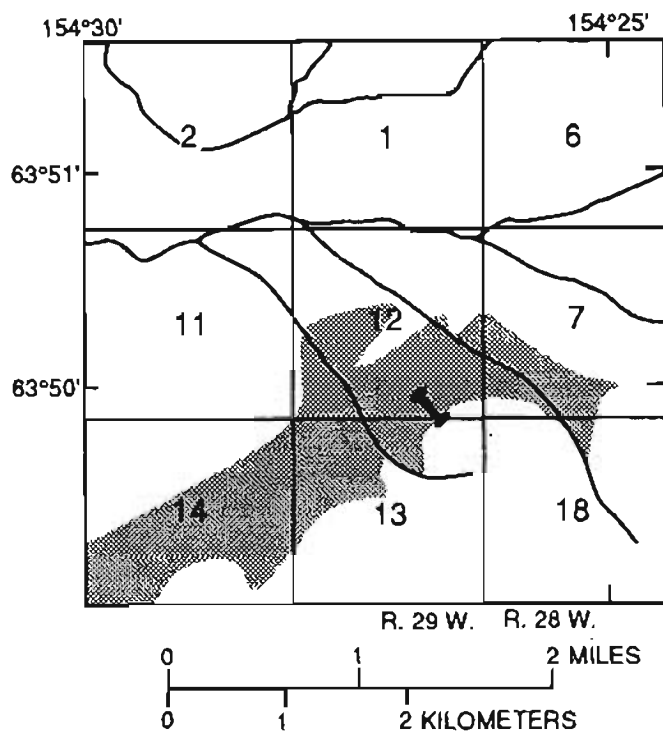


Figure 2. Location of measured section (see fig. 3) of unnamed lower Upper Devonian siliciclastic marine strata in Lime Hills D-4 quadrangle. Stippled pattern shows distribution of Ds unit of Gilbert and others (1990). Base at northwest end of section. Base map from U.S. Geological Survey, 1958 (minor revisions 1975), Lime Hills D-4 1:63,360 topographic map.

to the type species, *Orecoxia mccoysi* (Walcott, 1884) from the Devils Gate Limestone of central Nevada and its stratigraphic equivalents elsewhere in the Great Basin. The species resemblance is especially strengthened by the mutual occurrence of a strong angulation at the juncture between the upper and outer whorl surfaces. According to Pedder (1966, p. 144), the Nevada species ranges in age from early Frasnian (*argentarius* Zone) to possibly middle Frasnian. The gastropod genus *Aglaoglypta* is nearly wholly restricted to strata of Frasnian age, though a single species occurs in the late Givetian (late Middle Devonian) of Germany. Biogeographically, the megafauna is closely allied with other Frasnian faunas from western North America, the

Russian Platform, Novaya Zemlya, Taimyr, and Kolyma, as shown by the presence of the genera *Eleutherokomma* and *Orecoxia*. Several of the Frasnian megafauna species occurring in the upper part of the measured section are identical to species found in USGS fossil collections from Frasnian strata of the Shellabarger Pass region, northwestern Talkeetna quadrangle (R.B. Blodgett, personal observation, 1991).

Conodonts recovered from 1.7 kg of limestone at USGS locality 11938-SD yielded specimens identified by Robert Stamm (USGS, written commun., 1991) as *Polygnathus* aff. *P. aspelundi* Savage and Funai [four platform (Pa) elements with broken blades, six platform (Pa) elements with broken platforms, and one platform

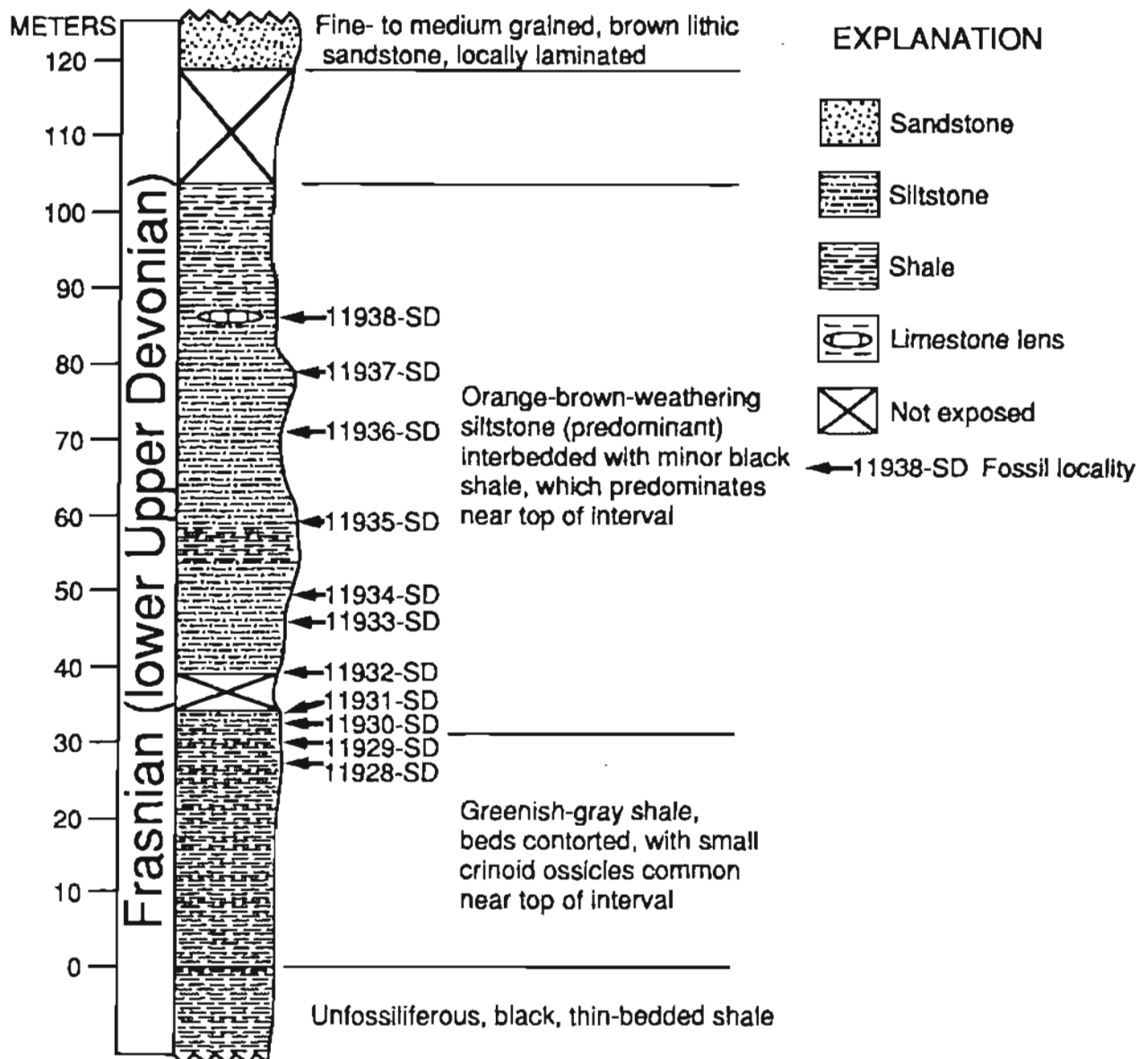


Figure 3. Columnar measured section of unnamed lower Upper Devonian siliciclastic marine strata. Location of section shown on figure 2. Arrows to right of column indicate USGS fossil localities (see descriptions in appendix).

(Pa) blade fragment]. All specimens were slightly abraded, with argillaceous and silt material attached. According to Stamm, "the complete stratigraphic and consequent age of *P. aspelundi* is poorly constrained. The faunal assemblage of Savage and Funai (1980) was assigned a probable early Frasnian age (Lower *asymmetricus* Zone) based on occurrences of *P. aff. P. dengleri* and *Pandorinellina insita*. Klapper and Lane (1985) feel that Savage and Funai's collections are of late Frasnian age (Lower to Upper *gigas* Zones) based on the occurrence of *P. unicornis* which was misidentified as *P. aff. P. dengleri* by Savage and Funai."

Environment of Deposition

The abundance, but low diversity, of the brachiopods, along with the relative abundance and diversity of gastropods, suggest an extremely shallow-water, open-marine, nearshore environment for that part of the section above 32.0 m. The presence of brachiopods and crinoid ossicles throughout this interval indicates conditions of normal marine salinity. The abundance of the charophyte *Sycidium* (a green alga) at USGS locality 11930-SD indicates very shallow (upper end of the photic zone) depths. Although charophytes are strictly found in nonmarine or brackish-water environments today, some of their earliest Devonian antecedents appear to have inhabited shallow-water, marine environments (Racki, 1982). Large, fragmentary vascular plant remains were noted in abundance near and at the levels of USGS localities 11931-SD and 11935-SD. It seems plausible that their abundance would require the nearby presence of a land area from which such vegetation could have been introduced.

The lower part of the measured section, from 0 to 32.0 m above the base, is interpreted to represent relatively deeper water, as it is much finer grained (being a shale) and thinner bedded. This interpretation is supported by the absence of fossils from the lower, greater part of this interval, as well as by the transition further below into unfossiliferous black shale, and then even further below into shale and chert (Dsc unit of Gilbert and others, 1990).

REGIONAL CORRELATION

Laterally equivalent to the Frasnian siliciclastic strata in the study area are platform carbonates that are exposed 30 to 65 km to the west and northwest in the Lyman Hills (loc. 2 in fig. 1). Most, if not all, of the thick, carbonate platform succession (uDI unit of Gilbert, 1981) appears to be of Frasnian age. These strata consist almost wholly of carbonate rocks, but a thin basal

sandstone bed has been recognized at several localities in the McGrath A-5 quadrangle (R.B. Blodgett, personal observation, 1979) (loc. 2 in fig. 1). This basal sandstone may represent a distal tongue of the thicker, clastic succession recognized to the southwest in the Lime Hills D-4 quadrangle. It and the overlying thick Frasnian carbonate succession form the base of the Mystic sequence in the Lyman Hills and appear to rest unconformably upon older deep-water strata of the Dillinger sequence. No Emsian and (or) Middle Devonian strata typical of the basal Mystic sequence in the study area and elsewhere have been recognized in the Lyman Hills. The lower Upper Devonian carbonate platform succession crops out nearly continuously along the south side of the Cheeneetuk River from the McGrath A-4 quadrangle in the northeast (15 to 20 km northeast of loc. 2 in fig. 1), southward to the vicinity of VABM Steep (loc. 4 in fig. 1) in the Lime Hills D-8 quadrangle. Other areas of exposure within the vicinity of the Lyman Hills include prominent exposures just east of North Lime Lake (loc. 5 in fig. 1) (Lime Hills B-6 and B-7 quadrangles) and also in a southwest-northeast-trending synclinalorium in the headwater region of the Gagaryah River (loc. 3 in fig. 1) (Lime Hills C-6 quadrangle). North of the Farewell fault this same succession can be recognized in the area of Farewell Mountain (loc. 8 in fig. 1) and St. Johns Hill (loc. 7 in fig. 1) (McGrath B-2 and B-3 quadrangles). Fossil algae have been described from this succession (Mamet and Plafker, 1982) based on five sample localities, three situated in the northern Lyman Hills, and the remaining two localities being situated approximately 6 km south-southwest of the town of Farewell (loc. 7 in fig. 1). Also, some limited discussion of a silicified ostracode fauna from this sequence in the McGrath A-5 quadrangle was given by W.K. Braun in Blodgett (1983, p. 128).

CONCLUSIONS

The measured section in the Lime Hills D-4 quadrangle documents the existence of Frasnian shallow-water siliciclastic strata equivalent to platform carbonate rocks to the west and northwest in the Lyman Hills. This contrast in facies is further evidence for the heterogeneity of the Mystic sequence in southwestern Alaska (Bundtzen and Gilbert, 1983; Gilbert and Bundtzen, 1984). The presence of older (pre-Frasnian) Mystic sequence strata in the study area, but absent in the Lyman Hills, implies more continuous marine sedimentation during the Devonian in the former area. The Frasnian siliciclastic strata may represent an orogenic clastic wedge derived from nearby tectonic highlands. The presence of a coeval Frasnian carbonate platform to the north in the Lyman Hills, as well as the regional trend of

this siliciclastic stratal succession (with strikingly similar rocks and fauna occurring in Shellabarger Pass, northwestern Talkeetna quadrangle), suggest that these highlands were probably located to the southeast.

REFERENCES CITED

- Blodgett, R.B., 1983, Paleobiogeographic affinities of Devonian fossils from the Nixon Fork terrane, southwestern Alaska, in Stevens, C.H., ed., Pre-Jurassic rocks in western North American suspect terranes: Los Angeles, Calif., Society of Economic Paleontologists and Mineralogists, Pacific Section, p. 125-130.
- Blodgett, R.B., and Clough, J.G., 1985, The Nixon Fork terrane—Part of an in-situ peninsular extension of the Paleozoic North American continent [abs.]: Geological Society of America Abstracts with Programs, v. 17, no. 6, p. 342.
- Blodgett, R.B., and Gilbert, W.G., 1983, The Cheeneetuk Limestone, a new Early(?) to Middle Devonian formation in the McGrath A-4 and A-5 quadrangles, west-central Alaska: Alaska Division of Geological and Geophysical Surveys Professional Report 85, 6 p., 1 sheet, scale 1:63,360.
- Bundtzen, T.K., and Gilbert, W.G., 1983, Outline of geology and mineral resources of the upper Kuskokwim region, Alaska: Journal of the Alaska Geological Society, v. 3, p. 101-119.
- in press, The geology and geochemistry of the Gagaryah barite deposit, western Alaska Range, Alaska, in Reger, R.D., ed., Short notes on Alaskan Geology-1991: Alaska Division of Geological and Geophysical Surveys Professional Report 111.
- Bundtzen, T.K., Kline, J.T., and Clough, J.G., 1982, Preliminary geology of the McGrath B-2 quadrangle, Alaska: Alaska Division of Geological and Geophysical Surveys Open-File Report 149, 22 p., 1 sheet, scale 1:63,360.
- Bundtzen, T.K., Kline, J.T., Smith, T.E., and Albanese, M.D., 1987, Geologic map of the McGrath A-2 quadrangle, Alaska: Alaska Division of Geological and Geophysical Surveys Professional Report 91, 20 p., 1 sheet, scale 1:63,360.
- Crickmay, C.H., 1950, Some Devonian Spiriferidae from Alberta: Journal of Paleontology, v. 24, p. 219-225.
- Decker, John, Bergman, S.C., Blodgett, R.B., Box, S.E., Bundtzen, T.K., Clough, J.G., Coonrad, W.L., Gilbert, W.G., Miller, M.L., Murphy, J.M., Robinson, M.S., and Wallace, W.K., in press, Geology of southwestern Alaska: Boulder, Colo., Geological Society of America, Geology of North America, v. F1, chapter II-F.
- Dutro, J.T., Jr., and Patton, W.W., Jr., 1982, New Paleozoic formations in the northern Kuskokwim Mountains, west-central Alaska: U.S. Geological Survey Bulletin 1529-H, p. H13-H22.
- Gilbert, W.G., 1981, Preliminary geologic map and geochemical data, Cheeneetuk River area, Alaska: Alaska Division of Geological and Geophysical Surveys Open-File Report 153, 10 p., 2 pls.
- Gilbert, W.G., and Bundtzen, T.K., 1983, Paleozoic stratigraphy of Farewell area, southwest Alaska Range, Alaska [abs.]: Alaska Geological Society Symposium, New Developments in the Paleozoic Geology of Alaska and the Yukon, Anchorage, Alaska, 1983, Program and Abstracts, p. 10-11.
- 1984, Stratigraphic relationships between Dillinger and Mystic terranes, western Alaska Range, Alaska [abs.]: Geological Society of America Abstracts with Programs, v. 16, no. 5, p. 286.
- Gilbert, W.G., Bundtzen, T.K., Kline, J.T., and G.M. Laird, 1990, Preliminary geology and geochemistry of the southwest part of the Lime Hills D-4 quadrangle, Alaska: Alaska Division of Geological and Geophysical Surveys Report of Investigations 90-6, 1 sheet, scale 1:63,360.
- Gilbert, W.G., Solie, D.N., and Kline, J.T., 1988, Geologic map of the McGrath A-3 quadrangle, Alaska: Alaska Division of Geological and Geophysical Surveys Professional Report 92, 2 sheets, scale 1:63,360.
- Gilbert, W.G., Solie, D.N., Kline, J.T., and Dickey, D.B., 1989, Geologic map of the McGrath B-3 quadrangle, Alaska: Alaska Division of Geological and Geophysical Surveys Professional Report 102, 2 sheets, scale 1:63,360.
- Jones, D.L., and Silberling, N.J., 1979, Mesozoic stratigraphy—The key to tectonic analysis of southern and central Alaska: U.S. Geological Survey Open-File Report 79-1200, 41 p.
- Jones, D.L., Silberling, N.J., Berg, H.C., and Plafker, George, 1981, Map showing tectonostratigraphic terranes of Alaska, columnar sections, and summary description of terranes: U.S. Geological Survey Open-File Report 81-792, 20 p., 2 sheets, scale 1:2,500,000.
- Jones, D.L., Silberling, N.J., Coney, P.J., and Plafker, George, 1987, Lithotectonic terrane map of Alaska (west of the 141st Meridian): U.S. Geological Survey Map MF-1874-A, 1 sheet, scale 1:2,500,000.
- Jones, D.L., Silberling, N.J., Gilbert, Wyatt, and Coney, Peter, 1982, Character, distribution, and tectonic significance of accretionary terranes in the central Alaska Range: Journal of Geophysical Research, v. 87, p. 3709-3717.
- Klapper, Gilbert, and Lane, H.R., 1985, Upper Devonian (Frasnian) conodonts of the *Polygnathus* biofacies, N.W.T., Canada: Journal of Paleontology, v. 59, p. 904-951.
- Kline, J.T., Gilbert, W.G., and Bundtzen, T.K., 1986, Preliminary geologic map of McGrath C-1 quadrangle, Alaska: Alaska Division of Geological and Geophysical Surveys Report of Investigations 86-25, 1 sheet, scale 1:63,360.
- Mamet, B.L., and Plafker, G., 1982, A Late Devonian (Frasnian) Microbiota from the Farewell-Lyman Hills area, west-central Alaska: U.S. Geological Survey Professional Paper 1216-A, p. A1-A10.
- Pedder, A.E.H., 1966, The Upper Devonian gastropod *Oreocopia* in western Canada: Palaeontology, v. 9, p. 142-147.
- Racki, Grzegorz, 1982, Ecology of the primitive charophyte algae; a critical review: Neues Jahrbuch für Geologie und Paläontologie Abhandlungen, v. 162, p. 388-399.
- Savage, N.M., and Funai, C.A., 1980, Devonian conodonts of probable early Frasnian age from the Coronados Islands of

southeastern Alaska: *Journal of Paleontology*, v. 54, p. 806-813.

Walcott, C.D., 1884, *Paleontology of the Eureka District*: U.S. Geological Survey Monograph 8, 298 p.

Reviewers: Bruce M. Gamble and J.G. Johnson

APPENDIX—FOSSIL LOCALITIES AT MEASURED SECTION

Collections of R.B. Blodgett

- USGS locality 11928-SD (field station 90ABd4), 27.4 m (90 ft) above base of section: *Eleutherokomma* n. sp., crinoid ossicles.
- USGS locality 11929-SD (field station 90ABd5), 30.2 m (99 ft.) above base of section, collection from small outcrop: undetermined rhynchonellid brachiopod.
- USGS locality 11930-SD (field station 90ABd6), 33.2 m (109 ft) above base of section, collection mostly from in situ rubble: *Spinatrypa* sp., *Eleutherokomma* n. sp., n. gen., n. sp. of gastropod (a similar, probably conspecific form occurs in the Frasnian of Shellabarger Pass, northwestern Talkeetna quadrangle), crinoid ossicles, *Sycidium* sp.
- USGS locality 11931-SD (field station 90ABd7), 34.1 m (112 ft) above base of section, collection from locally derived rubble: *Eleutherokomma* n. sp., undetermined high-spined gastropod, undetermined solitary rugose coral, crinoid ossicles, vascular plant debris.
- USGS locality 11932-SD (field station 90ABd8), 39.0 m (128 ft) above base of section, collection from locally derived rubble: *Schizophoria* sp., *Spinatrypa* sp., *Eleutherokomma* n. sp., undetermined gastropods.
- USGS locality 11933-SD (field station 90ABd9), 46.3 m (152 ft) above base of section, collection from locally derived rubble near base of prominent resistant knoblike exposure:

Schizophoria sp., *Eleutherokomma* n. sp., *Aglaoglypta* n. sp., bellerophontid gastropod with spiral ornament, *Straparollus* (*Straparollus*) sp., *S.* (*Euomphalus*) sp., undetermined bivalve, crinoid ossicles.

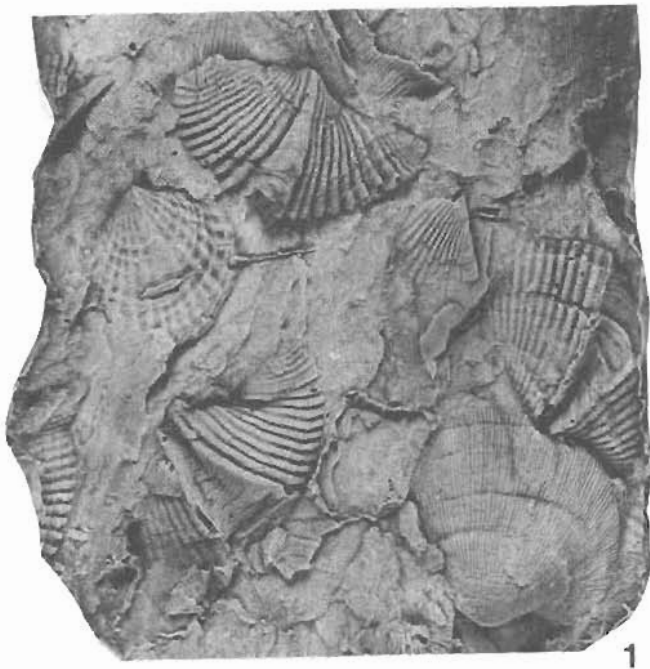
- USGS locality 11934-SD (field station 90ABd10), 49.4 m (162 ft) above base of section, collection from thin, laterally continuous, fossiliferous lens in lower part of resistant exposure: *Schizophoria* sp., *Eleutherokomma* n. sp., crinoid ossicles.
- USGS locality 11935-SD (field station 90ABd11), 59.4 m (195 ft) above base of section, collection from fossiliferous lens from upper part of resistant exposure: *Schizophoria* sp., *Eleutherokomma* n. sp., crinoid ossicles, vascular plant debris.
- USGS locality 11936-SD (field station 90ABd12), 71.6 m (235 ft) above base of section, collection made from locally derived rubble: *Schizophoria* sp., *Spinatrypa* sp., *Eleutherokomma* n. sp., crinoid ossicles.
- USGS locality 11937-SD (field station 90ABd13), 79.2 m (260 ft) above base of section, collection made from more or less in place lens: *Schizophoria* sp., *Spinatrypa* sp., *Eleutherokomma* n. sp., undetermined bellerophontid gastropod, *Straparollus* (*Straparollus*) sp., *Oreocopia* cf. *O. mccoyi* (Walcott, 1884), undetermined gastropods, undetermined bivalve, crinoid ossicles.
- USGS locality 11938-SD (field station 90ABd14), 86.6 m (284 ft) above base of section, collection made in locally derived rubble: *Schizophoria* sp., *Eleutherokomma* n. sp., indeterminate bellerophontid gastropod, crinoid ossicles.

Collection of W.G. Gilbert

- USGS locality 11939-SD (field station 89WG112): collection made from rubble between 32.0 to 62.5 m (105 to 205 ft) above base of section: *Schizophoria* sp., *Spinatrypa* sp., *Eleutherokomma* n. sp., crinoid ossicles.

Figure 4. Early Late Devonian (Frasnian) fossils from measured section in SE $\frac{1}{4}$ SW $\frac{1}{4}$ SE $\frac{1}{4}$ sec. 12, T. 20 N., R. 29 W., Lime Hills D-4 quadrangle.

1. Latex replica of siltstone block, USNM 460756, x1.5, containing impressions of *Eleutherokomma* n. sp., *Spinatrypa* sp., and *Schizophoria* sp., USGS loc. 11939-SD.
- 2-5. *Eleutherokomma* n. sp.
 2. Latex replica of a brachial valve, x4.0 (same specimen as in upper-left-hand corner of fig. 4.1), USGS loc. 11939-SD.
 3. Latex replica of pedicle valve, USNM 460757, x2, USGS loc. 11937-SD.
 4. Latex replica of two partially exposed pedicle valves, USNM 460758, x2, USGS loc. 11934-SD.
 5. Latex replica of pedicle valve, USNM 460759, x2, USGS loc. 11934-SD.
- 6, 7. *Schizophoria* sp.
 6. Partially decorticated pedicle valve showing internal structure, USNM 460760, x2, USGS loc. 11937-SD.
 7. Latex replica of free valve, showing external ornament of fine radial costellae, USNM 460761, x2, USGS loc. 11934-SD.
8. Latex replica of *Aglaoglypta* n. sp., USNM 460762, x8, USGS loc. 11933-SD.
9. Latex replica of *Orecoxia* cf. *O. mccoysi* (Walcott, 1884), USNM 460763, lateral view, x5, USGS loc. 11937-SD.
- 10, 11. N. gen. aff. *Acanthonema*, n. sp., USGS loc. 11937-SD.
 10. Apertural view of latex replica, USNM 460764, x6.
 11. Same view, x10.
- 12, 13. Latex replicas of the gyrogonites of the charophyte *Sycidium*, all specimens from a single hand specimen, USNM 460765, USGS loc. 11930-SD.
 12. Apical view of a single gyrogonite, x9.
 13. Scattered gyrogonites in differing orientations, x9.



1



3



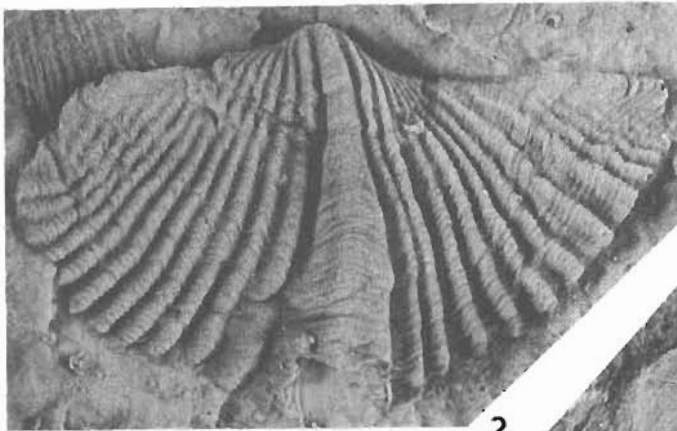
10



4



11



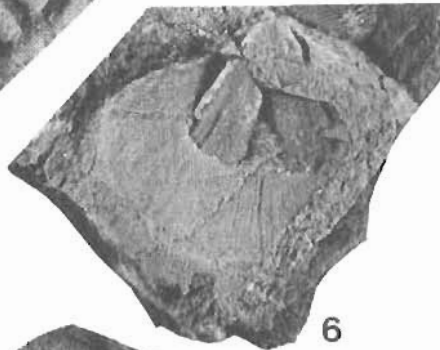
2



5



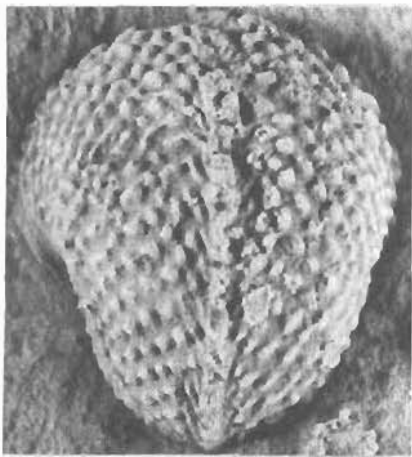
12



6



13



8



7



9

Petrography and Provenance of Sandstones from the Nation River Formation (Devonian) and the Step Conglomerate (Permian), Kandik Region, East-Central Alaska

By Thomas Brocculeri, Michael B. Underwood, and David G. Howell

Abstract

The Kandik region of east-central Alaska can be subdivided into two major fault-bounded geologic units (herein referred to as the Tatonduk "belt" and the Kandik River "belt"), plus three smaller tectonostratigraphic terranes. Within this overall framework are sandstones of the Devonian Nation River Formation and the Permian Step Conglomerate. These sandstones are composed mostly of monocrystalline quartz grains and chert clasts, together with modest percentages of sedimentary and metasedimentary rock fragments. All of the petrographic data and detrital modes are consistent with a recycled-orogenic tectonic provenance, and the detritus probably was eroded from a northern source area. The Step Conglomerate displays a slight increase in compositional maturity, which may be related to intrabasinal recycling. However, because of the petrographic similarities between the two formations, detrital modes do not provide definitive criteria for tectonostratigraphic assignment.

INTRODUCTION

Most of east-central Alaska is a composite of tectonostratigraphic terranes (Churkin and others, 1982; Coney and Jones, 1985). The Kandik region (fig. 1) has been described and interpreted by some workers within the conceptual framework of terrane analysis (for example, Howell and Wiley, 1987; Laughland and others, 1990; Howell and others, 1992). Conversely, other geologists regard most or all of these rocks as thrust-faulted continental-margin deposits of North American affinity (Dover, 1990; D. Bradley, written commun., 1992). Regardless of which concept is favored, there are two major belts of strata to consider, herein referred to as the Tatonduk "belt" and the Kandik River "belt" (following the suggestion of D. Bradley, written commun., 1992). A southeast-verging, younger-over-older thrust

fault (Glenn Creek fault zone) serves as the structural boundary between the two belts (fig. 1; Brabb and Churkin, 1969; Dover and Miyaoka, 1988). Both belts are overlain unconformably by unit TKs of Brabb and Churkin (1969), and both belts appear to be parautochthonous with respect to North America. In this paper, we make no inferences regarding the distance of tectonic transport for either belt with respect to the Proterozoic edge of North America.

The primary purpose of this brief paper is to present compositional data for sandstones assigned to the Nation River Formation (Devonian) and the Step Conglomerate (Permian). Detrital modes are used to describe the generic tectonic provenance. Comparisons between the Devonian and Permian formations also serve as a means of assessing temporal variations among the inferred detrital sources, as well as possible differences between the Paleozoic depositional histories of the Tatonduk and Kandik River belts. Within this report, the formational assignments of Brabb and Churkin (1969) and Foster (1976) have been retained. We note, however, that ambiguities exist in the tectonostratigraphic identity of certain samples (Churkin and others, 1982; Dover and Miyaoka, 1988; Howell and others, 1992).

GEOLOGIC SETTING

The Tatonduk belt includes basement rocks of the Tindir Group (Middle Proterozoic to Lower Cambrian) and extends upsection through Triassic to Lower Cretaceous strata of the Glenn Shale (Churkin and others, 1982; Howell and Wiley, 1987; Howell and others, 1992; see Underwood and others, this volume, for stratigraphic column). Stratigraphic and facies relations are consistent with a continental rifting event, followed by progressive deepening of depositional environments from

Late Proterozoic through Late Devonian time; lower Paleozoic carbonate strata, which include intervals of carbonate turbidites, grade upsection into ribbon chert and siliciclastic turbidite deposits (Payne and Allison, 1981; Howell and Wiley, 1987).

The Nation River Formation is a Devonian deep-marine turbidite sequence consisting of rhythmically interbedded chert-rich conglomerate, sandstone, and mudstone (Brabb and Churkin, 1967; Howell and Wiley, 1987). This diverse succession has been interpreted as a submarine-fan complex sandwiched between a deep-water chert (McCann Hill Chert) and a siliceous shale unit known as the Ford Lake Shale (Brabb, 1969; Brabb and Churkin, 1969; Payne and Allison, 1981). Nilsen and others (1976) described occurrences of west-directed paleocurrent indicators and linked the sediment source to

uplift in the Northwestern Cordillera, coupled with westward progradation of a deep-sea fan system. In contrast, Howell and Wiley (1987) documented a radial pattern of current indicators and concluded that paleoflow was directed predominantly toward the south and southeast (that is, toward the North American craton). Accordingly, a northern landmass may have been the sediment source for the Nation River Formation.

The Kandik River belt is dominated by Jurassic to Lower Cretaceous deep-marine deposits assigned to the Glenn Shale, Keenan Quartzite, Biederman Argillite, and Kathul Graywacke (see Underwood and others, this volume, for stratigraphic column; see Howell and others, 1992, for preliminary petrographic data for Cretaceous sandstones). Most of these rocks display a pronounced slaty cleavage, and Laughland and others (1990) docu-

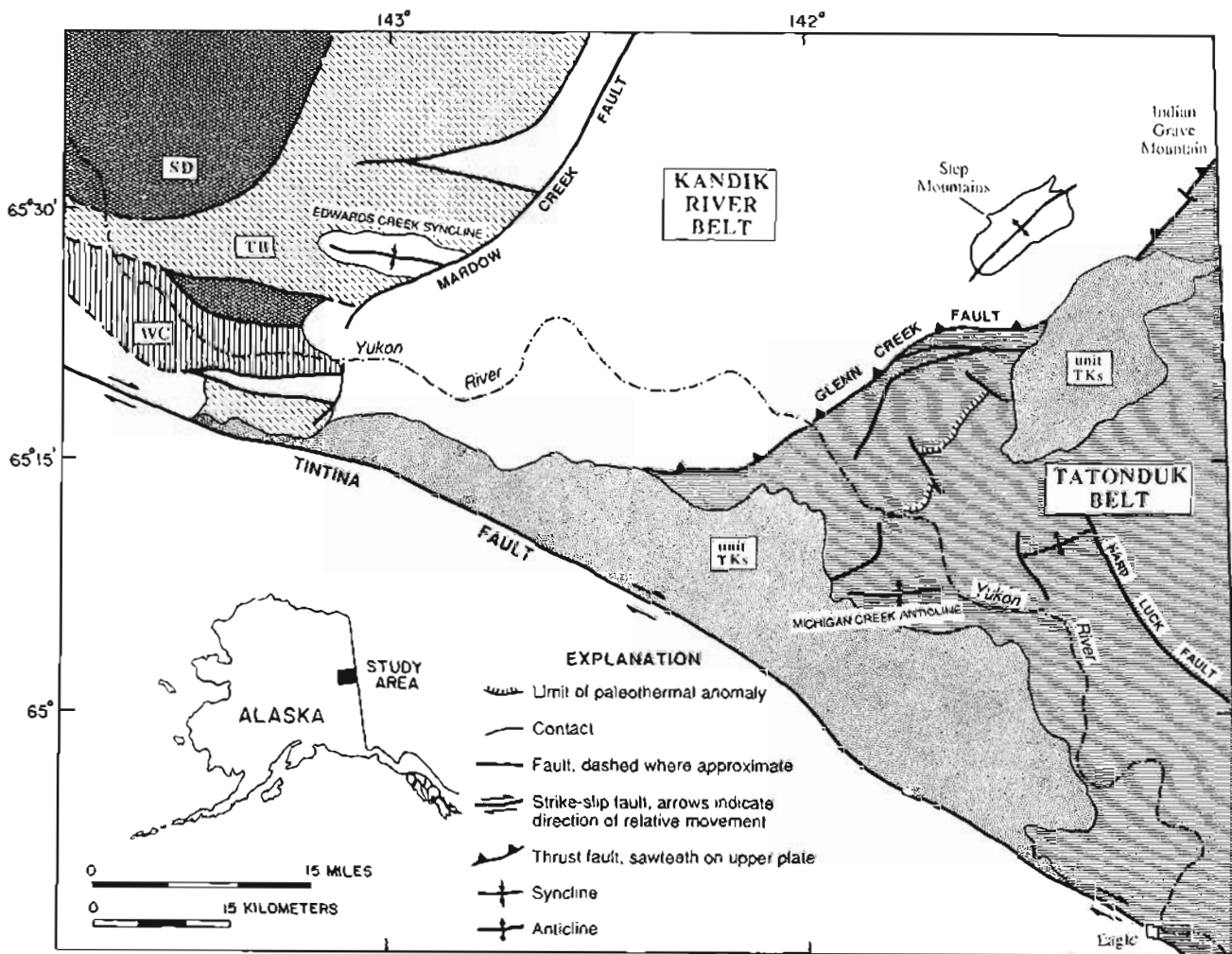


Figure 1. Geologic index map of east-central Alaska showing Kandik River belt (no pattern) and Tatonduk belt (horizontal lined pattern). Hachured line southeast of Glenn Creek fault delineates boundary of thermal-maturity anomaly (see Underwood and others, this volume). Also shown are unit TKs of Brabb and Churkin (1969), and Woodchopper Canyon (WC), Slaven Dome (SD), and Tacoma Bluff (TB) terranes of

Churkin and others (1982). Rocks southwest of Tintina fault zone are assigned to Yukon-Tanana composite terrane (Coney and Jones, 1985). Modified from Brabb and Churkin (1969) and Foster (1976). For relevant fossil control and alternative interpretations of structural geology, see Dover and Miyaoka (1988) and Miyaoka (1990).

mented much higher levels of thermal maturity in Mesozoic rocks of the Kandik River belt as compared with older strata of the Tatonduk belt. In the western portion of the study area (fig. 1), the Kandik River belt is in fault contact with the Woodchopper Canyon terrane, the Slaven Dome terrane, and the Takoma Bluff terrane of Churkin and others (1982).

Pre-Mesozoic sandstones and conglomerates occur in two general regions to the northwest of the Glenn Creek fault zone: (1) in the core of the Step Mountains anticline, and (2) west of the Mardow Creek fault (fig. 1). Based upon a single occurrence of poorly preserved spores (Miyaoka, 1990), Devonian conglomerates have been identified in the core of the Step Mountains anticline (Brabb and Churkin, 1969; Dover and Miyaoka, 1988). These strata, however, may correlate with poorly dated rocks of the Takoma Bluff terrane of Churkin and others (1982), rather than the widespread Nation River turbidite successions to the southeast of the Glenn Creek fault zone (Howell and others, 1992).

The Step Conglomerate (Lower Permian) consists primarily of massive, chert-rich sandstone and chert-pebble conglomerate, plus lenses of bioclastic limestone. The type locality of this formation is located in the Step Mountains (Brabb, 1969), but most of the mapped localities of the Step Conglomerate (Brabb and Churkin, 1969) are located within the Takoma Bluff terrane of Churkin and others (1982). The correlation between the Takoma Bluff terrane and the type section in the Step Mountains remains uncertain. Moreover, portions of the Takoma Bluff terrane have been remapped as Devonian (Nation River Formation?) by Dover and Miyaoka (1988). Locally, the Step Conglomerate lies above an angular unconformity that resulted from regional uplift and erosion prior to the Early Permian Epoch (Payne and Allison, 1981). A northern source has been inferred for the Permian gravels, but no specific provenance has been identified (Nilsen and others, 1976).

METHODS

Outcrop samples of sandstone (fine to coarse grained) were collected from a field area bounded to the southwest by the Tintina fault zone, to the north and west by the loess deposits of the Yukon Flats, and to the east by the international border with Canada (fig. 2). Two samples from Canada were provided by ARCO Alaska, Inc. Detrital modes were determined for 33 sandstone samples from the Nation River Formation and 7 sandstone samples from the Step Conglomerate (table 1). As stated previously, all of the formational assignments follow the maps of Brabb and Churkin (1969) and Foster (1976). Thin sections were impregnated with blue epoxy to identify pore space and stained for both

plagioclase and potassium feldspar, using a modified version of Houghton's (1980) technique. The Gazzi-Dickinson point-counting method was followed, in which only aphanitic grains are classified as lithic fragments (Ingersoll and others, 1984). This technique is advantageous because it minimizes the effect of grain size changes on modal data. At least 500 grid points were counted per specimen.

PETROGRAPHIC GRAIN DESCRIPTIONS

The following brief descriptions pertain to sandstone constituents in both the Nation River Formation and the Step Conglomerate. Monocrystalline quartz grains are common in all of these sandstones; extinction varies from straight to strongly undulose. Minute inclusions of sericite(?) occur within many of the quartz grains. Chert (cryptocrystalline quartz) is consistently the most abundant type of framework grain. Finely crystalline chert typically contains clay and mica impurities plus stains of metallic oxides. Outlines and spherical ghosts of radiolaria are rare. The feldspar content of some samples may be underestimated as a result of diagenetic alteration to albite, clay minerals, and calcium carbonate. Pure albite did not stain and was identified based on its characteristic cleavage. Potassium feldspar occurs as orthoclase, microcline, and perthite; the presence of K-feldspar suggests shallow burial depths and (or) minimal thermal alteration.

Most of the metamorphic rock fragments are slates and phyllites with a subtle to obvious planar fabric. Foliated mica-schist fragments are relatively rare. Fine-grained metaquartzites display both crude planar fabrics and strongly sutured grain boundaries. Fragments of quartz-mica tectonite exhibit undulose extinction and a foliation defined by parallel to subparallel alignment of micas. A gradation exists from strongly compacted shales to their low-grade metamorphic equivalents. Micaceous, quartz-rich siltstone fragments and clay-rich mudstones are both common. Volcanic rock fragments occur in only trace amounts; these fragments contain small plagioclase laths surrounded by strongly altered matrix, which is probably the weathering product of devitrified glass.

Sandstone matrix is composed of undifferentiated clay minerals, fine-grained mica grains, dark organic material, and dispersed silt-sized quartz. The matrix content tends to increase in samples containing a relatively high percentage of sedimentary and metamorphic rock fragments, suggesting that much of the material is pseudomatrix (that is, not original detrital material). Chemical cement also is more abundant in samples enriched in metasedimentary rock fragments; for example, calcium carbonate occurs as a replacement of framework

grains, as a filling of intergranular pores, and as pore-lining cement. Authigenic clay minerals also fill pore cavities and partially replace chemically unstable framework grains. Chalcedony and polycrystalline quartz cements exist in minor amounts, both within intergranular pores and as microveins. Silica cementation evidently occurred subsequent to pore-lining carbonate cementation. The abundance of clay-rich lithic fragments and the presence of clay matrix and clay coatings collectively served to absorb stresses during compaction, thereby inhibiting pressure solution along grain contacts. Visible porosity (open spaces filled with blue epoxy) is extremely low for both formations (0–3 percent). Because of the abundance of pore-filling matrix and the absence of visible porosity, it appears that the Nation River and Step sandstones have rather limited potential as reservoirs for oil or gas.

PROVENANCE ANALYSIS

Provenance interpretations for the Nation River Formation and the Step Conglomerate are based on standard ternary plots of framework constituents (fig. 3) and comparisons with empirical analogs (for example, Dickinson and others, 1983). QFL ternary diagrams (where Q is total quartz, F is total feldspar, and L is total unstable aphanitic lithic fragments) indicate the survivability of framework grains and the compositional maturity of sandstones. Shifting polycrystalline quartz (Q_p) to the L_t mode of the Q_mFL_t diagram sometimes helps emphasize detrital provenance better than QFL modes alone (Graham and others, 1976). The amounts and types of feldspar can be valuable provenance discriminators, but they are not useful in this particular study. The limiting factor for Q_mPK analysis (where P is plagioclase and K

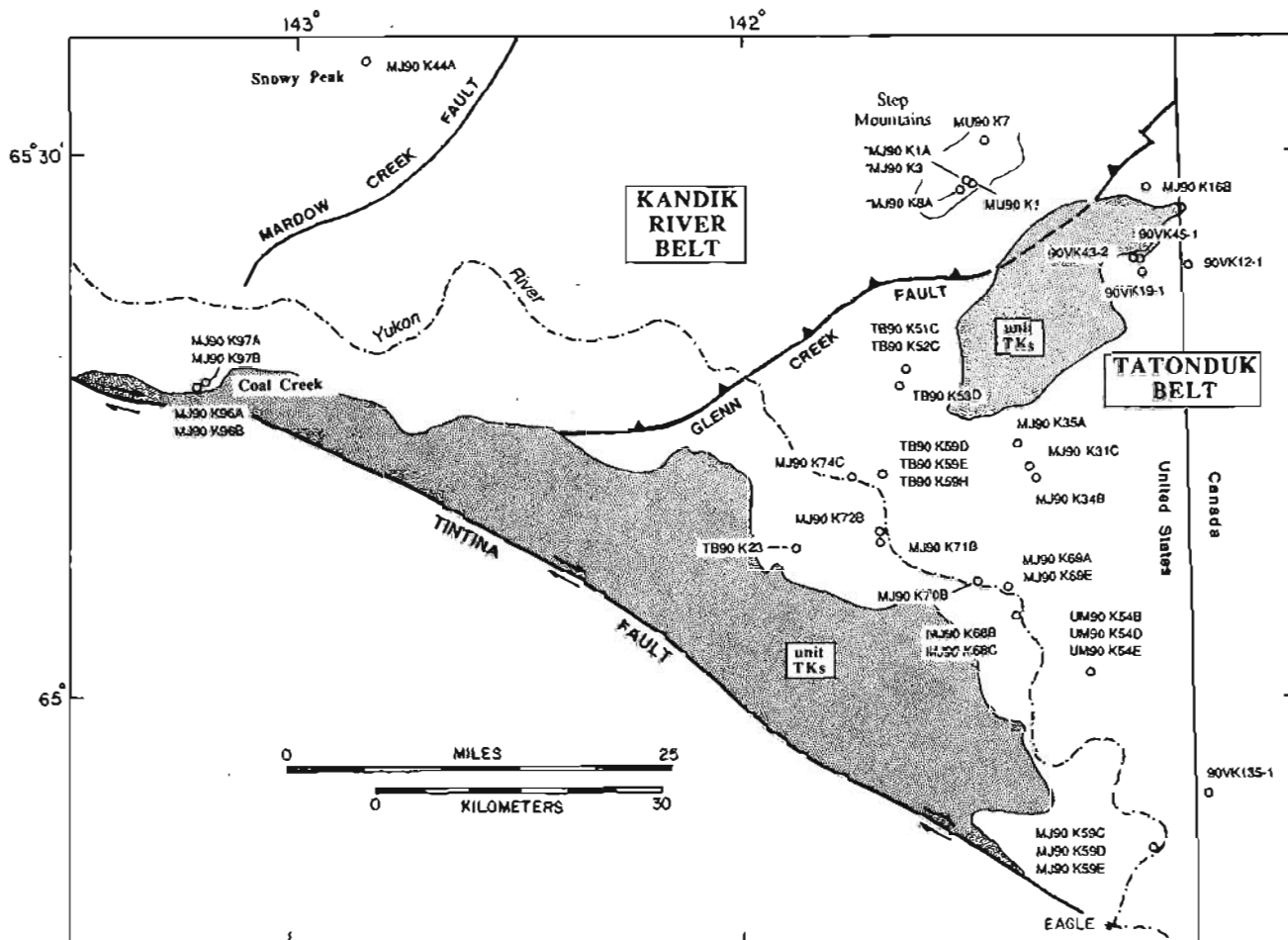


Figure 2. Sample localities for analyses of sandstone composition. See table 1 for formational assignments of each sample. Sample numbers with an asterisk (*) are associated with the Nation River Formation (as mapped by Brabb and Churkin, 1969) northwest of Glenn Creek fault zone. See figure 1 for explanation of symbols.

Table 1. Sandstone point-count data, Nation River Formation and Step Conglomerate, Kandik region, east-central Alaska—Continued

[See figure 2 for sample localities. Abbreviations: GZ, mean visual grain-size estimate (VC, very coarse; C, coarse; M, medium; F, fine; VF, very fine); Ch, chert; Ls, sedimentary rock fragments; Lm, metasedimentary rock fragments; Pore, visible pore space (blue epoxy); Cmt, chemical cement; Mx, fine-grained matrix; Alt, altered/unidentified grains. See figure 3 for definition of other abbreviations]

SAMPLE	TOTAL POINTS COUNTED													DETRITAL MODES (PERCENT)													
	GZ	Qm	Qp	Ch	P	K	Ls	Lm	Lv	Pore	Cmt	Mx	Alt	Q	F	L	Q _m	F	L _t	Q _m	P	K	Q _p	L _v	L _{sm}		
STEP CONGLOMERATE (italic indicates sample from Step Mountains anticline)																											
<i>MU90 K1</i>	M	100	44	156	14	2	112	22	3	1	23	11	12	66	04	30	22	04	74	86	12	02	59	01	40		
<i>MU90 K7</i>	C	78	46	189	6	2	87	33	0	2	67	21	5	71	02	27	18	02	80	91	07	02	66	00	34		
<i>MJ90 K44A</i>	C	128	59	138	6	7	72	31	13	0	20	17	9	72	03	26	28	03	69	91	04	05	63	04	33		
<i>MJ90 K96A</i>	VC	97	27	186	10	0	95	33	0	6	13	24	9	69	02	29	22	02	76	91	09	00	62	00	38		
<i>MJ90 K96B</i>	C	29	58	212	6	1	109	21	1	15	24	14	10	68	02	30	07	02	92	81	17	03	67	00	32		
<i>MJ90 K97A</i>	VC	61	53	252	2	1	76	14	9	0	12	8	12	78	01	21	13	01	86	95	03	02	75	02	22		
<i>MJ90 K97B</i>	C	73	39	238	9	0	62	29	0	6	24	12	8	78	02	20	16	02	82	89	11	00	75	00	25		
MEAN DETRITAL MODES														72	02	26	18	02	80	89	09	02	67	01	32		
MEAN PERCENT		16.2	9.3	39.2	1.5	0.4	17.5	5.2	0.7	0.9	5.2	3.1	1.9														
LOW PERCENT		5.8	5.4	27.6	0.4	0.0	12.4	2.8	0.0	0.0	2.4	1.6	1.0														
HIGH PERCENT		25.6	11.8	50.4	2.8	1.4	22.4	6.6	2.6	3.0	13.4	4.8	2.4														

is potassium feldspar) is the relative depletion of monoclinic constituents. The relative amounts and types of lithic fragments are probably the most valuable discriminators for interpreting sandstone provenance (Graham and others, 1976). The $Q_p L_{sm}$ diagram illustrates the predominance of Q_p (including chert), and sedimentary and metamorphic rock fragments (L_{sm}) with respect to volcanic rock fragments (L_v).

The mean QFL value for the Nation River Formation is $Q=62$, $F=5$, and $L=33$. These data are consistent with a recycled orogenic provenance (fig. 3). Interpretation of the $Q_m F L_t$ diagram suggests a transitional-recycled to lithic-recycled source, with a mean value of $Q_m=21$, $F=5$, and $L_t=74$. Average polycrystalline modes are $Q_p=55$, $L_v=1$, and $L_{sm}=44$ for the Nation River Formation, and these data are consistent with a sedimentary and low-grade metamorphic terrain as the principal source. However, rock fragments of this type could have been eroded from a variety of tectonic settings, including a collisional suture zone, a sedimentary fold-thrust belt, or an uplifted continental-margin succession with exposed metamorphic basement. The $Q_m PK$ data likewise support the interpretation of a continental-block provenance (fig. 3); there is no evidence, based on this plot, for significant input from either a dissected volcanic/plutonic terrain or comparable crystalline lithologies within continental basement.

Overall, we note only minor differences among the petrographic modes of the Step Conglomerate and the Nation River Formation. Some of the differences could be due to grain size, in that Step sandstones are generally coarser grained (table 1). However, the data set is too small to be statistically reliable. The Step Conglomerate yields a modal average of $Q=72$, $F=2$, and $L=26$. Percentages of chert are modestly higher in the Step Conglomerate, resulting in an average modes of $Q_m=18$, $F=2$, and $L_t=80$ and $Q_p=67$, $L_v=1$, and $L_{sm}=32$. Finally, both P and K values are slightly lower, on average, in the Step Conglomerate. Data for individual samples plot in the same tectonic-provenance fields as most of those described above for the Nation River Formation (fig. 3).

DISCUSSION

The identification of a specific geologic or geographic provenance for sandstones of the Nation River Formation and the Step Conglomerate requires some caution given the variety of factors influencing detrital modes. For example, the effects of distance of nonmarine transport, sediment recycling, transport energy and transport processes within the depositional setting, and diagenetic alteration of framework grains all must be considered. With this caveat in mind, we emphasize the obvious enrichment in both formations of to-

tal quartz and unstable lithic fragments relative to feldspar. Conversely, volcanic rock fragments and feldspar grains are rare. Collectively, these petrologic signatures define the quartzo-lithic suite (Dickinson, 1988). A logical conclusion is that sedimentary plus low-grade metasedimentary rocks dominated the provenance region. Based on the turbidite paleocurrent analysis of Howell and Wiley (1987), the source was probably located to the north. Paleoflow data of this type must be viewed with some caution, however, because turbidity

currents generally flow in directions parallel to a basin's axis during deposition, and that direction may not coincide with the initial sediment transport direction out of the subaerial source area.

The origin of the detrital chert grains is key to any provenance interpretation. This highly resistant debris may have been recycled from older sedimentary rocks within any of several types of geologic settings, such as an uplifted subduction complex, a fold-thrust belt, or a rifted continental-margin succession (Jones and

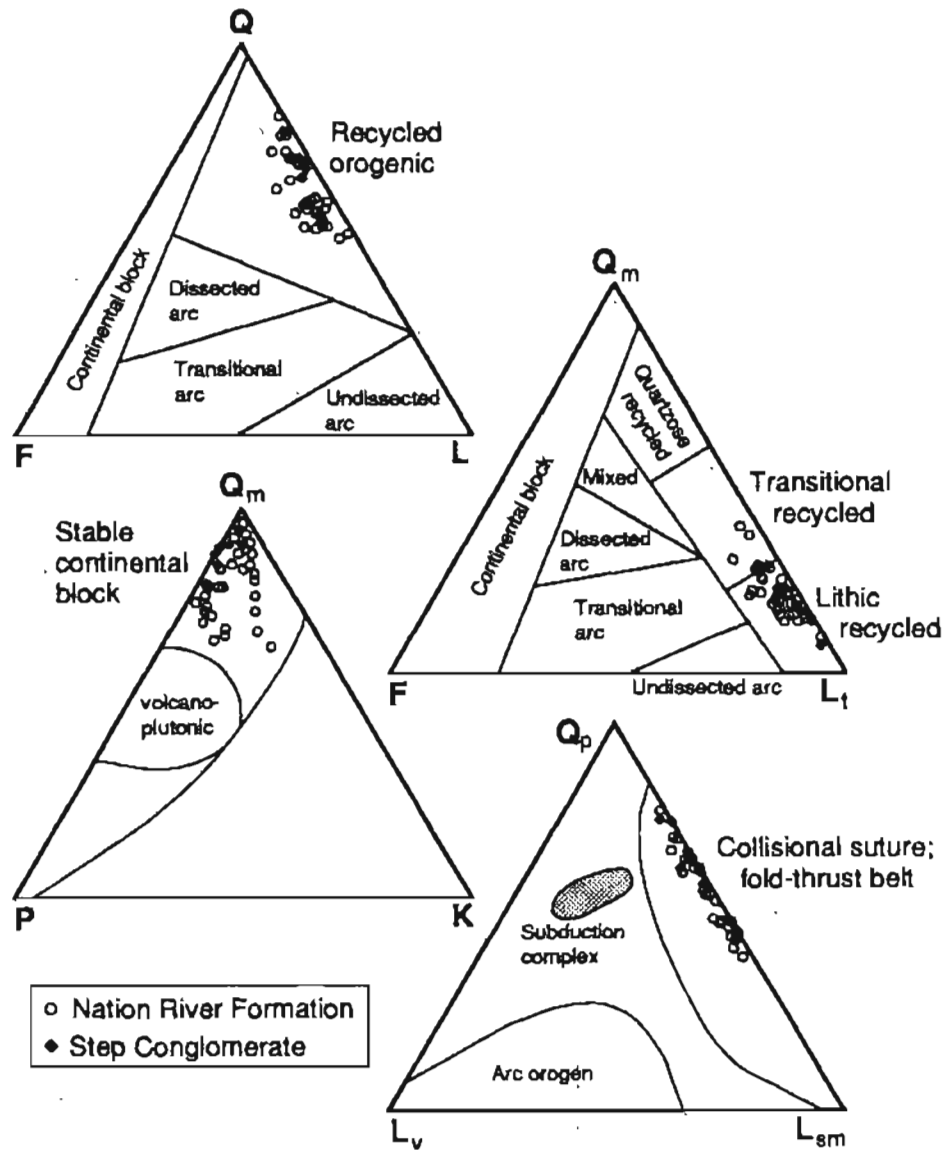


Figure 3. Ternary diagrams showing detrital modes for sandstones of Nation River Formation (open circles) and Step Conglomerate (solid diamonds), east-central Alaska. Abbreviations are as follows: Q, total quartz; Q_p , polycrystalline quartz (including chert); Q_m , monocrystalline quartz; P, plagioclase; K, potassium feldspar; F, total feldspar; L, unstable aphanitic rock fragments; L_v , total polycrystalline grains; L_v , volcanic rock fragments; L_{sm} , sedimentary and metasedimentary rock fragments. Boundaries for tectonic-provenance fields are from Dickinson and others (1983) and Dickinson (1988). See table 1 for complete petrographic data.

Murchey, 1986). The overall paucity of both volcanic debris and feldspar casts serious doubt on the subduction-zone hypothesis, and the scarcity of radiolaria tests and sponge spicules (or their diagenetic ghosts) leads us to suggest that most of the chert did not form through direct biogenic accumulation of silica ooze (that is, as a normal ribbon chert). Instead, we favor significant amounts of erosion from chert nodules that formed via diagenetic segregation of silica within shallow-water carbonate sequences (Knauth, 1979).

A significant difference in provenance between the Devonian Nation River Formation and the Permian Step Conglomerate is not supported by our petrographic analyses. Payne and Allison (1981) speculated that widespread Carboniferous uplift and intrabasinal erosion, including areas to the west and northwest of our study area (that is, in the vicinity of the Kaltag-Porcupine fault zone), may have provided the Step Conglomerate with some of the chert-rich gravel. The Step Conglomerate, on average, does contain greater percentages of resistant chert and slightly lesser amounts of mechanically unstable lithic fragments, so some intrabasinal recycling appears possible. Evidence for a major reduction in fragile metamorphic and sedimentary rock fragments is lacking, however, so we conclude that both units shared the same basic type of detrital source.

CONCLUSIONS

Detrital modes for 33 sandstones selected from the Nation River Formation and 7 from the Step Conglomerate define overlapping fields on all ternary plots of tectonic provenance. The high percentages of polycrystalline quartz (chert), sedimentary rock fragments, and metamorphic debris collectively point to a recycled-orogenic provenance for both formations. We speculate that the sediments were derived from an uplifted continental margin to the north of the Kandik region. Our data allow for a limited amount of intrabasinal recycling of older Paleozoic strata including, perhaps, the Devonian Nation River Formation as a partial source for the subtle enrichment of chert in the Permian Step Conglomerate. Because of the similarities in detrital modes, however, petrographic data cannot be used to provide definitive criteria for the assignment of individual Paleozoic sandstones and conglomerates to appropriate tectonostratigraphic units.

Acknowledgments.—Mark Johnsson and Lu Haufu assisted in the field. Samples and financial support to the University of Missouri were generously supplied by ARCO Alaska, Inc. We thank Gerry Van Kooten and his ARCO colleagues for their scientific cooperation and logistical aid. Superintendent Don Chase granted sampling permits and access to the Yukon-Charley Rivers National Preserve. Acknowledgment is also made to the

Donors of the Petroleum Research Fund, administered by the American Chemical Society, for partial support of this research (Grant #22773-AC2 to Underwood). Editorial suggestions by D. Bradley helped improve the manuscript.

REFERENCES CITED

- Brabb, E.E., 1969, Six new Paleozoic and Mesozoic formations in east-central Alaska: U.S. Geological Survey Bulletin 1274-I, p. 1-26.
- Brabb, E.E., and Churkin, M., Jr., 1967, Stratigraphic evidence for the Late Devonian age of the Nation River Formation, east-central Alaska: U.S. Geological Survey Professional Paper 575-D, p. D4-D15.
- , 1969, Geologic map of the Charlie River quadrangle, east-central Alaska: U.S. Geological Survey Miscellaneous Geologic Investigations Map I-973, scale 1: 250,000.
- Churkin, M., Jr., Foster, H.L., Chapman, R.H., and Weber, F.R., 1982, Terranes and suture zones in east-central Alaska: *Journal of Geophysical Research*, v. 87, p. 3718-3730.
- Coney, P.J., and Jones, D.L., 1985, Accretion tectonics and crustal structure in Alaska: *Tectonophysics*, v. 119, p. 265-283.
- Dickinson, W.R., 1988, Provenance and sediment dispersal patterns in relation to paleotectonic and paleogeography of sedimentary basins, in Kleinspehn, K.L., and Paola, C., eds., *New perspectives in basin analysis*: New York, Springer-Verlag, p. 331-351.
- Dickinson, W.R., Beard, L.S., Brakenridge, G.R., Erjavec, J.L., Ferguson, R.C., Inman, K.F., Knapp, R.A., Lindberg, F.A., and Ryberg, P.T., 1983, Provenance of North American Phanerozoic sandstones in relation to tectonic setting: *Geological Society of America Bulletin*, v. 94, p. 222-235.
- Dover, J.H., 1990, *Geology of east-central Alaska*: U.S. Geological Survey Open-File Report 90-289, 66 pp.
- Dover, J.H., and Miyaoka, R.T., 1988, Reinterpreted geologic map and fossil data, Charlie River quadrangle, east-central Alaska: U.S. Geological Survey Miscellaneous Field Studies Map MF-2004, 2 sheets, scale 1:250,000.
- Foster, H.L., 1976, Geologic map of the Eagle Quadrangle, Alaska: U.S. Geological Survey Miscellaneous Field Studies Map I-922, 1 sheet, scale 1:250,000.
- Graham, S.A., Ingersoll, R.V., and Dickinson, W.R., 1976, Common provenance for lithic grains in Carboniferous sandstones from the Ouachita Mountains and Black Warrior basin: *Journal of Sedimentary Petrology*, v. 46, p. 620-632.
- Houghton, H.F., 1980, Refined techniques for staining plagioclase and alkali feldspars in thin section: *Journal of Sedimentary Petrology*, v. 50, p. 629-630.
- Howell, D.G., Johnsson, M.J., Underwood, M.B., Lu Haufu, and Hillhouse, J.W., 1992, Tectonic evolution of the Kandik region, east-central Alaska: Preliminary interpretations, in Bradley, D.C., and Ford, A.B., eds., *Geologic studies in Alaska by the U.S. Geological Survey, 1990*: U.S. Geological Survey Bulletin 1999, p. 127-140.
- Howell, D.G., and Wiley, T.J., 1987, Crustal evolution of

- northern Alaska inferred from sedimentological and structural relations in the Kandik area: *Tectonics*, v. 6, p. 619-631.
- Ingersoll, R.V., Bullard, T.F., Ford, R.L., Grimm, J.P., Pickle, J.D., and Sares, S.W., 1984, The effect of grain size on detrital modes: A test of the Gazzi-Dickinson point-counting method: *Journal of Sedimentary Petrology*, v. 54, p. 103-116.
- Jones, D.L., and Murchey, B., 1986, Geologic significance of Paleozoic and Mesozoic radiolarian chert: *Annual Review of Earth and Planetary Sciences*, v. 14, p. 455-492.
- Klaath, L.P., 1979, A model for the origin of chert in limestone: *Geology*, v. 7, p. 274-277.
- Laughland, M.M., Underwood, M.B., and Wiley, T.J., 1990, Thermal maturity, tectostratigraphic terranes, and regional tectonic history: an example from the Kandik area, east-central Alaska, in Nuccio, V.F., and Barker, C.E., eds., *Applications of thermal maturity studies to energy exploration: Society of Economic Paleontologists and Mineralogists, Rocky Mountain Section, Special Publication*, p. 97-111.
- Miyaoka, R.T., 1990, Fossil locality map and fossil data for the southeastern Charley River quadrangle, east-central Alaska: U.S. Geological Survey Miscellaneous Field Studies Map MF-2007, 45 p., scale 1:100,000.
- Nilsen, T.H., Brabb, E.E., and Simoni, T.R., 1976, Deep sea fan deposition of the Devonian Nation River Formation, Yukon-Kandik area, Alaska: *Proceedings of the Alaska Geological Society Symposium*, p. E1-E20.
- Payne, M.W., and Allison, C.W., 1981, Paleozoic continental-margin sedimentation in east-central Alaska: *Geology*, v. 9, p. 274-279.
- Reviewers: H. McLean and M. Wilson

Magnetic Susceptibilities and Iron Content of Plutonic Rocks Across the Coast Plutonic-Metamorphic Complex near Juneau, Alaska

By James L. Drinkwater, Arthur B. Ford, and David A. Brew

Abstract

Magnetic susceptibility measurements and chemical data for granitoid samples collected from a transect across the Coast plutonic-metamorphic complex near Juneau help define and characterize 18 plutons and plutonic units that form three major belts and seven subbelts. Magnetic susceptibility values along the transect correlate moderately well with oxidation-state values but not well with total iron (FeO*) or normative magnetite. Very low magnetic susceptibility characterizes a group of 95-Ma plutons that lie along the western margin of the transect (Admiralty-Revillagigedo belt); these are ilmenite-bearing type granitoids that contain very little or no magnetite. Three small plutonic sills, which are part of the great tonalite sill belt east of the megalineament, are also ilmenite bearing and have very low magnetic susceptibility, but other major plutons of the same belt are magnetite-bearing types with very high magnetic susceptibility. East of the great tonalite sill belt, magnetic susceptibility generally decreases, oxidation states vary considerably, and most of the plutons are magnetite bearing. FeO* steadily decreases in the rocks as the SiO₂ and K-feldspar contents increase.

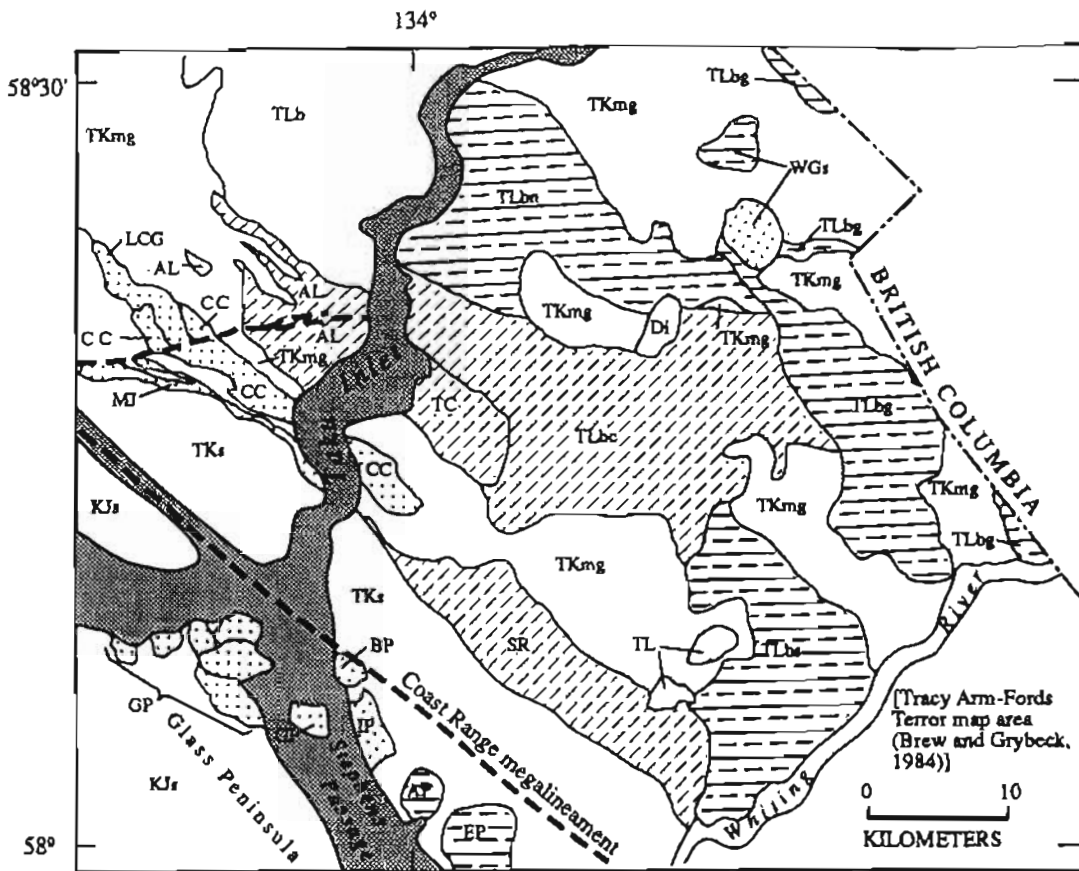
Differences in magnetic susceptibility are due to changes in composition, oxidation states, and Fe³⁺ mineralogy. Between the major plutonic belts these parameters are related to the different ages of the belts and the host terranes in which the plutons were emplaced, but the causes of these differences between subbelts is not well established. They may be related to the differentiation trends of the different groups of plutons. Geochemical and petrographic characteristics of the ilmenite-bearing plutons indicate that they are I-type granitoids that were generated either as reduced magmas or as oxidized magmas that became reduced during their magmatic history. An average oxidation value of 0.23 roughly separates ilmenite-bearing from magnetite-bearing type granitoids. Factors such as depth of magma generation, contamination, H₂O and sulfide content, and tectonic stresses during pluton emplacement may influence the extent of oxidation and reduction and the crystallization of magnetite and trivalent Fe-rich ferromagnesian silicate minerals. Trivalent Fe-rich silicate minerals such as biotite, epidote, allanite, and brown hornblende are much more common

in granitoids that have high FeO* and relatively high oxidation-state values but low magnetic susceptibility. Primary (magmatic) epidote is found mainly in the ilmenite-bearing (reduced) type plutons of the Admiralty-Revillagigedo plutonic belt.

INTRODUCTION

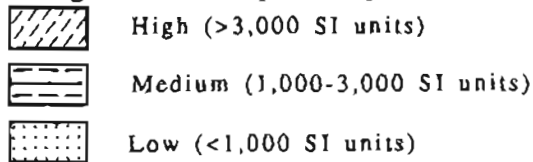
Magnetic susceptibility (MS) is an easily measured rock property that provides a semiquantitative measure of the magnetite content of a rock (Puranen, 1989; Ross, 1989; Tulloch, 1989). It is particularly useful in characterizing and delineating individual plutons for mapping purposes (Ross, 1989). Used in conjunction with iron content and iron oxidation states, the MS values may aid in the assessment of the magmatic and tectonic environment of emplacement (Ishihara, 1977; Takahashi and others, 1980; Tulloch, 1989; Bateman and others, 1991). Takahashi and others (1980) used MS data to separate granitic rocks into the magnetite and ilmenite series; these series, in turn, were interpreted to indicate different tectonic settings. Such interpretative use of MS data, however, may be weakened by significant differences in susceptibility that can occur between different plutons, parts of plutons, and lithologies. An example is the Idaho batholith, where the boundary between a western magnetite series and an eastern ilmenite series in the western part may partly reflect ages of intrusion (Piccoli and Hyndman, 1985). Some differences in MS are probably due to variable hydrothermal alteration (Criss and Champion, 1984).

This report provides data on the MS and iron content of granitic rocks of Late Cretaceous and Tertiary age in a northeast-trending transect (Taku Inlet transect) across the informally named Coast plutonic-metamorphic complex of Brew and Ford (1984a, b) (fig. 1). These data were derived from our ongoing investigations of the chemical and petrographic variations along the transect. The transect lies southeast of Juneau between Taku Inlet



EXPLANATION

Average magnetic susceptibility values of units —



Map Unit Abbreviations

<p>WGs - Wright Glacier stocks</p> <p>TLbg - Turner Lake batholith eastern unit</p> <p>TLbn - Turner Lake batholith northern unit</p> <p>TLbc - Turner Lake batholith central unit</p> <p>TLbs - Turner Lake batholith southern unit</p> <p>TLb - Turner Lake batholith undivided</p> <p>TL - Tease Lakes stocks</p> <p>SR - Speel River pluton</p> <p>TC - Taku Cabin pluton</p> <p>AL - Annex Lakes pluton</p> <p>CC - Carlson Creek pluton</p>	<p>LCG - Lemon Creek Glacier pluton</p> <p>MJ - Mount Juneau pluton</p> <p>EP - Everett Peak pluton</p> <p>AP - Arthur Peak pluton</p> <p>BP - Butler Peak pluton</p> <p>IP - Irving Peak pluton</p> <p>GI - Grand Island pluton</p> <p>GP - Glass Peninsula stocks</p> <p>TKmg - Migmatitic gneiss (Tertiary and Cretaceous)</p> <p>TKs - Schist (Tertiary and Cretaceous)</p> <p>KJs - Metasedimentary and metavolcanic rocks (Cretaceous and Jurassic)</p> <p>Di - Diorite</p>
---	---

Figure 1. Generalized geologic map of Taku Inlet transect area, southeastern Alaska, showing individual plutons and plutonic units discussed in text. Geology modified from Brew and Ford (1986).

and the Whiting River and extends from the Glass Peninsula of Admiralty Island northeastward to the Canadian border (fig. 1). The study area, or "transect area," includes MS data on the Annex Lakes pluton and for a group of plutonic sills (Mount Juneau, Carlson Creek, and Lemon Creek Glacier plutons) that lie east of Juneau and are just north of the Taku Inlet transect. Available age data for rocks in the transect are also summarized here. Descriptions of the plutons and country rocks in the transect area are found in Brew and Grybeck (1984), Brew and Ford (1986), Brew (1988), and Drinkwater and others (1989). Drinkwater and others (1990) used the informal term "Juneau sill group" for the Mount Juneau, Carlson Creek, Lemon Creek Glacier, Mendenhall Glacier, Annex Lakes and Taku Cabin plutons. We discontinue the usage of that informal term in this paper and refer to these plutons by their individual names. (The Mendenhall Glacier pluton is not shown on figure 1 and is not discussed in this paper.)

Methods

Magnetic susceptibility measurements were made from the same sawn slab surfaces from which modal compositions were determined. The measurements were made with a model JH-8 (Geoinstruments, Finland) hand-held susceptibility meter. The units of measurement for volume susceptibility readings, as used in this report, are dimensionless SI units (International standard units), $\times 10^{-5}$. One percent magnetite produces an MS of about $4,000 \times 10^{-5}$ SI units, which approximates $3,000 \times 10^{-6}$ cgs units (Ross, 1989). MS can be affected by grain size and chemistry of the magnetite (Tulloch, 1989) and commonly decreases with rock weathering (Puranen, 1989). Magnetite grains in samples from the Juneau transect show little size variation. For consistent results we used slabs of fresh rock with a minimum size of 10 cm by 8 cm by 2 cm. We scanned each sample by moving the meter around the surface of the slab and then used the highest reading, which reflects the closest approach to the actual value, according to the method of Tulloch (1989). We also multiplied the results by 2 to compensate for the use of hand samples rather than outcrops, in accordance with the JH-8 manual.

The MS values varied considerably in some samples, and those samples giving very heterogeneous readings were not used. Samples with anomalously high or low readings were also discarded unless they represented a distinct part of a pluton, such as the border zone or core phase. We measured MS on 148 samples, of which 137 were used in determining ranges and averages. Three to 18 samples were measured for each granitoid unit.

Total iron (FeO^*) was determined by X-ray fluorescence analysis in laboratories of the U.S. Geological Survey, and FeO was determined by wet chemical methods. The presence of sulfides, refractory oxides (magnetite and ilmenite), and organic material can obstruct the accuracy of FeO determinations because of problems of Fe oxidation or reduction during acid dissolution of samples in preparation for either coulometric or potentiometric titration methods (Jackson and others, 1987). Because of this potential problem, we did not use anomalously high or low oxidation-state values from sulfide- or oxide-rich samples. Chemical analyses that included FeO determinations were available for 120 samples, and both MS measurements and iron data were available for 54 samples.

GENERAL GEOLOGY

The granitic rocks investigated in this report are part of the Coast plutonic-metamorphic complex, which extends the length of southeastern Alaska and beyond into Canada. The granitoids of the Taku Inlet transect are part of the three plutonic belts (table 1) that, together with the intervening metamorphic rocks and the adjacent Gravina overlap assemblage, define the complex. The plutons along the western edge of the complex are part of the Admiralty-Revillagigedo belt of Brew and Morrell (1983) and are separated from other parts of the Coast plutonic-metamorphic complex by the northwest-trending Coast Range megalineament (Brew and Ford, 1978), a large fault zone with inferred east-side-up displacement and right-lateral offset (Stowell and Hooper, 1990; Hooper and others, 1990). These plutons intrude (1) metavolcanic rocks of the Douglas Island Volcanics and metasedimentary rocks of the Seymour Canal Formation of Late Jurassic and Early Cretaceous age (Brew and Ford, 1986) on the western side of Stephens Passage, and (2) high-grade schist (Brew and Ford, 1984a; Brew and others, 1989) on the eastern side. Collectively these units are referred to as the western metamorphic zone of the Coast plutonic-metamorphic complex (Brew and others, 1989). They were called parts of the Taku and Gravina tectonostratigraphic terranes by Berg and others (1978) and the Taku terrane and Gravina-Nutzotin overlap assemblage by Monger and Berg (1987); we, however, do not consider them to be a separate terrane. Gehrels and others (1990) argued that the eastern part of the western metamorphic zone (that part between the megalineament and the great tonalite sill belt) may belong to the Yukon crystalline terrane of eastern Alaska.

The great tonalite sill (Brew, 1988) is a northwest-trending belt of eastward-dipping plutonic sills of Late Cretaceous to early Tertiary age that forms the western boundary of the central granitic zone of the Coast plu-

Table 1. Major plutonic belts and subbelts of the Coast plutonic-metamorphic complex within the Taku Inlet transect, southeastern Alaska

Belt	Subbelt	Plutons	Main rock types	Age
Admiralty- Revillagigedo	Grand Island -----	Glass Peninsula stocks; Grand Island pluton; Irving Peak pluton; Butler Peak pluton	Quartz diorite; Tonallite; Diorite; Granodiorite	Late Cretaceous
	Taku Harbor -----	Everett Peak and Arthur Peak plutons	Quartz monzodiorite	Late Cretaceous
Great tonalite sill	Western subbelt -----	Speel River pluton; Mount Juneau, Carlson Creek, and Lemon Creek Glacier plutons	Tonalite; Quartz diorite, tonalite, and granodiorite	Early Tertiary, and Late Cretaceous to early Tertiary
	Eastern subbelt -----	Annex Lakes pluton; Taku Cabin pluton	Granodiorite, granite; Tonallite	Early Tertiary
Central granitic	Turner Lake batholith (western subbelt) -----	Northern, central, and southern granodiorite units	Granodiorite, and granite	Tertiary (Eocene)
	(eastern subbelt) -----	Undivided granite unit	Granite	Tertiary (Eocene)
	Foliated stocks -----	Tease Lake stocks	Quartz monzodiorite, Quartz monzonite	Early Tertiary
	Wright Glacier stocks ---	Two plutons	Granite, granodiorite	Late(?) Tertiary

tonic-metamorphic complex (Brew and Ford, 1984a, b). Within the transect area the sill belt is represented by the Speel River, Taku Cabin, and Annex Lakes plutons (Drinkwater and others, 1989, 1990) and by the largely more deformed and older Mount Juneau, Carlson Creek, and Lemon Creek Glacier plutons (Drinkwater and others, 1990).

East of the great tonalite sill, granodiorites and granites of Tertiary age form most of the central granitic belt of the Coast plutonic-metamorphic complex (Brew and Ford, 1984a, b). In the transect area these granitoids are grouped as the Turner Lake batholith and other units (table 1). They intrude high-grade metamorphic rocks and migmatites of Late Cretaceous to early Tertiary metamorphic age (Brew and Ford, 1986). These metamorphic host rocks are considered by Berg and others (1978) and Monger and Berg (1987) as part of the Tracy Arm terrane, although the tectonic affinity of these metamorphic rocks is inconclusive because of possible links to the Stikine terrane and to the older Alexander terrane (Brew and Ford, 1983, 1984a), as well as to the Yukon crystalline terrane (Gehrels and others, 1990). Brew and

Ford (1984b), Gehrels and others (1984), and Brew and others (1989) provide additional information on the timing of regional deformation, metamorphism, and pluton emplacement.

Plutonic Rocks of Transect Area

As noted above, the plutonic rocks of the transect area belong to three belts; from west to east they are: (1) the Admiralty-Revillagigedo belt of Late Cretaceous age (Brew and Morrell, 1983), (2) the great tonalite sill belt of Late Cretaceous to Paleocene age (Brew, 1988), and (3) the central granitic belt of Eocene age. The three belts are divided into seven separate subbelts (table 1). All of the plutonic rocks are calc-alkaline and I-types (Brew and Ford, 1986; Brew, 1988), and they vary in modal composition from quartz diorite to tonalite and granodiorite to granite northeastward along the transect (fig. 2). The major belts are characterized by an increase in SiO₂ from west to east along the transect (fig. 3). Exceptions to this trend are the quartz monzodiorite bodies at Everett and

Arthur Peaks, which are silica-poor (<60 percent SiO₂), K-feldspar-rich rocks.

The Admiralty-Revillagigedo belt is divided into two subbelts (table 1). The Grand Island subbelt consists of the Grand Island, Irving Peak, and Butler Peak plutons and six stocks of biotite-hornblende quartz diorite and tonalite on the Glass Peninsula. The rocks are typically well foliated to gneissic, contain primary-appearing garnet and epidote, and have traces of ilmenite and sulfides but contain no appreciable magnetite. A few thin sections of the Grand Island pluton contain traces of magnetite. Mafic and hornfelsic inclusions are common, particularly near the margins of the plutons. The epidote is magmatic according to the criteria of Zen and Hammarstrom (1984) and is typical of the 95-Ma plutons described by Brew and others (1984, 1989) and of the "Taku terrane" plutons in the Ketchikan area described by Arth and others (1988). The Taku Harbor subbelt consists of two stocklike bodies of foliated, porphyritic hornblende quartz monzodiorite. The stocks contain abundant brown hornblende, much sphene and magnetite, traces of sulfide minerals, phenocrystic K-feldspar, and primary epidote, but they lack biotite.

The great tonalite sill belt is divided into two subbelts (table 1). The Speel River, Mount Juneau, Carlson Creek, and Lemon Creek Glacier plutons form the western subbelt, and the Taku Cabin and Annex

Lakes plutons compose the eastern subbelt. The Speel River and Taku Cabin plutons are typical granitoids of the great tonalite sill (Brew, 1988); they are foliated, homogeneous, medium- to coarse-grained tonalites that carry much magnetite. The Mount Juneau, Lemon Creek Glacier, and Carlson Creek plutons are much more deformed and metamorphosed, show more heterogeneous textures and compositions, and lack magnetite or opaque minerals other than sulfides (Drinkwater and others, 1990). The Mount Juneau pluton, like the Grand Island subbelt, contains primary epidote and garnet. The Annex Lakes pluton consists mostly of foliated and inequigranular to porphyritic granodiorite, quartz monzodiorite, and tonalite. The pluton is very heterogeneous in texture and lithology, and it may well be a composite body of two to four individual sills (Drinkwater and others, 1990). Magnetite is commonly seen in most thin sections of the Annex Lakes pluton.

The central granitic belt lies east of the great tonalite sill belt; it contains three major units, including the Turner Lake batholith, which has two subbelts. Mapping has yet to determine the exact number of plutons that occur in this part of the Coast plutonic-metamorphic complex, but three granodioritic units form a western subbelt, and undivided granite forms an eastern subbelt. These units are distinguished by field and petrographic features, and by MS values (discussed later).

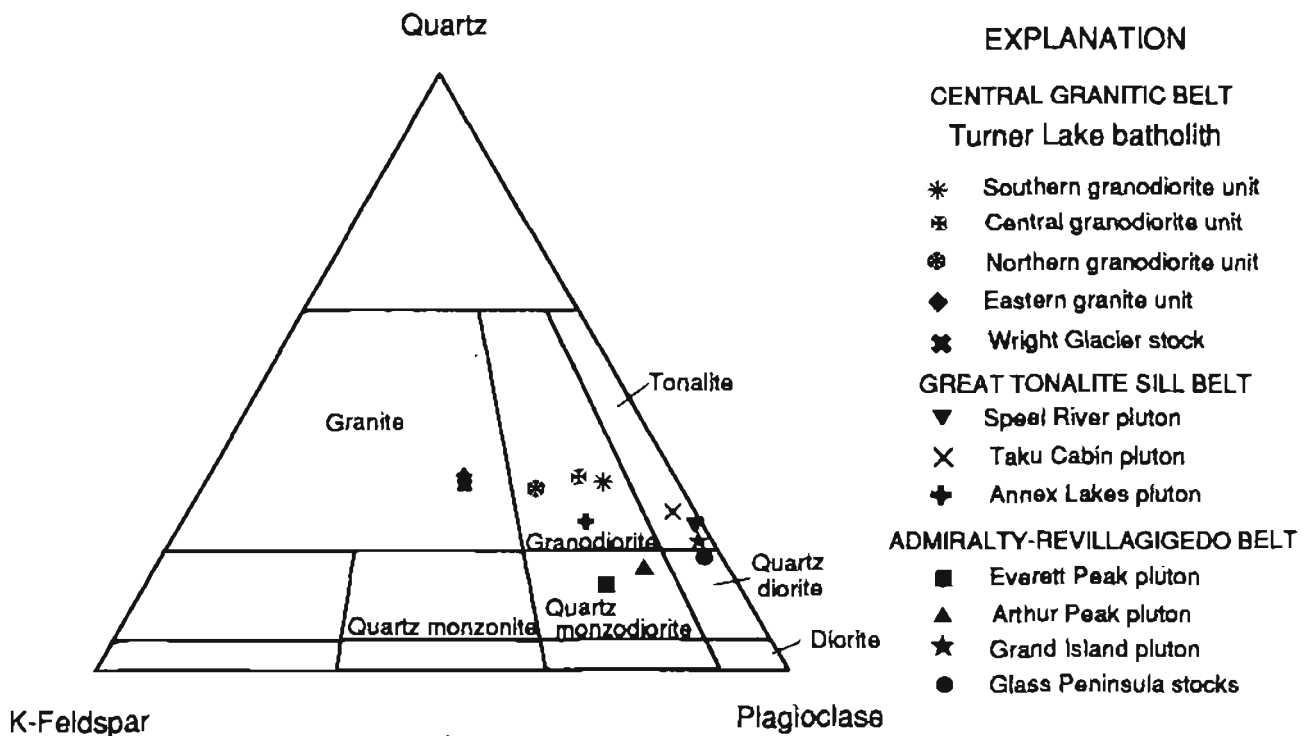


Figure 2. Quartz-potassium-feldspar-plagioclase diagram showing average modal composition of plutons or granitic units along Taku Inlet transect area, plotted on Streckeisen's (1973) plutonic rock classification diagram. Mount Juneau, Carlson Creek, and Lemon Creek Glacier plutons are tonalites according to average modal compositions from Drinkwater and others (1990). See table 1 for list of plutons and their belts.

The northern unit is intermediate in physical features and composition between the porphyritic biotite granite of the eastern subbelt and the typical massive equigranular biotite-hornblende granodiorite of the other two units of the western subbelt. K-feldspar occurs in different forms in the different subbelts and units. In the eastern subbelt, it is coarse granular to phenocrystic; in the central and southern units, it is intergranular and poikilitic; and in rocks of the northern unit, it occurs in all phases. In the western subbelt, granular clots of magnetite and apatite are typical of the central unit but are absent in the southern and northern units. Allanite is the most conspicuous accessory mineral of the eastern subbelt

granites, whereas sphene is more typical of the western subbelt granodiorites. Both allanite and sphene are common in the northern granodiorite unit. Several granitic stocks of late(?) Tertiary age occur within the Turner Lake batholith; they are typically massive, slightly porphyritic but otherwise fine- to medium-grained, magnetite-bearing hornblende-biotite granites. The two foliated stocks (Tease Lake stocks) are also considered part of the central granitic belt. Chemical and MS data are lacking on these foliated stocks, but generally they are heterogeneous in texture and range from granodiorite to monzodiorite in composition.

Ages

Granitoids of the Taku Inlet transect area are part of three major age groups that were emplaced between Late Cretaceous and Eocene time (Brew and Ford, 1986). The oldest group includes the plutons of the Grand Island and Taku Harbor subbelts, which belong to the Admiralty-Revillagigedo linear belt of 95-Ma dioritic and quartz dioritic plutons (Brew and Morrell, 1983; Brew and others, 1989) that extends most of the length of southeastern Alaska. The next oldest group includes the plutons of the great tonalite sill belt. The sill-belt plutons range in age from at least as old as 70 Ma to 55 Ma (Brew, 1988). Within the transect area, they are probably Paleocene in age based on a K-Ar hornblende age of 60.5 Ma from the Speel River pluton (recalculated age using newer standard constants; Drinkwater and others, 1989) and from U-Pb ages of 67.0 and 60.0 Ma (Gehrels and others, 1984) from the Carlson Creek and Annex Lakes plutons, respectively. Wood and others (1991) report a range of $^{40}\text{Ar}/^{39}\text{Ar}$ ages on biotite and hornblende of 63 to 53 Ma that systematically decrease from west to east across the Speel River pluton in the Holkham Bay area, which is located just south of the study area. A 66.5-Ma K-Ar hornblende age from the Mount Juneau pluton (Drinkwater and others, 1990) is considered a metamorphic age; although its emplacement age is unclear to us, we consider this body as the oldest pluton of the great tonalite sill group in this area. The youngest group consists of plutons of the Turner Lake batholith of the central granitic belt; they were emplaced from 54 to 49 Ma (K-Ar ages; Brew, 1988). A U-Pb zircon age of 50 Ma from granodiorite of the Turner Lake batholith near Taku Inlet was reported by Gehrels and others (1984). The westernmost of the Tease Lake stocks, which has an intrusive contact with the Speel River pluton, yielded a K-Ar hornblende age of 50.9 Ma (J.G. Smith and D.A. Brew, unpub. data); its field relationship to the Turner Lake batholith is uncertain because the Tease Lake stocks are mostly within metamorphic country rock.

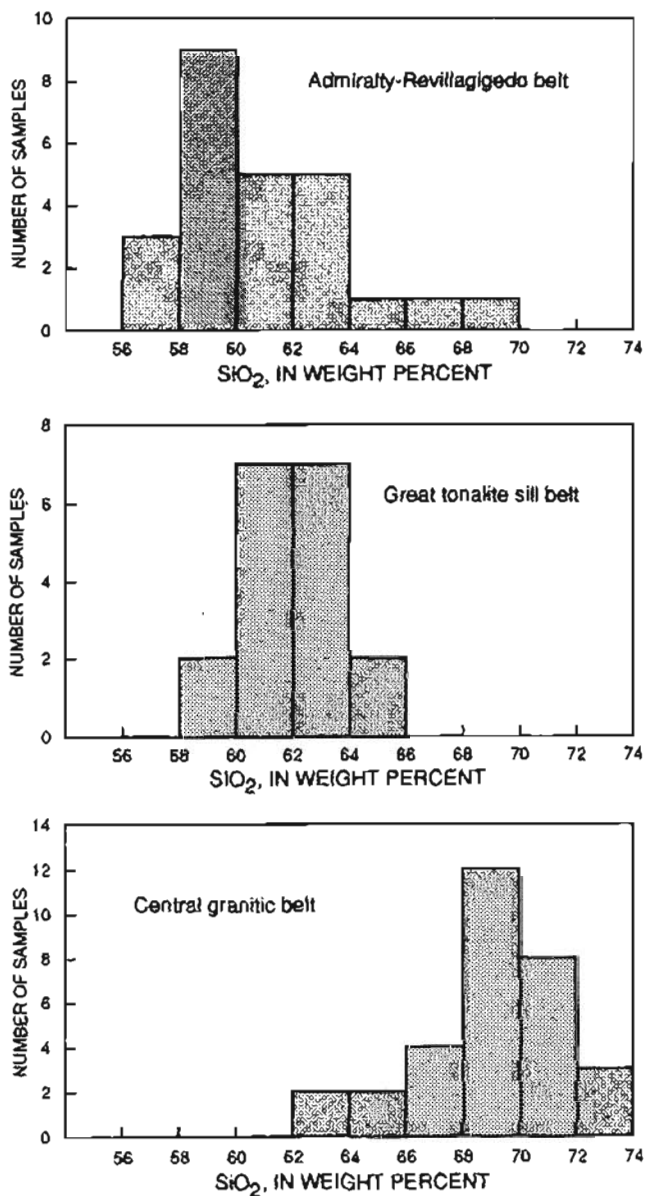


Figure 3. Frequency distribution of SiO₂ for major plutonic belts of Taku Inlet transect area.

MAGNETIC SUSCEPTIBILITIES

The results of 137 MS measurements (figs. 4, 5) define three different distribution patterns for rocks of the plutonic belts. The MS of the granitoids initially increases from southwest to northeast along the transect to the great tonalite sill belt, beyond which it decreases (with one exception) (fig. 5). The highest MS values of 2,500 to 5,000 $\times 10^{-5}$ SI units (hereafter abbreviated as 2,500–5,000) are found in rocks of the great tonalite sill belt (Speel River, Taku Cabin, and Annex Lakes plutons) and central granodiorite unit of the western subbelt of the Turner Lake batholith. The lowest MS values

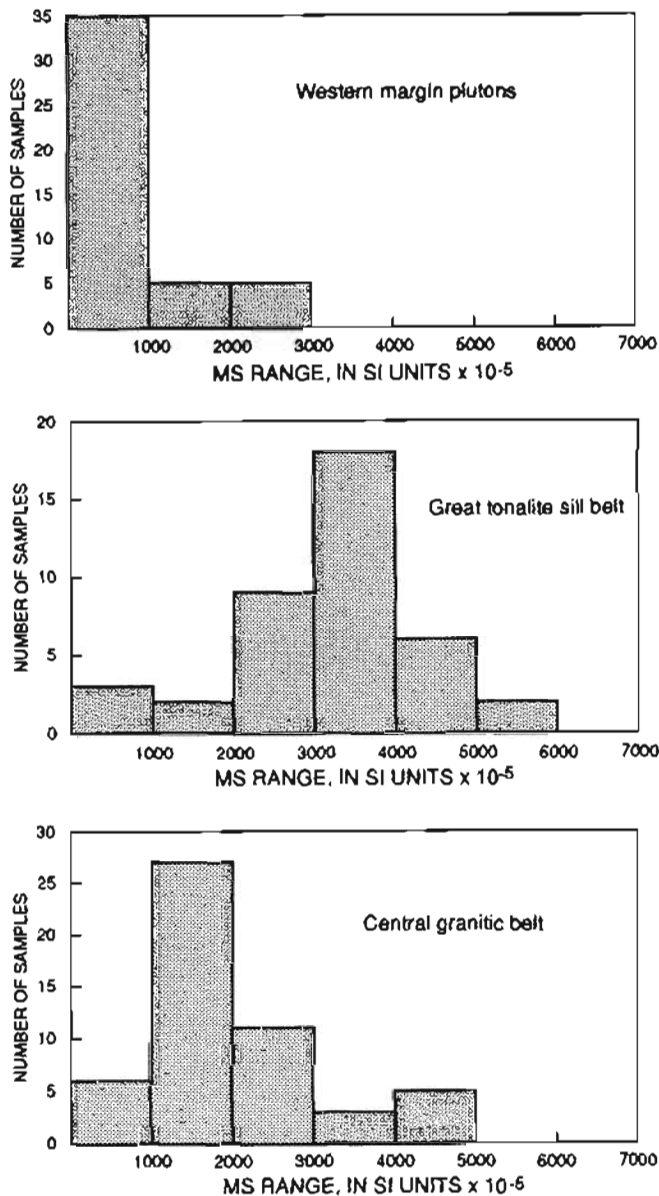


Figure 4. Frequency distribution of magnetic susceptibility for major belts of Taku Inlet transect area. Magnetic susceptibility measured in SI units, $\times 10^{-5}$.

(<250) are found in two groups of plutons that lie along the western edge of the complex, including the Grand Island pluton and Glass Peninsula stocks, and the Mount Juneau, Carlson Creek, and Lemon Creek Glacier plutons. Rocks from these plutons rarely show opaques in thin section; where present, they are generally sulfides or ilmenite, and more rarely magnetite. The small positive MS values of magnetite-free granitoids are attributed to biotite (Tulloch, 1989). These plutons with very low MS are similar to the ilmenite-series granitoids from the Japan area described by Ishihara (1977).

The MS range and average (fig. 5) are generally similar among the plutonic subbelts, but in many cases individual plutons or units have distinct MS signatures. The high MS values of the central granodiorite unit distinguish it from other units of the Turner Lake batholith. Granitic rocks of the eastern subbelt of the Turner Lake batholith generally show a relatively small range of low to intermediate MS values, but the two Wright Glacier stocks exhibit widely different MS values. The Speel River pluton has the widest range of MS values, but all main phases have values generally greater than 1,500. The highest average MS values are found in rocks of the Annex Lakes pluton and central granodiorite unit. Interestingly, three samples of border-zone rocks of the Speel River pluton have very low MS (<300) values similar to the ilmenite-bearing plutons. The Arthur Peak and Everett Peak plutons (Taku Harbor subbelt) show significant differences in their range and average MS values, with the Everett Peak body having the higher values.

CORRELATION WITH CHEMICAL PARAMETERS

The patterns of MS range values (fig. 5), surprisingly, show no systematic correlation with those of total iron (FeO^*) (fig. 6) or normative magnetite content (fig. 7). The MS of the ilmenite-bearing plutons of the western margin exhibit a positive correlation with FeO^* (fig. 8, lower band of points), and as a group, the plutons of the Turner Lake batholith also show a rough positive correlation between MS and FeO^* (fig. 8); however, no correlation is evident on figure 8 when all data points are considered. The granitoids with the highest FeO^* and normative magnetite values (Grand Island subbelt and Mount Juneau, Carlson Creek, and Lemon Creek Glacier plutons) actually contain no or only traces of magnetite. Conversely, the central granodiorite unit of the Turner Lake batholith, which contains abundant magnetite, has relatively low to moderate amounts of FeO^* and normative magnetite but yields very high MS values. This discrepancy is mostly explained by the iron oxidation state (OXS); here, OXS is calculated as the molecular ratio $\text{Fe}^{3+}/(\text{Fe}^{3+} + \text{Fe}^{2+})$ (fig. 9), which shows much better agreement with the MS trend (fig. 5) and

thus is a better indicator of magnetite content than normative magnetite. A general increase in MS with increase in OXS is indicated by figure 10 but with much scatter. Bateman and others (1991) also determined that the regional patterns and variations of magnetic susceptibility in the central Sierra Nevada batholith correlate with iron oxidation ratios but not with total iron content.

Most of the magnetite-bearing granitoids have oxidation-state values greater than 0.21, and most ilmenite-bearing (very low MS) granitoids have OXS values less than 0.23 (fig. 9); the overlap of OXS between these two pluton types is a small part of the total range of values and in part may be attributed to FeO analytical problems, as described by Jackson and others (1987). Average OXS values from figure 9 for ilmenite-bearing granitoids are 0.23 or less, and for most magnetite-bearing granitoids they are 0.23 or higher (fig. 9). Data from figure 10 (based on OXS vs MS) indicate a division at about 0.21 OXS between these two plutonic types of the

transect. MS values between 1,000 and 200 occur less frequently in these rocks, as evident from the gaps in data distribution in figures 5 and 10.

Admiralty-Revillagigedo Belt and Mount Juneau, Carlson Creek, and Lemon Creek Glacier Plutons

The granitoids along the western margin of the transect area include plutons of the Grand Island and Taku Harbor subbelts and the Mount Juneau, Carlson Creek, and Lemon Creek Glacier plutons. They are iron-rich rocks (> 4 percent FeO*) that have a range of very low to intermediate MS values. Although the Mount Juneau, Carlson Creek, and Lemon Creek Glacier plutons are spatially part of the great tonalite sill belt, their petrographic features (Drinkwater and others, 1990), high iron content, and very low MS values tie them (particularly the Mount Juneau pluton) to the

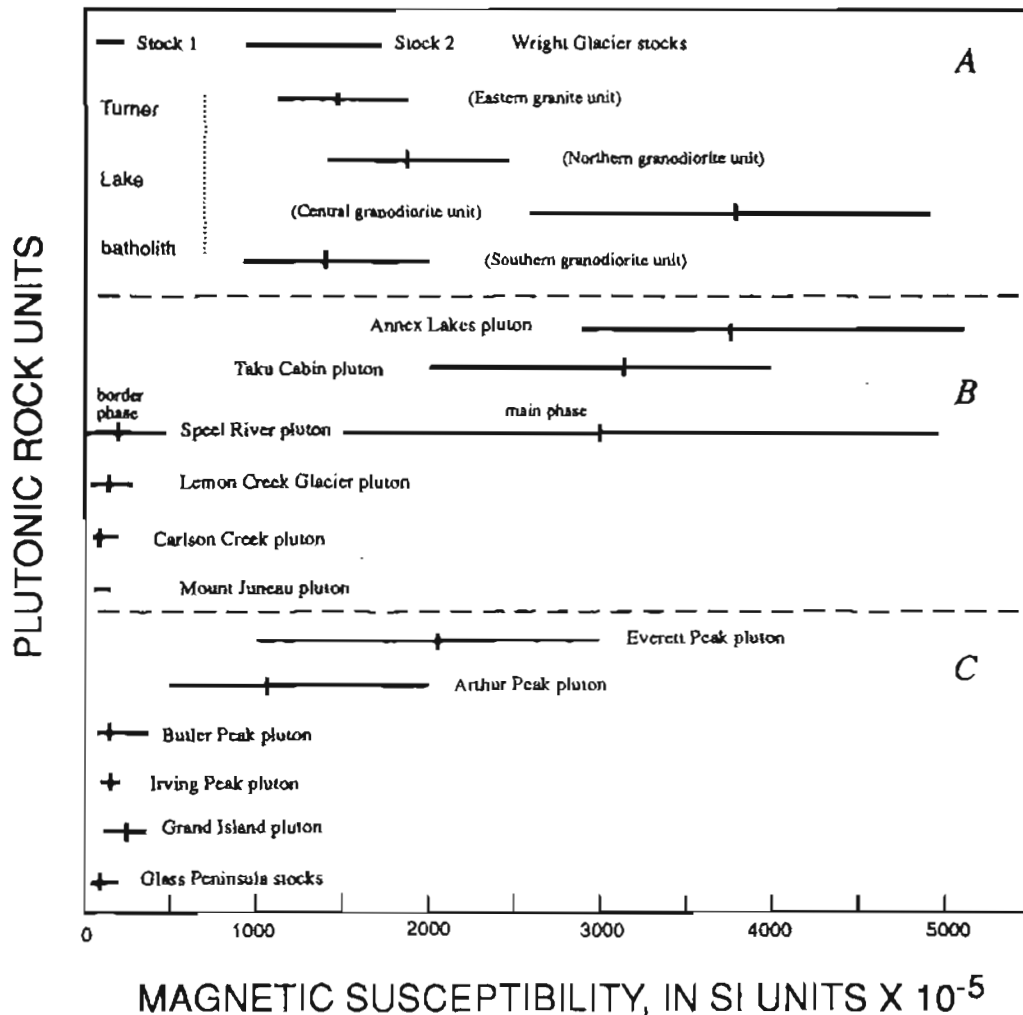


Figure 5. Ranges of magnetic susceptibility for plutons and granitic units of Taku Inlet transect area. Average magnetic susceptibility shown by vertical tick mark. See Appendix for individual sample data. A, Central granitic belt. B, Great tonalite sill belt. C, Admiralty-Revillagigedo belt.

Grand Island subbelt. More discriminating evidence, such as rare earth chemistry, isotopic attributes, and additional ages, is needed to fully compare these plutons. The Mount Juneau, Carlson Creek, and Lemon Creek Glacier plutons have the lowest OXS values, as is expected from ilmenite-series plutons (Takahashi and others, 1980). However, the ilmenite-bearing (very low MS) plutons of the Grand Island subbelt have a higher range of OXS (0.21–0.26) that is comparable to the range of OXS values of the Speel River, Taku Cabin, and Annex Lakes plutons, which have the most magnetite and the highest MS values. Evidently, other factors besides iron content and oxidation state can control the crystallization of Fe^{3+} -rich minerals (magnetite, biotite, epidote, and possibly garnet).

Granitoids of the Everett Peak and Arthur Peak plutons have the highest OXS values in the transect area as well as high total iron (4–6 percent), but they show only intermediate MS values. Much of the iron must have been incorporated into the epidote and hornblende that are common phases in these granitoids. Surprisingly, although the plutons are generally similar, the rocks of the Arthur Peak pluton have higher OXS values but generally lower MS values than rocks of the Everett Peak plu-

ton. The abundant K-feldspar and lack of biotite of these two plutons make them different from the typical 95-Ma dioritic plutons found in the western part of the Coast plutonic-metamorphic complex.

Great Tonalite Sill Belt (Speel River, Taku Cabin, and Annex Lakes Plutons)

The Speel River and Taku Cabin plutons are typical granitoids of the great tonalite sill belt; both show very similar MS ranges and averages as well as similar chemical, petrographic, and textural characteristics (Drinkwater and others, 1989, 1990). The iron data from the Taku Cabin pluton are within the narrow range of iron data shown for the Speel River pluton (figs. 6, 7). In contrast, the Mount Juneau, Carlson Creek, and Lemon Creek Glacier plutons differ by their much lower MS and OXS values but higher average FeO^* . In comparison, the Annex Lakes pluton has a large range of FeO^* with a lower average FeO^* value than the other great tonalite sill belt rocks but a higher average OXS value. Two samples from the Annex Lakes pluton not included in figures 4 and 5 because of their abundant

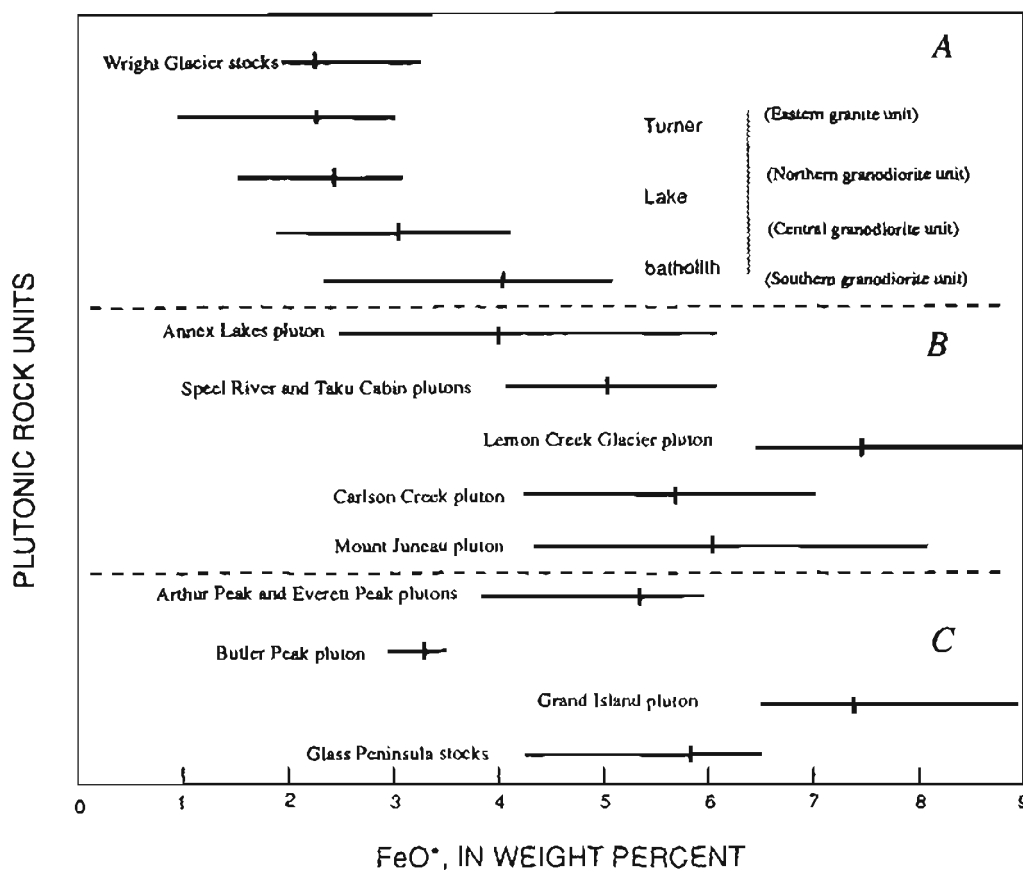


Figure 6. Ranges of FeO^* for plutons and granitic units of Taku Inlet transect. Averages shown by vertical tick marks. A, Central granitic belt. B, Great tonalite sill belt. C, Admiralty-Revillagigedo belt.

coarse-grained (>2 mm) magnetite yielded the highest MS values (8,000 and 7,000) of the complex.

Granitoids of the Central Granitic Belt

East of the great tonalite sill belt, the Coast plutonic-metamorphic complex is composed of magnetite-bearing calc-alkaline plutons of the Turner Lake batholith, late(?) Tertiary granitic stocks, and screens of metamorphic rock. Rocks of the Turner Lake batholith contain low FeO* (mostly <4 percent), but have relatively high OXS values and intermediate MS values. The much higher MS shown by rocks of the central granodiorite unit of the western subbelt reflects the abundant magnetite-apatite clots that are characteristic of this unit. Although the southern granodiorite unit has a higher average range of FeO* than other units of the Turner Lake batholith and similar OXS values as the central granodiorite unit, it contains less magnetite and lower MS values than the central granodiorite unit. The reason for this discrepancy is unknown but may be partially due to the more mafic-silicate-rich composition of

the southern unit. Tulloch (1989) argued that Fe³⁺ may be preferentially incorporated into biotite under certain conditions. The granite unit of the eastern subbelt contains only 1 to 3 percent FeO* but has a wide range of low to high OXS values and a relatively narrow and low range of MS values. The cause of this inconsistency is unclear but may be due in part to the abundant allanite in these rocks; allanite can accommodate varying amounts of trivalent iron (Deer and others, 1975). Analytical data are sufficient for consideration here of only one late(?) Tertiary granitic stock (southern Wright Glacier stock); these rocks have low to intermediate OXS and FeO* values and very low MS values. Whether this is typical of other late(?) Tertiary stocks in the region is unknown, but preliminary petrographic examination of available thin sections from these rocks reveal very few opaques such as magnetite.

DISCUSSION

The three major plutonic belts of the transect are characterized by plutons and plutonic units that are of

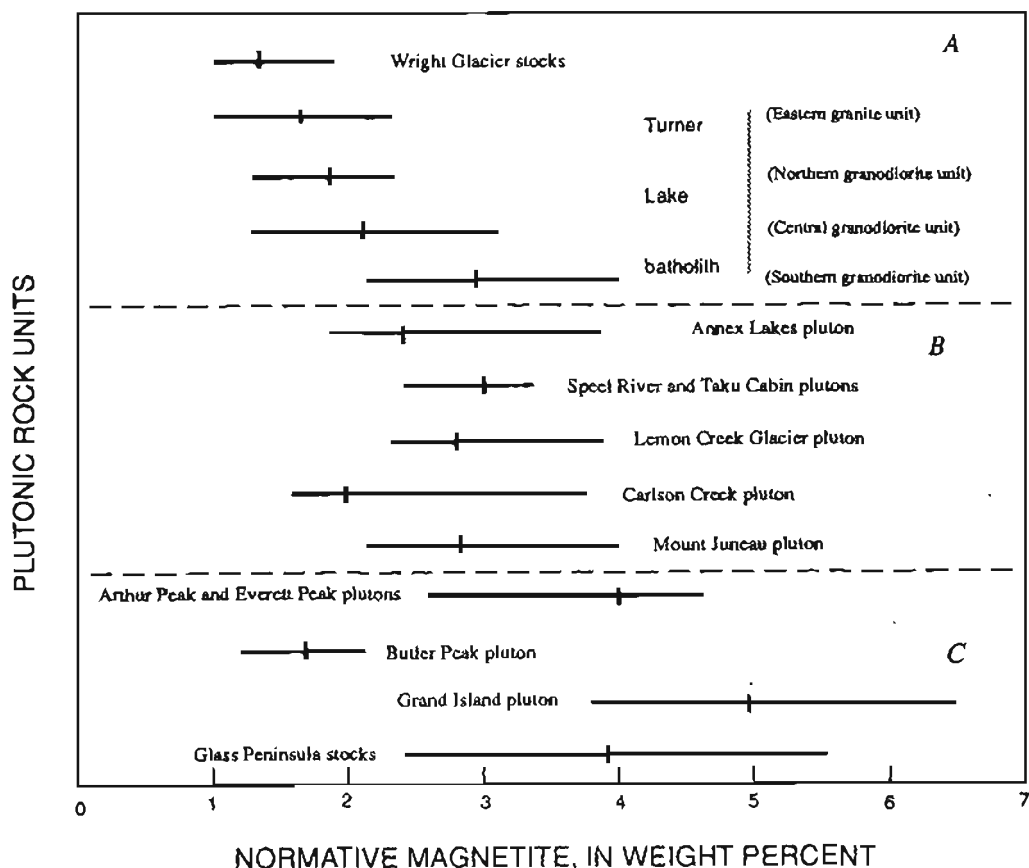


Figure 7. Ranges of normative magnetite for plutons and granitic units of Taku Inlet transect. Averages shown by vertical tick marks. A, Central granitic belt. B, Great tonalite sill belt. C, Admiralty-Revillagigedo belt.

similar age and have distinct MS values. The 95-Ma plutons in the western part of the transect are, in general, ilmenite-bearing types, and those of Tertiary age to the east are magnetite-bearing types. The larger plutons of the great tonalite sill belt, which separates the aforementioned western and eastern belts, are characterized by very high MS values and magnetite content and moderately high OXS values, whereas some (smaller ones) are more like the 95-Ma plutons. MS values, along the transect, correlate better with OXS values than with total FeO* or normative magnetite. An average OXS value of 0.23 roughly separates ilmenite-bearing plutons from magnetite-bearing plutons, but discrepancies in the MS-OXS correlation indicate that other factors may influence the crystallization of magnetite and Fe³⁺-rich silicate minerals. The Grand Island subbelt and Mount Juneau, Carlson Creek, and Lemon Creek Glacier plutons are not S-type granitoids according to the criteria of Chappell and White (1974), as would be expected for ilmenite-series rocks (Tulloch, 1989). They are instead SiO₂-poor (54–64 percent), Na₂O-rich (>3.2 percent) rocks with Al₂O₃/(Na₂O+CaO+K₂O) ratios <1. These are I-type granitoids that were generated either as reduced magmas or as oxidized magmas that became reduced during their magmatic history. The differences between the ilmenite- and magnetite-bearing type plu-

tons may bear on the nature of the bedrock terranes into which they were emplaced.

The ilmenite series of granitoids are believed to represent reduced magmas (Ishihara, 1977; Takahashi and others, 1980) and are generally associated with S-type granitoids (Chappell and White, 1974; Tulloch, 1989) or strongly contaminated reduced I-type granitoids (Ishihara and Sasaki, 1989). Magmas may be reduced at any stage—from site of generation, during ascent, or at shallow levels (Ishihara, 1977; Ishihara and Sasaki, 1989). At low oxygen fugacity, iron is not partitioned into Fe-Ti oxides but rather becomes incorporated into the ferromagnesian silicate phases (biotite, amphiboles, epidote, and garnet) and sometimes into iron sulfides (Puranen, 1989). Some workers (Ishihara, 1977; Ishihara and Sasaki, 1989) argue that the reduction of magma at the site of generation and during ascent is attributed to incorporation of carbon and sulfur by assimilation of carbonaceous and sulfur-rich sedimentary or metasedimentary rocks, resulting in lowered oxygen fugacity and reduction of iron. In their study of the central Sierra Nevada batholith, Bateman and others (1991) found no discernible relationship between free (noncarbonate) carbon and magnetic susceptibility and explained the regional variations in magnetic susceptibility and iron oxidation state as a function of the relative abundance of silicic crustal component in the magma. Local reduction of intrusive magma at margins of magnetite-bearing plutons can also occur by assimilation of pelitic wall rock (Ishihara and others, 1985). Magmas at shallower levels may be reduced by hydrothermal solutions. According to Ishihara (1977), Takahashi and others (1980), and Ishihara and Sasaki (1989), the ilmenite series of granitoids were generated at shallower levels than the magnetite series; the latter formed at deep levels in tensional tectonic settings where carbonaceous material is not stable, although Puranen (1989) argues that magnetite formation is possible at different depths, including shallow levels from reduced magmas.

The differences in MS signature between the ilmenite-bearing plutons of the Admiralty-Revillagigedo belt and the magnetite-bearing plutons of the central granitic belt may be largely explained by the differences in their ages and in the host terranes they intruded. Differences in source regime and emplacement history for the two plutonic groups could account for different oxidation histories. The rocks of the great tonalite sill belt were emplaced in a zone of compressional deformation represented by highly deformed, sheared, and moderately to highly metamorphosed rocks that form a boundary zone between two major composite terranes (Monger and others, 1982) considered by Rubin and others (1990) to be a former continental margin convergent zone. Brew and Ford (1983), in contrast, consider this zone essentially as a continent-continent collision zone. The

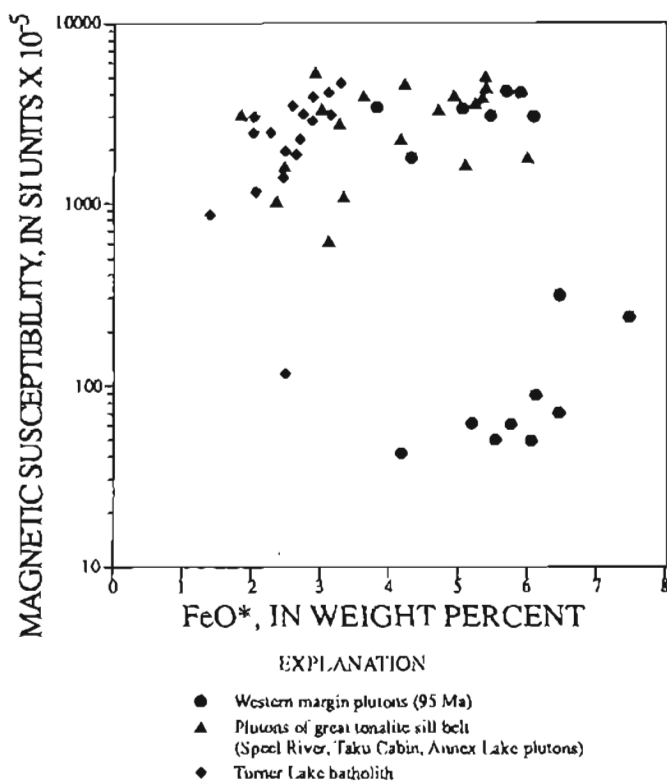


Figure 8. Magnetic susceptibility versus FeO* for granitic samples from major plutonic belts. Lower points from western margin plutons are samples of ilmenite-bearing plutons.

emplacement of rocks of the great tonalite sill belt occurred later and formed a suture between the two terranes; their age and MS signature are similar to those plutons of the central granitic belt. The MS variations in plutons of the central granitic belt follow more closely a pattern of decreasing MS with increasing differentiation (increasing SiO_2 and K_2O) that is probably related to extensional tectonics and the distance to the collision or convergent zone to the west. The Mount Juneau, Carlson Creek, and Lemon Creek Glacier plutons remain anomalous in being ilmenite-bearing plutons located east of the Coast Range megalineament. If these plutons represent an earlier phase of tonalitic sill plutonism and are unrelated to the 95-Ma Grand Island subbelt plutonism, then the relative spatial position of these two groups on opposite sides of the megalineament is coincidental.

Low MS values are reported for deformed granitoids in metamorphic terranes (for example, Ishihara, 1977; Tulloch, 1989). In Japan, low MS (ilmenite-type) foliated granitoids occur in high T/P grade zones of metamorphic belts (Ishihara, 1977). Tulloch (1989) describes mylonitic and cataclastically deformed plutonic rocks in New Zealand that have relatively high $\text{Fe}^{3+}/\text{Fe}^{2+}$ values but very low MS values. Gastil (1990), in his study of

the batholiths of southern California, also noted a correlation between grade of metamorphism of host rock and magnetic character of the intruded plutons, with non-magnetic plutons occurring in higher grade metamorphic rocks. The Mount Juneau, Carlson Creek, and Lemon Creek Glacier plutons, which are ilmenite bearing, occur with the highest grade metamorphic rocks in the transect (Brew and others, 1989). However, in the Taku Inlet transect, an increase in MS eastward from the Grand Island subbelt to the great tonalite sill belt (Speel River pluton) corresponds with northeast progressive metamorphic grade (Brew and others, 1989).

Contamination and tectonic stresses may have collectively influenced the production of the ilmenite-bearing plutons. The deep bedrock units beneath the moderately metamorphosed Gravina overlap assemblage, where the Grand Island subbelt is exposed, are uncertain but possibly include Alexander and Wrangellia terrane rocks that contain some graphite or other carbonaceous material (Brew and others, 1984; Brew and Ford, 1986; Brew and Karl, 1988). The plutons of the great tonalite sill belt were emplaced in higher grade metamorphic rocks, which we interpret to have been derived from the Alexander and Wrangellia terranes and Gravina overlap

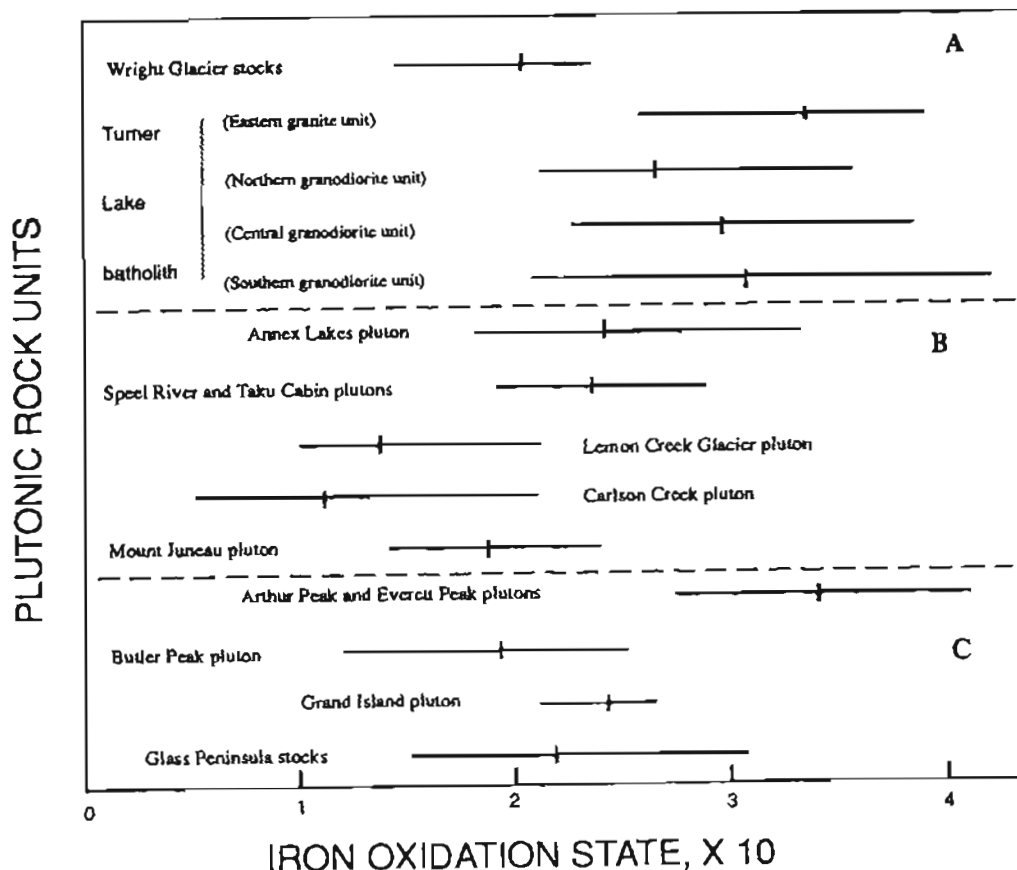


Figure 9. Ranges in oxidation state [molecular ratio of $\text{Fe}^3/(\text{Fe}^3 + \text{Fe}^2) \times 10$] for plutons and granitic units of Taku Inlet transect. Average shown by vertical tick marks. A, Central granitic belt. B, Great tonalite sill belt. C, Admiralty-Revillagigedo belt.

assemblage. The common occurrence of hornfelsed sedimentary and volcanic rock inclusions, and of sulfide minerals, which according to Ishihara and others (1985) are common in contaminated reduced magma types, implies that contamination was a factor in the formation of the ilmenite-bearing type plutons of the western margin. Because the ilmenite-bearing Mount Juneau, Carlson Creek, and Lemon Creek Glacier plutons in the belt are the most deformed and metamorphosed, we conclude that high compressional stresses may have also contributed to the development of reduced magmas and ilmenite-bearing plutons in the western part of the Juneau transect. An alternate explanation is that the Mount Juneau, Carlson Creek, and Lemon Creek Glacier plutons are analogous to the deformed and metamorphosed (and very low MS) border-phase rocks of the Speel River pluton, as defined by Drinkwater and others (1989). This suggests that the chemical and physical features of these plutons are a function of size more than age. The smaller size of the Mount Juneau, Carlson Creek, and Lemon Creek Glacier plutons may have allowed for more complete contamination.

Many of the ilmenite-bearing granitoids of the transect contain primary (magmatic) epidote, which according to the criteria of Zen and Hammarstrom (1984) indicates formation under oxidizing conditions at pressures greater than 8 kbars or at depths greater than 25 km. This conclusion conflicts with the contention of Takahashi and others (1980) and Ishihara and Sasaki (1989) that ilmenite-series granitoids, if formed at sites of magma generation, form at shallower depths and pressures under reducing conditions. If these particular

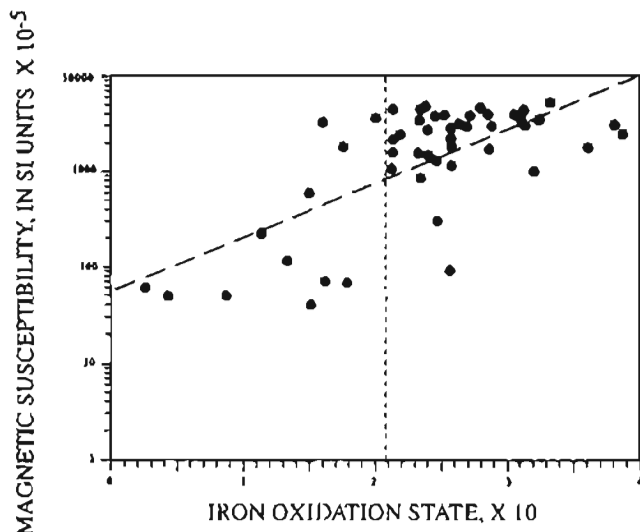


Figure 10. Magnetic susceptibility versus oxidation state values ($\times 10$) for granitic samples from Taku Inlet transect. Long dashed line is best-fit line based on simple exponential regression equation. Short dashed line shows arbitrary division between magnetite- and ilmenite-bearing granitic samples according to oxidation state.

granitoids indeed formed at great depths, then they must have been reduced during their ascent to upper crustal levels. The occurrence of magmatic epidote in the Mount Juneau pluton but not in the other two similar ilmenite-bearing sills (Lemon Creek Glacier and Carlson Creek plutons) is perplexing. All three sills consist of iron-rich granitoids, but the OXS of the Mount Juneau pluton is slightly higher, overlapping the OXS of the Grand Island subbelt plutons; this suggests a possible genetic link between the Mount Juneau pluton and plutons of the Grand Island subbelt.

As far as we know, epidote-bearing ilmenite-type plutons are unique and are seldom described in the published literature; it is not known whether other 95-Ma epidote-bearing plutons of this belt are ilmenite- or magnetite-bearing types, but petrographic descriptions from Burrell (1984) and Douglass and others (1989) reveal a conspicuous absence of magnetite and opaques from most rocks of the 95-Ma plutons in the Petersburg region (Brew and others, 1984). We examined many of the opaque-bearing sections from this group and observed that the opaques are chiefly sulfides or secondary magnetite. Zen and Hammarstrom (1984) report that the Ecstall and Moth Bay plutons farther away at the very southern end of this belt contain magnetite and primary epidote. This observation suggests that a large part of the 95-Ma plutonic belt in central and northern southeastern Alaska may be ilmenite-bearing type granitoids.

The Everett Peak pluton is unusual in that it contains both magnetite and epidote and no primary biotite. The crystallization history of this pluton is apparently different from that of the magnetite-absent/poor, biotite-rich, epidote-bearing Mount Juneau and Grand Island subbelt plutons. The fact that well-developed (primary) epidote and sulfides do not occur together in the same thin section may bear on the origin of this pluton. The lack of a hydrous silicate phase (biotite) in this pluton implies that its magma crystallized under either low water pressure or high load pressure, with the second possibility being compatible with the presence of primary epidote.

The magnetite-bearing granitoids of the Coast plutonic-metamorphic complex were emplaced in a terrane of high-grade metamorphic rocks and are interpreted to have formed under conditions of higher oxidation state than the plutons along the western margin. The decrease in MS east of the great tonalite sill belt correlates with an increase in K-feldspar and SiO_2 content across the complex. Oxidation-state values remain relatively high, but total iron is rapidly depleted eastward, resulting in lower MS values. These trends may reflect variations in the depth of magma generation and thus the distance from the subduction or collision zone to the west.

In conclusion, we believe that the magnetic susceptibility data demonstrate significant differences between

the granitoids in the three major plutonic belts of the Taku Inlet transect area. Differences in total iron content may explain variations in MS within subbelts or larger suites, but they do not explain the differences in MS on a larger regional scale; rather, the presence and amount of magnetite in these rocks depend largely on the degrees of oxidation and magmatic differentiation, grade of metamorphism, and amount of deformation during synkinematic emplacement. These factors are also affected by many variables, including the depth of magma generation, composition of the host country rock, amount of crustal assimilation, and hydrothermal alteration. We are uncertain if the reduced oxidation state of the magmas that formed the ilmenite-bearing plutons is a primary magmatic feature or if it is related to synkinematic emplacement under conditions of strong tectonic stress. This question may be resolved when more physical and chemical data become available for these plutons from the entire Admiralty-Revillagigedo belt.

REFERENCES CITED

- Arb, J.G., Barker, F., and Stern, T.W., 1988, Coast batholith and Taku plutons near Ketchikan, Alaska: Petrography, geochronology, geochemistry, and isotopic character: *American Journal of Science*, v. 288-A, p. 461-489.
- Bateman, P.C., Dodge, F.C., and Kistler, R.W., 1991, Magnetic susceptibility and relation to initial $87\text{Sr}/86\text{Sr}$ for granitoids of the central Sierra Nevada, California: *Journal of Geophysical Research*, v. 96, no. B12, p. 19,555-19,568.
- Berg, H.C., Jones, D.L., and Coney, P.J., 1978, Map showing pre-Cenozoic tectonostratigraphic terranes of southeastern Alaska and adjacent areas: U.S. Geological Survey Open-File Report 78-105, scale 1:1,000,000.
- Brew, D.A., 1988, Latest Mesozoic and Cenozoic magmatism in southeastern Alaska—A synopsis: U.S. Geological Survey Open-File Report 88-405, 41 p.
- Brew, D.A., and Ford, A.B., 1978, Megalineament in southeastern Alaska marks southwest edge of Coast Range batholithic complex: *Canadian Journal of Earth Science*, v. 15, no. 11, p. 1763-1772.
- 1983, Comment on "Monger, J.W.H., Price, R.A., and Tempelman-Kluit, D.J., 1982, Tectonic accretion and the origin of two major metamorphic and plutonic belts in the Canadian Cordillera": *Geology*, v. 11, p. 427-429.
- 1984a, Tectonostratigraphic terranes in the Coast plutonic-metamorphic complex, southeastern Alaska, in Reed, K.M., and Bartsch-Winkler, S., eds., *The United States Geological Survey in Alaska: Accomplishments during 1982*: U.S. Geological Survey Circular 939, p. 90-93.
- 1984b, The northern Coast plutonic complex, southeastern Alaska and northwestern British Columbia, in Coonrad, W.L., and Elliott, R.L., eds., *The United States Geological Survey in Alaska: Accomplishments during 1981*: U.S. Geological Survey Circular 868, p. 120-124.
- 1986, Preliminary reconnaissance geologic map of the Juneau, Taku River, Atlin and parts of the Skagway 1:250,000 quadrangles, southeastern Alaska: U.S. Geological Survey Open-File Report 85-395, 23 p., 2 sheets.
- Brew, D.A., Ford, A.B., and Himmelberg, G.R., 1989, Evolution of the western part of the Coast plutonic-metamorphic complex, southeastern Alaska, USA—A summary, in Daly, J.S., and others, eds., *Evolution of metamorphic belts*: Geological Society of America Special Publication 42, p. 447-452.
- Brew, D.A., and Grybeck, D., 1984, Geology of the Tracy Arm-Fords Terror Wilderness study area and vicinity, in U.S. Geological Survey and U.S. Bureau of Mines, *Mineral resources of the Tracy Arm-Fords Terror Wilderness Study Area and vicinity, Alaska*: U.S. Geological Survey Bulletin 1525, p. 19-52.
- Brew, D.A., and Karl, S.M., 1988, A reexamination of the contacts and other features of the Gravina belt, southeastern Alaska, in Galloway, J.P., and Hamilton, T.D., eds., *Geologic studies in Alaska by the U.S. Geological Survey during 1987*: U.S. Geological Survey Circular 1016, p. 143-146.
- Brew, D.A., and Morrell, R.P., 1983, Intrusive rocks and plutonic belts of southeastern Alaska, U.S.A., in Roddick, J.A., ed., *Circum-Pacific plutonic terranes*: Geological Society of America Memoir 159, p. 171-193.
- Brew, D.A., Ovenshine, A.T., Karl, S.M., and Hunt, S.J., 1984, Preliminary reconnaissance geologic map of the Petersburg and parts of the Port Alexander and Sumdum 1:250,000 quadrangles, southeastern Alaska: U.S. Geological Survey Open-File Report 84-405, 43 p., 2 pls.
- Burrell, P.D., 1984, Late Cretaceous plutonic rocks, Petersburg quadrangle, southeast Alaska, in Reed, K.M., and Bartsch-Winkler, S., eds., *The United States Geological Survey in Alaska: Accomplishments during 1982*: U.S. Geological Survey Circular 939, p. 93-96.
- Chappell, B.W., and White, A.J.R., 1974, Two contrasting granite types: *Pacific Geology*, v. 8, p. 173-174.
- Criss, R.E., and Champion, D.E., 1984, Magnetic properties of granitic rocks from the southern half of the Idaho batholith: Influences of hydrothermal alteration and implications of aeromagnetic interpretation: *Journal of Geophysical Research*, v. 89, no. B8, p. 7061-7076.
- Deer, W.A., Howie, R.A., and Zussman, J., 1975, *An Introduction to the rock-forming minerals*: London, Longman, 528 p.
- Douglass, S.L., Webster, J.H., Burrell, P.D., Lanphere, M.I., and Brew, D.A., 1989, Major-element chemistry, radiometric ages, and locations of samples from the Petersburg and parts of the Port Alexander and Sumdum quadrangles, southeastern Alaska: U.S. Geological Survey Open-File Report 89-527, 66 p.
- Drinkwater, J.L., Brew, D.A., and Ford, D.A., 1989, Petrographic and chemical description of the variably deformed Speel River pluton, south of Juneau, southeastern Alaska, in Dover, J.H., and Galloway, J.P., eds., *Geological studies in Alaska by the U.S. Geological Survey, 1988*: U.S. Geological Survey Bulletin 1903, p. 104-112.
- 1990, Petrographic and chemical data for the large Mesozoic and Cenozoic plutonic sills east of Juneau,

- southeastern Alaska: U.S. Geological Survey Bulletin 1918, 47 p.
- Gastil, G., 1990, The boundary between the magnetite-series and ilmenite-series granitic rocks in Peninsular California: University Museum, University of Tokyo, Nature and Culture, no. 2., p. 91-99.
- Gehrels, G.E., Brew, D.A., and Saleeby, J.B., 1984, Progress report on U-Pb (zircon) geochronologic studies in the Coast plutonic-metamorphic complex east of Juneau, southeastern Alaska, in Reed, K.M., and Bartsch-Winkler, S., eds., The United States Geological Survey in Alaska: Accomplishments during 1982: U.S. Geological Survey Circular 939, p. 100-102.
- Gehrels, G.E., McClelland, W.C., Samson, S.D., Patchett, P.J., and Jackson, J.L., 1990, Ancient continental margin assemblage in the northern Coast Mountains, southeast Alaska and northwest Canada: *Geology*, v. 18, no. 3, p. 208-211.
- Hooper, R.J., Brew, D.A., Himmelberg, G.R., Stowell, H.H., Bauer, R.L., and Ford, A.B., 1990, The nature and significance of post-thermal-peak shear zones west of the great tonalite sill near Juneau, southeastern Alaska, in Dover, J.H., and Galloway, J.P., eds., *Geologic studies in Alaska by the U.S. Geological Survey, 1989*: U.S. Geological Survey Bulletin 1946, p. 88-94.
- Ishihara, S., 1977, The magnetite-series and Ilmenite-series granitic rocks: *Mining Geology*, v. 27, p. 293-305.
- Ishihara, S., Matsuhisa, Y., Sasaki, A., and Terashima, S., 1985, Wall rock assimilation by magnetite-series granitoid at the Miyako pluton, Kitakami, northeastern Japan: *Journal of the Geological Society of Japan*, v. 91, no. 10, p. 679-690.
- Ishihara, S., and Sasaki, A., 1989, Sulfur isotopic ratios of the magnetite-series and ilmenite-series granitoids of the Sierra Nevada batholith—A reconnaissance study: *Geology*, v. 17, p. 788-791.
- Jackson, L.L., Brown, F.W., and Neil, S.T., 1987, Major and minor elements requiring individual determination, classical whole rock analysis, and rapid rock analysis, in Baedeker, P.A., ed., *Methods for geochemical analysis*: U.S. Geological Survey Bulletin 1770, p. G1-G23.
- Monger, J.W.H., and Berg, H.C., 1987, Lithotectonic terrane map of western Canada and southeastern Alaska: U.S. Geological Survey Miscellaneous Field Studies Map MF-1874B, scale 1:2,500,000.
- Monger, J.W.H., Price, R.A., and Tempelman-Kluit, D.J., 1982, Tectonic accretion and the origin of two major metamorphic and plutonic belts in the Canadian Cordillera: *Geology*, v. 10, p. 70-75.
- Piccoli, P.M., and Hyndman, D.W., 1985, Magnetite/ilmenite boundary in the western Atlanta lobe of the Idaho batholith: *Northwest Geology*, v. 14, p. 1-5.
- Puranen, Risto, 1989, Susceptibilities, iron and magnetite content of Precambrian rocks in Finland: Geological Survey of Finland, Report of Investigations no. 90, 45 p.
- Ross, D.C., 1989, Magnetic susceptibilities of modally analyzed granitic rocks from the southern Sierra Nevada, California: U.S. Geological Survey Open-File Report 89-204, 53 p.
- Rubin, C.M., Saleeby, J.B., Cowan, D.S., Brandon, M.T., and McGroder, M.F., 1990, Regionally extensive mid-Cretaceous west-vergent thrust system in the northwestern Cordillera: Implications for continent-margin tectonism: *Geology*, v. 18, p. 276-280.
- Stowell, H.H., and Hooper, R.J., 1990, Structural development of the western metamorphic belt adjacent to the Coast plutonic complex, southeastern Alaska: Evidence from Holkham Bay: *Tectonics*, v. 9, p. 391-407.
- Strecheisen, A.L., 1973, Plutonic rocks—classification and nomenclature recommended by the I.U.G.S. subcommission on the systematics of igneous rocks: *Geotimes*, v. 18, no. 10, p. 26-30.
- Takahashi, M., Aramaki, S., and Ishihara, S., 1980, Magnetite-series/ilmenite series vs. I-type/S-type granitoids: *Mining Geology*, Special Issue no. 8, p. 13-28.
- Tulloch, A.J., 1989, Magnetic susceptibilities of Westland-Nelson plutonic rocks: Discrimination of Paleozoic and Mesozoic granitoid suites: *New Zealand Journal of Geology and Geophysics*, v. 32, p. 197-203.
- Wood, D.J., Stowell, H.H., Onstott, T.C., and Hollister, 1991, $^{40}\text{Ar}/^{39}\text{Ar}$ constraints on the emplacement, uplift and cooling of the Coast plutonic complex sill, Southeastern Alaska: *Geological Society of America Bulletin*, v. 103, p. 849-860.
- Zen, E-an, and Hammarstrom, J.M., 1984, Magmatic epidote and its petrologic significance: *Geology*, v. 12, p. 515-518.

Reviewers: James G. Moore and Robert C. Jachens

High-Pressure Amphibolite-Facies Metamorphism and Deformation Within the Yukon-Tanana and Taylor Mountain Terranes, Eastern Alaska

By Cynthia Dusel-Bacon and Vicki L. Hansen

Abstract

Ductilely deformed amphibolite-facies tectonites comprise two adjacent terranes in the eastern part of the Yukon-Tanana upland in eastern Alaska. These terranes differ in protoliths, structural level, and cooling ages. A structurally complex zone of ductilely deformed, gently north-dipping tectonites separates the two terranes. The northern, structurally higher Taylor Mountain terrane includes garnet amphibolite, biotite±hornblende gneiss, marble, quartzite, metachert, pelitic schist, and crosscutting granitoids of intermediate composition (including the Taylor Mountain batholith). Lithologic associations and isotopic data from the granitoids suggest an oceanic or marginal basin origin for the Taylor Mountain terrane. $^{40}\text{Ar}/^{39}\text{Ar}$ metamorphic cooling ages from the Taylor Mountain terrane are latest Triassic to earliest Middle Jurassic. The southern, structurally lower Lake George subterrane of the Yukon-Tanana terrane is made up of quartz-biotite schist and gneiss, augen gneiss, pelitic schist, garnet amphibolite, and quartzite; we interpret it to comprise a continental margin and granitoid belt built on North American crust. Metamorphic cooling ages from the Lake George subterrane are almost entirely Early Cretaceous.

Geothermobarometric analysis of garnet rims and adjacent phases in garnet amphibolite and pelitic schist from the Taylor Mountain terrane and Lake George subterrane yields the following results: Taylor Mountain terrane: 7 to 12.5 kbar at 560°C to 685°C within a northern structural zone in which displacement is consistently top-to-the-northeast, and 6 to 7 kbar at 560°C to 605°C within a southern structural zone in which lineations and shear-sense directions are more variable; Lake George subterrane: 8.2 to 12.5 kbar at 625°C to 750°C. Preservation of growth zoning in garnet and the absence of partial melting in both terranes suggest metamorphic temperatures did not exceed 600°C to 650°C. Tectonites of the Lake George subterrane record dominantly top-to-the-northwest displacement in the northern part of the study area and top-to-the-southeast displacement within the southern part of the area. Where the two shear-sense directions occur together, top-to-the-northwest displacement preceded top-to-the-southeast displacement and was more penetrative.

We interpret the pressure, temperature, kinematic, and age data to indicate that metamorphism of the Taylor Mountain terrane and Lake George subterrane took place during different phases of a latest Paleozoic through early Mesozoic shortening episode, resulting from closure of an ocean basin now represented by klippen of the Seventymile-Slide Mountain terrane. High-pressure metamorphism of the Taylor Mountain terrane took place within a southwest-dipping (present-day coordinates) subduction system. High-pressure metamorphism of the Lake George subterrane occurred during continentward overthrusting of the Taylor Mountain and Seventymile-Slide Mountain terranes and imbrication of the continental margin in Jurassic time. The difference in metamorphic cooling ages between the Taylor Mountain terrane and adjacent parts of the Lake George subterrane is best explained by Early Cretaceous unroofing of the Lake George subterrane caused by crustal extension, recorded in its younger top-to-the-southeast fabric. Extension was probably related to the development of a northeast-dipping (present-day coordinates) subduction system outboard of the continental margin.

Although our geothermobarometric and kinematic data are from the eastern Yukon-Tanana upland, several lines of evidence suggest that Early to Middle Jurassic obduction of the outboard Seventymile-Slide Mountain and Taylor Mountain terranes onto the lower-plate Lake George subterrane was also a major tectonic and metamorphic event in the western Yukon-Tanana upland.

INTRODUCTION

The Yukon-Tanana terrane has commonly been defined as the broad elongate band of heterogeneous metamorphic and igneous rocks that lies between the right-lateral Tintina and Denali faults in east-central Alaska and Yukon Territory (Jones and others, 1987; Monger and Berg, 1987). Numerous workers have recognized the composite nature of this complex and extensive terrane and have proposed various subdivisions of it (Churkin and others, 1982; Aleinikoff and others, 1987;

Wheeler and McFeely, 1987; Wheeler and others, 1988; Hansen and others, 1991). The origin and history of the composite Yukon-Tanana terrane are clouded not only by its heterogeneity, structural complexity, poor exposure, and paucity of fossil-age control, but also because it occupies a suspect position in the northern Cordillera, being fault bounded along most of its length and lying between autochthonous or slightly displaced North America to the northeast and the innermost far-travelled terranes to the southwest (fig. 1). A flap of the terrane has been offset by approximately 450 km of dextral offset along the Tintina fault and lies northeast of the Tintina fault (Roddick, 1967; Tempelman-Kluit, 1979).

Recent detailed kinematic, metamorphic, and isotopic studies in the Teslin suture zone of southern Yukon (fig. 1) and kinematic and isotopic studies in eastern Alaska (Hansen, 1990; Hansen and others, 1991) have resulted in a subdivision of the Yukon-Tanana terrane into two separate structural levels, with differing cooling histories, that originated on opposite sides of an ancient ocean basin, the Anvil Ocean of Tempelman-Kluit (1979). The Teslin suture zone forms the fundamental boundary between the parautochthonous rocks to the east and allochthonous terranes to the west; it is marked by elongate, northwest-trending belts of the Teslin-Taylor Mountain and Nisutlin terranes (fig. 1). Deformational fabrics of the Teslin-Taylor Mountain and Nisutlin terranes are steeply dipping within the Teslin suture zone, whereas elsewhere in Yukon and east-central Alaska, the metamorphic fabrics and terrane boundaries are generally gently dipping. The interpretation of structural levels presented in this paper follows that presented by Hansen and her coworkers; however, rather than considering the upper structural levels as subdivisions of the Yukon-Tanana terrane, we have retained the Yukon-Tanana terrane name only for the structurally lower packages (subterrane) and consider the upper-level packages as terranes in their own right (fig. 2).

Although metamorphic rocks compose the major part of the formerly, broadly defined Yukon-Tanana terrane, and although knowledge of the conditions and tectonic setting of metamorphism is crucial to unraveling the tectonic evolution of this terrane, few geothermobarometric studies have been conducted on these rocks in Alaska. Geothermobarometry of lower-level rocks in the western part of the Yukon-Tanana terrane in Alaska has indicated medium-pressure (~5 kbar) metamorphism in two areas (Keskinen, 1989; Sisson and others, 1990). In southern Yukon, medium- to high-pressure (5–17 kbar) metamorphism is recorded in structurally higher rocks (correlative with the Taylor Mountain terrane), and high-pressure (7–13 kbar) metamorphism is recorded in structurally lower rocks (correlative with the Lake George subterrane) (Hansen, 1992b). In this paper, we present the preliminary results

of our combined geothermobarometric and kinematic study of tectonites of the structurally higher Taylor Mountain terrane and the structurally lower Lake George subterrane of the Yukon-Tanana terrane (subterrane terminology proposed in Nokleberg and others, 1989). Our primary focus is on the pressure and temperature (P - T) estimates from garnet amphibolite and pelitic schist, but the kinematic and cooling histories of these rocks also are briefly outlined because these histories are critical to our metamorphic and tectonic interpretation of the quantitative P - T calculations. We also speculate about the importance and applicability of the protracted late Paleozoic to early Mesozoic contractional episode and the Early Cretaceous extensional episode we recognize in eastern Alaska to the geologic evolution of the western part of the Yukon-Tanana upland.

Age designations used in this report are based on the Decade of North American Geology geologic time scale (Palmer, 1983).

GEOLOGIC FRAMEWORK

The Yukon-Tanana upland, a physiographic province of moderately dissected hills and mountains bounded by the Tintina fault on the north and the Tanana River on the south, is composed primarily of greenschist- and amphibolite-facies rocks of Paleozoic and probable Proterozoic protolith age that are intruded by postkinematic granitoids of latest Triassic to Early Jurassic, mid-Cretaceous, and early Tertiary age (Foster and others, 1987). The general geology of the major part of the Yukon-Tanana upland in Alaska is shown in figure 2, which elucidates the relationships that we discuss in this paper. Mylonitic and blastomylonitic textures are common in most metamorphic rocks, and many medium-grade rocks are sufficiently foliated and lineated to be classified as L-S tectonites (Turner and Weiss, 1963). Many metamorphic-unit boundaries, as defined on a metamorphic facies map of the region (Dusel-Bacon and others, in press), also are terrane or subterrane boundaries marked by low-angle faults. Metamorphic grade changes abruptly across many of the faults, indicating that major metamorphism predated final emplacement of the fault-bounded units (Foster and others, 1987; Dusel-Bacon and others, in press).

Structurally higher terranes all yield pre-Cretaceous metamorphic cooling ages both in Alaska and in presumably equivalent rocks in Yukon Territory (Hansen and others, 1991). The highest structural level, shown in figure 2, comprises a dismembered ophiolite composed of fault-bounded slices of serpentinized peridotite and weakly metamorphosed mafic volcanic and sedimentary rocks (Keith and others, 1981); sedimentary rocks are Mississippian to Late Triassic in age (Foster and others,

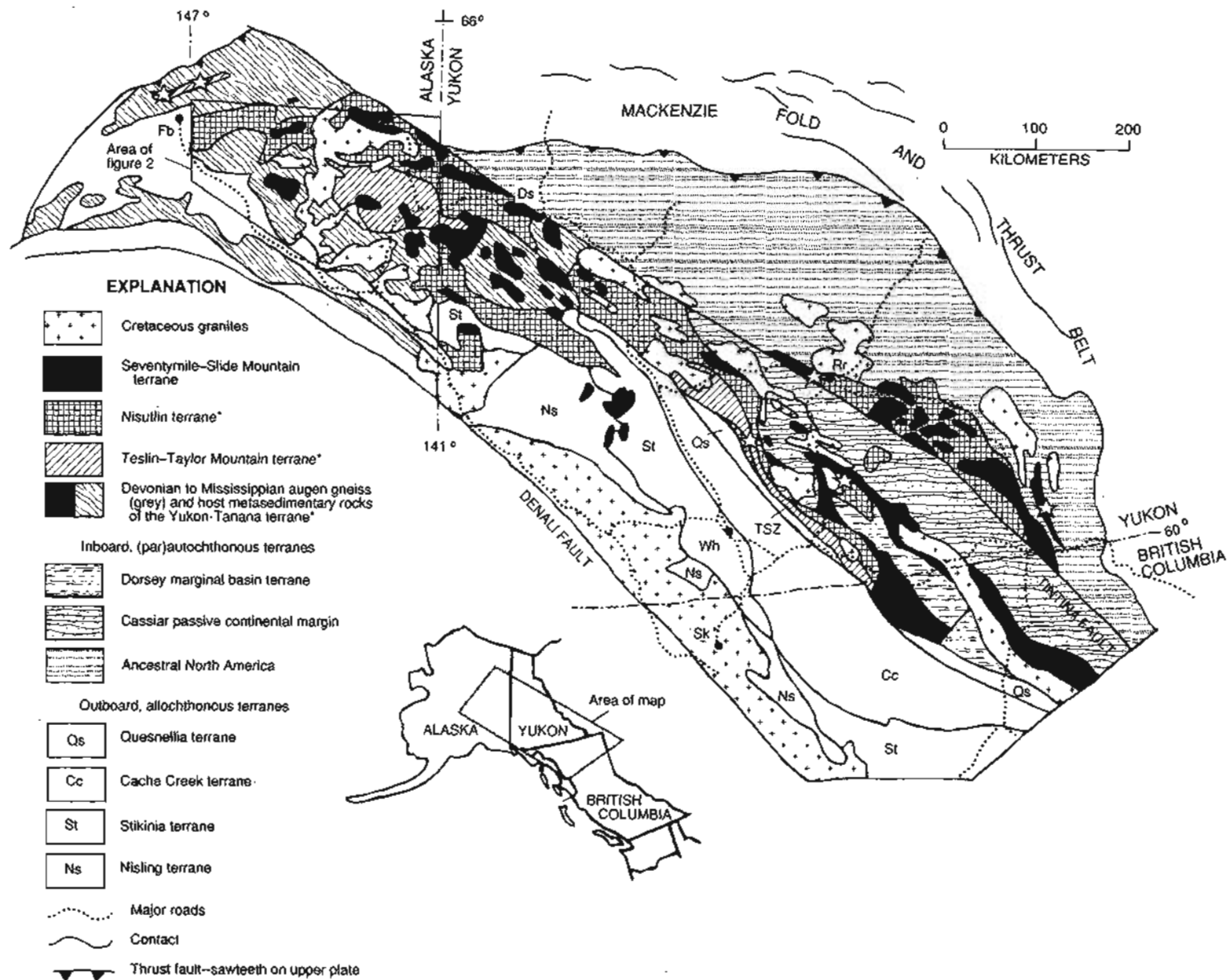


Figure 1. Simplified terrane map of northern Canadian and Alaskan Cordillera (modified from Hansen and others, 1991; data sources listed therein). Town abbreviations: Fb, Fairbanks; Ds, Dawson; Rr, Ross River; Wh, Whitehorse; Sk, Skagway. Location of eclogite (Erdmer and Helmstaedt, 1983; Laird and others, 1984; Brown and Forbes, 1986; Erdmer, 1987) shown by stars. * denotes terranes formerly included as subterrane of Yukon-Tanana terrane. TSZ, Teslin suture zone (see text for explanation). Unlabeled area surrounding Fairbanks is alluvium and unlabeled area north of Denali fault in Alaska comprises various terranes not discussed in this paper.

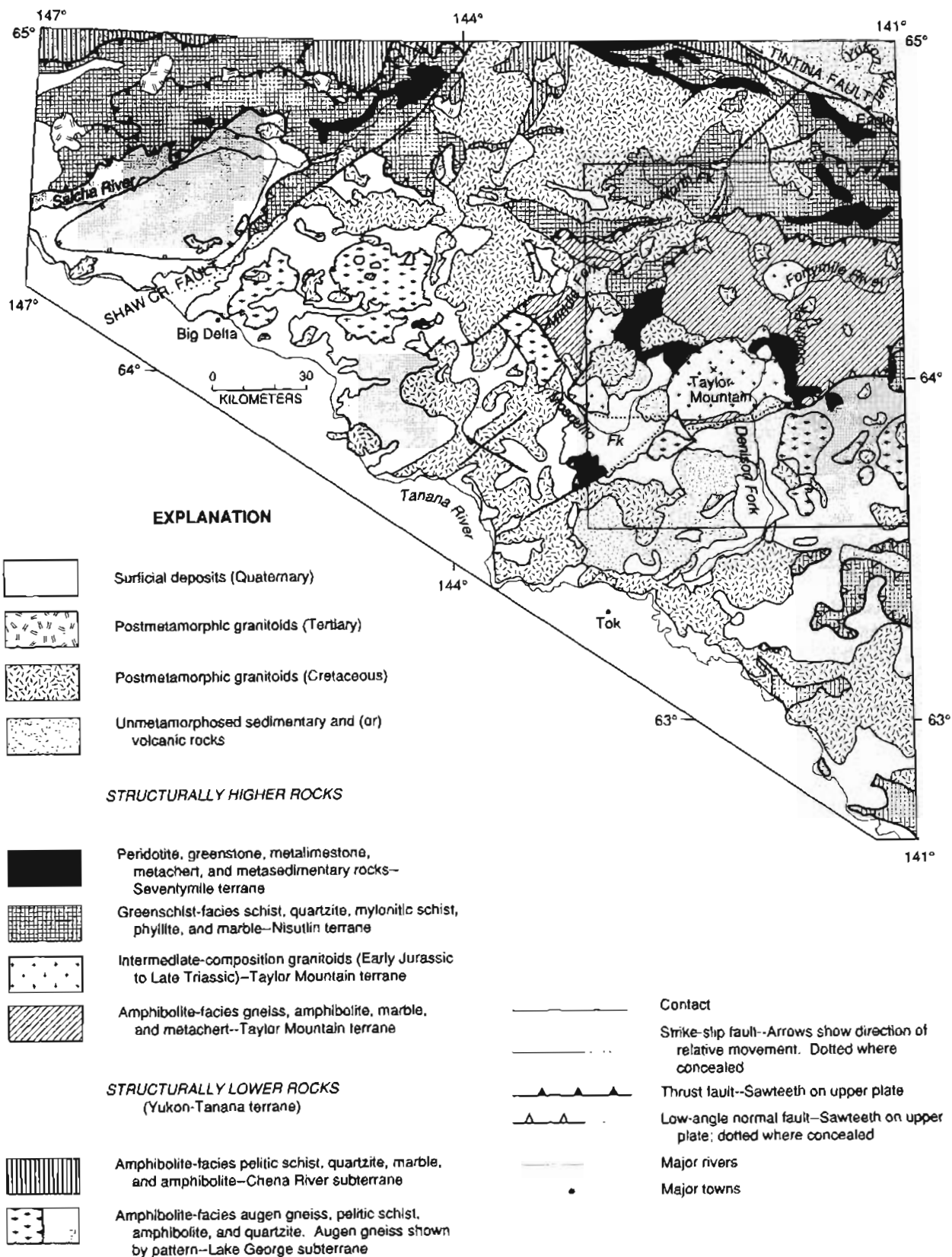


Figure 2. Simplified geologic map of part of Yukon-Tanana upland within Big Delta, Eagle, Tanacross, and northeastern Nabesna 1° by 3° quadrangles (modified from Dusel-Bacon and others, in press; data sources given therein). Box outlines area of figure 3. Closed line with double ticks shows sillimanite isograd that outlines sillimanite gneiss dome referred to in text.

1987). These rocks are included in the Seventymile terrane in Alaska and are considered equivalent to the Slide Mountain terrane in Canada, which is composed of weakly metamorphosed Devonian to Triassic oceanic rocks and Permian arc-related rocks (Harms and others, 1984; Harms, 1985; Nelson and Bradford, 1987; Nelson and others, 1988). Most Seventymile terrane rocks are not penetratively deformed, and they structurally overlie rocks of the Nisutlin or Taylor Mountain terranes. These oceanic rocks generally have been metamorphosed under prehnite-pumpellyite- to lower greenschist-facies conditions, but at one locality, near the northern edge of the area shown in figure 2, they have been metamorphosed under blueschist-facies conditions (Foster and Keith, 1974; Dusel-Bacon and others, in press). Small, well-foliated bodies of ultramafic rocks that reach lower amphibolite-facies metamorphic grade crop out in a discontinuous belt across the southwestern part of the Lake George subterrane west of the study area (Weber and others, 1978). Only one of these bodies is extensive enough to show in figure 2 (near the southeastern edge of the large body of augen gneiss).

Commonly associated with the Seventymile terrane, and structurally underlying it, is a sequence of greenschist-facies, quartz-rich clastic metasedimentary rocks and mafic and intermediate metavolcanic rocks. Common lithologies are quartz-chlorite-white mica schist, carbonaceous quartzite, calc-phyllite, mylonitic quartzofeldspathic schist, and marble. Protolith ages are unknown, but a Devonian and Mississippian age is likely on the basis of regional correlations (Foster and others, 1987) and a U-Pb age of 375 Ma on zircon from a meta-andesite in the Big Delta quadrangle (J.N. Aleinikoff and W.J. Nokleberg, unpub. data, 1989, reported in Dusel-Bacon and others, in press). Metamorphic cooling ages have not been determined for these rocks in Alaska, but at least part of this greenschist-facies sequence is thought to be correlative with the Klondike Schist in Canada, which has yielded Late Triassic to Early Jurassic metamorphic ages [175 ± 14 -Ma K-Ar age on muscovite (Tempelman-Kluit and Wanless, 1975) and 202 ± 11 -Ma Rb-Sr whole-rock age (Metcalfe and Clark, 1983)]. The greenschist-facies rocks of this generalized unit are assigned to the Nisutlin terrane as proposed by Hansen (1990) and Hansen and others (1991). In Canada, rare occurrences of blueschist and eclogite are associated with Nisutlin terrane rocks (Erdmer, 1987).

Amphibolite-facies garnet amphibolite, biotite±hornblende±garnet gneiss and schist, marble, quartzite, metachert, and pelitic schist constitute the metamorphic rocks of the Taylor Mountain terrane. Geothermobarometric data presented in this paper and previously in abstract form (Dusel-Bacon and Douglass, 1990; Dusel-Bacon and Hansen, 1991) indicate high-*P* amphibolite-facies conditions during metamorphism of this terrane.

Intrusive into these rocks are latest Triassic to Early Jurassic plutons of mostly granodioritic composition, including the Taylor Mountain batholith from which this terrane derives its name. Abundant marble, sparse manganeseiferous metachert, and initial common Pb ratios from plutonic rocks (Aleinikoff and others, 1987) suggest an oceanic or marginal-basin origin. Metamorphic cooling ages from $^{40}\text{Ar}/^{39}\text{Ar}$ incremental heating experiments are latest Triassic and Early Jurassic (Hansen and others, 1991; fig. 3). Similarities in metamorphic-protolith assemblages, high-*P* metamorphic conditions, and metamorphic cooling ages of the metamorphic rocks of the Taylor Mountain terrane to those in southern Yukon Territory led Hansen to correlate these two areas and to refer to them collectively as the Teslin-Taylor Mountain terrane (Hansen, 1990) (fig. 1).

Structurally lower rocks (fig. 2) consist of two similar amphibolite-facies subterrane of the Yukon-Tanana terrane. The Lake George subterrane is characterized by augen gneiss derived from dynamothermal metamorphism of a belt of Mississippian granitoids (Dusel-Bacon and Aleinikoff, 1985), as well as quartz-biotite schist and gneiss, pelitic schist, garnet amphibolite, and quartzite. A similar lithologic assemblage, albeit differing in the relative abundances of rock types (specifically, having very little augen gneiss and more quartzite) makes up the Chena River subterrane of the Yukon-Tanana terrane (terminology proposed in Nokleberg and others, 1989). Both of these subterrane, as well as other quartz-rich amphibolite- and greenschist-facies rocks north and northwest of the area shown in figure 2 (shown in fig. 1 as the Devonian to Mississippian augen gneiss and host sedimentary rocks of the Yukon-Tanana terrane), yield Early Cretaceous metamorphic cooling ages (Wilson and others, 1985). In Alaska, as well as in Yukon Territory, these rocks give Proterozoic U-Pb inheritance ages (Aleinikoff and others, 1984, 1986; Mortensen and Jilson, 1985; Mortensen, 1990) and Sm-Nd model ages (Aleinikoff and others, 1981b; Bennett and Hansen, 1988) consistent with North American cratonal basement values. We interpret these lower structural-level rocks (Yukon-Tanana terrane in our restricted application of the name) to comprise a continental margin and granitoid belt built on (par)autochthonous North American basement as previously proposed by Hansen (1990).

STRUCTURAL AND METAMORPHIC-COOLING-AGE SUBDIVISIONS IN THE AREA OF STUDY

Our study area (fig. 3) was chosen so we could examine both the Taylor Mountain terrane and Lake George subterrane and the nature of the structural contact between the two. Our data, combined with those

from previous structural and $^{40}\text{Ar}/^{39}\text{Ar}$ studies (Foster, 1970, 1976; Cushing and others, 1984; Cushing, 1984; Hansen and others, 1991), indicate two different structural and metamorphic-cooling-age zones within the Taylor Mountain terrane and two different structural zones within the Lake George subterrane.

Within the northern zone of the Taylor Mountain terrane, shear-sense indicators record top-to-the-northeast tectonic displacement, and metamorphic cooling ages are Early Jurassic. The $^{40}\text{Ar}/^{39}\text{Ar}$ hornblende plateau age (204 ± 4 Ma) in this zone is approximately 10 m.y. older than the oldest hornblende plateau age in the southern zone of the Taylor Mountain terrane. At the same locality

from which the 204-Ma age was determined, biotite from an actinolite-biotite schist yields a $^{40}\text{Ar}/^{39}\text{Ar}$ plateau age of 187 ± 2 Ma. The dated actinolite-biotite schist occurs within a shear zone that is parallel to, and probably of similar origin to, the south-dipping thrust contact that placed the amphibolite-facies rocks of the Taylor Mountain terrane onto the greenschist-facies rocks of the Nisutlin terrane; hence, the metamorphic cooling age probably dates the juxtaposition of these two metamorphic packages (Cushing and others, 1984). A 186 ± 2 -Ma plateau age on muscovite from an undeformed, unmetamorphosed dike that crosscuts metamorphic foliation within this northern zone (Cushing and others, 1984; Cushing, 1984) establishes a

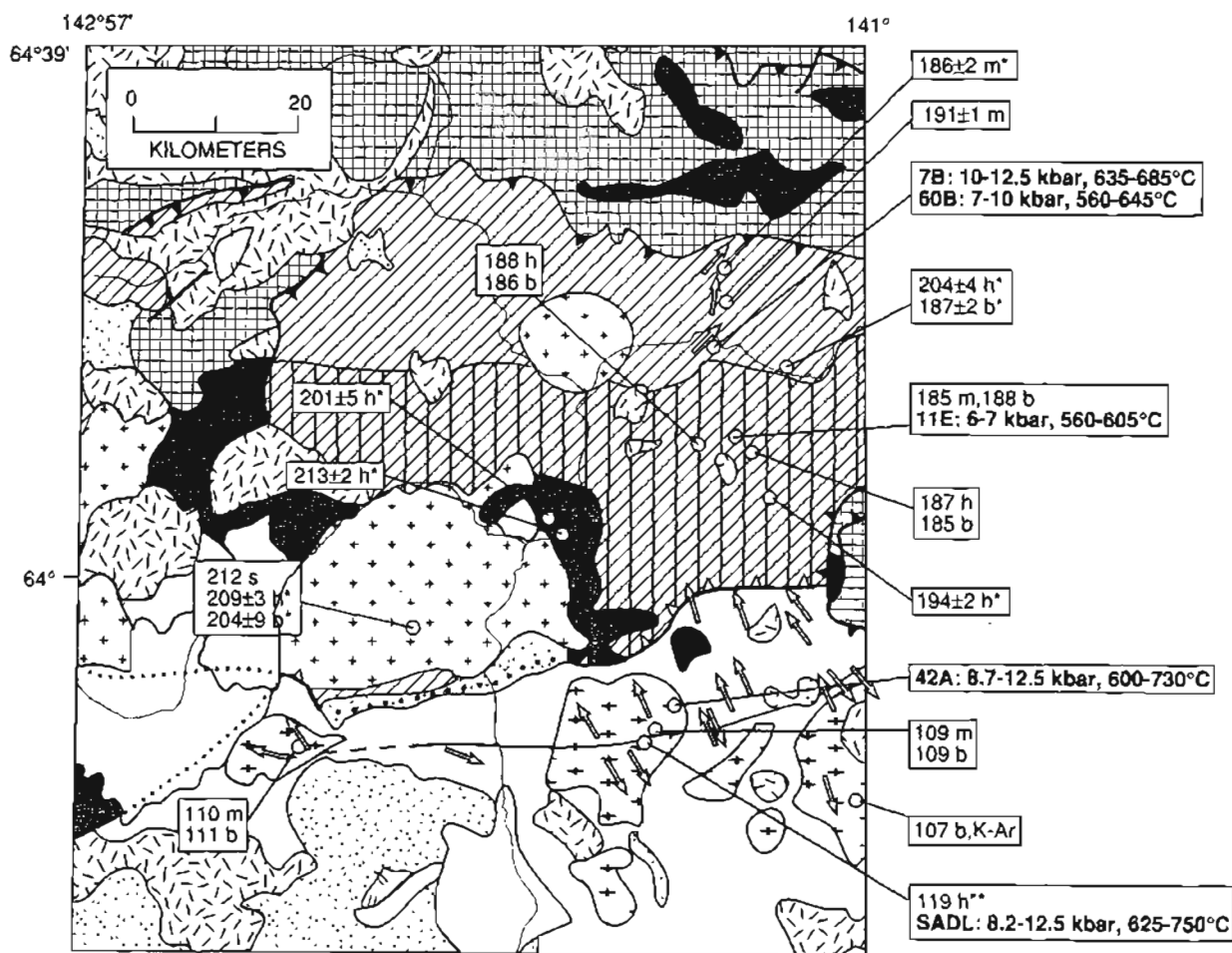


Figure 3. Taylor Mountain area showing location of samples and pressure-temperature estimates discussed in this report, direction of tectonic transport of upper plate rocks (arrows) determined by shear-sense indicators, and metamorphic or, in the case of the Taylor Mountain batholith, igneous cooling ages (Ma). Isotopic age abbreviations: m, b, and h indicate muscovite, biotite, and hornblende $^{40}\text{Ar}/^{39}\text{Ar}$ incremental heating ages, respectively; * indicates data from Cushing and others (1984) and Cushing (1984); ** indicates data from T.M. Harrison; unmarked $^{40}\text{Ar}/^{39}\text{Ar}$ data from Hansen and others

(1991); s, U-Pb sphene age from Aleinikoff and others (1981a); b, K-Ar, biotite K-Ar age from Nora Shew (written commun., 1985). Unit patterns are same as those shown for figure 2. Vertical-ruled overprint of Taylor Mountain terrane shows area of heterogeneous kinematics and unknown tectonic-transport directions in which azimuths of elongation lineations trend east-west, northeast-southwest, and northwest-southeast. East-west-trending line within Lake George subterrane (of Yukon-Tanana terrane) shows axis along which displacement changes from northwest- to southeast-vergent.

minimum metamorphic cooling age (to ~300°C, muscovite blocking temperature) for this zone.

The southern zone of the Taylor Mountain terrane (shown by a vertical-ruled overprint in fig. 3) is characterized by heterogeneous kinematics and metamorphic cooling ages. Only one shear-sense indicator has been determined thus far, but mineral stretching lineations are quite variable in azimuth. Metamorphic cooling ages in this zone straddle the boundary between the Early and Middle Jurassic epochs, with the exception of one older Early Jurassic age (194±2-Ma ⁴⁰Ar/³⁹Ar plateau age on hornblende). Two ⁴⁰Ar/³⁹Ar hornblende-biotite pairs indicate rapid cooling (100°C/m.y.) from 500°C (hornblende blocking temperature) at ~187 Ma to 300°C (biotite blocking temperature) at ~185 Ma (Hansen and others, 1991). We interpret the metamorphic cooling data to indicate rapid exhumation.

We also define two apparent structural zones in the lower-plate Lake George subterrane to the south. North of an east-west-trending line shown on figure 3, shear-sense indicators show top-to-the-northwest tectonic displacement, whereas south of the line, tectonic displacement is top-to-the-southeast. Along the line, tectonites locally record both top-to-the-northwest and top-to-the-southeast displacement. Preliminary data indicate that top-to-the-northwest displacement preceded top-to-the-southeast displacement and is associated with a more penetrative fabric. Metamorphic cooling ages from this area are Early Cretaceous (fig. 3), similar to ages elsewhere in the Lake George subterrane to the west. Comparison of ⁴⁰Ar/³⁹Ar plateau ages on hornblende (119 Ma) and biotite (109 Ma) from nearby outcrops indicates more gradual cooling (20°C/m.y.) from ~500°C to ~300°C that we interpret to indicate moderately rapid exhumation.

SAMPLE SELECTION AND ANALYTICAL PROCEDURES

Garnet amphibolite and pelitic schist from both the Taylor Mountain terrane and the Lake George subterrane of the Yukon-Tanana terrane were evaluated for apparent textural equilibrium, presence of phases necessary to apply multiple geothermometers and geobarometers, and representative coverage of the various structural and metamorphic age domains. Five samples (three garnet amphibolites and two pelitic schists) were chosen for microprobe analysis. Samples are discussed from north to south; their locations are shown on figure 3.

Major element analyses were obtained for garnet, biotite, hornblende, plagioclase, ilmenite, and muscovite using an ARL-SEM-Q electron microprobe equipped with nine wavelength-dispersive spectrometers. Synthetic and natural mineral standards were analyzed before, during,

and after mineral analyses in order to monitor drift. Data were reduced using the corrections of Bence and Albee (1968) and Albee and Ray (1970). In order to increase the probability that the analyzed compositions are representative of equilibrium compositions at peak metamorphic conditions, the following analytical technique, suggested by Hodges and Spear (1982) was used. Two to four domains were identified in each polished section such that all minerals to be analyzed in a given domain were either in contact or less than 1 mm apart. Mineral rims were then analyzed at points of mutual contact. For each mineral grain, three to six closely spaced analyses were averaged to arrive at mean compositions at each spot. An accelerating voltage of 15 kV was used. With the exception of plagioclase, analyses of all phases were obtained from 10-s counting times with a sample current of 25 nA; counting durations on plagioclase were 20 s with an accelerating voltage of 20 nA. The mineral compositions reported in tables 1-4 are typical of the mineral composition in the rocks, although minor compositional variations occur.

SAMPLE DESCRIPTION

TH7B

Garnet-biotite-amphibole gneiss was collected along the Taylor Highway within the northern zone of the Taylor Mountain terrane, in which tectonic displacement is top-to-the-northeast; asymmetric fabrics at this locality indicate N. 50° E. tectonic transport. Subhedral garnet porphyroblasts, 1.5 to 2 mm in diameter, occur in a well-foliated and lineated matrix defined by tabular, 1- to 2-mm-long porphyroblasts of reddish-brown biotite and medium-green (bluish- to yellowish-green to tan pleochroism) amphibole of ferroan pargasite composition [modified classification of Leake (1978), presented in Hawthorne (1981)]. Quartz and plagioclase occur as fine-grained (0.25-mm-long) mosaics; accessory phases are titanite, ilmenite, and rutile.

TH60B

Garnet-biotite-amphibole gneiss also was collected along the Taylor Highway in the northern zone of the Taylor Mountain terrane, approximately 1 km south of sample 7B. Tectonites at this locality record N. 40° E. tectonic transport. This sample is similar in composition to sample 7B but contains slightly more biotite and amphibole and garnet porphyroblasts are larger (3-4 mm) in diameter. Biotite and amphibole porphyroblasts are 1.5 mm long; the former are reddish brown, and the latter show a light- to medium-bluish-green to tan pleochroism. Amphibole

Table 1. Representative analyses of garnet

Sample	Taylor Mountain terrane			Lake George subterrane	
	7B-domain 2 (amphibolite)	60B-domain 2 (amphibolite)	11E-domain 3 (metapelite)	42A-domain 2 (amphibolite)	SADL-domain 3 (metapelite)
SiO ₂ -----	38.00	37.84	36.99	36.77	36.93
TiO ₂ -----	.14	.05	.02	.09	.03
Al ₂ O ₃ -----	21.00	20.96	20.84	21.15	20.83
FeO-----	27.51	31.32	36.73	29.97	34.53
MnO-----	4.85	.44	1.86	.73	1.97
MgO-----	1.88	2.69	2.37	2.71	2.70
CaO-----	8.89	7.90	2.58	8.73	3.25
Total-----	102.27	101.20	101.39	100.15	100.24
Formula normalized to 12 oxygens:					
Si-----	2.98	2.99	2.96	2.93	2.98
Al ^{IV} -----	.03	.02	.04	.07	.03
Al ^{VI} -----	1.92	1.93	1.93	1.91	1.95
Ti-----	.01	.01	.00	.01	.01
Fe-----	1.73	2.00	2.39	1.92	2.28
Mn-----	.32	.03	.13	.05	.14
Mg-----	.22	.32	.29	.32	.33
Ca-----	.75	.67	.22	.75	.28
Pyrope-----	.08	.11	.10	.11	.11
Almandine-----	.59	.68	.82	.65	.77
Spessartine-----	.11	.01	.04	.02	.05
Grossular-----	.22	.20	.04	.22	.07

Table 2. Representative analyses of biotite

Sample	Taylor Mountain terrane			Lake George subterrane
	7B-domain 2 (amphibolite)	60B-domain 2 (amphibolite)	11E-domain 3 (metapelite)	SADL-domain 3 (metapelite)
SiO ₂ -----	35.48	36.32	34.59	34.82
TiO ₂ -----	2.66	1.95	2.62	1.67
Al ₂ O ₃ -----	16.97	18.10	20.32	21.01
FeO-----	21.62	17.13	19.69	20.11
MnO-----	.03	.04	.07	.08
MgO-----	9.03	12.24	8.50	9.10
CaO-----	.00	.07	.04	.00
Na ₂ O-----	.09	.04	.07	.22
K ₂ O-----	10.00	9.57	9.44	9.16
Total-----	95.88	95.46	95.34	96.17
Formula normalized to 11 oxygens:				
Si-----	2.73	2.73	2.64	2.63
Al ^{IV} -----	1.27	1.27	1.37	1.37
Al ^{VI} -----	.27	.33	.46	.50
Ti-----	.15	.11	.15	.10
Fe-----	1.39	1.08	.26	1.27
Mn-----	.00	.00	.01	.01
Mg-----	1.04	1.37	.97	1.02
Ca-----	.00	.01	.00	.00
Na-----	.01	.01	.01	.03
K-----	.98	.92	.92	.88
Mg/(Mg+Fe)-----	.43	.56	.79	.45

Table 3. Representative analyses of hornblende

Sample	Taylor Mountain terrane		Lake George subterrane
	7B-domain 2 (amphibolite)	60B-domain 2 (amphibolite)	42A-domain 2 (amphibolite)
SiO ₂ -----	39.63	40.02	40.82
Al ₂ O ₃ -----	15.23	20.46	17.47
TiO ₂ -----	.43	.36	.44
MgO-----	6.32	6.75	8.30
FeO-----	21.74	16.89	16.71
MnO-----	.54	.06	.11
CaO-----	11.13	11.76	11.03
Na ₂ O-----	2.09	1.37	1.78
K ₂ O-----	.85	.53	.50
Total-----	97.96	98.20	97.16

Formula normalized to 23 oxygens:

Si-----	6.07	5.93	6.12
Al ^{IV} -----	1.93	2.07	1.88
Al ^{VI} -----	.82	1.50	1.20
Ti-----	.50	.04	.05
*Fe ³⁺ -----	.22	.00	.00
Mg-----	1.45	1.49	1.85
Fe ²⁺ -----	2.57	2.09	2.09
Mn-----	.07	.01	.01
Ca-----	1.83	1.87	1.77
Na(M4)-----	.00	.00	.02
Na(A)-----	.62	.39	.50
K-----	.17	.10	.10
Fe ²⁺ /(Mg + Fe ²⁺)--	.64	.58	.53

*Fe³⁺ calculated according to the method of Spear and Kimball (1984).

composition is ferroan tschermakite. Quartz and plagioclase are fine grained (0.25 mm long) and less abundant than in sample 7B. Ilmenite and trace amounts of rutile are accessory phases.

TH11E

Staurolite-kyanite-garnet-quartz mica schist also was collected along the Taylor Highway but from the southern, mixed kinematic zone of the Taylor Mountain terrane; lineation has an azimuth of N. 70° E. and plunges moderately to the northeast or southwest. Garnet porphyroblasts (1-2 mm in diameter) occur in a compositionally layered matrix composed of folia of intergrown and equally abundant 1-mm-long red-brown biotite and white mica that alternate with folia of 0.5- to 1-mm-long subhedral quartz and much less abundant plagioclase. Porphyroblasts of euhedral to subhedral kyanite (1-2 mm long) and subhedral staurolite (0.5 mm long) are present in minor amounts, and ilmenite, tourmaline, zircon, and rutile occur in trace amounts. Very minor alteration of biotite or garnet to chlorite occurs in a few areas of the thin section.

83ADb42A

Garnet amphibolite was collected within an area of the Lake George subterrane in which augen gneiss is the predominant rock type. This sample was collected from the zone in which kinematic indicators record top-to-the-

Table 4. Representative analyses of plagioclase

Sample	Taylor Mountain terrane			Lake George subterrane	
	7B-domain 2 (amphibolite)	60B-domain 2 (amphibolite)	11E-domain 3 (metapelite)	42A-domain 2 (amphibolite)	SADL-domain 3 (metapelite)
SiO ₂ -----	62.91	60.45	60.93	61.18	62.76
Al ₂ O ₃ -----	24.20	26.68	25.21	25.51	24.34
CaO-----	4.50	7.54	5.85	6.26	4.79
Na ₂ O-----	9.43	7.59	8.55	8.42	9.23
K ₂ O-----	.09	.07	.06	.04	.08
Total-----	101.13	102.33	100.60	101.41	101.20

Formula normalized to 8 oxygens:

Si-----	2.75	2.62	2.68	2.68	2.74
Al-----	1.25	1.37	1.31	1.32	1.25
Ca-----	.21	.35	.28	.29	.22
Na-----	.80	.64	.73	.71	.78
K-----	.01	.00	.00	.00	.00
An-----	21.1	35.0	27.5	29.4	22.5
Ab-----	80.2	63.7	72.7	71.6	78.5
Or-----	.5	.3	.3	.2	.4

northwest tectonic transport. Euhedral to subhedral garnet porphyroblasts (1 mm in diameter) lie in a well-foliated matrix of 0.5-mm-long grains of medium-bluish-green (to yellowish-tan) amphibole (ferroan pargasite), quartz, and plagioclase; there is no apparent compositional layering. Ilmenite, rutile, and titanite are accessory phases.

SADL

Staurolite-garnet-quartz mica schist was also collected within the augen gneiss-bearing part of the Lake George subterrane, but about 7 km to the southwest of sample 42A and near the boundary between northwest- and southeast-vergent fabrics; lineation at this locality is essentially flat lying, and nearby outcrops record S. 25° E. tectonic transport. Subhedral to euhedral porphyroblasts of garnet (1.5–4 mm in diameter) and staurolite (1–2 mm long) are enclosed in a matrix composed of folia of red-brown biotite and white mica (equal amounts of 1–1.5-mm-long grains) alternating with similar-sized grains of quartz and minor plagioclase. Ilmenite, rutile, tourmaline, and zircon are present in trace amounts.

GEOOTHERMOMETRY AND GEOBAROMETRY

Peak metamorphic temperatures and pressures corresponding to peak temperatures were determined by geothermometry and geobarometry using compositions determined by microprobe analysis of garnet rims and adjacent matrix phases as described above. Garnet zoning profiles (Cynthia Dusel-Bacon and Neena Bashir, unpub. data, 1991) show a core-to-rim decrease in Mn and an increase in Mg indicative of growth zoning. The profiles support our interpretation that garnet-rim compositions record maximum temperatures. It has not been possible to determine *P-T* conditions during early garnet growth because the only inclusions observed within garnet have been quartz and ilmenite.

Temperatures of final equilibration of the samples were calculated using the garnet-biotite (GT-BT) geothermometer (Hodges and Spear, 1982) and the garnet-hornblende (GT-HB) geothermometer (Graham and Powell, 1984). Pressures of final equilibration were derived using the garnet-plagioclase-hornblende-quartz (GPHQ) geobarometer for both tschermakite (TSCH) and its Fe end-member equivalent (FE TSCH) (Kohn and Spear, 1990); the garnet-rutile-ilmenite-plagioclase-quartz (GRIPS) geobarometer (Bohlen and Liotta, 1986); the garnet-rutile-Al₂SiO₅ (kyanite)-ilmenite (GRAIL) geobarometer (Bohlen and others, 1983); the garnet-Al₂SiO₅ (kyanite)-plagioclase-quartz (GASP) geobarometer (Kozioł and Newton, 1988); and the

garnet-plagioclase-muscovite-biotite (GPMB) geobarometer (Hodges and Crowley, 1985). Our calculations used the garnet activity model of Hodges and Spear (1982). Fe³⁺ in amphibole (table 3) was calculated to a minimum value consistent with amphibole stoichiometry using the method of Spear and Kimball (1984).

Results of the geothermobarometry for all the domains of the five samples are plotted in figure 4. The Al₂SiO₅ phase boundaries of Holdaway (1971) are shown for reference; the overlap in *P-T* results for all samples occurs in the kyanite field. Taken at face value, the following range of pressures and temperatures are indicated for each sample: Taylor Mountain terrane: garnet amphibolite, 10 to 12.5 kbar, 635°C to 685°C and 7 to 10 kbar, 560°C to 645°C; staurolite-kyanite-garnet-quartz-mica schist, 6 to 7 kbar, 560°C to 605°C; Lake George subterrane: garnet amphibolite, 8.7 to 12.5 kbar, 600°C to 730°C; garnet-staurolite-quartz-mica schist, 8.2 to 12.5 kbar, 625°C to 750°C.

In general, there is close agreement between the results of the various geobarometers applied to the same sample and of the same geobarometer applied to mineral suites from different domains. Agreement is poorer between the results of the GT-BT and GT-HB geothermometers where applied to the same sample and between the results of the same geothermometer applied to mineral pairs from different domains within the same sample. For the two samples in which both GT-HB and GT-BT temperatures were determined, GT-HB temperatures are higher. Generally, the highest GT-HB temperatures correspond to the hornblende with the highest Fe# (Fe²⁺/Fe²⁺+Mg) value. Graham and Powell (1984) warn that significant overestimates of temperature may arise in using their GT-HB geothermometer if the hornblende compositions are unusually rich in Fe³⁺. Potential problems related to the ferric iron content of our hornblendes could be minimized by the fact that estimates of the Fe³⁺ contents based only on stoichiometry tend to produce minimum values. The empirical experience of M. J. Kohn (written commun., 1990) suggests that when the Fe# is above 0.6 or 0.65, GT-HB temperatures become progressively higher than those indicated by other geothermometers and are inconsistent with phase equilibria. This is the case with the two GT-HB temperatures for sample 7B (Fe#'s=0.67 and 0.64) and the three highest GT-HB temperatures for sample 42A (Fe#'s=0.63 and 0.61). Additional problems with accurate temperature estimates for sample 7B come from the fact that the mole fraction of Mn in garnets (0.3) used in the application of the GT-HB geothermometer exceed the compositional range for garnet for which the calibration is recommended ($X_{Mn} < 0.1$ for GT-HB; Graham and Powell, 1984). If the three highest temperatures for sample 42A are ignored because of their high Fe#'s and the lower three temperatures ranging from 600–625 °C

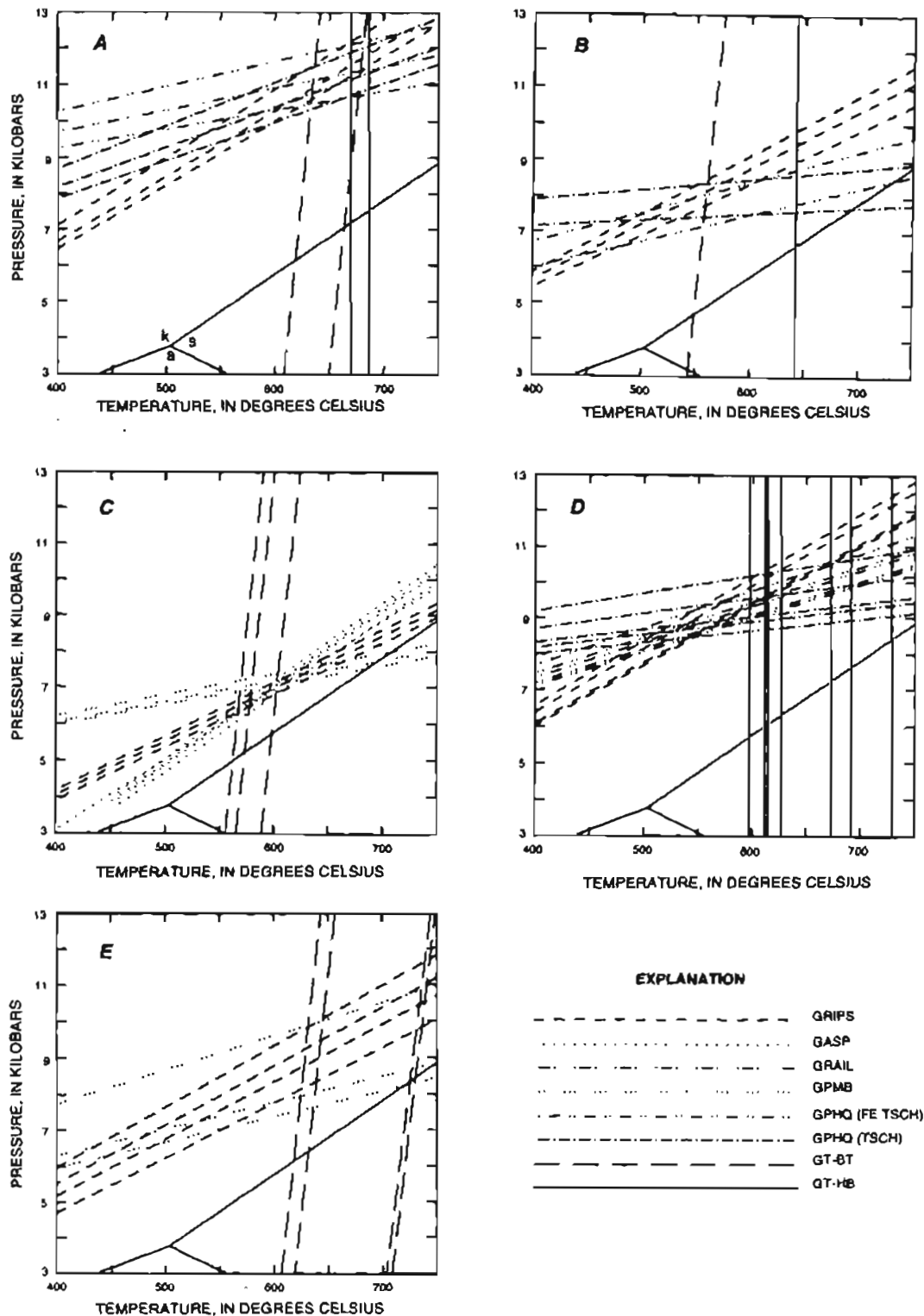


Figure 4. Pressure-temperature (P - T) diagrams showing results of geothermobarometric calculations for samples analyzed in this study. P - T estimates for each sample discussed in text are based on area of overlap of K_{eq} (equilibrium constant) lines. Each line represents a different K_{eq} based either on same geothermometer or geobarometer applied to multiple domains in each sample or on different geothermometers and

geobarometers applied to various domains; abbreviations for geothermometers and geobarometers explained in text. Heavy lines show Al_2SiO_5 phase diagram of Holdaway (1971). Abbreviations: k, kyanite; s, sillimanite, a, andalusite. A, Sample 7B. B, Sample 60B. C, Sample 11E. D, Sample 42A. E, Sample SADL. See figure 3 for location of samples.

(for which $Fe\#s=0.51-0.53$) are considered only, there is better correspondence between the pressures determined by the GRIPS and GPHQ geobarometers.

Although there is a considerable range in calculated temperatures for most samples, the relatively flat slopes of the equilibrium constant (K_{eq}) lines for the various equilibria on which the geobarometers are based cause the uncertainty in temperature to have little effect on overall pressure estimates. A realistic estimate of $-600^{\circ}C$ to $650^{\circ}C$ for maximum metamorphic temperatures is suggested by the preservation of garnet zoning profiles, indicating that temperatures were not high enough for modification of chemical zonation by diffusion during cooling from peak temperatures, and by the absence of evidence for partial melting in Taylor Mountain terrane and Lake George subterrane tectonites. Another argument that suggests that maximum metamorphic temperatures were in the range of $-600\pm 50^{\circ}C$ is that this is the approximate range of temperatures over which different geobarometers for the same sample intersect (fig. 4A-E).

The simultaneous solution of the various equilibria used as geothermometers and geobarometers in this study (represented by the areas of overlap of the K_{eq} lines for each sample) is shown in figure 5. The temperature and pressure ranges shown in figure 4 have been expanded in figure 5 by $\pm 30^{\circ}C$ and 0.5 kbar, respectively. Although absolute uncertainties in the calculated $P-T$ conditions have been suggested to be as high as $\pm 50^{\circ}C$ and ± 1 to 2 kbar for each of the calibrations, relative uncertainties are probably significantly smaller (Hodges and McKenna, 1987). Therefore, $P-T$ conditions that were obtained using the same geothermobarometers can be compared. As mentioned above, the upper temperature ranges allowed by the uncertainty in temperature estimates are shown to extend well into the range of partial melting (fig. 5), a relation not seen in the field. The consistency in estimated $P-T$ conditions for pelitic schist (SADL) and garnet amphibolite (42A) of the Lake George subterrane indicates that geothermobarometers using different bulk compositions can give the same result. This observation supports the

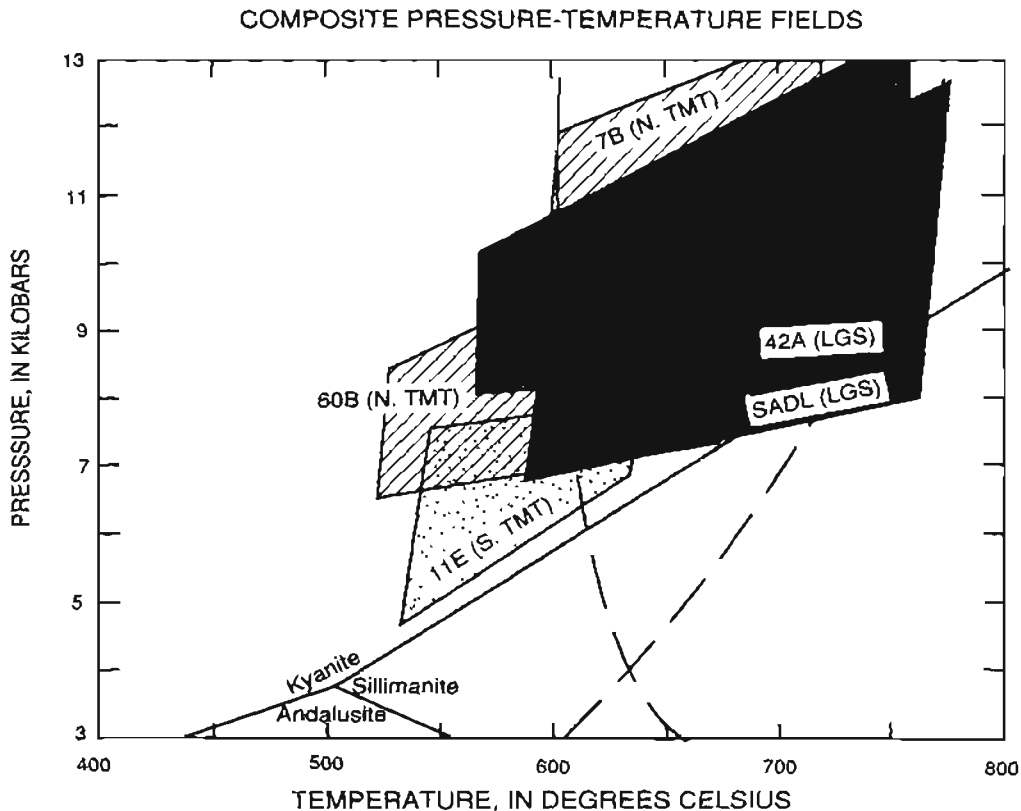


Figure 5. Estimated pressure-temperature ($P-T$) fields for samples 7B, 60B, 11E, 42A, and SADL, expanded to allow for temperature uncertainty of $30^{\circ}C$ and pressure uncertainty of 0.5 kbar. Dashed lines show initial melting of wet and dry pelite (lower and higher temperature lines, respectively; Thompson and Tracy, 1979). Abbreviations: LGS, Lake George subterrane of the Yukon-Tanana terrane ($P-T$ fields shown in gray); N. TMT, northern zone of the Taylor Mountain terrane ($P-T$ fields shown in diagonal ruled pattern); S. TMT, southern zone of Taylor Mountain terrane ($P-T$ field shown in stippled pattern).

real difference in P - T conditions indicated by our geothermobarometry of pelitic schist (11E) and garnet amphibolite (7B and 60B) from the Taylor Mountain terrane.

We are presently investigating possible explanations for the differences in pressures determined for the compositionally similar samples 7B and 60B. Our current hypothesis is that the calculated pressure differences are valid, for if these tectonites were indeed metamorphosed within a subduction-zone environment as we propose, one can envision displacement paths (within the subduction channel; Cloos and Shreve, 1988) that could juxtapose tectonites of different peak P - T conditions (for example, Cloos, 1985; Hansen, 1992a).

DISCUSSION

High-Pressure Metamorphism in the Eastern Yukon-Tanana Upland

The P - T conditions indicated by geothermobarometry reported above are consistent with high- P , moderate- T metamorphism and penetrative ductile deformation within a subduction-zone setting. Kinematic and thermochronometric (primarily $^{40}\text{Ar}/^{39}\text{Ar}$ incremental-heating ages) differences between Taylor Mountain terrane and Lake George subterrane rocks in the area of our study suggest that although similar P - T conditions (8–12 kbar) were determined for the northern zone of the Taylor Mountain terrane and the Lake George subterrane to the south, the timing and tectonic setting of metamorphism in these two areas differed. Ongoing P - T studies should help elucidate the tectonic model.

In the northern zone of the Taylor Mountain terrane, postmetamorphic and postkinematic cooling to about 500°C (hornblende-blocking temperature) took place as early as 204±4 Ma and deformation was top-to-the-northeast, perpendicular to regional strike. Similar high- P , moderate- T metamorphic conditions, orogen-normal tectonic transport, and Early Jurassic metamorphic cooling ages have been documented in correlative rocks in the Teslin suture zone of central Yukon (fig. 1) (Hansen, 1989, 1992b; Hansen and others, 1991). Considering our data in conjunction with those from the structurally and metamorphically similar rocks in the Teslin suture zone, we conclude that metamorphism and deformation within the northern zone of the Taylor Mountain terrane took place within the deep-seated part of a southwest-dipping (present-day coordinates) subduction zone outboard of western North America. A Permian Rb-Sr muscovite cooling age on blueschist-facies rocks associated with eclogite north of the town of Ross River in central Yukon (fig. 1) places a minimum age on initiation of subduction (Erdmer and Armstrong, 1988).

The single, and significantly lower (6–7 kbar), pressure determined for the staurolite-kyanite-garnet-quartz-mica schist from the southern zone of the Taylor Mountain terrane is more difficult to interpret. Rapid cooling and exhumation of this structural zone at about 188 to 186 Ma is indicated by the hornblende and mica $^{40}\text{Ar}/^{39}\text{Ar}$ cooling ages. We interpret the cooling and exhumation to have resulted from collision and obduction of these rocks onto the margin of western North America, including the Lake George subterrane and other associated lower-plate rocks of the Yukon-Tanana terrane. This interpretation of ages, presented previously by Hansen and others (1991), is supported by the 187±2-Ma $^{40}\text{Ar}/^{39}\text{Ar}$ muscovite cooling age from the shear zone that is parallel to the thrust fault along which the Taylor Mountain terrane was emplaced above the greenschist-facies rocks of the Nisutlin terrane during collision. Kinematic analysis from the southern zone of the Taylor Mountain terrane has not been completed, but the presence of northeast-, northwest-, and east-west-trending elongation lineations suggests a complex structural history. Our tentative interpretation of the structural data is that the rocks in this package, being closer to the plate boundary between the hanging wall (Taylor Mountain terrane) and the footwall (Lake George subterrane), were affected both by precollision deformation (northeast-directed tectonic transport) that we assume was dominant for the rocks of the northern structural zone and by syn-collision deformation (perhaps northwest-directed tectonic transport, as discussed below). The east-west-trending lineation also observed within this southern zone, and at the locality from which this P - T determination was made, may be analogous to the lineation developed within a zone of dextral strike-slip deformation within the Teslin suture zone. Metamorphic pressures from within the dextral strike-slip zone were significantly lower (5–8 kbar) than elsewhere within the Taylor Mountain terrane-equivalent rocks of the Teslin suture zone (12±4 kbar) (Hansen, 1992b). Our lower P determination from the southern Taylor Mountain terrane zone, relative to the two determinations from the northern package, may record either a later and shallower phase of accretion or dextral transpression that was shown to be an important process during the early Mesozoic accretion of Taylor Mountain terrane-equivalent rocks in southern Yukon (Hansen, 1989), or pressure that accompanied underthrusting of the Lake George subterrane, as discussed below.

High- P metamorphism of the Lake George subterrane is most reasonably explained by subduction of continental crust beneath the overriding, accreted rocks of the Taylor Mountain, Seventymile-Slide Mountain, and (probably) Nisutlin terranes. Rapid cooling and exhumation of the upper-plate Taylor Mountain terrane from about 500°C to 300°C around 186 Ma establishes a

likely age for initiation of tectonic burial of the lower plate. Crustal thickening of the Lake George subterrane undoubtedly would have continued after collision and initial obduction of upper-plate rocks, since continued contraction would have resulted in imbrication and folding of the lower plate. We interpret the Early Cretaceous metamorphic cooling ages in the eastern Lake George subterrane, and probably in much of the lower-plate Yukon-Tanana terrane as well, to reflect cooling and exhumation of these rocks as a result of crustal extension following obduction of the overlying terranes, as previously proposed by Hansen and others (1991). As mentioned above, comparison of hornblende and biotite $^{40}\text{Ar}/^{39}\text{Ar}$ ages (119 and 109 Ma, respectively) from nearby localities in the eastern Lake George subterrane (fig. 3) indicates a cooling rate of $20^\circ\text{C}/\text{m.y.}$, which, in turn suggests moderately rapid exhumation. The Lake George subterrane was apparently at the surface by ~ 93 Ma because it forms the country rock into which calderas of that age (shown on fig. 2 as the area of unmetamorphosed rocks north of Tok) were emplaced (Bacon and others, 1990).

Kinematic data from the eastern Lake George subterrane can be interpreted in two ways. In our first, and preferred, interpretation, the older, top-to-the-northwest, displacement records deformation during contraction accompanying accretion of obducted terranes and imbrication within lower-plate rocks, and the younger, top-to-the-southeast, deformation records shallower, subsequent extension. This interpretation is supported by a northwest-vergent shear sense recorded in quartzose rocks at the leading edge of the Yukon-Tanana terrane north of Fairbanks (fig. 1) during contraction, and by an east-southeast-directed transport direction measured in greenschist-facies mylonites at the base of the hanging wall above a sillimanite gneiss dome (fig. 2) that was exposed during major crustal extension (Pavlis and others, 1988, in press). In our second interpretation, both the top-to-the-northwest and top-to-the-southeast displacement occurred synchronously during extension. However, if upper-plate rocks were shed both to the northwest and to the southeast at the same time, one might expect a broad (>10 km) transitional zone dominated by coaxial shear deformation between the domains that record opposing ductile shear direction (for example, 10–20 km wide in the Albion, Grouse Creek, and Raft River Mountains, Idaho; Malavieille, 1987). However, the east-west-trending line (fig. 3) that separates opposing ductile shear fabrics in the study area is extremely sharp [in fact, opposing shear sense is recorded within a single outcrop at one locality (fig. 3, east of sample 42A)], and we also see no indication of coaxial deformation. In addition, kinematic analysis reveals that microstructures that record top-to-the-southeast shear consistently crosscut top-to-the-northwest microstructures.

Evidence for High-Pressure Metamorphism, Related to Jurassic Accretion, in the Western Yukon-Tanana Upland

Although our geothermobarometric and kinematic data are from the eastern part of the Yukon-Tanana upland in Alaska, several lines of evidence suggest that Early to Middle Jurassic obduction of the outboard Seventymile–Slide Mountain and Taylor Mountain terranes onto the lower-plate Lake George subterrane was also a major tectonic and metamorphic event in the western Yukon-Tanana upland. (1) Klippen of ultramafic and mafic Seventymile–Slide Mountain terrane rocks extend ~ 230 km westward into the center of the Big Delta quadrangle, attesting to the widespread original distribution of these oceanic rocks. (2) Rocks from an eclogite-bearing klippe of the Chatinika terrane northeast of Fairbanks (fig. 1) yield Middle Jurassic muscovite K-Ar cooling ages (Wilson and Shew, 1981). (3) The high- P assemblage garnet-hornblende-kyanite-staurolite occurs in schist (C. Dusel-Bacon and V.L. Hansen, unpub. data, 1991) within an area of amphibolite-facies mafic rocks that yield Early to Middle Jurassic hornblende K-Ar and $^{40}\text{Ar}/^{39}\text{Ar}$ cooling ages [188 ± 6 Ma (Wilson and others, 1985) and 181 ± 3 Ma (M.A. Lanphere and C. Dusel-Bacon, unpub. data, 1991), respectively], in contrast to the Early Cretaceous metamorphic cooling ages that are typical of the Lake George subterrane. We tentatively interpret this area of mafic rocks (shown on fig. 2 to occur within the large area of augen gneiss west of our area of study) as a klippe of the Taylor Mountain terrane above the Lake George subterrane. Our contention that these rocks record high- P conditions is based on P - T studies of kyanite+staurolite+hornblende amphibolites in other high- P metamorphic belts of the world, which indicate metamorphic pressures of 9 to 10 kbar (Selverstone and others, 1984, p. 514).

High- P metamorphism related to this same episode of plate convergence has been well documented in the Yukon by the high- P rocks in the Teslin suture zone (Hansen, 1989, 1992b; Hansen and others, 1991) and by isolated occurrences of eclogite (Erdmer and Helmstaedt, 1983) (fig. 1).

TECTONIC MODEL

The P - T estimates and kinematic and age data presented in this paper are consistent with a tectonic model proposed by Hansen (1990) and Hansen and others (1991) that is based to a large degree on the initial hypothesis of arc-continent collision made by Tempelman-Kluit (1979). A simplified two-dimensional version of this model is shown in figure 6. For clarity, no translational component

is shown, but we do not propose that movement was exactly normal to the continental margin.

Beginning in Devonian to Mississippian time, rifting commenced along the western margin of North America and a basin was formed. At about this same time, or perhaps before and possibly related to rifting, peraluminous Devonian and Mississippian granitoids intruded the continental crust. Rifting continued until Permian time, resulting in the development of the Anvil Ocean (a basin of unknown width, floored by oceanic crust) (fig. 6A). In this model, the peraluminous plutons shown northeast of the Anvil Ocean are the protoliths of the augen gneiss of the Lake George subterrane. We speculate that the rifted fragment of North American crust is the Nisling terrane, which lies outboard of the accreted terranes (fig. 1), and which is also intruded by Devonian and Mississippian peraluminous plutons (Gareau, 1989; McClelland and others, 1992).

By Late Permian time, southwest-dipping, right-oblique subduction (as indicated by precollision dextral shear zones within the Teslin suture zone; Hansen, 1989) of the Anvil Ocean lithosphere had begun (fig. 6B). This minimum age for initiation of subduction is provided by Rb-Sr and K-Ar age determinations of approximately 250 Ma for blueschist associated with eclogite near the town of Ross River, Yukon Territory (fig. 1). An arc, which includes the Triassic to Jurassic granitoids (including the Taylor Mountain batholith of the Taylor Mountain terrane) that characterize the Stikinia terrane, developed above the subduction zone. Multiple lines of evidence (summarized in Hansen and others, 1991, p. 72) suggest a composite oceanic/continental [Nisling(?) terrane] basement for the Stikinia arc, as we show in figure 6. According to this model, protoliths of the Taylor Mountain and Nisutlin terranes, the terranes that compose the intermediate and lower levels of the subduction complex associated with the Stikinia arc, include sedimentary clastic rocks derived from erosion of crustal and arc-related rocks, intermediate and siliceous volcanic rocks associated with arc activity, and sedimentary rocks deposited within the marginal basin. We propose that metamorphism of the Taylor Mountain terrane took place within the deep-seated part of the subduction zone where temperatures were highest. Nisutlin terrane rocks were metamorphosed and deformed at lower temperatures and, locally, at high pressures (only documented in Yukon; Hansen and others, 1991). The Seventymile terrane, the tectonic mixture of oceanic sedimentary rocks and crust, was only weakly metamorphosed in most areas.

In Early to Middle Jurassic time (~187 Ma), the outboard terranes were obducted onto North America (fig. 6C). Most of the obducted oceanic lithosphere (ultramafic rocks) of the Seventymile-Slide Mountain terrane were not penetratively deformed (represented by right-hand area of oceanic crust; fig. 6C). We propose that a

minor amount of the oceanic lithosphere from deeper within the subduction zone (middle sliver of oceanic lithosphere above the deformed augen gneiss bodies in fig. 6C) was ductilely deformed, and that the belt of outcrops of foliated ultramafic rocks in the southwestern part of the Lake George subterrane (west of our study area and described earlier in the paper) formed in this tectonic setting. Continued contraction resulted in further underthrusting of the continental margin. High-*P* metamorphism and ductile deformation occurred in the lower plate (Lake George subterrane) as a result of crustal thickening caused by a combination of obduction of outboard terranes and imbrication within the lower plate.

Subsequent development of a north- to northeast-dipping subduction system farther outboard was probably a major factor in widespread crustal extension that unroofed the Lake George subterrane and related basement rocks (Pavlis, 1989; Pavlis and others, in press)(fig. 6D). Extension resulted from gravitational collapse of overthickened crust, slab rollback and trench retreat, or a combination of these and other factors (Dewey, 1988; Pavlis and others, in press). Kinematic data in the western part of the Lake George subterrane indicate that the mylonites that form a partial sheath enveloping a domal structure in the footwall (sillimanite gneiss dome of the Lake George subterrane; fig. 2) record a uniform east-southeast transport direction of the hanging wall [greenschist-facies rocks of the Nisutlin terrane as defined by Hansen, 1990] (Pavlis and others, 1988, in press). Juxtaposition of these high- and low-grade rocks suggests removal of as much as 10 km of crustal section (Pavlis and others, in press). Decompression within the lower-plate gneiss dome also is indicated by the occurrence of andalusite-bearing quartz veins (Sisson and others, 1990), andalusite-bearing partial melts developed within the core of the gneiss dome (Dusel-Bacon and Foster, 1983), and the growth of texturally late andalusite that postdates kyanite growth in pelitic schist that flanks the gneiss dome (Sisson and others, 1990). A clastic wedge (Hauterivian to Cenomanian in age) that could represent the eroded material, stripped away during the postulated period of crustal extension, was shed to the east and deposited within the MacKenzie fold and thrust belt (Pavlis and others, in press).

In the eastern Lake George subterrane, the primary evidence for crustal extension is the juxtaposition of Taylor Mountain terrane tectonites with Early to Middle Jurassic cooling ages above Lake George subterrane tectonites with Early Cretaceous cooling ages, a relation best explained by the stripping away of upper-plate Taylor Mountain terrane along low-angle normal faults, resulting in exhumation and cooling of the lower-plate Lake George subterrane. This relation, as well as the

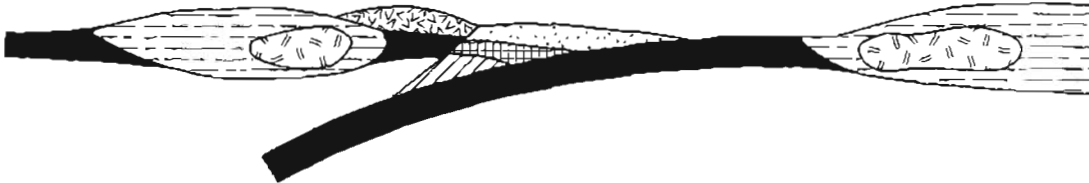
SOUTHWEST

NORTHEAST

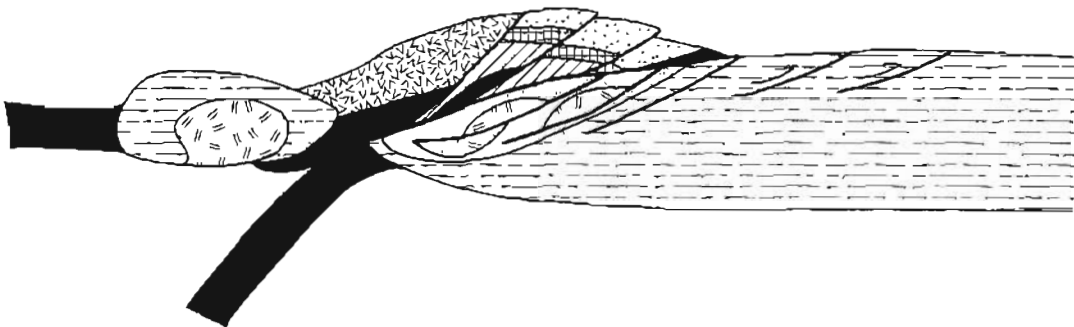
A. Devonian to Permian



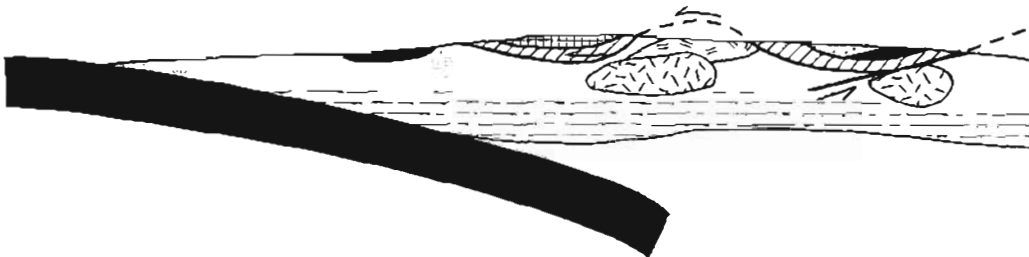
B. Permian and Triassic



C. Early to Middle Jurassic



D. Early to mid-Cretaceous



EXPLANATION


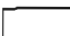

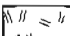

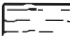

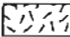
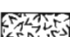
- | | | | |
|---|--|---|---|
|  | Seventymile-Slide Mountain terrane
sedimentary and volcanic rocks |  | Lake George subterrane
(of Yukon-Tanana terrane) |
|  | Seventymile-Slide Mountain terrane
oceanic crust |  | Devonian and Mississippian
peraluminous plutons |
|  | Nisutlin terrane |  | North American crust |
|  | Taylor Mountain terrane |  | Cretaceous plutons |
|  | Stikinia terrane | | |

Figure 6. Simplified tectonic model for Devonian to mid-Cretaceous evolution of accreted terranes and North American crust in east-central Alaska. Modified from Hansen and others (1991). See text for explanation, and Hansen and others (1991) for a more complete explanation of some of the data used in developing this model.

downdropping of the northern belt of unfoliated oceanic crust and the southern belt of foliated oceanic crust (shown by the right-hand and left-hand klippen of oceanic crust, respectively), is schematically displayed in figure 6D.

As shown in figure 6D, we speculate that mid-Cretaceous plutonism was probably associated with crustal extension, perhaps softening and further weakening the crust and thus facilitating the development of ductile shear zones such as those that we have observed in extremely attenuated rocks near the Lake George subterrane/Taylor Mountain terrane contact zone in the area of our study. The main period of plutonism (105–90 Ma; Wilson and others, 1985) postdates the ductile deformation but may have been related to melting facilitated by decreasing pressure during the later stages of extension-related uplift.

CONCLUSIONS

1. Geothermobarometric analysis of garnet rims and adjacent phases in garnet amphibolite and pelitic schist from the structurally higher Taylor Mountain terrane and structurally lower Lake George subterrane indicate high-*P*, moderate-*T* metamorphism in both tectonic units. *P-T* conditions were 7 to 12.5 kbar at ~560°C to 650°C within the northern structural zone of the Taylor Mountain terrane in which displacement is consistently top-to-the-northeast, and 6 to 7 kbar at 560°C to 605°C within the southern structural zone in which lineations and shear-sense directions are variable. Tectonites within the Lake George subterrane crystallized under conditions of 8.2 to 12.5 kbar at ~600°C to 650°C. Preservation of growth zoning in garnet and absence of partial melting in both terranes suggest that temperatures did not exceed 600°C to 650°C. Within the Lake George subterrane, tectonites record dominantly top-to-the-northwest displacement in a northern zone and top-to-the-southeast displacement within a southern zone. Where the two shear-sense directions occur together, top-to-the-northwest displacement preceded top-to-the-southeast displacement and was more penetrative.

2. We interpret metamorphic and kinematic data to indicate that metamorphism of the Taylor Mountain terrane and Lake George subterrane took place during different phases of late Paleozoic to Jurassic contraction, resulting from closure of an ocean basin now represented by klippen of the Seventymile–Slide Mountain terrane. High-*P* metamorphism of the Taylor Mountain terrane took place within a southwest-dipping subduction system. ⁴⁰Ar/³⁹Ar data indicate rapid cooling of the Taylor Mountain terrane at ~186 Ma, our interpreted age of accretion of the outboard terranes onto the leading edge of North America (Lake George subterrane). High-*P* meta-

morphism of the Lake George subterrane resulted from crustal thickening caused by overthrusting of the Seventymile–Slide Mountain, Taylor Mountain, and (probably) Nisutlin terranes and by imbrication of the continental margin during continued convergence. Subsequent development of a northeast-dipping subduction system was probably a major factor in widespread crustal extension that unroofed the Lake George subterrane basement in Early Cretaceous time.

3. Our working hypothesis to explain the kinematic data that we have obtained thus far is that the northeast-vergent fabric in the northern zone of the Taylor Mountain terrane formed prior to final accretion of the terrane, that the northwest-vergent fabrics in the Lake George subterrane record subduction of the lower-plate continental crust, and that the southeast-vergent fabrics in the Lake George subterrane are extension related.

4. Several lines of evidence suggest that high-*P*, moderate-*T* metamorphism resulting from obduction of the outboard Seventymile–Slide Mountain, Taylor Mountain, and (probably) Nisutlin terranes onto the lower-plate Lake George subterrane was also a major event in the western and northwestern parts of the Yukon-Tanana upland.

Acknowledgments.—We are especially grateful to Susan Douglass and Charles Bacon for invaluable assistance in the field and microprobe analyses. We also wish to express our respect and admiration for the detailed and insightful reconnaissance mapping of the region by Helen Foster and the unselfish sharing of her knowledge of the area with us. Acknowledgment is also made to Kari Cooper for her artful and rapid preparation of the illustrations.

REFERENCES CITED

- Albee, A.L., and Ray, L., 1970, Correction factors for electron microprobe microanalysis of silicates, oxides, carbonates, phosphates and sulfates: *Analytical Chemistry*, v. 42, p. 1408–1414.
- Aleinikoff, J.N., Dusel-Bacon, Cynthia, and Foster, H.L., 1981a, Geochronologic studies in the Yukon-Tanana Upland, east-central Alaska, in Albert, N.R.D., and Hudson, Travis, eds., *The United States Geological Survey in Alaska: Accomplishments during 1979*: U.S. Geological Survey Circular 823-B, p. 34–37.
- , 1986, Geochronology of augen gneiss and related rocks, Yukon-Tanana terrane, east-central Alaska: *Geological Society of America Bulletin*, v. 97, p. 626–637.
- Aleinikoff, J.N., Dusel-Bacon, Cynthia, Foster, H.L., and Futa, K., 1981b, Proterozoic zircon from augen gneiss, Yukon-Tanana upland, east-central Alaska: *Geology*, v. 9, p. 469–473.
- Aleinikoff, J.N., Dusel-Bacon, Cynthia, Foster, H.L., and Nokleberg, W.J., 1987, Lead isotopic fingerprinting of tectono-stratigraphic terranes, east-central Alaska: *Can-*

- dian Journal of Earth Sciences, v. 24, p. 2089–2098.
- Aleinikoff, J.N., Foster, H.L., Nokleberg, W.J., and Dusel-Bacon, Cynthia, 1984, Isotopic evidence from detrital zircons for early Proterozoic crustal material, east-central Alaska, in Coonrad, W.L., and Elliott, R.L., eds., *The United States Geological Survey in Alaska: Accomplishments during 1981*: U.S. Geological Survey Circular 868, p. 43–45.
- Bacon, C.R., Foster, H.L., and Smith, J.G., 1990, Rhyolitic calderas of the Yukon-Tanana Terrane, east central Alaska: Volcanic remnants of a mid-Cretaceous magmatic arc: *Journal of Geophysical Research*, v. 95, p. 21,451–21,461.
- Bence, A.E., and Albee, A.L., 1968, Empirical correction factors for the electron microanalysis of silicates and oxides: *Journal of Geology*, v. 76, p. 382–403.
- Bennett, V.C., and Hansen, V.L., 1988, Neodymium isotopic similarities between the Yukon-Tanana terrane, Yukon Territory and continental North America [abs.]: *Geological Society of America Abstracts with Programs*, v. 20, no. 7, p. A111.
- Bohlen, S.R., and Liotta, J.J., 1986, A barometer of garnet amphibolites and garnet granulites: *Journal of Petrology*, v. 27, p. 1025–1034.
- Bohlen, S.R., Wall, V.J., and Boettcher, A.L., 1983, Experimental investigations and geological applications of equilibria in the system $\text{FeO-TiO}_2\text{-Al}_2\text{O}_3\text{-SiO}_2\text{-H}_2\text{O}$: *American Mineralogist*, v. 68, p. 1049–1058.
- Brown, E.H., and Forbes, R.B., 1986, Phase petrology of eclogitic rocks in the Fairbanks district, Alaska, in Evans, B.W., and Brown, E.H., eds., *Blueschists and eclogites*: *Geological Society of America Memoir* 164, p. 155–167.
- Churkin, M., Jr., Foster, H.L., Chapman, R.M., and Weber, F.R., 1982, Terranes and suture zones in east-central Alaska: *Journal of Geophysical Research*, v. 87, no. B5, p. 3718–3730.
- Cloos, Mark, 1985, Thermal evolution of convergent plate margins: Thermal modeling and reevaluation of isotopic Ar-ages for blueschists in the Franciscan Complex of California: *Tectonics*, v. 4, p. 421–433.
- Cloos, Mark, and Shreve, R.L., 1988, Subduction-channel model of prism accretion, melange formation, sediment subduction, and subduction erosion at convergent plate margins: 1. Background and description: *Pure and Applied Geophysics*, v. 128, p. 454–489.
- Cushing, G.W., 1984, The tectonic evolution of the eastern Yukon-Tanana upland, Alaska: Albany, N.Y., State University of New York, M.S. thesis, 255 p.
- Cushing, G.W., Foster, H.L., Harrison, T.M., and Laird, Jo, 1984, Possible Mesozoic accretion in the eastern Yukon-Tanana upland, Alaska [abs.]: *Geological Society of America Abstracts with Programs*, v. 16, no. 6, p. 481.
- Dewey, J.F., 1988, Extensional collapse of orogens: *Tectonics*, v. 7, p. 1123–1139.
- Dusel-Bacon, Cynthia, and Aleinikoff, J.N., 1985, Petrology and tectonic significance of augen gneiss from a belt of Mississippian granitoids in the Yukon-Tanana terrane, east-central Alaska: *Geological Society of America Bulletin*, v. 96, no. 4, p. 411–425.
- Dusel-Bacon, Cynthia, Csejtey, Béla, Foster, H.L., Doyle, E.O., Nokleberg, W.J., and Plafker, George, in press, Distribution, facies, ages, and proposed tectonic associations of regionally metamorphosed rocks in east- and south-central Alaska: U.S. Geological Survey Professional Paper 1497-C, 100 ms p., 2 pls.
- Dusel-Bacon, Cynthia, and Douglass, S.L., 1990, New thermobarometric evidence for high-pressure, medium-temperature metamorphism of two subterrane of the Yukon-Tanana composite terrane (YTT) in easternmost Alaska [abs.]: *Geological Association of Canada Programs with Abstracts*, v. 15, p. A35.
- Dusel-Bacon, Cynthia, and Foster, H.L., 1983, A sillimanite gneiss dome in the Yukon crystalline terrane, east-central Alaska: Petrography and garnet-biotite geothermometry: U.S. Geological Survey Professional Paper 1170-E, 25 p.
- Dusel-Bacon, Cynthia, and Hansen, V.L., 1991, High-pressure, medium-temperature early Mesozoic metamorphism and deformation within the Yukon-Tanana composite terrane, eastern Alaska [abs.]: *Geological Society of America Abstracts with Programs*, v. 23, p. 20.
- Erdmer, Phillippe, 1987, Blueschist and eclogite in mylonitic allochthons, Ross River and Watson Lake areas, south-eastern Yukon: *Canadian Journal of Earth Sciences*, v. 24, p. 1439–1449.
- Erdmer, Phillippe, and Armstrong, R.L., 1988, Permo-Triassic isotopic dates for blueschist, Ross River area, Yukon, in *Yukon Geology*, v. 2: *Exploration and Geological Services Division, Yukon, Indian and Northern Affairs, Canada*, p. 33–36.
- Erdmer, Phillippe, and Helmstaedt, Herwart, 1983, Eclogite from central Yukon: a record of subduction at the western margin of ancient North America: *Canadian Journal of Earth Sciences*, v. 20, p. 1389–1408.
- Foster, H.L., 1970, Reconnaissance geologic map of the Tanacross quadrangle, Alaska: U.S. Geological Survey Miscellaneous Geologic Investigations Map I-593, scale 1:250,000.
- 1976, Geologic map of the Eagle quadrangle, Alaska: U.S. Geological Survey Miscellaneous Investigations Map I-922, scale 1:250,000.
- Foster, H.L., and Keith, T.E.C., 1974, Ultramafic rocks of the Eagle quadrangle, east-central Alaska: U.S. Geological Survey Journal of Research, v. 2, no. 6, p. 657–669.
- Foster, H.L., Keith, T.E.C., and Menzie, W.D., 1987, Geology of east-central Alaska: U.S. Geological Survey Open-File Report 87-188, 59 p.
- Gareau, S.A., 1989, Metamorphism, deformation and geochronology of the Ecstall-Quaal rivers area, Coast plutonic complex, British Columbia, in *Current Research, Part E, Geological Survey of Canada Paper* 89-1E, p. 155–162.
- Graham, C.M., and Powell, R., 1984, A garnet-hornblende geothermometer: Calibration, testing, and application to the Pelona Schist, southern California: *Journal of Metamorphic Geology*, v. 2, p. 13–31.
- Hansen, V.L., 1989, Structural and kinematic evolution of the Teslin suture zone, Yukon: Record of an ancient transpressional margin: *Journal of Structural Geology*, v. 11, p. 717–733.
- 1990, Yukon-Tanana terrane: A partial acquittal: *Geology*, v. 18, p. 365–369.

- 1992a, Backflow and margin-parallel shear within an ancient subduction complex: *Geology*, v. 20, no. 1, p. 71–74.
- 1992b, *P-T* evolution of the Teslin suture zone and Cassiar tectonites, Yukon, Canada: Evidence for A- and B-type subduction: *Journal of Metamorphic Geology*, v. 10, p. 239–263.
- Hansen, V.L., Heizler, M.T., and Harrison, T.M., 1991, Mesozoic thermal evolution of the Yukon-Tanana composite terrane: New evidence from $^{40}\text{Ar}/^{39}\text{Ar}$ data: *Tectonics*, v. 10, p. 51–76.
- Harms, T.A., 1985, Pre-emplacement thrust faulting in the Sylvester allochthon, northeast Cry Lake map area, British Columbia: Geological Survey of Canada Paper 85-1A, p. 301–304.
- Harms, T.A., Coney, P.J., and Jones, D.L., 1984, The Sylvester allochthon, Slide Mountain terrane, British Columbia: A correlative of oceanic terranes of northern Alaska [abs.]: Geological Society of America Abstracts with Programs, v. 16, p. 288.
- Hawthorne, F.C., 1981, Crystal chemistry of the amphiboles in Amphiboles and other hydrous pyriboles—Mineralogy: Mineralogical Society of America Reviews in Mineralogy, v. 9A, p. 1–102.
- Hodges, K.V., and Crowley, P.D., 1985, Error estimation and empirical geothermobarometry for pelitic systems: *American Mineralogist*, v. 70, p. 702–709.
- Hodges, K.V., and McKenna, L.W., 1987, Realistic propagation of uncertainties in geologic thermobarometry: *American Mineralogist*, v. 72, p. 671–680.
- Hodges, K.V., and Spear, F.S., 1982, Geothermometry, geobarometry and the Al_2SiO_5 triple point at Mt. Moosilauke, New Hampshire: *American Mineralogist*, v. 67, p. 1118–1134.
- Holdaway, M.J., 1971, Stability of andalusite and the aluminum silicate phase diagram: *American Journal of Science*, v. 271, p. 97–131.
- Jones, D.L., Silberling, N.J., Coney, P.J., and Plafker, G., 1987, Lithotectonic terrane map of Alaska (west of the 141st Meridian): U.S. Geological Survey Miscellaneous Field Studies Map MF-1874-A, scale 1:2,500,000.
- Keith, T.E.C., Foster, H.L., Foster, R.L., Post, E.V., and Lehmbeck, W.L., 1981, Geology of an alpine-type peridotite in the Mount Sorenson area, east-central Alaska in Shorter contributions to general geology: U.S. Geological Survey Professional Paper 1170-A, p. A1–A9.
- Keskinen, M., 1989, Lithological and fluid compositional control of amphibole compositions and their potential as *P-T* indicators of regional metamorphism: An illustration from the Fairbanks Schist, Yukon crystalline terrane, Alaska [abs.]: Geological Society of America Abstracts with Programs, v. 21, no. 6, p. A275.
- Kohn, M.J., and Spear, F.S., 1990, Empirical calibration of geobarometers for the assemblage garnet-hornblende-plagioclase-quartz: *American Mineralogist*, v. 75, p. 89–96.
- Koziol, A.M., and Newton, R.C., 1988, Redetermination of the anorthite breakdown reaction and improvement of the plagioclase-garnet- Al_2SiO_5 -quartz geobarometer: *American Mineralogist*, v. 73, p. 216–223.
- Laird, Jo, Foster, H.L., and Weber, F.R., 1984, Amphibole eclogite in the Circle quadrangle, Yukon-Tanana Upland, Alaska, in Coonrad, W.L., and Elliott, R.L., eds., The United States Geological Survey in Alaska: Accomplishments during 1981: U.S. Geological Survey Circular 868, p. 57–60.
- Leake, B.E., 1978, Nomenclature of amphiboles: *Canadian Mineralogist*, v. 16, p. 501–520.
- Malavieille, J., 1987, Kinematics of compressional and extensional ductile shearing deformation in a metamorphic core complex of the northeastern Basin and Range: *Journal of Structural Geology*, v. 9, p. 541–554.
- McClelland, W.C., Gehrels, G.E., Samson, S.D., and Patchett, P.J., 1992, Protolith relations of the Gravina belt and Yukon-Tanana terrane in central southeastern Alaska: *Journal of Geology*, v. 100, no. 1, p. 107–123.
- Metcalf, Paul, and Clark, G.S., 1983, Rb-Sr whole-rock age of the Klondike Schist, Yukon Territory: *Canadian Journal of Earth Sciences*, v. 20, no. 5, p. 886–891.
- Monger, J.W.H., and Berg, H.C., 1987, Lithotectonic terrane map of western Canada and southeastern Alaska: U.S. Geological Survey Miscellaneous Field Studies Map MF-1874-B, scale 1:2,500,000.
- Mortensen, J.K., 1990, Significance of U-Pb ages for inherited and detrital zircons from Yukon-Tanana terrane, Yukon and Alaska [abs.]: Geological Association of Canada Programs with Abstracts, v. 15, p. A91.
- Mortensen, J.K., and Jilson, 1985, Evolution of the Yukon-Tanana terrane: Evidence from southeastern Yukon Territory: *Geology*, v. 13, no. 11, p. 806–810.
- Nelson, J., and Bradford, J., 1987, Geology of the area around the Midway deposit, northern British Columbia (1040/16): Canada, British Columbia Ministry of Energy, Mines and Petroleum Resources, Geological Fieldwork, 1986, Paper 1987-1, p. 181–192.
- Nelson, J., Bradford, J.A., Green, K.C., and Marsden, H., 1988, Geology and patterns of mineralization, Blue Dome map area, Cassiar district (104P/12): British Columbia Ministry of Energy, Mines and Petroleum Resources, Geological Fieldwork, 1987, Paper 1988-1, p. 233–243.
- Nokleberg, W.J., Foster, H.L., and Aleinikoff, J.N., 1989, Geology of the northern Copper River Basin, eastern Alaska Range, and southern Yukon-Tanana Basin, southern and east-central Alaska, in Nokleberg, W.J., and Fisher, M.A., eds., Alaskan Geological and Geophysical Transect, Field trip guidebook T104: American Geophysical Union, Washington, D.C., p. 34–63.
- Palmer, A.R., 1983, The decade of North American geology 1983 geologic time scale: *Geology*, v. 11, no. 9, p. 503–504.
- Pavlis, T.L., 1989, Middle Cretaceous orogenesis in the northern Cordillera: A Mediterranean analog of collision-related extensional tectonics: *Geology*, v. 17, no. 10, p. 947–950.
- Pavlis, T.L., Sisson, V.B., Foster, H.L., Nokleberg, W.J., and Plafker, George, in press, Mid-Cretaceous extensional tectonics of the Yukon-Tanana terrane, Trans-Alaskan Crustal Transect (TACT), east-central Alaska: *Tectonics*.
- Pavlis, T.L., Sisson, V.B., Nokleberg, W.J., Plafker, George, and Foster, Helen, 1988, Evidence for Cretaceous crustal extension in the Yukon crystalline terrane, east-central

- Alaska [abs.]: *Eos* (American Geophysical Union, Transactions), v. 69, p. 1453.
- Roddick, J.A., 1967, Tintina trench: *Journal of Geology*, v. 75, p. 23-33.
- Selverstone, Jane, Spear, F.S., Franz, Gerhard, and Morteani, Giulio, 1984, High-pressure metamorphism in the Tauern window, Austria: *P-T* paths from hornblende-kyanite-staurolite schists: *Journal of Petrology*, v. 25, part 2, p. 501-531.
- Sisson, V.B., Pavlis, T.L., and Dusel-Bacon, Cynthia, 1990, Metamorphic constraints on Cretaceous crustal extension in the Yukon crystalline terrane, east-central Alaska [abs.]: Geological Association of Canada, Mineralogical Association of Canada Annual Meeting, Programs with Abstracts, v. 15, p. A-122.
- Spear, F.S., and Kimball, K.L., 1984, RECAMP-A FORTRAN IV program for estimating Fe^{3+} contents in amphiboles: *Computers and Geosciences*, v. 10, no. 2-3, p. 317-325.
- Tempelman-Kluit, D.J., 1979, Transported cataclasite, ophiolite and granodiorite in Yukon: evidence of arc-continent collision: Geological Survey of Canada Paper 79-14, 27 p.
- Tempelman-Kluit, D.J., and Wanless, R.K., 1975, Potassium-argon age determinations of metamorphic and plutonic rocks in the Yukon crystalline terrane: *Canadian Journal of Earth Sciences*, v. 12, no. 11, p. 1895-1909.
- Thompson, A.B., and Tracy, R.J., 1979, Model systems for anatexis of pelitic rocks. Part I. Theory of melting reactions in the systems $KAlO_2$ - $NaAlO_2$ - Al_2O_3 - SiO_2 - H_2O : *Contributions to Mineralogy and Petrology*, v. 70, p. 429-438.
- Turner, F.J., and Weiss, L.E., 1963, Structural analysis of metamorphic tectonites: New York, McGraw-Hill, 545 p.
- Weber, F.R., Foster, H.L., Keith, T.E.C., and Dusel-Bacon, Cynthia, 1978, Preliminary geologic map of the Big Delta quadrangle, Alaska: U.S. Geological Survey Open-File Report 78-529A, scale, 1:250,000.
- Wheeler, J.O., Brookfield, A.J., Gabrielse, H., Monger, J.W.H., Tipper, H.W., and Woodsworth, G.J., 1988, Tectonic assemblage map of the Canadian Cordillera and adjacent parts of the United States of America (rev. ed.): Geological Survey of Canada Open File 1894, scale 1:2,000,000.
- Wheeler, J.O., and McFeely, P., 1987, Tectonic assemblage map of the Canadian Cordillera and adjacent parts of the United States of America: Geological Survey of Canada Open File 1565, scale 1:2,000,000.
- Wilson, F.H., and Shew, Nora, 1981, Map and tables showing preliminary results for potassium-argon age studies in the Circle quadrangle, Alaska, with a compilation of previous dating work: U.S. Geological Survey Open-File Report 81-889, scale 1:250,000.
- Wilson, F.H., Smith, J.G., and Shew, Nora, 1985, Review of radiometric data from the Yukon crystalline terrane, Alaska and Yukon Territory: *Canadian Journal of Earth Sciences*, v. 22, p. 525-537.

Reviewers: Virginia B. Sisson and James O. Eckert, Jr.

Some Facies Aspects of the Upper Part of the Kenai Group, Southern Kenai Peninsula, Alaska

By Romeo M. Flores and Gary D. Stricker

Abstract

Detailed facies characteristics of the upper part of the Beluga Formation and the lower and middle parts of the Sterling Formation, Kenai Peninsula, indicate deposition in anastomosing and meandering streams, respectively. The presence of coeval channel sandstones and of abundant crevasse-overbank and flood plain mudstone-siltstone associations suggests deposition by suspended-load anastomosed streams. The fine-grained flood plain sediments, as well as coal-carbonaceous shale associations, laterally separate small sandstone bodies of merging and diverging fluvial channels. The abundance of narrow point-bar sandstone bodies and crevasse-flood plain sandstones, siltstones, and mudstones indicates deposition in mixed-load meandering streams.

In both depositional systems, raised platforms served as sites of peat accumulation. The peat bodies formed as narrow, lenticular deposits parallel to the length of the meander belt and as broad, elongate deposits in the crevasse splay of an anastomosing fluvial complex. Peat bodies, and the resulting coalbeds, in the meandering river systems of the Sterling Formation tended to be thin because of lateral migration of the sequence. Those peat bodies that developed in the anastomosing river systems of the Beluga Formation tended to be thick because of vertical accretion of the sequence.

INTRODUCTION

The upper part of the Kenai Group in the Cook Inlet, Alaska, which includes the Miocene Beluga Formation and the Miocene and Pliocene Sterling Formation, contains subbituminous coals and lignites (Merritt and others, 1987) and coalbed methane (Magoon, 1990). These formations are exposed in steep beach cliffs along the eastern coast of Cook Inlet near Clam Gulch, Ninilchik, Anchor Point, and Homer, and along the northern shore of Kachemak Bay (fig. 1).

The Beluga Formation in the southern Kenai Peninsula is more than 1,500 m thick and consists of interbedded conglomeratic sandstones, sandstones, siltstones, mudstones, carbonaceous shales, and coalbeds

(fig. 2; Calderwood and Fackler, 1972). The Sterling Formation is composed of sandstones, siltstones, mudstones, carbonaceous shales, and coalbeds and is as much as 2,100 m thick (Hayes and others, 1976; Merritt and others, 1987).

The upper part of the Beluga Formation and lower part of the Sterling Formation are exposed in the vicinity of McNeil Canyon along the northern shore of Kachemak Bay (fig. 1). Here, the Beluga Formation is gray and the Sterling Formation is buff or light brown. The color change occurs at about coalbed B (figs. 3, 4) of Barnes and Cobb (1959), which defines the Homerian (Upper Miocene) and Clamgulchian (Upper Miocene to Pliocene) floral boundary of Wolfe and others (1966). During the summer of 1991, facies characteristics that include lithofacies associations (groups of rocks with common physical properties) and facies sequences (a succession of genetically related lithofacies associations) of the upper part of the Beluga and the lower and middle parts of the Sterling were studied at 35 measured sections to assess relationships of coalbed occurrence and distribution to depositional environments. Differentiation of facies characteristics between the Beluga and Sterling Formations was utilized to compare their depositional setting.

GEOLOGIC HISTORY

The Kenai Peninsula is located in the southeastern part of the Cook Inlet basin—the active forearc basin of the Aleutian subduction zone. Cook Inlet basin lies between a volcanic-plutonic terrane of the Aleutian and Alaskan Ranges to the northwest and an uplifted accretionary wedge of graywacke, argillite, chert, and mafic and ultramafic igneous rocks of the Chugach and Kenai Mountains to the southeast.

During deposition of the Beluga Formation, episodic detrital influx from the Aleutian and Alaskan Ranges occurred; however, the Kenai-Chugach Mountains were the primary provenance (Hartman and others, 1972;

Kirschner and Lyon, 1973; Hite, 1975; Hayes and others, 1976; Magoon and others, 1976; Rawlinson, 1984; Magoon, 1986). During deposition of the Sterling For-

mation, the Aleutian and Alaskan Ranges were the primary source of sediments (Kirschner and Lyon, 1973). Reinink-Smith (1990a) suggested that these contrasting

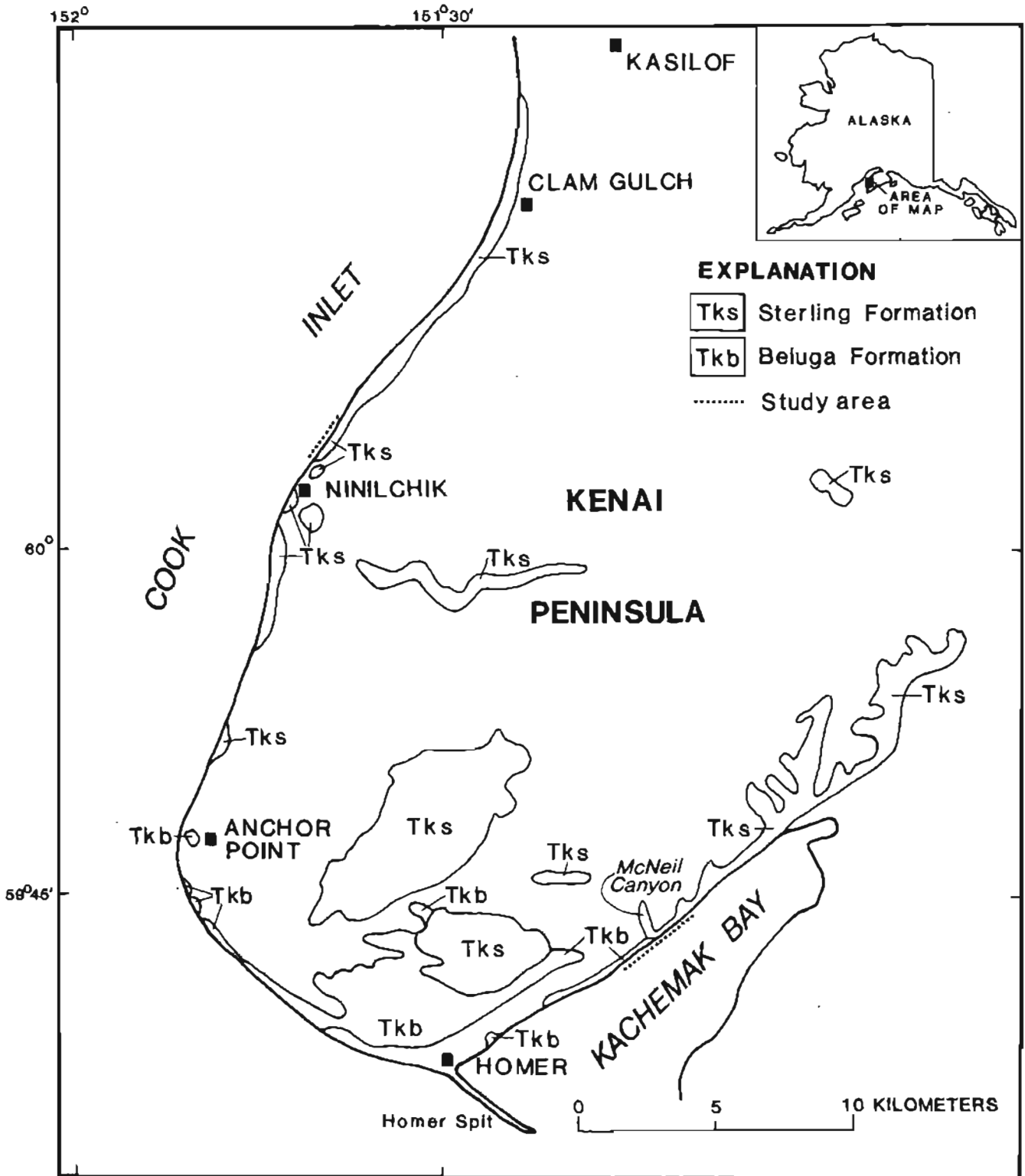


Figure 1. Location map of Kenai Peninsula showing outcrops of Beluga and Sterling Formations and study areas at eastern shore of Cook Inlet and along northern shore of Kachemak Bay (modified from Merritt and others, 1987).

sources for the Beluga and Sterling Formations were overprinted by volcanic activity related to the rise of the Alaska Range. Based on volcanic-ash partings in coalbeds, Reinink-Smith (1990a) indicated that an ash fall was recorded every 8,000 to 10,000 yr during deposition of the upper part of the Beluga and once every 11,000 yr during deposition of the lower part of the Sterling.

Previous interpretations of depositional environments of the Beluga and Sterling Formations were based on subsurface data (Hite, 1975, 1976; Hayes and others, 1976). Hayes and others (1976) suggested that deposition of the Beluga Formation was accomplished by small, high-gradient braided streams flowing on broad alluvial fans and plains, and that the Sterling Formation was deposited by large, meandering streams characterized by 9- to 14-m-thick point-bar sandstones.

LITHOFACIES ASSOCIATIONS

Lithofacies associations of the Beluga and Sterling Formations may be recognized as a combination of rock types with common lithologic properties (for example, color, grain size, mineral composition, internal structures, and body and ichno-fossil contents). The lithofacies associations include sandstone-dominated, mudstone-siltstone, and coal-carbonaceous shale associations.

ERA	PERIOD	EPOCH	GROUP	FORMATION THICKNESS (IN METERS)	DESCRIPTION	
Cenozoic	Tertiary	Upper Miocene to Pliocene	Kenai Group	Qual.	Alluvium and glacial deposits	
				Upper Miocene to Pliocene	Sterling Formation 0-2,100	Sandstone, siltstone, mudstone, carbonaceous shale, and lignites
				Upper Miocene	Beluga Formation >1,500	Sandstone, conglomeratic sandstone, siltstone, mudstone, carbonaceous shale, and subbituminous coalbeds
				Oligocene to upper Miocene	Tyonek Formation 1,200-2,350	Sandstone, mudstone, siltstone interbeds, and subbituminous coalbeds
				Oligocene	Hemlock Conglomerate 90-270	Sandstone and conglomerate
OLDER TERTIARY ROCKS						

Figure 2. Generalized stratigraphic column of Tertiary Kenai Group in Kenai Peninsula. Beluga and Sterling Formations comprise upper part of Kenai Group (modified from Calderwood and Fackler, 1972).

The mudstone-siltstone association consists of dark-gray mudstone and light- to dark-gray siltstone (figs. 3-5). The mudstone is either massive or crudely laminated, contains vertical and horizontal burrows, abundant finely macerated plant fragments, and plant root marks. The mudstone exhibits popcornlike weathered surfaces, indicating smectitic clay components (Reinink-Smith, 1990b). The siltstone exhibits current ripples, plant root marks, plant fragments, and vertical burrows. The mudstone-siltstone association may be randomly interbedded with current-rippled, rooted, burrowed, sandy siltstone; calcareous mudstone; and plant-rich ferruginous or hematite-rich sandy siltstone.

The mudstone-siltstone association is commonly capped by fine- to medium-grained sandstone of the sandstone-dominated association with which it constitutes a coarsening-upward sequence (figs. 3-5). The sandstone cap of the mudstone-siltstone association contains current-ripple laminations and small-scale (<7.5 cm thick) trough crossbeds and is frequently locally incised by trough-crossbedded sandstones with erosional bases. Several coarsening-upward sequences are vertically stacked to as thick as 30 m. In addition, the sandstone-dominated association consists of lag sandstones that fine upward (from pebbly to fine grained) and have erosional bases (figs. 3-5). Color varies from gray to light gray for the Beluga sandstones and buff for the Sterling sandstones. The sandstone-dominated association ranges from 3 to 15 m thick and varies from a single body to vertically stacked multiscoured (internally divided by erosional surfaces) and multilateral (laterally offset) bodies. The lower part of the sandstone bodies is trough crossbedded (1 m high and 13 m long) as well as convolute bedded (1.5 m high and 75 m long). The upper parts of the sandstone bodies exhibit current-ripple laminations and small- to medium-scale trough crossbeds ranging from 15 to 45 cm high. In places, some of the sandstone bodies are divided into smaller inclined subbodies by siltstone and mudstone drapes that extend from the margin to the interior of the body. A rare type of sandstone-dominated association is a basally erosional body consisting of inclined, rippled silty sandstone and siltstone-mudstone couplets that assumed the dominantly concave shape of the erosional surface (fig. 5), which lies about 15 m above the base of the section.

The coal-carbonaceous shale association comprises subbituminous coals and lignites intercalated with, as well as underlain and overlain by, black, plant-rich carbonaceous shale (figs. 3-5). The coals are mostly dull with vitrain bands distributed throughout the beds. Coal petrology work by Merritt and others (1987) indicated that vitrinite, representing the woody parts of trees, is relatively constant in percent in both the Beluga and Sterling coals. However, the higher quality coals of the Beluga Formation are richer in liptinites than the lower

UPPER BELUGA COMPOSITE SECTION (MCNEIL CANYON AREA)

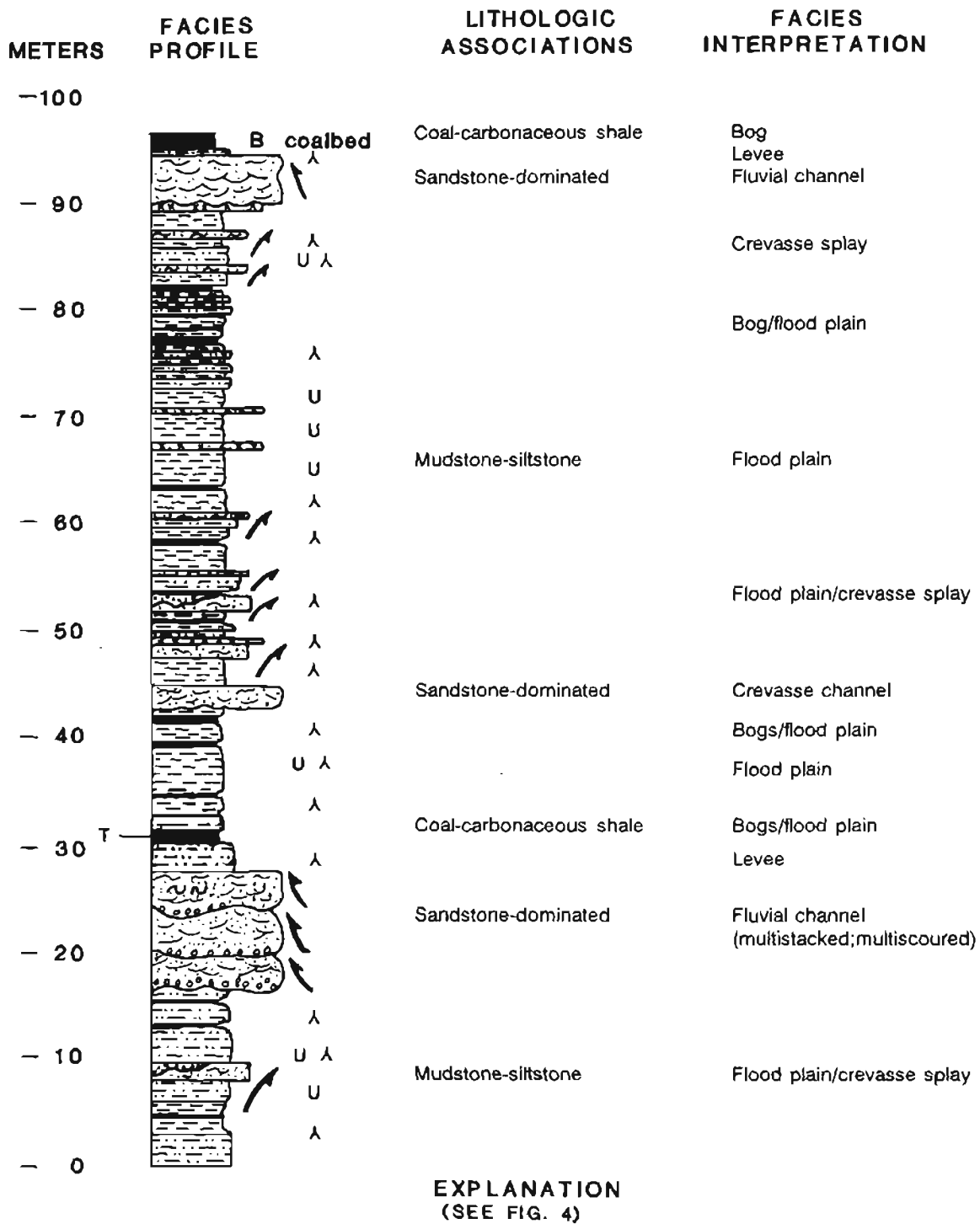
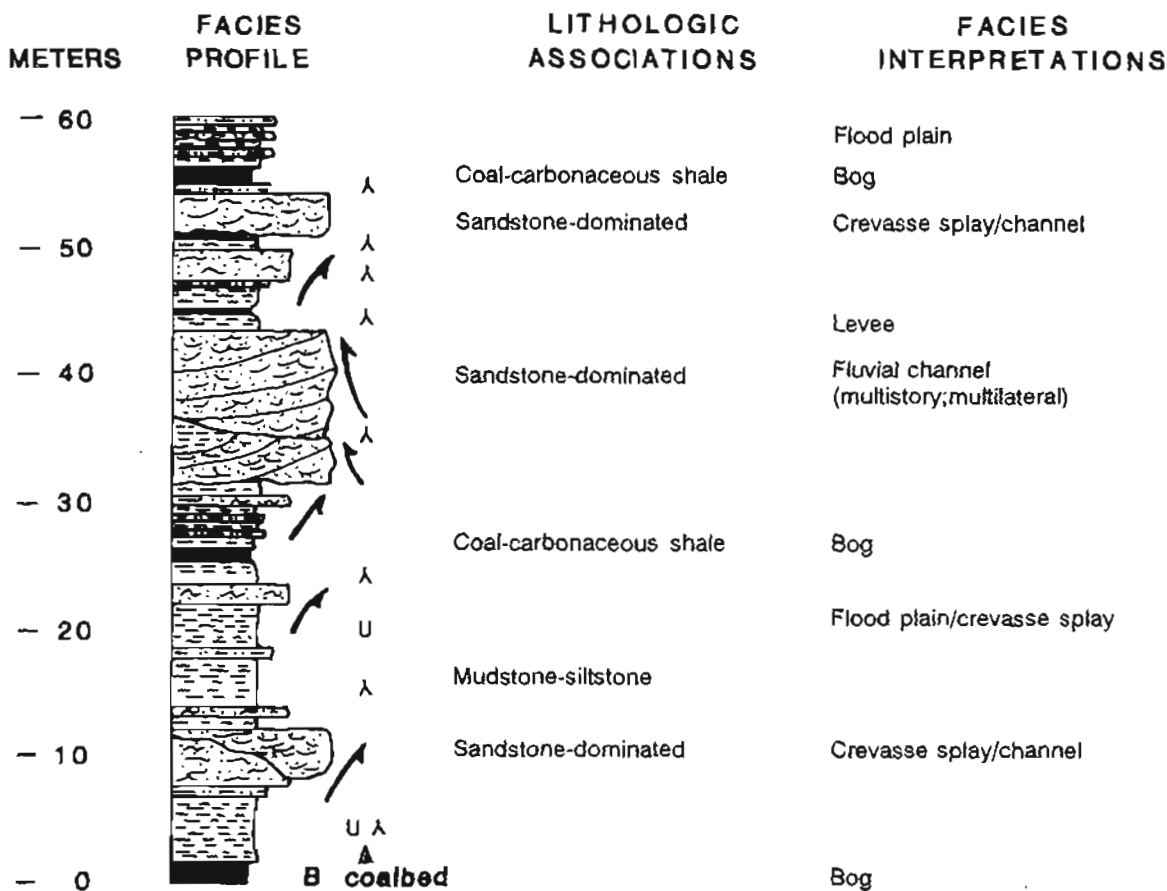


Figure 3. Facies profile, lithologic associations, and facies interpretations of upper part of Beluga Formation in McNeil Canyon area.

quality coals of the Sterling Formation. Beluga coals are low in inertinites, and the Sterling coals are high in inertinites (Merritt and others, 1987). The upper part of some coalbeds in the Sterling Formation have petrified tree trunks in growth position. The coalbeds are as thick

as 3.8 m and are laterally continuous (>3 km). Carbonaceous shales consist of fissile, mixed clay and very finely macerated plant fragments, and commonly they contain root marks. Carbonaceous shale is a common parting in coalbeds along with volcanic-ash partings (Reinink-Smith,

LOWER STERLING COMPOSITE SECTION (MCNEIL CANYON AREA)



EXPLANATION

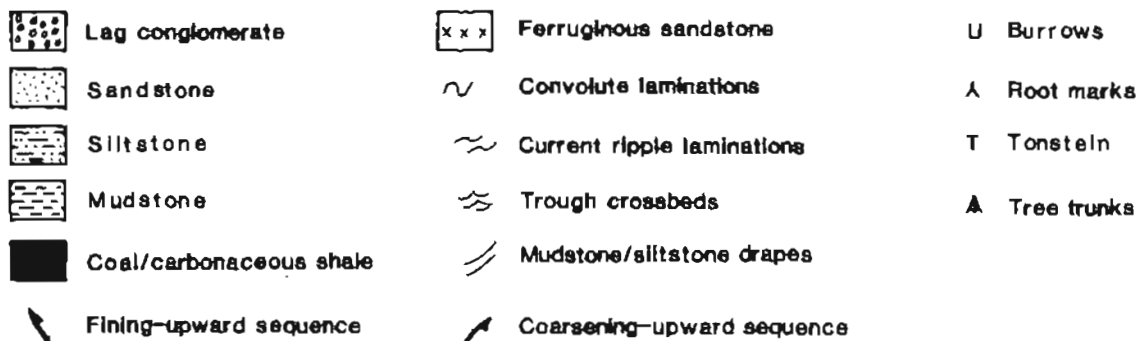


Figure 4. Facies profile, lithologic associations, and facies interpretations of lower part of Sterling Formation in McNeil Canyon area.

1990b). The volcanic-ash, or tonstein, partings are white to brownish in color, consist of pumice fragments, and are as thick as 0.3 m. The coalbeds in the lower part of the Sterling Formation contain more tonsteins than coalbeds of the upper part of the Beluga Formation. Mudstone and siltstone also are common partings in the coalbeds. They range from 0.005 to 3 m thick, are root marked, and contain dispersed smectite clays.

VERTICAL FACIES SEQUENCES

Upper Part of the Beluga Formation

The uppermost 100 m of the Beluga Formation at McNeil Canyon is largely composed of mudstone-siltstone associations with subordinate sandstone-dominated and coal-carbonaceous shale associations (fig. 3). The

MIDDLE STERLING COMPOSITE SECTION (NINILCHIK AREA)

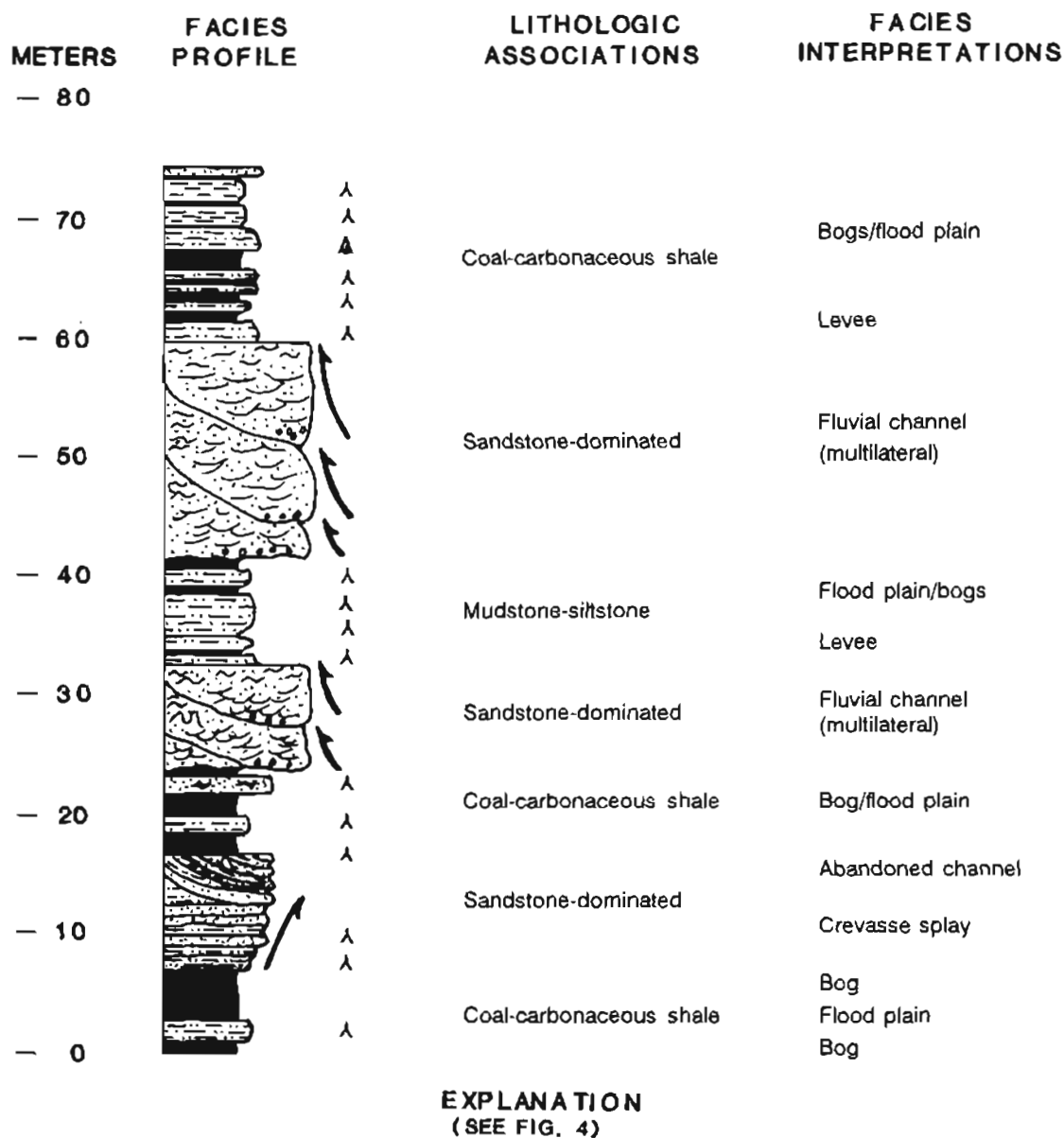


Figure 5. Facies profile, lithologic associations, and facies interpretations of middle part of Sterling Formation in Ninilchik area.

mudstone-siltstone associations, in the middle part of the study interval, contain caps of silty sandstone of the sandstone-dominated association, thus forming stacked, coarsening-upward facies sequences. Each silty sandstone cap includes a thin (1.5–3 m thick), fine-grained sandstone with a scoured base. This sandstone may also occur as a single body in the lower and middle parts of the coarsening-upward facies sequence.

The study interval contains sandstone-dominated and coal-carbonaceous shale associations at several stratigraphic levels (fig. 3). The sandstone-dominated association occurs either as thick, stacked, multiscoured, fining-upward conglomeratic sandstones or as individual fining-upward sandstone bodies. The stacked, multiscoured sandstone facies sequence is 13 m thick. This sandstone body is overlain by a thick (0.82 m) coal-carbonaceous shale association with 0.3-m-thick tonstein parting (fig. 3). The single, fining-upward sandstone is overlain by the 1.3-m-thick coal-carbonaceous shale association of the B coalbed (fig. 3).

The vertical and lateral variations of the lithofacies associations of the Beluga Formation below the B coalbed of Barnes and Cobb (1959) are shown in figure 6. The fining-upward, single and multiscoured sandstone in the upper

part of the cross section is coeval. These sandstone facies sequences are as thick as 5.5 m and 0.4 km in width and are overlain by a thick, coal-carbonaceous shale association. Also, they merge laterally with and are underlain by thick, stacked mudstone-siltstone associations with local sandstone caps of coarsening-upward facies sequences.

Lower and Middle Parts of the Sterling Formation

The lower and middle parts of the Sterling Formation in the McNeil Canyon and Ninilchik areas consist largely of sandstone-dominated and coal-carbonaceous shale associations and subordinately of a mudstone-siltstone association (figs. 4, 5). The sandstone-dominated association is mainly composed of multistory (stacked sandstone bodies separated by fine-grained deposits), multilateral (laterally offset sandstone bodies), fining-upward sandstone facies sequences as thick as 20 m and laterally traceable for as much as 0.4 km (figs. 4, 5, 7).

The lower part of the Sterling Formation studied in the McNeil Canyon area is 60 m thick and may be grouped into several facies sequences (fig. 4). The lower part of the studied interval is characterized by a

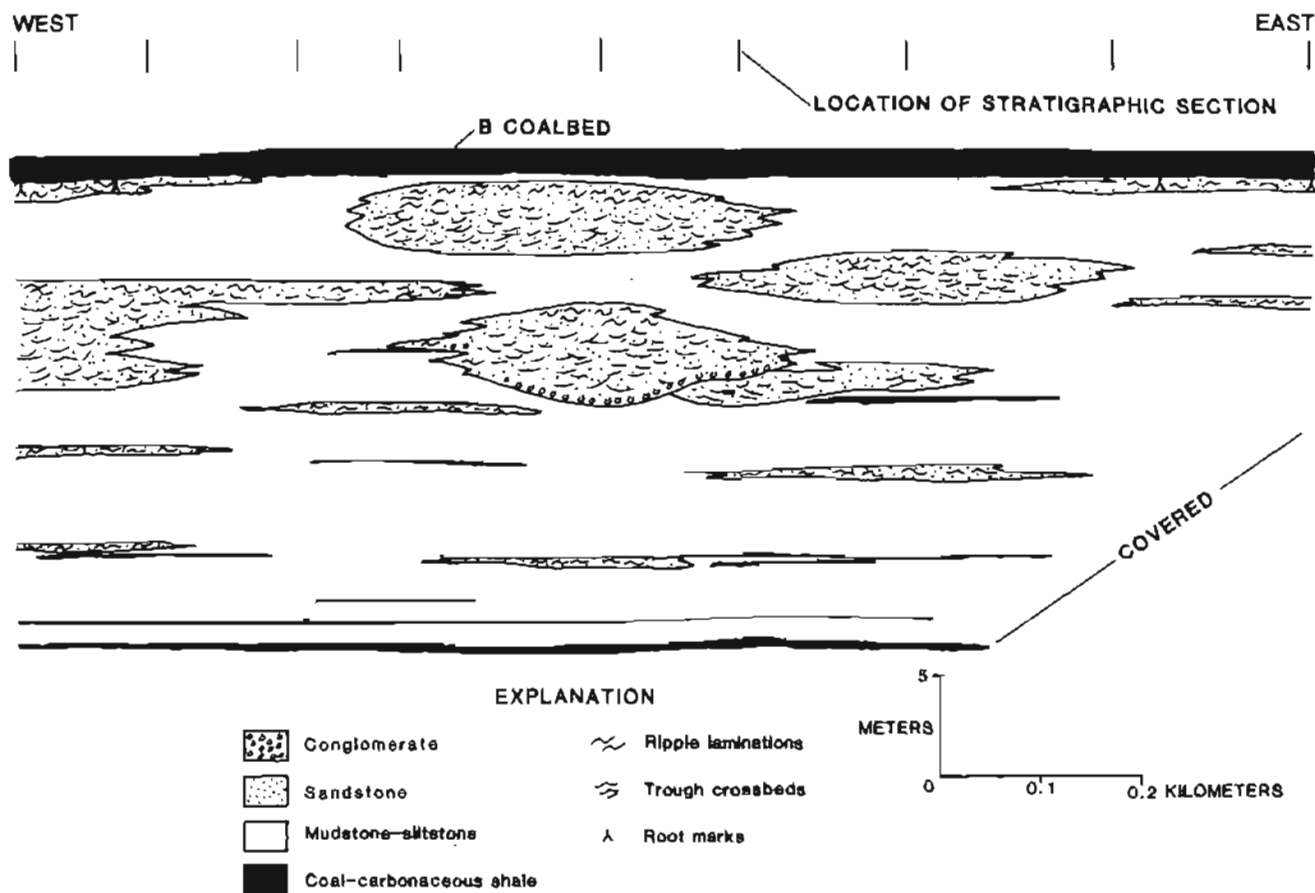


Figure 6. Stratigraphic cross section of uppermost part of Beluga Formation west of McNeil Canyon.

mudstone-siltstone association with sandstone caps forming a series of well-developed coarsening-upward facies sequences. The upper part of the studied interval consists mainly of a sandstone-dominated association containing multistory, multilateral, and fining-upward sandstone facies sequences that consist of small inclined sandstone bodies separated by very thin mudstone-siltstone drapes. In addition, these facies sequences are overlain by coarsening-upward sandstone and single-bodied fining-upward sandstone facies sequences. These sequences are interbedded with a 0.3- to 1.3-m-thick coal-carbonaceous shale association and a 6-m-thick mudstone-siltstone association.

Vertical and lateral lithofacies variations of the upper part of the Sterling Formation at McNeil Canyon are shown in figure 7. The sandstone bodies are multistory and multilateral in the upper part of the cross section. The sandstone bodies are stacked and are as thick as 10 m and as wide as 0.4 km. Each sandstone facies sequence contains inclined point-bar sandstones that are 3.5 m high. The sandstones grade laterally into the mudstone-siltstone association. The lower part of the cross section consists mainly of a coarsening-upward sandstone facies sequence that grades laterally into a mudstone-siltstone association.

The middle part of the Sterling Formation studied in the Ninilchik area is a 75-m-thick interval and may also

be grouped into several facies sequences (fig. 5). The lower part of the interval includes a coarsening-upward sandstone facies sequence. This sequence is capped by inclined beds of silty sandstone and siltstone-mudstone couplets of the sandstone-dominated association, which is marked by an erosional base. The upper part of the interval consists of fining-upward, multilateral, and multiscoured sandstone facies sequences. These facies sequences are interbedded with 0.2- to 3.8-m-thick sequence of the coal-carbonaceous shale association and 0.3- to 6-m-thick sequences of the mudstone-siltstone association.

FACIES INTERPRETATIONS AND CONCLUSIONS

Variations in the facies characteristics of the upper part of the Beluga and lower and middle parts of the Sterling Formations reflect differences in the depositional environments. The mudstone-siltstone, coal-carbonaceous shale, and sandstone-dominated associations of these formations were all deposited in a fluvial system. In general, these lithologic associations represent overbank-flood plain, bog, and channel deposits, respectively (fig. 8A, B).

The abundance of mudstone-siltstone association in the upper part of the Beluga Formation suggests that the

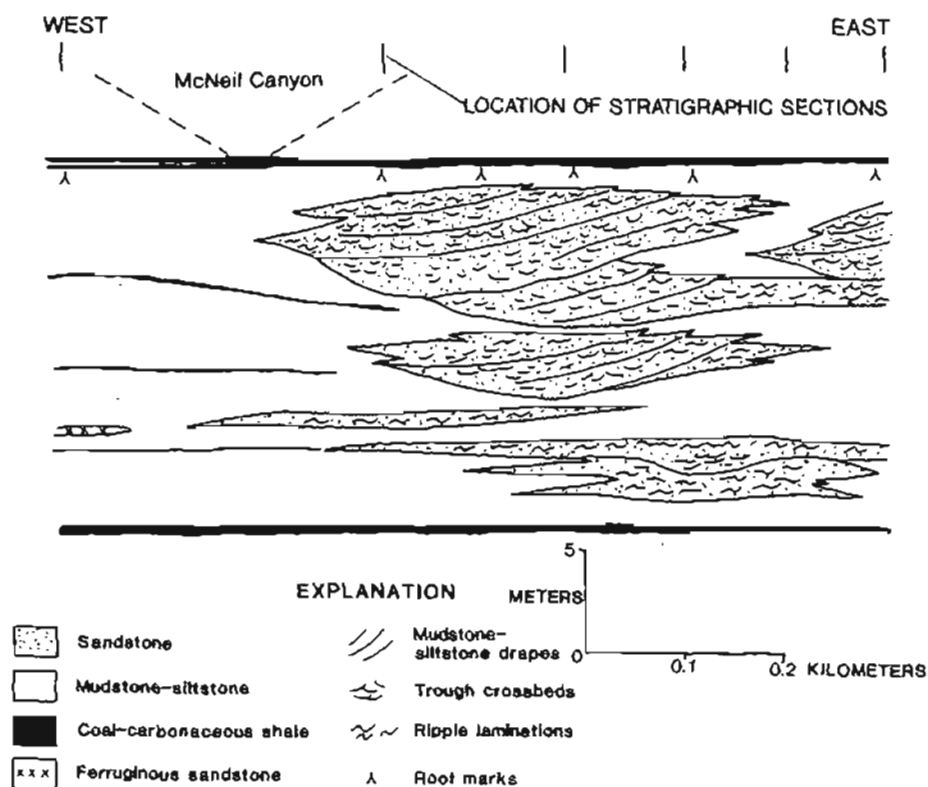


Figure 7. Stratigraphic cross section of upper part of study interval of Sterling Formation east of McNeil Canyon.

fluvial environment was dominated by suspended-load sediments (fig. 8A), which were mainly accreted vertically as thick overbank-flood plain deposits. The coarsening-upward facies sequences of the mudstone-siltstone association, which represent deposits of crevasse-splay channel complexes, suggest that the sediment load was transported into the flood plain via a breach in the levee during flood events. The vertically accreted mudstone-siltstone association reflects rapid subsidence by sediment compaction and basin subsidence. The occurrence of thick overbank-flood plain sediments that merge laterally with crevasse-splay sediments and thick, narrow, coeval sandstone bodies with erosional bases represents deposition

by an anastomosed fluvial system. In addition, confinement of fluvial channels by thick overbank-flood plain sediments resulted in deposition of narrow, stacked, fining-upward multiscoured sandstone facies sequences. The coal-carbonaceous shale association of the upper part of the Beluga Formation represents peat accumulation in bogs that formed on topographically high platforms built by overbank-flood plain crevasse fluvial channel sediments. These bog platforms were removed from detrital influx that allowed sufficient time for the accumulation of thick peat deposits. However, bogs formed on low-lying areas were commonly inundated by floodwaters that transported flocculated clays into the bog,

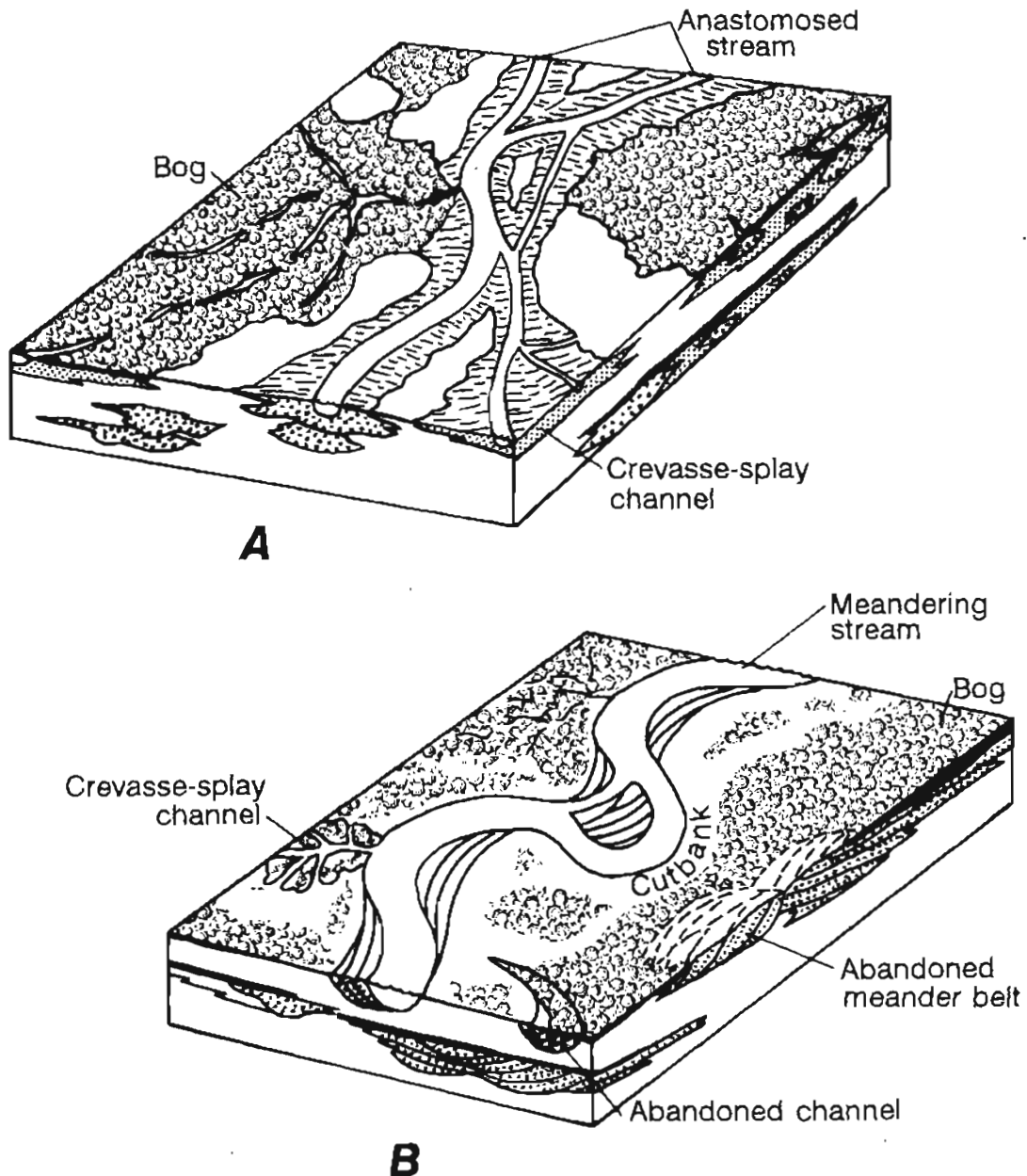


Figure 8. Diagrammatic depositional models in the McNeil Canyon and Ninilchik study areas. A, Beluga Formation. B, Sterling Formation.

which mixed with plant material and formed carbonaceous shale.

Our interpretation of deposition by anastomosing streams for the Beluga Formation at McNeil Canyon differs from that of Hayes and others (1976). They interpreted the Beluga as having been deposited by braided streams flowing on broad alluvial fans and plains. Two decades ago, Schumm (1968) suggested that braided streams refer to rivers in which flow diverges and rejoins around constantly shifting sand and gravel bars, whereas anastomosed streams reflect a river that divides into more permanent subchannels that are separated by fine-grained flood plain sediments. The largely fine-grained sediments juxtaposed with thin, narrow, coeval channel sandstones in the Beluga Formation at McNeil Canyon suggest deposition in anastomosed streams as defined by Schumm (1968). In addition, the fine-grained sediments formed in subaqueous flood plains, as indicated by associated animal burrows. The intervening flood plains of the anastomosed streams also formed low-lying bogs, as reflected by the coal-carbonaceous shale association interbedded with the mudstone-siltstone association. These depositional settings were described by Smith and Smith (1980) and Smith (1983) in their discussion of the anastomosing streams of the upper Columbia and Saskatchewan Rivers of Canada and the Magdalena River in Colombia.

In the lower and middle parts of the Sterling Formation, the development of thick, coarsening-upward sequences of the mudstone-siltstone association and moderately thick, fining-upward, multistory and multilateral sandstone facies sequences suggests deposition by a mixed-load fluvial system (fig. 8B). The mud, silt, and sand were deposited in small meandering fluvial systems, as indicated by moderately thick channel sandstones of limited width. Lateral migration developed by erosion on the cutbank side of meanders and deposition on point bars on the opposite side, as indicated by inclined sandstone bodies separated by mudstone-siltstone drapes. The presence of multilateral sandstone bodies provides evidence that the meandering fluvial channel migrated laterally by multiple cut-and-fill of channel cut-offs. However, lateral migration by avulsion via chute cutoff through necks of meander bends resulted in abandoned channels or channel plugs, as indicated by the inclined beds of the sandstone and siltstone-mudstone couplets with an erosional base. These sandstone bodies are similar to deposits of mixed-load or meandering fluvial systems described by Schumm (1977, p. 95-178) and Galloway (1985). Overbank-flood plain deposits associated with this fluvial system include sandy sediments that were transported into the flood plain by breaching through levees. Crevasse sedimentation via these breaches disrupted peat accumulation in bogs on the flood plain and resulted in formation of the thin coal-

carbonaceous shale associations. However, abandoned meander belts formed by avulsion and removed from detrital influx served as elevated platforms and permitted accumulations of thick peat bog deposits, as displayed in the Ninilchik section. That is, broad (wide and long) buildup of crevasse-splay and anastomosed stream deposits formed large platforms on which peat bogs accumulated.

Our interpretation of small meandering streams for the Sterling Formation at McNeil Canyon and Ninilchik differs from that of Hayes and others (1976), who suggested that the Sterling was deposited by large meandering streams. Development of point-bar sandstones with average thickness of 4 m in our study areas, compared with 9- to 14-m-thick point-bar sandstones observed elsewhere by Hayes and others (1976), clearly indicates deposition in small meandering fluvial channels. In addition, the 30-m width of channel-plug deposits and 400-m width of the channel sandstones support deposition of the Sterling Formation in a small, narrow, meandering fluvial system.

In conclusion, facies analysis of the Beluga and Sterling Formations suggests deposition in narrow-channelled, anastomosing (suspended load) and small meandering (mixed-load) fluvial systems, respectively. Vertical aggradation in the anastomosing fluvial system and lateral erosion and deposition in the meandering fluvial system probably controlled thick-to-thin peat accumulation in bogs of these fluvial systems. Thick and laterally extensive peats are more likely to be preserved in deposits in vertically aggrading anastomosing streams than in laterally aggrading meandering streams. Thus, the difference in depositional processes of the fluvial systems explains the original observation of Barnes and Cobb (1959), that coals are thicker in the Beluga Formation than in the Sterling Formation in the Kenai Peninsula.

REFERENCES CITED

- Barnes, F.F., and Cobb, E.H., 1959, Geology and coal resources of the Homer district, Kenai coal field, Alaska: U.S. Geological Survey Bulletin 1058-F, p. 217-260.
- Calderwood, K.W., and Fackler, W.C., 1972, Proposed stratigraphic nomenclature for the Kenai Group, Cook Inlet basin, Alaska: American Association of Petroleum Geologists Bulletin, v. 56, no. 4, p. 739-754.
- Galloway, W.E., 1985, Meandering streams—Modern and ancient, in Flores, R.M., Ethridge, F.G., Miall, A.O., Galloway, W.E., and Fouch, T.D., eds., Recognition of fluvial depositional systems and their resource potential: Society of Economic Paleontologists and Mineralogists Short Course No. 19, p. 145-166.
- Hartman, D.C., Pessel, G.H., and McGee, D.L., 1972, Preliminary report on stratigraphy of Kenai Group upper Cook Inlet, Alaska: Alaska Division of Geological and Geophysical Surveys Special Report 5, 4 p., 7 maps, 1 pl., scale 1:500,000.

- Hayes, J.B., Harms, J.C., and Wilson, T., Jr., 1976, Contrasts between braided and meandering stream deposits, Beluga and Sterling Formations (Tertiary), Cook Inlet, Alaska, in Miller, T.P., ed., *Recent and ancient sedimentary environments in Alaska*: Anchorage, Alaska Geological Society, p. J1-J27.
- Hite, D.M., 1975, Some sedimentary aspects of the Kenai Group, Cook Inlet, Alaska, in Sisson, A., ed., *Guide to the geology of the Kenai Peninsula, Alaska*: Anchorage, Alaska Geological Society, Anchorage, p. 3-19.
- 1976, Some sedimentary aspects of the Kenai Group, Cook Inlet, Alaska, in Miller, T.P., ed., *Recent and ancient sedimentary environments in Alaska*: Anchorage, Alaska Geological Society, p. I1-I23.
- Kirschner, C.E., and Lyon, C.A., 1973, Stratigraphic and tectonic development of Cook Inlet petroleum province, in Pitcher, M.G., ed., *Arctic geology*: American Association of Petroleum Geologists Memoir 19, p. 396-407.
- Magoon, L.B., 1990, Oil-source rock correlations using carbon isotope data and biological marker compounds, Cook Inlet-Alaska Peninsula, Alaska [abs.]: American Association of Petroleum Geologists Bulletin v. 74, p. 711.
- Magoon, L.B., Adkison, W.L., and Egbert, R.M., 1976, Map showing geology, wildcat wells, Tertiary plant fossil localities, K-Ar age dates, and petroleum operations, Cook Inlet area, Alaska: U.S. Geological Survey Miscellaneous Geologic Investigations Map I-1019, 3 sheets, scale 1:250,000.
- Magoon, L.B., ed., 1986, Geologic studies of the lower Cook Inlet COST No. 1 Well, Alaska outer continental shelf: U.S. Geological Survey Bulletin 1596, 99 p.
- Merritt, R.D., Lueck, L.L., Rawlinson, S.E., Belowich, M.A., Goff, K.M., Clough J.C., and Reinink-Smith, L.M., 1987, Southern Kenai Peninsula (Homer district) coal-resource assessment and mapping project: Alaska Division of Geological and Geophysical Surveys Public-Data File 87-15, 125 p.
- Rawlinson, S.E., 1984, Environments of deposition, paleocurrents, and provenance of Tertiary deposits along Kachemak Bay, Kenai Peninsula, Alaska: *Sedimentary Geology*, v. 38, p. 421-442.
- Reinink-Smith, L.M., 1990a, Relative frequency of Neogene volcanic events as recorded in coal partings from the Kenai lowland, Alaska: A comparison with deep-sea core data: *Geological Society of America Bulletin*, v. 102, p. 830-840.
- 1990b, Mineral assemblages of volcanic and detrital partings in Tertiary coalbeds, Kenai Peninsula, Alaska: *Clays and Clay Minerals*, v. 38, no. 1, p. 97-108.
- Schumm, S.A., 1968, Speculations concerning paleohydrologic controls of terrestrial sedimentation: *Geological Society of America Bulletin*, v. 79, p. 1573-1588.
- 1977, *The fluvial system*: New York, Wiley, 338 p.
- Smith, D.G., 1983, Anastomosed fluvial deposits—Modern examples from western Canada, in Collinson, J.D., and Lewin, J., eds., *Modern and ancient fluvial systems*: International Association of Sedimentologists Special Publication 6, p. 155-168.
- Smith, D.G., and Smith, N.D., 1980, Sedimentation in anastomosed river systems—Examples from alluvial valleys near Banff, Alberta: *Journal of Sedimentary Petrology*, v. 50, p. 157-164.
- Wolfe, J.A., Hopkins, D.M., and Leopold, E.B., 1966, Tertiary stratigraphy and paleobotany of the Cook Inlet region, Alaska: U.S. Geological Survey Professional Paper 398-A, p. A1-A29.

Reviewers: Edwin R. Landis and Richard G. Stanley

Sedimentology of the Bay of Pillars and Point Augusta Formations, Alexander Archipelago, Alaska

By Susan M. Karl and Closey F. Giffen

Abstract

The Bay of Pillars and Point Augusta Formations are Silurian marine siliciclastic units mapped in the Alexander archipelago in the southern part of the Alexander terrane. These rock units have been correlated and used to measure right-lateral offset on the Chatham Strait fault by previous workers. Our sedimentologic studies, measured sections, and point counts of these rocks indicate that the Bay of Pillars and Point Augusta Formations are lithologically similar but not identical, and that Silurian sandstone present in the Chilkat Mountains is identical in composition to the Point Augusta Formation, supporting correlation of these rock units by previous workers. The Point Augusta Formation is herein geographically extended to include the sandstone in the Chilkat Mountains. The Bay of Pillars Formation is significantly more volcanogenic than the Point Augusta Formation and consists largely of innerfan facies deposits. The Point Augusta Formation is more calcareous, thinner bedded, and has a greater proportion of midfan facies deposits than does the Bay of Pillars Formation. Both units, nonetheless, have similar sandstone compositions that indicate magmatic-arc provenances with dissected-arc orogen sources. Distinctive red syenitic cobbles suggest a similar source for conglomerates of the two units. Both units are interpreted to represent parts of turbidite aprons formed around volcanic islands with fringing limestone reefs. Distinctive deposits of interbedded black carbonaceous, calcareous mudstone and white limestone occur in both formations and are interpreted to represent an interchannel facies. It is likely that the Bay of Pillars and Point Augusta Formations are spatially related. Consequently, estimates of offset on the Chatham Strait fault are justified; however, the lack of marker beds precludes precise measurement. The significant granitic source component in both units suggests that the Alexander volcanic arc has continental rather than oceanic basement. Sandstone compositions indicate entirely local sources and support paleontologic studies that suggest that the Alexander arc was isolated from North America in the Silurian, despite its paleobiogeographic ties to North America.

INTRODUCTION

Paleozoic sedimentary rocks of the Alexander terrane are important because they are only mildly

deformed and their low metamorphic grade allows preservation of critical clues to the depositional and tectonic history of the Alexander arc. There has been debate about the oceanic versus continental nature of the crust underlying the Alexander arc (Armstrong, 1985; Samson and others, 1989), about whether or not the arc was originally part of North America (Gehrels and Saleeby, 1987a; Savage, 1988; Soja, 1991), and about where the arc was before collision and accretion to North America in the Cretaceous (Hillhouse and Grommé, 1980; Haeussler and others, in press). Also, because the rocks are relatively well preserved, they have been used as a basis for correlations made in measuring 150 to 200 km of offset on the right-lateral Chatham Strait fault (Lathram, 1964; Ovenshine and Brew, 1972; Loney and others, 1975; Hudson and others, 1982). The siliciclastic rocks of the Bay of Pillars and Point Augusta Formations compose part of the basis for these correlations (fig. 1). The composition of the sandstones in these units also provides information about source terranes and the nature of the basement of the Alexander volcanic arc.

Alexander Terrane

The Alexander terrane is an allochthonous crustal block with a long history of rifting, amalgamation, and accretion. It is composed of a succession of Precambrian(?) to Quaternary, dominantly sedimentary and volcanic rocks (fig. 2). The oldest rocks consist of pelitic schist, marble, metabasite, and metarhyolite of the Wales Group (Eberlein and others, 1983); these rocks are interpreted to represent a rift assemblage (S.M. Karl, unpub. data). The Wales Group was intruded by Late Cambrian diorite to granodiorite (Gehrels and Saleeby, 1987b). These rocks are metamorphosed to greenschist and amphibolite facies and are unconformably overlain by lower grade Ordovician and Silurian basaltic and andesitic flows and breccia and by volcanoclastic turbidites of the Descon Formation (Eberlein and others, 1983). The Descon Formation is gradationally overlain by the Silurian Heceta Limestone, a reef complex (Soja, 1991), and by the Silurian calcareous and volcanoclastic rocks

of the Bay of Pillars Formation. The older rocks are also intruded by Silurian to Devonian syenitic to trondhemitic plutons. The Devonian and older rocks are depositionally overlain by Devonian limestone, shallow-water calcarenite, or polymictic conglomerate that contains abundant red syenitic cobbles. The upper Paleozoic part of the sequence consists of Devonian basaltic, andesitic, and rhyolitic volcanic and volcanoclastic rocks, representing continuing arc activity, overlain by a thick section of Mississippian carbonate rocks and Permian carbonate and clastic rocks. Major unconformities throughout the Alexander terrane underlie Upper Triassic conglomerate, limestone, and bimodal basalt and rhyolite; Jurassic to Cretaceous mafic to intermediate volcanic and volcanoclastic rocks; Paleocene polymictic conglomerate; and Eocene to Quaternary basalt, andesite, and rhyolite.

Timing of amalgamation of the Alexander terrane with adjacent magmatic arc terranes is constrained by

Pennsylvanian tonalitic plutons that intruded its western contact with the Wrangellia terrane (Gardner and others, 1988) and by deposition of the Gravina belt overlap assemblage on its eastern contact with the Taku terrane (Berg and others, 1978; Brew and Karl, 1988). These amalgamated terranes were accreted to North America in the mid- to Late Cretaceous, based on the timing of deformation and metamorphism of the Jurassic and Cretaceous Gravina belt volcanic and volcanoclastic rocks.

Isotopic and chemical analyses of igneous rocks from the Alexander magmatic arc provide ambiguous results with respect to the nature of the crust underlying the Alexander terrane. Interpretation of Nd/Sm isotopes from a variety of sedimentary and igneous samples suggests a primitive origin (Samson and others, 1989). However, $^{87}\text{Sr}/^{86}\text{Sr}$ isotopes for Silurian plutons range from 0.7036 to 0.7212 (Armstrong, 1985) and are interpreted to indicate assimilation of older continental crust.

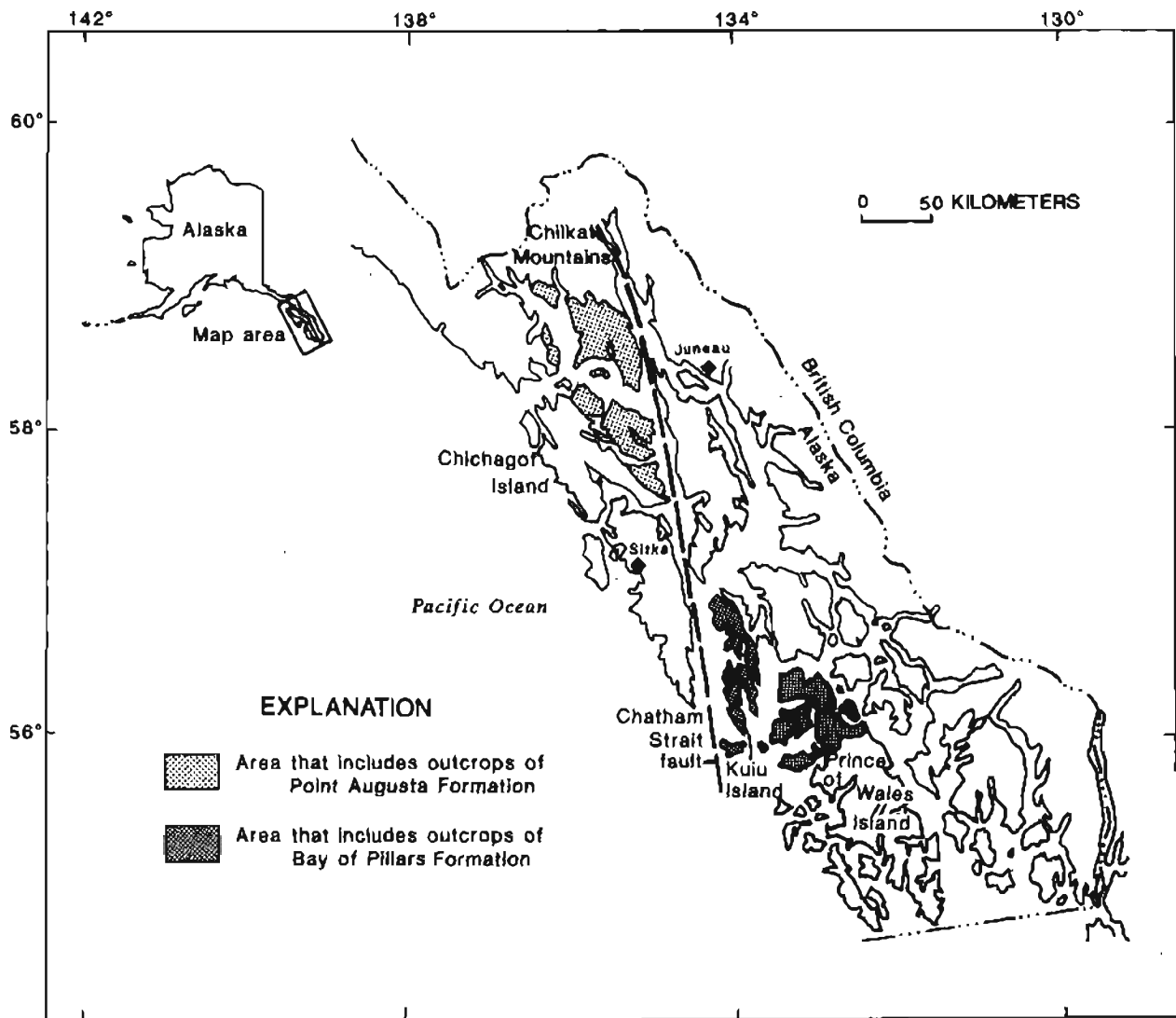


Figure 1. Location of Bay of Pillars and Point Augusta Formations.

Paleontologic studies of Silurian limestone identified a particular reef-building sponge, a phrosalpingid, that distinguishes these limestones from those of autochthonous western North America but ties them to rocks of the Nixon Fork terrane in southwestern Alaska, which are considered to be part of North America (Clough and Blodgett, 1989; Soja, 1991). Soja (1991) concludes that the Alexander terrane was isolated from North America but has biogeographic ties to the craton in the Silurian. This is supported by a recent study of Devonian faunas around the Pacific rim, which showed that the Devonian assemblage of the Alexander terrane is most like the Devonian assemblage of Nevada (Savage, 1988).

Paleomagnetic studies also give equivocal results that do not distinguish whether the Alexander terrane was in the Northern or Southern Hemisphere in the Paleozoic (Van der Voo, 1989). Haeussler and others (in press) interpreted their data to indicate that the Alexander terrane was in the Northern Hemisphere by the Permian, at about latitude 19° N. by the Late Trias-

ic, suggesting that it was probably at low latitudes during the early Paleozoic.

Methods of Study

This study represents preliminary results of extensive field work and petrographic work conducted under the auspices of the Petersburg and Juneau mineral resource assessment projects. Data collected by numerous project geologists were compiled from several hundred stations in the Point Augusta Formation on Chichagof Island and Silurian sandstone in the Chilkat Mountains, and from more than 500 stations in the Bay of Pillars Formation on Kuiu and Prince of Wales Islands. Turbidite facies associations according to the model of Mutti and Ricchi-Lucci (1972) were recorded at all stations where applicable. Bedding thicknesses were recorded in more than 50 estimated 3- to 10-m sections in the Bay of Pillars Formation; these sections were located

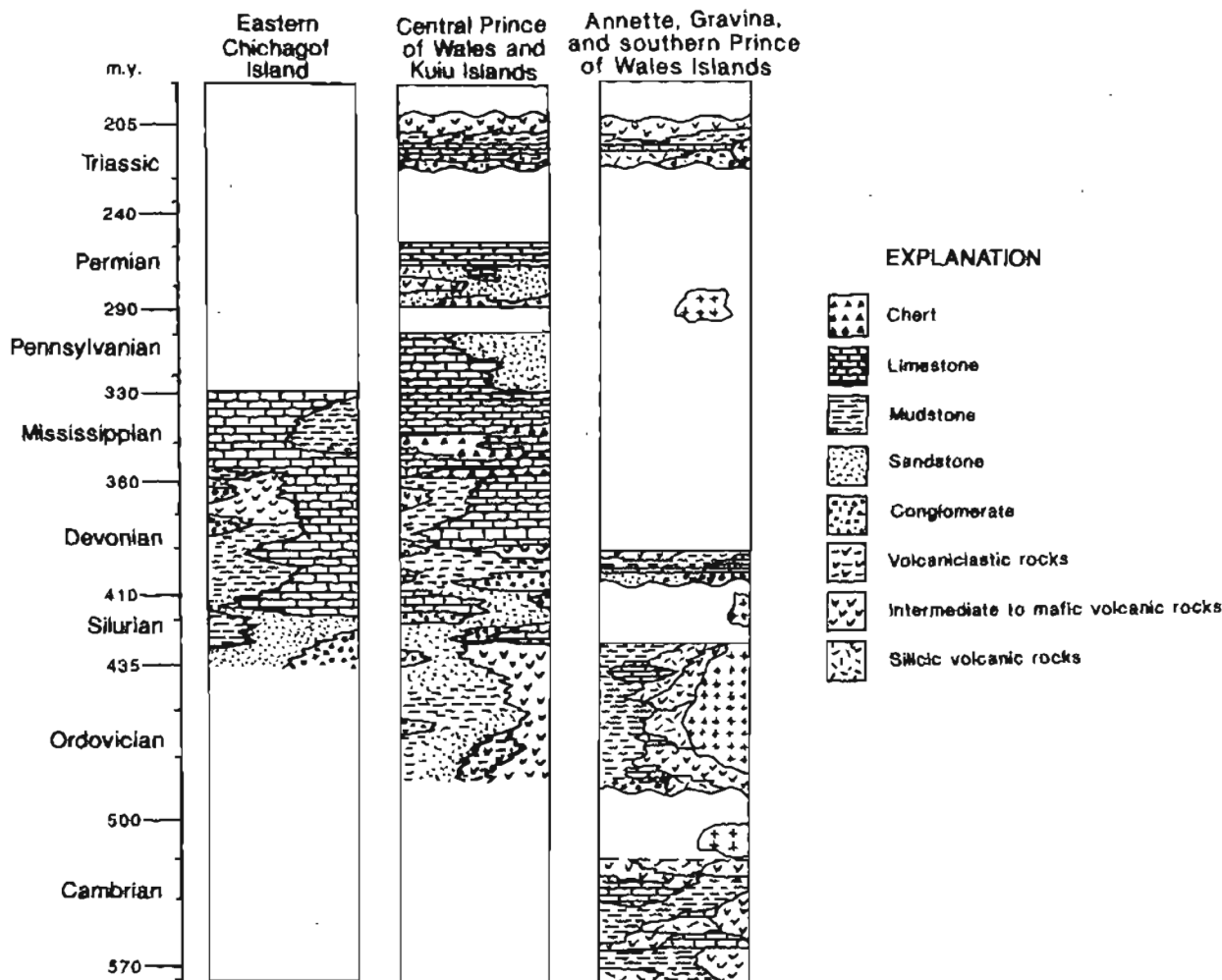


Figure 2. Columns showing stratigraphic sequences in Alexander terrane and geologic time scale used by U.S. Geological Survey (1986).

Table 1. Components of point-counted sandstones of the Bay of Pillars Formation

[Abbreviations: Quartz (m), monocrystalline quartz; Quartz (p), polycrystalline quartz; Quartz (c), chert; Feldspar (p), plagioclase; Feldspar (k), potassium feldspar; Biotite/Epidote (d), detrital; Foss. frag., fossil fragment; Amp, amphibole; Pyr, pyroxene; Pum, pumpellyite; c, calcite; w, graywacke or chloritic pseudomatrix, w(c), chloritic matrix with patches of calcite; tr, trace. Trace components were noted in thin section but did not fall under a counted point]

Sample number	Quartz (m)	Quartz (p)	Quartz (c)	Feldspar (p)	Feldspar (k)	Lithic (carbonate)	Lithic (mudstone)	Lithic (volcanic)	Lithic (plutonic)	Lithic (felsite)	Biotite (d)	Epidote (d)	Chlorite	Opaques	Foss. frag.	Glauconite	Amp	Pyr	Pum	Matrix
80SK455A	37	3	16	93		25	120	104	1	1			1							c
80SK461A	18	9	14	71		21	114	125	11	11	8									w
80SK462A	9	3	6	77		37	230		22	40										w
80SK465A	20		1	75		53	26	217	8	2				1						w(c)
80SK469A	22	1	6	86		38	20	192	18	10							3			c
80SK471A	10		11	98		72	13	192	16	8							20			w
82SK053A	13	4	5	96		37	26	209	1	5	4									w
82SK054A	12		17	240		73	26	70					8							w(c)
82SK056A	14	3	11	119		3	82	156		3			5							w(c)
82SK064A	100	4	11	125	44	5	20	65	13		16								tr	w(c)
82SK065A	23	12	33	89		47	130	51	3											c
82SK071A	1			12		20	8	331	1		tr	27								c
82SK073A	7	1	1	133		21	25	206												c
82SK075A	5	1	2	46		14	55	274						4						c

Table 2. Components of point-counted sandstones of the Point Augusta Formation and the Silurian sandstone of the Chilkat Mountains

[First seven samples listed are from the Point Augusta Formation; last five samples are from the Silurian sandstone unit of the Chilkat Mountains. Abbreviations: s(c), siliceous matrix with patches of calcite; all others as in table 1]

Sample number	Quartz (m)	Quartz (p)	Quartz (c)	Feldspar (p)	Feldspar (k)	L (carbonate)	L (mudstone)	L (volcanic)	L (plutonic)	L (felsite)	Biotite (d)	Epidote (d)	Chlorite	Opaques	Foss. frag.	Glauconite	Matrix
85SK003B	19			58	1		4	313	4	1				11			p
85SK013B	124	7	11	153	18		2	83	8		tr			2			p
85AK015A	117	7	6	121		19	40	83	1		7						c
85SK017A	85	5	4	92		57	37	112	4		1			3			c
85SK018A	80	5	40	44	16	1	98	76	33	8							s(c)
85SK018G	27		1	135			9	210	2	7	tr		8				w
85SK019A	96		10	92		19	86	97						1			c
85SK029A	17	3	1	260		6	11	100		4	1						w
85SK030A	41	5	7	102		41	97	101	2	1	3						c
85SK032A	44	3	10	96		36	98	114	2	5							c
85SK034A	26	11	15	103		54	115	64									c
85SK037A	35	2	8	113		38	90	173			1						c

mainly on Kuiu Island because rocks from this unit on Prince of Wales Island are principally conglomerates, olistostromes (sedimentary slump deposits), limestones, and calcareous mudstones. Twenty-one detailed 25- to 50-m sections were measured in the Point Augusta Formation on Chichagof Island and in Silurian sandstone in the Chilkat Mountains. Thin sections were collected at all stations. For this study, thin sections collected by the first author were examined, and from this data set 14 samples from the Bay of Pillars Formation, 7 samples from the Point Augusta Formation, and 5 samples from the sandstone in the Chilkat Mountains were chosen as suitable for point counting. Although a few samples contain prehnite or pumpellyite, primary clast compositions appear to be unaffected by the low metamorphic grade of these rocks (tables 1, 2). Approximately 500 points were counted on medium-grained sandstones with low matrix content by the traditional method (Dickinson, 1970); however, chert grains were combined with the sedimentary lithic parameter on ternary plots.

Paleocurrents were calculated from measured unidirectional and bidirectional sedimentary structures such as flute casts, asymmetric ripples, and groove casts. Measurements were rotated for plotting under the assumption of a horizontal fold axis because in most cases cleavage or fold axes were either not present or not measured at the outcrop where the paleocurrent indicator was measured. The regional structural style consists of broad, open folds. Measured and plotted fold axes plunge gently to moderately north or south (Karl and Hunt, 1983; S.M. Karl, unpub. data).

Owing to very poor age control and pervasive faulting, unit thicknesses are not known, but both the Bay of Pillars and Point Augusta Formations have been estimated to be approximately 1,500 m thick (Muffler, 1967; Loney and others, 1975). The broad geographic distribution of the samples and sections studied covers the full lithic variation within the units, and therefore the samples and sections are assumed to represent the full stratigraphic range of the units.

SEDIMENTOLOGY

Bay of Pillars Formation

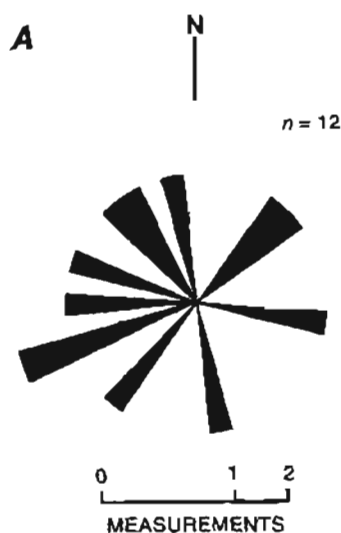
The Silurian Bay of Pillars Formation (Muffler, 1967) is mapped on Kuiu Island, Prince of Wales Island, and smaller islands east of the Chatham Strait fault (fig. 1), and it is inferred to gradationally overlie the Descon Formation on Prince of Wales Island (Brew and others, 1984). It is positionally overlain by the Silurian Kuiu Limestone on northern Kuiu Island (Muffler, 1967). The Bay of Pillars Formation consists dominantly of graywacke, mudstone, and calcareous mudstone, with subordinate

limestone, conglomerate, and mafic to intermediate volcanic flows, breccia, and tuff (Brew and others, 1984). The age of the unit is based on a few graptolite collections that range from middle Llandoveryan to early Ludlovian (late Early to Late Silurian) (C. Carter, in Brew and others, 1984). The stratigraphic position of the graptolite-bearing rocks is unknown.

The graywacke of the Bay of Pillars Formation is locally volcanoclastic, calcareous, or quartzofeldspathic (Brew and others, 1984). Rapid lateral and vertical compositional variations, poor sorting, and angular grains indicate sediment immaturity and local sources. All clast types can be tied to local sedimentary, volcanic, or plutonic sources in coeval or adjacent units. Distinctive pink to red syenite cobbles up to 50 cm in diameter are similar to nearby syenitic plutons that have yielded earliest Silurian U-Pb ages (Gehrels and Saleeby, 1987b). Meter-scale blocks of fossiliferous limestone in slump deposits within the unit are similar to the Heceta Limestone, an adjacent and coeval Silurian unit. Intercalated volcanic flows, agglomerate, and breccia indicate contemporaneous volcanic activity.

The sedimentary strata of the Bay of Pillars Formation were mainly deposited as turbidites, debris flows, olistostromes, and hemipelagic sediments. The turbidites are identified by full and partial Bouma (1962) sequences; graded bedding is ubiquitous. Soft-sediment deformation of beds is common. Debris flows are poorly organized, poorly sorted, matrix-supported conglomerate and breccia, with abundant internal soft-sediment deformation. Olistostromes consist of matrix-supported meter-scale angular blocks and meter-scale soft-sediment slump structures in the matrix. There is no cleavage or evidence of tectonic deformation in these deposits. Hemipelagic sediments consist of calcareous mudstones and limestones adjacent to, truncated by, and incorporated as blocks in the turbidites, debris flows, and olistostromes. The hemipelagic mudstones and limestones are more carbonaceous than the mudstones in the turbidite beds, and they tend to be deposited as planar beds with a uniform grain size. They are generally not turbiditic but contain rare, thin turbidite beds. The mudstones are black and the interbedded limestones are very light gray, providing a dramatic striped appearance that contrasts with the massive brown sandstone turbidites; consequently, they appear to represent a separate depositional facies. They are widely interspersed with the turbidites and are generally a few meters thick at most localities. In some places these beds are slumped as units into asymmetric, irregular folds, suggesting that they were deposited on a slope. For these reasons they are interpreted as slope or slope-basin deposits cut by the turbidite channels.

Measured sections and numerous field stations on Kuiu Island indicate sandstone/shale ratios consistently



in excess of 1 and commonly as high as 50:1. Beds range up to 12 m in thickness but average about 20 cm. Meter-scale channels and amalgamated beds are common. Both thickening-upward and thinning-upward sequences in cycles 1- to 10-m thick are recorded. Thinning-upward cycles are much more common, suggesting channel migration and (or) subsidence (Normark and Piper, 1969; Nelson, 1975). Paleocurrent studies do not indicate a clearly dominant direction of flow (fig. 3). There appears to be a few more measurements that fall in the northwest quadrant of the rose diagram for the asymmetric ripples (fig. 3A) and the flute casts (fig. 3B), but the most reasonable interpretation for the data set is radial current flow. This interpretation is consistent with the interpretation of a paleogeographic setting of volcanic islands for these lower Paleozoic rocks.

Turbidite facies analysis according to the model of Mutti and Ricchi-Lucci (1972) indicates dominantly inner-fan to midfan and slope facies deposits. Inner-fan facies include both matrix- and clast-supported conglomerate, locally with meter-scale crossbedding that suggests shallow-water deposition. Some conglomerates contain meter-scale angular or rounded boulders, indicating very nearby sources. Channel deposits consist dominantly of sandstone in graded or amalgamated beds of Bouma (1962) T_{ab} and T_{ac} units. Deposits interpreted as overbank and interchannel facies are generally more calcareous and finer grained than channel facies deposits. These beds consist of Bouma (1962) T_{be} and T_{ce} units. Centimeter-scale lenses of micritic limestone are present in many beds. The calcareous mudstone and micritic limestone may in part represent background hemipelagic sedimentation. These sediments may be related to prolific calcareous productivity or debris associated with nearby reefs represented by the adjacent and coeval Heceta limestone. Slump deposits and fine-grained black and light-gray hemipelagic calcareous and carbonaceous mudstone and limestone (described above) are interpreted to represent slope facies deposits between channel systems. These rocks of the Bay of Pillars Formation, with intercalated volcanic flows and reefs of the adjacent Heceta Formation (Brew and others, 1984), have been interpreted to represent a sedimentary apron around volcanic islands with fringing limestone reefs (Eberlein and others, 1983); this study concurs with that interpretation.

Sandstone compositions in the Bay of Pillars Formation vary greatly laterally and vertically on a scale of tens of meters. The three dominant types of sandstone include (1) calcareous graywacke containing carbonate

Figure 3. Rose diagrams of rotated paleocurrent directions for (A) asymmetric ripples, (B) flute casts, and (C) bidirectional groove casts measured in Bay of Pillars Formation. n , number of samples.

clasts and fossil fragments, with subordinate feldspar, quartz, chert, radiolarian mudstone, chalcedony, volcanic rock fragments, and a patchy, recrystallized calcite matrix; (2) volcanoclastic graywacke containing felted intermediate to mafic volcanic rock fragments with subordinate plagioclase, monocrystalline, embayed quartz, rare feldspar, epidote/clinozoisite, chlorite, clinopyroxene, amphibole, mudstone, red, green, gray or black chert, occasional fossil fragments, and a clayey to chloritic matrix; and (3) much less abundant quartzofeldspathic graywacke containing mudstone, mono- and polycrystalline quartz, plagioclase, potassium feldspar, detrital biotite, rare myrmekite, epidote/clinozoisite, and a locally calcareous or clayey matrix. Matrix of these sandstones ranges up to 35 percent of the sample. Secondary chlorite, white mica, pumpellyite, and pyrite were also identified in the various types of graywacke.

Sandstone samples of medium grain size (0.5 mm) were point counted (table 1) and compositions were plotted on Dickinson and Suczek (1979) diagrams. Results indicate that sandstones from the Bay of Pillars Formation are feldspatholithic to lithic and relatively low in quartz content. They fall in fields of magmatic-arc provenances (fig. 4), with arc orogen sources (fig. 5). Granitic components are greatly subordinate to volcanic components (fig. 6), but indicate a dissected arc source.

Point Augusta Formation

The Upper(?) Silurian Point Augusta Formation (Loney and others, 1975) has been mapped on Chichagof and smaller islands. Lithologically similar, age-equivalent deposits on the Chilkat Mountains, west of the

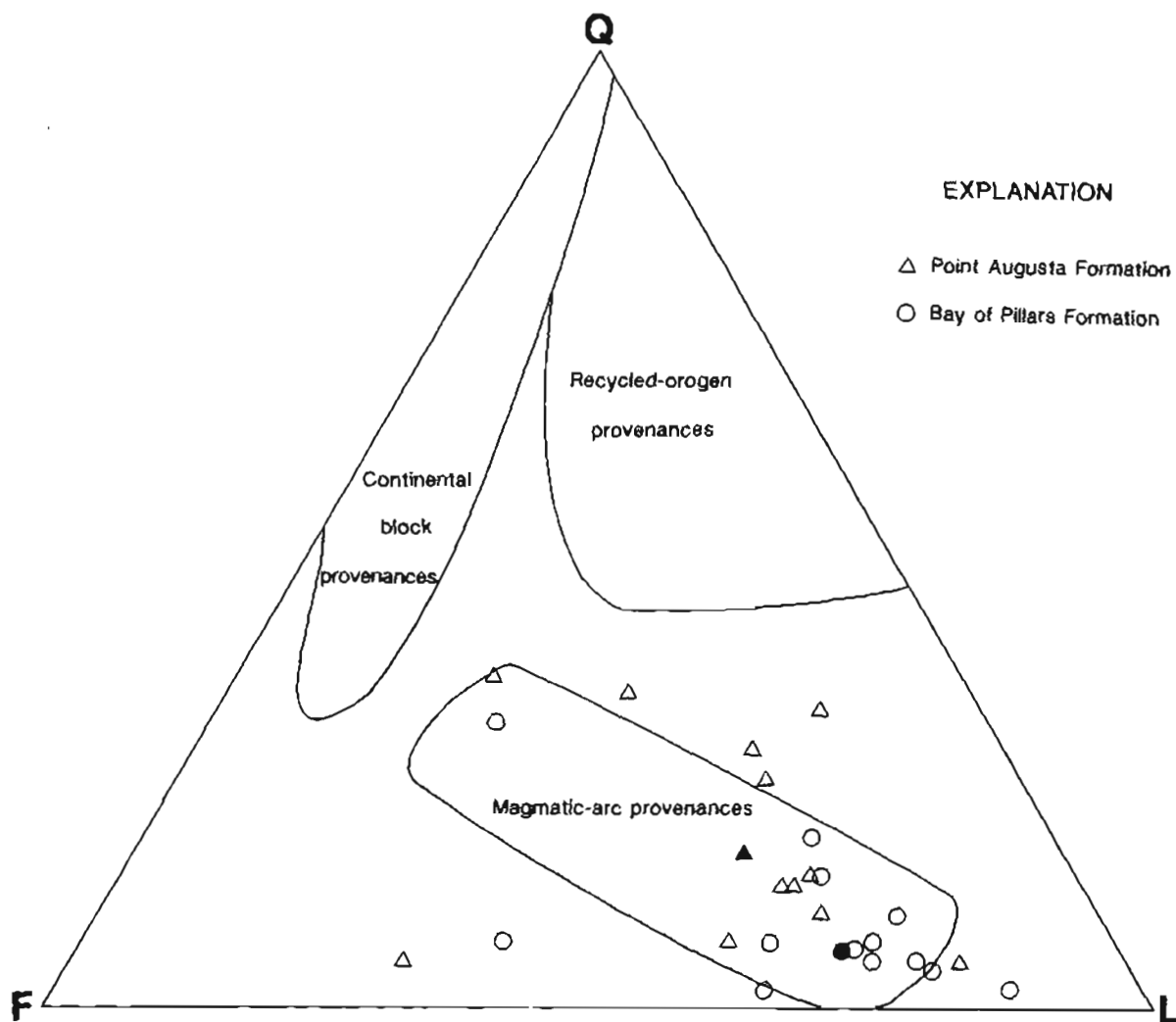


Figure 4. Quartz (Q)-feldspar (F)-lithics (L) diagram with provenance fields (after Dickinson and Suczek, 1979) showing compositions of point-counted sandstones from Bay of Pillars Formation, Point Augusta Formation, and Silurian sandstone of Chilkat Mountains (included with Point Augusta Formation; see table 2). Solid symbols indicate mean values for each unit.

Chatham Strait fault (fig. 1), were correlated with the Point Augusta Formation by Loney and others (1975) and Brew and Ford (1985), although these rocks have not formally been included in the unit. The lower contact of the Point Augusta Formation has not been observed; the unit grades laterally and vertically to the Silurian and (or) Devonian reefal Kennel Creek Limestone (Loney and others, 1963). The Point Augusta Formation consists dominantly of graywacke, argillite, and limestone turbidites, with subordinate conglomerate and limestone. Late Silurian graptolites have been recovered from the Chilkat Mountains and used to date the Point Augusta Formation (Loney and others, 1963, 1975). Distinctive pink to red syenite clasts in Point Augusta conglomerates have been used to correlate the Point Augusta Formation with the Bay of Pillars Formation (Ovenshine and Brew, 1972; Brew and others, 1984).

Syenites on eastern Chichagof Island at Sitkoh Bay have yielded Silurian K-Ar ages (Loney and others, 1975), but some bodies intrude Upper Devonian Freshwater Bay Formation (Ford and others, 1990a). However, the older phases of the syenite suite are still inferred to be the likely source of cobbles in conglomerates of the Point Augusta Formation (Ford and others, 1990b). It is possible that the red syenite bodies on southern Prince of Wales Island may be a source of the red syenite cobbles in both the Bay of Pillars and Point Augusta Formations. Paleocurrents measured from this unit do not indicate any dominant flow direction (fig. 7) and support an interpretation of radial current flow.

Sandstone/shale ratios in the Point Augusta Formation are high, generally in excess of 20:1, as shown by the measured section from the type locality at Point Augusta on Chichagof Island in figure 8. Turbidite facies analysis

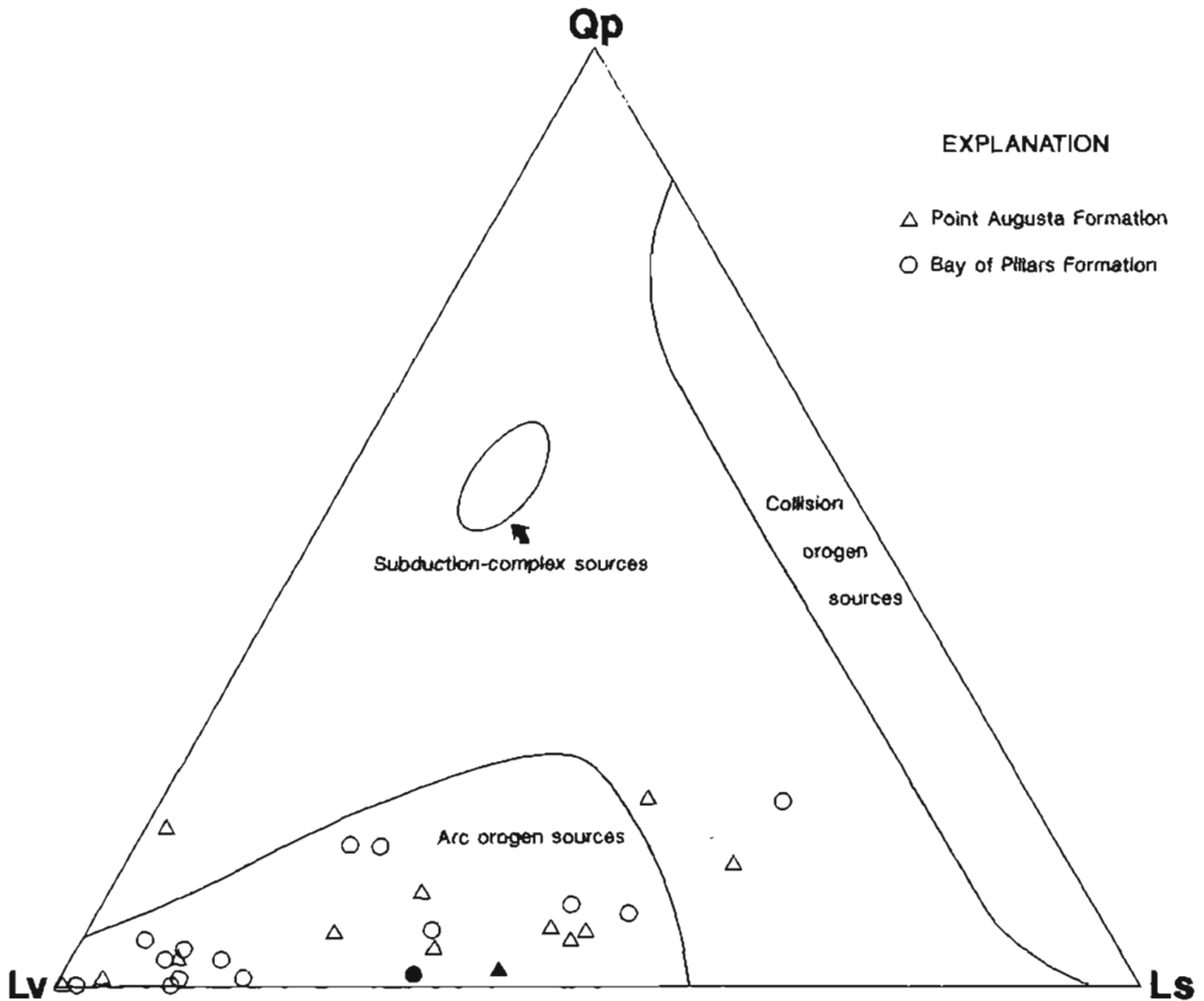


Figure 5. Polycrystalline quartz (Qp)-volcanic lithic grains (Lv)-sedimentary lithic grains (Ls) diagram (after Dickinson and Suczek, 1979) showing compositions of point-counted sandstones from Bay of Pillars Formation, Point Augusta Formation, and Silurian sandstone of Chilkat Mountains (included with Point Augusta Formation; see table 2). Solid symbols indicate mean values for each unit.

according to the model of Mutti and Ricchi-Lucci (1972) indicate dominantly mid- to inner-fan facies deposition. Conglomerates are mostly matrix supported; depositional cycles are mostly thinning-upward cycles. Interchannel deposits are black carbonaceous and calcareous mudstones alternating on a centimeter scale with light-colored limestone (fig. 9), identical to the striped rocks described from the Bay of Pillars Formation.

Sandstones in the Point Augusta Formation and the Silurian sandstones in the Chilkat Mountains are mainly calcareous graywacke containing clasts (in decreasing order of abundance) of volcanic rock fragments, mudstone and radiolarian mudstone, plagioclase, mono- and polycrystalline quartz, calcite, shelly debris, algae, chert, potassium feldspar, rare perthite, detrital biotite, epidote, chlorite, and glauconite(?) in a generally calcareous matrix (table 2). There are also some graywackes with a

tuffaceous matrix that contain volcanic rock fragments, felsite, monocrystalline quartz, mudstone, calcite, chert, epidote, and chlorite. Loney and others (1975) described one locality at False Bay on Chichagof Island where calcareous and chloritic layers alternate. These beds could reflect calcareous background sedimentation interrupted by sediment from volcanic events. Secondary minerals in both types of graywacke include chlorite, white mica, prehnite, pumpellyite, and pyrite.

Sandstone samples of medium grain size (0.5 mm) were point counted and plotted on ternary diagrams (after Dickinson and Suczek, 1979). Results suggest that these sandstones have magmatic-arc provenances (fig. 4) with arc orogen sources (fig. 5), similar in composition to the Bay of Pillars Formation. The Point Augusta Formation and Chilkat Mountains sandstones show a slightly higher sedimentary lithic component, a result that reflects the observed more cal-

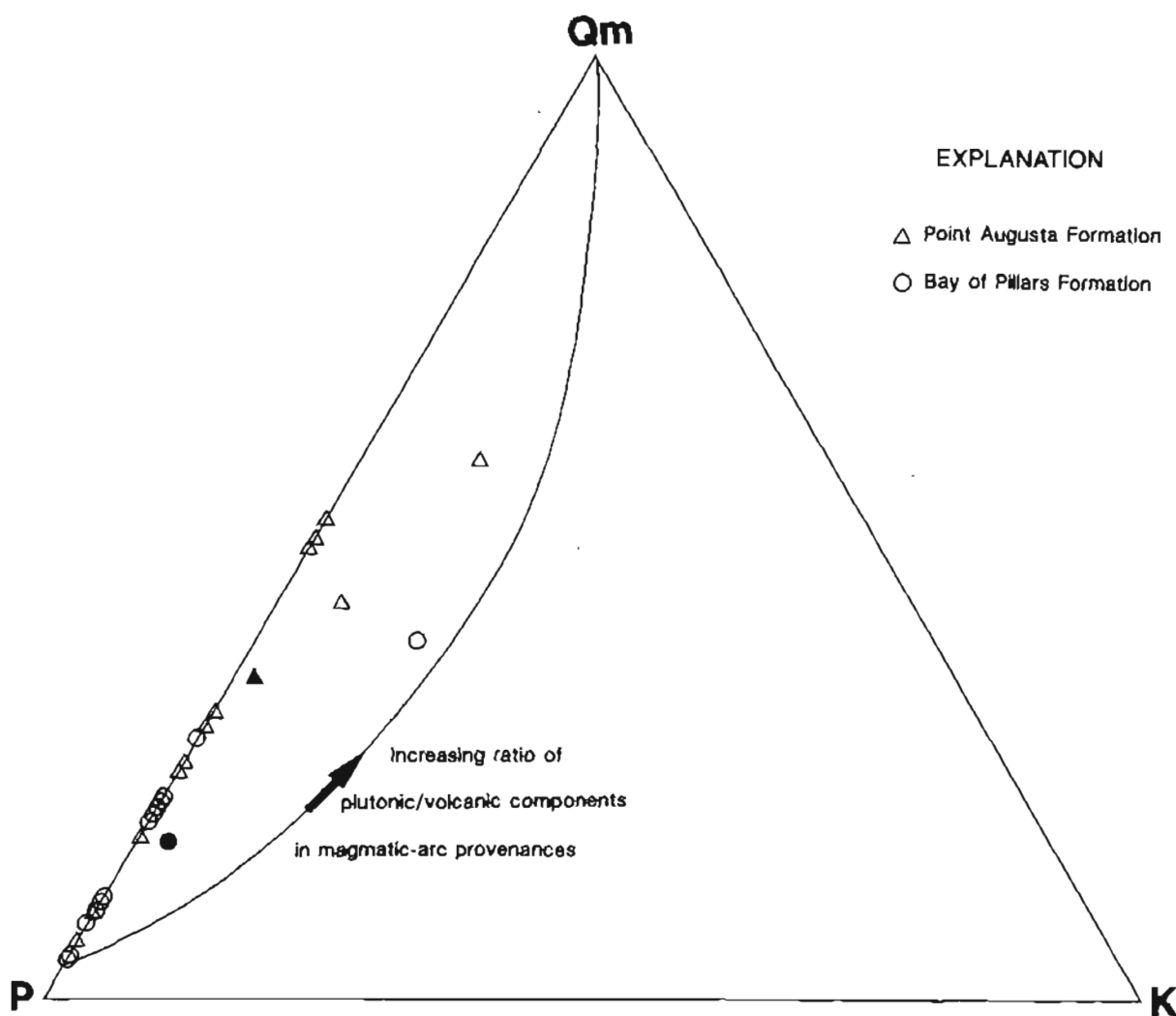
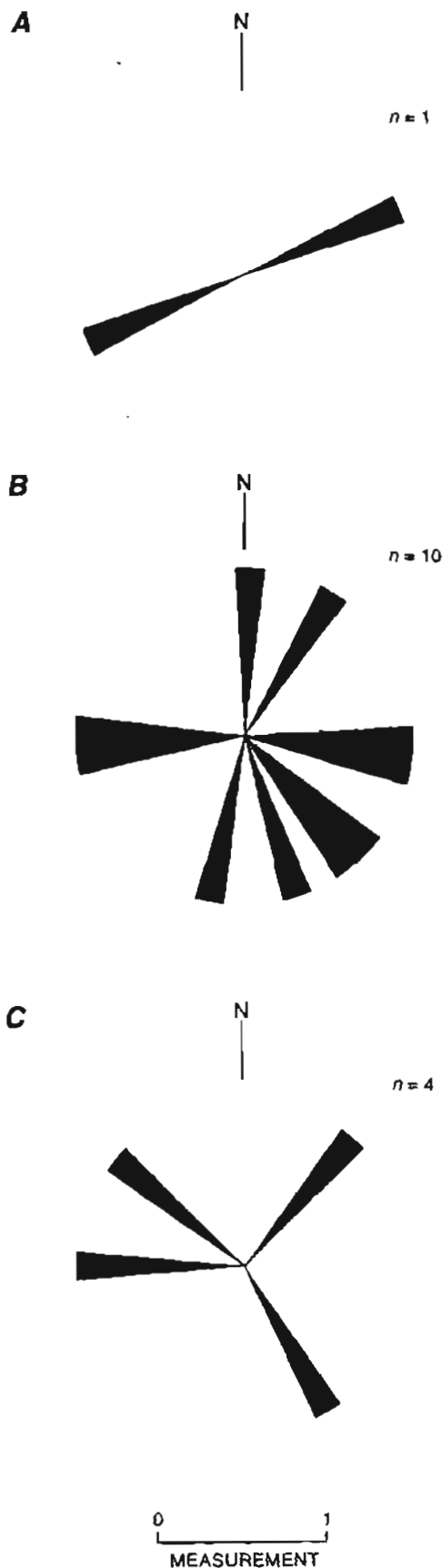


Figure 6. Monocrystalline quartz (Qm)-plagioclase (P)-potassium feldspar (K) diagram (after Dickinson and Suczek, 1979) showing compositions of point-counted sandstones from Bay of Pillars Formation, Point Augusta Formation, and Silurian sandstone in Chilkat Mountains (included with Point Augusta Formation; see table 2). Solid symbols indicate mean values for each unit.



careous composition of the graywackes relative to graywackes of the Bay of Pillars Formation. Point Augusta sandstones also have a higher proportion of plutonic components than those of the Bay of Pillars Formation.

The Point Augusta sandstones and sandstones of the Chilkat Mountains are so similar in composition (table 2), and in bedding habit (figs. 8, 10) that the Point Augusta Formation is here extended to include the sandstones of the Chilkat Mountains, as suggested by the correlation of Loney and others (1975), and Brew and Ford (1985).

Discussion

The petrography of the Bay of Pillars and Point Augusta Formations shows that the two units are very similar in composition, but that the Point Augusta Formation has generally more quartz, a greater sedimentary lithic component, a smaller volcanic lithic component, and a greater plutonic component than the Bay of Pillars Formation (figs. 4–6). Although sedimentary sources for these units are interpreted to be local, these observations may indicate a slightly more uplifted and dissected source for the Point Augusta Formation. Several possible explanations could allow for these differences. Paleocurrent directions appear to be radial for both the Bay of Pillars and Point Augusta Formations. Thus, there is no evidence to indicate the precise spatial relation between the two units when they were originally deposited. A hypothesis to explain the slight compositional differences might be that the Point Augusta Formation sandstones were separated from the main volcanic sources to the east by carbonate reefs, whereas the Bay of Pillars Formation may have been deposited closer to volcanic sources. Although there are massive channel conglomerates in the Point Augusta Formation, overall the beds are not as thick, sandstone/shale ratios are slightly lower, and a larger proportion of outcrops are interpreted as midfan facies turbidites than those in the Bay of Pillars Formation. For these reasons, it is possible that the two units were spatially related, with the Point Augusta Formation more distal to the same source as the Bay of Pillars Formation. Alternatively, the Point Augusta Formation could have been deposited along strike in the same island chain, adjacent to extinct or dormant volcanoes, with compositional differences reflecting local sources. Still another possibility, based on the slightly higher granitic component of the Point Augusta Formation, is that it overlaps in age with the Bay of Pillars Formation but ranges slightly younger in the Silurian, which is unrecognized owing to very sparse age control in both units.

Figure 7. Rose diagrams of 15 rotated paleocurrent directions for (A) groove casts, (B) flute casts, and (C) asymmetric ripples measured in Point Augusta Formation. *n*, number of samples.

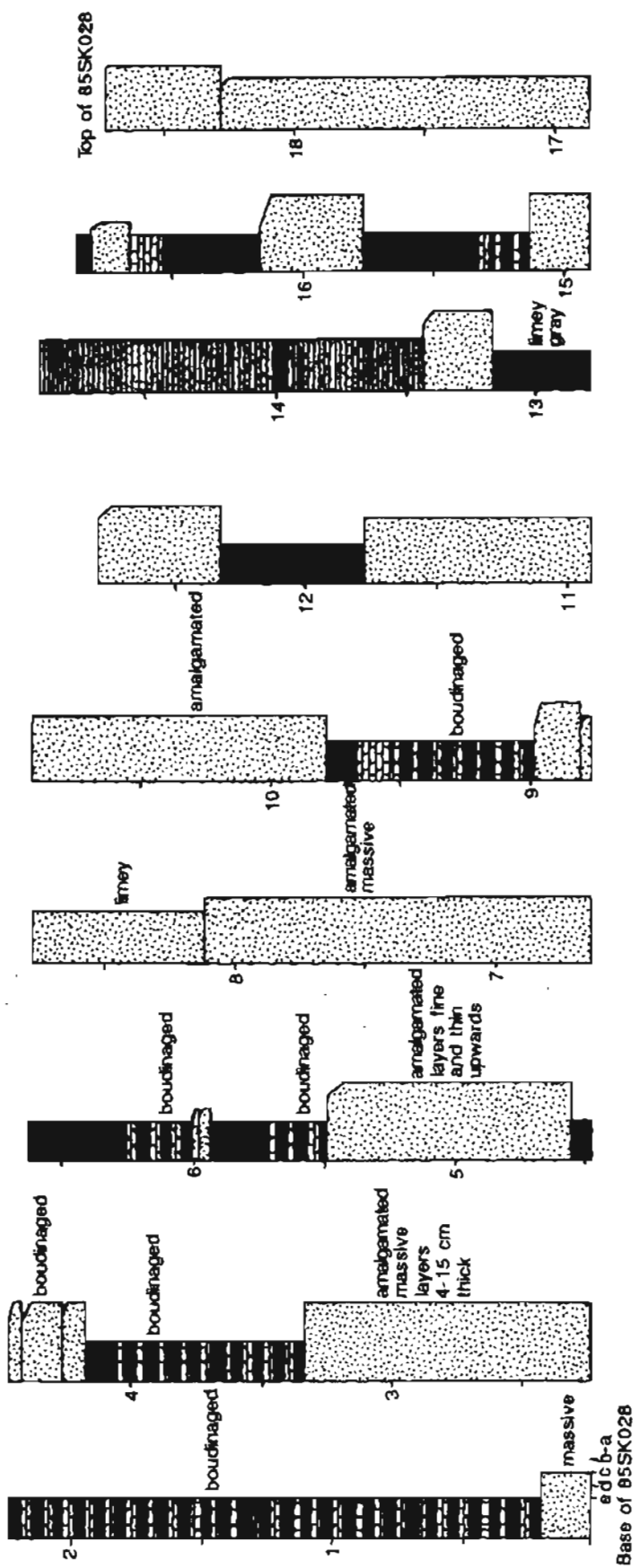


Figure 8. Measured section from Point Augusta Formation at its type locality on eastern Chichagof Island, showing typical bedding thicknesses and sandstone/shale ratios; section interpreted as midfan facies using model of Mutti and Ricchi-Lucci (1972). Solid color is mudstone; dotted pattern is sandstone. Scale in meters. Letters a, b, c, d, e refer to parts of the Bouma (1962) sequence present for each bed—beds extending to "a" contain full Bouma sequences.

Although petrologic analysis of these units clearly indicates magmatic-arc provenances, the quantity of granitic material present is significant (tables 1 and 2) and suggests basement to the Silurian Alexander magmatic arc is more evolved than would be expected for oceanic crust. Therefore, it seems improbable that this Silurian volcanic arc was a primitive intraoceanic arc as suggested by Samson and others (1989). Because paleontologic analyses indicate that Silurian reef-building faunas of the Alexander volcanic arc were isolated from but related to North America (Soja, 1991), the arc must have been located at some distance from North America; however, this scenario does not preclude the possibility that the Alexander terrane originally rifted away from North America or some nearby part of Pangea.

CONCLUSION

Both the Silurian Point Augusta and Bay of Pillars Formations were deposited as sedimentary aprons to volcanic islands with fringing carbonate reefs, but they are not lithologically identical. There is much overlap in bedding styles, sandstone compositions, and depositional environments. However, the Point Augusta Formation is more calcareous in nature, with slightly more mature or dissected arc sources than the Bay of Pillars Formation. The Silurian Chilkat Mountains sandstone is virtually identical in composition and depositional facies to the Point Augusta Formation, and the Point Augusta Formation is herein geographically extended to include these rocks. The Bay of Pillars Formation has a greater volcanic source and

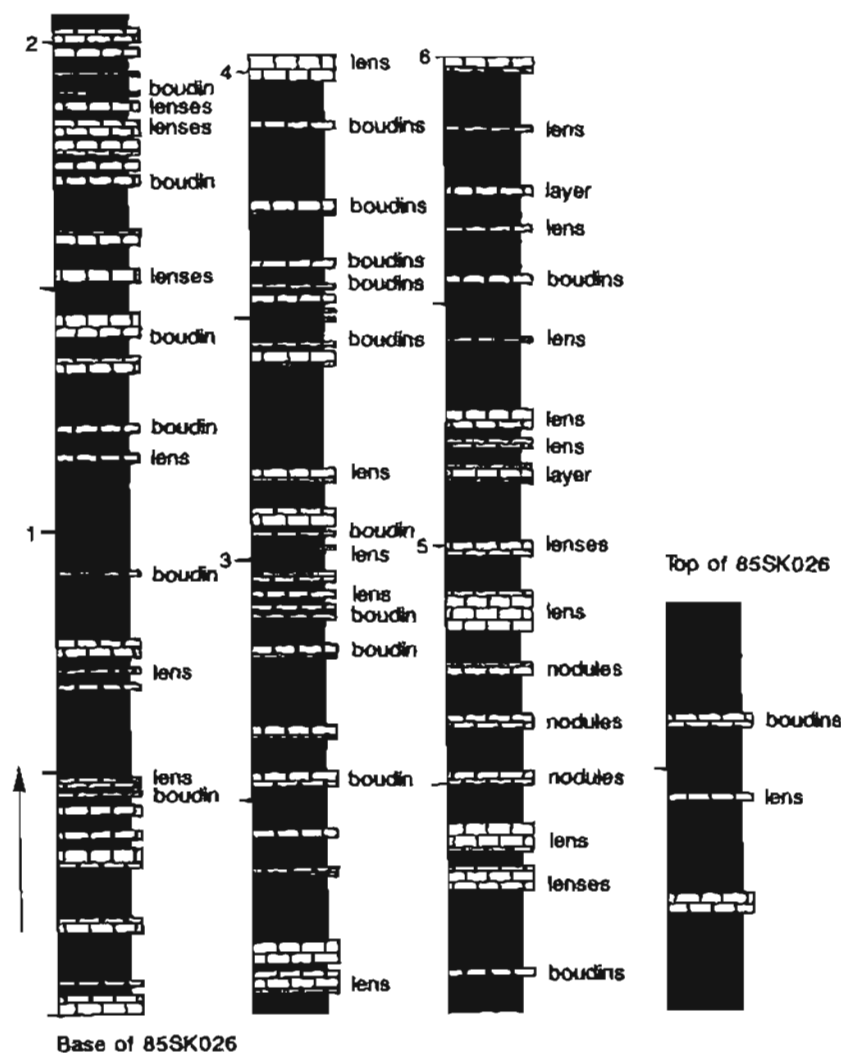


Figure 9. Measured section from Point Augusta Formation on northeastern Chichagof Island, showing typical bedding thicknesses for interchannel-slope facies rocks. Similar sections are also common in Bay of Pillars Formation. Solid color is mudstone; brick pattern is limestone. Arrow indicates up direction. Scale is in meters.

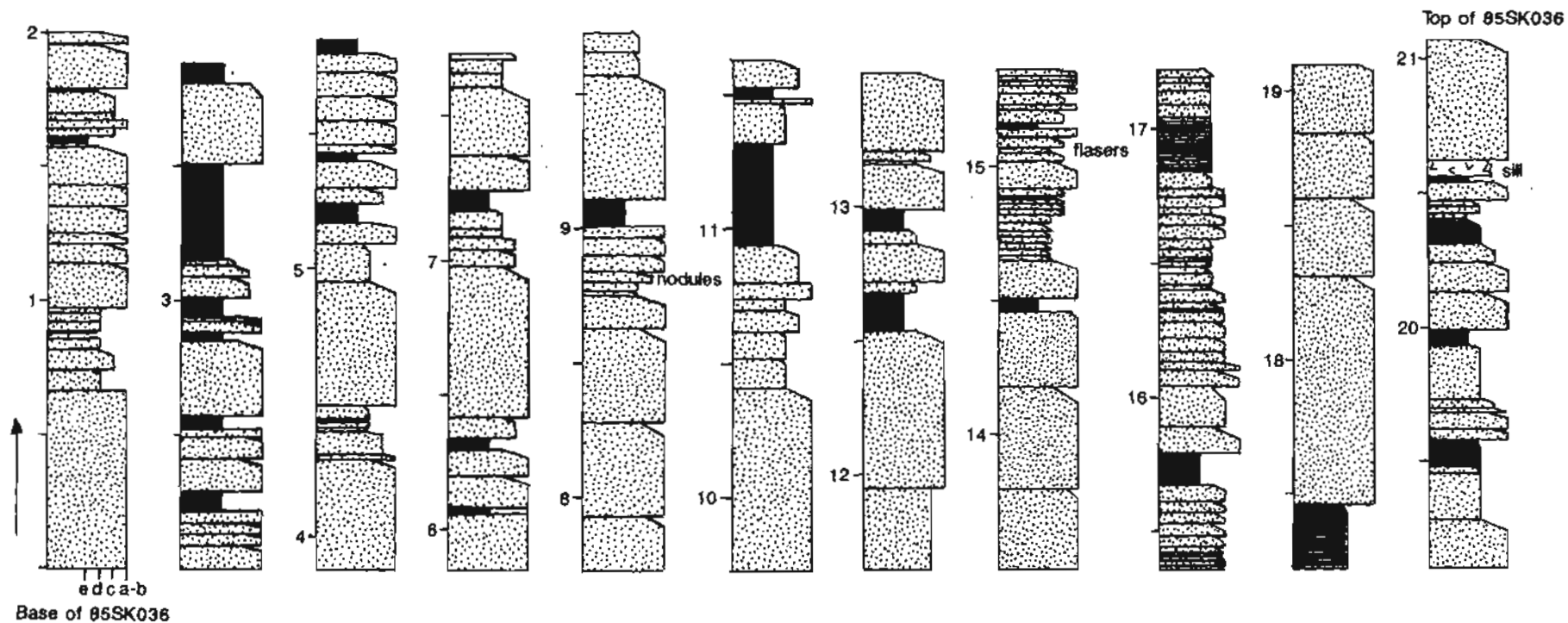


Figure 10. Measured section from Silurian sandstone in southern Chilkat Mountains. Solid color is mudstone, dotted pattern is sandstone, brick pattern is limestone, "V" pattern is andesite or dacite silt. Scale is in meters. Letters a, b, c, d, e refer to parts of the Bouma (1962) sequence present for each bed.

is represented by more proximal, inner-fan facies deposits than the Point Augusta Formation. Sediment compositions and facies relations clearly indicate that these units are related, but the exact lateral or vertical relationship between the units is not fully constrained. Estimates of 150-200 km of right-lateral offset on the Chatham Strait fault (Ovenshine and Brew, 1972; Hudson and others, 1982) based on correlation of Silurian clastic rocks are justified, but there is not an adequate marker for precise measurement of offset.

Acknowledgments.—Special thanks go to Dave Brew for field support for turbidite studies on the Petersburg and Juneau projects. Thanks also to Dave Brew, Sue Douglass, Art Ford, Glen Himmelberg, Sue Hunt, Rich Koch, Eric Lundin, and Willie Nelson for field collaboration and assistance in measuring sections, as well as to reviewers Julie Dumoulin and Peter Haeussler.

REFERENCES CITED

- Armstrong, R.L., 1985, Rb-Sr dating of the Bokan Mt. granite complex and its country rocks: *Canadian Journal of Earth Sciences*, v. 22, p. 1233-1236.
- Berg, H.C., Jones, D.L., and Coney, P.J., 1978, Map showing tectono-stratigraphic terranes of southeastern Alaska and adjacent areas: U.S. Geological Survey Open-File Report 78-1085, 2 sheets, scale 1:1,000,000.
- Bourma, A.H., 1962, *Sedimentology of some flysch deposits*: Amsterdam, Elsevier, 168 p.
- Brew, D.A., and Ford, A.B., 1985, Preliminary reconnaissance geologic map of the Juneau, Taku River, Adin, and part of the Skagway 1:250,000 quadrangles, southeastern Alaska: U.S. Geological Survey Open-File Report 85-395, 2 sheets, 23 p.
- Brew, D.A., and Karl, S.M., 1988, A reexamination of contacts and other features of the Gravina belt, southeastern Alaska, in Hamilton, T.D., and Galloway, J.P., eds., *Geologic studies in Alaska by the U.S. Geological Survey during 1987*: U.S. Geological Survey Circular 1016, p. 143-146.
- Brew, D.A., Ovenshine, A.T., Karl, S.M., and Hunt, S.J., 1984, Preliminary reconnaissance geologic map of the Petersburg and parts of the Port Alexander and Sumdum 1:250,000 quadrangles, southeastern Alaska: U.S. Geological Survey Open-File Report 84-405, 2 sheets, 43 p.
- Clough, J.G., and Blodgett, R.B., 1989, Silurian-Devonian algal reef mound complex of southwest Alaska, in Geldsetzer, H.H., Jr., James, N.P., and Tebbutt, G.E., eds., *Reefs, Canada and adjacent area*: *Canadian Society of Petroleum Geologists, Memoir 13*, p. 404-407.
- Dickinson, W.R., 1970, Interpreting detrital modes of graywacke and arkose: *Journal of Sedimentary Petrology*, v. 40, no. 2, p. 695-707.
- Dickinson, W.R., and Suczek, C.A., 1979, Plate tectonics and sandstone compositions: *American Association of Petroleum Geologists Bulletin*, v. 63, p. 2164-2182.
- Eberlein, G.D., Churkin, M., Jr., Carter, C., Berg, H.C., and Ovenshine, A.T., 1983, *Geology of the Craig quadrangle, Alaska*: U.S. Geological Survey Open-File Report 83-91, 28 p.
- Ford, A.B., Brew, D.A., and Koch, R.D., 1990, Alkalic plutonism of the Sitkoh Bay area (Chichagof Island), SE Alaska-Perplexities of age relations [abs.]: *Eos (American Geophysical Union Transactions)*, v. 71, no. 43, p. 1699.
- Ford, A.B., Brew, D.A., and Loney, R.A., 1990, The Sitkoh Bay alkalic plutonic suite: Silurian or older magmatism on eastern Chichagof Island, southeastern Alaska: U.S. Geological Survey Open-File Report 90-297, 10 p.
- Gardner, M.C., Bergman, S.C., Cushing, G.W., MacKevett, E.M., Jr., Plafker, G., Campbell, R.B., Dodds, C.J., McClelland, W.C., and Mueller, P.A., 1988, Pennsylvanian pluton stitching of Wrangellia and the Alexander terrane, Wrangell Mountains, Alaska: *Geology*, v. 16, p. 967-971.
- Gehrels, G.E., and Saleeby, J.B., 1987a, Geologic framework, tectonic evolution, and displacement history of the Alexander terrane: *Tectonics*, v. 6, no. 2, p. 151-173.
- 1987b, *Geology of southern Prince of Wales Island, southeastern Alaska*: *Geological Society of America Bulletin*, v. 98, p. 123-137.
- Haeussler, P.J., Coe, R.S., and Onstott, T.C., in press, Paleomagnetism of the Late Triassic Hound Island volcanics—Revisited: *Journal of Geologic Research*.
- Hillhouse, J.W., and Grommé, C.S., 1980, Paleomagnetism of the Triassic Hound Island volcanics, Alexander terrane, southeastern Alaska: *Journal of Geophysical Research*, v. 85, p. 2594-2602.
- Hudson, T., Plafker, G., and Dixon, K., 1982, Horizontal offset history of the Chatham Strait fault, in Coonrad, W.L., ed., *The U.S. Geological Survey in Alaska: Accomplishments during 1980*: U.S. Geological Survey Circular 844, p. 128-132.
- Karl, S.M., and Hunt, S.J., 1983, Stratigraphy and turbidite facies associations in the Bay of Pillars Formation, southeastern Alaska, in *New developments in the Paleozoic geology of Alaska and the Yukon*: Anchorage, Alaska, Alaska Geological Society Symposium, Proceedings, p. 18.
- Lathram, E.H., 1964, Apparent right-lateral separation on CSF, southeastern Alaska: *Geological Society of America Bulletin*, v. 75, no. 3, p. 249-252.
- Loney, R.A., Brew, D.A., Muffler, L.J.P., and Pomeroy, J.S., 1975, Reconnaissance geology of Chichagof, Baranof, and Kruzof Islands, southeastern Alaska: U.S. Geological Survey Professional Paper 792, 105 p.
- Loney, R.A., Condon, W.H., and Dutro, J.T., Jr., 1963, *Geology of the Freshwater Bay area, Chichagof Island, Alaska*: U.S. Geological Survey Bulletin 1108-C, p. C1-C51.
- Muffler, L.J.P., Jr., 1967, Stratigraphy of the Keku Islets and neighboring parts of Kuiu and Kupreanof Islands, southeastern Alaska: U.S. Geological Survey Bulletin 1241-C, 52 p.
- Mutti, E., and Ricchi-Lucci, F., 1972, Letorbidite dell'Appennino setentrionale—Introduzione all'analisi de facies: *Societa Geologica Italiana Memoir*, v. 11, p. 161-199.
- Nelson, C.H., 1975, Turbidite fans and other base-of-slope deposits, in Dickinson, W.R., ed., *Current concepts of*

- depositional systems with applications for petroleum geology: San Joaquin Geological Society Short Course, p 6-1-6-5.
- Normark, W.R., and Piper, D.J.W., 1969, Deep-sea fan valleys, past and present: Geological Society of America Bulletin, v. 80, p. 1859-1866.
- Ovenshine, A.T., and Brew, D.A., 1972, Separation and history of the CSF, southeast Alaska, North America: International Geological Congress, 24th, Montreal, 1972 Proceedings, sec. 3, p. 245-254.
- Samson, S.D., McClland, W.C., Patchett, P.J., Gehrels, G.E., and Anderson, R.G., 1989, Evidence from neodymium isotopes for mantle contributions to Phanerozoic crustal genesis in the Canadian cordillera: Nature, v. 337, no. 6209, p. 705-709.
- Savage, N.M., 1988, Devonian faunas and major depositional events in the southern Alexander terrane, southeastern Alaska, in McMillan, N.J., Embry, A.F., and Olan, D.J., eds., Devonian of the world: Canadian Society of Petroleum Geologists Memoir 14, v. 3, p. 257-264.
- Soja, C.M., 1991, Origin of Silurian reefs in the Alexander terrane of southeast Alaska: Palaios, v. 6, no. 2, p. 111-125.
- Van der Voo, R., 1989, Paleomagnetism of North America: The craton, its margins, and the Appalachian belt, in Pakiser, L.C., and Mooney, W.D., eds., Geophysical framework of the continental United States, Geological Society of America Memoir 172, p. 447-470.

Reviewers: Julie Dumoulin and Peter Haeussler

Depositional Environments and Some Aspects of the Fauna of Middle Ordovician Rocks of the Telsitna Formation, Northern Kuskokwim Mountains, Alaska

By Elizabeth A. Measures, David M. Rohr, and Robert B. Blodgett

Abstract

The northern Kuskokwim Mountains of west-central Alaska contain a thick sequence of Ordovician carbonate rocks, including the type section of the Telsitna Formation, which is in the Medfra D-2 quadrangle. Silicified, fossiliferous intervals from the Middle Ordovician part of the formation were sampled extensively in 1991. Two limestone intervals were measured and sampled in detail.

The limestones of the two measured sections are fundamentally different: section 1 is dominated by peloid-rich packstone and contains an abundant, silicified macrofauna; section 2 is dominated by recrystallized ooid, ostracode grainstone. Section 1 contains skeletal wacke-mudstone, peloid grain-packstone, and coated-grain, ooid grainstone; this composition indicates deposition in normal marine, middle-shelf conditions, including some inner-shelf shoals analogous to peloidal platform sediments of the Bahamas. The macrofauna of this section and lithologically similar underlying strata are dominated by gastropods and brachiopods. Gastropods from this limestone include abundant macluritid opercula and the carrier shell *Lytospira*. Brachiopod genera present include *Doleroides*, *Austinella*, *Strophomena*, *Macrocoelia*, n. gen. aff. *Macrocoelia*, and an undetermined rhynchonellid. Conodonts and brachiopods recovered in 1991 indicate a Llandeilian age for at least part of this section. Section 2 contains gastropod packstone, ooid and ostracode grainstone, mudstone, intraclast packstone, and peloid, intraclast grainstone. These lithologies indicate deposition in a restricted marine, shallow-water, inner-platform setting. Ooid shoals and beaches grade into a lagoon and then into tidal flats. We conclude that the Bahamian tidal flat model is a close analog to deposits of section 2. We propose that the deposits described represent formation under humid conditions similar to those found in the Bahamas today.

This is the first study of carbonate petrology of Middle Ordovician strata from west-central Alaska (Nixon Fork terrane), and the results derived here will be useful in comparing and contrasting these strata with other better known Middle Ordovician stratal sections elsewhere in Alaska and the Western Cordillera of North America in order to determine displacement of these rocks.

INTRODUCTION

The northern Kuskokwim Mountains of west-central Alaska contain a thick sequence of Ordovician carbonate rocks. Approximately 120 km northwest of McGrath, in the Medfra D-2 quadrangle, is a north-trending ridge adjacent to the Telsitna River. It is informally known among geologists familiar with the region as Telsitna Ridge. Rocks on this ridge have been included by Dutro and Patton (1982) in their 2,000-m-thick Telsitna Formation, which they reported to be of Middle and Late Ordovician age. A sparse silicified fauna is present, and collections by Dutro in 1977 and 1979 and by Blodgett in 1984 and 1985 have been published (Rohr and Blodgett, 1988; Rohr and others, 1991, 1992). In 1991, fossiliferous intervals at Telsitna Ridge were re-collected to further document the nature of the fossil assemblages. Detailed sections were measured to determine the microfacies of two adjacent, unnamed subunits ("members") of the Telsitna Formation.

Rocks included in the Telsitna Formation comprise part of the Nixon Fork terrane of Patton (1978), which is characterized primarily by lower and middle Paleozoic platform carbonate rocks. To the south and east this assemblage grades into equivalent, deeper water basinal strata (Blodgett and Clough, 1985) that have been variably mapped as belonging to other terranes (Dillinger, Minchumina, and East Fork terranes). Decker and others (in press) have recognized that these "terranes" are genetically related to one another, and they have proposed the term "Farewell Terrane" to unite them as a single tectonic entity.

Our primary purpose here is to document the carbonate microfacies found in Middle Ordovician strata of this region. Prior to this study, no published accounts existed on the carbonate petrology of Ordovician strata from either west-central or southwestern Alaska (see fig. 1 for distribution of Ordovician platform carbonate rocks in this region).

AGE

Samples collected in 1991 for conodonts have provided age determination for several of the localities. Preliminary study of conodonts (Anita G. Harris, U.S. Geological Survey, written commun., December 1991) from several samples that were processed for silicified macrofossils indicates an early Middle Ordovician age. A sample from U.S. Geological Survey (USGS) locality 11063-CO, north of section 1, however, produced abundant representatives of *Cahabagnathus sweeti* (Bergstrom), indicating a very latest Llanvirnian to at least middle Llandeilian age. Because this locality is inferred to lie stratigraphically below the interval including section 1, it can be assumed that the rocks in section 1 are Llandeilian or slightly younger Middle Ordovician age. Brachiopods from section 1 and lithologically similar underlying beds (comprising an unnamed subunit of the Telsitna Formation) are mostly represented by new species, making age determination difficult; however, closely related species are present in the Siberian platform and eastern cratonal North America, and these are mostly of Llandeilian or early Caradocian age.

Section 2 is from a sequence of strata that have been juxtaposed along a major fault opposite strata of section 1. However, strata of this interval are recognized farther to the north along the ridge, resting stratigraphically beneath the interval represented by section 1. Section 2 contains only a sparse, biostratigraphically nondiagnostic conodont fauna of Middle Ordovician age; the associated megafauna and its stratigraphic position beneath strata of

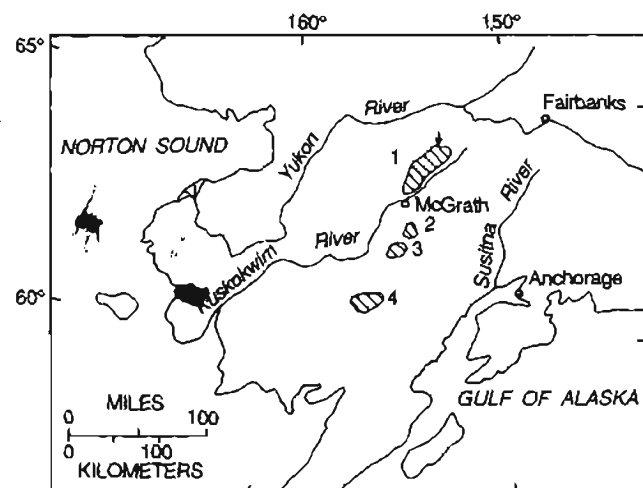


Figure 1. Distribution of Ordovician platform carbonate rocks in west-central and southwestern Alaska (modified from Churkin, 1973). Arrow indicates location of so-called Telsitna Ridge. 1, Northern Kuskokwim Mountains, Medfra quadrangle; 2, Lone Mountain area, McGrath quadrangle; 3, White Mountain area, McGrath quadrangle; 4, Holitna and Hoholitna Rivers, Sleetmute and Taylor Mountains quadrangles.

section 1 also indicate an early Middle Ordovician, probably pre-Llandeilian age for this interval.

CARBONATE MICROFACIES AND DEPOSITIONAL SETTING

Detailed sections were measured using a 1.5-m staff and Brunton compass along the two fossiliferous Middle Ordovician intervals on Telsitna Ridge (fig. 2). The sections are not complete because of structural complications and incomplete exposure, but they suggest relative lithologic uniformity throughout each interval. Surfaces of the limestone were weathered in such a way that few textures were observable, except on fresh-broken surfaces. Fresh surfaces from each bed were examined. Samples were collected at each lithologic change or every 1.5 m. Carbonate terminology established by Dunham (1962) is used to describe the carbonate rocks. Environmental interpretation from microfacies conforms to principles and models established by Wilson (1975), Flügel (1982), and Scholle and others (1983).

The limestones in the two sections are lithologically dissimilar. Section 1 is dominated by peloid-rich packstone and contains an abundant, silicified macrofauna (fig. 3). Section 2 is dominated by ooid, ostracode grainstone (fig. 4). The beds in section 1 are thicker than

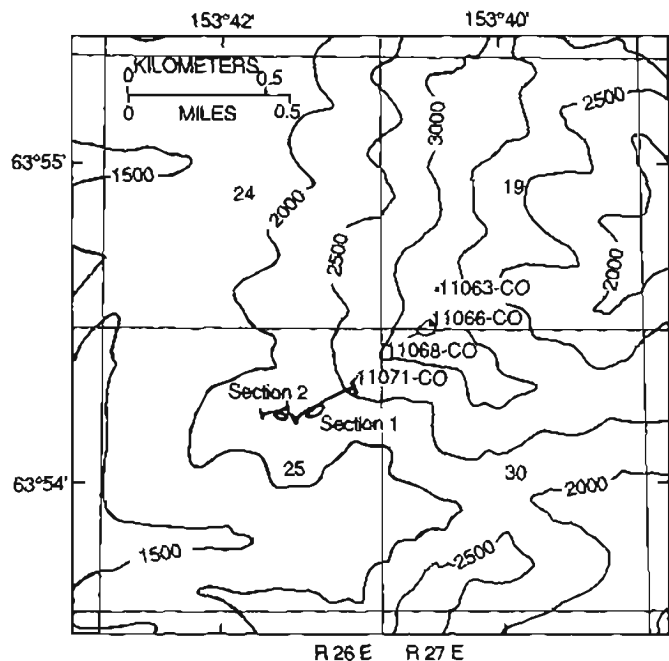


Figure 2. Location of measured sections and fossil-collection sites on so-called Telsitna Ridge. Section 1 (see fig. 3) has its base at northeast end. Section 2 (see fig. 4) also has its base at northeast end. U.S. Geological Survey (USGS) locality 11066-CO is at east end of area of USGS locality 11068-CO. Base map from Medfra D-2 quadrangle, 1958; contour interval 500 ft.

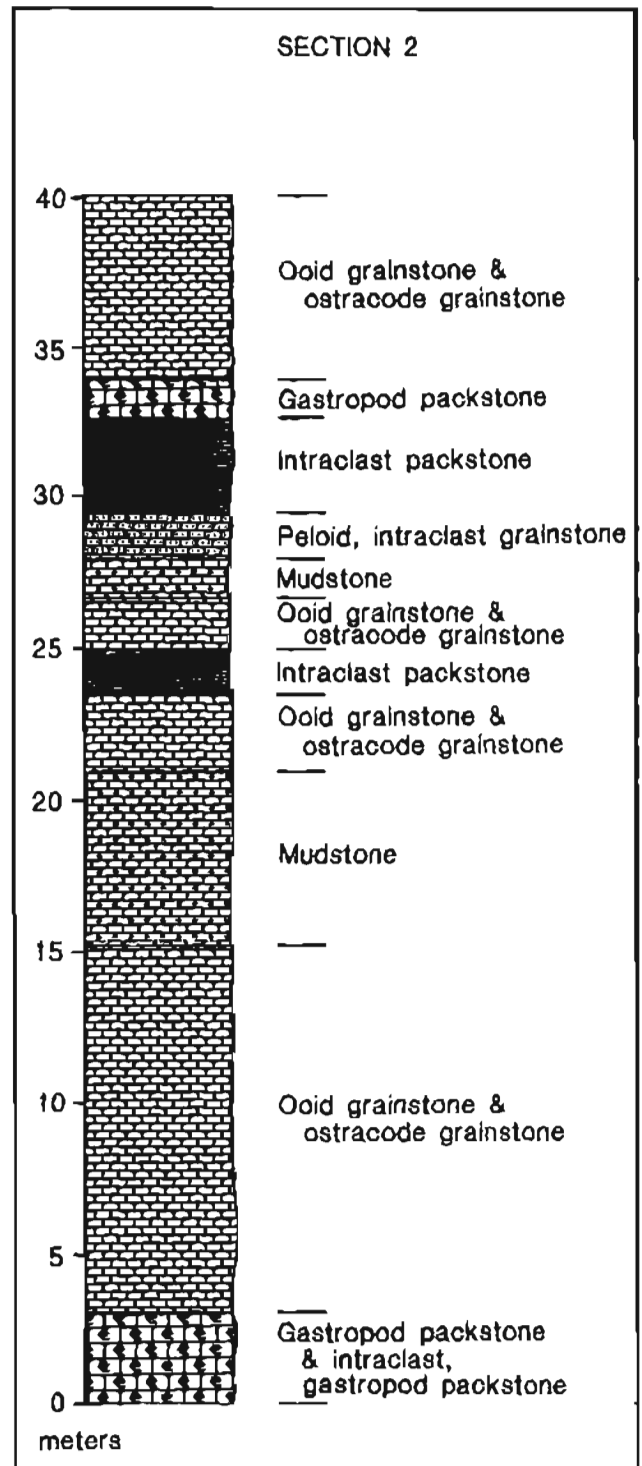
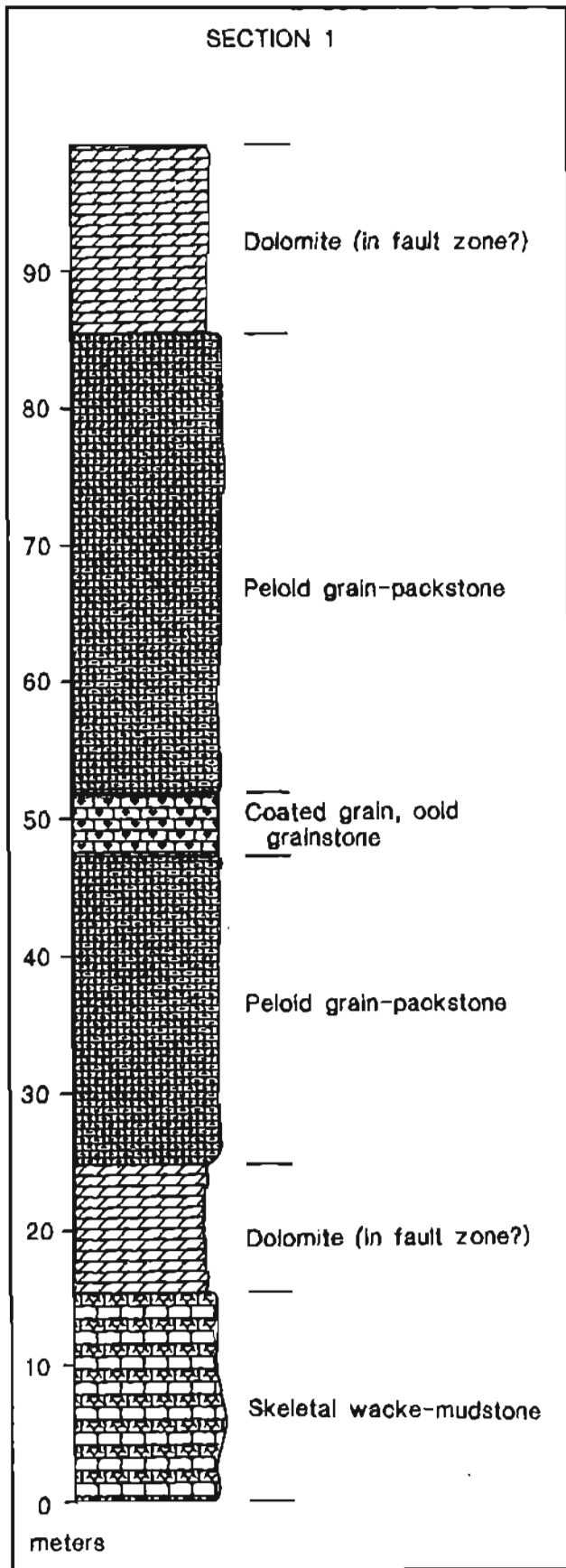


Figure 4. Columnar diagram of section 2 of Middle Ordovician carbonate rocks that form part of Telsitna Formation on so-called Telsitna Ridge.

←
Figure 3. Columnar diagram of section 1 of Middle Ordovician carbonate rocks that form part of Telsitna Formation on so-called Telsitna Ridge.

those in section 2. Section 1 is composed of fairly homogeneous carbonate lithologies, whereas section 2 is composed of interbedded distinct lithologies that appear cyclic. Section 2 has been extensively recrystallized, but section 1 carbonates have only minor recrystallization fabrics.

Section 1

The limestone in section 1 (fig. 3) can be grouped into the following three facies based upon petrographic and field observations: (1) skeletal wacke-mudstone, (2) peloid grain-packstone, and (3) coated-grain, ooid grainstone.

Skeletal Wacke-Mudstone Facies

The skeletal wacke-mudstone facies is characterized by a silicified fauna of brachiopods (*Doleroides*, *Austinella*, *Macrocoelia*, n. gen. aff. *Macrocoelia*, and *Strophomena*), straight nautiloids, and stromatoporoids. Silicified macluritacean gastropod opercula are present but uncommon. Trilobites, bryozoans, ostracodes, and cross sections of gastropods are also common but unsilicified. Thin, spaghetti-like trace fossils are very common on bedding planes and pieces of float. Bedding is very irregular to nodular and 7 to 15 cm thick.

The matrix of the wacke-mudstone is composed of micrite and contains small gastropods, trilobites, bryozoans, ostracodes, and pelmatozoans (fig. 5A). Microarchitecture is well preserved in all but the gastropods, which have been replaced by coarse spar. The most abundant material is bioclastic debris, up to 1.0 mm long, but very thin and broken. These fragments are unidentifiable but resemble spicules. Mottling was observed in thin section and is the result of recrystallization of burrow fill to coarse calcite spar.

The diverse fauna indicates normal marine, subtidal conditions (Wilson, 1975; Wilson and Jordan, 1983). The abundance of mud indicates that environmental energies—waves or currents—were not sufficiently high to remove the fine-grained carbonate. There is also a lack of high- or even moderate-energy sedimentary structures. These features and the abundant bioturbation mottling are indicative of middle-shelf conditions (Wilson and Jordan, 1983).

Peloid Grain-Packstone Facies

The peloid grain-packstone facies is characterized by both abundant macrofauna and peloids. Macrofauna consists of silicified stromatoporoids (laminar and bulbous), large gastropod opercula, and straight nautiloids. Silicified brachiopods occur rarely. Silicified burrows and bryozoans are apparent at a few horizons. Broken surfaces display ostracodes, trilobites, crinoids, bryozoans, gastropods, and intraclasts. In thin section, the bioclasts

display excellent preservation of microarchitecture (fig. 5E), although some bioclasts have micrite rims or coats of micrite. Peloids are rarely apparent on broken surfaces but are almost the exclusive allochem in thin section (fig. 5F). They are composed of homogeneous micrite in rounded, irregularly shaped bodies, 0.1 to 0.3 mm in diameter. Some lithologies contain poorly sorted allochems, smaller peloids, and larger skeletal grains. Rarely, the grain-packstone contains well sorted peloids, and these commonly lack bioclasts. Associated intraclasts, 3 mm to 2 cm in length, are commonly composed of skeletal mudstone to wackestone, or peloid packstone to wackestone. Intraclasts are rounded and irregularly ovoid shaped.

Matrix is commonly composed of micrite, and there is little evidence of recrystallization. This facies does contain abundant light-colored mottles. In thin section, these mottles contain peloids in a microspar matrix or even in poikilitic spar cement.

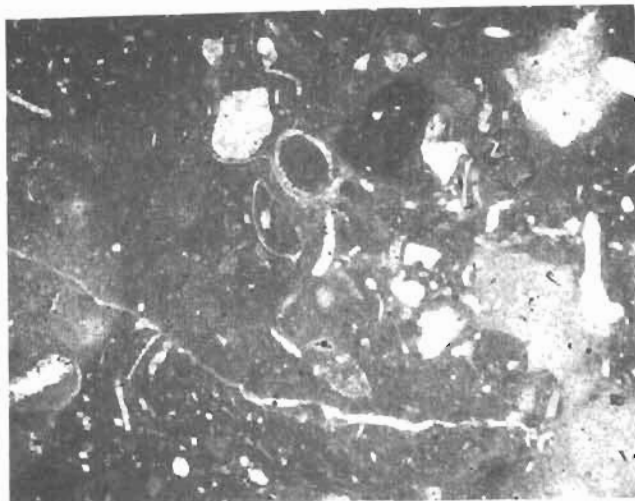
Normal marine, subtidal conditions are indicated by the diverse fauna (Wilson, 1975). The peloids indicate shallow subtidal conditions, ingestion of sediment by infauna, and probable physical reworking of semilithified substrate. Low sedimentation rates may also be indicated by the abundance of peloids (Enos, 1983). Low sedimentation rates and the presence of boring organisms are indicated by the micritized rims on many allochems. Intermittent conditions of moderate to high energy are indicated by the well sorted texture of some units and the occurrence of coated grains. Deposition in normal marine, middle-shelf conditions is consistent with these features (Wilson and Jordan, 1983).

Coated-Grain, Ooid Grainstone Facies

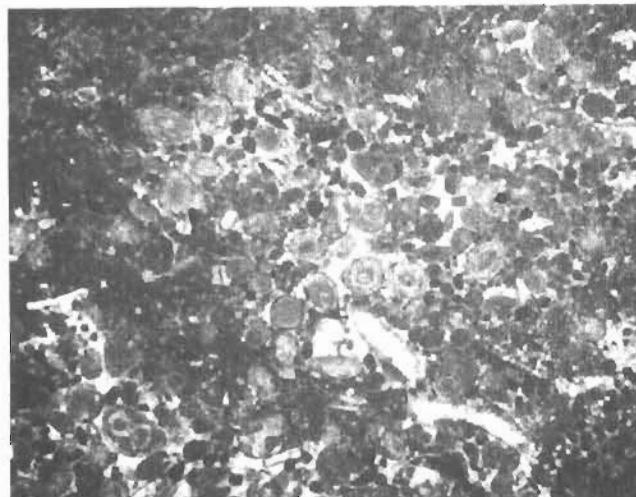
The coated-grain, ooid grainstone facies is characterized by very abundant coated grains and ooids. The coated grains are up to 0.4 mm in length and ovoid in shape. They have a nucleus composed of unidentifiable skeletal debris. The coating is composed of micrite and is up to 0.2 mm thick. The ooids are spherical, 0.3 to 0.1 mm in diameter, and have concentric laminae (fig. 5B, C). Some of the laminae appear to have been micritized. Overall they are moderately well sorted. The facies also contains intraclasts. These clasts are up to 1 cm in length and are composed of peloid pack-wackestone identical to the peloid grain-packstone facies. There is some microspar matrix as well as coarse spar cement.

In the field, this facies is massively bedded, 1 to 2 m thick. It contains some silicified stromatoporoids and *Murchisonia*. No opercula which otherwise are common in all other facies of this section, are found associated with this facies.

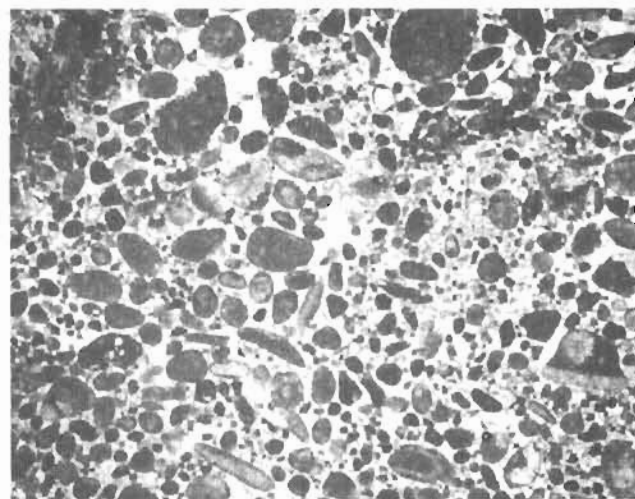
The limited fauna indicates environmental restriction (Wilson, 1975; Flügel, 1982). The occurrence of ooids also indicates restricted conditions of higher than average marine salinity and also formation within 2 m of sea level (Flügel,



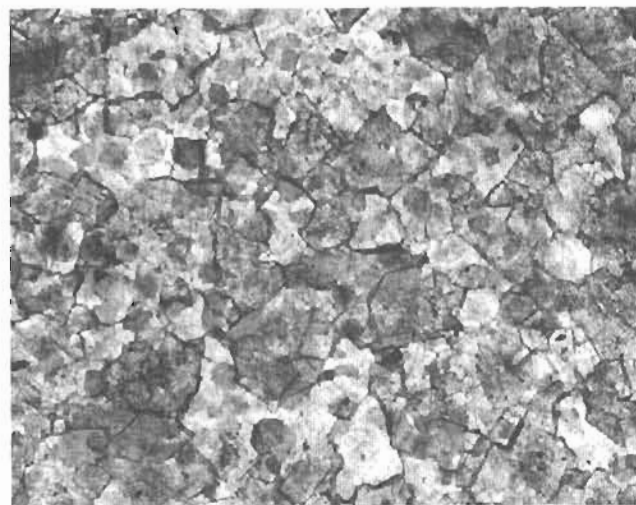
A



B



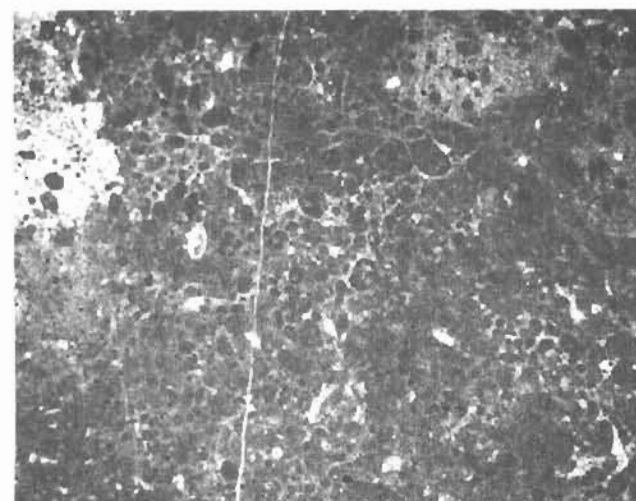
C



D



E



F



1982). The coated grains also indicate shallow-marine, high-energy conditions. Deposition took place as shoals on the muddy inner to middle shelf.

Depositional Sequence

The massive nature of these three facies and their noncyclical nature seen in section 1 (fig. 3) indicate persistence of depositional conditions. Deep subtidal, middle-shelf deposition was dominant, with minor deposition in shallow subtidal parts of the middle to inner shelf.

Section 2

The limestones of section 2 (fig. 4) can be grouped into five distinct facies based primarily upon petrographic differences: (1) gastropod packstone and intraclast, gastropod packstone; (2) ooid grainstone and ostracode grainstone; (3) mudstone; (4) intraclast packstone; and (5) peloid, intraclast grainstone.

Gastropod Packstone and Intraclast, Gastropod Packstone Facies

The gastropod packstone and intraclast, gastropod packstone facies is characterized by abundant, large (up to 3 cm in diameter), low-spired gastropods. In hand sample the gastropods appear to be the only allochem in this grain-supported lithology. They occur as casts and molds on broken surfaces. The shell material has been dissolved and replaced by large spar crystals. Other large allochems seen in hand sample include ostracodes and bivalves. Bedding varies from 15 to 30 cm thick.

The matrix is composed of an ooid packstone to ooid wackestone (fig. 6A). This is also the material that fills the whorls of the gastropods. The ooids are 0.1 to

0.2 mm in diameter. They are composed of single crystals of brownish calcite, but some concentric laminae have been preserved, indicating precursor allochem. The ooids are nearly perfectly circular and well sorted. The matrix also contains small (1 mm), disarticulated ostracodes. Fragments of trilobites, brachiopods, and bryozoans occur rarely in the matrix. The matrix is primarily cemented by spar crystals 5 mm in length. These spar crystals are poikilitic, but the enclosed ooids do not appear to be in optical continuity with the crystals. Poikilitic cement contains ooids that are not in grain contact but instead float in the spar. Boundaries of these ooids are not as well defined as ooids in nonpoikilitic cement. Most commonly the allochems are oriented randomly, but faint lamination may also be found.

A variation of this lithology contains intraclasts. The intraclasts are composed of ooid packstones, the same lithology that composes the matrix of this facies, and also mudstones (microspar). Some edges of the intraclasts are corroded and bored. Peloids occur associated with the intraclasts. Peloids are irregular in shape, composed of gray microspar, and are 0.2 to 0.4 mm in diameter.

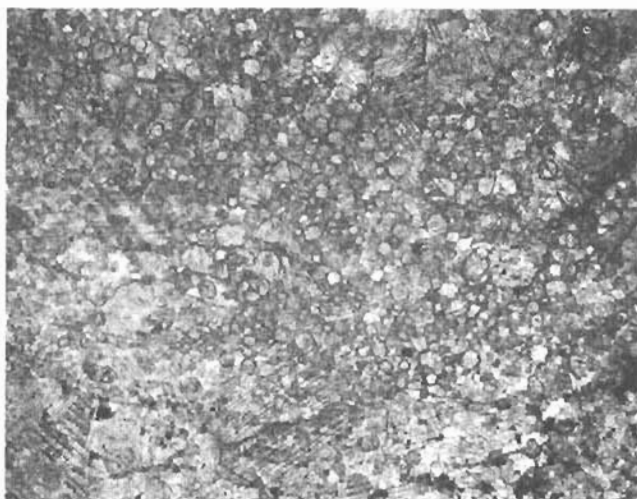
The fauna is typical of very shallow marine, restricted conditions (Wilson, 1975). The ooids indicate formation in very shallow (within normal wave base), restricted, hypersaline, marine conditions (Flügel, 1982). The intraclasts also indicate formation and subsequent deposition in very shallow marine conditions, supratidal to intertidal (Shinn, 1983). This association of allochems would be found in subtidal tidal channels. Intraclasts and gastropods are commonly concentrated in tidal channels (Shinn, 1983). The ooids probably formed offshore and were washed into channels by tides (Shinn, 1983). The grain-supported nature of these lithologies is also characteristic of tidal channels, as is the slightly muddy matrix (Wilson, 1975; Shinn, 1983). Tidal energy was high enough to move and concentrate large gastropods and intraclasts, and to transport subtidal sediment onshore, but not of a sufficient duration to winnow away the finer grain sizes.

Ooid Grainstone and Ostracode Grainstone Facies

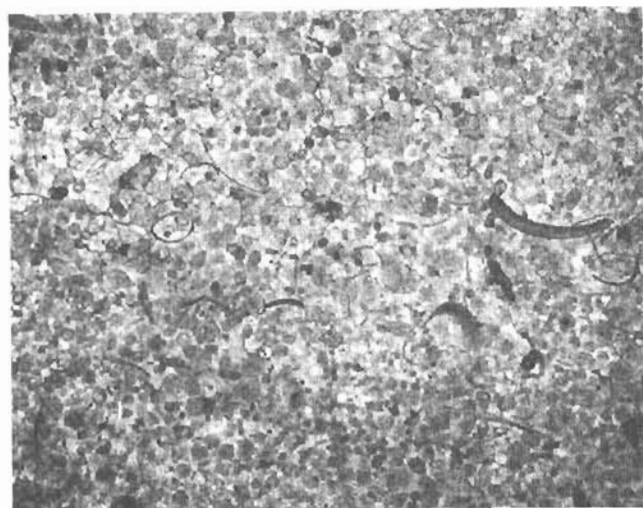
The ooid grainstone and ostracode grainstone facies is characterized by its grain-supported nature, ubiquitous ooids, and laminated texture (fig. 6B). The ooids are similar to those of the gastropod packstone facies and are composed of single crystals of brown calcite with preserved concentric laminae. The ooids vary in size between 0.1 and 0.5 mm, and they are circular and moderately well sorted. Ooids compose from 95 to 75 percent of the lithology. Laminae vary in thickness from 1 cm to 2 mm. Planar laminae and low-angle cross-laminae are both present and are primarily normally graded. Un-

←

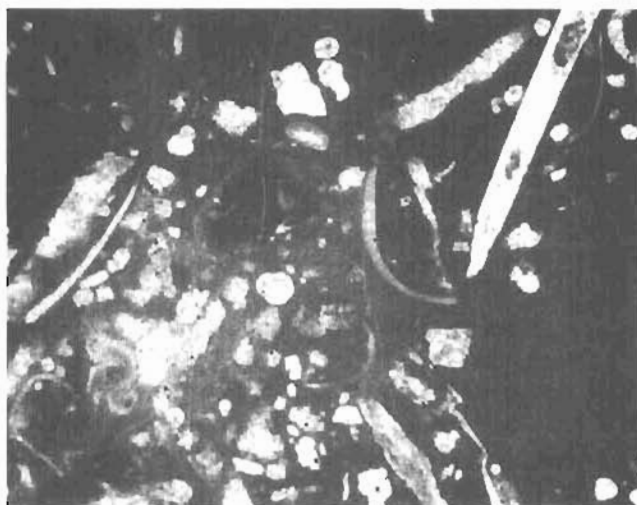
Figure 5. Photomicrographs (all under plane-polarized light) of samples from section 1, Telsitna Formation. Bar scale is 0.5 mm. A, Skeletal wacke-mudstone facies, 1 m above base of section. Skeletal wacke-mudstone showing coarse skeletal debris in micrite matrix. Debris includes pelmatozoan ossicles and trilobite fragments. B, Coated grain, ooid grainstone facies, 50 m above base of section. Coated grain, ooid grainstone showing ooids with concentric laminae and radial structure. Ooids (0.5 mm in diameter) display micritized rims. C, Coated grain, ooid grainstone facies, also 50 m above base. Coated grain, ooid grainstone showing peloidal interval. D, Fault zone 87 m above base of section. Dolomite with relict ooids or peloids. E, Peloid grain-packstone facies, 77 m above base of section. Peloid grain-packstone with skeletal elements of brachiopods, ostracodes, and trilobites in micrite matrix with poorly defined peloids. F, Peloid grain-packstone facies, 41 m above base of section. Peloid grain-packstone showing irregular-shaped peloids of various sizes in microspar matrix.



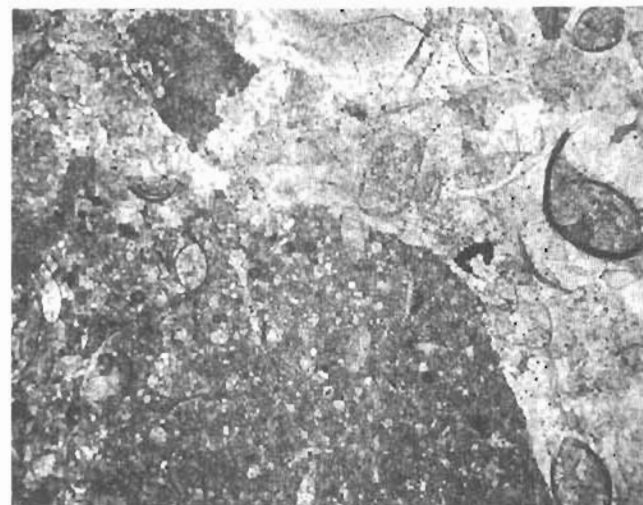
A



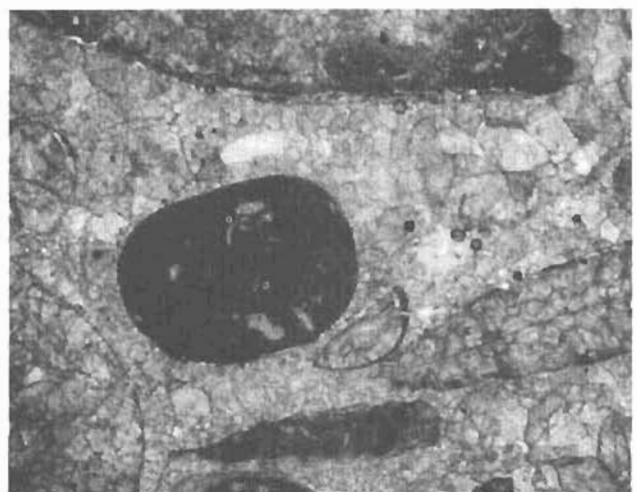
B



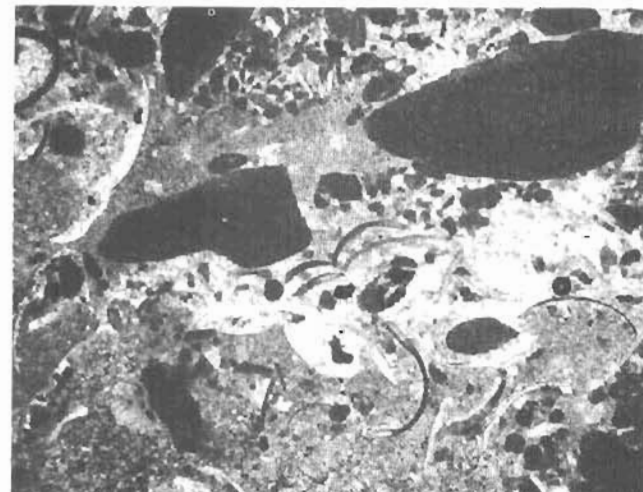
C



D



E



F

common, inverse grading occurs as well as combined inverse to normal grading. Contacts vary from sharp and well defined to gradational, and from planar to undulatory. In hand sample, the facies is easily distinguished by the coarse spar cement. In some instances, broken surfaces have spar-crystal faces 2 to 4 cm in length. Bedding is widely variable, from 8 to 60 cm.

Other allochems that occur in this facies include articulated and disarticulated ostracodes, trilobites, brachiopod debris, gastropods, bivalves, and peloids. Some beds contain as much as 25 percent ostracodes. Disarticulated ostracodes are commonly nested. Large macluritid gastropods rarely occur in this facies. They are poorly preserved and best seen on bedding planes as internal molds and casts.

Cement is composed of large, poikilitic spar crystals. The larger spar crystals enclose poorly defined, well separated, "floating" allochems. Large spar crystals occur with the larger ooids. Smaller ooids commonly occur in microspar cement. Lamination is accentuated by the presence of spar associated with coarse basal layers and microspar associated with the finer upper layers.

Bioturbation has disrupted laminae in several beds and creates structureless intervals. Small intraclasts are composed of ooid packstone. These intraclasts may be up to 1 cm in length, tabular in shape, and well rounded. Hardgrounds are common in the facies and are seen as laminae with coarse spar cement and an abrupt upper surface. The hardgrounds do not display any evidence of boring or encrustations.

Ooids indicate very shallow (<2 m) marine waters, within the influence of normal waves (Flügel, 1982). They also commonly indicate slightly elevated salinity (Flügel, 1982). The other allochems are also characteristic of restricted, hypersaline conditions (Wilson, 1975).

←

Figure 6. Photomicrographs (all under plane-polarized light) of samples from section 2, Telsitna Formation. Bars scale is 0.5 mm. *A*, Gastropod packstone facies, 0.3 m above base of section. Gastropod packstone showing matrix of ooid packstone-grainstone. Ooid in center (0.2 mm diameter) displays remnant concentric lamination and also shows cleavage traces of the calcite. *B*, Ooid grainstone facies, 9 m above base of section. Ooid grainstone with well sorted ooids (0.08 mm in diameter) and well preserved ostracodes. Ooids are poorly defined and are floating in poikilitic spar cement. *C*, Mudstone facies, 28 m above base of section. Skeletal wackestone showing trilobite and ostracode debris and a few recrystallized ooids. *D*, Intraclast packstone facies, 26 m above base of section. Intraclast packstone with intraclasts of ooid ostracode packstone. Edge of intraclast in contact with matrix, which is ostracode ooid packstone. *E*, Intraclast packstone facies, 41 m above base of section. Intraclast packstone showing small clast composed of slightly peloidal mudstone. Bryozoans also present. *F*, Peloid, intraclast grainstone facies, 29 m above base of section. Peloid, intraclast grainstone with mudstone intraclasts and peloids. Matrix contains abundant ostracodes and trilobites. Coarse, clear spar cements allochems but darker microspar also present.

The fine lamination and cross-lamination suggest deposition on the foreshore region of beaches (Inden and Moore, 1983) and intertidal levees, beach ridges, and tidal-flat overbank regions (Shinn, 1983). The sorting, nearly mud-free nature of the facies, nested ostracodes, and normal to inverse grading indicate continuous energy, with fluctuations in intensity, such as occur within the wave swash zone on beaches (Shinn, 1983). These features are common in beach deposits along with minor bioturbation and intraclasts (Shinn, 1983). Macluritid gastropods may have washed up on the beach after their death (Yochelson, 1975).

Mudstone Facies

The mudstone facies is characterized by micrite, which is unusual because the other four facies are extensively recrystallized. This facies is also unique because it contains mud-supported lithologies in a sequence dominated by grain-supported lithologies. Lithologies include mudstone and fossiliferous wackestone. In hand sample the facies is sometimes featureless but more commonly nodular. The nodular texture is composed of dark carbonate separated by light-brown crystalline carbonate. Bedding is very thin, 8 to 15 cm, but may be as thick as 30 cm.

Allochems include articulated and disarticulated ostracodes, trilobites, brachiopod debris, gastropods, ooids, and bryozoans (fig. 6C). Wackestones may have random orientation of allochems because of bioturbation; alternatively, wackestones may contain intervals of abundant allochems alternating with intervals of few allochems.

The mud-dominated nature and mud-supported lithology indicate conditions quite unlike those of the other four facies. This facies was deposited in a low-energy, subtidal environment. The allochems are a diverse mixture. Ooids were derived from the beach environment of the ooid grainstone facies and were washed into this environment. The fossils (abundant gastropods, ostracodes, bivalves) indicate restricted conditions. The nodular nature of the facies is the result of bioturbation and selective recrystallization of the burrow fill (Enos, 1983). Some of the fossils and mud of this facies were probably transported onto the tidal flats and through the tidal channels and contributed material to the rest of the facies. This facies is interpreted to represent a low-energy lagoon adjacent to tidal flats and beaches, which is a common association on inner shelves (Enos, 1983).

Intraclast Packstone Facies

The intraclast packstone facies is characterized by abundant intraclasts that are the main grain support. The intraclasts are composed of ooid grainstone and ostracode grainstone (fig. 6D, E) like those of the ooid

grainstone facies. Hand samples appear laminated. Bedding is 15 to 30 cm thick.

The matrix contains many different types of allochems: articulated and disarticulated ostracodes, trilobites, ooids, brachiopod debris, pelmatozoan ossicles, bryozoans, and gastropods. Ostracodes compose up to 40 percent of allochems in the matrix. Trilobites and ooids are the next most abundant. The remaining allochems form only a minor percentage. Fossil material is commonly 1 to 2 mm in size. This facies contains more biogenic material than other facies. The fossils are also coarser than in other facies.

Poikilitic spar cement is very common. It is similar to the poikilitic spar found in the other facies. Fine-grained micrite, not recrystallized to microspar, occurs as irregular blebs between allochems. This micrite also occurs commonly within articulated ostracode shells.

Intraclasts are commonly deposited in tidal channels or on supratidal flats (Shinn, 1983). They are formed by cementation of adjacent intertidal and shallow subtidal lithologies. The intraclasts are lithologically similar to the ooid grainstone facies and probably represent submarine cementation of that facies and subsequent reworking. The matrix between the intraclasts is similar to that of the gastropod packstone facies. This facies represents a tidal-channel deposit close to a beach.

Peloid, Intraclast Grainstone Facies

The peloid, intraclast grainstone facies is characterized by abundant peloids and intraclasts within the grain-supported lithology (fig. 6F). Furthermore, both the peloids and intraclasts are composed of fine-grained micrite, material similar to that of mudstone facies. The intraclasts are mudstones and contain no allochems. They are tabular and well rounded. The peloids compose up to 25 percent of the allochems. They are irregular in shape and quite variable in size, 0.5 to 1.0 mm.

The matrix contains some allochems. Trilobites and ostracodes make up approximately 20 percent of all allochems. In comparison to the other facies, this facies does not contain as diverse a fauna. Fossils are large, 1 to 2 mm, in comparison to fossils in the other facies.

Spar and microspar both occur as cement between allochems. The spar is not as coarse as in the other facies and does not have the poikilitic texture. Microspar is not abundant but does occur associated with the smaller peloids.

Lithologically this facies is similar to the gastropod packstone facies and the intraclast packstone facies, and it probably represents deposition in tidal channels. However, the lithology of the intraclasts is unlike those in the previously mentioned facies. The lithoclasts are lithologically similar to the lagoonal mudstone facies. The peloid, intraclast grainstone facies represents tidal-channel deposition near a lagoon.

Depositional Sequence

The distribution of facies in section 2 (fig. 4) is interpreted as follows. The base of the section represents a tidal-channel deposit. It is overlain by a thick section of beach deposits, which are in turn overlain by a thick deposit of lagoonal sediment. The upper part of the section is composed of interbedded beach deposits, tidal-channel deposits, and lagoonal deposits.

The thin-bedded nature of the entire section may indicate that the channels were broad, shallow features that migrated to form thin, blanket deposits. The thin beach deposits may have formed on the channel banks. Lack of typical tidal-flat features such as bird's-eyes, mudcracks, stromatolites, and cryptalgal laminites may result from insufficient sampling or may indicate that deposition took place on the outermost parts of the tidal flat in the lower intertidal zone. Therefore, upper intertidal and supratidal conditions are not represented in the section measured.

Sampling was insufficient to construct an idealized model of the interbedded or cyclic nature of the upper part of the section. Because the interval represented by section 2 was noted to underlie that of section 1, a deepening-upward succession is interpreted for these two unnamed subunits ("members") of the Telsitna Formation. Lack of adjacent, age-equivalent, described sections makes it impossible to form any conclusions about the nature of the carbonate platform or its paleogeography.

It can be concluded that the Bahamian tidal-flat model is a close analogy to these deposits. Ooid shoals and beaches graded into a lagoon, which then graded into tidal flats. Restricted conditions limited the fauna and allowed formation of ooids. The deposits described here were probably formed under humid conditions similar to those found in the Bahamas today.

PALEONTOLOGY

Gastropods

Gastropods are among the largest silicified fossils found at Telsitna Ridge. Both large shells (up to 15 cm in diameter) and opercula (10 cm high) are present. Previous collections indicated that several forms of "*Maclurites*" opercula are in the Ordovician section. Two of the purposes of the 1991 collecting were to determine if there was any systematic change in the opercula through the formation, and to determine if the opercula might have more biostratigraphic value than the shells to which they were once attached. At present, no biostratigraphic differentiation can be made within section 1 based upon opercula type. Two types of opercula are present: platelike to wedge shaped (fig. 7A-C, F, G),

and horn shaped (fig. 7D, E). Both have a projecting prong to which the retractor muscle of the gastropod was attached. This is a common feature of all *Maclurites* opercula. In addition, all of the forms of the Telsitna Formation show evidence of a secondary muscle attachment at the opposite end of the interior surface from the prong. This attachment is in the form of small pits or small digitate projections. This secondary attachment point was previously reported only from *M. logani* Salter. Both types of opercula are found in the same beds. The shells to which they correspond are not known. Macluritacean opercula were also found at USGS localities 11068-CO and 11063-CO. The genus *Maclurites* is rather widespread during the Middle Ordovician.

The gastropod genus *Lytopira* Koken was not known from the Middle Ordovician of Alaska previous to 1991. The genus is widespread during the Middle Ordovician, being reported from many localities in North America and the Baltics. Three large silicified specimens of the carrier shell were collected (fig. 7H-K). Linsley and Yochelson (1973) have reviewed the record of fossil and living carrier shells (gastropods that attach foreign material to their shells).

The oldest reported carrier shell is *Lytopira* Koken, 1896. *L. norvegica* Koken, 1925, has irregular attachment scars on the periphery and has been illustrated by Koken (1925) and Yochelson (1963) from the Llanvirnian-Llandeilian of Norway. *Lytopira* of Ibexian age, illustrated by Sando (1957) and Flower (1968), do not have attachment scars.

The Alaskan shell is an undescribed species of *Lytopira*. The shell is distinguished from other species by its large size, sharp crestal angulation, and spiral groove between two cords on the interior (fig. 7H). The cords are in a position suggesting that they may have been muscle attachment features corresponding to columellar folds in conspiral gastropods. Evidence of cementation of foreign objects is not known from all species of *Lytopira*, but all specimens of this species appear to have it.

The concave attachment scars on the exterior of the shell (fig. 7K) are smooth, and none of the foreign material is preserved. The curvature of the attachment scar suggests either a relatively large gastropod fragment or one of the strophomenid brachiopods present in the same beds. Linsley and Yochelson (1973) have shown that some Devonian and Holocene carrier shells are quite particular about the types of shells that they cement, often choosing only those of the same species.

Brachiopods

Silicified brachiopods are found in abundance at certain horizons within section 1, as well as in lithologi-

cally similar, underlying strata farther to the north along the ridge. Although the study of the recently acquired brachiopods is still preliminary, at least eight distinct species have been recognized from beds of this lithologic interval, including representatives of the following genera: *Doleroides*, *Austinella*, *Macrocoelia*, n. gen. aff. *Macrocoelia*, *Strophomena*, and an undetermined rhynchonellid. Many of these species are illustrated in figure 8. This moderate level of taxonomic diversity indicates relatively open-marine conditions for this interval. As noted earlier, the brachiopods show closest affinities with faunas described from eastern cratonal North America and the Siberian platform.

Brachiopods are almost wholly unknown from section 2, with only a few rare specimens of a single, undetermined orthoid being recognized from 13.4 to 13.7 m (44-45 ft) above the base of the section. The extreme low diversity of brachiopods here, usually considered to be stenohaline in environmental preference, coupled with the relatively high diversity of accompanying mollusks, suggest that the depositional environment of this section was subject to much more restricted, less open-marine conditions than section 1. Shallower water depth is also indicated by the dominance of such molluscan groups as gastropods and bivalves.

Acknowledgments.—Field work by Rohr, Blodgett, and Measures at Telsitna Ridge during 1991 was supported by The National Geographic Society. Subsequent laboratory preparation of thin sections and study of both the macrofauna and microfauna were conducted at the National Center (Reston, Va.) of the U.S. Geological Survey. We are grateful to William Beebe of the Alaska Department of Natural Resources, Division of Forestry at McGrath for providing helicopter support.

REFERENCES CITED

- Blodgett, R.B., and Clough, J.G., 1985, The Nixon Fork terrane—Part of an in-situ peninsular extension of the Paleozoic North American continent [abs.]: Geological Society of America Abstracts with Programs, v. 17, no. 6, p. 342.
- Churkin, M., Jr., 1973, Paleozoic and Precambrian rocks of Alaska and their role in its structural evolution: U.S. Geological Survey Professional Paper 740, 64 p.
- Decker, John, Blodgett, R.B., Box, S.E., Bundtzen, T.K., Clough, J.G., Coonrad, W.L., Gilbert, W.G., Miller, M.L., Murphy, J.M., Robinson, M.S., and Wallace, W.K., in press, Geology of southwestern Alaska, in Plafker, George, and Berg, H.C., eds., The Geology of Alaska: Boulder, Colo., Geological Society of America, Geology of North America, v. G1.
- Dunham, R.J., 1962, Classification of carbonate rocks according to depositional texture, in Ham, W.E., ed., Classification of carbonate rocks: American Association of Petroleum Geologists Memoir 1, p. 108-121.

- Dutro, J.T., Jr., and Patton, W.W., Jr., 1982, New Paleozoic formations in the northern Kuskokwim Mountains, west-central Alaska: U.S. Geological Survey Bulletin 1529-H, p. H13-H22.
- Enos, P., 1983, Shelf, in Scholle, P.A., Bebout, D.G., and Moore, C.H., eds., Carbonate depositional environments: American Association of Petroleum Geologists Memoir 33, p. 268-296.
- Flower, R.H., 1968, Part 1. Some El Paso guide fossils: New Mexico Bureau of Mines and Mineral Resources Memoir 22, p. 2-19.
- Flügel, Erik, 1982, Microfacies analysis of limestones: New York, Springer-Verlag, 633 p.
- Inden, R.F., and Moore, C.H., 1983, Beach, in Scholle, P.A., Bebout, D.G., and Moore, C.H., eds., Carbonate depositional environments: American Association of Petroleum Geologists Memoir 33, p. 211-265.
- Koken, Ernst, 1896, Die Leitfossilien: Leipzig, C.H. Tarnitz, 848 p.
- 1925, Die Gastropoden des Baltischen Untersilurs: Academie Science Russie Mémoire, Classe physico-mathématique, ser. 8, v. 37, no. 1, 326 p.
- Linsley, R.M., and Yochelson, E.L., 1973 Devonian carrier shells (*Euorophalidae*) from North America and Germany: U.S. Geological Survey Professional Paper 824, 25 p.
- Patton, W.W., Jr., 1978, Juxtaposed continental and oceanic-island arc terranes in the Medfra quadrangle, west-central Alaska, in Johnson, K.M., ed., The United States Geological Survey in Alaska: Accomplishments during 1977: U.S. Geological Survey Circular 772-B, p. B38-B39.
- Rohr, D.M., and Blodgett, R.B., 1988, First occurrence of *Helicotoma* Salter (Gastropoda) from the Ordovician of Alaska: Journal of Paleontology, v. 62, p. 304-306.
- Rohr, D.M., Dutro, J.T., Jr., and Blodgett, R.B., 1991, Gastropods and brachiopods from the Ordovician Telsitna Formation, northern Kuskokwim Mountains, west-central Alaska [abs.]: Australia Bureau of Mineral Resources, Geology and Geophysics, Record 1991/47, p. 29.
- 1992, Gastropods and brachiopods from the Ordovician Telsitna Formation, northern Kuskokwim Mountains, west-central Alaska, in Webby, B.D., and Laurie, J.R., eds., Global perspectives on Ordovician geology: Sixth International Symposium on the Ordovician System, Proceedings, University of Sydney, Australia: Rotterdam, A.A. Balkema Press.
- Sando, W.J., 1957, Beekmantown Group (Lower Ordovician) of Maryland: Geological Society of America Memoir 68, 161 p.
- Scholle, P.A., Bebout, D.G., and Moore, C.H., eds., 1983, Carbonate depositional environments: American Association of Petroleum Geologists Memoir 33, 708 p.
- Shinn, E.A., 1983, Tidal flat, in Scholle, P.A., Bebout, D.G., and Moore, C.H., eds., Carbonate depositional environments: American Association of Petroleum Geologists Memoir 33, p. 171-210.
- Wilson, J.L., 1975, Carbonate facies in geologic history: New York, Springer-Verlag, 471 p.
- Wilson, J.L., and Jordan, C., 1983, Middle shelf, in Scholle, P.A., Bebout, D.G., and Moore, C.H., eds., Carbonate depositional environments: American Association of Petroleum Geologists Memoir 33, p. 297-343.
- Yochelson, E.L., 1963, The Middle Ordovician of the Oslo region, Norway, 15. Monoplacophora and Gastropoda: Norsk Geologiske Tidsskrift, v. 43, p. 133-213.
- 1975, Early Ordovician gastropod opercula and epicontinental seas: U.S. Geological Survey Journal of Research, v. 3, p. 447-450.

Reviewers: William W. Patton, Jr. and Anita G. Harris

APPENDIX—FOSSIL LOCALITIES CITED IN TEXT (SEE FIG. 2 FOR LOCATION)

Collections of R.B. Blodgett

- USGS locality 11063-CO [=91ABd4 (=91T98 of Rohr)]: Rubble zone of silicified brachiopods (predominantly *Doleroides* n. sp.) trending northwest across ridge crest in the NE¼SW¼SW¼ sec. 19, T. 18 S., R. 27 E., Medfra D-2 quadrangle, lat 63°54'37" N., long 153°40'32" W. Elevation 3,250 ft. Locality in same unnamed lithologic unit of the Telsitna Formation as section 1 but is situated stratigraphically lower.
- USGS locality 11066-CO [=91ABd2]: Rubble containing abundant silicified brachiopods from northeast edge [3.0 to 6.1 m (10-20 ft) below ridge crest] of summit of hill in SE¼SW¼SW¼ sec. 19, T. 18 S., R. 27 E., Medfra D-2 quadrangle, lat 63°54'29" N., long 153°40'29" W. Locality situated stratigraphically above USGS locality 11063-CO but beneath base of section 1. However, this and the preceding locality are lithologically part of the same interval within the Telsitna Formation.
- USGS locality 11071-CO: Silicified brachiopods recovered from 0 to 1.2 m (0-4 ft) above the base of section 1, SE¼NE¼NE¼ sec. 25, T. 18 S., R. 26 E., Medfra D-2 quadrangle, lat 63°54'17" N., long 153°41'06" W.

Collections of D.M. Rohr

- USGS 11063-CO [=91T98 (=91ABd4 of Blodgett)]: See above.
- USGS 11068-CO [=91T99]: Summit of the ridge, 1,300-ft elevation, at the boundary between SW¼ sec. 19 and NW¼ sec. 30, T. 18 S., R. 26 E., Medfra D-2 quadrangle. The summit is a flat, circular area with a diameter of about 100 m. The shells are in medium- to thick-bedded, mollusk-brachiopod wackestone to packstone. Several types of macluritacean shells and opercula are found in the rocks as well as the brachiopods *Austinella*, *Doleroides*, *Macrocoelia*, n. gen. aff. *Macrocoelia*, and *Strophomena*.

FIGURES 7 AND 8

Figure 7. Middle Ordovician gastropods from USGS locality 11068-CO, Telsitna Formation.

A-C, F, G, Macluritacean operculum type 1:

A-C, Interior, exterior, and side views, respectively, x1.7, of platelike operculum with large, projecting retractor muscle process at lower right edge and secondary muscle scar near upper right edge, USNM 460982.

F, G, Interior and exterior views, x1.7, of a thicker specimen, USNM 460983.

D, E, Macluritacean operculum type 2, USNM 460984, exterior and oblique interior views, x1.7. Note the large projecting muscle process and the smaller, digitate secondary muscle attachment point.

H-K, Lytospira n. sp.:

H, I, USNM 460731, oblique side view showing spiral groove and cords on interior surface, x1.1, top view of shell with angular crest, x1.1.

J, K, Basal view of another shell, USNM 460732, x1.1, oblique basal view, x2.2, showing attachment scars and repaired break in shell near left edge of photograph.

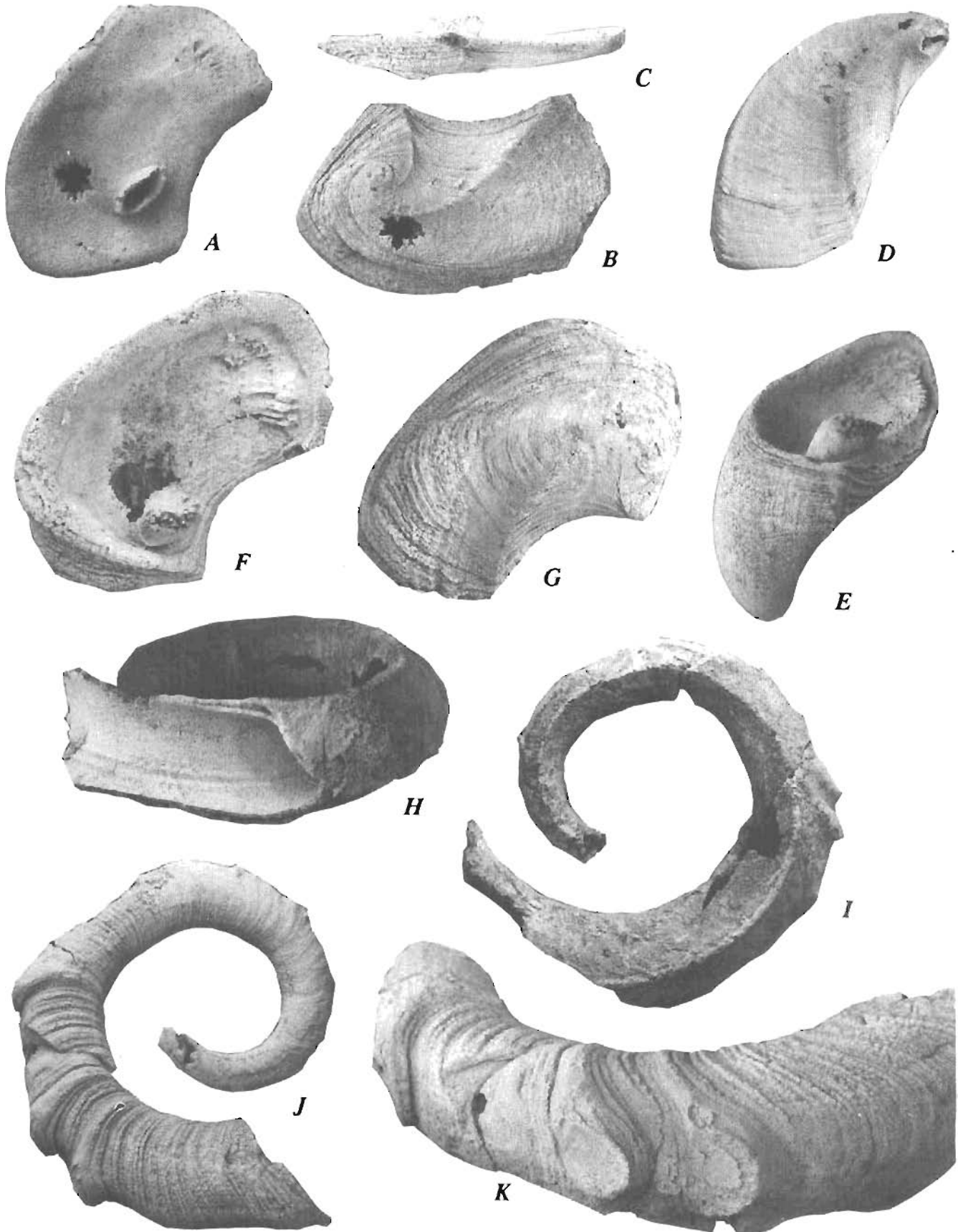


Figure 8. Brachiopods from Middle Ordovician strata of the Tetsina Formation.

A, B, Doleroides n. sp. aff. *D. panna* (Andreeva), exterior and interior views of free pedicle valve, USNM 460985, x2, USGS locality 11063-CO.

C–F, Austinella n. sp., ventral, dorsal, posterior, and lateral views of articulated specimen, USNM 460986, x2.6, USGS locality 11071-CO.

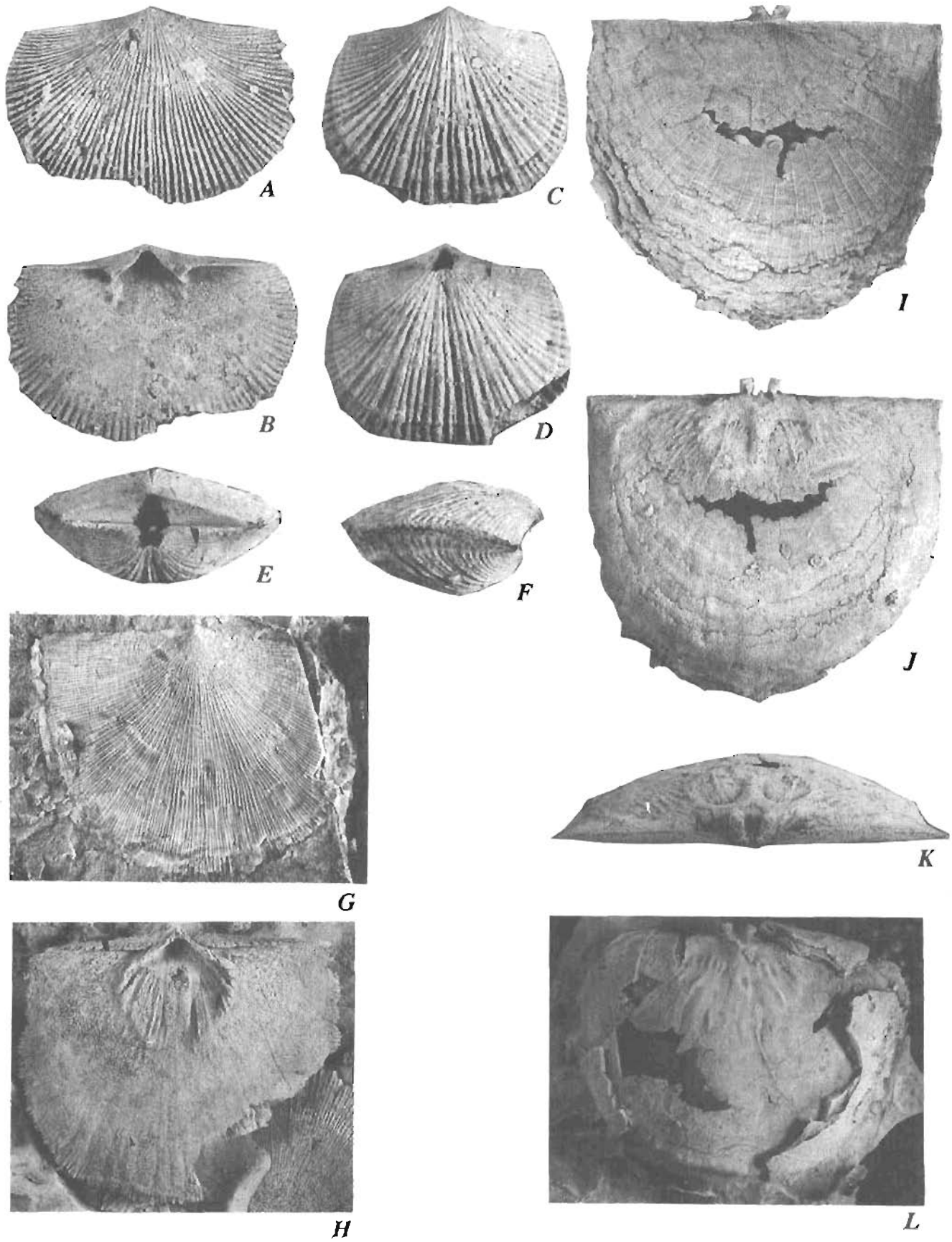
G, H, Strophomena sp., USGS locality 11071-CO:

G, Exterior view of a pedicle valve, USNM 460987, x2.

H, Interior view of another pedicle valve, USNM 460988, x2.

I–K, n. gen. aff. *Macrocoelia*, n. sp., exterior, interior, and posterior views of etched free brachial valve, USNM 460989, x2, USGS locality 11066-CO.

L, Macrocoelia n. sp., interior view of brachial valve (on right hand of specimen, some remnants of attached portions of the pedicle valve are visible), USNM 460990, x2, USGS locality 11071-CO.



Cenozoic Uplift History of the Mount McKinley Area in the Central Alaska Range Based on Fission-Track Dating

By George Plafker, Charles W. Naeser, Robert A. Zimmermann, John S. Lull, and Travis Hudson

Abstract

Fission-track dating of apatite and zircon from the Paleocene McKinley pluton at Mount McKinley, Mount Dan Beard, and Mount Huntington provides new data on uplift rates of this part of the western Alaska Range. Zircon ages of 52 to 39 Ma from the three mountains indicate rapid middle to late Eocene cooling—inferred to result from uplift and erosion. The apatite ages indicate relative stability during middle to late Miocene time. Rapid uplift and cooling of Mount McKinley began in the early Pliocene (about 4.2 Ma). Apatite ages (9.7–3.9 Ma) indicate that Mount McKinley has uplifted at an average rate of roughly 1.3 mm/yr for the last 4.2 m.y. Apatite and zircon ages from the same elevations on Mounts Huntington and Dan Beard are significantly older than those on Mount McKinley. This age difference indicates that Mount McKinley has been elevated by about 1,800 m relative to Mounts Huntington and Dan Beard during the late Cenozoic. This differential movement could be due to either regional tilting or to differential uplift along unidentified intervening faults.

INTRODUCTION

The rugged central Alaska Range has some of the greatest local topographic relief in the world and includes Mt. McKinley, the highest peak in North America (6,193 m, 20,320 ft). A suite of 13 granitoid rock samples was collected from Mounts McKinley, Dan Beard (3,127 m, 10,260 ft), and Huntington (3,731 m, 12,240 ft) by Geoff Radford and Bill Kitson during a climbing expedition in May 1981 (fig. 1). The samples were taken from a large vertical elevation range on the three mountains in order to obtain information on uplift/cooling rates by fission-track studies of apatite and zircon. Ten of the hand-specimen-size samples yielded zircon and apatite suitable for dating; the three highest samples collected on Mount McKinley at elevations of 5,305 m, 5,854 m, and 6,128 m did not contain adequate mineral assemblages for fission-track dating (samples A, B, C, fig. 1).

Fission-track samples from Mount McKinley were collected from the northern part of the McKinley pluton;

those from Mount Huntington and Mount Dan Beard are in the southern and eastern parts of the pluton, respectively (fig. 2). As described by Reed and Nelson (1977) and Lanphere and Reed (1985) mainly on the basis of float samples, the McKinley pluton is dominantly medium- to coarse-grained, hypidiomorphic-granular biotite granite. Petrographic data for the 7 samples collected from this pluton on Mount McKinley show compositional variation from leucocratic, tourmaline-bearing granite near the top of the mountain (samples A, B, C) to muscovite granite, biotite-muscovite granite, and biotite-muscovite granodiorite below (samples D, E, F, G, table 1). Ruth pluton, immediately to the east, is a large granitoid mass of weakly foliated, medium- to coarse-grained biotite with rare hornblende, coarse-grained biotite granite and granodiorite, and medium- to coarse-grained biotite and biotite-muscovite granite (Reed and Nelson, 1977). Except for the presence of reported rare hornblende in the Ruth pluton, it is essentially identical in composition with the McKinley pluton, and the two bodies likely merge at depth to form a continuous batholith.

Both the McKinley and Ruth plutons are considered to be part of the early Tertiary McKinley sequence of granitoid intrusions in the Alaska Range that have a late Paleocene emplacement age (average 57.3 Ma) based on K-Ar dating of nine samples of biotite and muscovite (Lanphere and Reed, 1985).

FISSION-TRACK DATA

Results of fission-track dating of zircons and apatites from the granitic rocks are presented in table 2. The analytical techniques used in this study are similar to those described in Bryant and Naeser (1991).

Significance of Fission-Track Ages in Interpreting Uplift Histories

The fission-track dating method is based on determination of the ratio of fission tracks spontaneously formed

in a mineral by decay of radioactive elements in the mineral to fission-tracks induced in the mineral by exposing it to a calibrated radioactive source. For a fission-track age to be geologically significant, the fission tracks must be retained once they are formed and be stable at ambient surface temperatures. Heating can cause partial to complete fading of the spontaneous tracks. Fission tracks are stable in most nonopaque minerals (opaque minerals do not retain tracks) at temperatures of 50°C or less. If a mineral is heated above a critical temperature and held there for a time, the fission tracks will begin to disappear (anneal). If the mineral is held at that temperature for a sufficiently long time, the tracks will completely disappear. The process of annealing is a time-temperature function (Fleischer and others, 1965); that is, a short time at a high temperature will have the same effect on the fission tracks as a long time at low temperature. As long as a mineral is held at or above its annealing temperature, it will not retain fission tracks. When this mineral is cooled to temperatures below which total annealing can take place, the mineral will again begin to accumulate tracks. Therefore, if an apatite or zircon is emplaced at depth in the crust where

the temperature is sufficient to cause total track annealing, it would have a zero apparent age. If it is then uplifted and cooled, it will yield a fission-track age that is related to the uplift event (Naeser, 1979a).

There is, however, a zone between total track loss and total track retention called the partial-annealing zone (PAZ) (Naeser, 1979a). In the case of apatite, this zone is about 30°C to 50°C wide (Naeser, 1981). If a mineral resides in this zone for any length of time, the fission tracks are only partially retained and the age calculated will be an intermediate age with no numerical significance in a strict geological context. There are several techniques that can be employed to test an apatite sample in order to determine whether or not the age from that sample is an intermediate "mixed" age or not. The best method is to determine the length distribution of confined fission tracks (Gleadow and others, 1986). In some studies, such as this one, the track densities are too low for lengths to be determined. This is in contrast to relatively slow uplift, where the blocking temperature for zircon could be around 160°C.

The annealing temperature for fission tracks in apatite under conditions of geologic heating is fairly well

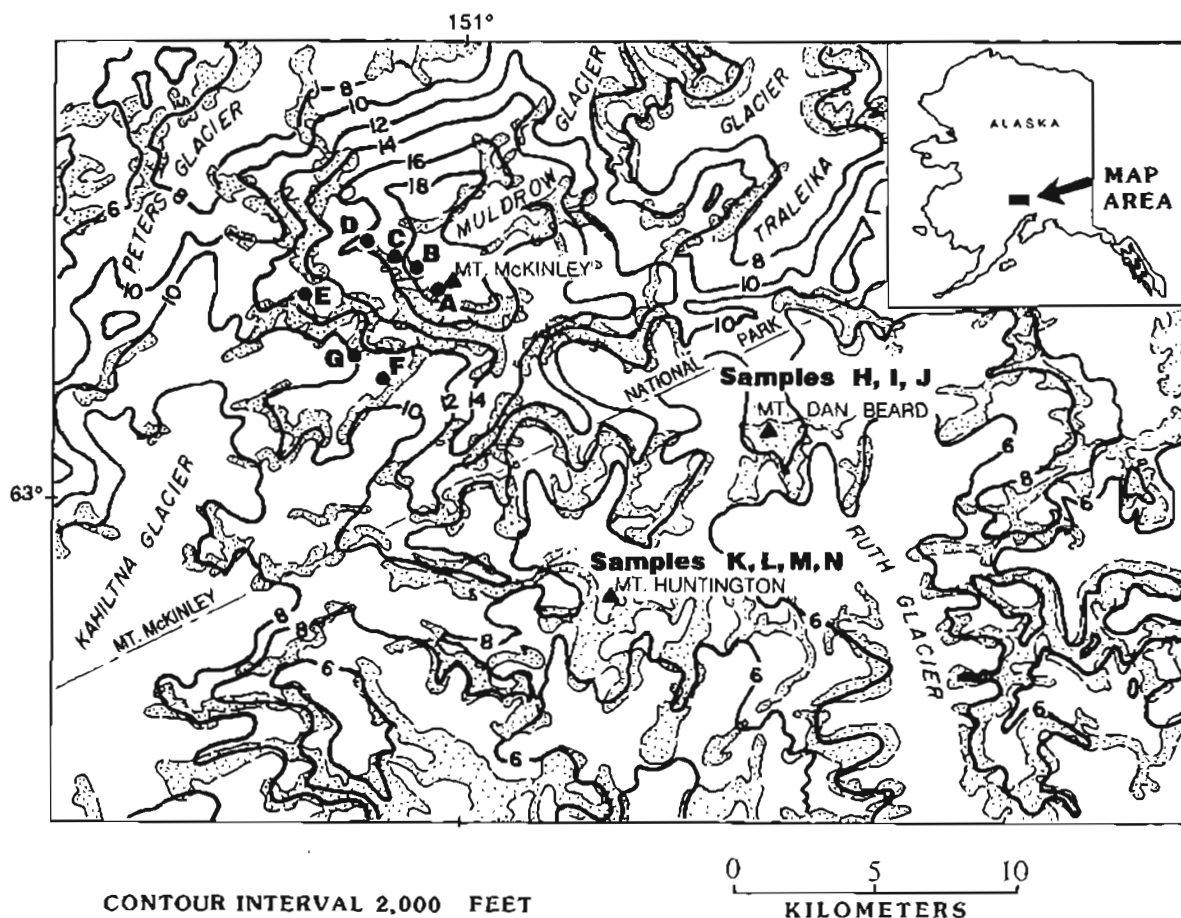
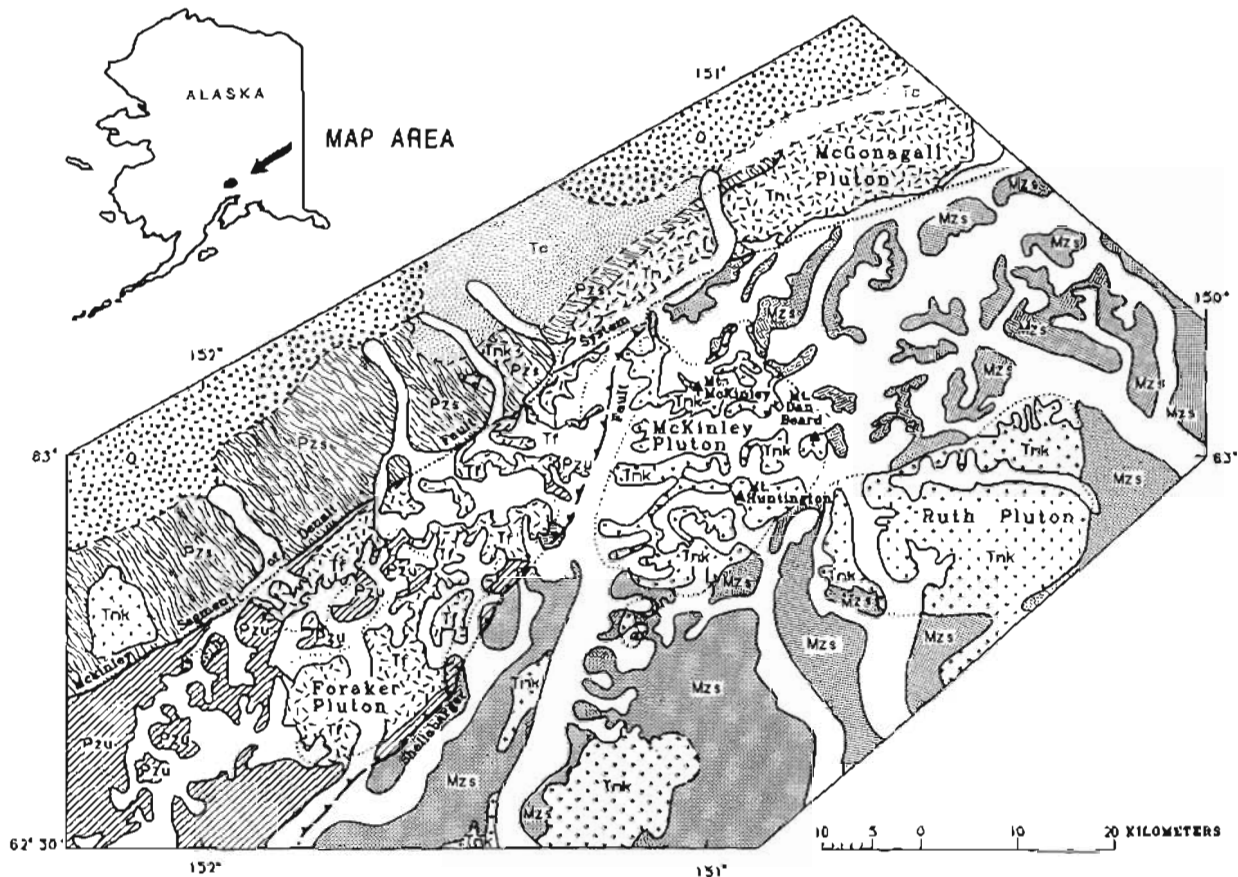


Figure 1. Topographic map showing locations of samples A through N from Mount McKinley, Mount Huntington, and Mount Dan Beard. Stippled pattern indicates area of exposed bedrock.



EXPLANATION

Q	Unconsolidated deposits (Quaternary)
Tm/Tf	Granodiorite of McGonagall (Tm) and Foraker (Tf) plutons (Oligocene)
Tmk	Granite and quartz monzonite of the Mount McKinley sequence of Reed and Lanphere (1972) (early Tertiary). Includes McKinley and Ruth plutons (Eocene)
Tc	Clastic sedimentary rocks, volcanic rocks, and minor coal of the Cantwell Formation (Paleocene)

Kahiltna terrane

Mzs	Mainly slate, argillite, and graywacke (Jurassic and Cretaceous)
-----	--

Mystic terrane

Pzu	Undifferentiated flysch, volcanogenic flysch, wildflysch, pillow basalt, chert, and ultramafic rocks; shelf- and slope-deposited clastic rocks and reef limestone; and subaerial clastic sedimentary rocks (late and middle Paleozoic)
Pzs	Argillite, slate, sandstone, schist, and limestone (Paleozoic)

— — — Contact—Dashed where approximate; dotted where concealed

— ····· Fault—Sawteeth on upper plate; dotted where concealed

Figure 2. Generalized map showing geologic setting of McKinley pluton, which underlies Mount McKinley, Mount Huntington, and Mount Dan Beard (modified from Reed and Lanphere, 1972; Reed and Lanphere, 1974, fig. 2; Reed and Nelson, 1977). Location shown on figure 5.

Table 1. Summary of lithologic and petrographic data for granitoids from Mount McKinley

Sample (fig. 1)	Elevation	Lithology	Granularity, texture, and structure	¹ Mineralogy			Plagioclase	² C.I.	Remarks
				Essential	Accessory	Secondary			
A	6,128 m (20,100 ft)	Granite	Medium- to coarse-grained, seriate; hypidiomorphic; massive.	<u>Plagioclase,</u> <u>quartz,</u> <u>K-feldspar,</u> biotite muscovite	Tourmaline, ³ zircon, garnet	Sericite	An ₂₀ -An ₁₀ : patchy normal and oscillatory zoning.	5	Tourmaline relatively abundant (~1%). Zircon with pleochroic haloes in biotite.
B	5,854 m (19,200 ft)	Granite	Medium-grained, equigranular to seriate; hypidiomorphic; massive.	<u>Plagioclase,</u> <u>quartz,</u> <u>K-feldspar,</u> muscovite	Tourmaline, ³ garnet, ³ topaz, ⁴ cassiterite, ±a patite. ±zircon (?)	Sericite	An ₁₅ -An ₁₀ : patchy zoning, complex twining.	2-3	Tourmaline abundant (2-3%), brown, color zoned. No biotite or hornblende.
C	5,305 m (17,400 ft)	Granite	Fine- to coarse-grained, seriate to porphyritic with K-feldspar phenocrysts; hypidiomorphic; massive.	<u>K-feldspar,</u> <u>plagioclase,</u> <u>quartz,</u> muscovite	Tourmaline, garnet	Sericite	An ₂₀ -An ₁₀ : patchy zoning. Some bent twin lamellae.	1-2	K-feldspar is perthitic. Tourmaline (1-2%).
D	4,907 m (16,100 ft)	Granite	Medium- to coarse-grained, seriate; hypidiomorphic; massive.	<u>Quartz,</u> <u>plagioclase,</u> <u>K-feldspar,</u> biotite, muscovite	Apatite, zircon, ³ garnet	Sericite, chlorite, white mica, fine-grained epidote	An ₂₀ -An ₁₀ : zoning not apparent. Altered.	5	Biotite mostly replaced by chlorite and white mica. Plagioclase largely replaced by sericite and epidote.
E	4,054 m (13,300 ft)	Grano-diorite	Fine- to medium-grained, seriate; hypidiomorphic; massive	<u>Quartz,</u> <u>plagioclase,</u> <u>K-feldspar,</u> biotite, muscovite	Apatite, zircon, ³ garnet	Sericite, chlorite, calcite	An ₃₀ -An ₂₀ : oscillatory zoning.	10	Minor chlorite after biotite; sericite and calcite after plagioclase.
F	3,444 m (11,300 ft)	Grano-diorite	Medium- to coarse-grained, equigranular; hypidiomorphic; massive	<u>Plagioclase,</u> <u>quartz,</u> <u>K-feldspar,</u> biotite	Apatite, zircon, tourmaline, epidote	Chlorite, sericite, fine-grained epidote	An ₂₀ -An ₁₀ : normal and oscillatory zoning.	15	Chlorite after biotite; sericite and epidote after plagioclase.
G	3,048 m (10,000 ft)	Granite	Medium- to coarse-grained, equigranular; hypidiomorphic; massive.	<u>Quartz,</u> <u>plagioclase,</u> <u>K-feldspar,</u> biotite	Apatite, zircon	Sericite, epidote, chlorite	An ₂₀ -An ₁₀ : fuzzy oscillatory zoning. Partly altered.	10	Chlorite after biotite; sericite and epidote after plagioclase. K-feldspar strongly perthitic.

¹ Visual estimate listed in order of decreasing abundance (underline indicates approximately equal abundance).

² Color index (C.I.); visual estimate.

³ Identified in mineral separates.

⁴ Identified by X-ray analysis.

known (Naeser, 1979b). With slow cooling it will begin to retain tracks at temperatures of about 100°C. If the cooling is rapid, as in an active tectonic region, a temperature of about 120°C can be used.

The annealing of fission tracks in zircon, under geological conditions, is not very well known. Limited data

suggest that temperatures between about 160°C (C.W. Naeser, unpub. data) and about 230°C (Hurford, 1986) will completely anneal fission tracks in zircon over periods of time in excess of several million years. The lower value of 160°C was determined from a metamorphic complex in the Yukon-Tanana upland between the Alaska

Table 2. Fission-track data for Mounts McKinley, Huntington, and Dan Beard

Sample (fig. 1)	Mineral (Z Zircon (A-Apatite))	Grains Counted	Observed Fossil Track Densities (10 ⁶ tracks/cm ²)	Track Densities Induced (#counted)	¹ Neutron Fluence (10 ¹⁵ n/cm ²)	² Age ± 95 percent CI (Ma)	Elevation
MOUNT MCKINLEY							
G-----	Z	6	9.09 (1,852)	6.61 (1,346)	.976 ¹	38.7 ± 4.8*	3,048 m
	A	20	.363 (37)	1.06 (1,082)	3.81 ²	3.9 ± 1.3	10,000 ft
F-----	Z	6	9.50 (1,848)	6.78 (1,317)	.976 ¹	40.9 ± 3.4	3,444 m
	A	20	.0333 (33)	.907 (898)	3.83 ²	4.2 ± 1.4	11,300 ft
E-----	Z	8	10.55 (2,980)	6.33 (1,787)	.976 ¹	45.5 ± 6.7*	4,054 m
	A	15	.106 (79)	2.13 (1,578)	3.84 ²	5.8 ± 1.4	13,300 ft.
D-----	Z	7	11.22 (1,927)	7.72 (1,320)	.976 ¹	40.9 ± 4.8*	4,907 m
	A	11	.0629 (34)	.744 (402)	3.86 ²	9.7 ± 3.5	16,100 ft
MOUNT HUNTINGTON							
K-----	Z	6	8.21 (1,179)	5.12 (734)	.976 ¹	46.7 ± 4.7	2,560 m
	A	15	.956 (71)	1.76 (1,309)	4.32 ³	7.0 ± 1.7	8,400 ft
L-----	Z	8	8.27 (1,130)	5.32 (727)	.976 ¹	45.2 ± 5.5	2,957 m
	A	15	.166 (123)	2.27 (1,685)	4.32 ³	9.4 ± 1.8	9,700 ft
M-----	Z	6	7.44 (1,378)	4.66 (863)	.976 ¹	46.5 ± 4.4	3,200 m 10,500 ft
N-----	Z	6	11.20 (1,037)	6.87 (636)	.976 ¹	45.2 ± 5.1*	3,414 m
	A	10	.234 (116)	2.66 (1,317)	4.32 ³	11.4 ± 2.3	11,200 ft
MOUNT DAN BEARD							
H-----	Z	6	6.15 (939)	4.30 (656)	.976 ¹	41.7 ± 4.5	2,438 m
	A	18	.229 (243)	2.38 (2,519)	4.32 ³	12.5 ± 1.7	8,000 ft
I-----	Z	6	9.87 (1,600)	5.59 (906)	.976 ¹	51.4 ± 4.7	2,743 m
	A	19	.244 (242)	2.34 (2,325)	3.79 ²	11.8 ± 1.7	9,000 ft
J-----	Z	7	9.71 (1,348)	5.11 (710)	.976 ¹	51.8 ± 7.8*	2,987 m
	A	15	.205 (124)	1.84 (1,113)	4.32 ³	14.3 ± 2.8	9,800 ft

¹ Samples irradiated in three different batches (superscripts 1, 2, and 3). For irradiation #1, 2,143 tracks were counted in the standard detectors and the uncertainty in neutron fluence is 2.2 percent. For irradiation #2, 2,489 tracks were counted in the two standard detectors and a significant neutron gradient was observed across the sample; neutron fluences are interpolated between the standard values and the uncertainties and are approximately 2.8 percent. For irradiation #3, 2,899 tracks were counted, no gradient was observed, and the uncertainty in neutron fluence is 1.9 percent.

² Age calculation formula is after Fleischer and others (1965) using the following constants:
 $\lambda_D = 1.55 \times 10^{-10} \text{ yr}^{-1}$; $\lambda_f = 7.03 \times 10^{-17} \text{ yr}^{-1}$; $U^{235}/^{238} = 0.00725$; $\sigma = 580.2 \text{ barns}$.
 Asterisk indicates that sample age failed the χ^2 test (5 percent level).

Range and the Fairbanks area that cooled very slowly (Naeser, 1981), while the higher value of Hurford (1986) is based on data from the Alps of Switzerland where the cooling rates are much higher. Zircons in the McKinley area probably record cooling from about 230°C because uplift rates are comparable to those encountered in the Alps.

Zircon Fission-Track Data

The zircon fission-track ages record rapid post-emplacement cooling during the Eocene (fig. 3). All of these ages have large error bars that range from 7.8 Ma

to 3.4 Ma. On Mount McKinley, ages are about 46 to 39 Ma for four samples through a vertical range of 1,859 m; on Mt. Huntington, ages are 47 to 45 Ma for four samples through a vertical range of 640 m; and on Mt. Dan Beard, the two highest samples are 52 to 51 Ma through a vertical range of 244 m. A possible exception is on Mount Dan Beard, where samples I (about 51 Ma) and H (about 42 Ma), with vertical separation of 305 m, suggest slowing of the cooling rate during the late Eocene. Cooling is assumed to result from post-emplacement uplift and erosion of the pluton. Concordancy of most of the ages from a single mountain indicates that the uplift was probably very rapid, but this cooling occurred at slightly different times on each of

these mountains. The large error bars for all the zircon samples preclude meaningful determination of uplift rates except possibly on Mt. Dan Beard, where it may be as low as 0.03 mm/yr for the interval between samples H and I (fig. 3).

Apatite Fission-Track Data

The apatite fission-track data provide information on the Neogene uplift history of Mounts McKinley, Huntington, and Dan Beard. We assume that cooling is a direct function of uplift and erosion. A plot of apatite fission-track age versus elevation for the three mountains is shown in figure 4. Straight lines are shown through all data points except I on Mt. Dan Beard, which we regard as probably anomalous. Alternative regression curves can be fit through the data points, but this was not done because the small number of samples from each mountain and the large error bars do not merit a more sophisticated analysis.

The data from Mount McKinley show a change in slope occurring at about 4.2 Ma, with apparent uplift rates of 0.2 to 0.4 mm/yr prior to 4.2 Ma. The elevation of this change in slope on Mt. McKinley is 3,444 m (11,300 ft). We interpret this to indicate that the

samples above 3,750 m on Mt. McKinley were in the partial-annealing zone prior to the most recent uplift and the samples from below 3,750 m were totally annealed prior to this latest period of uplift and cooling. Similarly, we interpret the apatite ages from Mounts Huntington and Dan Beard to be from an uplifted partial-annealing zone with apparent uplift rates of 0.1 to 0.3 mm/yr. However, if the apatite ages from above 3,750 m on Mount McKinley and all of the apatite ages from Mounts Huntington and Dan Beard represent uplifted partial-annealing zones, these ages can not be used to determine uplift/cooling rates.

An abrupt increase in the uplift rate on Mount McKinley occurred during the early Pliocene. The straight-line uplift rate defined by samples F and G is about 1.3 mm/yr since about 4.2 Ma and the y-intercept on the graph (fig. 4) would be at -2.1 km. Thus, for an apatite closure temperature of 120°C at a depth of 5.1 km below ground surface (difference in elevation between elevation of sample G and the y intercept), the indicated geothermal gradient is about 25°C/km. Alternative regression curves can be fit through the Mt. McKinley apatite data that tend to shift the curve toward the y-axis, thereby decreasing the average uplift rate and increasing the geothermal gradient. For example, a best-fit line between points F and G and the graph origin

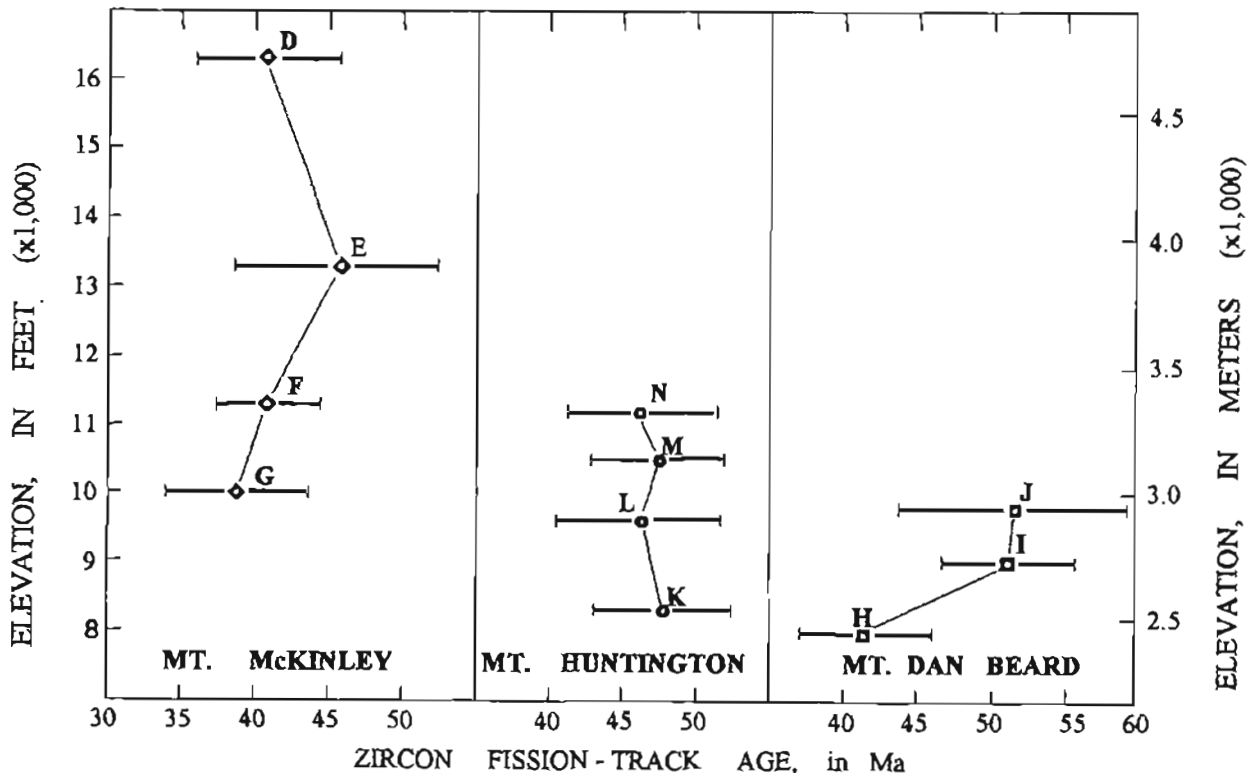


Figure 3. Zircon fission-track ages versus elevation for Mounts McKinley, Huntington, and Dan Beard (locations of samples on fig. 1; fission-track data in table 2). Vertical lines are error bars for each sample.

yields an apparent uplift rate of 0.80 mm/yr since about 4 Ma, with a geothermal gradient of 40°C/km. Although the geothermal gradient in this area is unknown, data from geologically comparable regions in the western Cordillera suggest it is likely to be less than 40°C/km and that the corresponding average uplift rate of 0.80 mm/yr is likely to be an approximate minimum rate for Mt. McKinley.

The recent uplift rate of about 1.3 mm/yr for Mt. McKinley, although high, is considerably slower than the 10 mm/yr rate determined for the tectonically active Nanga Parbat area in the Himalaya Mountains (Zeitler and others, 1982) or known Holocene uplift rates of up to 10+ mm/yr in some areas along the Gulf of Alaska coast (Plafker and Rubin, 1978).

Apatite fission-track ages comparable to those on Mount McKinley are found approximately 1,800 m lower on Mount Huntington and even lower on Mount Dan Beard. Although there is more scatter in the zircon fission-track data, they show the same general relationship. Thus, the combined apatite and zircon data indicate that Mount McKinley has undergone differential uplift of at least 1,800 m in the Neogene relative to Mounts Huntington and Dan Beard. This difference suggests either regional southeastward tilting or the presence of an unidentified fault between Mount McKinley

and Mounts Huntington and Dan Beard, with the Mount McKinley side relatively uplifted.

TECTONIC SETTING

Reconnaissance geologic mapping in the study area by Reed and Lanphere (1974), Reed and Nelson (1977), and Jones and others (1983) shows that the McKinley pluton lies in a structurally complex southwest-trending zone of thrust faults that splay off the Denali fault system within and east of the study area (figs. 2, 5).

Neotectonic Data

The long Denali fault system marks the northern boundary of the Saint Elias and Wrangell blocks with the remainder of Alaska (fig. 5). Seismicity is low along most of the fault, and there is no evidence of historic slip. In the segment between the Wrangell block and North America, however, the fault is dominantly dextral strike slip with geologically determined Holocene slip rates of 9 to 20 mm/yr with an overall decrease from east to west along the northern margin of the Wrangell block (Plafker and others, 1977). The slip rate is close

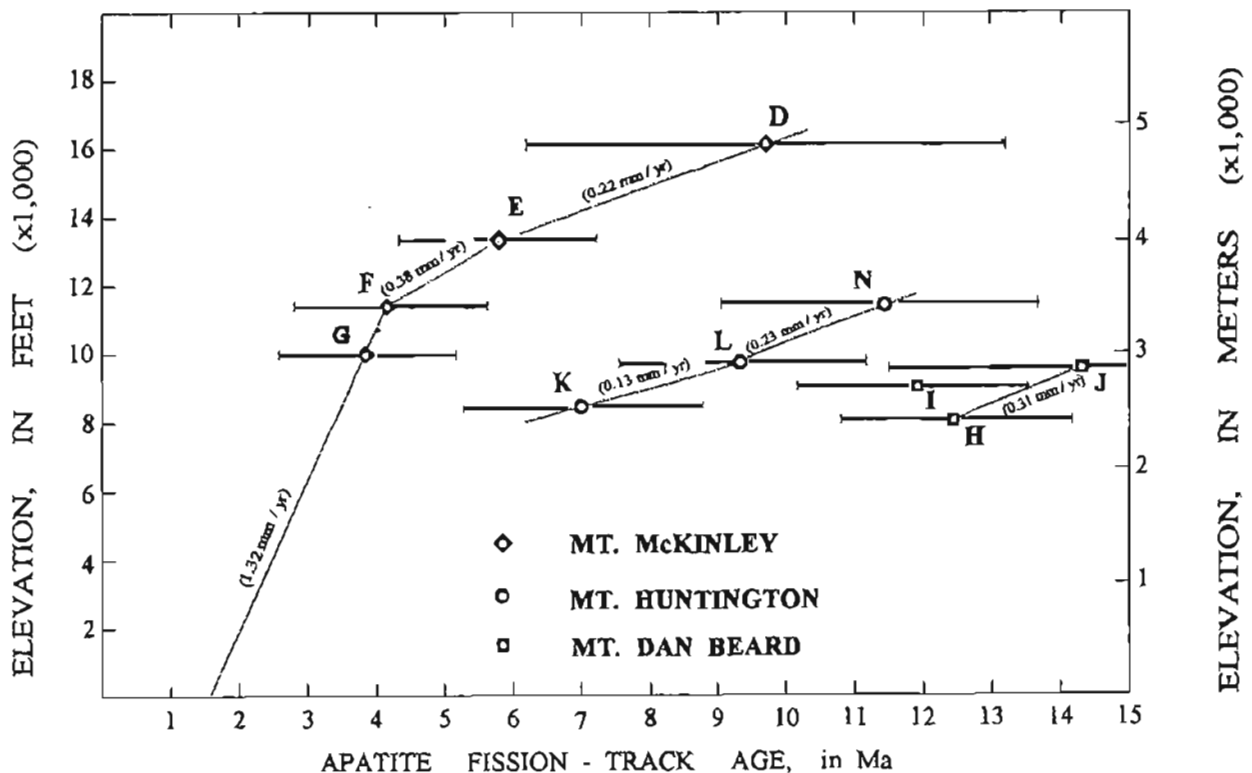


Figure 4. Neogene uplift rates of Mounts McKinley, Huntington, and Dan Beard based on apatite fission-track dating (locations of samples on fig. 1; fission-track data in table 2). Vertical lines are error bars for each sample.

to 9 mm/yr along the Denali fault 30 km east of the map area; there is no evidence for Holocene dextral displacements west of the point where the Shellabarger fault splays off the Denali fault just north of the McKinley pluton (fig. 2).

A kinematic interpretation of Holocene Pacific-North American plate interaction in southern Alaska has been made by Lahr and Plafker (1980) and Plafker and others (in press) based on integrated slip rates from fault, seismologic, and plate-motion data (fig. 5). This analysis suggests that the Wrangell tectonic block is rotating counterclockwise about an axis near the southwestern end of the block. The Denali fault is the northern boundary of the block, and a diffuse zone of seismicity and inferred faulting (dot pattern on fig. 5) is inferred to bound the block on the northwest. This boundary, as defined by seismicity, extends southwest through the central Alaska Range and through Cook Inlet and Shelikof Strait to merge with the Aleutian megathrust southwest of Kodiak Island (Lahr and Plafker, 1980). As a consequence of the block rotation, dextral slip on the Denali fault is inferred to be taken up on the northwestern boundary of the block in the central and western Alaska Range by contractional folding and

faulting. The present stress regime probably dates from about 3.9 to 3.4 Ma, when there was a change to a more northerly relative motion between the Pacific and North American plates as recorded in oceanic magnetic anomalies (Harbert and Cox, 1989).

Stratigraphic Record of Late Cenozoic Uplift

Late Cenozoic uplift of part of the Alaska Range is suggested by the stratigraphic record in the Cook Inlet basin and in local basins on the north side of the Alaska Range.

In the upper Cook Inlet region, Oligocene and Miocene units (mainly the Hemlock Conglomerate and Tyonek Formation) consist of fluvial, deltaic, and estuarine sandstone, siltstone, and coal deposited in cyclic fining-upward sequences (Kirschner and Lyons, 1973). Sandstone in these middle Tertiary units has abundant quartz and a distinctive heavy mineral assemblage that together indicate a high-grade metamorphic provenance of the type that occurs north of the Alaska Range. In contrast, the overlying middle Miocene to Pliocene sequence (Beluga and Sterling Formations) includes over 3,000 m of thick-bedded sandstone and conglomerate in which the predominant heavy-mineral fraction is hornblende derived from erosion of Alaska Range plutonic rocks and hypersthene from volcanic rocks of the Alaska Peninsula segment of the Aleutian magmatic arc. Kirschner and Lyon (1973) interpreted these data as indicating that the middle Tertiary sequence was deposited by an ancestral major river system that drained much of interior Alaska (comparable to the present Yukon and Tanana Rivers), and that this system was cut off as a result of uplift of the Alaska Range in late Miocene time.

The change in sandstone petrology within the Cook Inlet region also approximately coincides with a sedimentary change in the Nenana basin north of the central Alaska Range. In this basin, early and middle Tertiary fluvial and lacustrine coal-bearing strata are unconformably overlain by as much as 640 m of conglomerate and conglomeratic sandstone containing minor lenticular interbeds of shale and lignite of the Nenana Gravel (Wahrhaftig and others, in press). The gravel was derived from the rising Alaska Range and was deposited in large alluvial fans along the north flank of the range (Kirschner, in press; Wahrhaftig and others, in press).

The age of the Nenana Gravel is bracketed by isotopic dates from ash layers below and above the unit of 8.3 Ma and 2.75 Ma, respectively, and recent preliminary studies of the contained pollen assemblages suggest that it is of early Pliocene age (T. Agar, written comm., 1991). Thus, the formation is at least partly contempo-

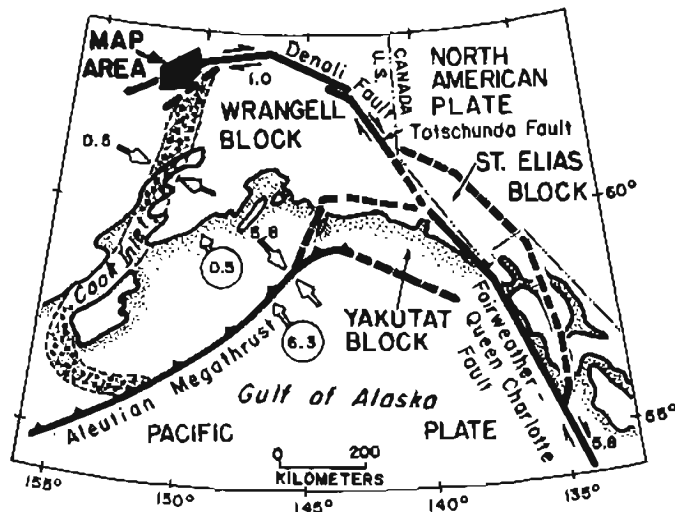


Figure 5. South-central Alaska showing relationship of Mount McKinley area to principal tectonic features, including Wrangell block, Denali fault, and main Denali fault splays in map area and southeast of map area. Open arrows with numerals in circles indicate direction and amount of motion of Pacific plate (6.3 cm/yr) and Wrangell block (0.5 cm/yr) relative to North America; paired facing open arrows and numerals indicate direction and rate of convergence across southeastern (Aleutian megathrust) and western (dot pattern indicating diffuse zone of seismicity) boundaries of Wrangell block; paired arrows along Denali fault and numeral indicate sense and amount of relative displacement on northwestern boundary of Wrangell block, and paired arrows along the Fairweather/Queen Charlotte faults and numeral indicate sense and amount of relative displacement between Pacific plate and Saint Elias block. Modified from Lahr and Plafker (1980) and Plafker and others (in press).

aneous with the Beluga and Sterling Formations of the Cook Inlet basin (Wahrhaftig and others, in press).

Assuming that gravel deposition began during or shortly after uplift of the Alaska Range, the early Pliocene age (between 5.2 and 3.4 Ma) is compatible with fission-track data suggesting onset of rapid uplift of Mt. McKinley at about 4.2 Ma. Furthermore, these data yield an approximate uplift rate of 1.2 to 1.8 mm/yr, assuming 6 km of differential uplift between the base of the Nenana Gravel and the present height of Mt. McKinley, and an early Pliocene age for the gravel. The calculated uplift rates bracket the rate of 1.3 mm/yr obtained for Mt. McKinley. However, these rates can only be considered crude approximations because they do not incorporate a probable time lag between onset of uplift and deposition of the gravel (which would tend to lower the calculated uplift rates), or the amount of erosion off the top of Mt. McKinley (which would tend to increase the rates).

POSSIBLE CAUSE OF THE LATE CENOZOIC UPLIFT OF MOUNT MCKINLEY

Stratigraphic data cited above suggest that prior to late Cenozoic time the central and western Alaska Range was not a major topographic high. The combined fission-track and stratigraphic data suggest to us that the late Cenozoic uplift was largely tectonic in origin.

In the study area, the geometric relationships between the Denali fault and the northeast-trending struc-

tures that appear to splay off it on the south side would result in a contractional horizontal component of 3.1 mm/yr and a vertical component of about 1.8 mm/yr if all the strike-slip motion were taken up by slip on a single thrust fault dipping at an average angle of 30° (fig. 6). This is more than enough to account for the 1.3 mm/yr average late Cenozoic uplift rate of Mount McKinley indicated by fission-track dating. Thus, the uplift inferred from fission-track studies could result from oblique underthrusting along one or more northeast-trending faults that splay off the Denali fault within the western Alaska Range.

The abrupt increase in uplift/cooling rates for the Mount McKinley region at about 4.2 Ma could be related to a change in relative Pacific-North American plate motion between about 3.2 and 3.9 Ma that involved clockwise rotation of about 15° in the eastern Aleutian arc (Harbert and Cox, 1989; DeMets and others, 1990). The inferred rotation would result in an increased component of compression across the Denali fault in the central Alaska Range. An alternative possibility, for which there is no direct evidence, is that the accelerated uplift/cooling at Mt. McKinley resulted from a change in the degree of coupling between the Pacific plate and the Yakutat block relative to the Wrangell block.

Earthquake data suggest that active faults other than the Denali fault may be present in the Mt. McKinley area (Lahr and Plafker, 1980). However, geologic mapping in the rugged and extensively glaciated central Alaska Range has been reconnaissance in nature, and few faults other than the Denali fault have been recognized.

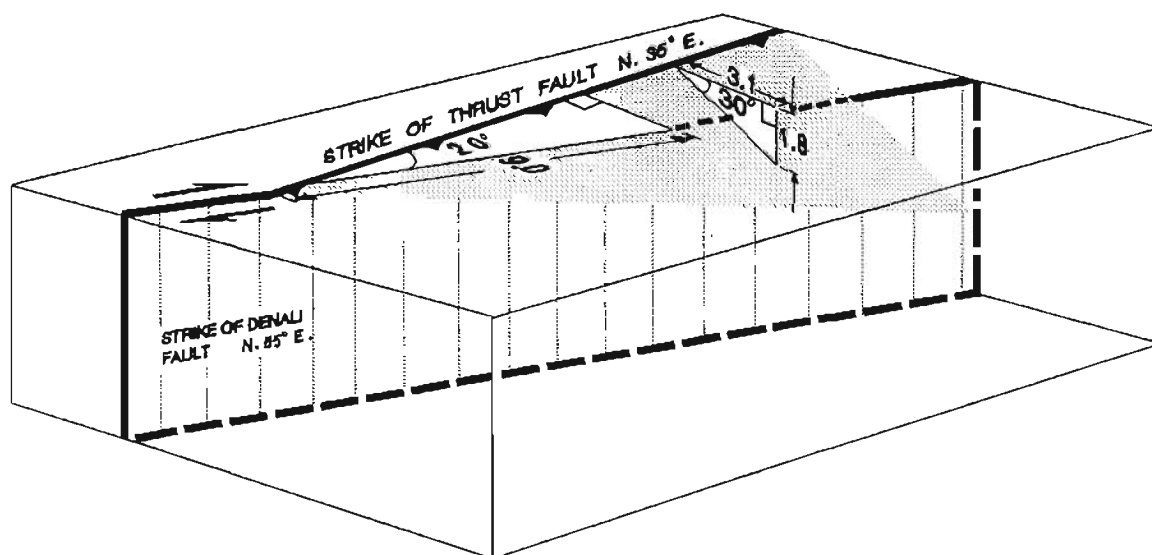


Figure 6. Diagram illustrating how strike-slip displacement averaging 9 mm/yr on Denali fault could produce 3.1 mm/yr contraction and 1.8 mm/yr uplift on a thrust splay dipping 30° northwest that intersects Denali fault at an angle of 20°.

One major thrust fault identified by Reed and Nelson (1977) and Jones and others (1983), the Shellabarger fault, extends northeast along the Kahiltna and Peters Glaciers to an acute intersection with the Denali fault (fig. 2). The Shellabarger fault has been interpreted as a terrane boundary that juxtaposes a basement complex of predominantly Paleozoic rocks on the northwest (Mystic terrane of Jones and others, 1983) against a sequence of Mesozoic flysch that comprises the Kahiltna terrane on the southeast (Reed and Nelson, 1977; Jones and others, 1983). Numerous faults and folds with comparable orientation occur east of the map area in the Healy quadrangle (Csejtey and others, 1992). Some of these faults have had late Cenozoic displacements and could represent active splays off the Denali fault (indicated schematically on fig. 5 by a dashed fault line).

SUMMARY AND CONCLUSIONS

Fission-track dating provides new data on the uplift history of mountains within the highest part of the Alaska Range. This area is uniquely suited for determination of uplift rates because local topographic relief is among the highest in the world, there is ample stratigraphic evidence for Neogene uplift, and the highest parts of the range are underlain by the McKinley pluton, which is made of rocks suitable for fission-track dating. The most important implications are the following:

1. The zircon data indicate an episode of rapid cooling and presumed uplift of Mounts McKinley, Huntington, and Dan Beard in Eocene time following late Paleocene emplacement of the McKinley pluton.

2. On Mount McKinley, the uplift rate increased dramatically to about 1.3 mm/yr from 4.2 Ma to the present; data are not available to determine whether comparable uplift occurred at Mounts Huntington and Dan Beard.

3. The cause of the dramatic change in uplift rate on Mount McKinley is uncertain, although it most likely reflects an increase in contractional deformation within the western Alaska Range fold-fault system, possibly resulting from late Cenozoic changes in the Pacific-North American relative plate motion.

4. The apatite and zircon data require that Mount McKinley was elevated about 1,800 m (6,000 ft) relative to Mounts Huntington and Dan Beard during the late Cenozoic. This differential uplift may reflect either regional southeastward tilting or the presence of an unidentified up-to-the-northwest fault between Mount McKinley and Mounts Huntington and Dan Beard.

Acknowledgments.—This study was made possible by the scientific interest and mountaineering skill of geologists Geoff Radford and Bill Kitson, who collected the samples described in this paper. We especially ac-

knowledge B.L. Reed's detailed and thoughtful technical review of the manuscript.

REFERENCES CITED

- Bryant, Bruce, and Naeser, C.W., 1991, Implications of low-temperature cooling history on a transect across the Colorado Plateau-Basin and Range boundary, west central Arizona: *Journal of Geophysical Research*, v. 96, no. B7, p. 12,375-12,388.
- Csejtey, Béla, Jr., Mullen, M.W., Cox, D.P., and Stricker, G.D., 1992, Geology and geochronology of the Healy quadrangle, south-central Alaska: U.S. Geological Survey Miscellaneous Investigations Series Map, I-1961, 63 p., 2 pls., scale 1:250,000.
- DeMets, D.C., Gordon, R.G., Argus, D.F., and Stein, S.A., 1990, Current plate motions: *Geophysical Journal International*, v. 101, no. 2, p. 425-478.
- Fleischer, R.L., Price, P.B., and Walker, R.M., 1965, Effects of temperature, pressure, and ionization on the formation and stability of fission tracks in minerals and glasses: *Journal of Geophysical Research*, v. 70, p. 1497-1502.
- Harbert, William, and Cox, Allan, 1989, Late Neogene motion of the Pacific plate: *Journal of Geophysical Research*, v. 94, no. B3, p. 3052-3064.
- Hurford, A.J., 1986, Cooling and uplift patterns in the Lepontine Alps south-central Switzerland and an age of vertical movement on the Insubric fault line: *Contributions to Mineralogy and Petrology*, v. 92, p. 413-427.
- Gleadow, A.J.W., Duddy, I.R., Green, P.F., and Lovering, J.F., 1986, Confined fission track lengths in apatite: A diagnostic tool for thermal analysis: *Contributions to Mineralogy and Petrology*, v. 94, p. 405-415.
- Jones, D.L., Silberling, N.J., and Coney, P.J., 1983, Tectono-stratigraphic map and interpretive bedrock geologic map of the Mount McKinley region, Alaska: U.S. Geological Survey Open-File Report 83-11, 8 sheets, scale 1:250,000.
- Kirschner, C.E., in press, Interior basins of Alaska, in Plafker, G., and Berg, H.C., eds., *Geology of Alaska: Boulder, Colo., Geological Society of America, Geology of North America*, v. G1.
- Kirschner, C.E., and Lyon, C.A., 1973, Stratigraphic and tectonic development of Cook Inlet Petroleum Province, in Pitcher, M.G., ed., *Arctic geology: American Association of Petroleum Geologists Memoir 19*, p. 396-407.
- Lahr, J.C., and Plafker, George, 1980, Holocene Pacific-North America plate interaction in southern Alaska: Implications for the Yakataga seismic gap: *Geology*, v. 8, p. 483-486.
- Lanphere, M.A. and Reed, B.L., 1985, The McKinley sequence of granitic rocks: A key element in the accretionary history of southern Alaska: *Journal of Geophysical Research*, v. 90, no. B13, p. 11,413-11,430.
- Naeser, C.W., 1979a, Thermal history of sedimentary basins: Fission-track dating of subsurface rocks: *Society of Economic Paleontologists and Mineralogists Special Publication 26*, p. 109-112.
- 1979b, Fission-track dating and geologic annealing of fission tracks, in Jaeger, E., and Hunziker, J.C., eds., *Lec-*

- tures in Isotope Geology: New York, Springer-Verlag, p. 154-169.
- 1981, The fading of fission tracks in the geologic environment—data from deep drill holes: *Nuclear Tracks*, v. 5, p. 248-250.
- Plafker, George, and Rubin, Meyer, 1978, Uplift history and earthquake recurrence as deduced from marine terraces on Middleton Island, Alaska, in *Proceedings of Conference VI, Methodology for identifying seismic gaps and soon-to-break gaps*: U.S. Geological Survey Open-File Report 78-943, p. 687-721.
- Plafker, George, Hudson, Travis, and Richter, D.H., 1977, Preliminary observations on late Cenozoic displacements along the Totschunda and Denali fault systems, in Blean, K.M., ed., *The United States Geological Survey in Alaska: Accomplishments during 1976*: U.S. Geological Survey Circular 751-B, p. B67-B69.
- Plafker, George, Gilpin, L.M., and Lahr, J.C., in press, Neotectonic map of Alaska, in Plafker, G., and Berg, H.C., eds., *Geology of Alaska*: Boulder, Colo., Geological Society of America, *Geology of North America*, scale 1:2,500,000, 1 sheet and text.
- Reed, B.L., and Lanphere, M.A., 1972, Generalized geologic map of the Alaska-Aleutian Range batholith showing potassium-argon ages of the plutonic rocks: U.S. Geological Survey Miscellaneous Field Studies Map MF-372, scale 1:1,000,000, 2 sheets.
- 1974, Offset plutons and history of movement along the McKinley segment of the Denali fault system, Alaska: *Geological Society of America Bulletin*, v. 85, p. 1883-1892.
- Reed, B.L., and Nelson, S.W., 1977, Geologic map of the Talkeetna quadrangle, Alaska: U.S. Geological Survey Miscellaneous Field Studies Map MF-870-A, scale 1:250,000.
- Zeitler, P.K., Johnson, N.M., Naeser, C.W., and Tahirkheli, Rashid A.K., 1982, Fission-track evidence for Quaternary uplift of the Nanga Parbat region, Pakistan: *Nature*, v. 298, p. 255-257.
- Wahrhaftig, Clyde, Bartsch-Winkler, S., and Stricker, G.D., in press, Coal in Alaska, in Plafker, G., and Berg, H.C., eds., *Geology of Alaska*: Boulder, Colo., Geological Society of America, *Geology of North America*, v. G1.

Reviewers: Marvin A. Lanphere and Bruce L. Reed

Isotopic Variations in Calcite Veins from the Kandik Region of East-Central Alaska

By Kevin L. Shelton, Michael B. Underwood, Deborah Bergfeld, and David G. Howell

Abstract

The Kandik River and Tatonduk belts of east-central Alaska are juxtaposed along the Glenn Creek fault zone. Measurements of oxygen and carbon isotopic compositions of vein-filling calcite in each belt, together with calculations of $\delta^{18}\text{O}_{\text{water}}$ values, indicate that the parent fluids in the Kandik River section were enriched in ^{18}O relative to fluids that moved through the Tatonduk stratigraphy. The Kandik River fluid reservoir equilibrated with a large volume of metasedimentary and volcanic rocks at elevated temperatures (up to 300°C) and low water-to-rock ratios (that is, the veins are broadly synmetamorphic). Tatonduk veins, in contrast, precipitated at lower temperatures (generally below 150°C) from less evolved meteoric waters; these fluids most likely attained their isotopic compositions under conditions of moderate to high water-to-rock ratios and modest amounts of interaction with intrabasinal carbonate, siliciclastic, and volcanic rocks. The exchange of fluids across the Glenn Creek fault zone (in either direction) appears to have been very limited, and the isotopic compositions provide additional supporting evidence for the emplacement of a hot Kandik River hanging wall over a cooler Tatonduk footwall. Conversely, veins from basaltic rocks assigned to the Woodchopper Canyon terrane yield isotopic values similar to those of the neighboring Kandik River belt. Evidently, both of these units were affected by the same high-temperature fluids, with vein precipitation occurring after the Woodchopper Canyon terrane and Kandik River belt had been amalgamated.

INTRODUCTION

The Kandik region of east-central Alaska (fig. 1) has been the site of a multidisciplinary study of the effects of thrust faulting on thermal structure. As outlined by Underwood and others (this volume), the study area contains two major tectono-stratigraphic units, herein referred to as the Kandik River "belt," which is dominated by Mesozoic deep-marine strata, and the Tatonduk "belt," which is mostly Proterozoic to Permian in age (see also Churkin and others, 1982; Howell and Wiley, 1987; Dover, 1990; Howell and others, 1992). Pelitic

rocks of the Kandik River belt (Glenn Shale and Biederman Argillite) typically have well-developed pressure-solution cleavage and (or) pencil structure, plus relatively high ranks of organic metamorphism; conversely, the Tatonduk belt is mildly deformed and much lower in thermal maturity (Laughland and others, 1990). In essence, the Tatonduk stratigraphy is a relatively straightforward example of a rifted continental margin that experienced thermal subsidence during the Paleozoic (Payne and Allison, 1981; Howell and Wiley, 1987; Dover, 1990). The western portion of the study area contains diverse sequences of rock that Churkin and others (1982) assigned to the Woodchopper Canyon, Slaven Dome, and Takoma Bluff terranes. Rock units within these smaller terranes include the Step Conglomerate (Permian); sequences of Paleozoic argillite, chert, limestone, and dolomite (units P_{2a} and P_{2l} of Brabb and Churkin, 1969); the Woodchopper Volcanics (Devonian); and argillite, dolomite, and volcanic rocks of Proterozoic(?) age.

Stratigraphic and structural relations are uncertain between the Mesozoic siliciclastic rocks of the Kandik River belt and Devonian to Permian strata that crop out in the Step Mountains region (fig. 1). Fault contacts separate the Kandik River belt from the Woodchopper Canyon, Slaven Dome, and Takoma Bluff terranes; Churkin and others (1982) referred to this complicated region as the Eureka suture zone. Some of the Paleozoic strata within the suture zone may have formed the depositional basement of the Kandik River belt (Howell and others, 1992). The Glenn Creek fault zone marks the structural boundary between the Kandik River and Tatonduk belts (fig. 1). Past field investigations of the region have resulted in conflicting interpretations of the geometry and sense of slip on the Glenn Creek fault (Brabb and Churkin, 1969; Howell and Wiley, 1987; Dover and Miyaoka, 1988; Laughland and others, 1990). Recent measurements of kinematic indicators, however, provide evidence that the fault is a southeast-verging thrust, with younger rocks of the Kandik River belt thrust over the older Tatonduk rocks (Howell and others,

1992). This orogenic event evidently occurred during late Early Cretaceous time.

In-depth analyses of vitrinite reflectance and illite crystallinity (Underwood and others, this volume) uphold interpretations derived from an earlier reconnaissance-level investigation of regional thermal maturity (Laughland and others, 1990). These data are important because they provide independent confirmation of the widespread occurrence of low-grade metamorphic rocks in the hanging wall of the Glenn Creek fault; the footwall sequences, in contrast, are much lower in thermal maturity. For example, the average value of mean random vitrinite reflectance (percent R_m) is 3.8 percent for the Kandik River belt, whereas a comparable average percent R_m value for the Tatonduk belt is only 1.2 percent (Underwood and others, this volume). Using the

correlation between percent R_m and paleotemperature established by Barker (1988), these data correspond to average temperature estimates of about 285°C (Kandik River) and 165°C (Tatonduk). Likewise, values of illite-crystallinity index for the Kandik River belt typically fall within the boundaries of the zone of anchimetamorphism (transition into lowermost greenschist facies). In contrast, the Tatonduk belt displays a great deal of scatter and inconsistency in illite crystallinity due to the effects of mixing among authigenic clay minerals and detrital populations of illite and muscovite inherited from a variety of source rocks (Underwood and others, this volume).

A complete understanding of the regional thermal history and its relation to the history of rock deformation cannot be determined without considering the role of

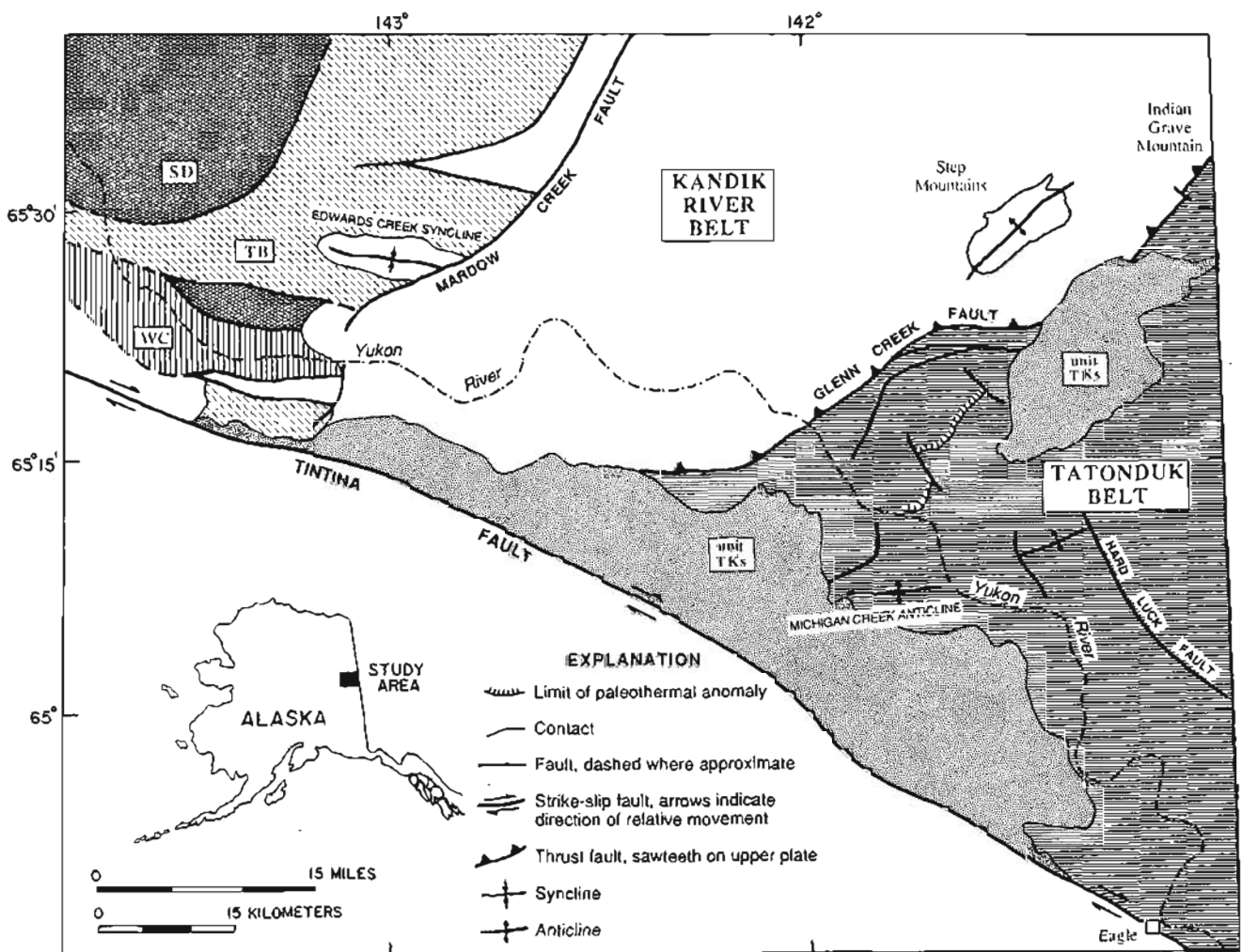


Figure 1. Geologic index map of east-central Alaska showing Kandik River belt (no pattern) and Tatonduk belt (horizontal lined pattern). The hachured line to the southeast of the Glenn Creek fault depicts the limit of a paleothermal anomaly detected in the Tatonduk footwall. Also shown are unit TKs of Brabb and Churkin (1969) and the Woodchopper Canyon (WC), Slaven Dome (SD), and Tacoma Bluff (TB) terranes of

Churkin and others (1982). Rocks southwest of Tintina fault zone are assigned to Yukon-Tanana composite terrane (Coney and Jones, 1985). Modified from Brabb and Churkin (1969) and Foster (1976). For relevant fossil control and alternative interpretations of the structural geology, see Dover and Miyaoka (1988) and Miyaoka (1990).

fluid migration. Perhaps the best evidence for the fluid-migration history comes from the mineral phases that were precipitated as vein fillings. Veins containing calcite, quartz, and quartz-calcite intergrowths are ubiquitous in the cleaved and complexly folded sequences of the Kandik River belt. Although we made a concerted effort to sample and measure both common and unusual vein orientations (fig. 2), most of the veins are aligned at high angle to bedding and (or) cleavage, locally filling conjugate sets of extension fractures. On the other hand, calcite veins in the Tatonduk belt occur sporadically, and there is little sense of systematic orientation (fig. 2).

In this paper we present initial results and tentative interpretations of isotopic analyses of calcite veins. Research in progress will establish the isotopic signature of quartz veins and microthermometric data for fluid inclusions. From these data, we expect to be able to estimate the temperatures of vein precipitation, the fluid compositions and salinities, the isotopic character of parent fluids (from which the veins precipitated), the degree of fluid-rock interaction, and the ultimate source or sources of the fluids.

METHODS

Previous studies have shown the utility of stable isotopes in elucidating the origin and history of hydrother-

mal fluids and fluid-rock interactions in tectonically disturbed terranes (Magaritz and Taylor, 1976; Dietrich and others, 1983; Wickham and Taylor, 1987; Rye and Bradbury, 1988; Burkhard and Kerrich, 1988; Bebout and Barton, 1989; Nesbitt and Muehlenbachs, 1989). In this study we measured the carbon and oxygen isotopic compositions of vein-filling calcites. Techniques of mineral extraction and analysis followed those of McCrea (1950), and the data are reported in conventional δ notation as per mil deviations relative to the Pee Dee Belemnite (PDB) standard for C and the Vienna standard mean ocean water (SMOW) standard for O. The standard error for each analysis is approximately ± 0.1 per mil, using the University of Missouri's automated Finnigan MAT Delta E mass spectrometer.

Specimens of calcite from calcite and calcite-quartz veins were extracted from a wide variety of lithologies and stratigraphic positions (table 1; fig. 3). Most of the Kandik River specimens (20) came from fractured sandstone beds in the Biederman Argillite (Cretaceous); in addition, we analyzed three samples from the Glenn Shale. Within the Woodchopper Canyon terrane (of Churkin and others, 1982), we selected one sample from a shale interval and four veins cutting through the Devonian basaltic rocks. We collected a total of 10 samples from the following units within the Tatonduk belt: shale and basalt of the Tindir Group (Proterozoic and Cambrian); Adams Argillite (Cambrian); argillite of the Road River Formation (Ordovician and Silurian); turbidite sequences of the Nation River Formation (Devonian); limestone and shale interbeds of the Calico Bluff Formation (Mississippian and Pennsylvanian); and the Tahkandit Limestone (Permian). All formational assignments (table 1) conform to the maps of Brabb and Churkin (1969) and Foster (1976).

RESULTS

If all of the samples from the study area are considered collectively, the $\delta^{18}\text{O}$ values of calcite veins range from 4.4 to 21.3 per mil; $\delta^{13}\text{C}$ values range from -7.6 to $+7.6$ per mil (table 1). A comparison of the isotopic data from the Tatonduk belt, the Kandik River belt, and the Woodchopper Canyon terrane indicates several noteworthy features (fig. 4). First, although the three data sets show some overlap of $\delta^{13}\text{C}$ values, veins from the Tatonduk belt are enriched in ^{13}C (average = 0.1 per mil) relative to those of the Kandik River belt and Woodchopper Canyon terrane (average = -3.5 per mil). Most of the overlap is associated with a single site in the Nation River Formation (MJ90-K59), where values of vitrinite reflectance are somewhat higher than normal for this particular formation (Underwood and others, this volume). Second, with one exception, calcite in veins

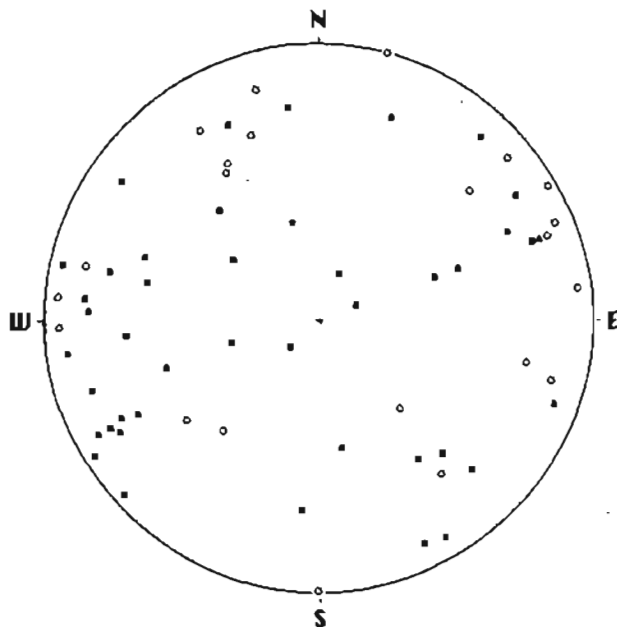


Figure 2. Schmidt equal-area projection (lower hemisphere) of poles to veins for calcite veins in Tatonduk belt (open circles) and composite Kandik River belt and Woodchopper Canyon terrane (closed squares). Statistical distribution of data for Kandik River belt is biased in that a concerted effort was made to sample and measure unusual vein orientations. Most veins are aligned at high angle to bedding and (or) cleavage.

Table 1. Isotopic data for calcite veins, Kandik region, east-central Alaska

[Values given in per mil]

Tatonduk belt					Kandik River belt/Woodchopper Canyon terrane				
Sample	Formation	Lithology ¹	$\delta^{13}\text{C}$	$\delta^{18}\text{O}$	Sample	Formation	Lithology ¹	$\delta^{13}\text{C}$	$\delta^{18}\text{O}$
mj90-k29b	Tindir	shale	+0.6	18.9	mj90-k80b	Biederman	ss/argillite	-6.0	17.9
mj90-k77c	Tindir	basalt	-2.1	15.4	mj90-k82e	Biederman	ss/argillite	-2.3	17.9
mj90-k77d	Tindir	basalt	-2.3	12.9	mj90-k82f	Biederman	ss/argillite	-3.8	17.6
um90-k34b	Tindir	lms/shale	+7.6	21.3	mj90-k82g	Biederman	ss/argillite	-3.1	18.0
mj90-k32c	Road River	shale	-1.8	6.5	mj90-k82h	Biederman	ss/argillite	-3.0	13.9
mj90-k33c	Adams	argillite	+2.9	6.2	mj90-k83g	Biederman	ss/argillite	-3.7	17.1
mj90-k59f	Nation River	ss/shale	-3.2	18.1	mj90-k84d	Biederman	ss/argillite	-1.3	17.8
mj90-k59g	Nation River	ss/shale	-2.6	18.6	mj90-k84e	Biederman	ss/argillite	-2.8	17.2
mj90-k64c	Calico Bluff	lms/shale	-0.2	20.2	mj90-k85c	Biederman	ss/argillite	-4.2	18.1
mj90-k73b	Tahkandit	limestone	+1.8	16.2	mj90-k85d	Biederman	ss/argillite	-2.2	18.1
					mj90-k87c	Biederman	ss/argillite	-4.4	19.2
					mj90-k88e	Biederman	ss/argillite	-5.6	17.6
					mj90-k88f	Biederman	ss/argillite	-3.5	18.2
					mj90-k88g	Biederman	ss/argillite	-3.2	18.2
					mj90-k90g	Biederman	ss/argillite	-2.1	18.4
					mj90-k90h	Biederman	ss/argillite	-3.8	18.6
					mj90-k90j	Biederman	ss/argillite	-4.0	18.9
					mj90-k91d	Biederman	ss/argillite	-5.8	18.5
					mj90-k91e	Biederman	ss/argillite	-2.4	18.3
					db91-k24d	Biederman	ss/argillite	-2.9	17.7
					um90-k24b	Glenn Shale	shale	-1.0	17.3
					um90-k25b	Glenn Shale	shale	-4.2	17.3
					um90-k25f	Glenn Shale	shale	-2.6	19.8
					dh91-k20	Woodchopper	basalt	-2.4	17.8
					dh91-k22c	Woodchopper	shale	-0.2	4.4
					dh91-k23a	Woodchopper	basalt	-3.9	17.7
					dh91-k23b	Woodchopper	basalt	-4.1	18.2
					dh91-k25b	Woodchopper	basalt	-7.6	20.4

¹Abbreviations: lms, limestone; ss, sandstone.

from northwest of the Glenn Creek fault show no consistent deviation in isotopic values as a function of the host-rock lithology or age; in other words, values from veins in basaltic rocks of the Woodchopper Volcanics (Devonian) are virtually identical to those from the Biederman Argillite (Cretaceous) and the Glenn Shale (Triassic-Cretaceous). The one exception (sample DH91-K22c) comes from a thin shale interval of the Woodchopper Volcanics (fig. 3); this specimen yielded the lowest $\delta^{18}\text{O}$ value (4.4 per mil) and the highest $\delta^{13}\text{C}$ value (-0.2 per mil). Third, calcite from veins in argillites and basalts of the Tatonduk belt display consistently lower $\delta^{18}\text{O}$ values than veins in Tatonduk limestone, sandstone, and (or) interbedded shale units (table 1). Thus, calcite veins from the Kandik River belt and the Woodchopper Canyon terrane display a much narrower isotopic range than vein-filling calcite in the Tatonduk belt. If reasonable inferences are made regarding temperature conditions at the time of vein emplacement, then we can demonstrate that the pore waters that deposited calcites in the two geologic domains were isotopically distinct.

INTERPRETATION

Oxygen Isotopes

Based on measurements of vitrinite reflectance (Underwood and others, this volume), it is certain that the average and the range of maximum paleotemperatures were quite different in the Kandik River and Tatonduk belts. Most of the calcite veins from the Kandik River belt have $\delta^{18}\text{O}$ values within the narrow range of 17 to 19 per mil (fig. 4). In comparison, Magaritz and Taylor (1976) showed that carbonate veins in a wide variety of rocks from the Franciscan Complex in coastal California produce $\delta^{18}\text{O}$ values of carbonates that concentrate between 14 and 16 per mil, and these data demonstrate a slight enrichment in ^{18}O with respect to the whole-rock values of the host lithologies. If we assume that the Kandik River calcite veins were precipitated at temperatures approximately equal to the average belt maxima, then it is possible to calculate $\delta^{18}\text{O}$ values

for the parent waters responsible for the vein fillings (O'Neil and others, 1969; Friedman and O'Neil, 1977; O'Neil, 1986).

The average paleotemperature for the entire Kandik River belt is approximately 285°C; if the paleotemperature calculation is restricted to the cleaved rocks within the Biederman Argillite (from which most veins were collected), then the average value rises to almost 300°C. A comparable average value for the Tatonduk belt is only 165°C; however, this statistic may be inappropriate for the purposes of calculating values of $\delta^{18}\text{O}_{\text{water}}$ because it includes a disproportionate concentration of data points from an aureole of elevated thermal maturity located to the southeast of the surface trace of the Glenn Creek fault (fig. 1). We believe that this anomaly was caused by syntectonic conductive heat transfer from hanging wall to footwall (see Laughland and others, 1990). A skewed population of data shifts the mean paleotemperature to a higher value than might be expected given equal spatial distribution of samples throughout the belt. If the footwall anomaly is eliminated from the calculation, then the Tatonduk mean drops to roughly 130°C. We believe that a value of

150°C is a reasonable compromise that takes into account the possibility of slightly elevated paleotemperatures near the thrust.

Calculated $\delta^{18}\text{O}_{\text{water}}$ values (using an approximate temperature of 300°C) for the Woodchopper Canyon and Kandik River veins (excluding sample DH91-K22c) range from 8.2 to 14.7 per mil, with a mean of 12.4 per mil (fig. 5). A $\delta^{18}\text{O}_{\text{water}}$ value near 12 per mil is consistent with a metamorphic parent fluid (Sheppard, 1986); in other words, the fluids must have equilibrated isotopically with a large volume of metamorphic or sedimentary rocks at elevated temperatures and low water-to-rock ratios (Valley, 1986). Similar calculations of $\delta^{18}\text{O}_{\text{water}}$ values in the Catalina Schist of California yielded average values of about 13 per mil for both greenschist-facies and blueschist-facies units (Bebout and Barton, 1989). We suggest that dehydration reactions within pelitic and basaltic rocks during lowermost greenschist-facies metamorphism (Valley, 1986) provided the source for fluids moving through the Kandik River belt and the Woodchopper Canyon terrane.

The extreme scatter of $\delta^{18}\text{O}$ values in Tatonduk calcite veins indicates that the fluids were possibly affected

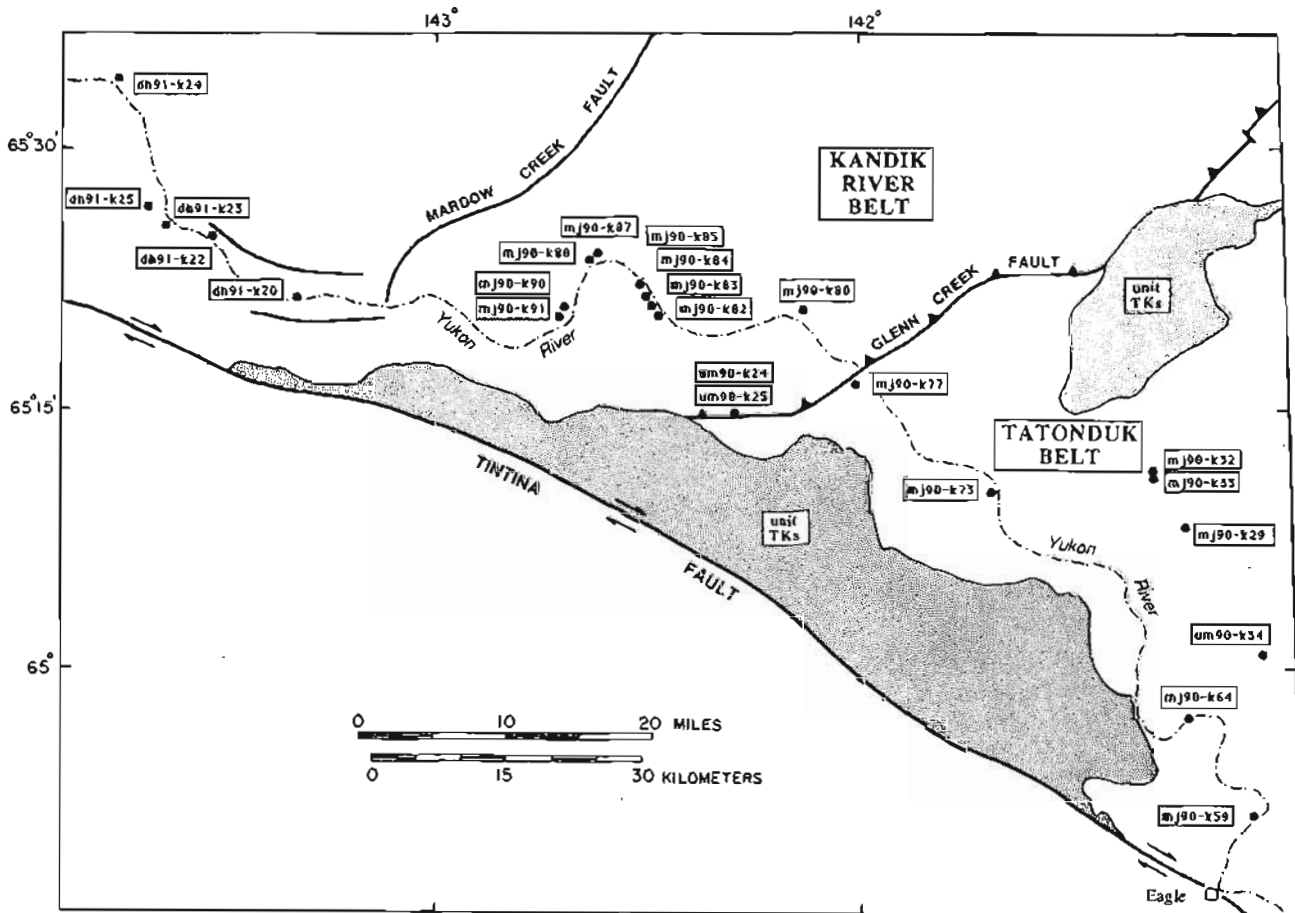


Figure 3. Sample localities for calcite veins in Tatonduk belt, Kandik River belt, and Woodchopper Canyon terrane (of Churkin and others, 1982). See figure 1 for a complete geologic base.

by several types of rocks, including marine carbonate rocks, which typically yield relatively high $\delta^{18}\text{O}$ values (25 ± 2 per mil, Keith and Weber, 1964). Using a temperature of 150°C , calculated $\delta^{18}\text{O}_{\text{water}}$ values for the Tatonduk belt are -6.5 to $+8.6$ per mil, with an average of 2.7 per mil (fig. 5). These estimates are significantly depleted in ^{18}O relative to the $\delta^{18}\text{O}_{\text{water}}$ values estimated for the geologic domain to the west, such that almost no overlap exists between the two data sets (fig. 5). Assuming a constant temperature of calcite-vein formation, the Tatonduk results are consistent with precipitation dominantly from less evolved meteoric waters whose isotopic compositions were attained through interaction with carbonate, siliciclastic, and basaltic rocks under moderate to high water-to-rock ratio conditions (Sheppard, 1986). Because similar $\delta^{18}\text{O}_{\text{water}}$ values are associated with host formations containing interbeds of limestone and shale, chert and shale, and sandstone and shale, we suggest that an open system of vein-forming fluids probably crossed many of the formational boundaries within the Tatonduk stratigraphy. The lowest $\delta^{18}\text{O}$ values come from mudrock and chert-shale units (Adams Argillite, Røad River Formation), where low formation permeabilities evidently inhibited significant isotopic exchange between fluids and the host rock. Thus, the ^{18}O -depleted signature of the source meteoric-water reservoir was dominantly preserved in these strata. Also, at temperatures below 150°C , exchange reactions are controlled by kinetics (O'Neil, 1986); equilibration with the silicic host rocks under these circumstances is unlikely.

The one anomalous sample in the Woodchopper Canyon terrane, extracted from the shale member of the

Woodchopper Volcanics, probably precipitated during a later stage, lower temperature emplacement event. This sample has a $\delta^{13}\text{C}$ value of -0.2 per mil, which is very close to the average value for the Tatonduk belt. In addition, if a lower paleotemperature of 150°C is used to calculate the $\delta^{18}\text{O}_{\text{water}}$ value for this specimen, it yields a value of -8.3 per mil, which likewise indicates a relatively unexchanged meteoric water. This vein probably precipitated late in the paragenetic history.

Carbon Isotopes

The $\delta^{13}\text{C}$ values for calcite veins in the Kandik River belt and Woodchopper Canyon terrane (average = -3.4 per mil) are compatible with a fluid source that incorporated oxidized carbon from a mixed source (marine limestone with minor input from degradation of organic carbon). The enrichment of ^{13}C in calcite veins from the Tatonduk belt (average $\delta^{13}\text{C} = 0.1$ per mil) may be due to lower temperatures of calcite-vein formation (Emrich and others, 1970).

If we again assume average calcite depositional temperatures of 150°C and 300°C for the Tatonduk belt and the composite Kandik River/Woodchopper Canyon domain, respectively, then it is possible to calculate the $\delta^{13}\text{C}$ values of dissolved CO_2 in equilibrium with calcite (Friedman and O'Neil, 1977). Calculated average $\delta^{13}\text{C}$ values of dissolved CO_2 are as follows: Kandik River/Woodchopper Canyon, -1.3 per mil; Tatonduk belt, -1.4 per mil. These values indicate that calcite-depositing fluids in each belt contained dissolved CO_2 of similar

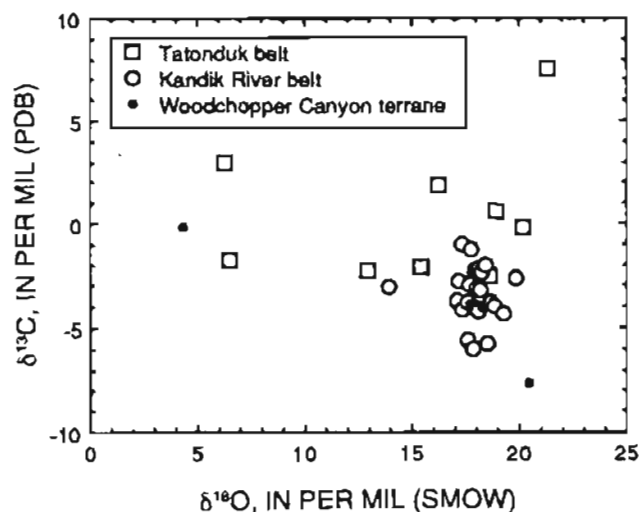


Figure 4. Values of $\delta^{13}\text{C}$ [relative to the Pee Dee Belemnite (PDB) standard] and $\delta^{18}\text{O}$ [relative to Standard Mean Ocean Water (SMOW)] for vein-filling calcite extracted from rocks of Tatonduk belt, Kandik River belt, and Woodchopper Canyon terrane, east-central Alaska. See table 1 for values and identification of host lithologies.

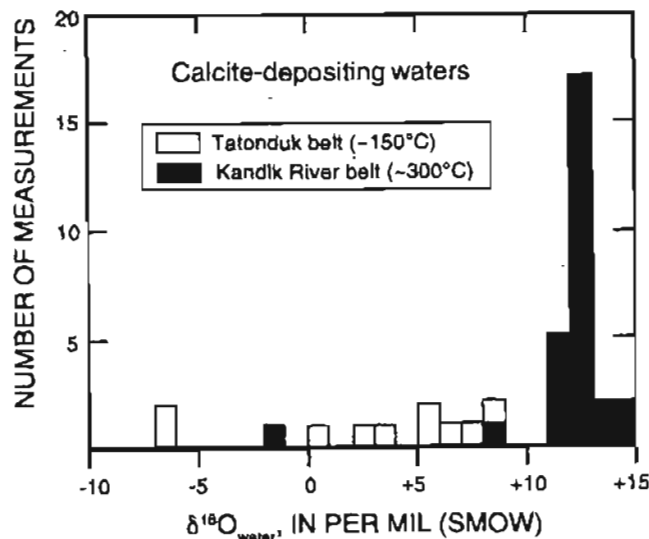


Figure 5. Calculated values of $\delta^{18}\text{O}_{\text{water}}$ for calcite veins in Tatonduk belt (open bars) and composite Kandik River belt and Woodchopper Canyon terrane (black bars) of east-central Alaska. Calculations follow technique outlined by O'Neil and others (1969) and Friedman and O'Neil (1977).

isotopic composition. Furthermore, these calculations support the idea that calcite veins were deposited at significantly different temperatures in the two belts.

The highest $\delta^{13}\text{C}$ value of 7.6 per mil occurs in a calcite vein extracted from a shale unit of the Tindir Group of the Tatonduk belt. Although this carbon-isotope signature could have been affected by the presence of ^{13}C -enriched interbedded carbonate rocks, another possible cause is the presence of methane. Methane concentrates ^{12}C relative to oxidized carbon species and thus causes the coexisting CO_2 in a mixed-carbon fluid to become enriched in ^{13}C ; precipitation of calcite from the dissolved CO_2 component in this type of fluid would cause an increase in $\delta^{13}\text{C}$ values. In contrast, oxidation of methane will result in carbonates depleted in ^{13}C (for example, Hudson, 1977; Ritger and others, 1987). There is no evidence to indicate that any calcite in veins of the Kandik study area was precipitated from a ^{13}C -depleted fluid reservoir containing abundant hydrocarbons or their oxidized equivalents.

Tectonic Evolution

The distinct isotopic compositions of calcite-depositing fluids in the Kandik River belt and the Tatonduk belt allow us to place additional constraints on models of regional tectonic evolution (for example, Dover, 1990; Laughland and others, 1990; Howell and others, 1992). Tatonduk veins produce a wide scatter in both $\delta^{13}\text{C}$ and $\delta^{18}\text{O}$ values, whereas the Kandik River data cluster tightly, with average values of about $\delta^{18}\text{O} = +18$ per mil and $\delta^{13}\text{C} = -4$ per mil. There is almost no overlap between the two data sets, particularly if one calculates the $\delta^{18}\text{O}$ values of the parent waters from which the veins precipitated (fig. 5). Thus, calcite veins in the Tatonduk belt did not share a common emplacement history with veins of the Kandik River belt; these two belts, moreover, did not share common fluid reservoirs or common pathways of fluid migration.

All but one of the Woodchopper and Kandik River samples show the effects of considerable isotopic exchange within a rock-dominated hydrothermal system. Fluids within this geologic domain probably were derived from dehydration reactions of pelitic rocks and basalt under conditions of subgreenschist facies metamorphism (Valley, 1986). Calcite veins in Woodchopper basaltic rocks (Devonian), moreover, are virtually identical to those in the Biederman Argillite (Cretaceous); this evidence strongly supports the idea that the two tectono-stratigraphic units were linked structurally prior to the peak heating and fluid-migration events. Most of the Biederman veins are aligned at a high angle to pressure-solution cleavage; precipitation occurred mostly within extension fractures in the sand-

stone interbeds, rather than within the pelitic rocks. Because of this, we believe that the vein emplacement was broadly synchronous with the formation of cleavage; furthermore, fluid movement and vein precipitation were byproducts of regional metamorphism, not the cause. If fluid migration had occurred long after low-temperature metamorphism, then we would expect to see evidence of fracture propagation through both sandstone beds and cleaved pelites. We see no evidence for preferential concentration of veins along pathways of enhanced permeability, such as fault zones.

The absolute age of Kandik River vein precipitation and its relative timing with respect to veins of the Tatonduk belt remain debatable. In the Tatonduk belt, fluid flow and local vein formation definitely occurred at lower temperatures, with various degrees of isotopic exchange between fluids and host rocks. The Tatonduk veins could have precipitated long before the two belts were juxtaposed along the Glenn Creek fault zone; alternatively, some or all of the veins may have formed late in the diagenetic history, after the hanging wall of the thrust system had cooled. We favor the former interpretation, for the following reasons. First, except for the narrow thermal anomaly beneath the thrust fault (fig. 1), vitrinite reflectance within the Tatonduk belt was not reset to higher values during the Cretaceous orogenic event (Laughland and others, 1990; Underwood and others, this volume). All of the veining was not necessarily synchronous with peak heating, but because we find only local evidence for a syntectonic thermal overprint, burial temperatures within most of the Tatonduk belt probably reached peak values prior to thrusting. Veins in the Nation River Formation at site MJ90-K59 (fig. 1) may represent an exception. Second, there is no evidence to suggest that hot fluids escaped the Kandik River belt and penetrated downdip into the Tatonduk belt. In fact, we did not recognize obvious increases in the spatial density of veining near the fault zone in either the hanging wall or the footwall. More importantly, there are no isotopic anomalies associated with veins in rocks on either side of the Glenn Creek fault and there is no detectable gradient in isotopic values with distance from the fault. One or more of these occurrences might be expected if the fault had served as a major pathway of syntectonic fluid movement. Instead, isotopic compositions are different on either side of the fault zone. Third, if widespread fluid migration had occurred after thrusting, then one might expect some updip penetration of a later stage, lower temperature plumbing system from the underlying Tatonduk strata into the overlying Kandik River section. Instead, we note that veins in basalt of the Tindir Group just to the southeast of the Glenn Creek fault are isotopically distinct with respect to veins in the overlying Glenn Shale and Biederman Argillite. The one unusual sample (DH91-

K22c; $\delta^{18}\text{O} = 4.4$ per mil) from shale of the Woodchopper Canyon terrane probably did precipitate very late in the thermal history as meteoric fluids migrated through the section.

CONCLUSIONS

The isotopic data from calcite veins amplify previous interpretations of the regional thermal structure of the Kandik region, particularly with regard to the emplacement of a hot Kandik River hanging wall over cooler footwall sequences of the Tatonduk belt. Fluid reservoirs in these two belts were not connected during the principal phases of vein precipitation, and most of the veins were formed before the belts were juxtaposed along the Glenn Creek fault zone. Conversely, similarities in isotopic data support the idea that the Woodchopper Canyon terrane and the Kandik River belt had been amalgamated prior to vein precipitation. These results should be regarded as preliminary, but they demonstrate the utility of stable-isotope geochemistry in deciphering the geodynamic and hydrogeologic histories of neighboring tectono-stratigraphic domains.

Acknowledgments.—Mark Johnsson, Tom Brocculeri, and Lu Haufu assisted in the field. Financial support to the University of Missouri was generously supplied by ARCO Alaska, Inc. We thank G. Van Kooten and his ARCO colleagues for their scientific cooperation and logistical aid. Superintendent Don Chase granted permission to sample in the Yukon-Charley Rivers National Preserve. Acknowledgment is also made to the Donors of the Petroleum Research Fund, administered by the American Chemical Society, for partial support of this research (grant #22773-AC2 to Underwood). Editorial suggestions by D. Bradley and C. Dusel-Bacon helped improve the manuscript.

REFERENCES CITED

- Barker, C.E., 1988, Geothermics of petroleum systems: Implications of the stabilization of kerogen maturation after a geologically brief heating duration at peak temperature, in Magoon, L.B., ed., *Petroleum systems of the United States*: U.S. Geological Survey Bulletin 1870, p. 26-29.
- Bebout, G.E., and Barton, M.D., 1989, Fluid flow and metasomatism in a subduction zone hydrothermal system: Catalina Schist terrane, California: *Geology*, v. 17, p. 976-980.
- Brabb, E.E., and Churkin, M., Jr., 1969, Geologic map of the Charlie River quadrangle, east-central Alaska: U.S. Geological Survey Miscellaneous Geologic Investigations Map I-973, scale 1:250,000.
- Burkhard, M., and Kerrich, R., 1988, Fluid regimes in the deformation of the Helvetic nappes, Switzerland, as inferred from stable isotope data: *Contributions to Mineralogy and Petrology*, v. 99, p. 416-429.
- Churkin, M., Jr., Foster, H.L., Chapman, R.H., and Weber, F.R., 1982, Terranes and suture zones in east-central Alaska: *Journal of Geophysical Research*, v. 87, p. 3718-3730.
- Coney, P.J., and Jones, D.L., 1985, Accretion tectonics and crustal structure in Alaska: *Tectonophysics*, v. 119, p. 265-283.
- Dietrich, D., McKenzie, J.A., and Song, H., 1983, Origin of calcite in syntectonic veins as determined from carbon-isotope ratios: *Geology*, v. 11, p. 547-551.
- Dover, J.H., 1990, *Geology of east-central Alaska*: U.S. Geological Survey Open-File Report 90-289, 66 pp.
- Dover, J.H., and Miyaoka, R.T., 1988, Reinterpreted geologic map and fossil data, Charley River quadrangle, east-central Alaska: U.S. Geological Survey Miscellaneous Field Studies Map MF-2004, 2 sheets, scale 1:250,000.
- Emrich, K., Ehhalt, D.H., and Vogel, J.C., 1970, Carbon isotope fractionation during the precipitation of calcium carbonate: *Earth and Planetary Science Letters*, v. 8, p. 363-371.
- Foster, H.L., 1976, Geologic map of the Eagle quadrangle, Alaska: U.S. Geological Survey Miscellaneous Geologic Investigations Map I-922, 1 sheet, scale 1:250,000.
- Friedman, I., and O'Neil, J.R., 1977, Compilation of stable isotope fractionation factors of geochemical interest: U.S. Geological Survey Professional Paper 440-KK, p. 1-12.
- Howell, D.G., Johnsson, M.J., Underwood, M.B., Lu, Haufu, and Hillhouse, J.W., 1992, Tectonic evolution of the Kandik region, east-central Alaska: Preliminary interpretations, in Bradley, D.C. and Ford, A.B., eds., *Geologic studies in Alaska by the U.S. Geological Survey During 1990*: U.S. Geological Survey Bulletin 1999, p. 127-140.
- Howell, D.G., and Wiley, T.J., 1987, Crustal evolution of northern Alaska inferred from sedimentological and structural relations in the Kandik area: *Tectonics*, v. 6, p. 619-631.
- Hudson, J.D., 1977, Stable isotopes and limestone lithification: *Journal of the Geological Society of London*, v. 133, p. 637-660.
- Keith, M.L., and Weber, J.N., 1964, Carbon and oxygen isotopic composition of selected limestones and fossils: *Geochimica et Cosmochimica Acta*, v. 28, p. 1787-1816.
- Laughland, M.M., Underwood, M.B., and Wiley, T.J., 1990, Thermal maturity, tectonostratigraphic terranes, and regional tectonic history: An example from the Kandik area, east-central Alaska, in Nuccio, V.F., and Barker, C.E., eds., *Applications of thermal maturity studies to energy exploration*: Society of Economic Paleontologists and Mineralogists, Rocky Mountain Section, Special Publication, p. 97-111.
- Magaritz, M., and Taylor, H.P., Jr., 1976, Oxygen, hydrogen and carbon isotope studies of the Franciscan Formation, Coast Ranges, California: *Geochimica et Cosmochimica Acta*, v. 40, p. 215-234.
- McCrea, J.M., 1950, The isotope chemistry of carbonates and a paleotemperature scale: *Journal of Chemical Physics*, v. 18, p. 849-857.
- Miyaoka, R.T., 1990, Fossil locality map and fossil data for the

- southeastern Charley River quadrangle, east-central Alaska: U.S. Geological Survey Miscellaneous Field Studies Map MF-2007, 1 sheet, scale 1:63,360.
- Nesbitt, B.E., and Muehlenbachs, K., 1989, Origin and movement of fluids during deformation and metamorphism in the Canadian Cordillera: *Science*, v. 245, p. 733-736.
- O'Neil, J.R., 1986, Theoretical and experimental aspects of isotopic fractionation, in Valley, J.W., Taylor, H.P., Jr., and O'Neil, J.R., eds., *Stable isotopes in high temperature geological processes: Reviews in Mineralogy*, v. 16, p. 1-40.
- O'Neil, J.R., Clayton, R.N., and Mayeda, T.K., 1969, Oxygen isotope fractionation in divalent metal carbonates: *Journal of Chemical Physics*, v. 51, p. 5547-5558.
- Payne, M.W., and Allison, C.W., 1981, Paleozoic continental-margin sedimentation in east-central Alaska: *Geology*, v. 9, p. 274-279.
- Ritger, S., Carson, B., and Suess, E., 1987, Methane-derived authigenic carbonates formed by subduction-induced pore-water expulsion along the Oregon/Washington margin: *Geological Society of America Bulletin*, v. 98, p. 147-156.
- Rye, D.M., and Bradbury, H.J., 1988, Fluid flow in the crust: An example from a Pyrenean thrust ramp: *American Journal of Science*, v. 288, p. 197-235.
- Sheppard, S.M.F., 1986, Characterization and isotopic variations in natural waters, in Valley, J.W., Taylor, H.P. Jr., and O'Neil, J.R., eds., *Stable isotopes in high temperature geological processes: Reviews in Mineralogy*, v. 16, p. 165-184.
- Valley, J.W., 1986, Stable isotope geochemistry of metamorphic rocks, in Valley, J.W., Taylor, H.P., Jr., and O'Neil, J.R., eds., *Stable isotopes in high temperature geological processes: Reviews in Mineralogy*, v. 16, p. 445-490.
- Wickham, S.M., and Taylor, H.P., Jr., 1987, Stable isotope constraints on the origin and depth of penetration of hydrothermal fluids associated with Hercynian regional metamorphism and crustal anatexis in the Pyrenees: *Contributions to Mineralogy and Petrology*, v. 95, p. 255-268.
- Reviews: William Carothers and Robert G. Bohannon

Statistical Comparison Between Illite Crystallinity and Vitrinite Reflectance, Kandik Region of East-Central Alaska

By Michael B. Underwood, Thomas Brocculeri, Deborah Bergfeld, David G. Howell, and Mark Pawlewicz

Abstract

Measurements of mean random vitrinite reflectance (R_m) and illite crystallinity index (CI) show that the Kandik River belt of east-central Alaska reached higher levels of thermal maturity than its neighbor, the Tatonduk belt. A statistical correlation between all available pairs of R_m and CI data yields a best-fit curve that passes through the domain of the anchizone (that is, the transition into lowermost greenschist-facies metamorphism). The equation to this curve is: $R_m = 0.31 - 6.79[\log(CI)]$, with the CI parameter measured in units of $\Delta^\circ 2\theta$. Individual data points from both belts display a considerable amount of scatter on either side of the correlation curve, and the correlation coefficient is only $r = 0.60$. We attribute the relatively poor statistical correlation to the effects of several internal and external variables: (1) contamination of the authigenic illite signal by detrital illite/muscovite; (2) differences in both the precursor clay-mineral assemblages and the bulk geochemistry of the diverse host rocks; (3) variations in the rate and (or) physical mechanism of heating; (4) fluctuations in the hydrogeochemistry and hydrogeology at the time of peak heating; and (5) differences in tectonic history, particularly the effects of deformation fabrics such as slaty cleavage and pencil structure.

INTRODUCTION

The Kandik region of east-central Alaska (fig. 1) contains a wide variety of geologic units that are parautochthonous with respect to the North American continent (Brabb and Churkin, 1969; Foster, 1976; Payne and Allison, 1981; Howell and Wiley, 1987; Dover and Miyaoka, 1988). This part of Alaska has been described and interpreted within the conceptual framework of terrane analysis (Churkin and others, 1982; Coney and Jones, 1985; Howell and Wiley, 1987; Laughland and others, 1990; Howell and others, 1992). Conversely, other geologists regard the Kandik region as a thrust-faulted continental-margin succession of North American

affinity (Dover, 1990; D. Bradley, 1992, written commun.). Regardless of which concept is favored, there are two major fault-bounded domains of strata to consider within the Kandik region, herein referred to as the Tatonduk "belt" and the Kandik River "belt" (following the suggestion of D. Bradley, 1992, written commun.). The structural boundary between the Kandik River and Tatonduk belts is the younger-over-older Glenn Creek fault zone (fig. 1), which is part of a complicated system of southeast-verging thrust faults (Dover and Miyaoka, 1988; Howell and others, 1992). In this paper, we make no inferences regarding the absolute distance of tectonic transport for either belt with respect to the Proterozoic edge of North America.

The Tatonduk belt (fig. 2) contains a Middle Proterozoic to Lower Cambrian basement complex (Tindir Group) composed largely of basalt, carbonate rocks, and shale (Young, 1982; Allison, 1988). These strata are overlain by a Paleozoic sequence of sedimentary rocks that records the rifting and progressive subsidence of the North American continental margin (Payne and Allison, 1981; Churkin and others, 1982; Howell and Wiley, 1987; Howell and others, 1992). The Kandik River belt (fig. 3), in contrast, is dominated by deep-marine deposits of Mesozoic age (Churkin and others, 1982). The principal rock units include the Glenn Shale (Triassic to Lower Cretaceous) and the Lower Cretaceous Kandik Group (Keenan Quartzite, Biederman Argillite, and Kathul Graywacke). Fossil localities for these and all other units in the Kandik study area have been summarized by Dover and Miyaoka (1988) and Miyaoka (1990).

Pre-Mesozoic strata occur in two general localities west of the Glenn Creek fault zone: in the core of the Step Mountains antiform, and west of the Mardow Creek fault (fig. 1). Three Paleozoic formations have been mapped in the Step Mountains: (1) conglomerate and fossiliferous limestone lenses of the Permian Step Conglomerate (Brabb, 1969); (2) undated mudrocks correlated by Brabb (1969) with the Ford Lake Shale (Upper

Devonian and Mississippian); and (3) poorly dated chert-pebble conglomerates, assigned to the Devonian Nation River Formation by Brabb and Churkin (1967). West of the Mardow Creek fault, within the so-called Eureka suture zone of Churkin and others (1982), the pre-Mesozoic units include (1) the Devonian Woodchopper Volcanics [named the Woodchopper Canyon terrane by Churkin and others (1982)]; (2) poorly dated interbeds of argillite and chert, sandstone and conglomerate, and limestone and dolomite [mostly units P_{2a} and P_{2l} of Brabb and Churkin (1969)]—these strata were assigned to the Slaven Dome terrane by Churkin and others (1982); and (3) the Permian Step Conglomerate, plus Proterozoic(?) deposits of undivided sedimentary rocks, dolomite, and volcanic rocks [the Takoma Bluff terrane of Churkin and others (1982)]. The map of Dover and Miyaoka (1988) shows widespread occurrences of Devo-

nian conglomerates (Nation River Formation rather than Step Conglomerate) within the Takoma Bluff terrane, but fossil control for these rocks is poor.

The youngest rocks within the study area are assigned to the unit TKs of Brabb and Churkin (1969). These strata are Albian to early Tertiary in age (Dover and Miyaoka, 1988; Miyaoka, 1990). Unit TKs unconformably overlies both the Tatonduk and Kandik River belts and consists of poorly indurated interbeds of conglomerate, sandstone, and mudrock, plus local lenses of coal and plant fragments.

One of the principal goals of our research in the Kandik region is to establish a clearly defined tectonic history, including the thermal evolution of all pertinent rock units. Preliminary accomplishments within this framework included reconnaissance-level measurements of vitrinite reflectance and illite "crystallinity"

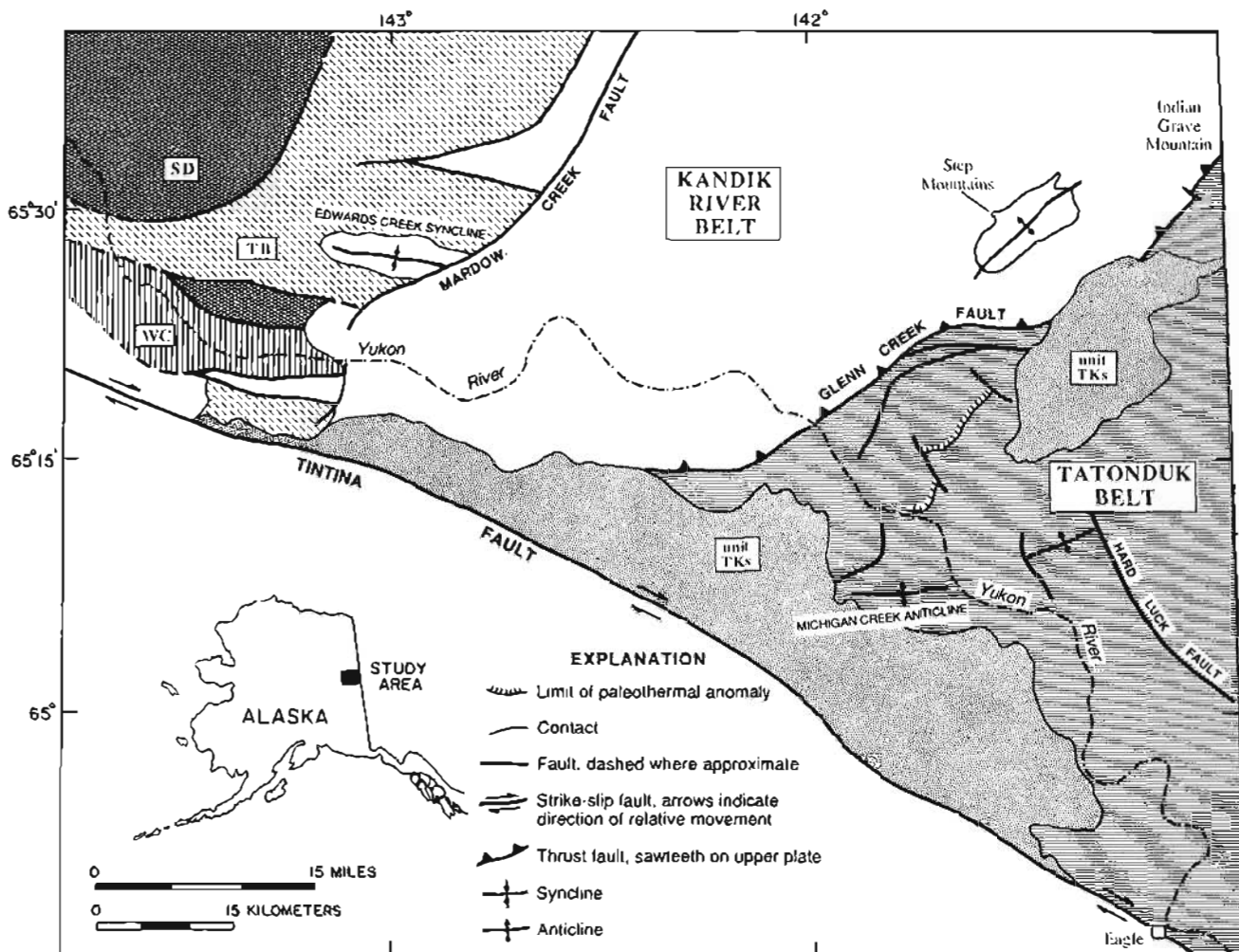


Figure 1. Geologic index map of east-central Alaska showing Kandik River belt (no pattern) and Tatonduk belt (horizontal lined pattern). Hachured line southeast of Glenn Creek fault represents detected limit of a footwall thermal aureole. Also shown are unit TKs of Brabb and Churkin (1969), and the Woodchopper Canyon (WC), Slaven Dome (SD), and the Tacoma

Bluff (TB) terranes of Churkin and others (1982). Rocks southwest of Tintina fault zone are assigned to Yukon-Tanana composite terrane (Coney and Jones, 1985). Modified from Brabb and Churkin (1969) and Foster (1976). For relevant fossil control and alternative interpretations of structural geology, see Dover and Miyaoka (1988) and Miyaoka (1990).

(Underwood and others, 1989; Laughland and others, 1990). Those studies showed that most of the rocks within the Kandik River belt attained significantly higher ranks of thermal maturity than those of the Tatonduk belt. We are now expanding on the analytical techniques and initial interpretations by including isotopic assessments of fluid-rock interactions (for example, Shelton and others, this volume) and microthermometric data from fluid inclusions.

Many techniques are available to help document peak burial temperatures (T) and pressures (P). Most traditional mineralogic studies suffer from a lack of precision with respect to P - T estimates because paragenetic sequences respond to a complex array of variables, and most of the common index minerals are stable over wide ranges of burial conditions (for example, Kisch, 1983; Liou and others, 1987; Frey, 1987). One widely used method for characterizing specific levels of diagenesis and incipient metamorphism is the measurement of illite

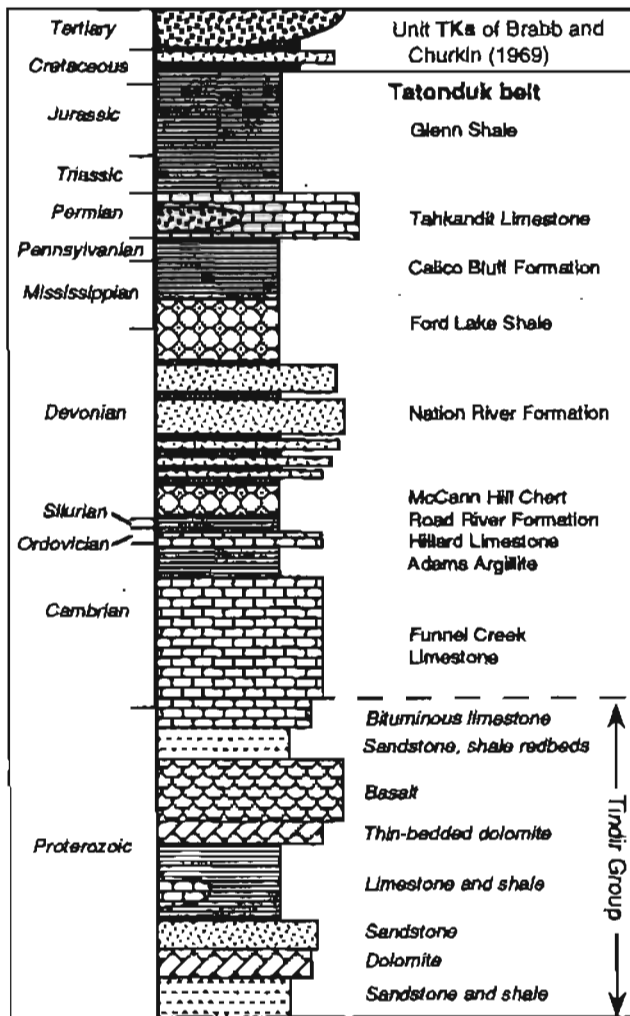


Figure 2. Schematic stratigraphic section for Tatonduk belt [otherwise known as Tatonduk terrane of Churkin and others (1982)]. Modified from Howell and others (1992).

“crystallinity” by X-ray diffraction (XRD). This procedure is rapid, simple, inexpensive, applicable over a wide variety of geologic conditions, and useful for documenting relatively subtle differences among individual samples. XRD data are especially helpful when combined with analyses of organic metamorphism, as measured, for example, by vitrinite reflectance [for general descriptions of this technique, see Dow (1977); Bostick (1979); Barker and Pawlewicz (1986)].

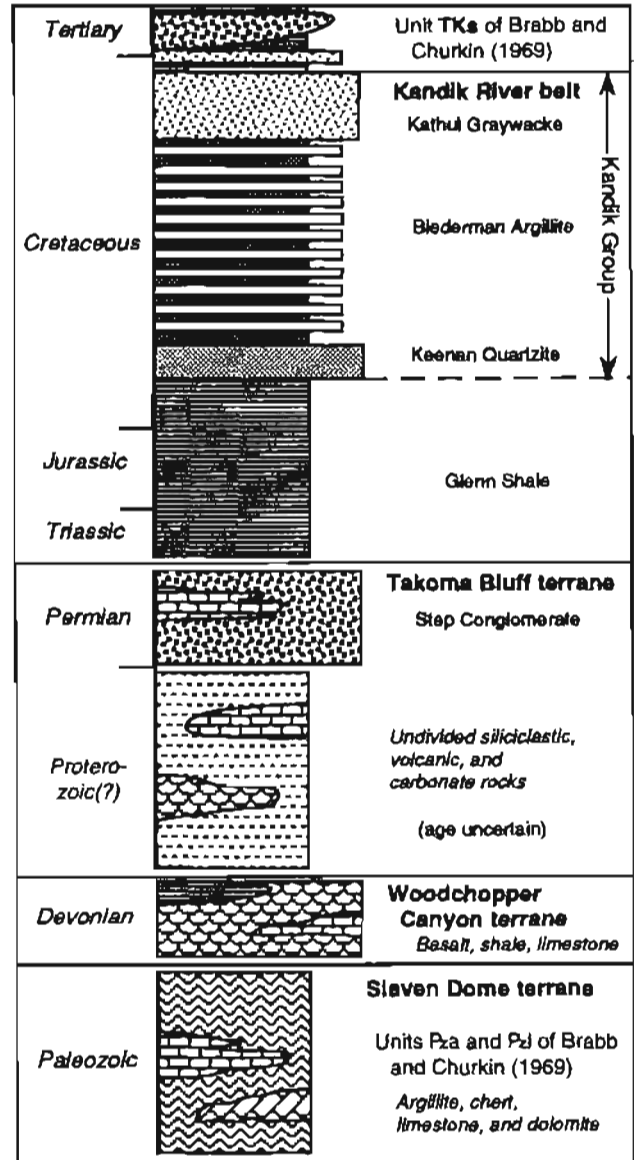


Figure 3. Schematic stratigraphic section for Kandik River belt and rocks of Eureka suture zone. Following the terminology of Churkin and others (1982), Precambrian rocks and Step Conglomerate would be assigned to Takoma Bluff terrane, Woodchopper Volcanics would be assigned to Woodchopper Canyon terrane, and units Pza and Pz1 of Brabb and Churkin (1969) would be assigned to Slaven Dome terrane. Modified from Howell and others (1992).

In this paper, we report on the responses of both organic and inorganic matter to conditions of diagenesis and low-temperature metamorphism within the Kandik region of east-central Alaska (fig. 1). So that meaningful comparisons can be made among many rock units with different burial histories, we have restricted the discussion to two types of data: mean random vitrinite reflectance (R_m), and illite "crystallinity" (CI). This paper establishes a statistical correlation between R_m and CI that is specific to the Kandik study area and compares the Kandik curve to trends established in other orogenic belts. Discussions of spatial variations in thermal maturity, and how they relate in detail to the stratigraphy and geodynamic evolution of the Kandik region, will be presented at a later date.

BASIC PRINCIPLES

Illite Crystallinity

Many studies of clay mineralogy have demonstrated that detrital and authigenic smectites are replaced gradually by illite during sediment diagenesis; in addition, a mixed-layer illite-smectite phase, which is the intermediate product of illitization, displays improved degrees of "ordering" as diagenesis proceeds, together with progressive increases in the ratio of illite to smectite (Dunoyer de Segonzac, 1970; Perry and Hower, 1970; Reynolds and Hower, 1970; Kisch, 1983; Moore and Reynolds, 1989). Weaver (1960) was the first to relate systematic variations in the shape of the 10 Å (001) illite X-ray diffraction peak to the lattice reorganization of illite. In reality, however, this process is quite complicated, in that it involves an increase in the size of crystallites, changes in chemical composition, and a progression toward greater regularity of the structural layers (Kisch, 1983). Frey (1970) demonstrated that increases in illite "crystallinity" can be accompanied by changes in several rock and mineral properties, including the intensity ratio of the illite basal reflections [$I(002)/I(001)$], the color of the host rock, the mean bulk density, and microscopic rock texture due to reactions between clastic quartz grains and clay matrix. Hunziker and others (1986) showed that four chemical modifications occur as illite is transformed into well-crystalline K-mica: (1) expandable layers decrease in relative abundance and eventually disappear; (2) the 1Md illite polymorph (disordered monoclinic) is replaced by the 2M₁ form (two octahedral layers with an overall monoclinic symmetry); (3) the total layer charge and the potassium content in illite interlayer positions both increase; and (4) the chemical variability of individual illite/mica grains decreases. Other authors have pointed out that the term illite "crystallinity" is not perfectly appropriate to describe this

complicated structural and chemical reorganization (Kisch, 1983; Frey, 1987), but it will be used in the remainder of this paper without quotation marks.

Many workers have used illite crystallinity data as part of detailed studies of regional and local structural evolution (for example, Frey and others, 1980; Kemp and others, 1985; Roberts and Merriman, 1985; Awan and Woodcock, 1991; Hesse and Dalton, 1991). Some caution is warranted in this regard, however, particularly if XRD data serve as the only indicator of paleotemperature. One might assume that crystallinity values respond in a linear fashion to increases in temperature or burial depth, as suggested by some borehole data (Yang and Hesse, 1991). Nevertheless, the inorganic reactions are complicated by the effects of many additional variables, including the duration or rate of heating, fluid pressure, fluid composition (K^+ must be available), rates of fluid migration, tectonic stress, original composition of the host sediment (inhibiting effects of Na^+ and Mg^{2+}), the content of organic matter, and the chemical make-up of illite and (or) mixed-layer precursors (Frey, 1987). In addition, data from regions of intermediate-level diagenesis can be notoriously unreliable because of a "contamination" effect caused by mixtures of authigenic illite, illite-smectite mixed-layer phases, and higher grade detrital micas eroded from metamorphic terrains.

As reviewed by Blenkinsop (1988), there are several procedures to quantify the shape of the 10-Å illite peak. To be consistent with most other studies of this type, we have employed the Kubler index (otherwise known as crystallinity index, or CI), which is defined as the width of the 10-Å peak at one-half the peak height (Kubler, 1968). Blenkinsop (1988) considered the Kubler crystallinity index to be marginally superior to the other indices at all grades of diagenesis and metamorphism. The crystallinity index decreases as the diagenetic/metamorphic grade increases, and values can be calculated very precisely using digital XRD data. The original units of crystallinity index were millimeters, but most subsequent workers have converted to angular units of $\Delta^{\circ}2\theta$ to minimize the effects of variable machine settings (for example, Kisch, 1980).

Robinson and others (1990) completed additional studies of error and precision and concluded that geologic interpretations of CI gradients and anomalies should be based on differences of at least $0.1\Delta^{\circ}2\theta$. The most reliable application, therefore, is simply to define broad zones or stages of advanced diagenesis and low-temperature metamorphism. A five-fold subdivision was introduced by Weaver (1960), but most workers follow the system of Kubler (1968), who defined the zones as diagenesis, anchimetamorphism (transition into lowermost greenschist-facies metamorphism), and epimetamorphism (lowermost greenschist facies). Pin-

pointing the zonal boundaries has been problematic because of operational inconsistencies in sample preparation, analytical equipment, and analytical technique [see Kisch (1987, 1990), Kisch and Frey (1987), and Robinson and others (1990) for comprehensive discussions of these problems]. With these problems in mind, Blenkinsop (1988) advocated the following values of CI for the two principal boundaries of thermal alteration: diagenesis-to-anchizone = $0.42\Delta^{\circ}2\theta$ and anchizone-to-epizone = $0.25\Delta^{\circ}2\theta$.

Vitrinite Reflectance and Paleotemperature

The goal of correlating CI zones with other indicators of low-grade metamorphism (both inorganic and organic) has been discussed in detail by Kisch (1987). Most noteworthy, for the purposes of our study, is the relation between CI values and coal rank, which is typically quantified in terms of vitrinite reflectance. To establish a universal CI- R_m correlation is troublesome, however, because the organic and inorganic systems quite clearly respond to different (though overlapping) sets of external variables. Unlike illite crystallinity, for example, vitrinite reflectance increases primarily in response to higher burial temperatures, thereby serving as a more direct indicator of maximum heating (Barker, 1989, 1991).

Time-dependent models of organic metamorphism (Hood and others, 1975; Bostick and others, 1978; Waples, 1980; Middleton, 1982; Ritter, 1984; Wood, 1988; Hunt and others, 1991) are useful for studies of first-cycle sedimentary basins. However, serious problems are inherent in the application of these models if one's goal is to calculate maximum paleotemperatures with any degree of accuracy, particularly within uplifted orogenic sequences where the tectonic and thermal histories can be very complicated and poorly constrained. In addition to the guesswork involved in the selection of an appropriate value of activation energy for a given rock unit (Antia, 1986; Wood, 1988), large uncertainties usually exist in the inferred reaction rates for time-temperature integrals (Issler, 1984; Ritter, 1984), not to mention in the choices of effective heating time. Conversely, many empirical and theoretical studies over the past decade have demonstrated that vitrinite reflectance is affected most by maximum temperature and almost imperceptibly by the duration of heating, at least under geologic situations where time is measured in millions of years (Wright, 1980; Gretener and Curtis, 1982; Suggate, 1982; Barker, 1983, 1989, 1991; Price, 1983; Barker and Pawlewicz, 1986). These workers, in other words, have argued that the time required for stabilization of kerogen maturation, at a given burial temperature, is usually on the order of 1 m.y. or less.

Several statistical correlations now exist between R_m and absolute paleotemperature, with the temperature scales established through direct borehole measurements (Barker, 1983, 1988; Price, 1983; Barker and Pawlewicz, 1986). The Barker (1988) correlation yields the lowest temperature estimates for a given value of R_m as compared with other time-independent methods. Recent models based on chemical kinetics (Burnham and Sweeney, 1989; Sweeney and Burnham, 1990) match the curve of Barker (1988) quite closely, provided the inferred heating time is limited to around 1 m.y. Furthermore, Barker and Goldstein (1990) arrived at a close match between homogenization temperatures of fluid inclusions (which are not affected by heating duration) and estimates of paleotemperature derived from the Barker and Pawlewicz (1986) regression analysis. The Barker (1988) equation is based on the same set of data as Barker and Pawlewicz (1986), but the statistical model is more defensible. Thus, for the purposes of providing a straightforward estimate of peak burial temperature, we prefer the equation of Barker (1988). The relevant equation is: $T (^{\circ}\text{C}) = 148 + 104[\ln(R_m)]$, and the error associated with paleotemperature estimates is roughly $\pm 30^{\circ}\text{C}$.

No universal agreement has been reached on the anchizone boundaries in terms of mean vitrinite reflectance or paleotemperature values. The boundaries suggested by various workers are diagenesis-to-anchizone = 2.5 percent R_m to 3.1 percent R_m [see numerous studies summarized by Kisch (1987)], and anchizone-to-epizone = 3.7 percent R_m to 5.5 percent R_m (Frey and others, 1980; Kisch, 1980; Ogunyomi and others, 1980; Duba and Williams-Jones, 1983). The lower and upper temperature limits of the anchizone have been approximated only vaguely at 200°C and 300°C , respectively (Kisch, 1987).

METHODS

Specimens of shale and their low-grade metamorphic equivalents were collected from fresh outcrop exposures. Virtually all of the mudrock-bearing formations within the Kandik region were sampled (table 1). The standard U.S. Geological Survey and University of Missouri techniques for preparation and optical measurements of vitrinite reflectance have been described at length elsewhere (Barker and Pawlewicz, 1986; Underwood and others, 1989) and are not repeated here. We report the data as mean values based on measurements (in oil) of at least 25 individual randomly oriented particles per specimen. Although a few coal specimens were analyzed during the investigation (particularly common in unit TKs), all of the reported data come from dispersed organic particles that were concentrated from mudstones, shales, and argillites.

Illite Sample Preparation

The rocks were ground to a fine powder using a mortar and pestle; the powder then was washed in distilled water and disaggregated further using an ultrasonic cell disrupter. A pinch of sodium phosphates and sodium carbonates was added to prevent flocculation of suspended clay minerals, and the <2- μm size fraction was segregated by centrifugation (770 rpm for 3.3 min.; then 1,500 rpm for 15 min.). Oriented aggregates of the clay-sized material were placed on glass slides using the vacuum-filtration and peel technique (Moore and Reynolds, 1989). Prior to XRD analysis, the slides were placed in a chamber containing ethylene glycol for 12 h at approximately 60°C to saturate any existing expandable clay phases; this step was necessary to prevent seasonal changes in atmospheric humidity from affecting the results.

Diffraction Settings and Digital Data Processing

All XRD measurements were completed at the University of Missouri using a Scintag PAD V microprocessor-controlled diffractometer, interfaced with a Microvax 2000 microcomputer. X-ray scans were run under the following machine settings: voltage = 30 kV; amperage = 20 mA; radiation = $\text{CuK}\alpha$; filters = none; receiving slits = 0.3° (close to detector); scatter slits = 2° (close to beam emission); scan = continuous with 0.03° chopper increment; time constant = 1.8 second/step; scan rate = 1°2 θ /min; rate meter = automatic control. The (101) quartz peak (3.342 Å) was used as a standard for internal calibration of 2 θ peak positions. The scan for illite (and other clay minerals) was run from 2°2 θ to 15°2 θ with the sample holders spun. The resulting digital output was processed first for a background correction and $\text{K}\alpha_2$ stripping, using Scintag software. The illite (001) peaks then were identified and deconvoluted using an interactive graphics subroutine. The deconvolution program is designed to fit XRD peaks to models, based on a Split Pearson VII profile shape (Gaussian-Lorentzian hybrid). Automatic computations yield peak positions and d -spacings (in °2 θ and Å values), peak intensities (counts per second), integrated peak areas (total counts), and full peak width at half maximum (Δ °2 θ).

The analytical sensitivity for measurements of peak width using the Scintag PAD V diffractometer is 0.001°2 θ . However, prior tests of internal reproducibility (Underwood and others, 1993) resulted in standard deviations about the mean ranging from 0.009°2 θ to 0.015°2 θ . We conclude, therefore, that the data are meaningful only to the nearest 0.01°2 θ .

RESULTS

All of the sample numbers, formational designations, values of illite crystallinity index, plus corresponding data from measurements of vitrinite reflectance are listed in table 1. All formational assignments conform to the maps of Brabb and Churkin (1969) and Foster (1976). Many of the specimens did not yield R_m data, either because they are too old to have incorporated debris from terrestrial plants or because the organic matter is too lean to produce reliable results.

Pre-Devonian Strata

Results from the older rock units within the Tatonduk belt (that is, stratigraphically below the Nation River Formation) are shown in figure 4. The principal epiclastic units within this part of the stratigraphic column (fig. 2) include interbeds of sandstone and shale or dolomite and shale within the Tindir Group, mudrocks of the Adams Argillite, and interbeds of chert, siliceous shale, and graptolitic shale of the Road River Formation. These CI data define an extremely wide range of apparent burial conditions, extending from the upper limit of the anchizone (0.25 Δ °2 θ) to the zone of early diagenesis (0.80 Δ °2 θ). Because these specimens do not contain appropriate organic constituents, we have no means of establishing comparable ranks of organic metamorphism or assessing the reliability of CI values as indicators of in situ burial conditions.

Nation River Formation

The Nation River Formation is an important Devonian unit of inferred submarine-fan deposits (sandstone turbidites, conglomerate, and shale). Vitrinite is fairly abundant in the mudrocks, which supports the idea of a continental provenance for the sediment. With one exception, CI values from the Nation River Formation all fall within the confines of the diagenetic zone (fig. 5). Similarly, ranks of organic metamorphism are generally low (below 1.0 percent R_m). Consistent exceptions to the low organic rank occur at two localities: (1) within the Step Mountains region, where R_m = 2.5 percent to 3.7 percent; and (2) within a relatively narrow zone (exposed along the Nation River) immediately to the southeast of the Glenn Creek fault, where R_m values are between 2.0 percent and 2.8 percent (see fig. 1 for general localities). Two samples of the Ford Lake Shale at Step Mountains also produced anomalously high values of R_m (table 1).

Structural and tectono-stratigraphic interpretations of the Step Mountains region are controversial. This feature could represent a simple faulted anticline (Brabb and

Table 1. Values of mean random vitrinite reflectance (R_m) and illite crystallinity (CI), Kandik region, east-central Alaska

Sample	Formation	R_m	CI	Sample	Formation	R_m	CI
Pre-Devonian strata							
mj90-k26a	Tindir		.30	tb90-k50b	Nation River	2.8	.51
mj90-k26b	Tindir		.27	tb90-k51a	Nation River	2.8	.53
mj90-k27a	Tindir		.53	tb90-k52a	Nation River	2.6	.52
mj90-k28	Tindir		.61	tb90-k53c	Nation River	2.5	.46
mj90-k29a	Tindir		.30	tb90-k59c	Nation River	.8	.44
mj90-k75a	Tindir		.36	786-3-2d	Nation River	.9	.52
mj90-k76a	Tindir		.25	786-3-3a	Nation River		.53
um90-k34a	Tindir		.63	786-4-2c	Nation River	.7	.51
um90-k35b	Tindir		.81	786-29-1	Nation River	2.0	.57
um90-k37c	Tindir		.45	85jcr-15a	Nation River		.67
um90-k39b	Tindir		.51	85jcr-24	Nation River	.8	.59
786-7-2	Tindir		.33	Glenn Shale			
85jcr-67	Tindir		.43	mj90-k17a	Glenn	3.4	.21
886-1-1	Funnel Creek		.54	mj90-k41a	Glenn	3.9	.42
mj90-k33a	Adams		.53	mj90-k41b	Glenn	4.4	.39
mj90-k63a	Adams		.65	mj90-k42a	Glenn		.50
um90-k33	Adams		.47	mj90-k43b	Glenn	4.3	.39
um90-k41a	Adams		.67	mu90-k9a	Glenn	2.7	.61
tb90-k56b	Adams		.47	um90-k17	Glenn	1.7	.56
tb90-k57b	Adams		.39	um90-k18	Glenn	3.0	.58
tb90-k58a	Adams		.39	um90-k20	Glenn	3.4	.68
um90-k44a	Hillard		.54	um90-k21	Glenn	2.3	.54
um90-k46	Hillard		.45	um90-k24a	Glenn	4.3	.30
um90-k47b	Hillard		.58	um90-k25c	Glenn	3.9	.58
mj90-k15a	Road River		.29	um90-k26b	Glenn	4.8	.28
um90-k50a	Road River		.48	um90-k28a	Glenn	4.6	.40
um90-k51a	Road River		.43	um90-k30a	Glenn		.78
um90-k52a	Road River		.78	um90-k31a	Glenn	4.1	.58
tb90-k54b	Road River		.49	um90-k32c	Glenn		.56
tb90-k55a	Road River		.51	um90-k78f	Glenn	4.1	.39
85jcr-25b	Road River	1.0	.53	um90-k78h	Glenn		.29
				tb90-k18	Glenn		.31
Nation River Formation				786-7-3a	Glenn	2.8	.33
mj90-k5	Nation River	2.5	.57	786-7-3b	Glenn		.39
mj90-k6	Nation River	3.7	.52	786-23-1a	Glenn	2.1	.58
mj90-k31b	Nation River	.7	.45	786-23-1b	Glenn	1.8	.62
mj90-k34a	Nation River	.8	.39	786-31-3a	Glenn		.78
mj90-k35c	Nation River	.7	.47	786-31-3b	Glenn	1.8	.74
mj90-k59a	Nation River	1.6	.47	786-31-3c	Glenn	1.6	.83
mj90-k68a	Nation River		.71	Kandik Group			
mj90-k69d	Nation River	.6	.54	mu90-k10a	Keenan	1.6	.62
mj90-k70a	Nation River	.6	.46	mj90-k18b	Biederman	2.2	.49
mj90-k71a	Nation River	.9	.56	mj90-k23a	Biederman	3.5	.47
mj90-k72a	Nation River	.8	.50	mj90-k37a	Biederman	2.8	.45
mj90-k74a	Nation River	1.2	.52	mj90-k38a	Biederman	2.9	.41
um90-k54c	Nation River	.7	.54				
tb90-k49c	Nation River	2.4	.56				

Table 1. Values of mean random vitrinite reflectance (R_m) and illite crystallinity (CI), Kandik region, east-central Alaska—Continued

Sample	Formation	R_m	CI	Sample	Formation	R_m	CI
Kandik Group				786-24-1b	Kathul		.44
mj90-k39a	Biederman	4.5	.30	786-24-2b	Kathul		.46
mj90-k40a	Biederman	4.7	.33	786-24-3a	Kathul		.37
mj90-k54	Biederman	3.4	.38	786-24-3b	Kathul		.40
mj90-k56a	Biederman		.33	786-25-8a	Kathul	2.2	.47
mj90-k79c	Biederman	4.4	.34	786-25-8b	Kathul	1.8	.42
mj90-k79g	Biederman	4.4	.36	786-25-10	Kathul	1.6	.37
mj90-k80c	Biederman	3.0	.37	85jcr-14	Kathul		.54
mj90-k81b	Biederman	2.7	.40	Miscellaneous			
mj90-k82b	Biederman	5.0	.32	mj90-k50	Pza	3.2	.40
mj90-k83d	Biederman	4.7	.27	mj90-k51a	Pza		.26
mj90-k84b	Biederman	4.8	.35	mj90-k51b	Pza		.32
mj90-k85b	Biederman	5.0	.35	mj90-k51c	Pza		.33
mj90-k86b	Biederman	4.2	.35	mj90-k94a	Pza	4.2	.33
mj90-k87b	Biederman	4.4	.39	mj90-k98b	Pza	3.7	.22
mj90-k89c	Biederman	5.1	.40	mj90-k99	Pza	4.0	.24
mj90-k90d	Biederman	4.9	.29	mj90-k4	Ford Lake	2.5	.38
mj90-k91b	Biederman	5.0	.30	mj90-k11	Ford Lake	3.9	.54
mj90-k92a	Biederman	4.8	.33	mj90-k62a	Ford Lake		.74
mj90-k93a	Biederman	4.7	.31	mu90-k2	Ford Lake		.36
um90-k27a	Biederman	4.3	.26	mu90-k3	Ford Lake		.38
786-8-2b	Biederman	3.3	.31	mu90-k4	Ford Lake		.36
786-12-1d	Biederman	3.7	.28	mu90-k8a	Ford Lake		.38
786-13-1	Biederman	2.1	.41	mu90-k11a	Ford Lake		.48
786-14-1	Biederman	3.3	.31	85jcr-11	Ford Lake		.37
786-14-3	Biederman	3.6	.32	mj90-k64a	Calico Bluff		.58
786-14-4	Biederman	4.2	.35	mj90-k67b	Calico Bluff		.50
786-23-2	Biederman	1.7	.50	um90-k16	Step	2.7	.27
786-23-3	Biederman	2.2	.58	mj90-k36a	TKs	.5	.51
786-26-1b	Biederman	2.9	.55	mj90-k58b	TKs	.7	.68
786-26-3a	Biederman		.48	mj90-k65a	TKs	.6	.51
786-27-1a	Biederman	1.9	.39	mj90-k66a	TKs		.57
786-27-1b	Biederman	1.6	.50	mj90-k95b	TKs		.34
786-27-4a	Biederman	2.7	.37	um90-k22j	TKs		.31
786-27-4b	Biederman	3.5	.32	tb90-k17	TKs		.26
mj90-k20a	Kathul		.48				
mj90-k21b	Kathul	2.2	.41				
mj90-k22a	Kathul		.38				

Churkin, 1969; Dover and Miyaoka, 1988), or a window into the Tatouduk belt, with the Paleozoic footwall strata exposed by erosion through a folded Glenn Creek fault (Laughland and others, 1990). Alternatively, Howell and others (1992) have speculated that the Devonian and Permian strata at Step Mountains could be part of a separate nappe composed of basement rocks that crop out to the west in the Eureka suture zone [that is, the Takoma Bluff and (or) Slaven Dome terranes of Churkin and others,

1982]. The existing thermal-maturity data fail to resolve these conflicting hypotheses, as any one of the scenarios would explain the generally higher values of thermal maturity in the core of the structure.

The second group of anomalous R_m data from the Nation River Formation confirms the existence of a thermal aureole created by displacement along the Glenn Creek fault (fig. 1). Laughland and others (1990) first suggested that this anomaly was caused by heat conduc-

tion as a hot hanging wall (Kandik River belt) was uplifted and thrust over the cooler footwall (Tatonduk belt). The southeastward termination of the paleothermal anomaly may be related to wedging out of the hanging wall (Laughland and others, 1990) or to a transition from a thrust ramp or associated fault-bend fold in the hanging wall to a flat in the hanging wall. The values of illite crystallinity within the aureole ($0.57\Delta^{\circ}2\theta$ to $0.46\Delta^{\circ}2\theta$) do not deviate with respect to the Nation River average of $0.52\Delta^{\circ}2\theta$. Thus, even though thrusting evidently reset R_m to higher values, the temperature increase was insufficient [in magnitude and (or) duration] to change CI beyond the levels inherited from detrital source rocks and (or) earlier stages of diagenesis.

Glenn Shale

CI values for the Glenn Shale vary considerably (fig. 6). This stratigraphic unit has been mapped without ambiguity within both the Kandik River belt and the Tatonduk belt (figs. 2 and 3; Churkin and others, 1982; Howell and others, 1992). One group of samples yielding higher CI values (sites 786-23 and 786-31) was obtained from a poorly mapped region on the Canadian side of the international border (see Underwood and others, 1989); these rocks are provisionally included in the Tatonduk belt, which is generally lower in thermal maturity. Based upon one datum (site um90-k30), CI values associated with shale outcrops on the flanks of the Michigan Creek anticline (see fig. 1 for location) are also consistent with low thermal maturity, as are specimens of the Nation River Formation obtained from the fold's core (sites 786-3 and 786-4).

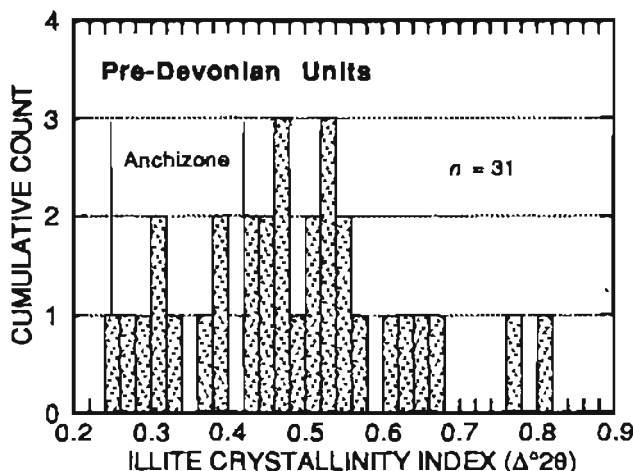


Figure 4. Illite crystallinity (CI) histogram for pre-Devonian strata of Tatonduk belt. Rock units consist of Tindir Group, Funnel Creek Limestone, Adams Argillite, and Road River Formation. See table 1 for complete listing of data. *n*, number of samples.

Within the Kandik River belt, one anomalous zone of relatively low thermal maturity (sites um90-k17 to um90-k21) is associated with an unusual east-west trending syncline (cored by the Glenn Shale and Keenan Quartzite); this structure is located to the west of and is truncated by the Mardow Creek fault (fig. 1; Brabb and Churkin, 1969). Most of the remaining data, particularly in the vicinity of the Glenn Creek fault zone, fall within the confines of the anchizone. These samples of Glenn Shale display excellent slaty cleavage or pencil structure, formed by the intersection of cleavage and fissility. One fault-zone specimen (mj90-k17a), a semi-schist from Indian Grave Mountain (fig. 1), falls within the zone of epimetamorphism. In general, the inorganic and organic data are consistent, in that most anchizone samples yield correspondingly high R_m values of 3.4 percent to 4.8 percent (table 1).

Kandik Group

Data from the Kandik Group (which forms the bulk of the Kandik River belt) display the most consistent cluster of any stratigraphic unit within the study area (fig. 7). Most of these samples were obtained from the Biederman Argillite; all of the interbeds of mudrock that we sampled from Biederman Argillite display excellent slaty cleavage, and sandstone interbeds typically contain extension fractures filled with quartz and calcite veins. The ubiquitous development of cleavage is consistent with the fact that most of the Biederman data fall within the boundaries of the anchizone; a few data points are

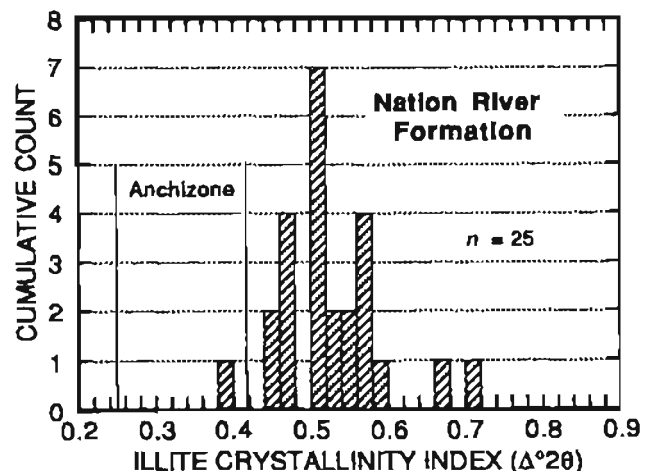


Figure 5. Illite crystallinity (CI) histogram for Nation River Formation (Devonian). See table 1 for complete listing of CI data and corresponding values of vitrinite reflectance. Included in this compilation are two data from Step Mountains (sites mj90-k5 and mj90-k6). All other samples were collected southeast of Glenn Creek fault zone. With one exception (site mj90-k59), all samples yielding R_m values above 1.0 percent were collected within inferred footwall aureole of the Glenn Creek fault (see fig. 1). *n*, number of samples.

within the uppermost zone of diagenesis (fig. 7). The corresponding values of vitrinite reflectance range from 1.6 percent to 5.1 percent, and most of the samples within the anchizone are above 3.0 percent R_m (table 1).

Miscellaneous

Two additional rock units deserve specific mention, even though data are relatively sparse. Unit P_{2a} of Brabb and Churkin (1969) occurs to the west of the Mardow Creek fault (that is, within the Slaven Dome terrane of Churkin and others, 1982). The original stratigraphic position of these poorly dated argillites remains uncertain, as all contacts with the Glenn Shale and the Kandik Group have been mapped as faults (Brabb and Churkin, 1969). CI values for unit P_{2a} are uniformly low, ranging between $0.40\Delta^{\circ}2\theta$ and $0.22\Delta^{\circ}2\theta$ (table 1); R_m values range from 3.2 percent to 4.2 percent. These results are consistent with the phyllitic appearance of hand specimens and the hypothesis that assigns unit P_{2a} to the depositional basement of the Kandik River belt (Howell and others, 1992).

CI values from unit TKs of Brabb and Churkin (1969) are extremely erratic and inconsistent with respect to levels of organic metamorphism. These poorly indurated and mildly deformed alluvial and fluvial deposits unconformably overlie rocks within both the Tatonduk and Kandik River belts (fig. 1). Coal specimens (unpublished U.S. Geological Survey and University of Missouri data) and dispersed organic matter from this unit consistently fall below 0.6 percent R_m , yet values of CI for the mudstones range from $0.26\Delta^{\circ}2\theta$ to $0.68\Delta^{\circ}2\theta$ (table 1). Clearly, most of the illite and well-crystalline K-mica incorporated into these mudstones is

detrital in origin, rather than a product of diagenetic alteration of the host rocks.

DISCUSSION

The following discussion places the available data from the Kandik region within the context of comparable studies completed elsewhere, particularly as they apply to calibrations of the anchizone. A cross plot of all pairs of CI and R_m data is shown in figure 8. In this diagram, we have adopted the following boundaries for the anchizone: CI boundaries set at $0.42\Delta^{\circ}2\theta$ and $0.25\Delta^{\circ}2\theta$; R_m boundaries set at 2.6 percent and 4.5 percent. These R_m limits agree with most of the data sets cited by Kisch (1987), but they are more specifically dictated by the results of several studies summarized by Underwood and others (1991). Using the correlation between R_m and paleotemperature established by Barker (1988), the temperature boundaries for the anchizone are 245°C and 305°C. These temperatures seem reasonable in light of the widespread acceptance of the 300°C isotherm as an approximate lower limit for greenschist-facies metamorphism (for example, Ernst, 1974).

We believe that a logarithmic regression is appropriate because of the well-established exponential relationship between R_m and temperature, with or without the hypothesized linear response to time or heating rate (Dow, 1977; Bostick, 1979; Barker and Pawlewicz, 1986). The precise numerical relationship between CI and paleotemperature is impossible to isolate, however, because of the many variables involved in illitic reactions. Nevertheless, diagenetic progressions in illite-smectite mixed-layer phases typically follow linear depth

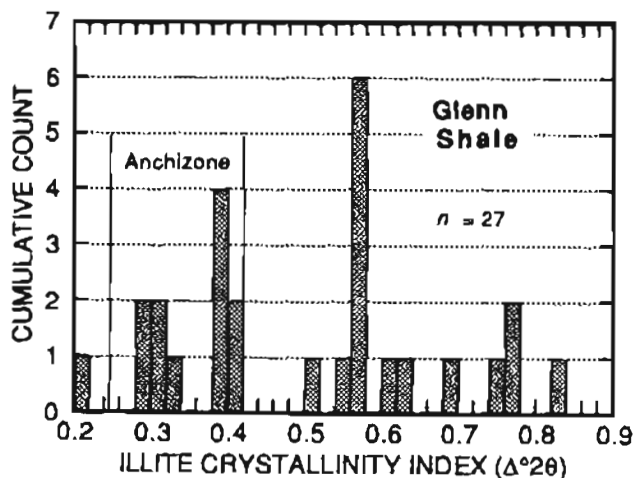


Figure 6. Illite crystallinity (CI) histogram for Glenn Shale (Triassic to Lower Cretaceous). Results from both Kandik River belt and Tatonduk belt are included. See table 1 for complete listing of CI data and corresponding values of vitrinite reflectance. n , number of samples.

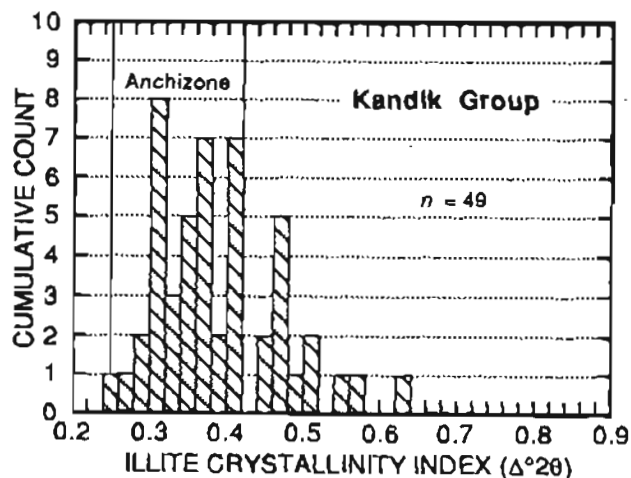


Figure 7. Illite crystallinity (CI) histogram for Kandik Group (Lower Cretaceous). Rock units consist of Keenan Quartzite, Biederman Argillite, and Kathul Graywacke. See table 1 for complete listing of CI data and corresponding values of vitrinite reflectance. n , number of samples.

trends (Perry and Hower, 1970; Freed and Peacor, 1989), and borehole gradients in CI are usually linear (for example, Yang and Hesse, 1991). Consequently, at least for the purpose of regression analysis, we assume that CI values change as a linear function of temperature, whereas R_m values change exponentially with temperature.

The equation to a best-fit curve for the Kandik data is $R_m = 0.31 - 6.79[\log(\text{CI})]$. This result closely matches similar curves established for two study areas within the Franciscan Complex of California (King Range terrane and Sur-Obispo terrane) and one site within the Shimanto Belt of Japan (fig. 9). It is important to point out, however, that a great deal of scatter exists in individual data points from the Kandik study area (fig. 8). As a measure of this scatter, the correlation coefficient for the Kandik curve is only $r = 0.60$. If both CI and R_m had responded in kind to the same set of external and (or) internal variables, then one might expect the correlation to be much tighter. As statistics for comparison, values of r for the Sur-Obispo terrane and the Shimanto data are 0.89 and 0.84, respectively (Underwood and others, 1991). Geologic reasons for the scatter of data in the Kandik study area need to be assessed.

Sample preparation methods, optical equipment, and operator technique will affect values of vitrinite reflectance, as will statistical manipulations of the resulting data (Dembicki, 1984). Beyond these possible influences, sev-

eral geologic and geochemical parameters appear to have influenced our results, particularly with respect to the CI data. One obvious reason for the poor statistical correlation is the fact that many of the rock units were exposed to only moderate degrees of diagenesis, and those mudstones contain mixed populations of illite/mica and illite-smectite mixed-layer clays. This is particularly obvious for samples within unit TKs, but low-rank sequences within most of the Tatonduk belt probably contain mixtures of detrital muscovite eroded from a broad spectrum of metamorphic source rocks. In support of this conclusion, petrographic analyses of sandstones from the Nation River Formation show that the detritus includes significant percentages of low-grade metasedimentary rock fragments (Brocculeri and others, this volume). Because of this recycling phenomenon, absolute values of CI within the field of diagenesis are not reliable as indicators of in situ thermal history. At the very least, we believe that CI data from any samples yielding R_m values less than 1.0 percent must be viewed as suspect (fig. 8). Furthermore, because the pre-Devonian units within the Tatonduk belt cannot be evaluated for vitrinite reflectance (fig. 4), we would caution against overinterpretation of those CI data unless some other measure of thermal maturity can provide independent confirmation.

A second factor to consider is the effect of clay-mineral precursors and bulk geochemistry of the host

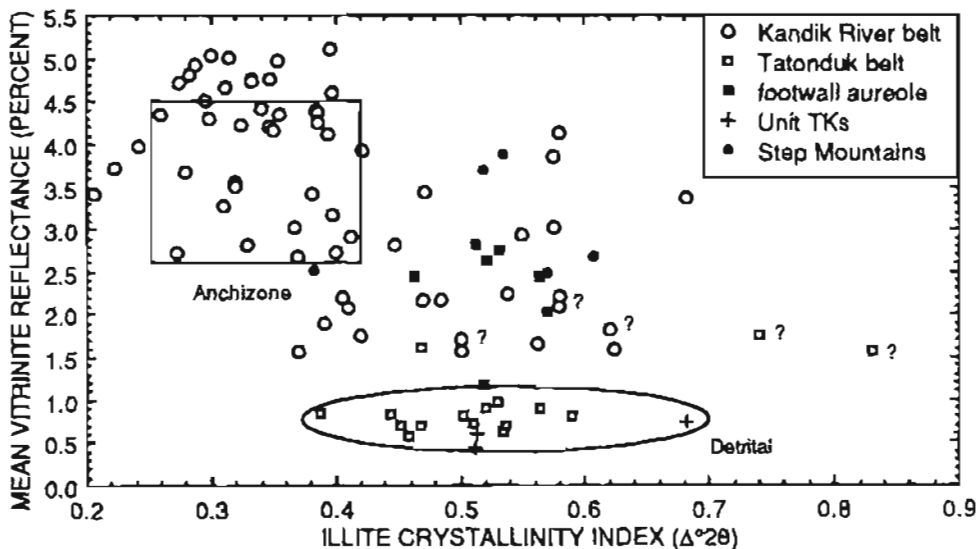


Figure 8. Scatter diagram and illite crystallinity (CI)-vitrinite reflectance (R_m) correlation curve for Kandik River and Tatonduk belts of east-central Alaska. CI boundaries for anchizone conform to designations of Blenkinsop (1988). R_m boundaries of 2.6 percent and 4.5 percent correspond to paleotemperatures of approximately 245°C and 305°C, based on the correlation of Barker (1988). Data from unit P2a of Brabb and Churkin (1969) have been combined with those of Kandik River belt. Samples from Step Mountains include Nation River Formation, Ford Lake Shale, and Glenn Shale. Inferred footwall aureole associated with Glenn Creek fault is based on data from seven sites within Nation River Formation. Data points with question marks refer to sample sites in Canada, where belt designations are uncertain (see Underwood and others, 1989). CI values are considered unreliable below equivalent R_m values of about 1.0 percent because of probable contamination by detrital illite/muscovite. Unit TKs of Brabb and Churkin (1969).

rock on illite diagenesis. Although we have no chemical data to provide quantitative constraints on this argument, it is obvious that the Tadonduk and Kandik River belts both contain a wide variety of rock types spanning long periods of geologic time. For example, interbeds between the mudrocks vary from chert, to dolomite and limestone, to sandstone and chert-pebble conglomerate; the mudrocks themselves differ considerably in color, texture, content of organic matter (see Underwood and others, 1989), carbonate content, and so on. Maintaining uniform geochemical conditions under these circumstances is not realistic. In comparison, the Franciscan and Shimanto study areas (fig. 9) are representative of relatively limited time intervals, consistent arc-related sediment sources, and uniform environments of deep-marine deposition. By increasing the variability of the host-rock lithologies, the scatter in CI data is bound to expand.

Other published studies have led to the suggestion that unusual heating events can affect the relationship between R_m and CI. In particular, CI values tend to be suppressed with respect to R_m under conditions of rapid heating, such as the emplacement of igneous intrusions (Pevear and others, 1980; Smart and Clayton, 1985; Kisch, 1987). This is because inorganic reactions are relatively sluggish compared with changes in the organic constituents. Within the King Range terrane of California, a similar lag in CI has been documented in an apparent response to localized hy-

drothermal discharge and mineralization around a vent site (Laughland, 1991). Another factor in hydrothermal systems is the chemical effect of hot fluids (Duba and Williams-Jones, 1983). The retardation of several different clay-mineral reactions is unequivocal in Holocene water-dominated geothermal systems, and this effect has been attributed to disequilibrium conditions triggered by rapid heating (Barker and others, 1986). Thus, the effects of both rapid conductive heating and advective heat transfer, by either focused or diffuse hydrothermal systems, need to be considered during interpretations of data from east-central Alaska, particularly for high-rank strata within the Kandik River belt.

Preliminary assessments of fluid-rock interactions within our study area show that the Tadonduk and Kandik River belts were affected by different systems of fluid (Shelton and others, this volume). For example, syntectonic quartz and calcite veins are widespread within the cleaved rocks of the Kandik Group and the Glenn Shale; our studies show that the calcite veins precipitated from metamorphic fluids that reached isotopic equilibration under conditions of low water-to-rock ratios and relatively high temperature. In contrast, calcite veins in the Tadonduk belt are quite rare, and those that do occur precipitated from low-temperature waters with isotopic signatures much closer to meteoric values (Shelton and others, this volume). Based on these data,

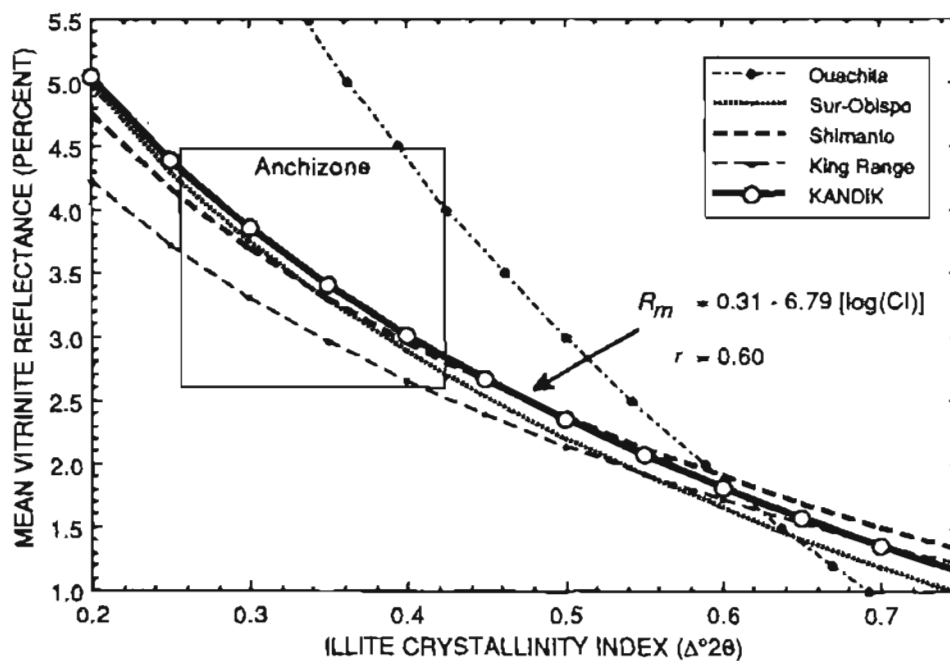


Figure 9. Comparison among Kandik illite crystallinity - vitrinite reflectance curve and equivalent correlations for other orogenic belts. Boundaries for anchizone are same as those defined in figure 8. Sources of data and statistical correlations are as follows: Ouachita Mountains, Arkansas and Oklahoma (Guthrie and others, 1986; Houseknecht and others, 1987); Shimanto Belt, Japan (Underwood and others, in press); King Range terrane, Franciscan Complex, California (Laughland, 1991; Underwood and others, 1991); Sur-Obispo terrane, Franciscan Complex, California (Laughland, 1991; Underwood and others, 1991). R_m , mean random vitrinite reflectance; r , correlation coefficient.

it is clear that the two terranes experienced fundamentally different histories of fluid migration; some of the scatter in the R_m -CI correlation, therefore, probably was caused by responses of different illite populations to the variations in pore-fluid chemistry, as well as to rates of fluid migration during the respective episodes of peak heating.

A final possibility is the effect of tectonic deformation. Stress regimes across the entire study area varied drastically at the time of peak heating, from environments of passive burial by sedimentation at one end of the spectrum to zones of complex folding, pressure solution, and thrust imbrication at the other. Studies completed elsewhere show that CI values can decrease within shear zones and toward the hinges of small folds, presumably in response to increases in effective stress (Nyk, 1985; Aldahan and Morad, 1986). Similarly, Kreuzberger and Peacor (1988) demonstrated that CI can be affected by pressure solution, even under isothermal conditions. Merriman and Roberts (1985), Kemp and others (1985), and Mitra and Yonkee (1985) noted obvious connections between values of illite crystallinity and zones of weak or strong cleavage, and Kisch (1991) has compiled an extensive data set showing how CI data vary with different types of cleavage. On the other hand, Robinson and Bevins (1986) were unable to recognize a regular association of well-cleaved rocks and more advanced stages of illite crystallinity, so the link between cleavage and CI is not universal. One key appears to be the timing of peak heating with respect to the development of cleavage.

The compilation of data shown on figure 8 does not discriminate perfectly between zones with well-developed folds and slaty cleavage and zones without any penetrative structural fabrics. In general, however, there is a clear connection between higher ranks of thermal maturity and cleavage. Virtually all of the high-rank samples that we selected from the Biederman Argillite, for example, display excellent slaty cleavage and (or) pencil structure, as do most samples of the Glenn Shale from the Kandik River belt. Many of the R_m values, particularly for rocks of the Biederman Argillite, are actually higher than expected for given values of CI (that is, data points plot above the correlation curve). The intensity and geometry of cleavage appear to be fairly uniform across the Kandik River belt, although we have not attempted to document these structural fabrics in great detail. Unfortunately, for the purposes of statistical analysis, high-rank rocks (>3.0 percent R_m) are not present in the Tatonduk belt, and low-rank rocks (<2.0 percent R_m) are quite rare in the Kandik River belt. Therefore, our ability to make meaningful comparisons between cleaved and uncleaved rocks of the same starting composition, and over a consistent gradient in paleotemperature, is limited. Perhaps the best evidence to refute a universal link between cleavage,

paleotemperature, and lower CI values comes from the anomalous zone of higher thermal maturity within the Nation River Formation (just to the southeast of the Glenn Creek fault). These specimens yield elevated values of vitrinite reflectance (due to conductive heat transfer across the thrust), but there is no demonstrable change in CI relative to the formational average, and no cleavage. We believe that additional studies must be completed at a variety of scales before the effects of deformation fabrics on both CI and R_m can be assessed properly, but this variable undoubtedly contributed to the inconsistent results displayed in figure 8.

CONCLUSIONS

Values of CI and R_m collectively show that the Tatonduk belt of east-central Alaska has been exposed to significantly lower levels of thermal maturity than its neighbor, the Kandik River belt. A best-fit statistical correlation between all available pairs of R_m and CI values is consistent with limits established elsewhere for the anchizone. The equation to this curve is: $R_m = 0.31 - 6.79[\log(CI)]$. However, the amount of scatter of individual data points is unusually large, as shown by the value of the correlation coefficient ($r = 0.60$). The relatively poor match between these popular indicators of thermal maturity probably was influenced by several factors: (1) widespread "contamination" of the illite signature due to mixing among detrital populations, authigenic illite, and illite-smectite mixed-layer phases; (2) changes in both the precursor clay-mineral assemblages and the bulk geochemistry of the host rocks; (3) pronounced fluctuations in both the chemical composition of pore fluids and the rates of fluid flow during peak heating events; (4) variations in both the rates and the physical causes of peak heating; and (5) differences in both the timing and the degree of structural disruption with respect to peak heating, particularly the presence or absence of cogenetic slaty cleavage and pencil structure. The technique of illite crystallinity works best where variations in geologic and geochemical parameters can be reduced to a minimum, and this ideal situation did not develop during the tectono-thermal evolution of east-central Alaska.

Acknowledgments.—Mark Johnsson and Lu Haufu assisted in the field. Eric Hathon provided guidance during the XRD analyses. Superintendent Don Chase granted permission to sample in the Yukon-Charley Rivers National Preserve. Financial support to the University of Missouri was generously supplied by ARCO Alaska, Inc. We thank Gerry Van Kooten and his ARCO colleagues for their scientific cooperation and logistical aid. Acknowledgment is also made to the Donors of the Petroleum Research Fund, administered by

the American Chemical Society, for partial support of this research (Grant #22773-AC2 to Underwood). Dwight Bradley and Cynthia Dusel-Bacon provided many helpful editorial suggestions.

REFERENCES CITED

- Aldahan, A.A., and Morad, S., 1986, Mineralogy and chemistry of diagenetic clay minerals in Proterozoic sandstones from Sweden: *American Journal of Science*, v. 286, p. 29-80.
- Allison, C.W., 1988, Paleontology of Late Proterozoic and Early Cambrian rocks of east-central Alaska: U.S. Geological Survey Professional Paper 1449, 50 p., 18 plates.
- Antia, D.D.J., 1986, Kinetic method for modeling vitrinite reflectance: *Geology*, v. 14, p. 606-608.
- Awan, M.A., and Woodcock, N.H., 1991, A white mica crystallinity study of the Berwyn Hills, North Wales: *Journal of Metamorphic Geology*, v. 9, p. 765-773.
- Barker, C.E., 1983, The influence of time on metamorphism of sedimentary organic matter in selected geothermal systems, western North America: *Geology*, v. 11, p. 384-388.
- 1988, Geothermics of petroleum systems: Implications of the stabilization of kerogen thermal maturation after a geologically brief heating duration at peak temperature, in Magoon, L.B., ed., *Petroleum systems of the United States*: U.S. Geological Survey Bulletin 1870, p. 26-29.
- 1989, Temperature and time in the thermal maturation of sedimentary organic matter, in Naeser, N.D., and McCulloh, T.H., eds., *Thermal history of sedimentary basins, methods and case histories*: New York, Springer-Verlag, p. 73-98.
- 1991, Implications for organic maturation studies of evidence for a geologically rapid increase and stabilization of vitrinite reflectance at peak temperature: Cerro Prieto geothermal system, Mexico: *American Association of Petroleum Geologists Bulletin*, v. 75, p. 1852-1863.
- Barker, C.E., Crysedale, B.L., and Pawlewicz, M.J., 1986, The relationship between vitrinite reflectance, metamorphic grade, and temperature in the Cerro Prieto, Salton Sea, and East Mesa geothermal systems, Salton Trough, United States and Mexico, in Mumpton, F.A., ed., *Studies in diagenesis*: U.S. Geological Survey Bulletin 1578, p. 83-95.
- Barker, C.E., and Goldstein, R.H., 1990, Fluid-inclusion technique for determining maximum temperature in calcite and its comparison to the vitrinite reflectance geothermometer: *Geology*, v. 18, p. 1003-1006.
- Barker, C.E., and Pawlewicz, M.J., 1986, The correlation of vitrinite reflectance with maximum temperature in humic organic matter, in Buntebarth, G., and Stegena, L., eds., *Paleogeothermics*: New York, Springer-Verlag, p. 79-93.
- Blenkinsop, T.G., 1988, Definition of low-grade metamorphic zones using illite crystallinity: *Journal of Metamorphic Geology*, v. 6, p. 623-636.
- Bostick, N.H., 1979, Microscopic measurement of the level of catagenesis of solid organic matter in sedimentary rocks to aid exploration for petroleum and to determine former burial temperatures—A review, in Scholle, P.A., and Schluger, P.R., eds., *Aspects of diagenesis: Society of Economic Paleontologists and Mineralogists Special Publication 26*, p. 17-43.
- Bostick, N.H., Cashman, S., McCulloh, T.H., and Wadell, C.T., 1978, Gradients of vitrinite reflectance and present temperature in the Los Angeles and Ventura basins, California, in Oltz, D., ed., *Symposium in geochemistry: Low temperature metamorphism of kerogen and clay minerals: Society of Economic Paleontologists and Mineralogists, Pacific Section, Special Publication*, p. 65-96.
- Brabb, E.E., 1969, Six new Paleozoic and Mesozoic formations in east-central Alaska: U.S. Geological Survey Bulletin 1274-I, p. 1-26.
- Brabb, E.E., and Churkin, M., Jr., 1967, Stratigraphic evidence for the Late Devonian age of the Nation River Formation, east-central Alaska: U.S. Geological Survey Professional Paper 575-D, p. D4-D15.
- 1969, Geologic map of the Charlie River Quadrangle, east-central Alaska: U.S. Geological Survey Miscellaneous Geological Investigations Map I-973, scale 1:250,000.
- Burnham, A.K., and Sweeney, J.J., 1989, A chemical kinetic model of vitrinite maturation and reflectance: *Geochimica et Cosmochimica Acta*, v. 53, p. 2649-2657.
- Churkin, M., Jr., Foster, H.L., Chapman, R.H., and Weber, F.R., 1982, Terranes and suture zones in east-central Alaska: *Journal of Geophysical Research*, v. 87, p. 3718-3730.
- Coney, P.J., and Jones, D.L., 1985, Accretion tectonics and crustal structure in Alaska: *Tectonophysics*, v. 119, p. 265-283.
- Dembicki, H., Jr., 1984, An interlaboratory comparison of source rock data: *Geochimica et Cosmochimica Acta*, v. 48, p. 2641-2649.
- Dover, J.H., 1990, Geology of east central Alaska: U.S. Geological Survey Open-File Report 90-289, 66 p.
- Dover, J.H., and Miyaoka, R.T., 1988, Reinterpreted geologic map and fossil data, Charley River Quadrangle, east-central Alaska: U.S. Geological Survey Miscellaneous Field Studies Map MF-2004, 2 sheets, scale 1:250,000.
- Dow, W.G., 1977, Kerogen studies and geological interpretations: *Journal of Geochemical Exploration*, v. 7, p. 79-87.
- Duba, D., and Williams-Jones, A.E., 1983, The application of illite crystallinity, organic matter reflectance, and isotopic techniques to mineral exploration: A case study in southwestern Gaspe, Quebec: *Economic Geology*, v. 78, p. 1350-1363.
- Dunoyer de Segonzac, G., 1970, The transformation of clay minerals during diagenesis and low-grade metamorphism: A review: *Sedimentology*, v. 15, p. 281-346.
- Ernst, W.G., 1974, Metamorphism and ancient continental margins, in Burk, C.A., and Drake, C.L., eds., *The geology of continental margins*: New York, Springer-Verlag, p. 907-919.
- Foster, H.L., 1976, Geologic map of the Eagle Quadrangle, Alaska: U.S. Geological Survey Miscellaneous Geological Investigations Map I-922, 1:250,000, 1 sheet.
- Freed, R.L., and Peacor, D.R., 1989, Geopressed shale and sealing effect of smectite to illite transition: *American Association of Petroleum Geologists Bulletin*, v. 73, p.

- Frey, M., 1970, The step from diagenesis to metamorphism in pelitic rocks during Alpine orogenesis: *Sedimentology*, v. 15, p. 261-279.
- 1987, Very low-grade metamorphism of clastic sedimentary rocks, in Frey, M., ed., *Low-temperature metamorphism*, New York, Chapman and Hall, p. 9-58.
- Frey, M., Teichmüller, M., Teichmüller, R., Mullis, J., Kunzi, B., Breitschmid, A., Gruner, U., and Schwizer, B., 1980, Very low-grade metamorphism in external parts of the Central Alps: Illite crystallinity, coal rank and fluid inclusion data: *Eclogae Geologicae Helveticae*, v. 73, p. 173-203.
- Gretener, P.E., and Curtis, C.D., 1982, Role of temperature and time on organic metamorphism: *American Association of Petroleum Geologists Bulletin*, v. 66, p. 1124-1129.
- Guthrie, J.M., Houseknecht, D.W., and Johns, W.D., 1986, Relationships among vitrinite reflectance, illite crystallinity, and organic geochemistry in Carboniferous strata, Ouachita Mountains, Oklahoma and Arkansas: *American Association of Petroleum Geologists Bulletin*, v. 70, p. 26-33.
- Hesse, R., and Dalton, E., 1991, Diagenetic and low-grade metamorphic terranes of Gaspé Peninsula related to the geologic structure of the Taconian and Acadian orogenic belts, Quebec Appalachians: *Journal of Metamorphic Geology*, v. 9, p. 775-790.
- Hood, A., Gutjahr, C.C.C., and Heacock, R.L., 1975, Organic metamorphism and the generation of petroleum: *American Association of Petroleum Geologists Bulletin*, v. 59, p. 986-996.
- Houseknecht, D.W., Johns, W.D., and Guthrie, J.M., 1987, Relationships among vitrinite reflectance, illite crystallinity, and organic geochemistry in Carboniferous strata, Ouachita Mountains, Oklahoma and Arkansas: Reply: *American Association of Petroleum Geologists Bulletin*, v. 71, p. 347.
- Howell, D.G., Johnsson, M.J., Underwood, M.B., Lu Haufu, and Hillhouse, J.W., 1992, Tectonic evolution of the Kandik region, east central Alaska: Preliminary interpretations, in Bradley, D.C., and Ford, A.B., eds., *Geologic studies in Alaska by the U.S. Geological Survey, 1990: U.S. Geological Survey Bulletin 1999*, p. 127-140.
- Howell, D.G., and Wiley, T.J., 1987, Crustal evolution of northern Alaska inferred from sedimentological and structural relations in the Kandik area: *Tectonics*, v. 6, p. 619-631.
- Hunt, J.M., Lewan, M.D., and Hennet, R.J.-C., 1991, Modeling oil generation with time-temperature index graphs based on the Arrhenius equation: *American Association of Petroleum Geologists Bulletin*, v. 75, p. 795-807.
- Hunziker, J.C., Frey, M., Clauer, N., Dallmeyer, R.D., Friedrichsen, H., Flehmig, W., Hochstrasser, K., Roggwiler, P., and Schwander, H., 1986, The evolution of illite to muscovite: Mineralogical and isotopic data from the Glarus Alps, Switzerland: *Contributions to Mineralogy and Petrology*, v. 92, p. 157-180.
- Issler, D.R., 1984, Calculation of organic maturation levels for offshore eastern Canada—Implications for general application of Lopatin's method: *Canadian Journal of Earth Science*, v. 21, p. 283-304.
- Kemp, A.E.S., Oliver, G.H.J., and Baldwin, J.R., 1985, Low-grade metamorphism and accretion tectonics: Southern Uplands terrane, Scotland: *Mineralogical Magazine*, v. 49, p. 335-344.
- Kisch, H.J., 1980, Illite crystallinity and coal rank associated with lowest-grade metamorphism of the Tavayanne graywacke in the Helvetic zone of the Swiss Alps: *Eclogae Geologicae Helveticae*, v. 73, p. 753-777.
- 1983, Mineralogy and petrology of burial diagenesis (burial metamorphism) and incipient metamorphism in clastic rocks, in Larsen, G., and Chilingar, G.V., eds., *Diagenesis in sediments and sedimentary rocks, part 2, Developments in sedimentology*, v. 25B: Amsterdam, Elsevier, p. 289-493.
- 1987, Correlation between indicators of very low-grade metamorphism, in Frey, M., ed., *Low-temperature metamorphism*: New York, Chapman and Hall, p. 227-300.
- 1990, Calibration of the anchizone: A critical comparison of illite 'crystallinity' scales used for definition: *Journal of Metamorphic Geology*, v. 8, p. 31-46.
- 1991, Development of slaty cleavage and degree of very-low grade metamorphism: A review: *Journal of Metamorphic Geology*, v. 9, p. 735-750.
- Kisch, H.J., and Frey, M., 1987, Appendix: Effect of sample preparation on the measured 10Å peak width of illite (illite 'crystallinity'), in Frey, M., ed., *Low temperature metamorphism*: New York, Chapman and Hall, p. 301-304.
- Kreutzberger, M.E., and Peacor, D.R., 1988, Behavior of illite and chlorite during pressure solution of shaly limestone of the Kalkberg Formation, Catskill, New York: *Journal of Structural Geology*, v. 10, p. 803-811.
- Kubler, B., 1968, Evaluation quantitative du métamorphisme par la cristallinité de l'illite: *Bulletin Centre de Recherches de Pau - SNPA*, v. 2, p. 385-397.
- Laughland, M.M., 1991, Organic metamorphism and thermal history of selected portions of the Franciscan accretionary complex of coastal California: Columbia, Mo., University of Missouri, Ph.D. dissertation, 318 pp.
- Laughland, M.M., Underwood, M.B., and Wiley, T.J., 1990, Thermal maturity, tectonostratigraphic terranes, and regional tectonic history: An example from the Kandik area, east-central Alaska, in Nuccio, V.F., and Barker, C.E., eds., *Applications of thermal maturity studies to energy exploration*: Society of Economic Paleontologists and Mineralogists, Rocky Mountain Section, Special Publication, p. 97-111.
- Liou, J.G., Maruyama, S., and Cho, M., 1987, Very low-grade metamorphism of volcanic and volcanoclastic rocks - mineral assemblages and mineral facies, in Frey, M., ed., *Low temperature metamorphism*: New York, Chapman and Hall, p. 59-113.
- Merriman, R.J., and Roberts, B., 1985, A survey of white mica crystallinity and polytypes in pelitic rocks of Snowdonia and Llyn, North Wales: *Mineralogical Magazine*, v. 49, p. 305-319.
- Middleton, M.F., 1982, Tectonic history from vitrinite reflectance: *Geophysical Journal of the Royal Astronomical Society*, v. 68, p. 121-132.
- Mitra, G., and Yonkee, W.A., 1985, Relationship of spaced

- cleavage to folds and thrusts in the Idaho-Utah-Wyoming thrust belt: *Journal of Structural Geology*, v. 7, p. 361-373.
- Miyaoka, R.T., 1990, Fossil locality map and fossil data for the southeastern Charley River quadrangle, east-central Alaska: U.S. Geological Survey Miscellaneous Field Studies Map MF-2007, 1:100,000, p. 1-46.
- Moore, D.M., and Reynolds, R.C., Jr., 1989, X-ray diffraction and the identification and analysis of clay minerals: New York, Oxford University Press, 332 pp.
- Nyk, R., 1985, Illite crystallinity in Devonian slates of the Meggen mine (Rhenish Massif): *Neues Jahrbuch für Mineralogie Monatshefte*, v. 1985, p. 268-276.
- Ogunyomi, O., Hesse, R., and Heroux, Y., 1980, Pre-orogenic and synorogenic diagenesis and anchi-metamorphism in Lower Paleozoic continental margin sequences of the northern Appalachians in and around Quebec City, Canada: *Bulletin of Canadian Petroleum Geology*, v. 28, p. 559-577.
- Payne, M.W., and Allison, C.W., 1981, Paleozoic continental-margin sedimentation in east-central Alaska: *Geology*, v. 9, p. 274-279.
- Perry, E., and Hower, J., 1970, Burial diagenesis in Gulf Coast pelitic sediments: *Clays and Clay Minerals*, v. 18, p. 165-177.
- Pevear, D.R., Williams, V.E., and Mustoe, G.E., 1980, Kaolinite, smectite, and K-rectorite in bentonites: Relation to coal rank at Tulameen, British Columbia: *Clays and Clay Minerals*, v. 28, p. 241-254.
- Price, L.C., 1983, Geologic time as a parameter in organic metamorphism and vitrinite reflectance as an absolute paleogeothermometer: *Journal of Petroleum Geology*, v. 6, p. 5-38.
- Reynolds, R.C., Jr., and Hower, J., 1970, The nature of interlayering in mixed-layer illite-montmorillonites: *Clays and Clay Minerals*, v. 18, p. 25-36.
- Ritter, U., 1984, The influence of time and temperature on vitrinite reflectance: *Organic Geochemistry*, v. 6, p. 473-480.
- Roberts, B., and Merriman, R.J., 1985, The distinction between Caledonian burial and regional metamorphism in metapelites from North Wales: An analysis of isocryst patterns: *Journal of the Geological Society of London*, v. 142, p. 615-624.
- Robinson, D., and Bevins, R.E., 1986, Incipient metamorphism in the Lower Palaeozoic marginal basin of Wales: *Journal of Metamorphic Geology*, v. 4, p. 101-113.
- Robinson, D., Warr, L.N., and Bevins, R.E., 1990, The illite 'crystallinity' technique: A critical appraisal of its precision: *Journal of Metamorphic Geology*, v. 8, p. 333-344.
- Smart, G., and Clayton, T., 1985, The progressive illitization of interstratified illite-smectite from Carboniferous sediments of northern England and its relationship to organic maturity indicators: *Clay Minerals*, v. 20, p. 455-466.
- Suggate, R.P., 1982, Low-rank sequences and scales of organic metamorphism: *Journal of Petroleum Geology*, v. 4, p. 377-392.
- Sweeney, J.J., and Burnham, A.K., 1990, Evaluation of a simple model of vitrinite reflectance based on chemical kinetics: *American Association of Petroleum Geologists Bulletin*, v. 74, p. 1559-1570.
- Underwood, M.B., Laughland, M.M., and Kang, S.M., 1993, A comparison between organic and inorganic indicators of diagenesis and metamorphism, Upper Shimanto Group, Muroto Peninsula, Shikoku, Japan, in Underwood, M.B., ed., *Thermal evolution of the Tertiary Shimanto Belt, southwest Japan: An example of ridge-trench interaction*: Geological Society of America Special Paper 273 [in press].
- Underwood, M.B., Laughland, M., Shelton, K., Solomon, R., Kang, S.M., Orr, R., Brocculeri, T., Bergfeld, D., and Pawlewicz, M., 1991, Correlations among paleotemperature indicators within orogenic belts: Examples from pelitic rocks of the Franciscan Complex (California), the Shimanto Belt (Japan), and the Kandik Basin (Alaska) [abs.]: *Eos (American Geophysical Union, Transactions)*, v. 72, p. 549.
- Underwood, M.B., Laughland, M.M., Wiley, T.J., and Howell, D.G., 1989, Thermal maturity and organic geochemistry of the Kandik Basin region, east-central Alaska: U.S. Geological Survey Open-File Report 89-353, 41 p.
- Waples, D.W., 1980, Time and temperature in petroleum exploration: Application of Lopatin's method to petroleum exploration: *American Association of Petroleum Geologists Bulletin*, v. 64, p. 916-926.
- Weaver, C.E., 1960, Possible uses of clay minerals in search for oil: *American Association of Petroleum Geologists Bulletin*, v. 44, p. 1505-1518.
- Wood, D.A., 1988, Relationships between thermal maturity indices calculated using Arrhenius equation and Lopatin method; Implication for petroleum exploration: *American Association of Petroleum Geologists Bulletin*, v. 72, p. 115-135.
- Wright, N.J.R., 1980, Time, temperature, and organic maturation: The evolution of rank within a sedimentary pile: *Journal of Petroleum Geology*, v. 2, p. 411-425.
- Yang, C., and Hesse, R., 1991, Clay minerals as indicators of diagenetic and anchimetamorphic grade in an overthrust belt, External Domain of southern Canadian Appalachians: *Clay Minerals*, v. 26, p. 211-231.
- Young, G.M., 1982, The late Proterozoic Tindir Group, east-central Alaska: Evolution of a continental margin: *Geological Society of America Bulletin*, v. 93, p. 759-783.

Reviewers: Mark Johnsson and Zenon Valin

The Arctic Alaska Superterrane

By Thomas E. Moore

INTRODUCTION

A recent major synthesis by Moore and others (1992, in press) on the geology of northern Alaska utilizes the tectonostratigraphic terrane classification of Jones and others (1987). Moore and others (1992, in press) extensively revised the terrane boundaries and stratigraphic definitions for northern Alaska shown by Jones and others (1987) in order to incorporate recent geologic mapping and observations. However, a debate occurred among the coauthors of Moore and others (1992, in press) concerning the use of the subterrane nomenclature used by Jones and others (1987). Some authors (and reviewers) expressed the view that subdivision of the Arctic Alaska terrane into subterrane emphasized the differences between tectonic units and downplayed evidence that the various parts of the Arctic Alaska terrane originated as a single paleogeographically connected body. Other authors argued that the terrane and subterrane units mapped by Jones and others coincide with independently mapped tectonic units of northern Alaska and hence represent a useful classification of constituent lithotectonic units. In the first view, the division of the Arctic Alaska terrane into subterrane is regarded as spurious and even misleading to an understanding of the largely known geologic history of the region. In the second view, the subterrane units provide a nomenclature that facilitates discussion and understanding of mappable bodies of rocks with distinctive stratigraphic aspects that have demonstrably undergone significant displacement relative to neighboring units, without prejudicing the discussion by using a genetic classification.

In this article I comment on some problems of the subterrane nomenclature as applied in northern Alaska and compare current usage there with the nomenclature developed for other situations in the northern Cordillera. I conclude that (1) tectonostratigraphic subdivisions of the Arctic Alaska terrane are a useful tool for tectonic investigations in northern Alaska; (2) the subdivisions of the Arctic Alaska terrane should be designated as terranes rather than subterrane, and (3) the entire entity, which has been displaced relative to North America, should be designated the Arctic Alaska superterrane.

TERRANE TERMINOLOGY USED IN THIS PAPER

The definition of terranes as "fault-bounded geologic packages of regional extent characterized by a geologic history which differs from that of neighboring terranes" of Howell and others (1985) is used in this article. The definition of Howell and others (1985) is preferred to the earlier one of Coney and others (1980), which has been construed by some to mean that tectonostratigraphic units are not terranes if they may be explained or interpreted as facies equivalents of one another or of cratonal North America. Howell and others (1985) also defined a composite terrane as consisting of "two or more distinct parts that became amalgamated and subsequently shared a common geologic history prior to their accretion." The terms "subterrane" and "superterrane," although in widespread use (for example, Jones and others, 1987; Csejtey and others, 1982), were not discussed in print until Coney (1989) wrote that "composite terranes***sometimes have been referred to as superterrane[s], which [are] made up of two or more 'subterrane[s]'. I utilize herein Coney's interpretation of a superterrane as an aggregate of subordinate terranes but regard a superterrane as a designation for combinations of terranes grouped on the basis of interpretation of similar kindred or affinity as well as those that share the same geologic history after an amalgamation event.

LITHOTECTONIC UNITS (TERRANES) OF NORTHERN ALASKA

The Arctic Alaska terrane (Jones and others, 1987) is one of the largest lithotectonic units in Alaska. It underlies about 20 percent of the state and consists of Proterozoic to Cretaceous rocks of continental affinity (Jones and others, 1986, 1987; Plafker, 1990). The southern part of the Arctic Alaska terrane is exposed in the Brooks Range, a Mesozoic fold-thrust belt, whereas its northern part occurs under the North Slope and Beaufort Sea continental shelf, which are the foreland for the orogen. The Arctic Alaska terrane is flanked to the north by Cretaceous oceanic crust of the Canada basin and terminates to the east at high angle against cratonic

North America under Cenozoic sedimentary rocks of the MacKenzie delta. To the south, it is structurally overlain by oceanic rocks of the Angayucham terrane. Grantz and others (1991) estimated from potential field data a thickness of 30 to 45 km for the terrane under the North Slope and Brooks Range, respectively. These estimated thicknesses have recently been confirmed by seismic-refraction studies of the Trans-Alaska Crustal Transect (TACT) program of the U.S. Geological Survey (Levander and others, 1991).

The stratigraphy of the Arctic Alaska terrane under the North Slope consists of three major rock sequences: structurally and stratigraphically complex pre-Mississippian rocks (the Franklinian sequence of Lerand, 1973), the Mississippian to Lower Cretaceous Ellesmerian sequence, and the Lower Cretaceous and younger Brookian sequence. The Ellesmerian sequence consists of northerly derived quartzose clastic and carbonate sedimentary rocks, whereas the Brookian sequence consists of lithic clastic material shed northward from the Brookian orogen (Lerand, 1973). Because the Arctic Alaska terrane is bordered to the north by the oceanic Canada basin of Cretaceous age, the northern quartz-rich source region for Paleozoic and lower Mesozoic rocks demonstrates that the Arctic Alaska terrane has been displaced relative to a once-contiguous continental area that lay to the north (present coordinates).

Stratigraphic studies of the upper Paleozoic and lower Mesozoic section in the Brooks Range have shown that while many of the same stratigraphic units exposed there are present under the North Slope, thrust slices in the frontal part of Brooks Range consist of coeval but contrasting facies that were juxtaposed against each other and the North Slope sequence by extensive thrust faulting in Jurassic and Cretaceous time (Tailleur and Brosgé, 1970; Martin, 1970; Mayfield and others, 1988). Estimates of shortening cannot be precisely constrained because of the reconnaissance nature of the mapping, but reconstructed facies suggest about 500 km of shortening (Oldow and others, 1987; Mayfield and others, 1988). Nonetheless, evidence of stratigraphic links between these thrust slices contrasted with the apparent absence of such links between terranes elsewhere in the Cordillera. Accordingly, Jones and others (1987) recognized five continental tectonostratigraphic units in northern Alaska which they designated as subterrane (North Slope, Endicott Mountains, De Long Mountains, Coldfoot, and Hammond) of the Arctic Alaska terrane. Most of these units in the western Brooks Range were adapted from tectonostratigraphic units defined independently by Martin (1970) and Mayfield and others (1988). In addition, Jones and others (1987) identified three other continental lithotectonic units in northern Alaska (Venetie, Sheenjek, Kagvik) as separate terranes on the basis of their own work and the controversial

investigation of Churkin and others (1979). Moore and Mull (1989) and Moore and others (1992, in press) interpreted these terranes to be the same as some of the subterrane of the Arctic Alaska terrane and defined the Slate Creek subterrane as consisting of the Venetie and southern part of the Coldfoot subterrane.

A terrane map for northern Alaska and a tectonostratigraphic correlation diagram are shown in figures 1 and 2. These diagrams, modified from Moore and Mull (1989) and Moore and others (1992, in press), are revised to show the subterrane of the Arctic Alaska terrane as separate terranes and the Arctic Alaska terrane as a superterrane as proposed below. In the remainder of this paper, the discussion will be according to the nomenclature shown in these figures, except where noted.

The largest terrane of the Arctic Alaska superterrane is the North Slope terrane. It consists of deformed, stratigraphically disrupted, lower Paleozoic rocks, some of which may be correlative with coeval North American rocks, and the extensive covering succession of upper Paleozoic and Mesozoic shelfal strata of the Ellesmerian sequence. This terrane is the benchmark to which all of the others of the Arctic Alaska superterrane are compared. The Endicott Mountains and De Long Mountains terranes consist of thrust slices composed of allochthonous upper Paleozoic and Mesozoic shelfal strata that are assigned to many of the same stratigraphic units as the North Slope terrane but are stratigraphically and lithologically distinct from one another and from the North Slope terrane. The Hammond and Coldfoot terranes encompass the metamorphic rocks of the southern Brooks Range and consist of lower Paleozoic rocks mostly older than those of the Endicott Mountains and De Long Mountains terranes but coeval with the older rocks of the North Slope terrane. The southernmost terrane of the Arctic Alaska terrane is the Slate Creek terrane, which is a phyllitic unit that separates the continental rocks of the Arctic Alaska superterrane from the structurally overlying oceanic rocks of the Angayucham terrane.

Of particular significance for the terrane nomenclature in northern Alaska are the stratigraphies of the Coldfoot and Hammond terranes of the southern Brooks Range. These units are metamorphosed, highly deformed, and, as far as known, consist mostly of pre-Mississippian rocks; in contrast, the North Slope, Endicott Mountains, and De Long Mountains terranes contain sedimentary upper Paleozoic and early Mesozoic successions. The Coldfoot terrane consists of penetratively deformed quartzose schist, calc-schist, metavolcanic rocks, and marble, all metamorphosed (first to blueschist and subsequently to greenschist facies) in Mesozoic time (Dusel-Bacon and others, 1989). Moore and others (1992, in press) divided the Coldfoot terrane into two regional quartz-rich schist units distin-

guished by the presence or absence of calc-schist and marble. The subjacent calc-schist unit locally yields Silurian to Devonian conodonts, but the protolith age of the noncalcareous schist unit is uncertain. The original stratigraphic relations of these units to each other are unknown, and their boundary is shown as a fault on most maps. Both units are intruded by metagranitic rocks of Proterozoic and Devonian age.

The extensive Hammond terrane consists of a variety of possibly unrelated units that includes at least two distinctive lower Paleozoic carbonate platform sequences (Dumoulin and Harris, 1987a, b), Devonian mixed clastic and carbonate units, volcanoclastic rocks of presumed Devonian age, a belt of granitic batholiths of Devonian age, amphibolite-facies lower Paleozoic metamorphic rocks, and Proterozoic metagranitic rocks. The carbonate platform sequences, juxtaposed in the Baird Mountains in the southwestern Brooks Range, overlap in age but differ in the amount of time represented; where rocks of the sequences are coeval, they display contrasting facies. Dumoulin and Harris (1987b) suggested that

one carbonate sequence is correlative with rocks of the Seward Peninsula, whereas the other sequence appears to extend eastward throughout much of the southern Brooks Range. Amphibolite and quartz-rich schists of Proterozoic protolith age have also been identified in structural highs in the Hammond terrane, and in the Schwatka Mountains, an upper Paleozoic sequence lithologically similar to the Ellesmerian sequence is present (Mull and Tailleir, 1977). All rocks of the Hammond terrane are partially to completely metamorphosed, structurally imbricated, and isoclinally folded so that original stratigraphic relationships are ambiguous. The Hammond terrane may eventually be found to comprise two or more tectonostratigraphic units that are yet to be recognized (for example, the two carbonate sequences of Dumoulin and Harris, 1987a, b).

The continental affinity of protoliths, the structural position beneath the oceanic Angayucham terrane, and the absence of included ophiolitic belts are evidence for incorporation of the Hammond and Coldfoot terranes in the Arctic Alaska superterrane. However, the correlation

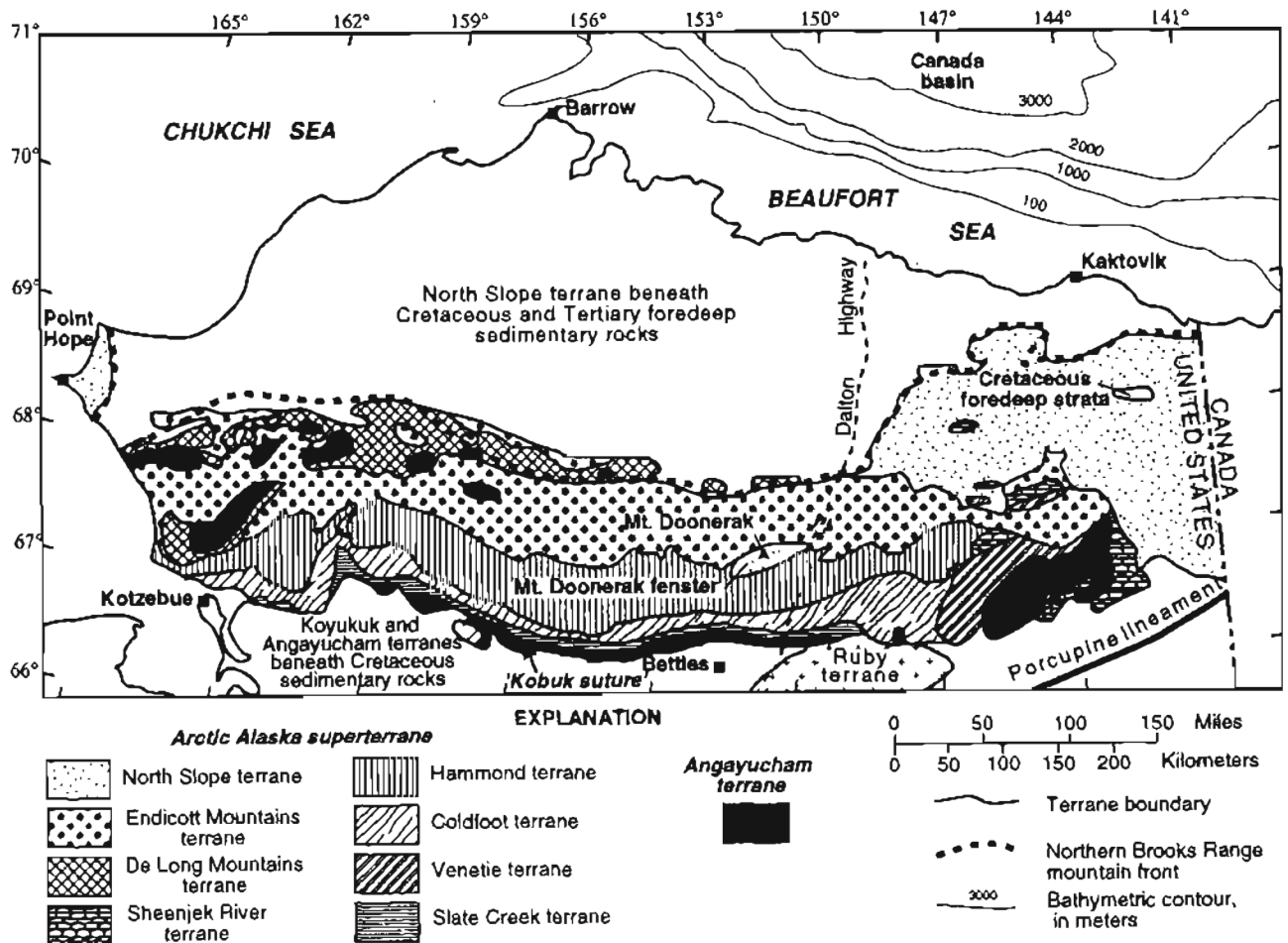


Figure 1. Distribution of constituent terranes of Arctic Alaska superterrane in northern Alaska according to terrane nomenclature proposed in this paper (terrane boundaries from Moore and others, 1992).

of the Coldfoot terrane with the North Slope terrane is tenuous, since they share no major stratigraphic units. Likewise, the Hammond terrane shares few stratigraphic units with the North Slope terrane, although correlation of the Hammond with the North Slope terrane is plausible because of the presence of Ellesmerian rocks in the Schwatka Mountains. More detailed mapping in that small area, however, could prove, in time, that those rocks occur in a fenster much like the Ellesmerian sequence at the Mt. Doonerak fenster (figure 1) and thus may not be part of the Hammond terrane. The Coldfoot, Hammond, and North Slope terranes all contain Devonian plutonic rocks that may be interpreted as a magmatic belt that links the terranes, but restoration of the terranes by undoing Mesozoic shortening would increase the distance between the plutonic belts. This consideration led Hubbard and others (1987) to conclude that two Devonian plutonic belts of different origins are present in northern Alaska. Because the Devonian and older stratigraphy for the North Slope terrane is complex and possibly partly of accretionary origin, linkages between the terranes are plausible but must be considered to be conjectural.

The designation of the Hammond and Coldfoot as subterrane of the Arctic Alaska terrane as shown by

Jones and others (1987) and Moore and others (1992, in press) clearly implies that these units have an integral stratigraphic and paleogeographic relationship to the remainder of the Arctic Alaska terrane. This implication is deceiving, however, because the stratigraphy and structure of these regions are complex and have been studied only at reconnaissance scale, and because the nature of their premetamorphic relationship has not been demonstrated. For example, the paleogeographic relationship of the contrasting carbonate platform sequences of the Hammond terrane described by Dumoulin and Harris (1987a, b) has not been investigated in detail and might indicate substantial amounts of shortening that is not explained by current stratigraphic models. Designation of both carbonate sequences as part of a single subterrane of a larger terrane implies that the observed stratigraphic differences and absence of firm tectonic correlation are a nuance of little importance to tectonic models. I suggest that the tectonic significance of these carbonate units, as well as the stratigraphic complexity and lithological diversity of the Hammond and Coldfoot terranes, are not presently understood and are a subject for careful consideration. Classification of the Hammond and Coldfoot as terranes, as I propose here, rather than as subterrane highlights rather than obscures this uncertainty.

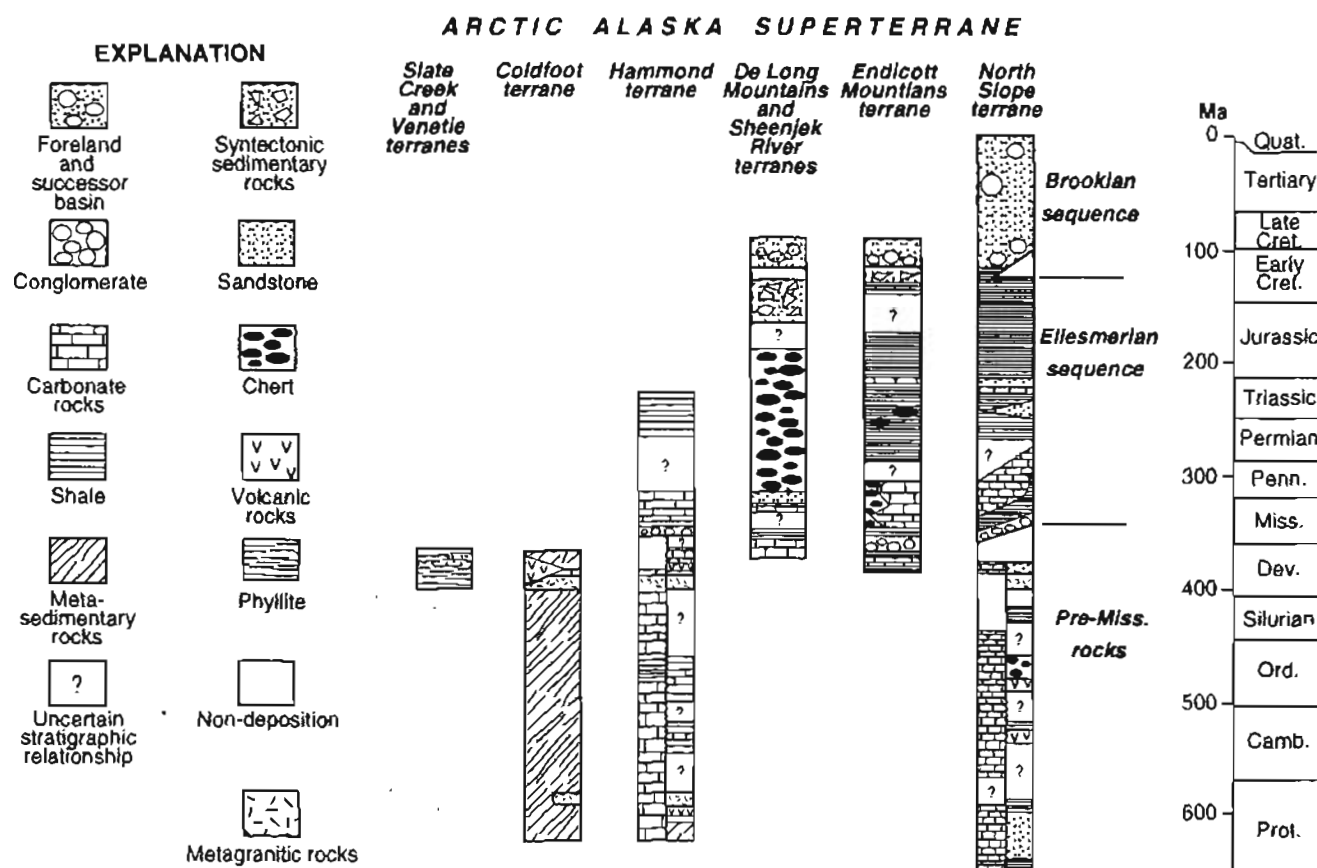


Figure 2. Terrane correlation diagram for terranes of Arctic Alaska superterrane according to terrane nomenclature proposed in this paper (modified from Moore and others, 1992). Geologic time scale used in this figure is from Palmer (1983).

Similarly, the relationship of the Slate Creek terrane, which consists of Devonian quartz-rich turbidites, phyllonite, and mélangé, to the other terranes of the Arctic Alaska superterrane is unclear. This unit has been interpreted as representing a deep-marine equivalent of part of the Endicott Mountains terrane (Murphy and Patton, 1988), but recent work suggests that it may be a tectonic unit produced by deformation associated with down-to-the-south extensional deformation in mid-Cretaceous time (Miller and Hudson, 1991; Moore and others, 1991). Patton and Box (1989) classified the Slate Creek as a thrust panel of the Angayucham terrane, whereas Moore and others (1992, in press) interpreted it as a subterrane of the Arctic Alaska terrane. Because there is uncertainty about its nature and correlation, the Slate Creek should be regarded as a separate terrane so that all models for its origin may be considered.

PROPOSED NEW TERRANE TERMINOLOGY FOR NORTHERN ALASKA

On the basis of the foregoing discussion, I conclude that the subterrane nomenclature of Jones and others (1987) as used in northern Alaska is misleading because it implies a genetic relationship between and within tectonostratigraphic units that, at least in the southern Brooks Range, cannot be firmly established on the basis of critical examination of observed field relations. The stratigraphies of the Endicott Mountains terrane, De Long Mountains terrane, and stratigraphically higher part of the North Slope terrane, in contrast, are structurally and stratigraphically less complicated and are more thoroughly investigated than the Hammond, Coldfoot, and Slate Creek terranes. Although these terranes of the northern Brooks Range display many distinctive stratigraphic and lithologic differences, they have been interpreted to be stratigraphically related and to represent different parts of an upper Paleozoic and Lower Mesozoic continental margin that was collapsed in Jurassic and Early Cretaceous time (for example, Oldow and others, 1987; Mayfield and others, 1988; Moore and Mull, 1989; Grantz and others, 1991; Moore and others, 1992, in press). This is the basis for their designation as subterranes of the Arctic Alaska terrane as shown by Jones and others (1987), Moore and Mull (1989), and Moore and others (1992, in press). However, if these allochthonous units are to be regarded as subterranes on the basis of their inferred origin, how well documented by geological data must the interpretation of their common origin be? Because the answer to this question is debatable, not easily measured by any standard, and could be revised in the light of new data, I suggest that the genesis of these units should not be considered at all for the purpose of their classification, but instead, classi-

fication should be based on map and stratigraphic data alone. This descriptive approach results in a terminology that is based on observed geologic data rather than on a specific paleogeographic model. Thus, because the tectonostratigraphic units of the northern Brooks Range have distinctive stratigraphies and have been displaced a significant but undetermined distance relative to each other (for example, Martin, 1970; Mayfield and others, 1988), I suggest that they also should be regarded as separate terranes rather than subterranes.

If, for the purpose of a tectonic synthesis or other regional investigation, there is a need to discuss combinations of terranes by their inferred origin, what nomenclature should then be used? Elsewhere in the northern Cordillera, groups of terranes have been discussed as composite terranes or superterranes. For example, Jones and others (1987) divided southern Alaska south of the Denali fault into about 10 terranes. Based on geologic data, Csejtey and others (1982) argued that two of the largest terranes in this area, the Peninsular and Wrangellia terranes, were geologically connected by Middle Jurassic time, on this basis, they combined the terranes into the Talkeetna superterrane. Later work showed that the Wrangellia and Alexander terranes have been contiguous since Pennsylvanian time (Gardner and others, 1988), and most workers now regard the Peninsular, Wrangellia, and Alexander terranes as the Peninsular-Alexander-Wrangellia (PAW) superterrane (Plafker and others, 1989). This superterrane composes about 20 percent of Alaska. Similarly, Monger and Berg (1987) divided the Canadian Cordillera into 12 terranes (including the Alexander and Wrangellia terranes). Monger and others (1982) concluded on the basis of stratigraphic evidence that most of these terranes can be combined into two composite terranes, which they designated composite terrane I and composite terrane II (the Peninsular-Alexander-Wrangellia superterrane). Recently, Plafker (1990) has grouped the terranes of the northern Cordillera into eight composite terranes in order to discuss his tectonic model for the development of the region.

These cases show that recent classifications have retained previously defined terranes as building blocks that can be combined in various ways as the genetic relations between terranes are reinterpreted or as new data are reported. This nomenclatural system retains mapped terranes as separate entities and presents hypotheses of their inferred paleogeographic origin as combinations of terranes by designating them as composite terranes or superterranes. This nomenclature has been utilized by a number of workers (for example, Oldow and others, 1989; Nokleberg and others, 1992) for the purpose of grouping terranes for regional analysis where simplifying assumptions are useful for discussions of the larger tectonic features. It is also consistent with Coney's (1989) view that subterranes are terranes that compose composite terranes

and superterrane. Thus, for purposes of consistency and comparability with terminology in use elsewhere in the northern Cordillera, I propose that the subterrane of the Arctic Alaska terrane of Jones and others (1987) should be regarded as independent terranes and that their Arctic Alaska terrane should be regarded as a superterrane or composite terrane.

CONCLUSION

The nomenclature of natural systems should not presuppose a particular genetic model, regardless of the degree of acceptance of the model by knowledgeable scientists, because it discourages formulation of alternative hypotheses. In the case of the terrane nomenclature of northern Alaska, the classification of its mapped constituent tectonostratigraphic units as subterrane on the basis of the prevailing interpretation of their common origin constitutes such a presupposition. Despite the conclusion of many workers, including myself, that at least some of the tectonostratigraphic units of northern Alaska originated as part of the same continental margin, the present structural position is that of displaced and fault-bounded stratigraphically distinct bodies of rock. Thus, they should be classified as independent terranes whose interrelationships in the future can be reevaluated free of the specific model implied by the nomenclature established by Jones and others (1987). For consideration as a single entity the combination of terranes in northern Alaska that are interpreted as fragments of a continental margin and for the purpose of comparison of this entity with groups of terranes of common origin established elsewhere in the northern Cordillera, I propose that the combined terranes be designated the Arctic Alaska superterrane.

REFERENCES CITED

- Churkin, M., Jr., Nokleberg, W.J., and Huie, C., 1979, Collision-deformed Paleozoic continental margin, western Brooks Range, Alaska: *Geology*, v. 7, no. 8, p. 379-383.
- Coney, P.J., 1989, Structural aspects of suspect terranes and accretionary tectonics in western North America: *Journal of Structural Geology*, v. 11, p. 107-125.
- Coney, P.J., Jones, D.L., and Monger, J.W.H., 1980, Cordilleran suspect terranes: *Nature*, v. 288, p. 329-333.
- Csejtey, Béla, Jr., Cox, D.P., and Evarts, R.C., 1982, The Cenozoic Denali fault system and the Cretaceous accretionary development of southern Alaska: *Journal of Geophysical Research*, v. 87, p. 3741-3754.
- Dumoulin, J.A., and Harris, A.G., 1987a, Lower Paleozoic carbonate rocks of the Baird Mountains quadrangle, western Brooks Range, Alaska, in Tailleux, I.L., and Weimer, Paul, eds., *Alaskan North Slope geology: Bakersfield, Calif., Pacific Section, Society of Economic Paleontologists and Mineralogists*, v. 50, p. 311-336.
- , 1987b, Cambrian through Devonian carbonate rocks of the Baird Mountains, western Brooks Range, Alaska [abs.]: *Geological Society of America Abstracts with Programs*, v. 19, no. 6, p. 373-374.
- Dusel-Bacon, Cynthia, Brosgé, W.P., Till, A.B., Doyle, E.O., Mayfield, C.F., Reiser, H.N., and Miller, T.P., 1989, Distribution, facies, ages, and proposed tectonic associations of regionally metamorphosed rocks in northern Alaska: *U.S. Geological Survey Professional Paper 1497-A*, 44 p., 2 sheets, scale 1:1,000,000.
- Gardner, M.C., Bergman, S.C., MacKevett, E.M., Jr., Plafker, George, Campbell, R.C., Cushing, G.W., Dodds, C.J., and McClelland, W.D., 1988, Middle Pennsylvanian pluton stitching of Wrangellia and the Alexander terrane, Wrangell Mountains, Alaska: *Geology*, v. 16, p. 967-971.
- Grantz, Arthur, Moore, T.E., and Roeske, Sarah, 1991, Gulf of Alaska to Arctic Ocean: Boulder, Colo., Geological Society of America, Centennial Continent/Ocean Transect #15, 72 p., scale 1:500,000, 3 sheets.
- Howell, D.G., Jones, D.L., and Schermer, E.R., 1985, Tectonostratigraphic terranes of the circum-Pacific region, in Howell, D.G., ed., *Tectonostratigraphic terranes of the circum-Pacific region: Houston, Texas, Circum-Pacific Council for Energy and Mineral Resources, Earth Science Series*, v. 1, p. 3-30.
- Hubbard, R.J., Edrich, S.P., and Rattey, R.P., 1987, Geologic evolution and hydrocarbon habitat of the Arctic Alaska microplate, in Tailleux, I.L., and Weimer, Paul, eds., *Alaskan North Slope geology: Bakersfield, Calif., Pacific Section, Society of Economic Paleontologists and Mineralogists*, v. 50, p. 797-830.
- Jones, D.L., Silberling, N.J., and Coney, P.J., 1986, Collision tectonics in the Cordillera of western North America: Examples from Alaska, in Coward, M.P., and Ries, A.C., eds., *Collision tectonics: Geological Society of London Special Publication 19*, p. 367-387.
- , 1987, Lithotectonic terrane map of Alaska (west of the 141st meridian): *U.S. Geological Survey Miscellaneous Field Studies Map MF-1874-A*, 1 sheet, scale 1:2,500,000.
- Lerand, Monti, 1973, Beaufort Sea, in McCrossan, R.G., ed., *The future petroleum provinces of Canada—Their geology and potential: Canadian Society of Petroleum Geology Memoir 1*, p. 315-386.
- Levander, A.R., Wissinger, E.S., Fuis, G.S., and Lutter, W.J., 1991, The 1990 Brooks Range seismic experiment: Near vertical incidence reflection images [abs.]: *Eos (American Geophysical Union Transactions)*, v. 72, no. 44 suppl., p. 296.
- Martin, A.J., 1970, Structure and tectonic history of the western Brooks Range, De Long Mountains, and Lisburne Hills, northern Alaska: *Geological Society of America Bulletin*, v. 81, p. 3605-3622.
- Mayfield, C.F., Tailleux, I.L., and Ellersieck, Inyo, 1988, Stratigraphy, structure, and palinspastic synthesis of the western Brooks Range, northwestern Alaska, in Gryc, George, ed., *Geology and exploration of the National Petroleum Reserve in Alaska, 1974 to 1982: U.S.*

- Geological Survey Professional Paper 1399, p. 143-186.
- Miller, E.L., and Hudson, T.L., 1991, Mid-Cretaceous extensional fragmentation of a Jurassic-Early Cretaceous compressional orogen, Alaska: *Tectonics*, v. 10, p. 781-796.
- Monger, J.W.H., and Berg, H.C., 1987, Lithotectonic terrane map of western Canada and southeastern Alaska: U.S. Geological Survey Miscellaneous Field Studies Map MF-1874-B, 1 sheet, scale 1:2,500,000, 12 p.
- Monger, J.W.H., Price, R.A., and Tempelman-Kluit, D.J., 1982, Tectonic accretion and the origin of the two major metamorphic and plutonic belts in the Canadian Cordillera: *Geology*, v. 10, p. 70-75.
- Moore, T.E., and Mull, Gil, 1989, Geology of the Brooks Range and North Slope, in Schmidt, R.A.M., Nokleberg, W.J., and Page, R.A., Alaska geological and geophysical transect, Valdez to Coldfoot, Alaska: American Geophysical Union, Field Trip Guidebook T104, p. 107-131.
- Moore, T.E., Nokleberg, W.J., Jones, D.L., Till, A.B., and Wallace, W.K., 1991, Contrasting structural levels of the Brooks Range orogen along the Trans-Alaska Crustal Transect (TACT) [abs.]: *Eos (American Geophysical Union Transactions)*, v. 72, no. 44 suppl., p. 295.
- Moore, T.E., Wallace, W.K., Bird, K.J., Karl, S.M., Mull, C.G., and Dillon, J.T., 1992, Stratigraphy, structure, and geologic synthesis of northern Alaska: U.S. Geological Survey Open-File Report 92-330, 283 p., 1 pl.
- in press, Geology of northern Alaska, in Plafker, George, and Berg, H.C., eds., *The geology of Alaska: Boulder, Colo., Geological Society of America, The geology of North America*, v. G1.
- Mull, C.G., and Tailleir, I.L., 1977, Sadlerochit(?) Group in the Schwatka Mountains, south-central Brooks Range, in Blean, K.M., ed., *The United States Geological Survey in Alaska: Accomplishments during 1976: U.S. Geological Survey Circular 751-B*, p. B27-B29.
- Murphy, J.M., and Patton, W.W., Jr., 1988, Geologic setting and petrography of the phyllite and metagraywacke thrust panel, north-central Alaska, in Galloway, J.P., and Hamilton, T.D., eds., *Geologic studies in Alaska by the U.S. Geological Survey during 1987: U.S. Geological Survey Circular 1016*, p. 104-108.
- Nokleberg, W.J., and sixteen others, 1992, Circum-North Pacific tectono-stratigraphic terrane map [abs.]: Submitted to International Geologic Congress, Kyoto, Japan.
- Oldow, J.S., Bally, A.W., Avé Lallemant, H.G., and Leeman, W.P., 1989, Phanerozoic evolution of the North American Cordillera; United States and Canada, in Bally, A.W., and Palmer, A.R., eds., *The geology of North America—An overview: Boulder, Colo., Geological Society of America, Geology of North America*, v. A, p. 139-232.
- Oldow, J.S., Seidensticker, C.M., Phelps, J.C., Julian, F.E., Gottschalk, R.R., Boler, K.W., Handschy, J.W., and Avé Lallemant, H.G., 1987, Balanced cross sections through the central Brooks Range and North Slope, Arctic Alaska: American Association of Petroleum Geologists Publication, 19 p., 8 pls., scale 1:200,000.
- Palmer, A.R., 1983, The Decade of North American Geology 1983 time scale: *Geology*, v. 11, p. 503-504.
- Patton, W.W., Jr., and Box, S.E., 1989, Tectonic setting of the Yukon-Koyukuk basin and its borderlands, western Alaska: *Journal of Geophysical Research*, v. 94, no. B11, p. 15,807-15,820.
- Plafker, George, 1990, Regional geology and tectonic evolution of Alaska and adjacent parts of the northeast Pacific Ocean margin: Pacific Rim Congress 90, Proceedings: Australasian Institute of Mining and Metallurgy, Queensland, Australia, p. 841-853.
- Plafker, George, Nokleberg, W.J., and Lull, J.S., 1989, Bedrock geology and tectonic evolution of the Wrangellia, Peninsular, and Chugach terranes along the Trans-Alaska crustal transect in the Chugach Mountains and southern Copper River basin, Alaska: *Journal of Geophysical Research*, v. 94, no. B4, p. 4255-4295.
- Tailleir, I.L., and Brosgé, W.P., 1970, Tectonic history of northern Alaska, in Adkison, W.L., and Brosgé, M.M., eds., *Geological seminar on the North Slope of Alaska, Proceedings: American Association of Petroleum Geologists Pacific Section Meeting, Los Angeles, Calif.*, p. E1-E19.

Reviewers: Warren J. Nokleberg and Arthur Grantz

BIBLIOGRAPHIES

U.S. Geological Survey Reports on Alaska Released in 1991*

Compiled by Ellen R. White

[Some reports dated 1990 did not become available until 1991; they are included in this listing.]

* Also listed is the 1992 release (Bulletin 1999) because it covers research done in 1990.

ABBREVIATIONS

- B1950 Goldfarb, R.J., Nash, J.T., and Stoesser, J.W., eds., 1990, Geochemical studies in Alaska by the U.S. Geological Survey, 1989: U.S. Geological Survey Bulletin 1950, Chaps. A-F, variously paged. [Chapters are not available separately but are indexed in this bibliography.]
- B1999 Bradley, D.C., and Ford, A.B., eds., 1992, Geologic studies in Alaska by the U.S. Geological Survey, 1990: U.S. Geological Survey Bulletin 1999, 244 p.
- C1062 Good, E.E., Slack, J.F., and Kotra, R.K., 1991, USGS research on mineral resources—1991, program and abstracts: U.S. Geological Survey Circular 1062, 99 p. [Annual V.E. McKelvey Forum on Mineral and Energy Resources, 7th, Reno, Nevada, 1991.]
- C1065 Casadevall, T.J., ed., 1991, First International Symposium on Volcanic Ash and Aviation Safety, Program and Abstracts, Seattle, Washington, July 8-12, 1991: U.S. Geological Survey Circular 1065, 58 p.
- OF90-680 Jacobson, M.L., compiler, 1990, National Earthquake Hazards Reduction Program; Summaries of technical reports, v. XXXI: U.S. Geological Survey Open-File Report 90-680, 603 p.
- OF91-352 Jacobson, M.L., compiler, 1991, National Earthquake Hazards Reduction Program; Summaries of technical reports, v. XXXII: U.S. Geological Survey Open-File Report 91-352, 707 p.
- OF91-631 Carlson, P.R., ed., 1991, Sediment of Prince William Sound, beach to deep fjord floor, a year after the *EXXON Valdez* oil spill: U.S. Geological Survey Open-File Report 91-631, 101 p.

Abers, G.A., 1990, Seismic monitoring of the Shumagin seismic gap, Alaska, in OF90-680, p. 1-3.

———1991, Seismic monitoring of the Shumagin seismic gap, Alaska, in OF91-352, p. 1-4.

Abers, G.A., and Jacob, K.H., 1991, Analysis of seismic data from the Shumagin seismic gap, Alaska, in OF91-352, p. 70-73.

Allen, M.S., 1990, Gold anomalies and newly identified gold occurrences in the Lime Hills quadrangle, Alaska, and their association with the Hartman sequence plutons: B1950, Chap. F., p. F1-P16.

Arbogast, B.F., Erickson, B.M., Gray, J.E., and McNeal, J.M., 1991, Analytical results and sample locality map of moss, moss-sediment, and willow samples from the Iditarod quadrangle, Alaska: U.S. Geological Survey Open-File Report 91-380-A (paper version) 101 p., scale 1:250,000; 91-380-B (5 1/4 inch diskette version, text in ASCII file format, IBM compatible computer required, using MS DOS.)

Barker, J.C., 1991, Investigation of rare-earth and associated

elements, Zane Hills pluton, northwestern Alaska: U.S. Geological Survey Open-File Report 36-91, 39 p. including foldout maps.

Barnes, D.F., 1991, Map showing geologic interpretation of aeromagnetic data for the Chugach National Forest, Alaska: U.S. Geological Survey Miscellaneous Field Studies Map MF-1645-H, 8 p., scale 1:250,000.

Barnes, D.F., and Kelley, J.S., 1991, Applications of gravity data to studies of framework geology, evaluation of mineral deposits, and mineral prospecting in northwestern Alaska [abs.]: C1062, p. 3-4.

Beavan, John, 1990, Crustal deformation measurements in the Shumagin seismic gap, Alaska, in OF90-680, p. 176-180.

———1991, Crustal deformation measurements in the Shumagin seismic gap, Alaska, in OF91-352, p. 229-231.

Begét, J.E., Swanson, S.E., and Stone, David, 1991, Frequency and regional extent of ash eruptions from Alaskan volcanoes [abs.]: C1065, p. 13.

Bering Sea EEZ-Scan Scientific Staff, 1991, Atlas of the U.S. Exclusive Economic Zone, Bering Sea: U.S. Geological

- Survey Miscellaneous Investigations Series Map I-2053, 147 p. [10x22 inches, in color.]
- Bird, K.J., 1991, Geology, play descriptions, and petroleum resources of the Alaskan North Slope (petroleum provinces 58-60): U.S. Geological Survey Open-File Report 88-450-Y, 52 p.
- Blodgett, R.B., Clough, J.G., Harris, A.G., and Robinson, M.S., 1992, The Mount Copleston Limestone, a new Lower Devonian formation in the Shublik Mountains, northeastern Brooks Range, Alaska: B1999, p. 3-7.
- Box, S.E., and Elder, W.P., 1992, Depositional and biostratigraphic framework of the Upper Cretaceous Kuskokwim Group, southwestern Alaska: B1999, p. 8-16.
- Boyd, T.M., 1990, Analysis of the 1957 Andreanof Islands earthquake, in OF90-680, p. 54-60.
- 1991, Analysis of the 1957 Andreanof Islands earthquake, in OF91-352, p. 76-85.
- Bradley, D.C., and Ford, A.B., 1992, Introduction: B1999, p. 1-2.
- Bradley, D.C., and Kusky, T.M., 1992, Deformation history of the McHugh Complex, Seldovia quadrangle, south-central Alaska: B1999, p. 17-32.
- Brew, D.A., Drew, L.J., Schmidt, J.M., Root, D.H., and Huber, D.F., 1991, Assessment of undiscovered mineral resources, Tongass National Forest, southeastern Alaska [abs.]: C1062, p. 6.
- 1991, Undiscovered locatable mineral resources of the Tongass National Forest and adjacent lands, southeastern Alaska: U.S. Geological Survey Open-File Report 91-10, 370 p., 12 pls., scale 1:250,000.
- Brew, D.A., and Drinkwater, J.L., 1991, Tongass Timber Reform Act Wilderness areas, supplement to U.S. Geological Survey Open-File Report 91-10 (Undiscovered locatable mineral resources of the Tongass National Forest and adjacent lands, southeastern Alaska): U.S. Geological Survey Open-File Report 91-343, 35 p., foldout map.
- Bronston, M.A., 1990, A view of sea-floor mapping priorities in Alaska from the mining industry: C1052, p. 86-91.
- Cady, J.W., 1990, Aeromagnetic map of Alaska from lat 65°-68° N., long 141°-162° W.: Color-shaded relief: U.S. Geological Survey Geophysical Investigations Map GP-992, 2 sheets, scale 1:500,000.
- Carlson, P.R., 1991, Conclusions and recommendations: 1989 Prince William Sound oil spill, the following year, in OF91-631, p. 99-101.
- Carlson, P.R., Barnes, P.W., Hayden, Eran, and Carkin, B.A., 1991, Morphology of bottom sediment of Prince William Sound along the oil spill trajectory, in OF91-631, p. 1-30.
- Carter, L.D., and Hillhouse, J.W., 1992, Age of the late Cenozoic Bigbendian marine transgression of the Alaskan Arctic coastal plain: Significance for permafrost history and paleoclimate: B1999, p. 44-51.
- Cathrall, J.B., and Antweiler, J.C., 1992, Occurrence of platinum-group elements in some gold-mining districts of Alaska: B1999, p. 33-43.
- Cathrall, J.B., Carlson, R.R., Antweiler, J.C., and Mosier, B.L., 1991, Platinum group elements in native gold, alluvium concentrates, and mineralized rock concentrates from some gold mining districts of Alaska: U.S. Geological Survey Open-File Report 91-348, 36 p., 1 sheet.
- Clendenen, W.S., Sliter, W.V., and Byrne, Tim, 1992, Tectonic implications of the Albatross sedimentary sequence, Sitkinak Island, Alaska: B1999, p. 52-70.
- Coel, R.J., Crock, J.G., and Kyle, J.R., 1991, Biogeochemical studies of gold in a placer deposit, Livengood, Alaska: U.S. Geological Survey Open-File Report 91-142, 51 p.
- Combellick, R.A., and Reger, R.D., 1991, Investigation of peat stratigraphy in estuarine flats near Anchorage, Alaska, as a means of determining recurrence intervals of major earthquakes, in OF91-352, p. 162-163.
- Cooper, A.K., Marlow, M.S., Geist, E.L., and Smith, G.L., 1991, Multichannel seismic-reflection profiles collected in 1980 from the southern Bering Sea, Alaska: U.S. Geological Survey Open-File Report 91-317, 5 p.
- Cronin, T.M., Briggs, W.M., Jr., Brouwers, E.M., Whatley, R.C., Wood, Adrian, and Cotton, M.A., 1991, Modern arctic Podocypid ostracode database: U.S. Geological Survey Open-File Report 91-385, 51 p.
- Crowe, D.E., Shanks, W.C., III, and Valley, J.W., 1991, Laser-microprobe studies of sulfur isotopes in stockwork and massive sulfide ores, Rua Cove Mine, south-central Alaska [abs.]: C1062, p. 13-14.
- Csejtey, Béla, Jr., 1992, Discrepancies between geologic evidence and rotational models—Talkeetna Mountains and adjacent areas of south-central Alaska: B1999, p. 71-80.
- Curtis, S.M., Ellersieck, Inyo, Mayfield, C.F., and Tailleux, I.L., 1990, Reconnaissance geologic map of the De Long Mountains A-1 and B-1 quadrangles and part of the C-1 quadrangle, Alaska: U.S. Geological Survey Miscellaneous Investigations Series Map I-1930, 2 sheets, scale 1:63,360, color. [This map supersedes USGS Open-File Report 83-185.]
- Dean, K.G., and Whiting, Larry, 1991, Analysis of satellite images of Redoubt Volcano plumes [abs.]: C1065, p. 17.
- Detterman, R.L., 1990, Stratigraphic correlation and interpretation of exploratory wells, Alaska Peninsula: U.S. Geological Survey Open-File Report 90-279, 56 p., 2 pls. [correlation charts.]
- Dickinson, K.A., and Skipp, G.L., 1992, Clay mineral depositional facies and uranium resource potential in part of the Tertiary Kenai Group, Kenai Peninsula, Alaska: B1999, p. 81-99.
- Dusel-Bacon, Cynthia, 1991, Metamorphic history of Alaska: U.S. Geological Survey Open-File Report 91-556, 48 p., 2 sheets, scale 1:2,500,000.
- Dusel-Bacon, Cynthia, Brew, D.A., and Douglass, S.L., 1991, Metamorphic facies map of southeastern Alaska—Distribution, facies, and ages of regionally metamorphosed rocks: U.S. Geological Survey Open-File Report 91-29, 46 p., 2 sheets, scale 1:1,000,000.
- Elder, W.P., and Miller, J.W., 1991, Maps showing fossil localities and checklists of Jurassic and Cretaceous macrofauna of western Alaska: U.S. Geological Survey Open-File Report 91-629, 71 p., 7 pls., scale 1:500,000.
- Ellersieck, Inyo, Curtis, S.M., Mayfield, C.F., and Tailleux, I.L., 1990, Reconnaissance geologic map of the De Long Mountains A-2 and B-2 quadrangles and part of the C-2 quadrangle, Alaska: U.S. Geological Survey Miscellaneous Investigations Series Map I-1931, 2 sheets, scale 1:63,360, color. [This map supersedes USGS Open-File

- Report 83-184.]
- Feist, Monique, and Brouwers, Elisabeth, 1991, A new *Tolypella* from the Ocean Point dinosaur locality, North Slope, Alaska, and the Late Cretaceous to Paleocene Nitelloid charophytes: U.S. Geological Survey Bulletin 1990-F, 7 p., 1 pl.
- Ferrians, O.J., Jr., 1991, Bibliography of Quaternary geology, Copper River basin and adjacent areas, south-central Alaska: U.S. Geological Survey Open-File Report 91-107-A, 20 p. (paper version); 91-107-B (IBM PC, XT, AT, or compatible diskette version).
- Frederiksen, N.O., 1990, Pollen zonation and correlation of Maastrichtian marine beds and associated strata, Ocean Point dinosaur locality, North Slope, Alaska: U.S. Geological Survey Bulletin 1990, 31 p., 7 pls.
- Frost, G.M., and Stanley, R.G., 1991, Compiled geologic and Bouguer gravity map of the Nenana basin area, central Alaska: U.S. Geological Survey Open-File Report 91-562, 30 p., 2 pls., scale 1:250,000.
- Frost, T.P., 1990, Geology and geochemistry of mineralization in the Bethel quadrangle, southwestern Alaska: B1950, Chap. C, p. C1-C9.
- Frost, T.P., and Box, S.E., 1991, Lithologic and tectonic controls on mercury mineralization in the Bethel 1° x 3° quadrangle, southwestern Alaska [abs.]: C1062, p. 29-31.
- Gaccetta, J.D., and Church, S.E., 1989, Lead isotope data base for sulfide occurrences from Alaska, December 1989: U.S. Geological Survey Open-File Report 89-688, 60 p.
- Galloway, J.P., Huebner, Mark, Lipkin, Robert, and Dijkmans, J.W.A., 1992, Early Holocene calcretes from the subarctic active Nogahabara Sand Dune field, northern Alaska: B1999, p. 100-111.
- Gehrels, G.E., 1991, Geologic map of Long Island and southern and central Dall Island, southeastern Alaska: U.S. Geological Survey Miscellaneous Field Studies Map MF-2146, scale 1:63,360.
- Goldfarb, R.J., Bailey, E.A., Folger, P.F., and Schmidt, J.M., 1991, The use of heavy-mineral concentrate data to show geochemical favorability for zinc-lead-silver and copper-(cobalt) mineral occurrences in the Baird Mountains quadrangle, northwest Alaska: U.S. Geological Survey Miscellaneous Field Studies Map MF-2151, scale 1:250,000.
- Goldfarb, R.J., Gray, J.E., Pickthorn, W.J., Gent, C.A., and Cieutat, B.A., 1990, Stable isotope systematics of epithermal mercury-antimony mineralization, southwestern Alaska: B1950, Chap. E, p. E1-E9.
- Goldfarb, R.J., and Pickthorn, W.J., 1991, Synorogenic auriferous fluids of the Juneau gold belt, southeast Alaska—Stable-isotope evidence for a deep crustal origin [abs.]: C1962, p. 32-33.
- Gough, L.P., Severson, R.C., Harms, T.F., Papp, C.S.E., and Shacklette, H.T., 1991, Biogeochemistry of selected plant materials, Alaska: U.S. Geological Survey Open-File Report 91-292, 30 p.
- Gray, J.E., Detra, D.E., Goldfarb, R.J., and Slaughter, K.E., 1991, Geochemical exploration criteria for epithermal cinnabar and stibnite deposits, southwestern Alaska [abs.]: C1062, p. 34-35.
- Gray, J.E., Frost, T.P., Goldfarb, R.J., and Detra, D.E., 1990, Gold associated with cinnabar- and stibnite-bearing deposits and mineral occurrences in the Kuskokwim River region, southwestern Alaska: B1950, Chap. D, p. D1-D6.
- Grybeck, D.J., 1991, Tapping the potential mineral resources of Alaska, in United States Geological Survey Yearbook 1990, p. 45-47.
- Grybeck, D.J., Nokleberg, W.J., and Bundtzen, T.K., 1991, Comparative metallogeny of the Soviet Far East and Alaska [abs.]: C1062, p. 36.
- Hill, P.L., 1991, Bibliographies and location maps of publications on aeromagnetic and aeroradiometric surveys for Hawaii and Alaska: U.S. Geological Survey Open-File Report 91-370-E, 35 p. [revised 3-1-91.]
- Hobbs, P.V., Radke, L.P., and Coffman, D.J., 1991, Airborne lidar detection and in situ measurements of ash emissions from the 1990 volcanic eruptions of Mount Redoubt [abs.]: C1065, p. 24.
- Hoblitt, R.P., 1991, Lightning detection and location as a remote ash-cloud monitor at Redoubt Volcano, Alaska [abs.]: C1065, p. 24.
- Hopkins, D.M., Gray, J.E., Hageman, P.L., McDougal, C.M., and Slaughter, K.E., 1991, Gold, mercury, tellurium, and thallium data and sample locality map of stream-sediment samples from the Iditarod quadrangle, Alaska: U.S. Geological Survey Open-File Report 91-283-A, 37 p., 1 sheet, scale 1:250,000 (paper version); 91-283-B (5.25 inch, 360K diskette version).
- Hopkins, D.M., Gray, J.E., and Slaughter, K.E., 1991, Low-level gold determinations by use of flow injection analysis-atomic absorption spectrophotometry—An application to precious-metal-resource assessment in the Iditarod 1° x 3° quadrangle, southwestern Alaska [abs.]: C1062, p. 39.
- Howell, D.G., Bird, K.J., Huafo, Lu, and Johnsson, M.J., 1992, Tectonics and petroleum potential of the Brooks Range fold and thrust belt—A progress report: B1999, p. 112-126.
- Howell, D.G., Johnsson, M.J., Underwood, M.B., Huafo, Lu, and Hillhouse, J.W., 1992, Tectonic evolution of the Kandik region, east-central Alaska: Preliminary interpretations: B1999, p. 127-140.
- Karl, S.M., 1992, Arc and extensional basin geochemical and tectonic affinities for the Maiyumerak basalts in the western Brooks Range: B1999, p. 141-155.
- Karl, S.M., Goldfarb, R.J., Kelley, K.D., Sutphin, D.M., Finn, C.A., Ford, A.B., and Brew, D.A., 1991, Mineral-resource potential of the Sitka 1° x 3° quadrangle, southeastern Alaska [abs.]: C1062, p. 45-46.
- Kelley, J.S., 1990, Generalized geologic map of the Chandler Lake quadrangle, north-central Alaska: U.S. Geological Survey Miscellaneous Field Studies Map MF-2144-A, 19 p., scale 1:250,000.
- Kelley, K.D., 1990, Interpretation of geochemical data from Admiralty Island, Alaska—Evidence for volcanogenic massive sulfide mineralization: B1950, Chap. A, p. A1-A9.
- Kilburn, J.E., Box, S.E., Goldfarb, R.J., and Gray, J.E., 1992, Geochemically anomalous areas in the eastern Goodnews Bay 1° by 3° quadrangle, southwest Alaska: B1999, p. 156-162.

- Kilburn, J.E., Box, S.E., Goldfarb, R.J., Gray, J.E., and Jones, J.L., 1991, Mineral-resource assessment of the Goodnews 1° x 3° quadrangle and parts of the Hagemester Island and Nushagak Bay quadrangles, southwestern Alaska [abs.]: C1062, p. 46.
- Kisslinger, Carl, Hill, Julie, and Kindel, Bruce, 1991, Central Aleutians Islands seismic network, in OF91-352, p. 24-27.
- Kisslinger, Carl, Kubichek, Sharon, Kindel, Bruce, and Hill, Julie, 1990, Central Aleutians Islands seismic network, in OF90-680, p. 15-17.
- Kvenvolden, K.A., Rapp, J.B., and Hostettler, F.D., 1991, Tracking hydrocarbons from Prince William Sound, Alaska—About one year after the *EXXON Valdez* oil spill, in OF91-631, p. 69-98.
- Lahr, J.C., Stephens, C.D., Page, R.A., and Fogleman, K.A., 1990, Alaska seismic studies, in OF90-680, p. 18-23.
- 1991, Alaska seismic studies, in OF91-352, p. 28-34.
- Lipscomb, S.W., 1991, Streamflow and sediment transport characteristics of the lower Campbell Creek basin, Anchorage, Alaska, 1986-88: U.S. Geological Survey Water-Resources Investigations Report 91-4074, 38 p.
- Lisowski, M., Savage, J.C., Prescott, W.H., King, N.E., and Svarc, J.L., 1991, Crustal strain, in OF91-352, p. 295-304. [Has section on Alaska.]
- Lynch, J.S., 1991, Mount Redoubt: Tracing volcanic ash plumes from space [abs.]: C1065, p. 30.
- Madden, D.J., 1991, Geochemical maps showing distribution of anomalously abundant elements in stream-sediment and glacial-moraine samples from the Anchorage 1° x 3° quadrangle, southern Alaska: U.S. Geological Survey Miscellaneous Investigations Series Map I-1976, scale 1:250,000.
- 1991, Geochemical maps showing distribution of anomalously abundant elements in the nonmagnetic, heavy-mineral-concentrate fraction of stream sediment from the Anchorage 1° x 3° quadrangle, southern Alaska: U.S. Geological Survey Miscellaneous Investigations Series Map I-1977, scale 1:250,000.
- Madden-McGuire, D.J., and Winkler, G.R., 1991, Areas of mineral-resource favorability (with emphasis on gold and chromite) in the Anchorage 1° x 3° quadrangle, southern Alaska [abs.]: C1062, p. 50-51.
- Mann, D.M., and Fisher, M.A., 1991, Multichannel seismic-reflection data collected in 1980 in Norton Sound, Alaska: U.S. Geological Survey Open-File Report 91-254, 5 p., 1 pl., scale 1:250,000.
- Marincovich, Louie, Jr., and Moriya, Shigehiro, 1992, Early middle Miocene mollusks and benthic foraminifers from Kodiak Island, Alaska: B1999, p. 163-169.
- Mayfield, C.F., Curtis, S.M., Ellersieck, Inyo, and Tailleur, I.L., 1990, Reconnaissance geologic map of the De Long Mountains A-3 and B-3 quadrangles and parts of the A-4 and B-4 quadrangles, Alaska: U.S. Geological Survey Miscellaneous Investigations Series Map I-1929, 2 sheets, color, scale 1:63,360. [This map supersedes USGS Open-File Report 83-183.]
- McDanal, S.K., Arbogast, B.P., and Cathrall, J.B., 1991, Analytical results and sample locality map of stream-sediment, heavy-mineral-concentrate, pebble, and rock samples from the Craig Study Area; Craig, Dixon Entrance, Ketchikan, and Prince Rupert quadrangles, Alaska: U.S. Geological Survey Open-File Report 91-36-A, 122p., 2 sheets, scale 1:250,000 (paper copy), 91-36-B (DS/HB IBM compatible diskette version).
- McGimsey, R.G., Richter, D.H., DuBois, G.D., and Miller, T.P., 1992, A postulated new source for the White River Ash, Alaska: B1999, p. 212-218.
- McLean, Hugh, and Stanley, R.G., 1992, Reconnaissance sandstone petrology and provenance of the Cantwell Formation, central Alaska: B1999, p. 170-179.
- Miller, T.P., 1991, Redoubt Volcano, Alaska, in United States Geological Survey Yearbook Fiscal Year 1990, p. 12-15.
- Miller, T.P., and Davies, J.N., 1991, The 1989-90 eruption of Redoubt Volcano: Chronology, character and effects [abs.]: C1065, p. 33.
- Mullen, M.W., and Grantz, Arthur, 1991, Bathymetric map of southern Northwind Ridge and vicinity, Arctic Ocean: U.S. Geological Survey Open-File Report 91-136, scale 1:250,000.
- Murray, T.L., Bauer, C.I., and Paskievitch, J.F., 1991, Using a personal computer to obtain predicted plume trajectories during the 1989-1990 eruption of Redoubt Volcano, Alaska [abs.]: C1065, p. 34.
- Nelson, R.E., and Carter, L.D., 1992, Preliminary interpretation of vegetation and paleoclimate in northern Alaska during the late Pliocene Colvillian marine transgression: B1999, p. 219-222.
- Nelson, S.W., and Blome, C.D., 1991, Preliminary geochemistry of volcanic rocks from the McHugh Complex and Kachemak terrane, southern Alaska: U.S. Geological Survey Open-File Report 91-134, 14 p.
- Nokleberg, W.J., Lange, I.M., Roback, R.C., Yeend, Warren, and Silva, S.R., 1991, Map showing locations of metalliferous lode and placer mineral occurrences, mineral deposits, prospects, and mines, Mount Hayes quadrangle, eastern Alaska Range, Alaska: U.S. Geological Survey Miscellaneous Field Studies Map MF-1996-C, 42 p., scale 1:250,000.
- Nokleberg, W.J., Patton, W.W., Jr., and Hearn, P.P., 1991, The Soviet Far East and Alaska, in United States Geological Survey Yearbook 1990, p. 72-73.
- Palmer, I.F., Jr., 1990, Mapping requirements for planning the Outer Continental Shelf mining program Norton Sound, Alaska, lease sale: C1052, p. 97-105.
- Phillips, R.L., Grantz, Arthur, Mullen, M.W., and White, J.M., 1991, Preliminary lithostratigraphy of piston cores from the Beaufort Sea continental slope off northeastern Alaska: U.S. Geological Survey Open-File Report 91-34, 2 sheets.
- Quintero, P.J., 1991, Benthic foraminifera from Prince William Sound, Alaska—About one year after the *EXXON Valdez* oil spill, in OF91-631, p. 31-68.
- Riehle, J.R., Church, S.E., and Magoon, L.B., 1991, Resource assessment of the Mount Katmai 1° x 3° quadrangle and adjacent parts of the Naknek and Afognak quadrangles, Alaska Peninsula [abs.]: C1062, p. 65-66.
- Roberts, S.B., 1991, Subsurface cross section showing coal beds in the Sagavanirktok Formation, vicinity of Prudhoe Bay, east-central North Slope, Alaska: U.S. Geological

- Survey Coal Investigations Map C-139-A.
- Roberts, S.B., Stricker, G.D., and Affolter, R.H., 1991, Stratigraphy and chemical analysis of coal beds in the Upper Cretaceous and Tertiary Sagavanirktok Formation, east-central North Slope, Alaska: U.S. Geological Survey Coal Investigations Map C-139-B.
- 1992, Reevaluation of coal resources in the Late Cretaceous-Tertiary Sagavanirktok Formation, North Slope, Alaska: B1999, p. 196-203.
- Roeske, S.M., Pavlis, T.L., Snee, L.W., and Sisson, V.B., 1992, $^{40}\text{Ar}/^{39}\text{Ar}$ isotopic ages from the combined Wrangellia-Alexander terrane along the Border Ranges fault system in the eastern Chugach Mountains and Glacier Bay, Alaska: B1999, p. 180-195.
- Rowan, E.L., Bailey, E.A., and Goldfarb, R.J., 1990, Geochemical orientation study for identification of metallic mineral resources in the Sitka quadrangle, southeastern Alaska: B1950, Chap. B, p. B1-B12.
- Sampson, J.A., Labson, V.F., and Long, C.L., 1992, Electrical resistivity cross sections in east-central Alaska: B1999, p. 223-227.
- Sass, J.H., Lachenbruch, A.H., and Williams, C.F., 1991, Heat flow and tectonic studies, in OF91-352, p. 494-498. [Section on North Slope and on Colville Basin, Alaska.]
- Schlatter, T.W., and Benjamin, S.G., 1991, A mesoscale data assimilation system adapted for trajectory calculations over Alaska [abs.]: C1065, p. 38-39.
- Schneider, D.J., and Rose, W.I., 1991, Utility of AVHRR sensor for remote sensing of Alaskan eruption clouds [abs.]: C1065, p. 38.
- Schneider, J.L., 1990, 1990 annual report on Alaska's mineral resources: U.S. Geological Survey Circular 1056, 67 p.
- 1991, 1991 Annual report on Alaska's mineral resources: U.S. Geological Survey Circular 1072, 69 p.
- Scott, W.E., and McGimsey, R.G., 1991, Mass, distribution, grain size, and origin of 1989-1990 tephra-fall deposits of Redoubt Volcano, Alaska [abs.]: C1065, p. 39.
- Seitz, H.R., 1991, Hydrologic conditions at Anaktuvuk Pass, Alaska, 1989: U.S. Geological Survey Open-File Report 90-591, 17 p.
- Severson, R.C., and Gough, L.P., 1990, Geochemical studies of plants and soils in the Beluga coal field, Alaska: U.S. Geological Survey Circular 1033, p. 159-160.
- Shasby, M.B., 1991, Alaska disaster—Natural and manmade, in United States Geological Survey Yearbook 1990, p. 18.
- Snyder, E.R., 1990, Activities of the Alaska district, Water Resources Division, U.S. Geological Survey, 1990: U.S. Geological Survey Open-File Report 90-157, 21 p.
- 1991, Location maps and list of U.S. Geological Survey reports on water resources in Alaska, 1950 to 1990: U.S. Geological Survey Open-File Report 91-60, 44 p.
- Stanley, R.G., Flores, R.M., and Wiley, T.J., 1992, Fluvial facies architecture in the Tertiary Usibelli Group of Suntrana, central Alaska: B1999, p. 204-211.
- Stover, C.W., and Brewer, L.R., 1991, Earthquake descriptions: Alaska, in Stover, C.W., and Brewer, L.R., United States earthquakes, 1985: U.S. Geological Survey Bulletin 1954, p. 9-19. [See also: Summary of United States earthquakes: Alaska, p. 76-99.]
- Tanaka, H.L., 1991, Development of a prediction scheme for the volcanic ash fall from Redoubt Volcano [abs.]: C1065, p. 44-45.
- Theis, C.V., 1991, Short papers on water supplies and engineering geology, Alaska Highway, 1943-1944: U.S. Geological Survey Open-File Report 91-80, 61 p.
- Trabant, D.C., Krimmel, R.M., and Post, Austin, 1991, A preliminary forecast of the advance of Hubbard Glacier and its influence on Russell Fiord, Alaska: U.S. Geological Survey Water-Resources Investigations Report 90-4172, 34 p.
- Tripp, R.B., and Madden, D.J., 1991, Mineralogical maps showing distribution of ore-related minerals in the non-magnetic, heavy-mineral-concentrate fraction of stream sediment from the Anchorage 1° x 3° quadrangle, southern Alaska: U.S. Geological Survey Miscellaneous Investigations Series Map I-1975, 1 sheet, scale 1:250,000.
- Valin, Z.C., Bader, J.W., Barnes, D.F., Fisher, M.A., and Stanley, R.G., 1991, Simple Bouguer gravity anomaly maps of the Nenana basin area, Alaska: U.S. Geological Survey Open-File Report 91-33, 5 sheets. [Quads. included: Tanana, Kantishna River, Mt. McKinley, Livengood, Fairbanks, and Healy.]
- White, E.R., 1992, Reports about Alaska in non-USGS publications released in 1990 that include USGS authors: B1999, p. 236-242.
- 1992, U.S. Geological Survey reports on Alaska released in 1990: B1999, p. 231-235.
- Wilson, F.H., Detterman, R.L., and Harris, E.E., 1991, Generalized geologic map of the Port Moller, Stepovak Bay, and Simeonof Island quadrangles, Alaska Peninsula, Alaska: U.S. Geological Survey Miscellaneous Field Studies Map MF-2155-A, scale 1:250,000.
- Yeend, Warren, 1991, Gold placers of the Circle district, Alaska—Past, present, and future: U.S. Geological Survey Bulletin 1943, 42 p., 1 pl., scale 1:63,360.
- 1992, Gold placers, gold source, and high terrace gravels in the Fortymile River area, Alaska: B1999, p. 228-230.
- Yehle, L.A., Schmoll, H.R., and Dobrovolsky, Ernest, 1991, Geologic map of the Anchorage B-8 SW quadrangle, Alaska: U.S. Geological Survey Open-File Report 91-143, 30 p., 2 sheets, scale 1:25,000.

Reports About Alaska in Non-USGS Publications Released in 1991 That Include USGS Authors

Compiled by Ellen R. White

[Some reports dated 1989 and 1990 did not become available until 1991; they are included in this listing. USGS authors are marked with asterisks (*)]

ABBREVIATIONS

- Eos Eos (American Geophysical Union, Transactions), v. 72, no. 44, suppl.
GSA2 Geological Society of America Abstracts with Programs, v. 23, no. 2.
GSA5 Geological Society of America Abstracts with Programs, v. 23, no. 5.
Wood Wood, C.A., and Kienle, Jürgen, eds., 1990, *Volcanoes of North America*: New York, Cambridge University Press, 354 p.
Workshop Mesoscale Modeling, Circumpolar Climate Change, Arctic Science Conference, 42nd, Arctic Workshop, 21st, University of Alaska, Fairbanks, Alaska, 1991, Abstracts: University of Alaska Museum, Alaska Quaternary Center Occasional Paper 4, 97p.

- *Aleinikoff, J.N., *Moore, T.E., *Karl, S.M., and Dillon, J.T., 1991, Pb isotopic ratios in Late Proterozoic and Devonian granitic rocks of the Brooks Range, Alaska [abs.]: Eos, p. 299-300.
- *Barnes, D.F., 1991, Small or undetectable [undetectable] gravity changes accompany vertical crustal movements in northern southeast Alaska and adjacent Canada [abs.]: Eos, p. 111.
- *Barnes, D.F., *Nokleberg, W.J., and *Brocher, T.M., 1991, Gravitational and seismic evidence for Tertiary structural basins in the Alaska Range and Tanana lowland [abs.]: GSA2, p. 5.
- Beaudoin, B.C., *Fuis, G.S., *Mooney, W.D., *Nokleberg, W.J., *Lutter, W.J., and Christensen, N.I., 1991, Thin, low-velocity crust beneath the Yukon-Tanana terrane, east-central Alaska [abs.]: GSA2, p. 5.
- *Bird, K.J., 1991, North Slope of Alaska, in Gluskoter, H.J., Rice, D.D., and Taylor, R.B., eds., *Economic geology, U.S.: Boulder, Colo., Geological Society of America, Geology of North America*, v. P-2, Chap. 28, p. 447-462, pl. 6A.
- Boyd, T.M., *Engdahl, E.R., and *Spence, W., 1991, Aleutian earthquake catalog: 1957 through 1989 [abs.]: Eos, p. 348.
- *Brew, D.A., 1990, Behm Canal and Rudyerd Bay, southeastern Alaska, in Wood, p. 95-96.
- 1990, Duncan Canal, southeastern Alaska, in Wood, p. 94-95.
- 1990, Origin and distribution of granitic rocks in the Coast plutonic-metamorphic complex, northern Canadian-Alaskan Cordillera, southeastern Alaska, U.S.A. [abs.], in Chappell, B.W., ed., *Hutton Symposium on Granites and Related Rocks*, 2nd, Canberra [Australia], 1991, Abstracts: Canberra, Australia, Bureau of Mineral Resources, Geology and Geophysics, p. 14.
- 1990, Tlevak Strait and Suez Island, southeastern Alaska, in Wood, p. 95.
- 1991, Geology, tectonics, and metallogeny of southeastern Alaska and adjacent parts of the Pacific Ocean rim [abs.]: GSA5, p. 218.
- *Brew, D.A., *Drew, L.J., *Schmidt, J.M., *Root, D.H., and *Huber, D.F., 1991, Undiscovered locatable mineral resources of the Tongass National Forest and adjacent areas, southeastern Alaska [abs.]: Alaska Miners Association, Juneau Branch, Conference, Juneau, Alaska, 1991, Abstracts of Professional Papers, p. 45-46.
- *Brew, D.A., *Hammarstrom, J.M., Himmelberg, G.R., *Wooden, J.L., *Loney, R.A., and *Karl, S.M., 1991, Crawfish Inlet pluton, Baranof Island, southeastern Alaska—a north-tilted Eocene body or an untilted enigma? [abs.]: GSA2, p. 8.
- *Brew, D.A., *Karl, S.M., *Barnes, D.F., *Jachens, R.C., *Ford, A.B., and Horner, Robert, 1991, A northern Cordilleran ocean-continent transect: Sitka Sound, Alaska, to Atlin Lake, British Columbia: Canadian Journal of Earth Sciences, v. 28, no. 6, p. 840-853.

- *Brewer, Max, 1991, Research projects on the National Petroleum Reserve [abs.], in Geiselman, Joy, and Mitchell, K.L., eds., Federal Arctic Research Information Workshop, Anchorage, Alaska, 1991, Proceedings: U.S. Department of the Interior, Minerals Management Service, OCS Study MMS 91-0053, p. 73-74.
- *Brocher, T.M., *Fisher, M.A., *Geist, E.L., *Moses, M.J., and *Hart, P.E., 1990, Images of subducting oceanic lithosphere and a mid-crustal decollement beneath southern Alaska [abs.]: Terra Abstracts, v. 2, p. 192.
- *Brocher, T.M., *Fisher, M.A., *Luzitano, Robert, *Fuis, G.S., *Labson, V.F., *Stanley, W.D., and Christensen, N.I., 1991, Crustal structure and evolution of the Alaska Range, Alaska [abs.]: GSA2, p. 8.
- *Brocher, T.M., *Moses, M.J., *Fisher, M.A., *Stephens, C.D., and *Geist, E.L., 1991, Images of the plate boundary beneath southern Alaska, in Meissner, Rolf, Brown, Larry, Dürbaum, H.-J., Franke, Wolfgang, Fuchs, Karl, and Seifert, Friedrich, eds., Continental lithosphere: Deep seismic reflections: Washington, D.C., American Geophysical Union, Geodynamics Series v. 22, p. 241-246.
- *Brocher, T.M., *Nokleberg, W.J., Christensen, N.I., *Lutter, W.J., *Geist, E.L., and *Fisher, M.A., 1991, Seismic reflection/refraction mapping of faulting and regional dips in the eastern Alaska Range: Journal of Geophysical Research, v. 96, no. B6, p. 10,233-10,249.
- *Bruns, T.R., *Fisher, M.A., *Geist, E.L., and *Brocher, T.M., 1990, Deep crustal structure across the Yakutat terrane—Prince William terrane subduction suture, northern Gulf of Alaska, from multichannel seismic reflection data [abs.]: Terra Abstracts, v. 2, p. 192-193.
- Burns, L.E., Pessel, G.H., Little, T.A., Pavlis, T.L., Newberry, R.J., *Winkler, G.R., and Decker, John, 1991, Geology of the northern Chugach Mountains, southcentral Alaska: Alaska Division of Geological and Geophysical Surveys Professional Report 94, 63 p., 2 sheets, scale 1:63,360.
- *Cacchione, D.A., and *Drake, D.E., 1991, Bottom and near-bottom sediment dynamics in Norton Sound, Alaska in U.S. Department of Commerce and U.S. Department of the Interior, OCSEAP, Final reports of principal investigators v. 74: U.S. Department of the Interior, Minerals Management Service, OCS Study MMS 91-0085, p. 77-143.
- *Cady, J.W., 1991, Angayucham and Tozitna geophysical domains—Geophysical and geochemical ties between parts of the Angayucham and Tozitna terranes, northern Alaska [abs.]: Eos, p. 296.
- *Carlson, P.R., 1990, GLORIA imagery provides clues to Quaternary sedimentary history in the Gulf of Alaska [abs.], in American Association for the Advancement of Science, Arctic Division, Circumpolar Perspectives, Arctic Science Conference, Anchorage, Alaska, 1990, Proceedings, p. 46.
- *Carlson, P.R., *Bruns, T.R., and *Fisher, M.A., 1990, Development of slope valleys in the glacial environment of a complex subduction zone, northern Gulf of Alaska, in Dowdeswell, J.A., and Scourse, J.D., eds., Glacial marine environments: Processes and sediments: Geological Society of London Special Publication 53, p. 139-153.
- *Carlson, P.R., *Stevenson, A.J., *Mann, D.M., *Bruns, T.R., and Dobson, M., 1991, From glaciers to deep-sea fans: Quaternary sedimentation in Gulf of Alaska [abs.]: GSA5, p. 385.
- *Carter, L.D., and *Whelan, J.F., 1991, Isotopic evidence for restricted Arctic sea ice during a late Pleistocene warm period: Implications for sea ice during future climatic warming at high latitudes [abs.]: GSA5, p. 237.
- *Chouet, B.A., *Page, R.A., Davies, J.N., and Power, J.A., 1991, Forecasting eruptions at Redoubt Volcano, Alaska [abs.]: GSA2, p. 13.
- 1991, Forecasting eruptions at Redoubt Volcano, Alaska [abs.]: Seismological Research Letters, v. 62, no. 1, p. 25.
- *Clifton, H.E., 1990, Variation in sequence development in transgressive-regressive successions on the western margin of North America [abs.] in International Sedimentological Congress, 13th, Nottingham, England, 1990, Abstracts of Papers, p. 96. [Narrow Cape Formation on southern Kodiak Island is one of the four examples.]
- Crampin, Stuart. [Comment on] and, *Brocher, T.M., and Christensen, N.I., [Reply on] "Seismic anisotropy due to preferred mineral orientation observed in shallow crustal rocks in southern Alaska": Geology, v. 19, no. 8, 1991, p. 859-860. [Original article appeared in Geology, v. 18, 1990, p. 737-740.]
- *Deming, D., *Sass, J.H., and *Lachenbruch, A.H., 1991, Heat flow and subsurface temperature as evidence for basin-scale groundwater flow, N. Slope of Alaska [abs.]: Eos, p. 504.
- *Dorava, J.M., 1991, Generalized stream channel evolution resulting from the 1989-90 eruptions of Redoubt Volcano, Alaska [abs.]: Eos, p. 214.
- *Dumoulin, J.A., and *Harris, A.G., 1991, Lower and Middle Paleozoic metacarbonate rocks of the Snowden Mountain area, central Brooks Range, northern Alaska [abs.]: Eos, p. 300.
- *Dusel-Bacon, Cynthia, and Hansen, V.L., 1991, High-pressure, medium-temperature early Mesozoic metamorphism and deformation within the Yukon-Tanana composite terrane, eastern Alaska [abs.]: GSA2, p. 20.
- Ellas, S.A., Short, S.K., *Waythomas, C.F., and Ten Brink, N.W., 1991, Late Quaternary paleoenvironments of the north Alaska Range [abs.], in Workshop, p. 62.
- *Foster, H.L., 1990, Prindle, eastern Alaska, in Wood, p. 108-109.
- *Frost, G.M., and *Stanley, R.G., 1991, Preliminary geologic and Bouguer gravity map of the Nenana basin area, central Alaska [abs.]: GSA2, p. 26.
- *Frost, T.P., and *Box, S.E., 1991, Depth controls on magmatism-related gold and mercury mineralization, Bethel quadrangle, southwestern Alaska [abs.]: GSA2, p. 27.
- *Fuis, G.S., *Ambos, E.L., *Mooney, W.D., Christensen, N.I., and *Geist, Eric, 1991, Crustal structure of accreted terranes in southern Alaska, Chugach Mountains and Copper River basin, from seismic refraction results: Journal of Geophysical Research, v. 96, no. B3, p. 4187-4227.
- *Fuis, G.S., and Clowes, R.M., 1991, A comparison of deep continental-margin structure along transects in southern Alaska, southern Vancouver Island, and central California [abs.]: GSA2, p. 42.
- *Fuis, G.S., *Lutter, [*Moore, T.E.], W.J., Levander, A.R., and

- Wissinger, E.S., 1991, A preliminary seismic-velocity model for the uppermost crust of the Brooks Range, arctic Alaska [abs.]: *Eos*, p. 296.
- *Fuis, G.S., and *Plafker, George, 1991, Evolution of deep structure along the Trans-Alaska Crustal Transect, Chugach Mountains and Copper River basin, southern Alaska: *Journal of Geophysical Research*, v. 96, no. B3, p. 4229-4253.
- *Galloway, J.P., 1991, Development of an Alaskan radiocarbon data base as a subset of the international radiocarbon data base (IRDB) [abs.]: *GSA2*, p. 28.
- Gebrels, G.E., McClelland, W.C., Samson, S.D., Patchett, P.J., and *Brew, D.A., 1991, U-Pb geochronology of Late Cretaceous and early Tertiary plutons in the northern Coast Mountains batholith: *Canadian Journal of Earth Sciences*, v. 28, no. 6, p. 899-911.
- *Geist, E.L., *Scholl, D.W., and *Vallier, T.L., 1991, Collision of the Aleutian island arc with Kamchatka [abs.]: *Eos*, p. 440.
- *Goldfarb, R.J., 1989, Genesis of Iode gold deposits of the southern Alaskan Cordillera [abs.]: *Fluid Inclusion Research*, v. 22, p. 128. [Abstract of Ph.D. thesis, Boulder, Colo., Univ. of Colorado.]
- *Goldfarb, R.J., *Leach, D.L., *Rose, S.C., and *Landis, G.P., 1989, Fluid inclusion geochemistry of gold-bearing quartz veins of the Juneau gold belt, southeastern Alaska: Implications for ore genesis [abs.]: *Fluid Inclusion Research*, v. 22, p. 128.
- *Goldfarb, R.J., Newberry, R.J., *Pickthorn, W.J., and *Gent, C.A., 1991, Oxygen, hydrogen, and sulfur isotope studies in the Juneau gold belt, southeastern Alaska: Constraints on the origin of hydrothermal fluids: *Economic Geology*, v. 86, no. 1, p. 66-80.
- *Goldfarb, R.J., *Snee, L.W., Miller, L.D., and Newberry, R.J., 1991, New evidence for widespread fluid flow and gold deposition in southeast Alaska at 55 Ma [abs.]: *GSA2*, p. 29.
- 1991, Rapid dewatering of the crust deduced from ages of mesothermal gold deposits: *Nature*, v. 354, no. 6351, Nov. 28, p. 296-298.
- 1991, Timing of gold deposition within the Juneau gold belt [abs.]: Alaska Miners Association, Juneau Branch, Conference, Juneau, Alaska, 1991, Abstracts of Professional Papers, p. 12-13.
- *Grantz, Arthur, and *Moore, T.E., 1991, Crustal model of northern Alaska from the Brooks Range to the Arctic Ocean basin [abs.]: *GSA2*, p. 30.
- 1991, A prediction of the crustal structure of the Brooks Range, Alaska, based on regional geologic and gravity data [abs.]: *Eos*, p. 299.
- *Grantz, Arthur, *Moore, T.E., and Roeske, Sarah, 1991, Gulf of Alaska to Arctic Ocean: Boulder, Colo., Geological Society of America, Centennial Continent/Ocean Transect #15, 72 p., 3 pls., scale 1:500,000.
- *Gray, J.E., *Goldfarb, R.J., *Detra, D.E., and *Slaughter, K.E., 1991, Geochemistry and exploration criteria for epithermal cinnabar and stibnite vein deposits in the Kuskokwim River region, southwestern Alaska: *Journal of Geochemical Exploration*, v. 41, no. 3, p. 363-386.
- *Griscom, Andrew, and *Sauer, P.E., 1991, Tectonics of the Aleutian subduction fault in the northern Gulf of Alaska from magnetic data [abs.]: *GSA2*, p. 31.
- *Hamilton, T.D., 1991, The last interglaciation and the Old Crow tephra: Data from 10 Alaskan sites [abs.], in Workshop, p. 68-69.
- *Hamilton, T.D., Westgate, J.A., and Begét, J.E., 1991, The Old Crow tephra: A stratigraphic marker for the last interglaciation in Alaska and the Yukon Territory? [abs.]: *GSA5*, p. 62.
- *Heinrichs, T.A., *Mayo, L.R., Echelmeyer, K.E., and Harrison, W.D., 1991, Black Rapids Glacier, Alaska—Unexpected behavior during the quiescent phase of a surge-type glacier [abs.]: *Eos*, p. 158.
- *Hildreth, Wes, 1990, Griggs, Alaska Peninsula, in Wood, p. 72.
- 1990, Katmai, Alaska Peninsula, in Wood, p. 71-72.
- 1990, The Katmai eruption of 1912: a comparison with the Minoan eruption of Santorini, in Hardy, D.A., Keller, J., Galanopoulos, V.P., Flemming, N.C., and Druitt, T.H., eds., *Thera and the Aegean world III*: London, England, Thera Foundation, Earth, v. 2, p. 455-462. [Proceedings of the Third International Congress, Santorini, Greece, 1989.]
- 1990, Mageik, Alaska Peninsula, in Wood, p. 67-68.
- 1990, Novarupta, Falling Mountain, and Cerberus, Alaska Peninsula, in Wood, p. 70-71.
- 1990, Trident, Alaska Peninsula, in Wood, p. 68-69.
- 1991, The timing of caldera collapse at Mount Katmai in response to magma withdrawal toward Novarupta: *Geophysical Research Letters*, v. 18, no. 8, p. 1541-1544.
- Himmelberg, G.R., *Brew, D.A., and *Ford, A.B., 1991, Development of inverted metamorphic isograds in the western metamorphic belt, Juneau, Alaska: *Journal of Metamorphic Geology*, v. 9, no. 2, p. 165-180.
- *Hinkley, T.K., *Fitzpatrick, J.J., *Landis, G.P., *Rye, R.O., and Holdsworth, G., 1991, High-resolution paleoclimate reconstruction from Alaskan ice-core records [abs.]: *GSA5*, p. 352.
- *Horton, R.J., *Karl, S.M., *Griscom, Andrew, *Taylor, C.D., and *Bond, K.R., 1991, Annette Islands Reserve Mineral Assessment Project, southeast Alaska, in Manydeeds, S.A., and Smith, B.D., eds., *Mineral frontiers on Indian lands*, Annual Northwest Mining Convention, 97th, Spokane, Wash., 1991: U.S. Bureau of Indian Affairs, Division of Energy and Mineral Resources, p. 22-31, Introduction on p. 19-21.
- *Howell, D.G., Fehri, N., and *Bird, K.J., 1991, Thin- versus thick-skinned thrusting in the central Brooks Range orogen, Alaska—Constraints based on surface geology [abs.]: *Eos*, p. 295.
- *Johnson, M.J., *Howell, D.G., and *Bird, K.J., 1991, Use of vitrinite reflectance to constrain regional structural patterns: An example from the North Slope of Alaska [abs.]: *Eos*, p. 549-550.
- *Jolly, A.D., *Page, R.A., *Stephens, C.D., *Lahr, J.C., Power, J.A., and Cruse, G.R., 1991, Seismicity in the vicinity of Mt. Spurr volcano, south-central Alaska, based on revised velocity model [abs.]: *Eos*, p. 567.
- Kamata, Hiroki, Johnston, D.A., and *Waitt, R.B., 1991, Stratigraphy, chronology, and character of the 1976 pyro-

- clastic eruption of Augustine Volcano, Alaska: *Bulletin of Volcanology*, v. 53, no. 6, p. 407-419.
- *Karl, S.M., 1991, Regional geology of the Chichagof mining district, southeastern Alaska [abs.]: Alaska Miners Association, Juneau Branch, Conference, Juneau, Alaska, 1991, Abstracts of Professional Papers, p. 12-13.
- *Keith, T.E.C., 1991, Argillic alteration in the Novarupta vent region, Katmai National Park, Alaska: *Geophysical Research Letters*, v. 18, no. 8, p. 1549-1552.
- 1991, Fossil and active fumaroles in the 1912 eruptive deposits, Valley of Ten Thousand Smokes, Alaska: *Journal of Volcanology*, v. 45, no. 3-4, p. 227-254.
- *Keith, T.E.C., and *Ingebritsen, S.E., 1991, Advective flux of solutes and heat from the Valley of Ten Thousand Smokes, Katmai National Park, Alaska [abs.]: *Eos*, p. 551.
- *Kempema, E.W., *Reimnitz, Erk, and *Hunter, R.E., 1990, Flume studies and field observations of the interactions of frazil ice and anchor ice with sediment, in U.S. Department of Commerce, and U.S. Department of the Interior, Outer Continental Shelf Environmental Assessment Program, Final Reports of Principal Investigators, v. 72, p. 283-330. [“This is a report of flume experiments....Observations of frazil and anchor ice from the Alaskan Beaufort Sea also are presented.” This report has also been published as U.S. Geological Survey Open-File Report 86-515.]
- Kissling, Eduard, and *Lahr, J.C., 1991, Tomographic image of the Pacific slab under southern Alaska: *Eclogae Geologicae Helveticae*, v. 84, no. 2, p. 297-315.
- *Kleinman, J.W., and *Iwatsubo, E.Y., 1991, A geodetic network in the Novarupta area, Katmai National Park, Alaska: *Geophysical Research Letters*, v. 18, no. 8, p. 1517-1519.
- *Kvenvolden, K.A., *Collett, T.S., and *Williams, R.S., 1991, Methane in permafrost ice near Fairbanks, Alaska [abs.]: *Eos* (American Geophysical Union, Transactions), v. 72, no. 17, suppl., p. 67.
- *Kvenvolden, K.A., and *Lorenson, T.D., 1991, Varying amounts of methane in shallow permafrost cores from Alaska [abs.]: *Eos*, p. 162. [Three cores taken on the University of Alaska, Fairbanks, campus.]
- *Kvenvolden, Keith, *Lorenson, T.D., and *Collett, T.S., 1991, Arctic shelf gas hydrate as a possible source of methane [abs.]: *GSA5*, p. 238.
- *Labson, V.F., Rodriguez, B.D., Sampson, J.A., and Bisdorf, R.J., 1991, Deep crustal geoelectric structure in the vicinity of the Tintina fault zone, north-central Alaska [abs.]: *GSA2*, p. 43.
- *Labson, V.F., *Sampson, J.A., and *Heran, W.D., 1991, Magnetotelluric electrical resistivity profile across the Brooks Range, Alaska [abs.]: *Eos*, p. 300.
- *Landis, G.P., and *Hofstra, A.H., 1991, Fluid inclusion gas chemistry as a potential minerals exploration tool: Case studies from Creede, CO, Jerritt Canyon, NV, Coeur d'Alene district, ID and MT, southern Alaska mesothermal veins, and mid-continent MVT's: *Journal of Geochemical Exploration*, v. 42, no. 1, p. 25-59.
- Lange, I.M., *Nokleberg, W.J., and Newkirk, S.R., 1991, Primary and secondary textures in multiply deformed and metamorphosed Devonian age massive sulfide deposits, Yukon-Tanana terrane, Alaska [abs.]: *Geological Society of America Abstracts with Programs*, v. 23, no. 4, p. 40.
- Levander, A.R., Wissinger, E.S., *Fuis, G.S., and *Lutter, W.J., 1991, The 1990 Brooks Range seismic experiment: Near vertical incidence reflection images [abs.]: *Eos*, p. 296.
- Levander, A.R., Wissinger, E.S., Henrys, S.A., and *Fuis, G.S., 1991, Results from the 1988 and 1990 Brooks Range seismic experiments, arctic Alaska [abs.]: *Eos* (American Geophysical Union, Transactions), v. 72, no. 17, suppl., p. 273.
- *Light, T.D., *Brew, D.A., and *Ashley, R.P., 1989, The Alaska-Juneau and Treadwell lode gold systems, southeastern Alaska: U.S. Geological Survey Bulletin 1857, p. D27-D36 [Comment]: *Fluid Inclusion Research*, v. 22, p. 231.
- Lowell, R.P., and *Keith, T.E.C., 1991, Chemical and thermal constraints on models of thermal springs, Valley of Ten Thousand Smokes, Alaska: *Geophysical Research Letters*, v. 18, no. 8, p. 1553-1556.
- *Lutter, W.J., *Fuis, G.S., [*Moore, T.E.], Levander, A.R., and Wissinger, E., 1991, A simultaneous inversion of seismic travel-time data for the velocity and interface position for the 1990 Brooks Range experiment [abs.]: *Eos*, p. 300.
- *Major, J.J., 1991, Destructive geomorphic processes on volcanoes [abs.]: *Eos*, p. 228. [Redoubt Volcano is an example.]
- *Marincovich, Louie, Jr., and *Powell, C.L., II, [Comment on] and McNeil, D.H., and Miller, K.G., [Reply] “High-latitude application of $^{87}\text{Sr}/^{86}\text{Sr}$: Correlation of Nuwuk beds on North Slope, Alaska, to standard Oligocene chronostratigraphy”: *Geology*, v. 19, no. 5, 1991, p. 537-539. [Original article appeared in *Geology*, 1990, v. 18, no. 5, p. 415-418.]
- McNutt, S.R., *Miller, T.P., and Taber, J.J., 1991, Geological and seismological evidence of increased explosivity during the 1986 eruptions of Pavlov Volcano, Alaska: *Bulletin of Volcanology*, v. 53, no. 3, p. 86-98.
- Meen, J.K., *Snee, L.W., Ross, Kent, and Elthon, Don, 1991, Age and geologic relations of the Hall Cove Complex, Duke Island [abs.]: *GSA5*, p. 389.
- *Miller, M.L., *Bradshaw, J.Y., Kimbrough, D.L., *Stern, T.W., and Bundtzen, T.K., 1991, Isotopic evidence for Early Proterozoic age of the Idono Complex, west-central Alaska: *Journal of Geology*, v. 99, no. 2, p. 209-223.
- *Miller, T.P., 1990, Aniakchak, Alaska Peninsula, in Wood, p. 59-60.
- 1990, Black Peak, Alaska Peninsula, in Wood, p. 58-59.
- 1990, Dutton, Alaska Peninsula, in Wood, p. 51-52.
- 1990, Emmons and Hague, Alaska Peninsula, in Wood, p. 52-53.
- 1990, Fisher, eastern Aleutian Islands, in Wood, p. 46-48.
- 1990, Iliamna, Cook Inlet, Alaska, in Wood, p. 80-81.
- 1990, Pavlof and Pavlof Sister, Alaska Peninsula, in Wood, p. 53-54.
- 1990, Ugashik and Peulik, Alaska Peninsula, in Wood, p. 63-64.

- *Miller, T.P., and Davies, J.N., 1991, Volcanic hazards and earthquake potential of the North Pacific [abs.]: GSA5, p. 218. [Aleutian-Alaskan volcanic arc-trench system.]
- Moll, S.H., *Light, T.D., and *Bie, S.W., 1991, Digital methods for lode gold exploration in central Alaska [abs.]: GSA5, p. 414-415.
- *Moll-Stalcup, E.J., 1990, Kookooligit, Bering Sea, Alaska, in Wood, p. 104-105.
- 1990, St. Michael, western Alaska, in Wood, p. 103-104.
- 1990, Yukon Delta, western Alaska, in Wood, p. 99-102. [Ungulungwak Hill-Ingrihuak Hill, p. 100; Ingakslugwat Hills, p. 100-101; Nushkolik Mountain, p. 101; Ingrisarak Mountain, p. 102; Nelson Island, p. 102.]
- *Moll-Stalcup, E.J., and *Arth, J.G., 1991, Isotopic and chemical constraints on the petrogenesis of Blackburn Hills volcanic field, western Alaska: *Geochimica et Cosmochimica Acta*, v. 55, no. 12, p. 3753-3776.
- *Molnia, B.F., *Post, Austin, *Carlson, P.R., and *Trabant, D.C., 1991, Evolution and morphology of proglacial Vitus Lake, Bering Glacier, Alaska [abs.]: *Eos*, p. 158-159.
- *Molnia, B.F., *Trabant, D.C., *Post, Austin, and *Frank-Molnia, D.G., 1990, The potential for an irreversible calving retreat of Bering Glacier, Alaska [abs.], in American Association for the Advancement of Science, Arctic Division, Circumpolar Perspectives, Arctic Science Conference, Anchorage, Alaska, 1990, Proceedings, p. 44.
- Moore, J.C., Diebold, J., *Brocher, T.M., *Fisher, M.A., *Geist, E.L., *Moses, M.J., Talwani, M., Ewing, J.I., Davies, J., Stone, D., Sample, J., and von Huene, R., 1990, Comparison of EDGE and TACT images of subducting oceanic lithosphere and crustal reflectivity beneath southern Alaska [abs.]: *Terra Abstracts*, v. 2, p. 202.
- Moore, J.C., Diebold, John, *Fisher, M.A., Sample, J., *Brocher, T., Talwani, M., Ewing, John, von Huene, Roland, Rowe, C., Stone, D., *Stevens, Chris, and Sawyer, Dale, 1991, EDGE deep seismic reflection transect of the eastern Aleutian arc-trench layered lower crust reveals underplating and continental growth: *Geology*, v. 19, no. 5, p. 420-424.
- *Moore, T.E., *Nokleberg, W.J., Jones, D.L., *Till, A.B., and Wallace, W.K., 1991, Contrasting structural levels of the Brooks Range orogen along the Trans-Alaskan Crustal Transect (TACT) [abs.]: *Eos*, p. 295.
- *Moore, T.E., *Plafker, George, and *Weber, F.R., 1991, Evidence bearing on reconstruction of crystalline and sedimentary terranes in central Alaska [abs.]: GSA2, p. 80.
- *Moore, T.E., Wallace, W.K., and Jones, D.L., 1991, TACT geologic studies in the Brooks Range: Preliminary results and implications for crustal structure [abs.]: GSA2, p. 80.
- Motyka, R.J., *Trabant, D.C., and Noll, Rick, 1990, Preliminary analysis of the Taku Glacier advance [abs.], in American Association for the Advancement of Science, Arctic Division, Circumpolar Perspectives, Arctic Science Conference, Anchorage, Alaska, 1990, Proceedings, p. 13.
- Murphy, J.M., and *Patton, W.W., Jr., 1991, Apatite fission track studies on granitic plutons of the Yukon-Koyuk basin and Ruby geanticline, Alaska [abs.]: *Eos*, p. 505.
- Murphy, J.M., O'Sullivan, P.B., *Nelson, S., Miller, E.L., and *Moore, T.E., 1991, Apatite fission track thermochronology of the southern Brooks Range, Alaska: Evidence of episodic Tertiary uplift, segmentation and high-angle fault reactivation [abs.]: *Eos*, p. 299.
- Newberry, R.J., and *Brew, D.A., 1991, Stratabound sulfide deposits of uncertain origins in metamorphic rocks vs. Black box data: 3 Alaskan examples [abs.]: Alaska Miners Association, Juneau Branch, Conference, Juneau, Alaska, 1991, Abstracts of Professional Papers, p. 10-11. [Groundhog Basin prospect, 20 km east of Wrangell; Liberty Bell deposit, 25 km northeast of Healy; Dream prospect, 20 km northwest of Kensington.]
- *Nokleberg, W.J., *Foster, H.L., *Lanphere, M.A., *Aleinikoff, J.N., and Pavlis, T.L., 1991, Structure and tectonics of the Yukon-Tanana, Wickersham, Seventymile, and Stikinia terranes along the Trans-Alaska-Crustal-Transect (TACT), east-central Alaska [abs.]: GSA2, p. 84.
- *Nokleberg, W.J., and *Fisher, M.A., eds., 1989, Alaskan geological and geophysical transect, Valdez to Coldfoot, Alaska, June 24-July 5, 1989, in *Sedimentation and tectonics of western North America*, v. 1: Washington, D.C., American Geophysical Union, 28th International Congress Field Trip Series T104, p. T104:1-T104:131. [For detailed indexing of T104 see USGS Bulletin 1946, p. 116-121.]
- Oldow, J.S., Avé Lallemant, H.G., Gottschalk, R.R., and *Snee, L.W., 1991, Timing and kinematics of Cretaceous contraction and extension in the southern Brooks Range, Alaska [abs.]: *Eos*, p. 295.
- 1991, Timing and kinematics of Cretaceous contraction and extension in the southern Brooks Range, Alaska [abs.]: GSA2, p. 85.
- *Page, R.A., Biswas, N.N., *Lahr, J.C., and Pulpan, Hans, 1991, Seismicity of continental Alaska, in Slemmons, D.B., Engdahl, E.R., Zoback, M.D., and Blackwell, D.D., eds., *Neotectonics of North America: Boulder, Colo., Geological Society of America, DNAG series, Decade Map volume to accompany the neotectonic maps, part of the continent-scale maps of North America*, Chap. 4, p. 47-68.
- *Page, R.A., *Stephens, C.D., *Fogleman, K.A., *Brocher, T.M., *Fisher, M.A., and *Fuis, G.S., 1991, Seismicity and current tectonics of south-central Alaska [abs.]: GSA2, p. 86.
- Papike, J.J., *Keith, T.E.C., Spilde, M.N., Shearer, C.K., Galbreath, K.C., and Laul, J.C., 1991, Major and trace element mass flux in fumarolic deposits, Valley of Ten Thousand Smokes, Alaska, rhyolite-rich protolith: *Geophysical Research Letters*, v. 18, no. 8, p. 1545-1548.
- Papike, J.J., Spilde, M.N., and *Keith, T.E.C., 1991, Chemical mass flux in fumarolic deposits, Valley of Ten Thousand Smokes, Alaska: Influence of assumed protolith composition on enrichment/depletion systematics [abs.]: *Eos*, p. 551.
- Patrick, B.E., Dinklage, W.S., and *Till, A.B., 1991, Metamorphism and progressive deformation in the Walker Lake region of the southern Brooks Range, Alaska [abs.]: GSA2, p. 87.
- *Patton, W.W., Jr., 1991, Deep crustal composition of the

- Yukon-Koyukuk basin, Alaska [abs.]: GSA2, p. 88.
- Phillips, R.L., *Grantz, Arthur, *Mullen, M.W., *Chase, T., and *Young, J., 1990, Preliminary stratigraphy and sediment processes on southeastern Northwind Ridge, Arctic Ocean [abs.], in *Sediments 1990, International Sedimentological Congress, 13th, Nottingham, England, 1990, Abstracts of Posters*, p. 176.
- *Plafker, George, 1990, Regional vertical tectonic displacement of shorelines in south-central Alaska during and between great earthquakes: *Northwest Science*, v. 64, no. 5, p. 250-258.
- *Plafker, George, *Lajoie, K.R., and *Rubin, Meyer, 1991, New data on the recurrence interval and seismic cycle for great 1964-type earthquakes in the Copper River delta, Alaska [abs.]: *Seismological Research Letters*, v. 62, no. 1, p. 38.
- *Reimnitz, Erk, and *Kempema, E.W., 1990, Field observations on slush ice generated during freezeup in Arctic coastal waters, in U.S. Department of Commerce, and U.S. Department of the Interior, Outer Continental Shelf Environmental Assessment Program, Final Reports of Principal Investigators, v. 72, p. 331-355.
- *Reimnitz, Erk, *Kempema, E.W., and *Barnes, P.W., 1990, Anchor ice and bottom-freezing in high-latitude marine sedimentary environments: Observations from the Alaskan Beaufort Sea, in U.S. Department of Commerce, and U.S. Department of the Interior, Outer Continental Shelf Environmental Assessment Program, Final Reports of Principal Investigators, v. 72, p. 257-281. [This report has also been published as U.S. Geological Survey Open-File Report 86-298.]
- *Richter, D.H., 1990, Capital, Wrangell Mountains, Alaska, in Wood, p. 89-90.
- 1990, Drum, Wrangell Mountains, Alaska, in Wood, p. 86-87.
- 1990, Eastern Wrangell, Wrangell Mountains, Alaska, in Wood, p. 91-92.
- 1990, Sanford, Wrangell Mountains, Alaska, in Wood, p. 87.
- 1990, Tanada, Wrangell Mountains, Alaska, in Wood, p. 90-91.
- *Riehle, J.R., 1990, Chiginagak, Alaska Peninsula, in Wood, p. 61-62.
- 1990, Edgecumbe, southeastern Alaska, in Wood, p. 93-94.
- 1990, Hayes, Cook Inlet, Alaska, in Wood, p. 84-85.
- 1990, Kialagvik, southeast Alaska [should be "Alaska Peninsula"], in Wood, p. 62-63.
- 1990, Yantarni, Alaska Peninsula, in Wood, p. 60-61.
- Roeske, S.M., Murphy, J.M., and *Snee, L.W., 1991, Isotopic constraints on the metamorphic and cooling history of high P/low T and moderate P/high T metamorphic rocks and E. Cretaceous granites in the SW Ruby terrane, central Alaska [abs.]: *Eos*, p. 440.
- Roeske, S.M., *Snee, L.W., and Pavlis, T.L., 1991, Strike-slip and accretion events along the southern Alaska plate margin in the Cretaceous and early Tertiary [abs.]: GSA5, p. 428-429.
- Roeske, S.M., *Walter, Marianne, and *Aleinikoff, J.N., 1991, Cretaceous deformation of granitic rocks in the southwest Ruby terrane, central Alaska [abs.]: GSA2, p. 93.
- *Saltus, R.W., Stone, D.B., Kienle, J., and Goodliffe, A.M., 1991, New gravity data at Katmai National Park, Alaska, suggest a magma body analogue to that at the Geysers-Clear Lake region, California [abs.]: *Eos*, p. 429.
- *Savage, J.C., and *Lisowski, M., 1991, Strain accumulation along the Denali fault at the Nenana River and Delta River crossings, Alaska: *Journal of Geophysical Research*, v. 96, no. B9, p. 14,481-14,492.
- *Savage, J.C., and *Plafker, George, 1991, Tide gage measurements of uplift along the south coast of Alaska: *Journal of Geophysical Research*, v. 96, no. B3, p. 4325-4335.
- *Scholl, D.W., and *Stevenson, A.J., 1991, Exploring the idea that early Tertiary evolution of the Alaska orocline and the Aleutian-Bering Sea region is a manifestation of Kula-plate-driven Cordilleran tectonism and escape tectonics? [abs.]: GSA5, p. 435.
- 1991, Tectonic evolution of the Pacific's Alaska-Bering Sea rim in terms of large-scale plate-boundary driven transgressive deformation [abs.], in *Toronto 1991, Geological Association of Canada, Mineralogical Association of Canada and Society of Economic Geologists, Joint Annual Meeting, Toronto, Canada, 1991, Program with Abstracts*, p. A112.
- *Schoonmaker, J.W., Jr., *Jones, J.E., and *Molnia, B.F., 1989, Preliminary results of glacier studies from digital radar data, in *Agenda for the 90's, ASPRS/ACSM (American Society for Photogrammetry and Remote Sensing, and American Congress on Surveying and Mapping) Annual Convention, Baltimore, Md., 1989, Technical Papers*, v. 3, p. 1-9.
- *Stanley, W.D., *Nokleberg, W.J., and *Labson, V.F., 1991, Flysch belts and collisional processes: Eastcentral Alaska and Alpine-Carpathian regions [abs.]: GSA2, p. 100.
- *Starratt, S.W., 1991, Late Quaternary paleoceanography of the Navarin basin region, Bering Sea: Evidence from diatom floras and radiolarian faunas [abs.]: GSA2, p. 100.
- *Stricker, G.D., 1991, Economic Alaskan coal deposits, in Gluskoter, H.J., Rice, D.D., and Taylor, R.B., eds., *Economic geology, U.S.: Boulder, Colo., Geological Society of America, Geology of North America*, v. P-2, Chap. 37, p. 591-602, pl. 7.
- Swanson, S.E., Begét, J.E., and *McGimsey, R.G., 1991, Compositional equivalence of tephra and lava groundmass glasses in the 1989-90 eruption of Mount Redoubt, Alaska: Implications for eruption monitoring [abs.]: GSA5, p. 396.
- Taber, J.J., Billington, S., and *Engdahl, E.R., 1991, Seismicity of the Aleutian arc, in Slemmons, D.B., Engdahl, E.R., Zoback, M.D., and Blackwell, D.D., eds., *Neotectonics of North America: Boulder, Colo., Geological Society of America, DNAG series, Decade Map volume to accompany the neotectonic maps, part of the continent-scale maps of North America*, Chap. 3, p. 29-46.
- *Thompson, Ken, 1991, [USGS] Water Resources Division Arctic research [abs.], in Geiselman, Joy, and Mitchell, K.L., eds., *Federal Arctic Research Information Workshop, Anchorage, Alaska, 1991, Proceedings: U.S. Department of the Interior, Minerals Management Service, OCS Study MMS 91-0053*, p. 74-75.

- *Till, A.B., and *Moore, T.E., 1991, Tectonic relations of the schist belt, southern Brooks Range, Alaska [abs.]: *Eos*, p. 295-296.
- *Till, A.B., and Patrick, B.E., 1991, Ar-Ar evidence for a 110-105 MA amphibolite-facies overprint on blueschist in the south-central Brooks Range, Alaska [abs.]: *GSA5*, p. 436.
- *Trabant, D.C., *Molnia, B.F., and *Post, Austin, 1991, Bering Glacier, Alaska—Bed configuration and potential for calving retreat [abs.]: *Eos*, p. 159.
- Underwood, M.B., Laughland, M., Shelton, K., Solomon, R., Kang, S.M., Orr, R., Brocculeri, T., Bergfeld, D., and *Pawlewicz, M., 1991, Correlations among paleotemperature indicators within orogenic belts: Examples from pelitic rocks of the Franciscan Complex (California) and the Kandik Basin, Alaska [abs.]: *Eos*, p. 549.
- *Vallier, T.L., 1990, Koniujji, central Aleutian Islands, in Wood, p. 28-29.
- *Waitt, R.B., 1991, Repeated failures of summit domes of Augustine Volcano delivering tsunami-generating debris avalanches to Cook Inlet, Alaska [abs.]: *Eos*, p. 602.
- *Waitt, R.B., and Begét, J.E., 1991, Tsunami hazard from debris avalanches off Augustine Volcano, Alaska [abs.]: *Eos*, p. 227-228.
- Walker, H.J., and *Brewer, M.C., 1991, The Colville River delta: Hydrologic characteristics [abs.], in Workshop, p. 28.
- Walker, H.J., and *Brewer, M.C., 1991, The Colville River delta: Morphology [abs.], in Workshop, p. 27.
- Walker, H.J., and *Brewer, M.C., 1991, When Colville River water meets the sea [abs.], in Workshop p. 29.
- *Ward, P.L., *Pitt, A.M., and *Endo, Eliot, 1991, Seismic evidence for magma in the vicinity of Mt. Katmai, Alaska: *Geophysical Research Letters*, v. 18, no. 8, p. 1537-1540.
- Warne, J.E., Gardner, M.H., Ethridge, F.G., Houston, W.S., and *Flores, R.M., 1991, Tertiary non-marine stratigraphic section along Shelikof Straits, Katmai National Park, Alaska [abs.]: *GSA2*, p. 107.
- *Waythomas, C.F. and Kaufman, D.S., [Comment on] and Bigelow, N., Begét, J.E., and Powers, W.R., [Reply on], and Begét, J.E., Bigelow, Nancy, and Powers, Roger, 1991, [Reply to Comment on] "Latest Pleistocene increase in wind intensity recorded in eolian sediments from central Alaska": *Quaternary Research*, v. 36, no. 3, p. 329-338. [Original article appeared in *Quaternary Research*, v. 34, 1990, p. 160-168.]
- *White, Willis, 1991, Activities of the Branch of Alaska Geology [abs.], in Geiselman, Joy, and Mitchell, K.L., eds., Federal Arctic Research Information Workshop, Anchorage, Alaska, 1991, Proceedings: U.S. Department of the Interior, Minerals Management Service, Alaska OCS Region OCS Study MMS 91-0053, p. 71.
- *Wilson, F.H., 1990, Kupreanof (Stepovak Bay) Alaska Peninsula, in Wood, p. 55-56.
- 1991, Geology of the Alaska Peninsula, southwestern Alaska, and the Alaska Peninsula terrane [abs.]: *GSA5*, p. 435.
- *Wiltshire, D.A., and *Molnia, B.F., 1990, Arctic data interactive: A hypermedia system [abs.], in American Association for the Advancement of Science, Arctic Division, Circumpolar Perspectives, Arctic Science Conference, Anchorage, Alaska, 1990, Proceedings, p. 48.
- Wissinger, E.S., Levander, A.R., *Lutter, W.J., and *Fuis, G.S., 1991, The 1990 Brooks Range seismic experiment: Near vertical incidence reflection data processing [abs.]: *Eos*, p. 299.
- *Wong, F.L., 1990, St. George, Bering Sea, Alaska, in Wood, p. 97-98.
- 1990, St. Paul, Bering Sea, Alaska, in Wood, p. 96-97.
- *Yount, M.E., 1990, Dana, Alaska Peninsula, in Wood, p. 55.
- 1990, Redoubt, Cook Inlet, Alaska, in Wood, p. 81-82.
- 1990, Veniaminof, Alaska Peninsula, in Wood, p. 56-58.
- Zoback, M.D., and *Zoback, M.L., 1991, Tectonic stress field of North America and relative plate motions, in Slemmons, D.B., Engdahl, E.R., Zoback, M.D., and Blackwell, D.D., eds., *Neotectonics of North America: Boulder, Colo., Geological Society of America, DNAG series, Decade Map volume to accompany the neotectonic maps, part of the continent-scale maps of North America*, Chap. 19, p. 339-366.